LINKING STOMATAL DEVELOPMENT AND PHYSIOLOGY: FROM STOMATAL MODELS TO NON-MODEL SPECIES AND CROPS

EDITED BY: Caspar Christian Cedric Chater, Graham Dow, Elena D. Shpak, Scott McAdam and Michael T. Raissig

PUBLISHED IN: Frontiers in Plant Science

frontiers Research Topics

frontiers

ISSN 1664-8714
ISBN 978-2-88971-707-1
DOI 10.3389/978-2-88971-707-1

About Frontiers

Frontiers is more than just an open-access publisher of scholarly articles: it is a pioneering approach to the world of academia, radically improving the way scholarly research is managed. The grand vision of Frontiers is a world where all people have an equal opportunity to seek, share and generate knowledge. Frontiers provides immediate and permanent online open access to all its publications, but this alone is not enough to realize our grand goals.

Frontiers Journal Series

The Frontiers Journal Series is a multi-tier and interdisciplinary set of open-access, online journals, promising a paradigm shift from the current review, selection and dissemination processes in academic publishing. All Frontiers journals are driven by researchers for researchers; therefore, they constitute a service to the scholarly community. At the same time, the Frontiers Journal Series operates on a revolutionary invention, the tiered publishing system, initially addressing specific communities of scholars, and gradually climbing up to broader public understanding, thus serving the interests of the lay society, too.

Dedication to Quality

Each Frontiers article is a landmark of the highest quality, thanks to genuinely collaborative interactions between authors and review editors, who include some of the world's best academicians. Research must be certified by peers before entering a stream of knowledge that may eventually reach the public - and shape society; therefore, Frontiers only applies the most rigorous and unbiased reviews.
Frontiers revolutionizes research publishing by freely delivering the most outstanding research, evaluated with no bias from both the academic and social point of view. By applying the most advanced information technologies, Frontiers is catapulting scholarly publishing into a new generation.

What are Frontiers Research Topics?

Frontiers Research Topics are very popular trademarks of the Frontiers Journals Series: they are collections of at least ten articles, all centered on a particular subject. With their unique mix of varied contributions from Original Research to Review Articles, Frontiers Research Topics unify the most influential researchers, the latest key findings and historical advances in a hot research area! Find out more on how to host your own Frontiers Research Topic or contribute to one as an author by contacting the Frontiers Editorial Office: frontiersin.org/about/contact

LINKING STOMATAL DEVELOPMENT AND PHYSIOLOGY: FROM STOMATAL MODELS TO NON-MODEL SPECIES AND CROPS

Topic Editors:
Caspar Christian Cedric Chater, Royal Botanic Gardens, United Kingdom
Graham Dow, ETH Zürich, Switzerland
Elena D. Shpak, The University of Tennessee, Knoxville, United States
Scott McAdam, Purdue University, United States
Michael T. Raissig, Heidelberg University, Germany

Citation: Chater, C. C. C., Dow, G., Shpak, E. D., McAdam, S., Raissig, M. T., eds. (2021). Linking Stomatal Development and Physiology: From Stomatal Models to Non-Model Species and Crops. Lausanne: Frontiers Media SA.
doi: 10.3389/978-2-88971-707-1

Table of Contents

frontiers in Plant Science

EDITORIAL
published: 30 September 2021
doi: 10.3389/fpls.2021.743964

Editorial: Linking Stomatal Development and Physiology: From Stomatal Models to Non-model Species and Crops

Scott A. M. McAdam[1], *Caspar C. C. Chater*[2]*, *Elena D. Shpak*[3], *Michael T. Raissig*[4] and *Graham J. Dow*[5]

[1] Purdue Center for Plant Biology, Department of Botany and Plant Pathology, Purdue University, West Lafayette, IN, United States, [2] Royal Botanic Gardens, Kew, Richmond, United Kingdom, [3] Department of Biochemistry, Cellular and Molecular Biology, University of Tennessee, Knoxville, Knoxville, TN, United States, [4] Centre for Organismal Studies Heidelberg, Heidelberg University, Heidelberg, Germany, [5] Molecular Plant Breeding, Institute of Agricultural Sciences, ETH Zurich, Zurich, Switzerland

Keywords: stomata/guard cells < gas exchange < physiology, guard cell development, stomatal evolution and behavior, plant abiotic response, stomatal ABA response, guard cell (GC), stomata

OPEN ACCESS

Edited by:
Dongliang Xiong, Huazhong Agricultural University, China

Reviewed by:
Christopher David Muir, University of Hawaii, United States
Yujie Wang, California Institute of Technology, United States

***Correspondence:**
Caspar C. C. Chater
c.chater@kew.org

Specialty section:
This article was submitted to Plant Development and EvoDevo, a section of the journal Frontiers in Plant Science

Received: *19 July 2021*
Accepted: *01 September 2021*
Published: *30 September 2021*

Citation:
McAdam SAM, Chater CCC, Shpak ED, Raissig MT and Dow GJ (2021) Editorial: Linking Stomatal Development and Physiology: From Stomatal Models to Non-model Species and Crops. Front. Plant Sci. 12:743964. doi: 10.3389/fpls.2021.743964

Editorial on the Research Topic

Linking Stomatal Development and Physiology: From Stomatal Models to Non-model Species and Crops

Stomata are highly dynamic valves in the epidermis of plants. These microscopic structures regulate the exchange of gases with the atmosphere and are essential for plant survival on land (Raven, 2002). There is an enduring fascination with stomata because of their specialized nature: from their unique development out of undifferentiated epidermal cells; to the environmental and internal signals they respond to; and the impacts their function have on climate and global change. These key themes have been the topic of many classical compendiums and scientific conferences (Jarvis and Mansfield, 1981; Ziegler et al., 1987; Roelfsema and Kollist, 2013). Research in the past two decades has accelerated our understanding of stomatal function, particularly through the accumulation of a critical mass of knowledge on the genetic underpinnings of stomatal development and physiology in the model angiosperm *Arabidopsis* (Assmann and Jegla, 2016; Qi and Torii, 2018). In this Frontiers eBook, we sought to bring together the latest research and reviews on stomatal biology that span a vast continuum: from cells to ecosystems. The articles were solicited with four key themes in mind: (1) The coordination of stomatal development with plant growth, development, and environmental signaling; (2) The role of stomatal development in plant acclimation and adaptation to the environment; (3) The influence of stomatal development and function on plant resource use, ecosystem processes, and global climate; and (4) The selection for stomatal traits in plant evolution, crop domestication and breeding, and designing food for the future.

The research contributed to this eBook encompasses the wide diversity of topics studied by contemporary stomatal biologists. At a phylogenetic level, works describe the unique stomata of mosses (Caine et al.; Renzaglia et al.), grasses (Buckley et al.; Serna), and a species of C_3-CAM dicot *Mesembryanthemum* (Guan et al.). At the developmental level, articles describe critical stomatal developmental genes (Chen et al.), the physiological development of stomatal function in leaves (Kane et al.), and important signals for stomatal regulation in developing *Citrus* fruit (Lugassi et al.). At a functional scale, research spans the molecule to the leaf, with reports on the importance of aerosol deposition on stomatal function (Grantz et al.), the role of subsidiary cells in stomatal regulation (Gray et al.), the molecular link between reactive oxygen species (ROS) and abscisic

acid (ABA) signaling in guard cells (Postiglione and Muday), and the importance of ROS and salicylic acid (SA) on stomatal responses to CO_2 (He et al.). Novel and unexplored mechanisms are proposed by two papers, one which describes the evolutionary pressures placed on stomatal development by pathogens (Muir) and the other which finds divergent stomatal strategies driven by competition between species (Zenes et al.).

The bryophytes, including mosses, form a monophyletic group that is sister to all other land plants and represent the oldest extant lineage of plants to possess stomata, having diverged from the ancestor of vascular plants more than 400 million years ago (de Sousa et al., 2019). Caine et al. show shared and divergent control of stomatal ontogeny in the model moss species *Physcomitrium patens* through bHLH transcription factor and signaling peptide orthologs conserved in the angiosperm stomatal program (Chen et al.). In addition to the conserved one-cell spacing rule for moss stomata (**Figure 1**), the authors observe environmental plasticity in the development of moss substomatal cavities (Caine et al.), suggesting a more complex role for bryophyte stomata in the maturation of the reproductive sporophyte capsule. Insight into stomatal function in this lineage is scarce (Chater et al., 2016; Kubásek et al., 2021). In a comprehensive phylogenetic screening across mosses, Renzaglia et al. find that stomata have been lost more than 63 times across this lineage and there is considerable variation in the number of stomata per capsule within and between families. This discovery raises questions about the possible functions of stomata in bryophytes, and by extension in the common ancestor of all extant land plants. Renzaglia et al. suggest that stomata are functionally dispensable for spore dispersal in mosses, although their continued presence in species that do have stomata suggests that stomatal opening offers a fitness advantage by facilitating the desiccation of the sporophyte capsule (Caine et al.).

Grasses, of which domesticated cereal crops provide more than 50% of globally consumed calories (Yu and Tian, 2018), have long been recognized as having unique stomatal complexes comprised of dumbbell-shaped guard cells flanked by highly specialized subsidiary cells (Strasburger, 1866; **Figure 1**). This stomatal complex may have evolved to enhance stomatal response speed, and is only found in Poaceae and Cyperaceae (Raschke, 1975; Nunes et al., 2020). Only recently are we starting to reveal the genes responsible for the development of these unique stomatal complexes. Serna provides a contemporary perspective on our understanding of the genetic control of C_3 and C_4 grass stomatal complexes, in which orthologs of the bHLH transcription factor MUTE have been co-opted as regulators of subsidiary cell differentiation and specialization (Raissig et al., 2016; Wang et al., 2019; Wu et al., 2019). Buckley et al. provide a highly complementary review to this discussion on the unique developmental regulators of grass stomata, by detailing the possible gene targets in the stomatal development network that could be utilized for the generation of climate-ready cereal crops. The genetic regulation of stomatal development in grasses stands in contrast to the regulation of stomatal development in other

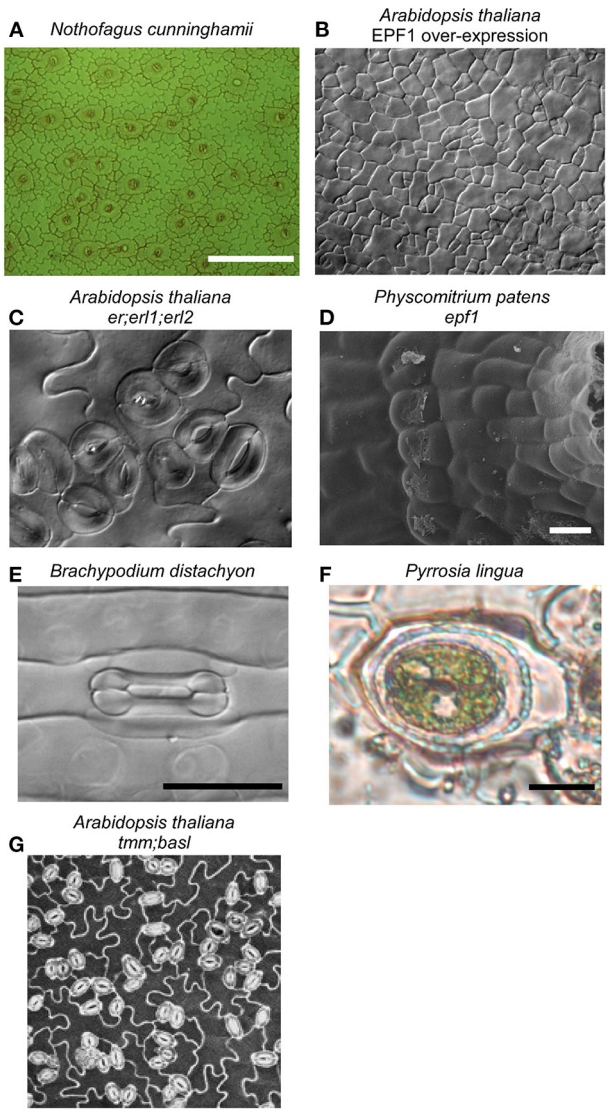

FIGURE 1 | Stomata are found on the aerial parts of most land plants, in the highest densities on the leaves of vascular plants, like the temperate rainforest tree *Nothofagus cunninghamii* **(A)**. Considerable insights into the molecular determinants of stomatal development have been made in *Arabidopsis thaliana*, with the discovery that SPEECHLESS is essential for stomata formation; when it is constitutively inhibited by the EPF/ERF signaling pathway, epidermal cells can not differentiate into stomata **(B)**. Mutants in this pathway, like the *er;erl1;erl2* triple mutant in *Arabidopsis* **(C)** and *epf1* mutant in the moss *Physcomitrium patens* (Caine et al., 2016) **(D)**, both having similarly clustered stomata, indicating that all land plants use the same pathway for stomatal development. Considerable diversity in stomatal form exists across land plants, exemplified by the dumbbell-shaped guard cells and associated subsidiary cells of some species of monocot, including the grass *Brachypodium distachyon* **(E)**. Subsidiary cell arrangement is highly diverse across land plants, in some ferns including *Pyrrosia lingua* both guard cells are surrounded by a single, encircling subsidiary cell **(F)**. Neighboring cells can impact stomatal function, with compromised stomatal responses reported in stomatal developmental mutant lines that have increased stomatal clustering (Dow et al., 2014), like the *tmm;basl* double mutant of *Arabidopsis* **(G)**.

species (Chen et al.), for example, provide a compelling case for the pivotal importance of the bHLH transcription factor SPEECHLESS in the development of stomata in *Arabidopsis* (**Figure 1**).

The grasses provide an extreme example of the subsidiary cells that flank guard cells (**Figure 1**). There are numerous unique subsidiary cell arrangements described across land plants (Baranova, 1987), yet their functional role and relevance remain mostly enigmatic. Gray et al. provide a modern synthesis on subsidiary cell development, diversity, and what little we know about subsidiary cell function. Gray et al. conclude that future work utilizing new model systems with highly complex subsidiary cell arrangements has the potential to advance our understanding of how they develop and their roles in stomatal function across diverse plants. It is tempting to speculate that subsidiary cell morphological complexity is indicative of a broad functional diversity as extensions of the stomatal complex; perhaps providing spatio-temporally distinct reservoirs of essential metabolites, ions, and signaling components for optimal guard cell responses or mechanically accommodating guard cell movement. Future single-cell transcriptomic and metabolomic studies may help determine exactly what these subsidiary cell functions are.

For over 150 years researchers have investigated the environmental and endogenous signals that cause stomata to open and close in mature tissue (von Mohl, 1856), however very little work has focused on how stomatal function develops (Pantin et al., 2013). To address this, Kane et al. investigated when stomata begin to function in developing leaves. Newly expanding leaves tend to have high rates of water loss and the authors show the majority originates from the immature cuticle and not stomata. In young leaves, stomata have not yet fully developed and remain shut; they only appear to open and control water loss once the leaf is approaching full expansion and cuticular conductance reaches a minimum (Kane et al.). Stomata are not only found on leaves; in many angiosperm species stomata are also found on the epidermis of fruit (Blanke and Lenz, 1989). Lugassi et al. investigated stomatal function as fruit develop and found that stomata on immature *Citrus* fruit are functional and responsive to sugars via hexokinase, just like a leaf. As fruit develop, stomata become plugged, which greatly reduces fruit transpiration. Lugassi et al. developed a transgenic *Citrus* plant that had guard cell specific expression of hexokinase and found that these plants had reduced seed development and more closed stomata during fruit formation, suggesting that functional stomata on immature *Citrus* fruit are critical for seed formation. Physiologically active stomata on green immature fruits likely contribute a carbon source for photosynthesis in this rapidly developing organ, prior to their switch from source to carbon sink duration maturation; correlating with the loss of the fruit's stomatal function and photosynthetic capacity. The timing of this transition could be a breeding target for the control of fruit ripening and flavor traits.

Since the advent of stomatal research, responses have been detected via direct measurement of single pores or gas exchange measurements providing mean approximations of the aperture of many thousands of stomata (Darwin, 1898). Grantz et al. show that while there is considerable variation in individual stomatal apertures across a large leaf surface area exposed to similar conditions, stomatal apertures are quasi-normally distributed, and remain so when responding to VPD and atmospheric pollutants. This result provides an important experimental bridge between measurements of stomatal responses made at a local, individual pore scale, with those measured at a leaf level (Grantz et al.).

Stomatal closure is a key adaptation to conserve water during periods of water deficit or to optimize water use relative to photosynthetic carbon gain (Cowan and Farquhar, 1977; Brodribb et al., 2017). Characterizing the signals of stomatal closure is a core target of modern stomatal biology and has great potential for increasing crop productivity via modern breeding techniques (Anjanappa and Gruissem, 2021; Horton et al., 2021). Halophytes, or plants that can survive in high salt environments, have evolved some of the most extreme adaptations to retain and use scarce available water, including adaptations to stomatal regulation (Shabala, 2013). *Mesembryanthemum crystallinum* is an emerging model system for discovering the molecular pathways of plant tolerance to salt or extremely limited available free-water (Guan et al.). Guan et al. characterized the unique ability of this plant to switch between C_3 and CAM photosynthesis under salt stress, finding the transition takes approximately 6 days and elicits a major switch in diurnal stomatal rhythm and photosynthetic regulation. The hormone abscisic acid (ABA) plays a critical role in stomatal closure during water deficit and the signaling pathway for this direct response is well described (Geiger et al., 2010; Brandt et al., 2012). Postiglione and Muday provide a thorough review of the role of ABA-induced ROS signaling in guard cell regulation, a signaling pathway that operates in parallel to the direct ABA pathway. Postiglione and Muday conclude that ROS are a critical component of guard cell ABA signaling and that future work will reveal the relative importance of the direct action of ABA and ROS on stomatal responses. In parallel to this work, He et al. demonstrate that both ROS and salicylic acid (SA) are essential in the stomatal response to elevated CO_2 in *Arabidopsis*. He et al. found that ROS originates from two different sources in the guard cells depending on whether stomata are closed by elevated CO_2 or if light-induced opening is inhibited by it. Furthermore, SA is required for elevated CO_2-induced stomatal closure (He et al.), increasing the complexity of the hormonal landscape of guard cell regulation (Jarvis and Mansfield, 1981).

Modeling continues to be a powerful tool to propose and test hypotheses related to stomatal function and development (Ziegler et al., 1987). To this end, Muir developed a new model that examines the trade-off between maximum anatomical stomatal conductance, as determined by stomatal size and density, and the risk of pathogen infection. This model proposes some non-intuitive, yet testable, hypotheses related to the evolution of stomatal development in response to pathogen infection risk and provides a new framework for understanding the developmental trade-offs between maximizing leaf gas exchange and minimizing infection (Muir). Zenes et al. also utilize a new model of plant water use to analyze experimental findings on the shift in plant water use strategies in response to

competition. The adaptation in water use strategy in response to competitors can be accurately predicted by a model that assumes plants maximize carbon gain while only mitigating water use that prevents the risk of hydraulic failure by embolism (Zenes et al.). This result shifts our understanding of how plants manage water use away from exclusively optimizing carbon gain relative to water use, toward maximizing carbon gain while preventing lethal hydraulic thresholds (Anderegg et al., 2018). The mechanism behind these shifts in water use strategy in response to competition remain uncharacterized and provides an exciting prospect for future studies. Although (Zenes et al.) focus on C3 tree seedlings, it would be interesting to see how this model fairs with C4 and CAM plant species.

CONCLUSION

Modern stomatal biology continues to investigate research questions that span a vast continuum of disciplines from the cell to the ecosystem. In this Research Topic "Linking Stomatal Development and Physiology: From Stomatal Models to Non-models and Crops," research articles and reviews cover much of this continuum. Among the topics included: ancient evolution of stomatal development and function; further description of the complex genetic models governing stomatal development; and the identification of breeding targets for improved water use and productivity in agricultural systems. Nevertheless, with such a broad topic as stomata, many themes inevitably remain unaddressed. For example, insights into C_2 and C_4 stomatal responses, circadian stomatal rhythms, and stomatal thermal responses are just some of the areas not covered here. However, a universal theme amongst this diverse stomatal research, linking plant gas exchange and photosynthetic mechanisms, is testament to the sheer importance that these tiny plant structures have on our understanding of plant development, function, and evolution.

AUTHOR CONTRIBUTIONS

SM wrote the first draft and all co-authors contributed equally to writing the manuscript and developing the figure. All authors contributed to the article and approved the submitted version.

REFERENCES

Anderegg, W. R. L., Wolf, A., Arango-Velez, A., Choat, B., Chmura, D. J., Jansen, S., et al. (2018). Woody plants optimise stomatal behaviour relative to hydraulic risk. *Ecol. Lett.* 21, 968–977. doi: 10.1111/ele.12962

Anjanappa, R. B., and Gruissem, W. (2021). Current progress and challenges in crop genetic transformation. *J. Plant Physiol.* 261, 153411. doi: 10.1016/j.jplph.2021.153411

Assmann, S. M., and Jegla, T. (2016). Guard cell sensory systems: recent insights on stomatal responses to light, abscisic acid, and CO_2. *Curr. Opin. Plant Biol.* 33, 157–167. doi: 10.1016/j.pbi.2016.07.003

Baranova, M. A. (1987). Historical development of the present classification of morphological types of stomates. *Bot. Rev.* 53, 53–79. doi: 10.1007/BF02858182

Blanke, M. M., and Lenz, F. (1989). Fruit photosynthesis. *Plant Cell Environ.* 12, 31–46. doi: 10.1111/j.1365-3040.1989.tb01914.x

Brandt, B., Brodsky, D. E., Xue, S., Negi, J., Iba, K., Kangasjärvi, J., et al. (2012). Reconstruction of abscisic acid activation of SLAC1 anion channel by CPK6 and OST1 kinases and branched ABI1 PP2C phosphatse action. *Proc. Natl. Acad. Sci. U.S.A.* 109, 10593–10598. doi: 10.1073/pnas.1116590109

Brodribb, T. J., McAdam, S. A., and Carins Murphy, M. R. (2017). Xylem and stomata, coordinated through time and space. *Plant Cell Environ.* 40, 872–880. doi: 10.1111/pce.12817

Caine, R. S., Chater, C. C. C., Kamisugi, Y., Cuming, A. C., Beerling, D. J., Gray, J. E., et al. (2016). An ancestral stomatal patterning module revealed in the non-vascular land plant Physcomitrella patens. *Development* 143, 3306–3314. doi: 10.1242/dev.135038

Chater, C. C., Caine, R. S., Tomek, M., Wallace, S., Kamisugi, Y., Cuming, A. C., et al. (2016). Origin and function of stomata in the moss *Physcomitrella patens*. *Nat. Plants* 2, 16179. doi: 10.1038/nplants.2016.179

Cowan, I. R., and Farquhar, G. D. (1977). Stomatal function in relation to leaf metabolism and environment. *Symp. Soc. Exp. Biol.* 31, 471–505.

Darwin, F. (1898). Observartions on stomata. *Proc. R. Soc. Lond* 63, 413–417. doi: 10.1098/rspl.1898.0053

de Sousa, F., Foster, P. G., Donoghue, P. C. J., Schneider, H., and Cox, C. J. (2019). Nuclear protein phylogenies support the monophyly of the three bryophyte groups (Bryophyta Schimp.). *New Phytol.* 222, 565–575. doi: 10.1111/nph.15587

Dow, G. J., Berry, J. A., and Bergmann, D. C. (2014). The physiological importance of developmental mechanisms that enforce proper stomatal spacing in *Arabidopsis thaliana*. *New Phytol.* 201, 1205–1217. doi: 10.1111/nph.12586

Geiger, D., Scherzer, S., Mumm, P., Marten, I., Ache, P., Matschi, S., et al. (2010). Guard cell anion channel SLAC1 is regulated by CDPK protein kinases with distinct Ca^{2+} affinities. *Proc. Natl. Acad. Sci. U.S.A.* 107, 8023–8028. doi: 10.1073/pnas.0912030107

Horton, P., Long, S. P., Smith, P., Banwart, S. A., and Beerling, D. J. (2021). Technologies to deliver food and climate security through agriculture. *Nat. Plants* 7, 250–255. doi: 10.1038/s41477-021-00877-2

Jarvis, P. G., and Mansfield, T. A. (1981). *Stomatal Physiology*. Cambridge: Cambridge University Press.

Kubásek, J., Hájek, T., Duckett, J., Pressel, S., and Šantruček, J. (2021). Moss stomata do not respond to light and CO_2 concentration but facilitate carbon uptake by sporophytes: a gas exchange, stomatal aperture, and 13C-labelling study. *New Phytol.* 230, 1815–1828. doi: 10.1111/nph.17208

Nunes, T. D. G., Zhang, D., and Raissig, M. T. (2020). Form, development and function of grass stomata. *Plant J.* 101, 780–799. doi: 10.1111/tpj.14552

Pantin, F., Renaud, J., Barbier, F., Vavasseur, A., Le Thiec, D., Rose, C., et al. (2013). Developmental priming of stomatal sensitivity to abscisic acid by leaf microclimate. *Curr. Biol.* 23, 1805–1811. doi: 10.1016/j.cub.2013.07.050

Qi, X., and Torii, K. U. (2018). Hormonal and environmental signals guiding stomatal development. *BMC Biol.* 16:21. doi: 10.1186/s12915-018-0488-5

Raissig, M. T., Abrash, E., Bettadapur, A., Vogel, J. P., and Bergmann, D. C. (2016). Grasses use an alternatively wired bHLH transcription factor network to establish stomatal identity. *Proc. Natl. Acad. Sci. U.S.A.* 113, 8326–8331. doi: 10.1073/pnas.1606728113

Raschke, K. (1975). Stomatal action. *Annu. Rev. Plant Physiol.* 26, 309–340. doi: 10.1146/annurev.pp.26.060175.001521

Raven, J. A. (2002). Selection pressures on stomatal evolution. *New Phytol.* 153, 371–386. doi: 10.1046/j.0028-646X.2001.00334.x

Roelfsema, M. R. G., and Kollist, H. (2013). Tiny pores with a global impact. *New Phytol.* 197, 11–15. doi: 10.1111/nph.12050

Shabala, S. (2013). Learning from halophytes: physiological basis and strategies to improve abiotic stress tolerance in crops. *Ann. Bot.* 112, 1209–1221. doi: 10.1093/aob/mct205

Strasburger, E. (1866). Ein beitrag zur entwicklungsgeschichte der spaltöffnungen. *Jahrb. Wiss. Bot* 5, 297–342.

von Mohl, H. (1856). Welche ursachen bewirken die erweiterung und verengung der spaltöffnungen? *Bot. Zeitung* 14, 697–704, 713–721.

Wang, H., Guo, S., Qiao, X., Guo, J., Li, Z., Zhou, Y., et al. (2019). BZU2/ZmMUTE controls symmetrical division of guard mother cell and specifies neighbor cell fate in maize. *PLoS Genet.* 15:e1008377. doi: 10.1371/journal.pgen.1008377

Wu, Z., Chen, L., Yu, Q., Zhou, W., Gou, X., Li, J., et al. (2019). Multiple transcriptional factors control stomata development in rice. *New Phytol.* 223, 220–232. doi: 10.1111/nph.15766

Yu, S., and Tian, L. (2018). Breeding major cereal grains through the lens of nutrition sensitivity. *Mol. Plant* 11, 23–30. doi: 10.1016/j.molp.2017.08.006

Ziegler, H., Farquhar, G. D., and Cowan, I. R. (1987). *Stomatal Function.* Stanford, CA: Stanford University Press.

Conflict of Interest: The authors declare that the research was conducted in the absence of any commercial or financial relationships that could be construed as a potential conflict of interest.

Publisher's Note: All claims expressed in this article are solely those of the authors and do not necessarily represent those of their affiliated organizations, or those of the publisher, the editors and the reviewers. Any product that may be evaluated in this article, or claim that may be made by its manufacturer, is not guaranteed or endorsed by the publisher.

frontiers in Plant Science

PERSPECTIVE
published: 11 February 2020
doi: 10.3389/fpls.2020.00055

The Role of Grass *MUTE* Orthologues During Stomatal Development

*Laura Serna**

Facultad de Ciencias Ambientales y Bioquímica, Universidad de Castilla-La Mancha, Toledo, Spain

Gas exchange between the plant and the atmosphere takes place through stomatal pores formed by paired guard cells. Grasses develop a unique stomatal structure that consists of two dumbbell-shaped guard cells flanked by lateral subsidiary cells. These structures confer a very efficient gas exchange capacity, which may have contributed to the evolutionary success of grasses. Recent works have identified orthologues of Arabidopsis *MUTE* in three grass species: *BdMUTE* in *Brachypodium distachyon*, *BZU2/ZmMUTE* in maize, and *OsMUTE* in rice. These genes induce the recruitment of subsidiary cells, and it appears to rely upon the ability of intercellular movement, from the guard mother cell to subsidiary mother cells, of the proteins encoded by them. Unexpectedly, this function of these grass *MUTE* genes contrasts with that of Arabidopsis *MUTE*, which promotes guard mother cell identity. These *MUTE* orthologues also appear to control guard mother cell fate progression, with the action of *BdMUTE* being less severe than those of *BZU2/ZmMUTE* and *OsMUTE*. The emerging picture unravels that grass *MUTE* genes have not only diverged, due to neo-functionalization, from Arabidopsis *MUTE*, but also among them.

Keywords: grasses, MUTE, orthologues, polarization, stomata, subsidiary cells

OPEN ACCESS

Edited by:
Michael T. Raissig,
Heidelberg University, Germany

Reviewed by:
Chun-Peng Song,
Henan University, China
Suiwen Hou,
Lanzhou University, China
Robert Spencer Caine,
University of Sheffield,
United Kingdom

***Correspondence:**
Laura Serna
laura.serna@uclm.es

Specialty section:
This article was submitted to Plant Development and EvoDevo, a section of the journal Frontiers in Plant Science

Received: *05 November 2019*
Accepted: *15 January 2020*
Published: *11 February 2020*

Citation:
Serna L (2020) The Role of Grass MUTE Orthologues During Stomatal Development. Front. Plant Sci. 11:55. doi: 10.3389/fpls.2020.00055

INTRODUCTION

Plants colonized land more than 400 million years ago (Edwards et al., 1998; Berry et al., 2010). One of the key innovations that enabled this to be possible was the development of a waxy cuticle to prevent water loss from the plant surface (Berry et al., 2010). The appearance of this impermeable layer coincides with the presence of stomatal pores, thus allowing the uptake of carbon dioxide to perform photosynthesis with a minimal loss of water vapor (Edwards et al., 1998; Berry et al., 2010). These microscopic innovations, bordered by a pair of kidney-shaped guard cells (GCs), are conserved across all land plants except liverworts and some mosses and hornworts (Chater et al., 2017; Renzaglia et al., 2017). Although to date no other structures has replaced the stoma, its shape, and its relationship with other epidermal cells have changed over time. Grasses, which develop a unique stomatal structure consisting of two dumbbell-shaped GCs flanked by two lateral subsidiary cells (SCs) (Stebbins and Shah, 1960; Rudall et al., 2017; Hepworth et al., 2018; Nunes et al., 2019), are a beautiful example of these changes. In addition, several works comparing stomatal responses between grasses and species with different stomatal morphology suggest that the stomatal complexes of grasses increase stomatal responsiveness with large and rapid GC movements

(Franks and Farquhar, 2007; Bertolino et al., 2019 and references therein). Moreover, it has even been proposed that this developmental innovation has contributed, at least in part, to the extraordinary evolutionary success of this plant group (Kellogg, 2001; Hetherington and Woodward, 2003; Chen et al., 2017).

In the leaves of grasses, stomatal development occurs only in some epidermal cell files and it proceeds acropetally, with early stages of this process taking place in the basal regions of the leaf and stomata developing later in the distal ones (Stebbins and Shah, 1960). The development of four-celled stomatal complexes takes place through a simple and invariant pattern of cell divisions (Stebbins and Shah, 1960; Serna, 2011; Hepworth et al., 2018; Nunes et al., 2019; **Figure 1A**). They initiate with an asymmetric cell division from a protodermal cells leading to a smaller guard mother cell (GMC) and a larger sister cell. Before GMC division, cells from files in either side of newly formed GMC acquire subsidiary mother cell (SMC) identity and divide asymmetrically. The smaller cells resulting from these divisions, which are always placed next to the GMC, differentiate as SCs. Following SCs recruitment, the GMC divides symmetrically, with the cell division plane being parallel to the main axis of leaf growth, and it yields the paired GCs. This cell division pattern differs from that taking place in Arabidopsis (Serna and Fenoll, 2000; Bergmann and Sack, 2007; **Figure 1A**). First, in Arabidopsis, stomatal precursors, named meristemoids, are self-renewing cells. They can undergo several rounds of cell division in an inward spiral, regenerating themselves in each division, before assuming GMC identity. In contrast, in grasses, an asymmetric division directly gives rise to the stomatal precursor. Thus, meristemoids appear to be absent in this plant group. Second, the GMC of Arabidopsis does not recruit SCs. In addition, while grasses form dumbbell-shaped GCs, eudicots and most monocots develop kidney-shaped GCs pairs (Stebbins and Shah, 1960).

The recruitment of SCs in grasses is preceded by a process of polarization of the SMC that is very well known in maize (Serna, 2015; Apostolakos et al., 2018; **Figure 2**). This begins with the accumulation of the SCAR/WAVE regulatory complex (WRC) at the cell surface of the SMC, specifically at the site of GMC

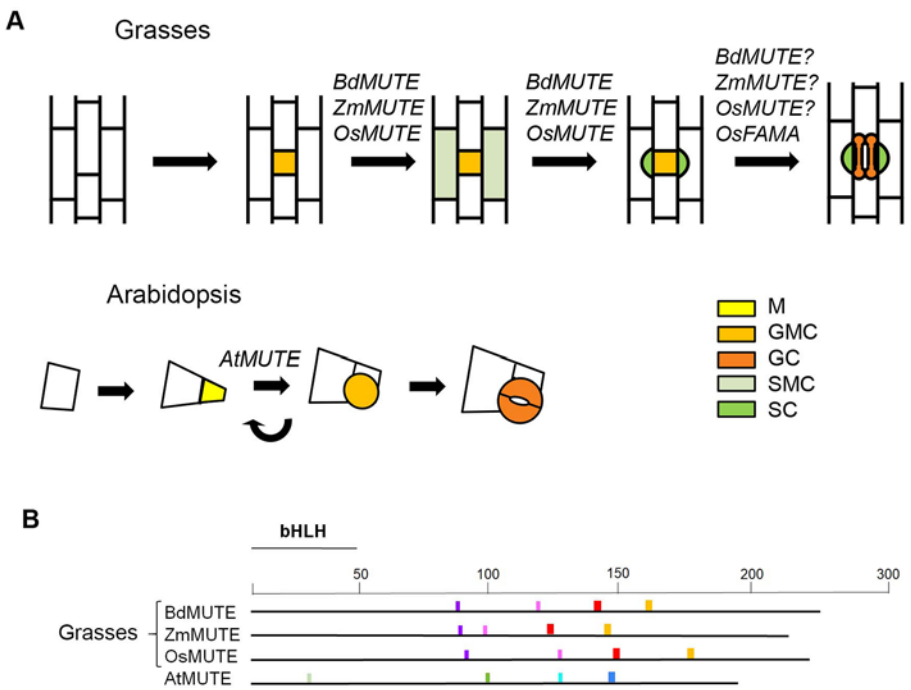

FIGURE 1 | Role of *MUTE* orthologues of grasses and *AtMUTE* during stomatal development. **(A)** Stomatal development in grasses starts with an asymmetric division that produces a guard mother cell (GMC). Before GMC division, cells from files on either side of the GMC assume subsidiary mother cell (SMC) identity. SMCs then divide asymmetrically to produce subsidiary cells (SCs) in direct contact with the GMC. Only when the GMC is flanked by the two SCs, a symmetric cell division produces the two dumbbell-shaped guard cells (GCs). Grass *MUTE* genes specify SMC identity. They also appear to control the fate of the GMC, with the action of *BdMUTE* being less severe than those of *ZmMUTE* and *OsMUTE*. *OsFAMA* regulates the last stage of stomatal development. In Arabidopsis, a protodermal cell divides asymmetrically to produce a meristemiod (M) and a larger pavement cell. Ms usually reiterate asymmetric division several times, in an inward spiral, until they assume GMC identity. The GMC divides symmetrically to produce the two kidney-shaped GCs. *AtMUTE* regulates the transition of the M to GMC. **(B)** Schematic diagram of potential mobility motifs in the MUTE protein sequences. Conserved motifs in grass MUTE proteins could promote the intercellular movement, from the GMC to SMC, of these transcriptional factors. In contrast, the motifs conserved in AtMUTE could prevent its intercellular movement. The different-coloured boxes represent different motifs. These motifs are conserved among grasses but not in eudicots or vice versa, or are different between grasses and eudicots. Arabidopsis motifs are shown as an example of eudicot ones. The position of the bHLH domain is indicated. GC, guard cell; GMC, guard mother cell; M, meristemoid. SMC, subsidiary mother cell; SC, subsidiary cell.

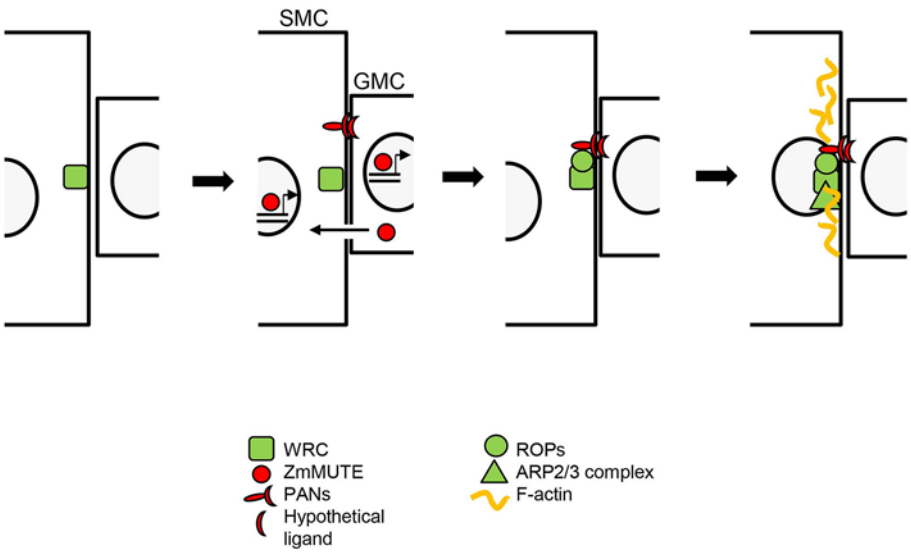

FIGURE 2 | ZmMUTE role during the polarization of the subsidiary mother cell (SMC) in maize. The WAVE regulatory complex (WRC) complex polarizes to the cell surface of the SMC, at the site of guard mother cell (GMC) contact. ZmMUTE moves from the GMC to SMCs, where it binds to *PANs* promoters and promotes their induction. PANs accumulate, in a WRC-dependent manner, at the SMC/GMC contact site. PANs then recruit and activate ROPs. Activated ROPs physically interact and activate the WRC, which activates the ARP2/3 complex. Finally, ARP2/3 activity produces a dense F-actin patch and promotes nuclear migration towards the GMC in an actin-dependent manner. ZmMUTE may also exert a cell-autonomous role inducing, directly or indirectly, the expression of the hypothetical ligands of PANs. GMC, guard mother cell. SMC, subsidiary mother cell.

contact (Facette et al., 2015). Unknown signals emanating from GMC activate PANs receptors, which also, in a WRC-dependent manner (Facette et al., 2015), accumulate at the SMC/GMC contact site (Cartwright et al., 2009; Zhang et al., 2012). Then PANs recruit and activate ROPs (Humphries et al., 2011), which activate the WRC complex (Facette et al., 2015). Finally, activated WRC activates the ARP2/3 complex giving rise to a dense T-actin and inducing the migration of the nucleus toward the GMC (Deeks and Hussey, 2005).

Over the last twenty-five years, the isolation and characterization of numerous genes have illuminated our understanding of stomatal development in Arabidopsis. In this model plant, three basic helix-loop-helix (bHLH) transcription factors, SPEECHLESS (SPCH), MUTE, and FAMA sequentially specify stomatal lineage identity, regulate the transition from meristemoids to GMCs, and promote GCs differentiation, respectively (Ohashi-Ito and Bergmann, 2006; MacAlister et al., 2007; Pillitteri et al., 2007). The function of these transcriptional factors requires heterodimerization with the functionally redundant bHLH proteins ICE1 or SCREAM2 (Kanaoka et al., 2008). With origins which predate the divergence of the mosses and hornworts, these bHLH proteins diverged prior to the monocot-dicot split (Chater et al., 2017; Hepworth et al., 2018, and references therein). This divergence enabled the emergence of new protein functions, which are essential for the unique stomatal development of grasses (Raissig et al., 2017; Wang et al., 2019; Wu et al., 2019).

Recent works have uncovered the role of three orthologues of Arabidopsis *MUTE* during stomatal development in three grass species (Raissig et al., 2017; Wang et al., 2019; Wu et al., 2019): *BdMUTE* of *Brachypodium distachyon*, *BZU2/ZmMUTE* of *Zea mays* (maize) and *OsMUTE* of *Oryza sativa* (rice). The role of these genes, regulating the formation of SCs (Raissig et al., 2017; Wang et al., 2019; Wu et al., 2019), differs from that of *AtMUTE*. These orthologues of *MUTE* also seem to regulate the identity of the GMC, with the action of *BdMUTE* in this process being less severe. Taken together, these recent discoveries suggest not only that *MUTE* orthologues of grasses have diverged from *AtMUTE*, but also that *MUTE* genes of domesticated grasses studied thus far have diverged comparatively to *BdMUTE*.

MUTE ORTHOLOGUES OF GRASSES RECRUIT SCs

In *Brachypodium*, maize and rice, like in other grass species, stomatal complexes comprise a pair of dumbbell-shaped GCs associated with two SCs (Campbell, 1881; Stebbins and Shah, 1960; Shoemaker and Srivastava, 1973; Kamiya et al., 2003; Raissig et al., 2017). Interestingly, the mutants *subsidiary cell identity defective* (*sid*) of *B. distachyon*, *bizui2* (*bzu2*) of maize and *c-osmute* of rice, in addition to having impaired other steps of the stomatal developmental, fail to recruit SCs (Raissig et al., 2017; Wang et al., 2019; Wu et al., 2019). These mutants have alterations in their orthologues of Arabidopsis *MUTE* (Raissig et al., 2017; Wang et al., 2019; Wu et al., 2019): *sid* in *BdMUTE*, *bzu2-1* in *BZU2/ZmMUTE* and *c-osmute* in *OsMUTE*. The function of these *MUTE* orthologues contrasts with that of *AtMUTE*, which triggers GMC formation only in Arabidopsis (MacAlister et al., 2007; Pillitteri et al., 2007; **Table 1**).

How do these grass orthologues of Arabidopsis *MUTE* recruit SCs? The expression of the *yellow fluorescent protein* (*YFP*) under the control of the *BdMUTE* promoter showed that its

induction is restricted to GMCs and GCs (Raissig et al., 2017). However, analysis of transgenic plants expressing the protein encoded by *YFP-BdMUTE* construct driven by the *BdSPCH2* promoter showed that BdMUTE locates not only in GMCs but also in SMCs (Raissig et al., 2017). Considering that the *BdSPCH2* promoter is active only in the stomatal lineage cells (Raissig et al., 2016), Raissig et al. (2017) inferred that BdMUTE protein moves from the GMC to epidermal cells of neighboring files. In consonance, successful complementation experiments of *sid* mutants with a fusion of the *BdMUTE* promoter to the *YFP-BdMUTE* construct lights up not only GMCs and young GCs, but also SMCs and young SCs (Raissig et al., 2017). In rice, *YFP-OsMUTE* expression driven by the *OsMUTE* promoter, whose induction in the developing four-celled complex is restricted to GMCs (Liu et al., 2009; Wang et al., 2019), lights up also GMCs and SMCs (Wang et al., 2019). This indicates that OsMUTE, like BdMUTE, also moves from the GMC to epidermal cells of neighboring files (Wang et al., 2019). Maize expressing *YFP-ZmMUTE* driven by the *ZmMUTE* promoter illuminates also GMCs, young GCs and SMCs (Wang et al., 2019). Assuming that the cellular localization of the *ZmMUTE* promoter induction is restricted to GMCs and young GCs, ZmMUTE would also move from the GMC to epidermal cells of neighboring files. Indeed, ZmMUTE protein is also able to move from the GMCs to SMCs in rice, and to epidermal cells adjacent to the stoma in Arabidopsis (Wang et al., 2019). These experiments strongly suggest that the recruitment of SCs in grasses depends on the intercellular movement of the grass MUTE proteins. Interestingly, the overexpression of *BdMUTE* driven by the *Ubi* constitutive promoter produces not only lateral, but also polar SCs (Raissig et al., 2017). This emphasizes the relationship between SCs recruitment and intercellular movement of MUTE orthologues in grasses. However, direct proof conclusively validating that the SCs formation relies upon the grass MUTE intercellular movement is lacking.

Multiple studies have shown that transcriptional factors move among cells *via* plasmodesmata (Han et al., 2014). GMCs of *Brachypodium* are symplastically connected with surrounding epidermal cells (Raissig et al., 2017). Therefore, BdMUTE may also move from the GMC to cells of neighboring files through plasmodesmata. But, what allows this protein to move laterally but not radially? Plasmodesmata continuously adjust their permeability in response to multiple cues (Sager and Lee, 2018). In addition, it is known that the control of this permeability is essential to the proper segregations of cell fate determinants during stomatal development in Arabidopsis (Guseman et al, 2010; Kong et al., 2012). Therefore, the lateral mobility of BdMUTE, and the unique design of the grass stomatal complexes, could depend on the restriction of the permeability of the plasmodesmata that symplastically connect cells of the same row. Future research should include delving in this direction.

TABLE 1 | Functions of *AtMUTE* and *MUTE* orthologues of grasses.

Gene name	Species	Gene function	References
AtMUTE	*Arabidopsis thaliana* (Eudicot)	Transition from M to GMC	MacAlister et al., 2007; Pillitteri et al., 2007
BdMUTE	*Brachypodium distachyon* (Monocot, Poaceae)	Recruitment of SCs. Less severely, GMC and GCs identities	Raissig et al., 2017
BZU2/ ZmMUTE	*Zea mays* (Monocot, Poaceae)	Recruitment of SCs and GMC identity. Early events in SMC polarization	Wang et al., 2019
OsMUTE	*Oryza sativa* (Monocot, Poaceae)	Recruitment of SCs and GMC identity	Wu et al., 2019

GCs, guard cells; GMC, guard mother cell; M, meristemoid; SMC, subsidiary mother cell; SCs, subsidiary cells.

ZmMUTE REGULATES EARLY EVENTS IN SMC POLARIZATION

MUTE orthologues of grasses move from the GMC to the cells of neighboring files and this is linked with the formation of SCs. But, what do they do there? Wang and co-workers (2019) examined the role of *ZmMUTE,* specifically with regard to the regulation of SMC polarization. They found that cells adjacent to stomata, placed in neighboring epidermal files, of the *bzu2-1* mutant, in contrast to the wild type, do not show enrichment of F-actin patches at the GMC contact sites or polarization of their nuclei (Wang et al., 2019). This indicates that SMC polarization is not cell-autonomous, and that *ZmMUTE* regulates this process (**Table 1**). The *bzu2-1* mutation downregulates the transcription of both *PAN1* and *PAN2*, indicating that ZmMUTE transcriptional factor positively regulates *PAN1* and *PAN2* expression (Wang et al., 2019). Because PAN1, whose polarization at the SMC/GMC interface requires PAN2 (Cartwright et al., 2009; Zhang et al., 2012), recruits and activates ROPs (Humphries et al., 2011), ZmMUTE must induce *PANs* expression before ROPs polarization (**Figure 2**). Interestingly, while the *bzu2-1* mutant is almost devoid of SCs (Wang et al., 2019), most of the SCs of *pan1* and *pan2* mutants show no defects and most probably they derive from normal asymmetric cell divisions (Gallagher and Smith, 2000; Cartwright et al., 2009; Zhang et al., 2012; Facette et al., 2015). Therefore, ZmMUTE, or its downstream transcriptional factors, controls the expression not only of *PANs*, but also of other unknown genes to induce the recruitment of SCs. Among these genes could be those that encode for the hypothetical ligands of PANs, and his discovery would reveal one of the best-kept secrets of SMC polarization. If this is so, and assuming that these ligands emanate from the GMC, ZmMUTE may have both cell-autonomous and non-cell-autonomous functions (**Figure 2**).

Yeast one-hybrid and EMSA experiments showed that ZmMUTE binds to the E-box P1 and P2 motifs of the *PAN1* and *PAN2* promoters respectively (Wang et al., 2019). This suggests that the action of ZmMUTE on the expression of these genes may be direct. This does not rule out that ZmMUTE could also indirectly affect the activity of *PAN1* and *PAN2* promoters through upregulation of positive regulators

and/or downregulation of repressors of *PANs* expression. For example, the transcriptional factor Glis3, directly and indirectly, regulates the expression of the insulin gene (Yang et al., 2009). The ZmMUTE protein does not bind the E-box P3 motif of the *PAN2* promoter *in vitro*, but ChlP-qPCR data indicate that it binds this motif *in vivo* (Wang et al., 2019). This suggests that the ZmMUTE protein physically interacts with other proteins to activate the E-box P3 of the *PAN2* promoter (Wang et al., 2019). Interestingly, yeast two-hybrid and bimolecular fluorescence complementation assays have just showed that its orthologue of rice, OsMUTE, interacts with OsICE1 and OsICE2 (Wu et al., 2019). Therefore, ZmMUTE may interact with their homologs to regulate the E-box P3 of the *PAN2* promoter.

AtMUTE AND GRASS *MUTE* ORTHOLOGUES FUNCTIONS HAVE DIVERGED

BdMUTE, ZmMUTE and OsMUTE conserve the motifs that could promote their intercellular movement or lack those that could prevent such movement (Raissig et al., 2017; Xu et al., 2018; **Figure 1B**). These proteins move from the GMC to epidermal cells of neighboring files, where they may specify SMC identity to recruit SCs (Raissig et al., 2017; Wang et al., 2019; Wu et al., 2019). In contrast, the Arabidopsis MUTE protein, whose gene is expressed in GMCs (MacAlister et al., 2007; Pillitteri et al., 2007), does not move among cells (Wang et al., 2019). As expected, AtMUTE does not have the conserved mobility motifs of grass MUTE proteins, but those conserved in eudicots (Raissig et al., 2017; **Figure 1B**). In accordance, the recruitment of SCs does not take place in Arabidopsis. The role of AtMUTE is restricted to control the meristemoid to GMC transition (MacAlister et al., 2007; Pillitteri et al., 2007).

The fact that the *YFP-BdMUTE* construct, driven by the GMC-specific *AtMUTE* promoter (MacAlister et al., 2007; Pillitteri et al., 2007), illuminates not only stomatal precursors but also adjacent epidermal cells in Arabidopsis (Raissig et al., 2017; Wang et al., 2019), underlines the very likely importance of the mobility motifs in the protein movement. Interestingly, this construct does not induce the recruitment of SCs in Arabidopsis (Raissig et al., 2017; Wang et al., 2019), highlighting that *AtMUTE* and *BdMUTE* have diverged. *AtMUTEp : YFP-ZmMUTE* in Arabidopsis also lights up GMCs and neighboring epidermal cells (Wang et al., 2019). Given that OsMUTE conserve the motifs that could promote its movement or lack those that could prevent it (Raissig et al., 2017), it is expected that this protein also moves from stomatal precursors to neighboring epidermal cells in Arabidopsis. *OsMUTE* and *ZmMUTE* expressed under the control of the *AtMUTE* promoter partially complement the defects of Arabidopsis *mute-1* by inducing the formation of stomata from some stomatal precursors (Liu et al., 2009), but, like *BdMUTE*, they do not induce the recruitment of SCs (Figure 4 in Liu et al., 2009). Although OsMUTE and ZmMUTE, and perhaps BdMUTE, retain the function of inducing stomata formation, they are unable to induce the recruitment of SCs in Arabidopsis. This underlies that these proteins have diverged from the AtMUTE protein acquiring of a new function: the recruitment of SCs.

ZmMUTE AND *OsMUTE* FUNCTION DIFFERS FROM THAT OF *BdMUTE*

Although the three orthologues of *MUTE* regulate the formation of SCs, their function during stomatal development is not identical (**Table 1**). The *bzu2-1* mutant forms GMCs but displays defects in their divisions, undergoing excessive, randomly oriented and/or asymmetric divisions (Wang et al., 2019). This gives rise to short columns of elongated cells instead of stomata, which results in a slower transpiration rate and in a decreased photosynthetic activity (Wang et al., 2019). *c-osmute* exhibits also columns of undifferentiated cells, produced by misoriented and/or asymmetric cell divisions (Wu et al., 2019). Morphologically, the phenotype of the *c-osmute* mutant is reminiscent of the *bzu2-1* one, and the physiology of *c-osmute* mutants must also be dramatically affected. Certainly, both mutants exhibit a lethal phenotype at the seedling stage (Wang et al., 2019; Wu et al., 2019).

The *sid* mutant is fully viable and fertile, although its stomatal physiology is also affected (Raissig et al., 2017). Like the *bzu2-1* and *c-osmute* mutants, the *sid* mutant also undergoes misoriented GMC divisions (Raissig et al., 2017). However, in contrast to these mutants, about 70% of the GMCs of this mutant develop dicot-like two celled stomata (Raissig et al., 2017). Therefore, while *bzu2-1* and *c-osmute* mutants exhibit a fully penetrant phenotype affecting the division of the GMC (Wang et al., 2019; Wu et al., 2019), many of GMC divisions of the *sid* mutant are normal (Raissig et al., 2017). The molecular nature triggering the lack of a fully penetrant phenotype in *sid* is unknown, and to delve into this question is one of the most exciting future directions. *OsFAMA* also controls GC morphogenesis, with *c-osmute* exhibiting stomata with swollen GCs (Wu et al., 2019). This mutant also exhibits a fraction of swollen SCs, suggesting that, in addition to *OsFAMA*, other genes regulate SC differentiation (Wu et al., 2019). Among these unknown genes could be *OsMUTE*.

The defects induced by mutations in the grass *MUTE* orthologues in the maintenance of the GMC identity could reflect a mechanism of cellular signaling from the SMC towards the GMC to induce stomatal formation. It has been proposed that, prior SC formation, high levels of a grass peptide similar to AtEPF1/2 may cause GMC arrest (Hughes et al., 2017; Hepworth et al., 2018), perhaps through the suppression of grass MUTE orthologues activity specifically in GMCs. Grass MUTE activity in SMC would allow SC formation. Then, signals from SCs may activate grass MUTE orthologues in GMCs, perhaps by reducing grass EPF1/2 production, to promote stomatal formation. Agree with this, 1) GMCs do not progress to become stomata until SC formation, and 2) barley overexpressing *HvEPF1* exhibits arrested GMCs (Hughes et al., 2017). It is then

likely that grass *MUTE* genes, in addition to having a non-cell-autonomous role specifying the SMC fate, have a cell-autonomous one triggering the progression of the GMC fate. The complementation of the Arabidopsis *mute-1* mutant phenotype, inducing stomatal development from some stomatal precursors, with at least the *OsMUTE* and *ZmMUTE* genes (Liu et al., 2009), also supports the cell-autonomous role of MUTE orthologues regulating GMC fate.

GRASS STOMATAL COMPLEXES IMPROVE STOMATAL FUNCTION

Several works comparing physiological stomatal behaviors among species with different stomatal complexes suggest that those of grasses are more efficient (Grantz and Zeiger, 1986; Franks and Farquhar, 2007; Vico et al., 2011; Merilo et al., 2014; McAusland et al., 2016; Haworth et al., 2018). The isolation of the *sid* mutant, the first grass mutant to date that disrupts the two main attributes of the grass stomatal complexes, the presence of dumbbell-shaped GCs and the recruitment of SCs (Raissig et al., 2017), underscores the important role of this innovative morphology in the stomatal function (Nunes et al., 2019). The maximum area of the open pore in the *sid* mutant, and its gas exchange capacity, were noticeably smaller than those in the wild type, even when stomatal opening was induced by the toxin fusicoccin (Raissig et al., 2017). The *sid* mutant also exhibited slower stomatal movements to fluctuating light conditions, and its stomata could not open as wide compared with the wild type (Raissig et al., 2017). Consequently, *sid* mutants produced less biomass than the wild types (Raissig et al., 2017). These results link the morphology of the stomatal complexes with its impact on gas exchange and biomass production in the wild grass *Brachypodium*, and strongly they suggest that this relationship may extend to the remaining grass species.

The improvement of stomatal function in grasses could have contributed to their expansion and diversification, 30 to 45 million years ago, when a progressive and global aridification took place (Kellogg, 2001; Hetherington and Woodward, 2003; Chen et al., 2017). The inability of the *sid* mutant to open widely its pores indicates that grass stomatal complexes are associated with greater stomatal openings and conductance. Interestingly, species with greater maximum stomatal conductance exhibit higher sensitivity to closure during drought (Henry et al., 2019). Under a global drought, a more sensitive stomatal closure could have allowed to capture carbon dioxide without losing too much water, thus favoring the successful diversification of this plant group. Certainly, Poaceae, with around 12,000 species, includes almost a quarter of all monocots of the planet, and it is one of the largest families of flowering plants. Curiously, the enrichment of species in genera of monocotyledons is associated with geographical variables, like larger ranges and lower elevations, rather than with biological attributes (Tang et al., 2016). It is likely that the success of the grasses lies partly in their morphology, including their unique stomatal complexes, and partly in the places they have occupied.

CONCLUDING REMARKS

The development of the unique grass stomatal complex is a great advantage, which may have contributed to the expansion of this plant group. Undoubtedly, *MUTE* orthologues of grasses provide a starting point to unravel not only the mechanism underlying stomatal complexes formation, but also the evolution of this essential trait. *MUTE* orthologues of grasses have not only functionally diverged, due to neo-functionalization, from *AtMUTE*, but also among them, with *BdMUTE* exhibiting divergence from *ZmMUTE* and *OsMUTE*. Certainly, protein phylogenetic analysis of bHLH regulators of stomatal development supports this view (Wu et al., 2019). The comparison of the grass *MUTE* function between domesticated plants and their wild relatives, will allow us to know if the agricultural practices have driven the divergence of these genes. Because grass stomatal complexes have largely contributed to the adaptive success in hotter and drier environment, delving into the function of these genes will also provide useful genetic tools for producing plants with better tolerance to drought caused by climate change.

AUTHOR CONTRIBUTIONS

LS wrote the article and designed the figures.

REFERENCES

Apostolakos, P., Livanos, P., Giannoutsou, E., Panteris, E., and Galatis, B. (2018). The intracellular and intercellular cross-talk during subsidiary cell formation in *Zea mays*: existing and novel components orchestrating cell polarization and asymmetric division. *Ann. Bot.* 122, 679–696. doi: 10.1093/aob/mcx193

Bergmann, D. C., and Sack, F. D. (2007). Stomatal development. *Annu. Rev. Plant Biol.* 58, 163–181. doi: 10.1146/annurev.arplant.58.032806.104023

Berry, J. A., Beerling, D. J., and Franks, P. J. (2010). Stomata: key players in the earth system, past and present. *Curr. Opin. Plant Biol.* 13, 233–240. doi: 10.1016/j.pbi.2010.04.013

Bertolino, L. T., Caine, R. S., and Gray, J. E. (2019). Impact of stomatal density and morphology on water-use efficiency in a changing world. *Front. Plant Sci.* 10, 225. doi: 10.3389/fpls.2019.00225

Campbell, D. H. (1881). On the development of the stomata of Tradescantia and Indian corn. *Amer. Nat.* 15, 761–766. doi: 10.1086/272919

Cartwright, H. N., Humphries, J. A., and Smith, L. G. (2009). PAN1: a receptor-like protein that promotes polarization of an asymmetric cell division in maize. *Science* 323, 649–651. doi: 10.1126/science.1161686

Chater, C. C. C., Caine, R. S., Fleming, A. J., and Gray, J. E. (2017). Origins and evolution of stomatal development. *Plant Physiol.* 174, 624–638. doi: 10.1104/pp.17.00183

Chen, Z. H., Chen, G., Dai, F., Wang, Y., Hills, A., Ruan, Y. L., et al. (2017). Molecular evolution of grass stomata. *Trends Plant Sci.* 22, 124–139. doi: 10.1016/j.tplants.2016.09.005

Deeks, M. J., and Hussey, P. J. (2005). Arp2/3 and SCAR: plants move to the fore. *Nat. Rev. Mol. Cell. Biol.* 6, 954–964. doi: 10.1038/nrm1765

Edwards, D., Kerp, H., and Hass, H. (1998). Stomata in early land plants: an anatomical and ecophysiological approach. *J. Exp. Bot.* 49, 255–278. doi: 10.1093/jxb/49.Special_Issue.255

Facette, M. R., Park, Y., Sutimantanapi, D., Luo, A., Cartwright, H. N., Yang, B., et al. (2015). The SCAR/WAVE complex polarizes PAN receptors and promotes division asymmetry in maize. *Nat. Plants* 1, 14024. doi: 10.1038/nplants.2014.24

Franks, P. J., and Farquhar, G. D. (2007). The mechanical diversity of stomata and its significance in gas-exchange control. *Plant Physiol.* 143, 78–87. doi: 10.1104/pp.106.089367

Gallagher, K., and Smith, L. G. (2000). Roles for polarity and nuclear determinants in specifying daughter cell fates after an asymmetric cell division in the maize leaf. *Curr. Biol.* 10, 1229–1232. doi: 10.1016/S0960-9822(00)00730-2

Grantz, D. A., and Zeiger, E. (1986). Stomatal responses to light and leaf-air water vapor pressure difference show similar kinetics in sugarcane and soybean. *Plant Physiol.* 81, 865–868. doi: 10.1104/pp.81.3.865

Guseman, J. M., Lee, J. S., Bogenschutz, N. L., Peterson, K. M., Virata, R. E., Xie, B., et al. (2010). Dysregulation of cell-to-cell connectivity and stomatal patterning by loss-of-function mutation in Arabidopsis chorus (glucan synthase-like 8). *Development* 137, 1731–1741. doi: 10.1242/dev.049197

Han, X., Kumar, D., Chen, H., Wu, S., and Kim, J.-Y. (2014). Transcription factor-mediated cell-to-cell signalling in plants. *J. Exp. Bot.* 65, 1737–1749. doi: 10.1093/jxb/ert422

Haworth, M., Scutt, C. P., Douthe, C., Marino, G., Gomes, M. T. G., Loreto, F., et al. (2018). Allocation of the epidermis to stomata relates to stomatal physiological control: stomatal factors involved in the evolutionary diversification of the angiosperms and development of amphistomaty. *Environ. Exp. Bot.* 151, 55–63. doi: 10.1016/j.envexpbot.2018.04.010

Henry, C., John, G. P., Pan, R., Bartlett, M. K., Fletcher, L. R., Scoffoni, C., et al. (2019). A stomatal safety-efficiency trade-off constrains responses to leaf dehydration. *Nat. Commun.* 10, 3398. doi: 10.1038/s41467-019-11006-1

Hepworth, C., Caine, R. S., Harrison, E. L., Sloan, J., and Gray, J. E. (2018). Stomatal development: focusing on the grasses. *Curr. Opin. Plant Biol.* 41, 1–7. doi: 10.1016/j.pbi.2017.07.009

Hetherington, A. M., and Woodward, F. I. (2003). The role of stomata in sensing and driving environmental change. *Nature* 424, 901–908. doi: 10.1038/nature01843

Hughes, J., Hepworth, C., Dutton, C., Dunn, J. A., Hunt, L., Stephens, J., et al. (2017). Reducing stomatal density in barley improves drought tolerance without impacting on yield. *Plant Physiol.* 174, 776–787. doi: 10.1104/pp.16.01844

Humphries, J. A., Vejlupkova, Z., Luo, A., Meeley, R. B., Sylvester, A. W., Fowler, J. E., et al. (2011). ROP GTPases act with the receptor-like protein PAN1 to polarize asymmetric cell division in maize. *Plant Cell* 23, 2273–2284. doi: 10.1105/tpc.111.085597

Kamiya, N., Itoh, J. I., Morikami, A., Nagato, Y., and Matsuoka, M. (2003). The *SCARECROW* gene's role in asymmetric cell divisions in rice plants. *Plant J.* 36, 45–54. doi: 10.1046/j.1365-313X.2003.01856.x

Kanaoka, M. M., Pillitteri, L. J., Fujii, H., Yoshida, Y., Bogenschutz, N. L., Takabayashi, J., et al. (2008). SCREAM/ICE1 and SCREAM2 specify three cell-state transitional steps leading to arabidopsis stomatal differentiation. *Plant Cell.* 20, 1775–1785. doi: 10.1105/tpc.108.060848

Kellogg, E. A. (2001). Evolutionary history of the grasses. *Plant Physiol.* 125, 1198–1205. doi: 10.1104/pp.125.3.1198

Kong, D., Karve, R., Willet, A., Chen, M.-K., Oden, J., and Shpak, E. D. (2012). Regulation of plasmodesmatal permeability and stomatal patterning by the glycosyltransferase-like protein KOBITO1. *Plant Physiol.* 159, 156–168. doi: 10.1104/pp.112.194563

Liu, T., Ohashi-Ito, K., and Bergmann, D. C. (2009). Orthologues of Arabidopsis thaliana stomatal bHLH genes and regulation of stomatal development in grasses. *Development* 136, 2265–2276. doi: 10.1242/dev.032938

MacAlister, C. A., Ohashi-Ito, K., and Bergmann, D. C. (2007). Transcription factor control of asymmetric cell divisions that establish the stomatal lineage. *Nature* 445, 537–540. doi: 10.1038/nature05491

McAusland, L., Vialet-Chabrand, S., Davey, P., Baker, N. R., Brendel, O., and Lawson, T. (2016). Effects of kinetics of light-induced stomatal responses on photosynthesis and water-use efficiency. *New Phytol.* 211, 1209–1220. doi: 10.1111/nph.14000

Merilo, E., Jõesaar, I., Brosché, M., and Kollist, H. (2014). To open or to close: species-specific stomatal responses to simultaneously applied opposing environmental factors. *New Phytol.* 202, 499–508. doi: 10.1111/nph.12667

Nunes, T. D. G., Zhang, D., and Raissig, M. T. (2019). Form, development and function of grass stomata. *Plant J.* doi: 10.1111/tpj.14552

Ohashi-Ito, K., and Bergmann, D. C. (2006). Arabidopsis FAMA controls the final proliferation/differentiation switch during stomatal development. *Plant Cell* 18, 2493–2505. doi: 10.1105/tpc.106.046136

Pillitteri, L. J., Sloan, D. B., Bogenschutz, N. L., and Torii., K. U. (2007). Termination of asymmetric cell division and differentiation of stomata. *Nature* 445, 501–505. doi: 10.1038/nature05467

Raissig, M. T., Abrash, E., Bettadapur, A., Vogel, J. P., and Bergmann, D. C. (2016). Grasses use an alternatively wired bHLH transcription factor network to establish stomatal identity. *Proc. Natl. Acad. Sci. U. S. A.* 113, 8326–8331. doi: 10.1073/pnas.1606728113

Raissig, M. T., Matos, J. L., Gil, M. X. A., Kornfeld, A., Bettadapur, A., Abrash, E., et al. (2017). Mobile MUTE specifies subsidiary cells to build physiologically improved grass stomata. *Science* 355, 1215–1218. doi: 10.1126/science.aal3254

Renzaglia, K. S., Villarreal, J. C., Piatkowski, B. T., Lucas, J. R., and Merced, A. (2017). Hornwort stomata: architecture and fate shared with 400-million-year-old fossil plants without leaves. *Plant Physiol.* 174, 788–797. doi: 10.1104/pp.17.00156

Rudall, P. J., Chen, E. D., and Cullen, E. (2017). Evolution and development of monocot stomata. *Am. J. Bot.* 104, 1122–1140. doi: 10.3732/ajb.1700086

Sager, R. E., and Lee, J. Y. (2018). Plasmodesmata at a glance. *J. Cell Sci.* 131, pii: jcs209346. doi: 10.1242/jcs.209346

Serna, L., and Fenoll, C. (2000). Stomatal development in Arabidopsis: how to make a functional pattern. *Trends Plant Sci.* 5, 458–460. doi: 10.1016/S1360-1385(00)01782-9

Serna, L. (2011). Stomatal development in Arabidopsis and grasses: differences and commonalities. *Int. J. Dev. Biol.* 55, 5–10. doi: 10.1387/ijdb.103094ls

Serna, L. (2015). Development: Early events in asymmetric division. *Nat. Plants* 1, 15008. doi: 10.1038/nplants.2015.8

Shoemaker, E. M., and Srivastava, L. M. (1973). The mechanics of stomatal opening in corn (*Zea mays* L.) leaves. *J. Theor. Biol.* 42, 219–225. doi: 10.1016/0022-5193(73)90086-6

Stebbins, G. L., and Shah, S. S. (1960). Developmental studies of cell differentiation in the epidermis of monocotyledons. II. Cytological features of stomatal development in the Gramineae. *Dev. Biol.* 2, 477–500. doi: 10.1016/0012-1606(60)90050-6

Tang, C. Q., Orme, C. D. L., Bunnefeld, L., Jones, F. A., Powell, S., Chase, M. W., et al. (2016). Global monocot diversification: geography explains variation in species richness better than environment or biology. *Bot. J. Linn. Soc.* 83, 1–15. doi: 10.1111/boj.12497

Vico, G., Manzoni, S., Palmroth, S., and Katul, G. (2011). Effects of stomatal delays on the economics of leaf gas exchange under intermittent light regimes. *New Phytol.* 192, 640–652. doi: 10.1111/j.1469-8137.2011.03847.x

Wang, H., Guo, S., Qiao, X., Guo, J., Li, Z., Zhou, Y., et al. (2019). BZU2/ZmMUTE controls symmetrical division of guard mother cell and specifies neighbor cell fate in maize. *PloS Genet.* 15, e1008377. doi: 10.1371/journal.pgen.1008377

Wu, Z., Chen, L., Yu, Q., Zhou, W., Gou, X., Li, J., et al. (2019). Multiple transcriptional factors control stomata development in rice. *New Phytol.* 223, 220–232. doi: 10.1111/nph.15766

Xu, M., Chen, F., Qi, S., Zhang, L., and Wu, S. (2018). Loss or duplication of key regulatory genes coincides with environmental adaptation of the stomatal complex in *Nymphaea colorata* and *Kalanchoe laxiflora*. *Hortic. Res.* 5, 42. doi: 10.1038/s41438-018-0048-8

Yang, Y., Chang, B. H., Samson, S. L., Li, M. V., and Chan, L. (2009). The Krüppel-like zinc finger protein Glis3 directly and indirectly activates insulin gene transcription. *Nucleic Acids Res.* 37, 2529–2538. doi: 10.1093/nar/gkp122

Zhang, X., Facette, M., Humphries, J. A., Shen, Z., Park, Y., Sutimantanapi, D., et al. (2012). Identification of PAN2 by quantitative proteomics as a leucine-rich repeat-receptor-like kinase acting upstream of PAN1 to polarize cell division in maize. *Plant Cell* 24, 4577–4589. doi: 10.1105/tpc.112.104125

Conflict of Interest: The author declares that the research was conducted in the absence of any commercial or financial relationships that could be construed as a potential conflict of interest.

frontiers in Plant Science

REVIEW
published: 11 February 2020
doi: 10.3389/fpls.2019.01783

Pores for Thought: Can Genetic Manipulation of Stomatal Density Protect Future Rice Yields?

*Christopher R. Buckley, Robert S. Caine and Julie E. Gray**

Department of Molecular Biology and Biotechnology, University of Sheffield, Sheffield, United Kingdom

Rice (*Oryza sativa* L.) contributes to the diets of around 3.5 billion people every day and is consumed more than any other plant. Alarmingly, climate predictions suggest that the frequency of severe drought and high-temperature events will increase, and this is set to threaten the global rice supply. In this review, we consider whether water or heat stresses in crops — especially rice — could be mitigated through alterations to stomata; minute pores on the plant epidermis that permit carbon acquisition and regulate water loss. In the short-term, water loss is controlled *via* alterations to the degree of stomatal "openness", or, in the longer-term, by altering the number (or density) of stomata that form. A range of molecular components contribute to the regulation of stomatal density, including transcription factors, plasma membrane-associated proteins and intercellular and extracellular signaling molecules. Much of our existing knowledge relating to stomatal development comes from research conducted on the model plant, *Arabidopsis thaliana*. However, due to the importance of cereal crops to global food supply, studies on grass stomata have expanded in recent years, with molecular-level discoveries underscoring several divergent developmental and morphological features. Cultivation of rice is particularly water-intensive, and there is interest in developing varieties that require less water yet still maintain grain yields. This could be achieved by manipulating stomatal development; a crop with fewer stomata might be more conservative in its water use and therefore more capable of surviving periods of water stress. However, decreasing stomatal density might restrict the rate of CO_2 uptake and reduce the extent of evaporative cooling, potentially leading to detrimental effects on yields. Thus, the extent to which crop yields in the future climate will be affected by increasing or decreasing stomatal density should be determined. Here, our current understanding of the regulation of stomatal development is summarised, focusing particularly on the genetic mechanisms that have recently been described for rice and other grasses. Application of this knowledge toward the creation of "climate-ready" rice is discussed, with attention drawn to the lesser-studied molecular elements whose contributions to the complexity of grass stomatal development must be understood to advance efforts.

Keywords: stomatal development, rice, crop yields, stomatal density, grasses, crop physiology

OPEN ACCESS

Edited by:
Graham Dow,
ETH Zürich, Switzerland

Reviewed by:
Yun-Kuan Liang,
Wuhan University, China
Danilo M. Daloso,
Federal University of Ceara, Brazil

****Correspondence:***
Julie E. Gray
j.e.gray@sheffield.ac.uk

Specialty section:
This article was submitted to Plant Development and EvoDevo, a section of the journal Frontiers in Plant Science

Received: *23 September 2019*
Accepted: *20 December 2019*
Published: *11 February 2020*

Citation:
Buckley CR, Caine RS and Gray JE (2020) Pores for Thought: Can Genetic Manipulation of Stomatal Density Protect Future Rice Yields? Front. Plant Sci. 10:1783. doi: 10.3389/fpls.2019.01783

INTRODUCTION

Feeding a global population expected to reach 9.8 billion by 2050 is one of the greatest challenges of our time (McGuire, 2015; United Nations, 2017). Together with rising temperatures and dwindling reserves of natural resources such as freshwater, the problem is exasperated by growing climate instabilities (Stott, 2016). The frequency and intensity of extreme weather events are projected to increase under future climate scenarios, which will likely lead to substantial losses of crop yields (Seneviratne et al., 2012; Challinor et al., 2014). Thus, to alleviate the risk of crop failures, the development of "climate-ready" crops that can withstand future climatic stresses should be prioritized.

Rice (*Oryza sativa* L.) is a major source of food and income for billions worldwide. In Asia, where over 90% of rice is grown and consumed (Brar and Khush, 2013; Elert, 2014), the primary climatic factor for the majority of the growing region is the monsoon, which contributes >80% of annual rainfall within a few months (Haefele et al., 2016). Rainfed cultivation accounts for ~20% of global rice supply yet, as a consequence of this irregular rainfall, productivity in rainfed regions is already constrained by drought (Wassmann et al., 2009; Maclean et al., 2013; Swain et al., 2017). Rice is also susceptible to heat stress, particularly during the reproductive and grain filling stages (Matsui et al., 2000; Lin et al., 2010), and there are concerns that both high-temperature events and droughts are expected to become more prevalent across the world's rice cultivation regions (Krishnan et al., 2011). Furthermore, there is an increasing requirement to limit water use for crop irrigation, which already accounts for around 70% of global freshwater usage (Foley et al., 2011). It is therefore important that water use efficiency (WUE; defined here as the amount of carbon assimilated per unit of water lost) and tolerances to heat-stress and drought are improved to ready rice for future climates.

Plants use microscopic epidermal openings called stomata to regulate the uptake of CO_2 and the release of water between internal tissue surfaces and the environment (Buckley, 2005). Typically consisting of a pair of specialised turgor-driven guard cells (GCs) surrounding a central pore, stomata also function to regulate plant temperature and to move solutes and water internally *via* the transpiration stream. Under water-limiting conditions stomata close, thereby restricting water loss *via* reduced stomatal conductance (g_s), with CO_2 uptake for photosynthesis (A), evaporative cooling, and nutrient transfer often diminished as a result (Arve et al., 2011; Urban et al., 2017). Because less cooling occurs, stomatal closure exacerbates the risk of plant organs reaching lethally high temperatures which, particularly for rice in lower latitudes, may lead to substantial crop losses (Long and Ort, 2010; Sánchez et al., 2014).

Adjustments to the size of the stomatal pore permit a near-immediate plant response to a change in the surrounding environment (Brownlee, 2001). However, when sustained environmental stimuli arise over longer durations, alterations to stomatal density (SD; the number of stomata that form per unit area) and size may also occur (Casson and Gray, 2008; Qi and Torii, 2018). By increasing SD, g_s might be increased, which in turn may lead to greater evaporative cooling and increases in A (Tanaka et al., 2013). Conversely, by reducing SD, g_s can be lowered, which may curb water loss and result in improved WUE and drought tolerance (Doheny-Adams et al., 2012; Caine et al., 2019). If reductions in SD do not have a significant detrimental impact on A or evaporative cooling, the overall benefits of increased water conservation could represent a viable strategy to protect certain crops, including rice, against future extreme weather events (Hepworth et al., 2018).

A deep understanding of the stomatal development program in rice is required for genetic manipulation of SD. The majority of our existing knowledge stems from the model plant Arabidopsis (*Arabidopsis thaliana*), and this is beginning to be translated into grass species (to name a few: Raissig et al., 2016; Raissig et al., 2017; Yin et al., 2017; Abrash et al., 2018; Lu et al., 2019; Mohammed et al., 2019; Wu et al., 2019). In this review, our current understanding of the molecular-level control of stomatal development in rice will be summarized, drawing comparisons and distinctions between Arabidopsis, the model grass Brachypodium (*Brachypodium distachyon*), and other grass species of agricultural importance such as maize (*Zea mays*) and barley (*Hordeum vulgare*). Then, translating this knowledge into action, recent advances towards "climate-ready" rice with altered SD will be discussed.

GRASSES HAVE CONSERVED AND DIVERGENT ELEMENTS OF STOMATAL MORPHOLOGY AND DEVELOPMENT

Rice and other cereal crops such as maize, barley, and wheat (Triticum aestivum) are monocot grasses and, relative to eudicot plants such as Arabidopsis, are defined by a number of distinctive features relating to where and how stomata develop (Raissig et al., 2016; Conklin et al., 2018; Hepworth et al., 2018). In grass leaves, stomata are organized into evenly distributed parallel files which are interspersed either side of leaf veins, with the origin of stomatal development primarily occurring at the leaf base (Conklin et al., 2018). Whereas stomatal development is primarily initiated at the leaf base in Arabidopsis, the location of development is not as constrained as in grasses and the spatial distribution of stomata appears more random as a result (Conklin et al., 2018). The culmination of stomatal development for grasses is a cellular complex composed of a pair of dumbbell-shaped GCs adjoined on either side by subsidiary cells (SCs) (**Figure 1**). These complexes are typically separated by at least one epidermal cell and thus development follows the one-cell spacing rule (Sachs, 1991; Chen et al., 2017; Hepworth et al., 2018). In Arabidopsis, stomatal GCs are kidney-shaped (**Figure 1**) and are without flanking SCs but, like grasses, the one-cell spacing rule is maintained (Hara et al., 2007).

For most plant species, including Arabidopsis and grasses, the stomatal lineage progresses in much the same way; originating from a set of undifferentiated epidermal cells at the base of the leaf known as protodermal cells (Stebbins and Shah, 1960; Yang et al., 1995; Luo et al., 2012; Pillitteri and Dong, 2013; Raissig et al., 2016; Hepworth et al., 2018; Endo and Torii, 2019). The

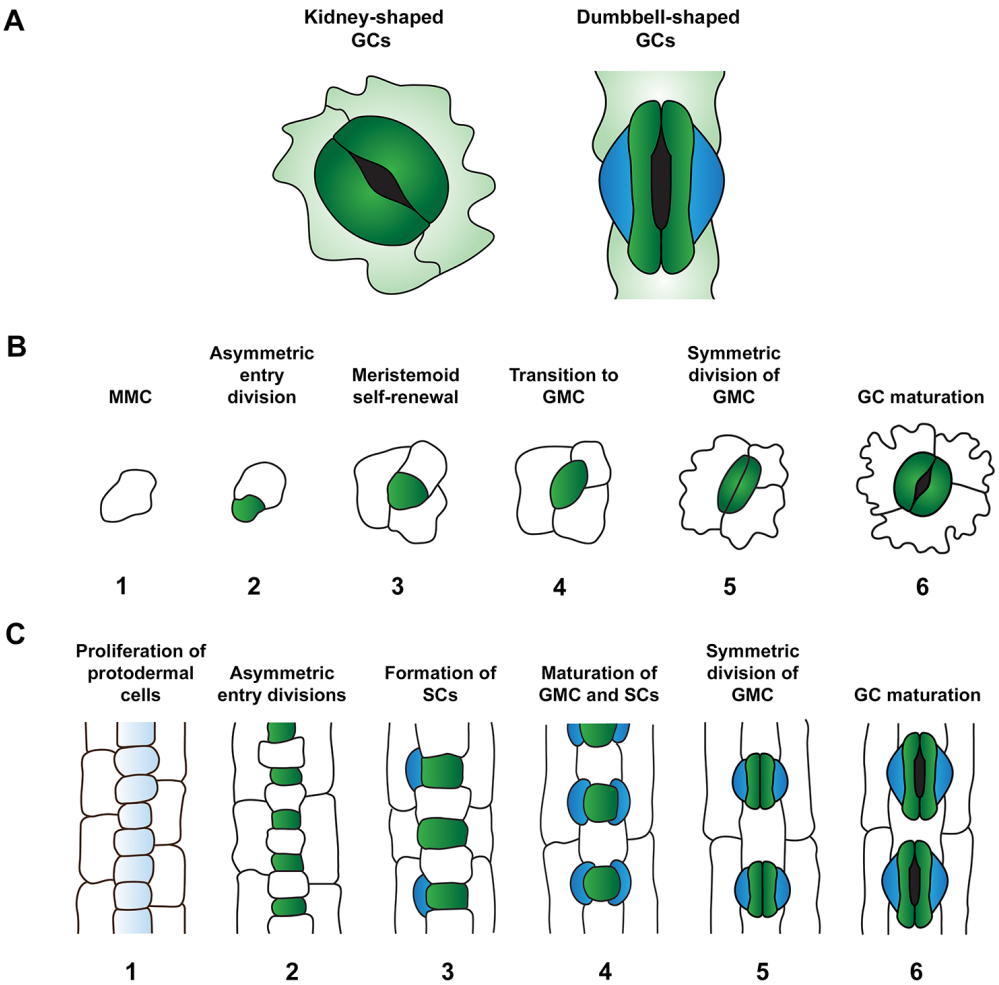

FIGURE 1 | Comparison of stomatal morphology and development in the leaves of the eudicot *Arabidopsis thaliana* and monocot grasses. **(A)** Comparison of guard cell (GC) morphology: kidney-shaped GCs of *A. thaliana* (left) and dumbbell-shaped GCs typical of monocot grasses (right). GCs and subsidiary cells (SCs) are depicted in dark green and blue respectively. **(B)** Stomatal development in *A. thaliana*. Meristemoid mother cells (MMCs) (1) divide asymmetrically to form meristemoids (green) (2). This process of asymmetric division is repeated in the self-renewing meristemoid phase (3). Note, asymmetric spacing divisions of MMCs occur around this developmental stage, with newly formed satellite meristemoids forming at least one-cell away from pre-existing meristemoids and stomata. Asymmetric divisions are then terminated and meristemoids transition to guard mother cell (GMC) state (4). GMCs undergo a single symmetric division to produce a pair of GCs (5) which mature to define the stomatal aperture amid the tessellated pavement cells of the leaf epidermis (6). **(C)** Stomatal development in grasses (modelled from barley, *Hordeum vulgare*). At the beginning of stomatal development, protodermal cells start to proliferate at a faster rate than surrounding cell files (1). Protodermal cells undergo just one round of asymmetric division, generating smaller GMCs (green) and larger epidermal cells (2). GMCs become enlarged and provide cues to induce asymmetric divisions in flanking subsidiary mother cells (SMCs) (3) which result in the production of SCs (blue) (4). Analogous to eudicot stomatal development, GMCs undergo a single symmetric division (5) to produce a pair of daughter cells that differentiate into mature GCs surrounded by columnar pavement cells (6).

stomatal lineage is initiated when individual protodermal cells (known in Arabidopsis as meristemoid mother cells, MMCs) gain the capacity to undergo asymmetric cell divisions (**Figure 1**). In both Arabidopsis and grasses an asymmetric entry division leads to the formation of one smaller daughter cell and one larger daughter cell (**Figure 1**). The larger cell in Arabidopsis is termed a stomatal lineage ground cell (SLGC), while in grasses this cell is typically referred to simply as a sister cell or long cell. The smaller cell in Arabidopsis is a meristemoid and retains the ability to undergo self-renewing amplifying divisions, often generating several new SLGCs as a result (**Figure 1**). Although Wu et al. (2019) refer to the smaller cells in grasses as meristemoids, there is no evidence in the literature to suggest that these cells possess the ability to undergo amplifying divisions; instead the smaller daughter cell expands slightly and transitions directly to a guard mother cell (GMC) (Raissig et al., 2016; Hepworth et al., 2018). For clarity, in this review we will refer to the smaller cells derived from grass asymmetric divisions as GMCs. While Arabidopsis SLGCs have the ability to undergo a spacing division to form satellite meristemoids (Pillitteri and Dong, 2013), similar

functionality has not been reported for the larger sister cells of grasses. However, since the proximal-distal development of grass stomata is not completely linear, and multiple large epidermal cells can develop adjacently without the presence of an intervening GMC (Hepworth et al., 2018), the possibility that larger sister cells can undergo infrequent satellite divisions to produce new GMCs cannot be ruled out.

The divergent developmental processes described above during the beginning of the stomatal lineage are briefly realigned when meristemoids in Arabidopsis transition to GMCs and take on a form similar to that of grass GMCs (**Figure 1**). However, while Arabidopsis GMCs are typically programmed to divide symmetrically to form a pair of GCs, grass GMC cell state is temporarily maintained (Luo et al., 2012; Pillitteri and Dong, 2013; Hepworth et al., 2018). This allows asymmetric divisions to occur in both of the adjacent subsidiary mother cells (SMCs), resulting in the production of a pair of SCs either side of the GMC. Once SCs have formed, grass GMCs — like Arabidopsis GMCs — undergo a single symmetric division to form a pair of GCs. The termination of stomatal development occurs when nascent Arabidopsis and grass GCs fully differentiate to become kidney-shaped and dumbbell-shaped cells respectively (Conklin et al., 2018) (**Figure 1**).

STOMATAL LINEAGE INITIATION AND ADVANCEMENT IS GOVERNED BY TRANSCRIPTIONAL REGULATORS

In Arabidopsis, five basic helix-loop-helix (bHLH) transcription factors are primarily responsible for regulating stomatal lineage entry and subsequent advancement to mature stomata. These bHLHs are known as SPEECHLESS (SPCH), its close paralogues MUTE and FAMA, and SCREAM (SCRM, also known as ICE1) and SCRM2 (Ohashi-Ito and Bergmann, 2006; MacAlister et al., 2007; Pillitteri et al., 2007; Kanaoka et al., 2008) (**Figure 2**). The formation of MMCs, asymmetric entry divisions and subsequent meristemoid self-renewal requires the first of these, SPCH (Pillitteri and Dong, 2013; Endo and Torii, 2019). MUTE activity is then required to terminate asymmetric divisions and promote the differentiation of meristemoids into GMCs (Pillitteri et al., 2007). Recent work by Han et al. (2018) has shown that MUTE also promotes the GMC-to-GC division by directly inducing the expression of a series of cell-cycle genes that trigger the symmetric divisions of GMCs. MUTE also promotes the transcriptional repressor of these genes, FAMA, which together with the closely related MYB proteins FOUR LIPS (FLP) and MYB88, acts to inhibit extraneous symmetric divisions of GMCs and promote GC maturation (Ohashi-Ito and Bergmann, 2006; Han et al., 2018). At each specific stage of cell division and transition, SPCH, MUTE, and FAMA form obligate heterodimer complexes with SCRM and SCRM2 (Kanaoka et al., 2008; Conklin et al., 2018). These complexes are crucial to the activity of SPCH, MUTE and FAMA; double Arabidopsis *scrm scrm2* knockout plants fail to produce cells that enter the stomatal lineage (Kanaoka et al., 2008).

There are many hormonal stimuli that directly and/or indirectly regulate stomatal development. For example, the abiotic stress signal abscisic acid (ABA), is known to be an important regulator of both stomatal development and stomatal closure (Chater et al., 2014). However, since our understanding of hormonal regulation in grass stomatal development is limited with respect to our knowledge from Arabidopsis, here we will focus primarily on the core transcription factor-driven stomatal development module. For further information on the hormonal control of stomatal development, see Qi and Torii (2018) or Zoulias et al. (2018).

NOVEL AND DISTINCT BHLH FUNCTIONS IN RICE AND OTHER GRASSES

Several phylogenetic studies have concluded that *SPCH*, *MUTE*, *FAMA*, *SCRM*, and *SCRM2* are highly conserved across land plants, with *SPCH* undergoing a duplication event in grass species (MacAlister and Bergmann, 2011; Ran et al., 2013; Chater et al., 2017; Qu et al., 2017) (**Figure 3**). Despite the divergence of stomatal morphology and development in grasses (**Figure 1**), bHLH orthologues have now been characterised in both rice (Liu et al., 2009; Wu et al., 2019) and Brachypodium (Raissig et al., 2016), with some discreet differences in functionality detected (**Figure 2**).

Recent research has shown that the two bHLH *SPCH* paralogues — *OsSPCH1* and *OsSPCH2* — both contribute to stomatal development in rice. Despite this, a reduction in GMC number and SD is only observed in single *osspch2* knockout plants (Liu et al., 2009; Wu et al., 2019). Analysis of downstream gene expression in *osspch1* and *osspch2* single mutants support this finding as *OsMUTE* and *OsFAMA* are only downregulated in *osspch2* plants (Wu et al., 2019). However, a more severe effect on development is observed in *osspch1 osspch2* double knockouts where no GMCs or stomata form, suggesting that OsSPCH1 does contribute to early stomatal development in the absence of OsSPCH2 (Wu et al., 2019). Genetic reporter analyses in Brachypodium further emphasize the importance of the grass *SPCH2* paralogue over *SPCH1* (Raissig et al., 2016). A BdSPCH2 signal can be strongly detected from the initiation of stomatal development until SC formation, whereas BdSPCH1 displays a lower overall activity, with the strongest signal occurring after the initial asymmetric division and declining before SC formation begins. Relative to the mild stomatal phenotype of *bdspch1* knockouts, *bdspch2* plants have a drastically reduced SD, consolidating SPCH2 as the main player in initiating stomatal development in grasses (Raissig et al., 2016). Nevertheless, as with rice double knockouts, *bdspch1 bdspch2* plants also fail to form GMCs or stomata, suggesting that in both grass species studied thus far, at least one *SPCH* gene must be present for cells to enter the stomatal lineage (**Figure 2**).

Functioning downstream of SPCH in Arabidopsis, MUTE stops meristemoid amplifying divisions, promotes GMC formation and subsequently promotes the symmetric GMC division which leads to the formation of GC pairs (Pillitteri

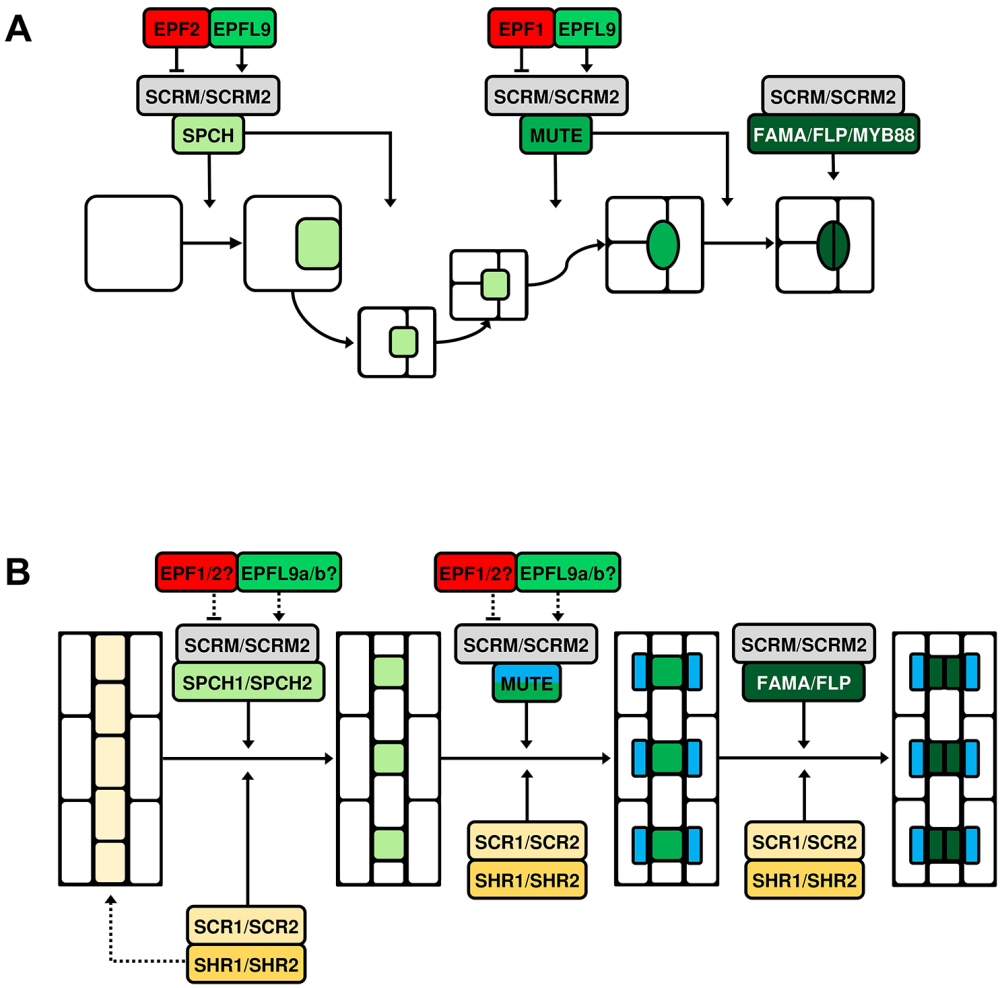

FIGURE 2 | Simplified models of bHLH-mediated stomatal cell lineage transitions in *Arabidopsis thaliana* and grasses. Five basic helix-loop-helix (bHLH) transcription factors, SPEECHLESS (SPCH), MUTE, FAMA, and their heterodimeric partners SCREAM (SCRM) and SCRM2 exhibit control over stomatal cell type transitions and are conserved across land plants. **(A)** Stomatal development in *A. thaliana*. SPCH directs asymmetric divisions of meristemoid mother cells (MMCs) and promotes the meristemoid self-renewing divisions. Epidermal patterning factor 2 (EPF2) and EPF-like protein 9 (EPFL9) are antagonistic regulators of SPCH; competing to suppress and promote its activity respectively. MUTE terminates the meristemoid self-renewing state and promotes guard mother cell (GMC) differentiation and GMC symmetric division. EPF1 primarily targets MUTE; by restraining its activity extra symmetric divisions of GMCs are prevented. EPF1, like EPF2, is assumed to compete with EPFL9 for the regulation of MUTE. FAMA also prevents ectopic symmetric divisions of GMCs and ultimately promotes guard cell (GC) maturation together with the closely related MYB proteins FOUR LIPS (FLP) and MYB88. At each stage of transition, SPCH, MUTE and FAMA form obligate heterodimer complexes with SCRM or SCRM2. **(B)** The molecular control of stomatal development is 'alternatively wired' in monocotyledonous grasses such as rice (*Oryza sativa*) and Brachypodium (*Brachypodium distachyon*). It has been suggested that the transcription factors SHORTROOOT1 and SHORTROOT2 (SHR1/2) are involved in the establishment of stomatal lineage cell files (dashed arrow). SPCH has been duplicated and both homologues act to induce asymmetric divisions in these stomatal lineage cells, with SPCH2 the more predominant actor. MUTE promotes GMC differentiation and is involved in the formation of subsidiary cells (SCs) in neighboring subsidiary mother cells (SMCs). As in Arabidopsis, FAMA inhibits supernumerary symmetric divisions of GMCs, probably in combination with a single FLP protein. SCRM and SCRM2 also appear to form heterodimer complexes with the aforementioned bHLHs throughout the lineage, as is observed in Arabidopsis. SHR1/2 and their partner transcription factors SCARECROW1/2 (SCR1/2) exert regulatory influence at each stage of transition. EPFs/EPFLs are also present during grass stomatal development and, while they can demonstrably constrain or promote development, exactly where and how they regulate the grass bHLHs has not been determined (dashed arrows).

et al., 2007; Han et al., 2018). Grasses are not thought to possess self-renewing meristemoids, yet by generating *osmute* gene knockout lines, Wu et al. (2019) reported that OsMUTE functions primarily to prevent ectopic divisions of GMCs (**Figure 2**), as GMCs appear to undergo further division(s) before arresting in *osmute* plants. Interestingly, like in rice, ZmMUTE has recently been shown to be responsible for preventing ectopic divisions in maize, with multiple aborted GMCs often found to be stacked within a stomatal file in maize *zmmute* (also termed *bizui2*) mutants (Wang et al.,

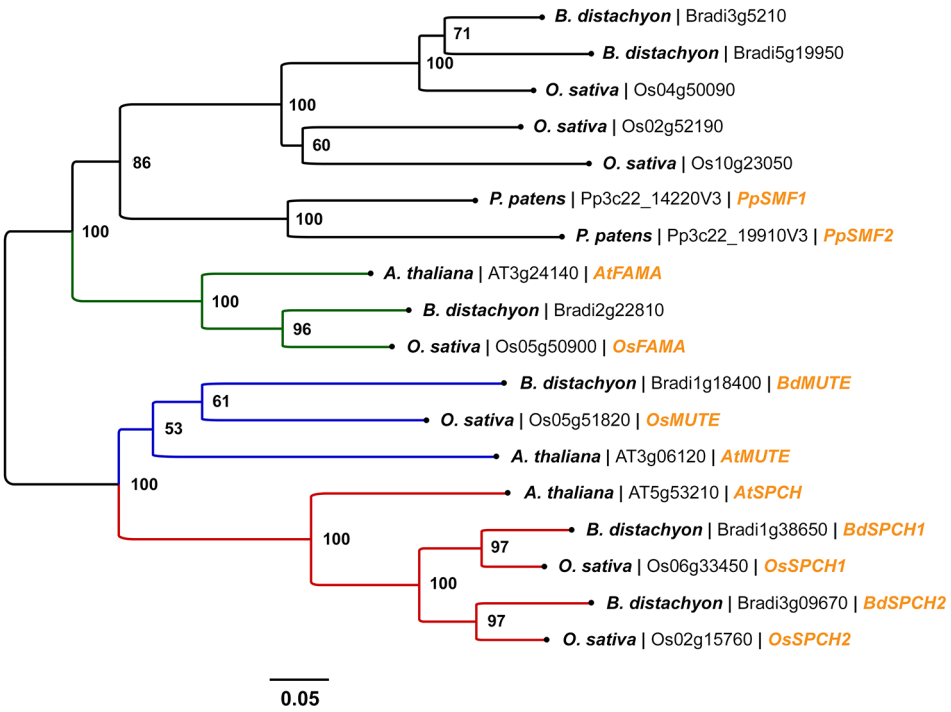

FIGURE 3 | Phylogenetic analysis of SPEECHLESS (SPCH), MUTE, and FAMA peptide sequences in Arabidopsis (*Arabidopsis thaliana*), rice (*Oryza sativa*), and Brachypodium (*Brachypodium distachyon*). Peptide sequences were obtained *via* BLAST searches of the rice and Brachypodium genomes using Phytozome v12. All peptide sequences with expect values (E-values) < 1 x 10^{-30} against AtSPCH, AtMUTE, and AtFAMA were used in the analysis. Stomatal bHLH peptide sequences PpSMF1 and PpSMF2 from the non-vascular moss *Physcomitrella patens* were included for evolutionary context; obtained from Chater et al. (2017). A total of 18 peptide sequences were involved in the phylogenetic analysis. Peptide sequences were aligned using the MUSCLE algorithm (Edgar, 2004). The phylogenetic tree was constructed using the neighbor-joining method (Saitou and Nei, 1987). The optimal tree with the sum of branch length = 4.05347046 is shown. A bootstrap test was performed (1,000 replicates) and the percentage of replicate trees that clustered taxa into the conformation displayed is shown adjacent to the nodes. Evolutionary distances between peptide sequences (in units of amino acid substitutions per site) were calculated using the Poisson correction method (Zuckerkandl and Pauling, 1965). The tree is drawn to scale, with branch lengths proportionate to the evolutionary distances used to infer the tree. All evolutionary analyses were performed in MEGA6. From left to right, species name, gene accession number and gene name (if characterised) are labeled at the branch tips. The clades comprising SPCH, MUTE, and FAMA orthologues are coloured red, blue and green respectively.

2019). Ectopic divisions of GMCs often occur in irregular orientations in *osmute* plants and it is unclear whether the stacking phenotype that is observed in maize *zmmute* mutants also occurs in the rice mutants. In both *osmute* and *zmmute*, neither GCs or SCs form, which for *zmmute* plants results in seedling lethality around 14 days post-germination. Taken together, these observations show that if MUTE functionality is compromised it is possible to invoke meristemoid-like activity in grasses. However, as mentioned previously, to date no grass species surveyed has naturally exhibited such a cell type.

In *OsMUTE*-overexpressing plants, Wu et al. (2019) report that all epidermal cells aside from silica and cork cells take on GC-like identity although, upon inspection of the images provided, this suggestion is difficult to interpret as the cells that form appear to be undifferentiated. This is especially apparent when the given examples are contrasted with overexpression studies of *MUTE* in Arabidopsis. In Arabidopsis, ectopic GCs form as part of a stoma and are more clearly GC-like (Pillitteri et al., 2007). To truly determine the identity of the cells generated *via OsMUTE* overexpression — and thus understand more about OsMUTE functionality and governance of cell state — it would be useful to repeat the genetic manipulation of *OsMUTE* in reporter plants that convey GMC, SC, and GC identity.

Whereas neither GCs or SCs form in *osmute* and *zmmute* knockout mutant plants, GC pairs do form in *bdmute* knockout mutant plants, but these GCs are devoid of SCs (Raissig et al., 2017). By generating YFP-BdMUTE reporter lines, it has been demonstrated that the BdMUTE protein is mobile and can promote asymmetric SC entry divisions by entering SMCs from neighboring GMCs (Raissig et al., 2017). Despite the phenotypic discrepancy between *bdmute* mutants and *zmmute* and *osmute* mutants, Wang et al. (2019) showed that ZmMUTE and OsMUTE are also capable of travelling from GMCs to SMCs. Similarly to what was initially described in Brachypodium YFP-BdMUTE reporter lines, YFP-ZmMUTE and YFP-OsMUTE signals are detectable in both GMCs and neighboring SMCs immediately prior to SC-forming divisions in maize and rice, respectively (Raissig et al., 2017; Wang et al., 2019). Yet, unlike *osmute* and *zmmute*, the course of GMC and GC development is

less perturbed in *bdmute* knockout plants, and thus MUTE's involvement in the regulation of GMC cell fate and divisions appears to show some variation amongst different grass species.

OsFAMA function has been analyzed *via* the production of both T-DNA and CRISPR *osfama* mutants, with both methods revealing that OsFAMA acts to promote GC maturation in rice (Liu et al., 2009; Wu et al., 2019) (**Figure 2**). Intriguingly, ectopic GMC divisions (as in *osmute*) and, in some cases, undivided SMC cells are detectable in *osfama* knockout plants (Wu et al., 2019). This implies that FAMA, perhaps in combination with MUTE, contributes to the regulation of SMC asymmetric divisions and GMC symmetric divisions in rice. There are no reports yet that describe how FAMA functions during Brachypodium or maize stomatal development, and so at present it is not possible to compare the function of other grass FAMA orthologues with that of OsFAMA. It will be interesting to learn whether BdFAMA and ZmFAMA also partake in events upstream of GC formation as has been shown in OsFAMA.

Genes with high sequence similarity to Arabidopsis *SCRM* and *SCRM2* have been identified in rice (*Os11g32100* and *Os01g71310* respectively), suggesting that the heterodimerisation of bHLH transcription factors observed in Arabidopsis also occurs in rice (Liu et al., 2009) (**Figure 2**). The proposed protein-protein interactions of these gene products — *OsSCRM* and *OsSCRM2* — with the aforementioned stomatal development genes (OsSPCH1/2, OsMUTE, and OsFAMA) have now been confirmed *in vitro via* bimolecular fluorescent complementation (BiFC) and yeast two-hybrid (Y2H) assays (Wu et al., 2019). Like Arabidopsis SCRM and SCRM2, OsSCRM and OsSCRM2 act redundantly during stomatal development, with double *scrm scrm2* knockouts leading to the absence of all stomatal lineage cell types and stomata in both species (Kanaoka et al., 2008; Wu et al., 2019). Whereas *osscrm* CRISPR knockout mutants fail to produce stomata (and only a few meristemoids form in early development), Arabidopsis T-DNA knockdown plants with little-to-no *SCRM* expression produce a range of stomatal lineage cells (at various aborted stages) as well as stomata (Kanaoka et al., 2008). However, when equivalent *osscrm* T-DNA knockouts are examined in rice (which display a weaker phenotype than CRISPR *osscrm* plants), the function of OsSCRM appears to more closely mirror that of AtSCRM. This is because aborted stomatal lineage cells can be observed throughout the development stages, implying that, together with OsSPCH1/2 in early development, OsSCRM probably associates with OsMUTE and OsFAMA *in vivo* (Wu et al., 2019). In contrast to *scrm* knockouts, stomatal development is unaffected in both *atscrm2* and *osscrm2* knockout mutants, suggesting that these paralogous proteins play a minor role in the development of stomata in their respective species (Kanaoka et al., 2008; Wu et al., 2019).

In Brachypodium, the roles of BdSCRM and BdSCRM2 are more distinct. Both *bdscrm* and *bdscrm2* single mutants produce a seedling lethal phenotype, owing to an inability to produce mature stomata (Raissig et al., 2016). While *bdscrm* plants fail to produce any stomatal lineage cells, entry to the stomatal lineage is not blocked in *bdscrm2* mutants; instead aborted four-cell complexes form which fail to progress to mature stomata (Raissig et al., 2016). This indicates that BdSCRM2 might fulfil a novel function later in development which is independent of BdSCRM (Raissig et al., 2016). It is conceivable that this function is to specifically interact with FAMA and drive the formation of mature stomata. Thus, it will be interesting to learn whether the stomatal phenotype of *bdfama* matches that of *bdscrm2*. Considered across the species discussed, there are clear similarities and some subtle differences in the function and coordination of the bHLH transcription factors; both between the grasses and Arabidopsis and within the grasses themselves.

SIGNALING PEPTIDES CAN ADJUST STOMATAL DEVELOPMENT IN GRASSES

For plants to adjust their leaf SD, succinct titration of bHLH activity is essential. This is particularly true of SPCH, which has a diverse range of transcriptional targets in Arabidopsis, with chromatin immunoprecipitation-sequencing (ChIP-Seq) experiments identifying over 8,000 genomic binding sites (Lau et al., 2014). To coordinate the activity of SPCH (and other bHLHs) during stomatal development, intra- and extracellular signalling are particularly important and, in Arabidopsis, much research has been conducted into these signalling modules.

Arabidopsis uses apoplastic cysteine-rich signalling peptides called epidermal patterning factors (EPFs) and EPF-like (EPFL) peptides to convey extracellular signals between stomatal lineage cells, mesophyll cells, and cells destined to become pavement cells (Simmons and Bergmann, 2016) (**Figure 2**). EPF2 and EPF1 negatively regulate SD; EPF2 primarily by preventing stomatal lineage entry and meristemoid amplifying divisions (Hara et al., 2009; Hunt and Gray, 2009); EPF1 by restricting meristemoid identity and facilitating the correct orientation of SLGC spacing divisions (Hara et al., 2007; Qi et al., 2017). On the other hand, EPFL9 promotes stomatal development in opposition to EPF2 and EPF1 (Hunt et al., 2010; Sugano et al., 2010). At the plasma membrane, EPF/EPFL signals are perceived by members of the ERECTA family (ERECTA, ER; ERECTA-LIKE1, ERL1; and ERECTA-LIKE2, ERL2) of receptor kinases along with the receptor protein TOO MANY MOUTHS (TMM) (Nadeau and Sack, 2002; Shpak et al., 2005; Lin et al., 2017).The binding of EPF2 to an ER/TMM complex in the presence of somatic embryogenesis receptor kinases (SERKs) promotes signal transduction across the plasma membrane into the cytoplasm; thereby activating the intracellular mitogen-activated protein kinase (MAPK) pathway (Meng et al., 2015). When activated, this pathway culminates in the phosphorylation and subsequent degradation of SPCH (Lampard et al., 2008). EPFL9 acts antagonistically to EPF2 by competing to bind to the ER/TMM complex (Lee et al., 2015). If successful in doing so, EPFL9 can prevent SPCH degradation by blocking activation of the MAPK pathway (Bergmann et al., 2004; Lampard et al., 2008). Rather than an ER/TMM complex, EPF1 preferentially binds to ERL1, which also associates with TMM and, like EPF2, probably competes with EPFL9 for binding (Lee et al., 2015).

Like with the bHLH transcription factors, functional orthologues of EPF/EPFLs are also present in grasses (Tanaka et al., 2013; Caine et al., 2016; Hughes et al., 2017; Yin et al., 2017; Lu et al., 2019) (**Figure 2**). Moreover, phylogenetic analysis also suggests that ERECTA and TMM genes are present, with OsERECTA already shown to be a governor of heat tolerance in rice (Shen et al., 2015). As in Arabidopsis, there are probably two *EPF* genes involved in negatively regulating stomatal development in grasses (Hepworth et al., 2018; Lu et al., 2019). However, rather than one *EPFL9* gene, grasses normally have two; *EPFL9a* and *EPFL9b* (Hepworth et al., 2018; Lu et al., 2019). Using CRISPR-Cas9 and CRISPR-Cpf1 genome editing, Yin et al. (2017) have shown that *OsEPFL9a* plays a major role in regulating rice stomatal development, with *osepfl9a* knockout plants having a ~90% reduction in SD. Conversely, overexpression of *OsEPFL9a* has been shown to moderately increase SD and reduce stomatal size (Mohammed et al, 2019). Interestingly, little-to-no clustering of stomata occurs upon *OsEPFL9a* overexpression in rice, whereas the large increase in density in *EPFL9*-overexpressing Arabidopsis plants is driven by stomatal clustering (Hunt et al., 2010). Despite this, exactly how, where and when *OsEPFL9a* contributes to stomatal lineage progression is still not well understood and requires further study. While no equivalent *OsEPFL9b* knockout or overexpressing rice plants have been generated thus far, recent work in Arabidopsis has shown that *OsEPFL9b* can moderately increase SD when overexpressed (Lu et al., 2019). In contrast to *OsEPFL9a* overexpression, *OsEPFL9b*-overexpressing plants have a tissue-specific clustering phenotype, with stomatal clusters forming in hypocotyls but not rosette leaves (Lu et al., 2019). Nevertheless, based on evidence that is currently available, it seems that *OsEPFL9a* is the dominant player in stomatal development, with *OsEPFL9b* perhaps playing a minor role.

In barley and wheat, Hughes et al. (2017) and Dunn et al. (2019) have shown that overexpression of *HvEPF1* and *TaEPF1B* leads to inhibition of multiple stages of the stomatal lineage, including asymmetric entry divisions, GMC development and the formation of SCs. Overexpression of *HvEPF1* in Arabidopsis produces a similar phenotype to that of Arabidopsis *EPF1* overexpression, whereby meristemoid differentiation is perturbed, resulting in a clustering of small cells around a central meristemoid (Hughes et al., 2017). Given that cells derived from asymmetric entry divisions in grasses are not believed to take on meristemoid-like identity, it is intriguing that HvEPF1 is capable of regulating meristemoid fate in Arabidopsis. This finding, together with findings from wheat, suggests that *EPF1* orthologues probably act relatively early in the stomatal lineage in grasses, but further investigation is required to ascertain exactly where and how these gene products are functioning. Subsequent work by Caine et al. (2019) and Lu et al. (2019), where *OsEPF1* was overexpressed in both rice and Arabidopsis, produced similar results to those in barley and in wheat, with strong overexpression of *OsEPF1* in rice resulting in the majority of protodermal cells failing to enter the stomatal lineage (Caine et al., 2019). As with *OsEPF1*, increasing the expression of *OsEPF2* effectively reduces the SD of both rice and Arabidopsis, with phenotypic similarities to *OsEPF1* overexpression in each instance (Lu et al., 2019). Clearly, assessment of how EPF/EPFLs regulate SD in rice has provided insight to their function, but more research (including generation of *osepf1*, *osepf2* single knockout and *osepf1 osepf2* double knockout plants) is required to enable a more succinct understanding of how rice stomatal development unfolds.

Little is known about how EPF signals are transduced to nuclear-residing bHLH transcription factors during grass stomatal development. However, a recent report has confirmed that like in Arabidopsis, a member of the MAPK pathway, YODA, is involved in regulating stomatal development in Brachypodium (Abrash et al., 2018). Abrash et al. (2018) show that *bdyda1* knockout mutants have a large increase in SD and a severe stomatal clustering phenotype, whereby approximately 86% of stomata are involved in cell clusters. Interestingly, rather than arising as a result of faulty physical asymmetry in cell divisions (as in Arabidopsis *yda* mutants), cell clusters in *bdyda* mutants result from a failure of differentiation and fate reinforcement after asymmetric entry divisions have already occurred (Bergmann et al., 2004; Abrash et al., 2018). Thus, although YDA proteins influence entry to the stomatal lineage in both Brachypodium and Arabidopsis, their roles appear to be distinct. In Arabidopsis, YDA is a pre-division regulator, whereas BdYDA acts post-division to reinforce cell fate in Brachypodium (Abrash et al., 2018).

MOVING AWAY FROM THE USUAL SUSPECTS: OTHER PLAYERS IN RICE STOMATAL DEVELOPMENT

SCARECROW and SHORTROOT Control Cell File Positioning

Until recently, the positional signals that prompt the specification of grass stomatal cell files remained unclear. Schuler et al.'s (2018) study of rice and maize *SHR* orthologues has shed new light onto this area. In Arabidopsis, SHR interacts with another transcription factor, SCARECROW (SCR), in the shoots to position bundle sheath cells around the developing vasculature (Cui et al., 2014). Given that *(i)* vascular patterning and stomatal patterning are coordinated, *(ii)* stomatal cell files are specified (laterally) adjacent to procambial centres in grasses, and *(iii) OsSHR1* and *OsSCR1* are expressed in stomatal lineage cells, it was proposed that SHR-SCR interactions might contribute to the specification and spacing of stomatal cell files in grasses (Kamiya et al., 2003; Schuler et al., 2018). Indeed, ectopic expression of *ZmSHR1* in the rice epidermis (chosen to avoid potentially silencing another SHR gene, *OsSHR2*) does lead to the formation of extra stomatal cell files positioned further from the leaf veins (Schuler et al., 2018). In line with these findings, double knockout *osshr1 osshr2* rice plants have been shown to have reduced SD, with phenotypes suggesting that OsSHR1/2 act redundantly at multiple points during the stomatal lineage (Wu et al., 2019) (**Figure 2**). Despite these

findings suggesting that OsSHR1/2 promote stomatal formation, Wu et al.'s (2019) study does not indicate that overexpression of *OsSHR1* or *OsSHR2* alters the number of stomatal cell files, nor does SD increase when either gene is overexpressed. It is unclear whether this is because of gene silencing (as alluded to above) or whether OsSHR1 or OsSHR2 are genuinely incapable of promoting new stomatal files in rice.

Wu et al. (2019) also investigated the function of OsSCR1 and OsSCR2 during rice stomatal development and found that like OsSHR1/2, OsSCR1 and OsSCR2 positively regulate SD at multiple stages (**Figure 2**). While OsSCR1 has a prominent role, OsSCR2 function is only noticeable in *osscr1 osscr2* double knockouts and not in single knockout *osscr2* mutants. Binding assays have confirmed the existence of OsSHR-OsSCR interactions *in vitro*, suggesting that rice replicates the functional link between SHRs and SCRs that is observed in Arabidopsis. Further analysis of the genomic targets of SHRs and SCRs in grasses might help to clarify exactly how and when they regulate stomatal development and thus may also have implications for the optimisation of SD in rice.

Cyclins and Cyclin-Dependent Kinases in the Rice Stomatal Lineage

Whereas the rice stomatal bHLHs are thought to invoke and regulate specific cell identities and divisions in the rice stomatal lineage, the precise mitotic control of these divisions has not been well-studied. Across life, specific cyclin-CDK (cyclin-dependent kinase) complexes are known to govern cell cycle transitions (Harashima et al., 2013; Han and Torii, 2019). In the Arabidopsis stomatal lineage, complexes of A2-type cyclins (CYCA2s) and a B-type CDK, CDKB1;1, promote symmetric divisions of GMCs (Boudolf et al., 2009; Vanneste et al., 2011). Undivided GCs are common in triple knockouts of *CYCA2s* (*cyca2;134* and *cyca2;234*) and in *cdkb1;1* mutants, and the nuclear DNA content of cells from the former is double that of normal GCs, suggesting that they are arrested at the G2-to-M phase (Boudolf et al., 2004; Vanneste et al., 2011).

While four CYCA2s are found in Arabidopsis, only one *CYCA2* gene, *OsCYCA2;1*, is present in the rice genome (La et al., 2006; Qu et al., 2018). BiFC assays have shown that OsCYCA2;1 and OsCDKB1;1 (orthologue of Arabidopsis CDKB1;1) form a functional complex in rice (Qu et al., 2018). Yet, in contrast to Arabidopsis, when *OsCYAC2;1* or *OsCDKB1;1* are knocked down, GMC divisions are uninterrupted (Qu et al., 2018). Intriguingly, fewer asymmetric entry divisions are observed in stomatal cell files in *OsCYCA2;1*-RNAi plants, leading to an overall reduction in SD (Qu et al., 2018). Nevertheless, both *OsCYCA2;1* and *OsCDKB1;1* can rescue the defective phenotypes of Arabidopsis *cyca2* and *cdkb1* mutants respectively (Qu et al., 2018). Thus, the functions of CYCA2s and CDKB1;1 must be somewhat conserved between rice and Arabidopsis despite the divergence in the timing of their activity (Qu et al., 2018).

Connections between the core bHLH module and cell-cycle regulators in the Arabidopsis stomatal lineage are beginning to be identified (Xie et al., 2010; Lau et al., 2014; Adrian et al., 2015; Han et al., 2018). In the early lineage, *CYCD3s* are upregulated in response to *SPCH* expression (Adrian et al., 2015), with *CYCD3;1* targeted directly by SPCH (Lau et al., 2014). Later in development, inducers of symmetric GMC divisions — *CYCD5;1*, *CYCA2s*, and *CDKB1;1* — are directly upregulated by MUTE; a recent finding that has implicated MUTE as a governor of the GMC symmetric division (Han et al., 2018). FAMA and FLP/MYB88 are responsible for negatively regulating this symmetric division by ensuring that GCs do not undergo further divisions (Lai et al., 2005; Lee et al., 2014). Whereas MUTE enhances the expression of *CDKB1;1*, FLP represses its expression by binding to a *cis*-regulatory region in its promoter sequence (Xie et al., 2010). A single orthologue of *FLP/MYB88*, *OsFLP*, is present in the rice genome (Wu et al., 2019). Akin to its role in Arabidopsis, OsFLP appears to be involved in the regulation of symmetric divisions in rice, as knocking out its expression leads to abnormal division of GMCs (Wu et al., 2019) (**Figure 2**). However, as described earlier, CDKB1;1 does not influence the GMC-GC transition in rice, so the genomic targets of OsMUTE and OsFLP must have diverged to some extent. Thus, exactly how the functions of other cyclins and CDKs are programmed in the rice stomatal lineage must now be determined. Furthermore, by investigating the cyclin-CDK-mediated regulation of asymmetric SC entry divisions, insight will be gained as to how the regulatory machinery of the plant cell-cycle has been adjusted in grasses to accommodate these unique cell divisions.

MANIPULATING GAS EXCHANGE IN RICE BY ALTERING STOMATAL DENSITY

Decreasing Stomatal Density Improves WUE and Drought Tolerance

Our extensive knowledge of stomatal development in Arabidopsis is gradually being translated into rice and other grasses. Now, by harnessing this knowledge, efforts are being made to alter the stomatal development of rice to create crops that might be better suited to future climate conditions. Decreasing the number of stomata on the leaves of rice could maintain its productivity in the future hotter, drier climate (Caine et al., 2019). Reducing SD in Arabidopsis, maize, and barley demonstrably improves WUE and/or drought tolerance (Hepworth et al., 2015; Liu et al., 2015; Hughes et al., 2017). However, until Caine et al.'s (2019) study, it was unclear whether this finding could be replicated in rice given the potentially negative impact of constraining the transpiration rate of such a water-intensive crop (Hoekstra and Chapagain, 2006). To test this hypothesis, Caine et al. (2019) engineered a rice cultivar (IR64) to overexpress *OsEPF1*, creating plants with up to an 88% reduction in stomata density (relative to wildtype SD). Direct examinations of whole-plant water use have shown that *OsEPF1*-overexpressing (*OsEPF1oe*) plants consume around 40% less water than control plants over equivalent periods, due primarily to reductions in g_s (Caine et al., 2019).

In future predictions of the climate, plants will be faced with a dilemma: close stomata to save water or keep them open to stay

cool (Chaves et al., 2016). Whereas both elevated atmospheric CO_2 or reduced water availability trigger stomatal closure in plants, exposure to increased temperatures could lead to lethal overheating or photoinhibition if transpirational cooling is not maintained (Bertolino et al., 2019). By this logic, plants engineered to have fewer stomata should be more susceptible to heat-stress (Urban et al., 2017). However, thermal imaging of *OsEPF1oe* and comparable control plants subjected to droughted conditions reveals a heightened capacity for evaporative cooling in *OsEPF1oe* plants during late-stage drought. Essentially, *OsEPF1oe* plants are able to restrict transpiration during the early stages of drought, meaning more water is available for maintenance of evaporative cooling later in the drought (Caine et al., 2019). Moreover, under well-watered conditions at elevated temperature, *OsEPF1oe* plants can increase the aperture of their stomata, thereby mitigating the potentially detrimental effect of having fewer stomata when conditions are more favorable (Caine et al., 2019).

Although results have not been replicated in the field, during laboratory-simulated drought treatments *OsEPF1oe* grain yields are at least equivalent to controls (Caine et al., 2019). Interestingly, when drought is introduced during flowering (after 88 days of growth), lines with moderate stomatal reductions (*OsEPF1oeW*) outperform both control plants and those with more severe reductions (*OsEPF1oeS*). In these plants, both grain yield and above-ground biomass are increased, suggesting that subtle adjustments to SD might be beneficial during drought at the flowering stage (Caine et al., 2019). After the same treatment, the 1,000 grain weight of all *OsEPF1oe* lines is significantly higher than that of controls (Caine et al., 2019). Exposure to high temperatures during grain filling is known to reduce the content of starch molecules and storage proteins in rice grains (Lin et al., 2010). Therefore, the observed maintenance of grain weight in *OsEPF1oe* lines in droughted conditions might be due to prolonged transpirational cooling of the heat-sensitive flowers (Morita et al., 2016).

Can Increases to Stomatal Density Improve Photosynthetic Efficiency?

It has been shown that changes to stomatal size and density can be correlated with g_s, and so it follows that genetic manipulation of SD has the potential to increase photosynthetic gas exchange (Franks et al., 2012). However, as pointed out by Harrison et al. (2019), such a coupling between SD and gas exchange does not always exist in practice. Nevertheless, Arabidopsis *EPFL9*-overexpressing plants (with ~600% increased SD) show enhanced A at both ambient and elevated CO_2, probably due to a much increased g_s (Tanaka et al., 2013). This is despite the occurrence of stomatal clustering, a trait that has been shown to negatively impact photosynthetic performance (Dow et al., 2014). In rice plants that overexpress *OsEPFL9a*, gas exchange (both A and g_s) is unchanged, although this may be a signature of the smaller increase in SD (~20%–30%) in these plants relative to Arabidopsis *EPFL9*-overexpressing plants (Mohammed et al., 2019). A similarly modest increase in SD in rice has been generated *via* the overexpression of a maize *SHORTROOT* gene, *ZmSHR1* (Schuler et al., 2018). Like with *OsEPFL9a* overexpression, higher SD in *ZmSHR1*-overexpressing plants does not lead to an enhancement of A or g_s (Schuler et al., 2018). For *OsEPFL9a* overexpression, the lack of increase in either parameter may be explained by a concurrent reduction in stomatal size (Mohammed et al., 2019). Perhaps if changes to the stomatal number were more significant — as in Tanaka et al. (2013) — the compensatory effect of reduced stomatal size in *OsEPFL9a*-overexpressing plants might have less of an impact in preventing g_s from increasing.

As discussed previously, manipulating SD will create a trade-off between the uptake of CO_2 and the control of transpirational water flow. Indeed, in Arabidopsis, enhancement of A in Tanaka et al.'s (2013) *AtEPFL9*-overexpressing plants is not translated to biomass gains. This is likely due to the plants being more prone to water loss, as transgenic plants with greater SD have significantly greater transpiration rates (Tanaka et al., 2013). Relative to Arabidopsis and other plants, rice might be more able to afford an increased rate of water loss, as the majority (~75%) of production is sourced from irrigated lowland systems (Zhao et al., 2011). Moreover, amongst lowland rice varieties, A is correlated with SD when plants are grown in flooded soils (Tsunoda and Fukoshima, 1986). In fact, the SD and g_s of 3 high-yielding rice cultivars (IR72, Takanari and LYPJ) are significantly higher than the corresponding average values from 69 lower-yielding accessions (Ohsumi et al., 2007).

Linking SD With Stomatal Size and Physiology to Improve WUE

Genetic manipulation of SD leads to a fixed change in the number of stomata that form per unit area in the epidermis. The stomata of Arabidopsis SD mutants (of multiple genotypic backgrounds) retain the capacity to open and close and changes in SD are often accompanied by inverse changes to stomatal size; i.e., reductions in SD are linked to increases in stomatal size and vice versa (Doheny-Adams et al., 2012). However, this size-density response is not consistently seen in grasses. For both barley and the IR64 rice cultivar (subspecies indica) the opposite response is observed, whereby reductions in SD result in co-reductions in stomata size (Hughes et al., 2017; Caine et al., 2019). In the Nipponbare rice cultivar (subspecies japonica), reduced SD leads to increased stomatal size and increased SD leads to reduced size; responses similar to those previously observed in Arabidopsis (Mohammed et al., 2019). Thus, within different subspecies of rice, the stomatal size responses to genetic manipulation of SD are different. Why this occurs is unclear, although there is evidence in grasses that smaller stomata can improve WUE by opening and closing quicker in response to environmental fluctuations (McAusland et al., 2016; Lawson and Vialet-Chabrand, 2019). For both subspecies, it would be interesting to assess how the stomata of low-SD *OsEPF1oe* plants perform under fluctuating conditions to ascertain the impact that size and density alterations have on the "speed" of stomatal movements and WUE.

By targeting the mechanisms that govern guard cell ion transportation across the plasma membrane and tonoplast, it is

possible to effectively alter stomatal opening and closing in response to both abiotic and biotic stress (Huang et al., 2009; Daszkowska-Golec and Szarejko, 2013; Li et al., 2017; Lawson and Vialet-Chabrand, 2019) and to enhance plant biomass accumulation (Papanatsiou et al., 2019). Because the SCs of grasses are thought to both enable a swifter transport of ions and osmolytes to GCs and to lend a mechanical advantage to their stomatal movements, grass stomatal complexes are viewed as being more responsive than other stomatal morphologies (Franks and Farquhar, 2006; Cai et al., 2017; Nunes et al., 2019). Indeed, the stomata of *bdmute* plants (which are devoid of SCs) respond more slowly to changes in light intensity (Raissig et al., 2017). However, to date no genetic manipulations that enhance the speed of grass stomata have been reported, and it is therefore not possible to compare the potential water savings that could be achieved by low-SD rice with those of rice manipulated to have enhanced stomatal closure. To address this unknown, future efforts to manipulate rice stomata should aim to target short-term stomatal responses, perhaps individually and in combination with SD, so that a more complete picture of the control of WUE in grass plants can be developed.

CONCLUSION

Rice is the world's most important human food crop and yields must be protected against future climate instabilities. As the "gatekeepers" of transpiration and carbon uptake, stomata represent an obvious target to improve *A* or water retention in rice (Lawson and Blatt, 2014). Although more detailed examinations of rice stomatal development will be required to match our understanding of stomatal development in Arabidopsis, the advances to our understanding of grass stomatal development discussed here have enabled high- and low-SD rice plants to be developed (Schuler et al., 2018; Caine et al., 2019; Mohammed et al., 2019). Contrary to expectation, rice plants with increased SD do not exhibit corresponding increases in *A* (Schuler et al., 2018; Mohammed et al., 2019), although this could be due to altered stomatal size and or aperture size. Thus, rice plants with more substantial increases in SD will be required to test the efficacy (or lack thereof) of targeting stomatal development for the enhancement of either *A* or evaporative cooling. On the other hand, given that freshwater insecurities and exposure to drought will likely become increasingly prevalent in areas of rice cultivation (Kang et al., 2009; Quentin Grafton, 2017), rice crops that use water more efficiently might be of greater importance in the future climate. This will be especially important in Africa where, as a result of water limitations, rainfed upland rice production is steadily increasing, despite this method being particularly susceptible to drought (Saito et al., 2018). Promisingly, *OsEPF1oe* lines with decreased SD exhibit improved water conservation and tolerance to drought without yield penalties (Caine et al., 2019). While this development is encouraging, these findings have not yet been reproduced in the field, and so it remains to be seen whether real-world fluctuations in environmental variables will influence the performance of these plants that have thus far only been tested under laboratory conditions.

AUTHOR CONTRIBUTIONS

CB, RC, and JG wrote the article and CB prepared the figures. All authors checked and approved the article before publication.

FUNDING

RC and JG acknowledge the BBSRC and Newton fund for the financial support. RC also acknowledges the University of Sheffield QR GCRF fellowship (Research England institutional allocation) for the fellows.

REFERENCES

Abrash, E., Anleu Gil, M. X., Matos, J. L., and Bergmann, D. C. (2018). Conservation and divergence of YODA MAPKKK function in regulation of grass epidermal patterning. *Dev. (Cambridge England)* 145 (14), dev.165860. doi: 10.1242/dev.165860

Adrian, J., Chang, J., Ballenger, C. E., Bargmann, B. O. R., Alassimone, J., Davies, K. A., et al. (2015). Transcriptome dynamics of the stomatal lineage: birth, amplification, and termination of a self-renewing population. *Dev. Cell* 33 (1), 107–118. doi: 10.1016/j.devcel.2015.01.025

Arve, L., Torre, S., Olsen, J., and Tanino, K. (2011). "Stomatal Responses to Drought Stress and Air Humidity," in *Abiotic Stress in Plants - Mechanisms and Adaptations* (Rijeka: IntechOpen), 268–280.

Bergmann, D. C., Lukowitz, W., and Somerville, C. R. (2004). Stomatal development and pattern controlled by a MAPKK kinase. *Science* 304 (5676), 1494–1497. doi: 10.1126/science.1096014

Bertolino, L. T., Caine, R. S., and Gray, J. E. (2019). Impact of stomatal density and morphology on water-use efficiency in a changing world. *Front. Plant Sci.* 10, 225. doi: 10.3389/fpls.2019.00225

Boudolf, V., Vlieghe, K., Beemster, G. T. S., Magyar, Z., Torres Acosta, J. A., Maes, S., et al. (2004). The plant-specific cyclin-dependent kinase CDKB1;1 and transcription factor E2Fa-DPa control the balance of mitotically dividing and endoreduplicating cells in Arabidopsis. *Plant Cell* 16 (10), 2683–2692. doi: 10.1105/tpc.104.024398

Boudolf, V., Lammens, T., Boruc, J., Van Leene, J., Van Den Daele, H., Maes, S., et al. (2009). CDKB1;1 forms a functional complex with CYCA2;3 to suppress endocycle onset. *Plant Physiol.* 150 (3), 1482–1493. doi: 10.1104/pp.109.140269

Brar, D. S., and Khush, G. S. (2013). Biotechnological approaches for increasing productivity and sustainability of rice production. In *Progress and Prospects in Crop Research*, (Cambridge, MA: Academic Press), 151–175.

Brownlee, C. (2001). The long and the short of stomatal density signals. *Trends Plant Sci.* 6 (10), 441–442. doi: 10.1016/S1360-1385(01)02095-7

Buckley, T. N. (2005). The control of stomata by water balance. *New Phytol.* 168 (2), 275–292. doi: 10.1111/j.1469-8137.2005.01543.x

Cai, S., Papanatsiou, M., Blatt, M. R., and Chen, Z.-H. (2017). Speedy grass stomata: emerging molecular and evolutionary features. *Mol. Plant* 10 (7), 912–914. doi: 10.1016/j.molp.2017.06.002

Caine, R. S., Chater, C. C., Kamisugi, Y., Cuming, A. C., Beerling, D. J., Gray, J. E., et al. (2016). An ancestral stomatal patterning module revealed in the non-vascular land plant Physcomitrella patens. *Development* 143 (18), 3306–3314. doi: 10.1242/dev.135038

Caine, R. S., Yin, X., Sloan, J., Harrison, E. L., Mohammed, U., Fulton, T., et al. (2019). Rice with reduced stomatal density conserves water and has improved

drought tolerance under future climate conditions. *New Phytol.* 221 (1), 371–384. doi: 10.1111/nph.15344

Casson, S., and Gray, J. E. (2008). Influence of environmental factors on stomatal development. *New Phytol.* 178 (1), 9–23. doi: 10.1111/j.1469-8137.2007.02351.x

Challinor, A. J., Watson, J., Lobell, D. B., Howden, S. M., Smith, D. R., and Chhetri, N. (2014). A meta-analysis of crop yield under climate change and adaptation. *Nat. Climate Change* 4 (4), 287–291. doi: 10.1038/nclimate2153

Chater, C. C., Oliver, J., Casson, S., and Gray, J. E. (2014). Putting the brakes on: abscisic acid as a central environmental regulator of stomatal development. *New Phytol.* 202 (2), 376–391. doi: 10.1111/nph.12713

Chater, C. C. C., Caine, R. S., Fleming, A. J., and Gray, J. E. (2017). Origins and evolution of stomatal development. *Plant Physiol.* 174 (2), 624–638. doi: 10.1104/pp.17.00183

Chaves, M. M., Costa, J. M., Zarrouk, O., Pinheiro, C., Lopes, C. M., and Pereira, J. S. (2016). Controlling stomatal aperture in semi-arid regions—the dilemma of saving water or being cool? *Plant Sci.* 251, 54–64. doi: 10.1016/j.plantsci.2016.06.015

Chen, Z.-H., Chen, G., Dai, F., Wang, Y., Hills, A., Ruan, Y.-L., et al. (2017). Molecular evolution of grass stomata. *Trends Plant Sci.* 22 (2), 124–139. doi: 10.1016/j.tplants.2016.09.005

Conklin, P. A., Strable, J., Li, S., and Scanlon, M. J. (2018). On the mechanisms of development in monocot and eudicot leaves. *New Phytol.* 221 (2), 706–724. doi: 10.1111/nph.15371

Cui, H., Kong, D., Liu, X., and Hao, Y. (2014). SCARECROW, SCR-LIKE 23 and SHORT-ROOT control bundle sheath cell fate and function in Arabidopsis thaliana. *Plant J.* 78 (2), 319–327. doi: 10.1111/tpj.12470

Daszkowska-Golec, A., and Szarejko, I. (2013). Open or close the gate - Stomata action under the control of phytohormones in drought stress conditions. *Front. Plant Sci.* 4, 138. doi: 10.3389/fpls.2013.00138

Doheny-Adams, T., Hunt, L., Franks, P. J., Beerling, D. J., and Gray, J. E. (2012). Genetic manipulation of stomatal density influences stomatal size, plant growth and tolerance to restricted water supply across a growth carbon dioxide gradient. *Philosophic Transact. Royal Soc. B.: Biol. Sci.* 367 (1588), 547–555. doi: 10.1098/rstb.2011.0272

Dow, G. J., Berry, J. A., and Bergmann, D. C. (2014). The physiological importance of developmental mechanisms that enforce proper stomatal spacing in Arabidopsis thaliana. *New Phytol.* 201 (4), 1205–1217. doi: 10.1111/nph.12586

Dunn, J., Hunt, L., Afsharinafar, M., Meselmani, M. A., Mitchell, A., Howells, R., et al. (2019). Reduced stomatal density in bread wheat leads to increased water-use efficiency. *J. Exp. Bot.* 70(18), 4737–4748. doi: 10.1093/jxb/erz248

Edgar, R. C. (2004). Muscle: multiple sequence alignment with high accuracy and high throughput. *Nucleic Acids Res.* 32 (5), 1792–1797. doi: 10.1093/nar/gkh340

Elert, E. (2014). Rice by the numbers: a good grain. *Nature* 514 (7524), S50–S51. doi: 10.1038/514S50a

Endo, H., and Torii, K. U. (2019). Stomatal development and perspectives toward agricultural improvement. *Cold Spring Harbor Perspect. Biol.* 11 (5), a034660. doi: 10.1101/cshperspect.a034660

Foley, J. A., Ramankutty, N., Brauman, K. A., Cassidy, E. S., Gerber, J. S., Johnston, M., et al. (2011). Solutions for a cultivated planet. *Nature* 478 (7369), 337–342. doi: 10.1038/nature10452

Franks, P. J., and Farquhar, G. D. (2006). The mechanical diversity of stomata and its significance in gas-exchange control. *Plant Physiol.* 143 (1), 78–87. doi: 10.1104/pp.106.089367

Franks, P. J., Leitch, I. J., Ruszala, E. M., Hetherington, A. M., and Beerling, D. J. (2012). Physiological framework for adaptation of stomata to CO2 from glacial to future concentrations. *Philosophic Transact. Royal Soc. B.: Biol. Sci.* 367 (1588), 537–546. doi: 10.1098/rstb.2011.0270

Haefele, S. M., Kato, Y., and Singh, S. (2016). Climate ready rice: augmenting drought tolerance with best management practices. *Field Crops Res.* 190, 60–69. doi: 10.1016/J.FCR.2016.02.001

Han, S.-K., and Torii, K. U. (2019). Linking cell cycle to stomatal differentiation. *Curr. Opin. Plant Biol.* 51, 66–73. doi: 10.1016/J.PBI.2019.03.010

Han, S.-K., Qi, X., Sugihara, K., Dang, J. H., Endo, T. A., Miller, K. L., et al. (2018). MUTE directly orchestrates cell-state switch and the single symmetric division to create stomata. *Dev. Cell* 45 (3), 303–315.e5. doi: 10.1016/j.devcel.2018.04.010

Hara, K., Kajita, R., Torii, K. U., Bergmann, D. C., and Kakimoto, T. (2007). The secretory peptide gene EPF1 enforces the stomatal one-cell-spacing rule. *Genes Dev.* 21 (14), 1720–1725. doi: 10.1101/gad.1550707

Hara, K., Yokoo, T., Kajita, R., Onishi, T., Yahata, S., Peterson, K. M., et al. (2009). Epidermal cell density is Autoregulated via a secretory peptide, epidermal patterning factor 2 in Arabidopsis leaves. *Plant Cell Physiol.* 50 (6), 1019–1031. doi: 10.1093/pcp/pcp068

Harashima, H., Dissmeyer, N., and Schnittger, A. (2013). Cell cycle control across the eukaryotic kingdom. *Trends Cell Biol.* 23 (7), 345–356. doi: 10.1016/J.TCB.2013.03.002

Harrison, E. L., Arce Cubas, L., Gray, J. E., and Hepworth, C. (2019). The influence of stomatal morphology and distribution on photosynthetic gas exchange. *Plant J.* tpj.14560. doi: 10.1111/tpj.14560

Hepworth, C., Doheny-Adams, T., Hunt, L., Cameron, D. D., and Gray, J. E. (2015). Manipulating stomatal density enhances drought tolerance without deleterious effect on nutrient uptake. *New Phytol.* 208 (2), 336–341. doi: 10.1111/nph.13598

Hepworth, C., Caine, R. S., Harrison, E. L., Sloan, J., and Gray, J. E. (2018). Stomatal development: focusing on the grasses. *Curr. Opin. Plant Biol.* 41, 1–7. doi: 10.1016/J.PBI.2017.07.009

Hoekstra, A. Y., and Chapagain, A. K. (2006). "Water footprints of nations: Water use by people as a function of their consumption pattern," in *Integrated Assessment of Water Resources and Global Change* (Dordrecht: Springer Netherlands), 35–48.

Huang, X. Y., Chao, D. Y., Gao, J. P., Zhu, M. Z., Shi, M., and Lin, H. X. (2009). A previously unknown zinc finger protein, DST, regulates drought and salt tolerance in rice via stomatal aperture control. *Genes Dev.* 23 (15), 1805–1817. doi: 10.1101/gad.1812409

Hughes, J., Hepworth, C., Dutton, C., Dunn, J. A., Hunt, L., Stephens, J., et al. (2017). Reducing stomatal density in barley improves drought tolerance without impacting on yield. *Plant Physiol.* 174 (2), 776–787. doi: 10.1104/pp.16.01844

Hunt, L., and Gray, J. E. (2009). The signaling peptide EPF2 controls asymmetric cell divisions during stomatal development. *Curr. Biol.* 19 (10), 864–869. doi: 10.1016/j.cub.2009.03.069

Hunt, L., Bailey, K. J., and Gray, J. E. (2010). The signalling peptide EPFL9 is a positive regulator of stomatal development. *New Phytol.* 186 (3), 609–614. doi: 10.1111/j.1469-8137.2010.03200.x

Kamiya, N., Itoh, J.-I., Morikami, A., Nagato, Y., and Matsuoka, M. (2003). The SCARECROW gene's role in asymmetric cell divisions in rice plants. *Plant J.* 36 (1), 45–54. doi: 10.1046/j.1365-313X.2003.01856.x

Kanaoka, M. M., Pillitteri, L. J., Fujii, H., Yoshida, Y., Bogenschutz, N. L., Takabayashi, J., et al. (2008). SCREAM/ICE1 and SCREAM2 specify three cell-state transitional steps leading to arabidopsis stomatal differentiation. *Plant Cell* 20 (7), 1775–1785. doi: 10.1105/tpc.108.060848

Kang, Y., Khan, S., and Ma, X. (2009). Climate change impacts on crop yield, crop water productivity and food security – a review. *Prog. Nat. Sci.* 19 (12), 1665–1674. doi: 10.1016/J.PNSC.2009.08.001

Krishnan, P., Ramakrishnan, B., Reddy, K. R., and Reddy, V. R. (2011). High-temperature effects on rice growth, yield, and grain quality. *Adv. Agron.* 111, 87–206. doi: 10.1016/B978-0-12-387689-8.00004-7

La, H., Li, J., Ji, Z., Cheng, Y., Li, X., Jiang, S., et al. (2006). Genome-wide analysis of cyclin family in rice (Oryza Sativa L.). *Mol. Genet. Genomics* 275 (4), 374–386. doi: 10.1007/s00438-005-0093-5

Lai, L. B., Nadeau, J. A., Lucas, J., Lee, E.-K., Nakagawa, T., Zhao, L., et al. (2005). The Arabidopsis R2R3 MYB Proteins FOUR LIPS and MYB88 restrict divisions late in the stomatal cell lineage. *Plant Cell* 17 (10), 2754–2767. doi: 10.1105/tpc.105.034116

Lampard, G. R., MacAlister, C. A., and Bergmann, D. C. (2008). Arabidopsis stomatal initiation is controlled by MAPK-mediated regulation of the bHLH SPEECHLESS. *Science* 322 (5904), 1113–1116. doi: 10.1126/science.1162263

Lau, O. S., Davies, K. A., Chang, J., Adrian, J., Rowe, M. H., Ballenger, C. E., et al. (2014). Direct roles of SPEECHLESS in the specification of stomatal self-renewing cells. *Science* 345 (6204), 1605–1609. doi: 10.1126/science.1256888

Lawson, T., and Blatt, M. R. (2014). Stomatal size, speed, and responsiveness impact on photosynthesis and water use efficiency. *Plant Physiol.* 164 (4), 1556–1570. doi: 10.1104/PP.114.237107

Lawson, T., and Vialet-Chabrand, S. (2019). Speedy stomata, photosynthesis and plant water use efficiency. *New Phytol.* 221 (1), 93–98. doi: 10.1111/nph.15330

Lee, E., Lucas, J. R., and Sack, F. D. (2014). Deep functional redundancy between FAMA and FOUR LIPS in stomatal development. *Plant J.* 78 (4), 555–565. doi: 10.1111/tpj.12489

Lee, J. S., Hnilova, M., Maes, M., Lin, Y.-C. L., Putarjunan, A., Han, S.-K., et al. (2015). Competitive binding of antagonistic peptides fine-tunes stomatal patterning. *Nature* 522 (7557), 439–443. doi: 10.1038/nature14561

Li, J., Li, Y., Yin, Z., Jiang, J., Zhang, M., Guo, X., et al. (2017). OsASR5 enhances drought tolerance through a stomatal closure pathway associated with ABA and H2O2 signalling in rice. *Plant Biotechnol. J.* 15 (2), 183–196. doi: 10.1111/pbi.12601

Lin, C.-J., Li, C.-Y., Lin, S.-K., Yang, F.-H., Huang, J.-J., Liu, Y.-H., et al. (2010). Influence of high temperature during grain filling on the accumulation of storage proteins and grain quality in rice (Oryza sativa L.). *J. Agric. Food Chem.* 58 (19), 10545–10552. doi: 10.1021/jf101575j

Lin, G., Zhang, L., Han, Z., Yang, X., Liu, W., Li, E., et al. (2017). A receptor-like protein acts as a specificity switch for the regulation of stomatal development. *Genes Dev.* 31 (9), 927–938. doi: 10.1101/gad.297580.117

Liu, T., Ohashi-Ito, K., and Bergmann, D. C. (2009). Orthologs of Arabidopsis thaliana stomatal bHLH genes and regulation of stomatal development in grasses. *Development* 136 (13), 2265–2276. doi: 10.1242/dev.032938

Liu, Y., Qin, L., Han, L., Xiang, Y., and Zhao, D. (2015). Overexpression of maize SDD1 (ZmSDD1) improves drought resistance in Zea mays L. by reducing stomatal density. *Plant Cell Tissue Organ Cult. (PCTOC)* 122 (1), 147–159. doi: 10.1007/s11240-015-0757-8

Long, S. P., and Ort, D. R. (2010). More than taking the heat: crops and global change. *Curr. Opin. Plant Biol.* 13 (3), 240–247. doi: 10.1016/J.PBI.2010.04.008

Lu, J., He, J., Zhou, X., Zhong, J., Li, J., and Liang, Y.-K. (2019). Homologous genes of epidermal patterning factor regulate stomatal development in rice. *J. Plant Physiol.* 234–235, 18–27. doi: 10.1016/J.JPLPH.2019.01.010

Luo, L., Zhou, W.-Q., Liu, P., Li, C.-X., and Hou, S.-W. (2012). The development of stomata and other epidermal cells on the rice leaves. *Biol. Plant.* 56 (3), 521–527. doi: 10.1007/s10535-012-0045-y

MacAlister, C. A., and Bergmann, D. C. (2011). Sequence and function of basic helix-loop-helix proteins required for stomatal development in Arabidopsis are deeply conserved in land plants. *Evol. Dev.* 13 (2), 182–192. doi: 10.1111/j.1525-142X.2011.00468.x

MacAlister, C. A., Ohashi-Ito, K., and Bergmann, D. C. (2007). Transcription factor control of asymmetric cell divisions that establish the stomatal lineage. *Nature* 445 (7127), 537–540. doi: 10.1038/nature05491

Maclean, J., Hardy, B., and Hettel, G. (2013). *Rice almanac: Source book for one of the most important economic activities on Earth* (Los Baños: International Rice Research Instituite).

Matsui, T., Omasa, K., and Horie, T. (2000). High temperature at flowering inhibits swelling of pollen grains, a driving force for thecae dehiscence in rice (Oryza sativa L.). *Plant Prod. Sci.* 3 (4), 430–434. doi: 10.1626/pps.3.430

McAusland, L., Vialet-Chabrand, S., Davey, P., Baker, N. R., Brendel, O., and Lawson, T. (2016). Effects of kinetics of light-induced stomatal responses on photosynthesis and water-use efficiency. *New Phytol.* 211 (4), 1209–1220. doi: 10.1111/nph.14000

McGuire, S. (2015). FAO, IFAD, and WFP. The State of Food Insecurity in the World 2015: Meeting the 2015 International Hunger Targets: Taking Stock of Uneven Progress. *Adv. Nutrition* 6 (5), 623–624. doi: 10.3945/an.115.009936

Meng, X., Chen, X., Mang, H., Liu, C., Yu, X., Gao, X., et al. (2015). Differential function of Arabidopsis SERK family receptor-like kinases in stomatal patterning. *Curr. Biol.* 25 (18), 2361–2372. doi: 10.1016/j.cub.2015.07.068

Mohammed, U., Caine, R. S., Atkinson, J. A., Harrison, E. L., Wells, D., Chater, C. C., et al. (2019). Rice plants overexpressing OsEPF1 show reduced stomatal density and increased root cortical aerenchyma formation. *Sci. Rep.* 9 (1), 5584. doi: 10.1038/s41598-019-41922-7

Morita, S., Wada, H., and Matsue, Y. (2016). Countermeasures for heat damage in rice grain quality under climate change. *Plant Prod. Sci.* 19 (1), 1–11. doi: 10.1080/1343943X.2015.1128114

Nadeau, J. A., and Sack, F. D. (2002). Control of stomatal distribution on the Arabidopsis leaf surface. *Science* 296 (5573), 1697–1700. doi: 10.1126/science.1069596

Nunes, T. D. G., Zhang, D., and Raissig, M. T. (2019). Form, development and function of grass stomata. *Plant J.* tpj.14552. doi: 10.1111/tpj.14552

Ohashi-Ito, K., and Bergmann, D. C. (2006). Arabidopsis FAMA controls the final proliferation/differentiation switch during stomatal development. *Plant Cell* 18 (10), 2493–2505. doi: 10.1105/tpc.106.046136

Ohsumi, A., Kanemura, T., Homma, K., Horie, T., and Shiraiwa, T. (2007). Genotypic variation of stomatal conductance in relation to stomatal density and length in rice (*Oryza sativa* L.). *Plant Prod. Sci.* 10 (3), 322–328. doi: 10.1626/pps.10.322

Papanatsiou, M., Petersen, J., Henderson, L., Wang, Y., Christie, J. M., and Blatt, M. R. (2019). Optogenetic manipulation of stomatal kinetics improves carbon assimilation, water use, and growth. *Science* 363 (6434), 1456–1459. doi: 10.1126/science.aaw0046

Pillitteri, L. J., and Dong, J. (2013). Stomatal development in Arabidopsis. *Arabidopsis Book* 11, e0162. doi: 10.1199/tab.0162

Pillitteri, L. J., Sloan, D. B., Bogenschutz, N. L., and Torii, K. U. (2007). Termination of asymmetric cell division and differentiation of stomata. *Nature* 445 (7127), 501–505. doi: 10.1038/nature05467

Qi, X., and Torii, K. U. (2018). Hormonal and environmental signals guiding stomatal development. *BMC Biol.* 16 (1), 21. doi: 10.1186/s12915-018-0488-5

Qi, X., Han, S.-K., Dang, J. H., Garrick, J. M., Ito, M., Hofstetter, A. K., et al. (2017). Autocrine regulation of stomatal differentiation potential by EPF1 and ERECTA-LIKE1 ligand-receptor signaling. *ELife* 6, e24102. doi: 10.7554/eLife.24102

Qu, X., Peterson, K. M., and Torii, K. U. (2017). Stomatal development in time: the past and the future. *Curr. Opin. Genet. Dev.* 45, 1–9. doi: 10.1016/J.GDE.2017.02.001

Qu, X., Yan, M., Zou, J., Jiang, M., Yang, K., and Le, J. (2018). A2-type cyclin is required for the asymmetric entry division in rice stomatal development. *J. Exp. Bot.* 69 (15), 3587–3599. doi: 10.1093/jxb/ery158

Quentin Grafton, R. (2017). Responding to the 'Wicked Problem' of water insecurity. *Water Resour. Manage.* 31 (10), 3023–3041. doi: 10.1007/s11269-017-1606-9

Raissig, M. T., Abrash, E., Bettadapur, A., Vogel, J. P., and Bergmann, D. C. (2016). Grasses use an alternatively wired bHLH transcription factor network to establish stomatal identity. *Proc. Natl. Acad. Sci. U.S.A.* 113 (29), 8326–8331. doi: 10.1073/pnas.1606728113

Raissig, M. T., Matos, J. L., Anleu Gil, M. X., Kornfeld, A., Bettadapur, A., Abrash, E., et al. (2017). Mobile MUTE specifies subsidiary cells to build physiologically improved grass stomata. *Science* 355 (6330), 1215–1218. doi: 10.1126/science.aal3254

Ran, J.-H., Shen, T.-T., Liu, W.-J., and Wang, X.-Q. (2013). Evolution of the bHLH genes involved in stomatal development: implications for the expansion of developmental complexity of stomata in land plants. *PloS One* 8 (11), e78997. doi: 10.1371/journal.pone.0078997

Sánchez, B., Rasmussen, A., and Porter, J. R. (2014). Temperatures and the growth and development of maize and rice: a review. *Global Change Biol.* 20 (2), 408–417. doi: 10.1111/gcb.12389

Sachs, T. (1991). *Pattern formation in plant tissues* (Cambridge, UK: Cambridge University Press).

Saito, K., Asai, H., Zhao, D., Laborte, A. G., and Grenier, C. (2018). Progress in varietal improvement for increasing upland rice productivity in the tropics. *Plant Prod. Sci.* 21 (3), 145–158. doi: 10.1080/1343943X.2018.1459751

Saitou, N., and Nei, M. (1987). The neighbor-joining method: a new method for reconstructing phylogenetic trees. *Mol. Biol. Evol.* 4 (4), 406–425. doi: 10.1093/oxfordjournals.molbev.a040454

Schuler, M. L., Sedelnikova, O. V., Walker, B. J., Westhoff, P., and Langdale, J. A. (2018). SHORTROOT-mediated increase in stomatal density has no impact on photosynthetic efficiency. *Plant Physiol.* 176 (1), 757–772. doi: 10.1104/PP.17.01005

Seneviratne, S. I., Nicholls, N., Easterling, D., Goodess, C. M., Kanae, S., Kossin, J., et al. (2012). "Changes in Climate Extremes and their Impacts on the Natural Physical Environment," in *Managing the Risks of Extreme Events and Disasters to Advance Climate Change Adaptation. A Special Report of Working Groups I and II of the Intergovernmental Panel on Climate Change (IPCC)* (Cambridge, UK: Cambridge University Press), 109–230.

Shen, H., Zhong, X., Zhao, F., Wang, Y., Yan, B., Li, Q., et al. (2015). Overexpression of receptor-like kinase ERECTA improves thermotolerance in rice and tomato. *Nat. Biotechnol.* 33 (9), 996–1003. doi: 10.1038/nbt.3321

Shpak, E. D., McAbee, J. M., Pillitteri, L. J., and Torii, K. U. (2005). Stomatal patterning and differentiation by synergistic interactions of receptor kinases. *Science* 309 (5732), 290–293. doi: 10.1126/science.1109710

Simmons, A. R., and Bergmann, D. C. (2016). Transcriptional control of cell fate in the stomatal lineage. *Curr. Opin. Plant Biol.* 29, 1–8. doi: 10.1016/j.pbi.2015.09.008

Stebbins, G. L., and Shah, S. S. (1960). Developmental studies of cell differentiation in the epidermis of monocotyledons: II. Cytological features of stomatal development in the Gramineae. *Dev. Biol.* 2 (6), 477–500. doi: 10.1016/0012-1606(60)90050-6

Stott, P. (2016). How climate change affects extreme weather events. *Science* 352 (6293), 1517–1518. doi: 10.1126/science.aaf7271

Sugano, S. S., Shimada, T., Imai, Y., Okawa, K., Tamai, A., Mori, M., et al. (2010). Stomagen positively regulates stomatal density in Arabidopsis. *Nature* 463 (7278), 241–244. doi: 10.1038/nature08682

Swain, P., Raman, A., Singh, S. P., and Kumar, A. (2017). Breeding drought tolerant rice for shallow rainfed ecosystem of eastern India. *Field Crops Res.* 209, 168–178. doi: 10.1016/J.FCR.2017.05.007

Tanaka, Y., Sugano, S. S., Shimada, T., and Hara-Nishimura, I. (2013). Enhancement of leaf photosynthetic capacity through increased stomatal density in Arabidopsis. *New Phytol.* 198 (3), 757–764. doi: 10.1111/nph.12186

Tsunoda, S., and Fukoshima, M. T. (1986). Leaf properties related to the photosynthetic response to drought in upland and lowland rice varieties. *Annals Bot.* 58 (4), 531–539. doi: 10.1093/annbot/58.4.531

United Nations. (2017). *World Population Prospects: The 2017 Revision* (New York, NY).

Urban, J., Ingwers, M. W., McGuire, M. A., and Teskey, R. O. (2017). Increase in leaf temperature opens stomata and decouples net photosynthesis from stomatal conductance in Pinus taeda and Populus deltoides x nigra. *J. Exp. Bot.* 68 (7), 1757–1767. doi: 10.1093/jxb/erx052

Vanneste, S., Coppens, F., Lee, E., Donner, T. J., Xie, Z., Van Isterdael, G., et al. (2011). Developmental regulation of CYCA2s contributes to tissue-specific proliferation in Arabidopsis. *EMBO J.* 30 (16), 3430–3441. doi: 10.1038/emboj.2011.240

Wang, H., Guo, S., Qiao, X., Guo, J., Li, Z., Zhou, Y., et al. (2019). BZU2/ZmMUTE controls symmetrical division of guard mother cell and specifies neighbor cell fate in maize. *PLOS Genet.* 15 (8), e1008377. doi: 10.1371/journal.pgen.1008377

Wassmann, R., Jagadish, S. V. K., Sumfleth, K., Pathak, H., Howell, G., Ismail, A., et al. (2009). Regional vulnerability of climate change impacts on Asian rice production and scope for adaptation. *Adv. Agron.* 102, 91–133. doi: 10.1016/S0065-2113(09)01003-7

Wu, Z., Chen, L., Yu, Q., Zhou, W., Gou, X., Li, J., et al. (2019). Multiple transcriptional factors control stomata development in rice. *New Phytol.* 223 (1), 220–232. doi: 10.1111/nph.15766

Xie, Z., Lee, E., Lucas, J. R., Morohashi, K., Li, D., Murray, J. A. H., et al. (2010). Regulation of cell proliferation in the stomatal lineage by the Arabidopsis MYB FOUR LIPS via direct targeting of core cell cycle genes. *Plant Cell* 22 (7), 2306–2321. doi: 10.1105/tpc.110.074609

Yang, M., Sack, F. D., Lucas, J., Lee, E.-K., Nakagawa, T., Zhao, L., et al. (1995). The too many mouths and four lips mutations affect stomatal production in Arabidopsis. *Plant Cell* 7 (12), 2227–2239. doi: 10.1105/tpc.7.12.2227

Yin, X., Biswal, A. K., Dionora, J., Perdigon, K. M., Balahadia, C. P., Mazumdar, S., et al. (2017). CRISPR-Cas9 and CRISPR-Cpf1 mediated targeting of a stomatal developmental gene EPFL9 in rice. *Plant Cell Rep.* 36 (5), 745–757. doi: 10.1007/s00299-017-2118-z

Zhao, L., Wu, L., Wu, M., and Li, Y. (2011). Nutrient uptake and water use efficiency as affected by modified rice cultivation methods with reduced irrigation. *Paddy Water Environ.* 9 (1), 25–32. doi: 10.1007/s10333-011-0257-3

Zoulias, N., Harrison, E. L., Casson, S. A., and Gray, J. E. (2018). Molecular control of stomatal development. *Biochem. J.* 475 (2), 441–454. doi: 10.1042/BCJ20170413

Zuckerkandl, E., and Pauling, L. (1965). Molecules as documents of evolutionary history. *J. Theor. Biol.* 8 (2), 357–366. doi: 10.1016/0022-5193(65)90083-4

Conflict of Interest: The authors declare that the research was conducted in the absence of any commercial or financial relationships that could be construed as a potential conflict of interest.

frontiers in Plant Science

MINI REVIEW
published: 21 February 2020
doi: 10.3389/fpls.2020.00114

SPEECHLESS Speaks Loudly in Stomatal Development

*Liang Chen, Zhongliang Wu and Suiwen Hou**

Key Laboratory of Cell Activities and Stress Adaptations, Ministry of Education, School of Life Sciences, Lanzhou University, Lanzhou, China

Stomata, the small pores on the epidermis of plant shoot, control gas exchange between the plant and environment and play key roles in plant physiology, evolution, and global ecology. Stomatal development is initiated by the basic helix-loop-helix (bHLH) transcription factor SPEECHLESS (SPCH), whose central importance in stomatal development has recently come to light. SPCH integrates intralineage signals and serves as an acceptor of hormonal and environmental signals to regulate stomatal density and patterning during the development. SPCH also plays a direct role in regulating asymmetric cell division in the stomatal lineage. Owing to its importance in stomatal development, *SPCH* expression is tightly and spatiotemporally regulated. The purpose of this review is to provide an overview of the SPCH-mediated regulation of stomatal development, reinforcing the idea that SPCH is the central molecular hub for stomatal development.

Keywords: SPCH, stomatal development, stomatal lineage, stomatal patterning, stomatal differentiatation

OPEN ACCESS

Edited by:
Elena D. Shpak,
The University of Tennessee, United States

Reviewed by:
On Sun Lau,
National University of Singapore, Singapore
Aarthi Putarjunan,
Howard Hughes Medical Institute (HHMI), United States

***Correspondence:**
Suiwen Hou
housw@lzu.edu.cn

Specialty section:
This article was submitted to Plant Development and EvoDevo, a section of the journal Frontiers in Plant Science

Received: *06 November 2019*
Accepted: *24 January 2020*
Published: *21 February 2020*

Citation:
Chen L, Wu Z and Hou S (2020) SPEECHLESS Speaks Loudly in Stomatal Development. Front. Plant Sci. 11:114. doi: 10.3389/fpls.2020.00114

INTRODUCTION

In *Arabidopsis*, stomata formation depends on a series of cell divisions and consecutive cell fate transitions, producing five major cell types of the stomatal lineage, including meristemoid mother cells (MMCs), meristemoids, stomatal lineage ground cells (SLGCs), guard mother cells (GMCs), and guard cells (GCs) (Nadeau and Sack, 2002b; Bergmann and Sack, 2007; Lau and Bergmann, 2012; Pillitteri and Torii, 2012; Pillitteri and Dong, 2013). A subset of protodermal cells in the epidermis acquire the fate of MMCs and initiate the stomatal lineage by undergoing asymmetric entry divisions to produce the small triangular meristemoids and larger sister cells called SLGCs (**Figure 1**). Meristemoids carry out a limited number of asymmetric amplifying divisions to increase the number of SLGCs, while also performing the process of self-renewal (**Figure 1**). Finally, meristemoids lose their ability of reiterative asymmetric division and differentiate into GMCs. Each GMC symmetrically divides to yield a pair of highly specialized GCs (**Figure 1**) (Nadeau and Sack, 2002b; Bergmann and Sack, 2007; Lau and Bergmann, 2012; Pillitteri and Torii, 2012; Pillitteri and Dong, 2013). SLGCs can also acquire the MMC fate and undergo asymmetric division to produce satellite meristemoids that are oriented away from preexisting stomata or

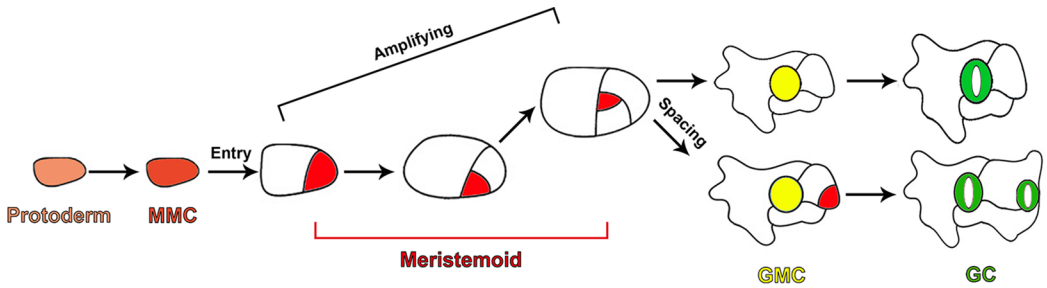

FIGURE 1 | Diagram depicting cell fate transitions during the stomatal development in *Arabidopsis*. A subset of protodermal cells (faint red) acquire the fate of an MMC (brick red) and undergo asymmetric entry division, producing a meristemoid (red) and SLGC (white). Meristemoids undergo asymmetric amplifying divisions to increase the number of SLGCs while also self-renewing. Eventually, meristemoids differentiate into GMCs (yellow). Each GMC symmetrically divides to yield a pair of highly specialized GCs (green). SLGCs can also initiate stomatal development through oriented asymmetric spacing divisions.

precursors. This asymmetric division, which prevents the direct contact between two stomata, is termed "oriented asymmetric spacing divisions". Alternatively, SLGCs can terminally differentiate into pavement cells (**Figure 1**) (Geisler et al., 2000; Bergmann and Sack, 2007).

SPEECHLESS (SPCH) INITIATES THE STOMATAL LINEAGE

A null stoma mutant named *spch-1* was identified in a sensitized genetic screen (MacAlister et al., 2007). *SPCH* encodes a bHLH transcription factor and has two closely related paralogues, *MUTE* and *FAMA*. *SPCH* is broadly transcribed in epidermal cells, but the SPCH protein is restricted to MMCs and meristemoids, suggesting that SPCH is strictly regulated at the posttranslational level (MacAlister et al., 2007). Closer observation showed that epidermal cells in *spch-1* did not undergo asymmetric entry division. In contrast, overexpression of *SPCH* induced ectopic entry division in the epidermis. These results suggest that *SPCH* is crucial for stomatal lineage initiation (**Figure 2**) (MacAlister et al., 2007; Pillitteri et al., 2007). The stomatal formation is also completely eliminated when both the two homologous bHLH-leucine zipper (bHLH-LZ) transcription factors, INDUCER OF CBF EXPRESSION1 (ICE1) and SCREAM2 (SCRM2), are knocked out (Kanaoka et al., 2008). Further research revealed that SPCH, MUTE, and FAMA heterodimerize with SCRMs (ICE1 and SCRM2) to trigger the successive MMC-meristemoid-GMC-GC fate transition (**Figure 2**) (Kanaoka et al., 2008). The direct targets of *SPCH* include *SPCH* itself and *ICE1*/*SCRM2*. SPCH and ICE1/SCRM2 can bind to their own promoters and enhance self-expression, thereby constituting a positive feedback loop that maintains the MMC and meristemoid fate (Lau et al., 2014; Horst et al., 2015) (**Figure 2**). In the grass *Brachypodium distachyon* and *Oryza sativa*, disabling either *SPCH* or *ICE1* eliminated stomata, suggesting that the *SPCH*/*ICE1* heterodimer also functions as a switch for the stomatal initiation in monocots (Raissig et al., 2016; Wu et al., 2019).

SPCH INTEGRATES INTRALINEAGE SIGNALS FOR PROPER STOMATAL DENSITY AND PATTERNING

SPCH activity is inhibited by its phosphorylation and consequent degradation (Lampard et al., 2008). Interestingly, although the phosphorylation of SPCH is known to be mediated by mitogen-activated protein kinase 3/6 (MPK3/6), a direct interaction between MPK3/6 and SPCH has not been detected to date. A recent study has found that ICE1/SCRM2 acts as a scaffolding partner for their interaction (Lampard et al., 2008; Putarjunan et al., 2019). The direct association of MPK3/6 and ICE1/SCRM2 is also required for the phosphorylation and consequent degradation of ICE1/SCRM2, and this process is crucial for the proper specification of the stomatal cell fate (Putarjunan et al., 2019). Accordingly, a direct link between the SPCH•SCRM module and a MAPK cascade consisting of YODA (YDA), four MAPKKs (MKK4/5/7/9), and two MAPKs (MPK3/6) is established during the stomatal development (Bergmann et al., 2004; Wang et al., 2007; Lampard et al., 2009; Putarjunan et al., 2019). Upstream of the YDA-MKK4/5/7/9-MPK3/6 cascade lies a multiprotein receptor complex composed of the leucine-rich repeat receptor-like protein TOO MANY MOUTHS (TMM), the ERECTA family (ERf) leucine-rich repeat receptor-like kinases [ERECTA (ER), ERECTA-LIKE1 (ERL1), and ERECTA-LIKE2 (ERL2)], and SOMATIC EMBRYOGENESIS RECEPTOR KINASEs (SERKs) (Yang and Sack, 1995; Nadeau and Sack, 2002a; Shpak et al., 2005; Lee et al., 2012; Lee et al., 2015; Meng et al., 2015). These receptors can recognize several specifically expressed ligands that belong to the EPIDERMAL PATTERNING FACTOR-LIKE (EPFL) family of secreted cysteine-rich peptides to either repress or promote stomatal development in specific regions (**Figure 2**) (Hara et al., 2007; Hara et al., 2009; Hunt and Gray, 2009; Abrash and Bergmann, 2010; Hunt et al., 2010; Kondo et al., 2010; Sugano et al., 2010; Abrash et al., 2011; Lee et al., 2012; Niwa et al., 2013; Lee et al., 2015; Meng et al., 2015). EPF1, the first such peptide to be identified, is mainly dependent on ERL1 to ensure the correct spacing and meristemoid differentiation (**Figure 2**) (Hara et al., 2007; Lee et al., 2012). EPF2 is detected primarily by ER, which

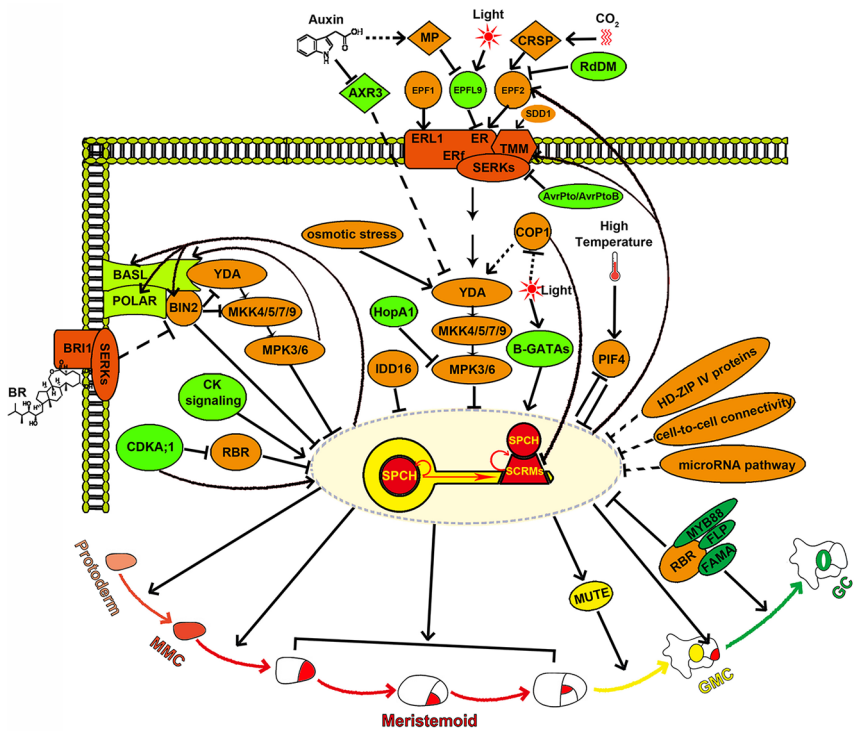

FIGURE 2 | SPCH is the molecular key that opens stomatal development and acts as a central molecular hub while specifying stomatal cell fate. SPCH determines the entry into the stomatal lineage and integrates diverse developmental and environmental signals mediated by the YDA-MKK4/5/7/9-MPK3/6 cascade, BIN2, CDKA;1, B-GATAs, and PIF4. SPCH also directly regulates asymmetric cell division in the stomatal lineage through activating the transcription of the key polarity proteins BASL and POLAR. *SPCH* expression is tightly and spatiotemporally regulated by HD-ZIP IV proteins, cell-to-cell connectivity, microRNA pathway, IDD16, and RBR. SPCH enhances its own activity by activating itself and SCRMs, thereby maintaining the MMC and meristemoid fate, and suppresses itself by activating the EPF2-TMM signaling to ensure proper stomatal density and patterning.

subsequently represses stomatal lineage initiation through the activation of the downstream MAPK cascade (Hara et al., 2009; Hunt and Gray, 2009; Lee et al., 2012; Lee et al., 2015). In contrast to EPF1 and EPF2, STOMAGEN/EPFL9 is a positive peptide that competes with EPF2 for ER association without triggering the downstream MAPK response (Hunt et al., 2010; Kondo et al., 2010; Sugano et al., 2010; Lee et al., 2015; Lin et al., 2017). In this way, STOMAGEN prevents the inhibitory activity of EPF2 (Lee et al., 2015) (**Figure 2**). In the stems, CHALLAH family peptides activate ERf receptors and inhibit stomatal development (Abrash and Bergmann, 2010; Abrash et al., 2011; Niwa et al., 2013). This ligand/receptor-mediated stomatal signaling pathway has also been reconstructed in mature *Nicotiana benthamiana* leaf cells (Jewaria et al., 2013). Epigenetic modifications on *EPF2* and *ERf* genes have been found to regulate stomatal development. The expression of *EPF2* is regulated by RNA-directed DNA methylation (RdDM), and the expression of *ERf* genes is regulated by histone modification and DNA methylation (Yamamuro et al., 2014; Wang et al., 2016). In addition, the subtilisin STOMATAL DENSITY AND DISTRIBUTION (SDD1), which is predicted to process peptide precursors that remain elusive, also acts upstream of TMM and YODA to repress stomatal formation (Berger and Altmann, 2000; von Groll, 2002; Lampard et al., 2008). The above intralineage signals are integrated by SPCH to regulate stomatal initiation and patterning. Moreover, *EPF2*, *TMM*, and *ERf* receptors are the direct targets of *SPCH* (Lau et al., 2014). SPCH and SCRMs directly activate the EPF2-TMM signaling, which in turn suppresses the SPCH•SCRM module, thus constituting a negative feedback loop that inhibits stomatal initiation and ensures the one-cell-spacing patterning (Lau et al., 2014; Horst et al., 2015) (**Figure 2**).

SPCH SERVES AS AN ACCEPTOR OF HORMONAL AND ENVIRONMENTAL SIGNALS TO REGULATE STOMATAL DENSITY AND PATTERNING

SPCH directly integrates hormonal and environmental signals for stomatal formation. SPCH can be directly phosphorylated by the brassinosteroid (BR) signaling intermediate the glycogen synthase kinase 3 (GSK3)-like kinase BRINSENSITIVE 2 (BIN2), which is itself a direct target of SPCH, and this phosphorylation promotes the degradation of SPCH. Thus, BR promotes stomatal formation in hypocotyls though suppression of BIN2 mediated SPCH phosphorylation and degradation (Gudesblat et al., 2012; Yang

et al., 2015). SPCH can also be directly phosphorylated by Cyclin-Dependent Kinases A;1 (CDKA;1). Unlike the negative regulation of SPCH by MAPK- and BIN2-mediated phosphorylation, CDKA;1 mediated phosphorylation of SPCH at Serine 186 promotes stomatal initiation, revealing that SPCH activity and stability are fine-tuned *via* phosphorylation by multiple kinases in response to various signals (Yang et al., 2015) (**Figure 2**). Increased cytokinin (CK) levels or signaling promotes SPCH expression, and SPCH directly induces the expression of the type-A ARABIDOPSIS RESPONSE REGULATOR16 (ARR16) and CLAVATA3/EMBRYO SURROUNDING REGION RELATED 9/10 (CLE9/10) (Lau et al., 2014; Vaten et al., 2018). ARR16 negatively regulates CK response and CLE9/10 represses type-A ARRs. The SPCH-dependent activities of the repressive type-A ARR16/17 and the secreted peptides CLE9/10 are essential for establishing local domains of low CK signaling, which inhibits both SLGC division and stomatal formation (Vaten et al., 2018). ARR16/17 and CLE9/10 counteract the proliferative effect of SPCH to customize the epidermal cell-type composition (Vaten et al., 2018). CLE9/10 peptides are also recognized by the receptor kinase HAESA-LIKE 1 (HSL1) to regulate the stomatal lineage cell division; however, the underlying mechanism is unknown (Qian et al., 2018). The heat-stress signaling induces the accumulation of PHYTOCHROME-INTERACTING FACTOR 4 (PIF4) in stomatal precursors. PIF4 can directly bind to *SPCH* and repress its expression, while the SPCH protein, in turn, inhibits the expression of *PIF4*, thus producing a negative feedback loop to control stomatal development in fluctuating temperatures (Lau et al., 2018). Red light can induce the expression of both *SPCH* and GATA factors of the B-subfamily (B-GATA) transcription factors. B-GATAs directly bind to the *SPCH* promoter and are required for the red-light-dependent induction of *SPCH* expression (Klermund et al., 2016).

SPCH also serves as a final acceptor of hormonal and environmental signals accepted by its upstream signaling factors. BR has also been shown to inhibit stomatal formation in the leaf epidermis through the inactivation of BIN2. In this scenario, BIN2 has been found to repress YDA and MKK4/5 activation, promoting SPCH stabilization (Kim et al., 2012; Khan et al., 2013) (**Figure 2**). Another phytohormone, auxin, negatively regulates stomatal formation partially by activating auxin response factor 5 (ARF5) and inhibiting AUXIN RESISTANT3 (AXR3). ARF5 suppresses stomatal formation by directly repressing STOMAGEN expression in the mesophyll, while AXR3 promotes stomatal production by functioning upstream of the YDA MAPK cascade in dark-grown seedlings (Balcerowicz et al., 2014; Le et al., 2014; Zhang et al., 2014) (**Figure 2**). Light signals are perceived by multiple photoreceptors to promote stomatal formation by inhibiting the RING E3 ubiquitin ligase CONSTITUTIVE PHOTOMORPHOGENIC 1 (COP1) (Lau and Deng, 2012). COP1 acts genetically upstream of YDA to repress the stomatal development and can also stimulate the degradation of SCRM proteins through ubiquitin/proteasome pathways in the dark (Kang et al., 2009; Lee et al., 2017) (**Figure 2**). In addition, increased light irradiation increases stomatal density by inducing the expression of *STOMAGEN* (Hronkova et al., 2015) (**Figure 2**). Elevated atmospheric carbon dioxide (CO_2) levels induce the expression of *CO2 RESPONSIVE SECRETED PROTEASE* (*CRSP*), and the encoded protein can cleave the pro-peptide EPF2 (**Figure 2**). Thus, high concentrations of CO_2 may repress stomatal formation primarily by the EPF2-mediated negative regulation pathway (Engineer et al., 2014). Osmotic stress decreases stomatal number by downregulating SPCH protein level. This process is mediated by the MAPK-SPCH core developmental pathway (Kumari et al., 2014) (**Figure 2**). Stomata also serve as bacterial entry gates (Melotto et al., 2006; Melotto et al., 2017). The pathogen *Pseudomonas syringae* invades hosts through stomatal pores and releases the effector HopA1 (Melotto et al., 2006; Zhang et al., 2007). Overexpression of HopA1 in plant specifically inactivates MPK3/6, leading to stomatal clustering (Kim et al., 2012) (**Figure 2**). In addition, the inducible overexpression of AvrPto and AvrPtoB, two effector proteins of *P. syringae pv. tomato* (*Pst*), also generates clustered stomata in *Arabidopsis* (Meng et al., 2015). AvrPto and AvrPtoB may promote stomatal formation through impairing the function of their target SERKs, which act as coreceptors along with the ER-TMM complex (**Figure 2**).

SPCH REGULATES ASYMMETRIC CELL DIVISION IN THE STOMATAL LINEAGE

SPCH induces the expression of *BREAKING OF ASYMMETRY IN THE STOMATAL LINEAGE* (*BASL*) and *POLAR* in the stomatal lineage. Both BASL and POLAR proteins exhibit a polarized peripheral localization during the stomatal lineage asymmetric cell division (ACD). Phosphorylation of BASL by MPK3/6 enhances its interaction with YDA, leading to the recruitment of YDA to the cell cortex (Dong et al., 2009; Zhang et al., 2015; Zhang et al., 2016). Thus, BASL serves as a scaffold protein that spatially concentrates MAPK signaling in the cortex and segregates MAPK signaling into SLGCs after ACD (Zhang et al., 2015). The enhanced YDA-MPK3/6 signaling in SLGCs promotes the phosphorylation and degradation of SPCH, leading to the differentiation of SLGCs into pavement cells. However, the low level of YDA-MPK3/6 signaling in meristemoids results in stable SPCH expression, triggering the subsequent developmental processes (Zhang et al., 2015). POLAR polarization requires BASL activity (Pillitteri et al., 2011), and POLAR appears to function together with BASL to regulate the stomatal lineage ACD by confining BIN2 to the cell cortex (Houbaert et al., 2018). This regulation can relieve the inhibition of SPCH by BIN2, thus freeing SPCH to drive ACD (Houbaert et al., 2018).

SPCH EXPRESSION IS TIGHTLY AND SPATIOTEMPORALLY REGULATED

The *HOMEODOMAIN LEUCINE ZIPPER CLASS IV* (*HD-ZIP IV*) family genes *MERISTEM LAYER 1* (*ML1*) and *HOMEODOMAIN GLABROUS2* (*HDG2*) function in establishing and maintaining epidermal identity. Their ectopic expression induces the formation of ectopic epidermal layers with *SPCH* expression and stomatal formation in internal leaf

tissues, suggesting that the acquisition of epidermal layer identity is required for *SPCH* expression and stomatal lineage fate (Peterson et al., 2013; Takada et al., 2013).

Plasmodesmatal permeability and cellular integrity in the epidermis confine SPCH to stomatal lineage cells during stomatal development (**Figure 2**). Mutating the callose synthase *GLUCAN SYNTHASE-LIKE 8* (*GSL8*/*CHORUS*) or the glycosyltransferase-like protein KOBITO1 disrupts cellular integrity or increases plasmodesmata permeability. These defects allow intercellular movement of SPCH protein in the leaf epidermis, resulting in clustered stomata formation and disorganized cell divisions in the stomatal lineage (Guseman et al., 2010; Kong et al., 2012).

A microRNA pathway is presumed to repress stomatal lineage initiation through regulating *SPCH* transcripts (**Figure 2**) (Kutter et al., 2007; Yang et al., 2014). In addition, IDD16, a C2H2 zinc finger transcription factor from the INDETERMINATE DOMAIN (IDD) family, and RETINOBLASTOMA RELATED (RBR), which is targeted by CDKA;1, have been shown to inhibit stomatal initiation by directly binding to *SPCH* and repressing *SPCH* transcription (**Figure 2**) (Weimer et al., 2012; Qi et al., 2019). The specific downregulation of *RBR* in GMCs and GCs leads to excess divisions in differentiated GCs and formation of the "Stoma-in-Stoma" (SIS) phenotype (Lee et al., 2014b; Matos et al., 2014). Histone3 K27 trimethylation (H3K27me3) is involved in maintaining the GC identity (Lee et al., 2019), and its reduced deposition on the *SPCH* and *MUTE* loci is responsible for the SIS phenotype (Lee et al., 2014b; Matos et al., 2014). Consistent with this, constitutive expression of CURLY LEAF (CLF), a member of Polycomb Repressive Complex 2 (PRC2) that functions in H2K27me3 and other chromatin modifications, suppresses the SIS phenotype (Lee et al., 2014b). RBR has been shown to interact with PRC2, FAMA, and FLP/MYB88, which redundantly functions with FAMA to inhibit GMC division (Desvoyes et al., 2010; Magyar et al., 2012; Lee et al., 2014a). Both RBR and FAMA target the promoters of *SPCH*, *EPF1*, and *FAMA* (Matos et al., 2014). Thus, a model in which RBR and the PRC2 components are recruited by FAMA to the promoters of *SPCH* and other stomatal lineage genes has been presented. This complex represses the re-expression of those genes and the reinitiation of stomatal lineage through chromatin modification (Matos et al., 2014).

CONCLUSION AND PERSPECTIVE

In summary, SPCH acts as a central molecular hub that integrates both developmental and environmental signals while specifying stomatal cell fate. However, many questions remain to be addressed. Firstly, more external and internal cues that are integrated into the SPCH node need to be identified to further understand how stomatal development adjusts to a fluctuating environment. Secondly, although SPCH mostly functions upstream of the stomatal lineage, little is known about how SPCH transcription is initiated and regulated. In addition, although the direct target genes of SPCH have been known for years, most of their functions remain elusive. Lastly, RNA polymerase II (Pol II) is essential for stomatal patterning and differentiation (Chen et al., 2016), and it is unknown how SPCH recruits Pol II for specific gene expression. SPCH is the core regulator of stomatal density. Genetic manipulation of stomatal density to improve plant productivity and water consumption efficiency has been proven to be feasible in barley and rice (Hughes et al., 2017; Caine et al., 2019). Future studies focusing on the above questions will provide invaluable potential targets for genetic improvement of agriculturally relevant species to promote sustainable agricultural development.

AUTHOR CONTRIBUTIONS

LC wrote the manuscript, drew figures, and edited its final form. ZW contributed critical evaluation of the text. LC and SH conceived the topic.

FUNDING

This work was supported by National Natural Science Foundation of China (NSFC) (grant numbers 31670185, 31870251, 31800237); the Ministry of Agriculture of the People's Republic of China (grant number 2016ZX08009003-002); the major project of Science and Technology of Gansu province (grant number 17ZD2NA016-5, 17ZD2NA015-06); China Postdoctoral Science Foundation Grant (grant number 2017M620478); and the Chang Jiang Scholars Program of China (2017).

ACKNOWLEDGMENTS

We thank the anonymous reviewers for suggestions on improvements to this review and apologize to colleagues whose work has not been mentioned because of space limitations.

REFERENCES

Abrash, E. B., and Bergmann, D. C. (2010). Regional specification of stomatal production by the putative ligand CHALLAH. *Development* 137, 447–455. doi: 10.1242/dev.040931

Abrash, E. B., Davies, K. A., and Bergmann, D. C. (2011). Generation of signaling specificity in Arabidopsis by spatially restricted buffering of ligand-receptor interactions. *Plant Cell* 23, 2864–2879. doi: 10.1105/tpc.111.086637

Balcerowicz, M., Ranjan, A., Rupprecht, L., Fiene, G., and Hoecker, U. (2014). Auxin represses stomatal development in dark-grown seedlings *via* Aux/IAA proteins. *Development* 141, 3165–3176. doi: 10.1242/dev.109181

Berger, D., and Altmann, T. (2000). A subtilisin-like serine protease involved in the regulation of stomatal density and distribution in Arabidopsis thaliana. *Genes Dev.* 14, 1119–1131. doi: 10.1101/gad.14.9.1119

Bergmann, D. C., and Sack, F. D. (2007). Stomatal development. *Annu. Rev. Plant Biol.* 58, 163–181. doi: 10.1146/annurev.arplant.58.032806.104023

Bergmann, D. C., Lukowitz, W., and Somerville, C. R. (2004). Stomatal development and pattern controlled by a MAPKK kinase. *Science* 304, 1494–1497. doi: 10.1126/science.1096014

Caine, R. S., Yin, X., Sloan, J., Harrison, E. L., Mohammed, U., Fulton, T., et al. (2019). Rice with reduced stomatal density conserves water and has improved drought tolerance under future climate conditions. *New Phytol.* 221, 371–384. doi: 10.1111/nph.15344

Chen, L., Guan, L., Qian, P., Xu, F., Wu, Z., Wu, Y., et al. (2016). NRPB3, the third largest subunit of RNA polymerase II, is essential for stomatal patterning and differentiation in Arabidopsis. *Development* 143, 1600–1611. doi: 10.1242/dev.129098

Desvoyes, B., Sanchez, M. P., Ramirez-Parra, E., and Gutierrez, C. (2010). Impact of nucleosome dynamics and histone modifications on cell proliferation during Arabidopsis development. *Heredity* 105, 80–91. doi: 10.1038/hdy.2010.50

Dong, J., MacAlister, C. A., and Bergmann, D. C. (2009). BASL controls asymmetric cell division in Arabidopsis. *Cell* 137, 1320–1330. doi: 10.1016/j.cell.2009.04.018

Engineer, C. B., Ghassemian, M., Anderson, J. C., Peck, S. C., Hu, H., and Schroeder, J. I. (2014). Carbonic anhydrases, EPF2 and a novel protease mediate CO2 control of stomatal development. *Nature* 513, 246–250. doi: 10.1038/nature13452

Geisler, M., Nadeau, J., and Sack, F. D. (2000). Oriented asymmetric divisions that generate the stomatal spacing pattern in Arabidopsis are disrupted by the too many mouths mutation. *Plant Cell* 12, 2075–2086. doi: 10.1105/tpc.12.11.2075

Gudesblat, G. E., Schneider-Pizon, J., Betti, C., Mayerhofer, J., Vanhoutte, I., van Dongen, W., et al. (2012). SPEECHLESS integrates brassinosteroid and stomata signalling pathways. *Nat. Cell Biol.* 14, 548–554. doi: 10.1038/ncb2471

Guseman, J. M., Lee, J. S., Bogenschutz, N. L., Peterson, K. M., Virata, R. E., Xie, B., et al. (2010). Dysregulation of cell-to-cell connectivity and stomatal patterning by loss-of-function mutation in Arabidopsis chorus (glucan synthase-like 8). *Development* 137, 1731–1741. doi: 10.1242/dev.049197

Hara, K., Kajita, R., Torii, K. U., Bergmann, D. C., and Kakimoto, T. (2007). The secretory peptide gene EPF1 enforces the stomatal one-cell-spacing rule. *Genes Dev.* 21, 1720–1725. doi: 10.1101/gad.1550707

Hara, K., Yokoo, T., Kajita, R., Onishi, T., Yahata, S., Peterson, K. M., et al. (2009). Epidermal cell density is autoregulated *via a* secretory peptide, EPIDERMAL PATTERNING FACTOR 2 in Arabidopsis leaves. *Plant Cell Physiol.* 50, 1019–1031. doi: 10.1093/pcp/pcp068

Horst, R. J., Fujita, H., Lee, J. S., Rychel, A. L., Garrick, J. M., Kawaguchi, M., et al. (2015). Molecular framework of a regulatory circuit initiating two-dimensional spatial patterning of stomatal lineage. *PloS Genet.* 11, e1005374. doi: 10.1371/journal.pgen.1005374

Houbaert, A., Zhang, C., Tiwari, M., Wang, K., de Marcos Serrano, A., Savatin, D. V., et al. (2018). POLAR-guided signalling complex assembly and localization drive asymmetric cell division. *Nature* 563, 574–578. doi: 10.1038/s41586-018-0714-x

Hronkova, M., Wiesnerova, D., Simkova, M., Skupa, P., Dewitte, W., Vrablova, M., et al. (2015). Light-induced STOMAGEN-mediated stomatal development in Arabidopsis leaves. *J. Exp. Bot.* 66, 4621–4630. doi: 10.1093/jxb/erv233

Hughes, J., Hepworth, C., Dutton, C., Dunn, J. A., Hunt, L., Stephens, J., et al. (2017). Reducing stomatal density in barley improves drought tolerance without impacting on yield. *Plant Physiol.* 174, 776–787. doi: 10.1104/pp.16.01844

Hunt, L., and Gray, J. E. (2009). The signaling peptide EPF2 controls asymmetric cell divisions during stomatal development. *Curr. Biol.* 19, 864–869. doi: 10.1016/j.cub.2009.03.069

Hunt, L., Bailey, K. J., and Gray, J. E. (2010). The signalling peptide EPFL9 is a positive regulator of stomatal development. *New Phytol.* 186, 609–614. doi: 10.1111/j.1469-8137.2010.03200.x

Jewaria, P. K., Hara, T., Tanaka, H., Kondo, T., Betsuyaku, S., Sawa, S., et al. (2013). Differential effects of the peptides stomagen, EPF1 and EPF2 on activation of MAP kinase MPK6 and the SPCH protein level. *Plant Cell Physiol.* 54, 1253–1262. doi: 10.1093/pcp/pct076

Kanaoka, M. M., Pillitteri, L. J., Fujii, H., Yoshida, Y., Bogenschutz, N. L., Takabayashi, J., et al. (2008). SCREAM/ICE1 and SCREAM2 specify three cell-state transitional steps leading to Arabidopsis stomatal differentiation. *Plant Cell* 20, 1775–1785. doi: 10.1105/tpc.108.060848

Kang, C. Y., Lian, H. L., Wang, F. F., Huang, J. R., and Yang, H. Q. (2009). Cryptochromes, phytochromes, and COP1 regulate light-controlled stomatal development in Arabidopsis. *Plant Cell* 21, 2624–2641. doi: 10.1105/tpc.109.069765

Khan, M., Rozhon, W., Bigeard, J., Pflieger, D., Husar, S., Pitzschke, A., et al. (2013). Brassinosteroid-regulated GSK3/Shaggy-like kinases phosphorylate mitogen-activated protein (MAP) kinase kinases, which control stomata development in Arabidopsis thaliana. *J. Biol. Chem.* 288, 7519–7527. doi: 10.1074/jbc.M112.384453

Kim, T. W., Michniewicz, M., Bergmann, D. C., and Wang, Z. Y. (2012). Brassinosteroid regulates stomatal development by GSK3-mediated inhibition of a MAPK pathway. *Nature* 482, 419–422. doi: 10.1038/nature10794

Klermund, C., Ranftl, Q. L., Diener, J., Bastakis, E., Richter, R., and Schwechheimer, C. (2016). LLM-domain B-GATA transcription factors promote stomatal development downstream of light signaling pathways in Arabidopsis thaliana hypocotyls. *Plant Cell* 28, 646–660. doi: 10.1105/tpc.15.00783

Kondo, T., Kajita, R., Miyazaki, A., Hokoyama, M., Nakamura-Miura, T., Mizuno, S., et al. (2010). Stomatal density is controlled by a mesophyll-derived signaling molecule. *Plant Cell Physiol.* 51, 1–8. doi: 10.1093/pcp/pcp180

Kong, D., Karve, R., Willet, A., Chen, M. K., Oden, J., and Shpak, E. D. (2012). Regulation of plasmodesmatal permeability and stomatal patterning by the glycosyltransferase-like protein KOBITO1. *Plant Physiol.* 159, 156–168. doi: 10.1104/pp.112.194563

Kumari, A., Jewaria, P. K., Bergmann, D. C., and Kakimoto, T. (2014). Arabidopsis reduces growth under osmotic stress by decreasing SPEECHLESS protein. *Plant Cell Physiol.* 55, 2037–2046. doi: 10.1093/pcp/pcu159

Kutter, C., Schob, H., Stadler, M., Meins, F.Jr., and Si-Ammour, A. (2007). MicroRNA-mediated regulation of stomatal development in Arabidopsis. *Plant Cell* 19, 2417–2429. doi: 10.1105/tpc.107.050377

Lampard, G. R., Macalister, C. A., and Bergmann, D. C. (2008). Arabidopsis stomatal initiation is controlled by MAPK-mediated regulation of the bHLH SPEECHLESS. *Science* 322, 1113–1116. doi: 10.1126/science.1162263

Lampard, G. R., Lukowitz, W., Ellis, B. E., and Bergmann, D. C. (2009). Novel and expanded roles for MAPK signaling in Arabidopsis stomatal cell fate revealed by cell type-specific manipulations. *Plant Cell* 21, 3506–3517. doi: 10.1105/tpc.109.070110

Lau, O. S., and Bergmann, D. C. (2012). Stomatal development: a plant's perspective on cell polarity, cell fate transitions and intercellular communication. *Development* 139, 3683–3692. doi: 10.1242/dev.080523

Lau, O. S., and Deng, X. W. (2012). The photomorphogenic repressors COP1 and DET1: 20 years later. *Trends Plant Sci.* 17, 584–593. doi: 10.1016/j.tplants.2012.05.004

Lau, O. S., Davies, K. A., Chang, J., Adrian, J., Rowe, M. H., Ballenger, C. E., et al. (2014). Direct roles of SPEECHLESS in the specification of stomatal self-renewing cells. *Science* 345, 1605–1609. doi: 10.1126/science.1256888

Lau, O. S., Song, Z., Zhou, Z., Davies, K. A., Chang, J., Yang, X., et al. (2018). Direct control of SPEECHLESS by PIF4 in the high-temperature response of stomatal development. *Curr. Biol.* 28, 1273–1280. doi: 10.1016/j.cub.2018.02.054

Le, J., Liu, X. G., Yang, K. Z., Chen, X. L., Zou, J. J., Wang, H. Z., et al. (2014). Auxin transport and activity regulate stomatal patterning and development. *Nat. Commun.* 5, 3090. doi: 10.1038/ncomms4090

Lee, J. S., Kuroha, T., Hnilova, M., Khatayevich, D., Kanaoka, M. M., McAbee, J. M., et al. (2012). Direct interaction of ligand-receptor pairs specifying stomatal patterning. *Genes Dev.* 26, 126–136. doi: 10.1101/gad.179895.111

Lee, E., Lucas, J. R., and Sack, F. D. (2014a). Deep functional redundancy between FAMA and FOUR LIPS in stomatal development. *Plant J.* 78, 555–565. doi: 10.1111/tpj.12489

Lee, E., Lucas, J. R., Goodrich, J., and Sack, F. D. (2014b). Arabidopsis guard cell integrity involves the epigenetic stabilization of the FLP and FAMA transcription factor genes. *Plant J.* 78, 566–577. doi: 10.1111/tpj.12516

Lee, J. S., Hnilova, M., Maes, M., Lin, Y. C., Putarjunan, A., Han, S. K., et al. (2015). Competitive binding of antagonistic peptides fine-tunes stomatal patterning. *Nature* 522, 439–443. doi: 10.1038/nature14561

Lee, J. H., Jung, J. H., and Park, C. M. (2017). Light inhibits COP1-mediated degradation of ICE transcription factors to induce stomatal development in Arabidopsis. *Plant Cell* 29, 2817–2830. doi: 10.1105/tpc.17.00371

Lee, L. R., Wengier, D. L., and Bergmann, D. C. (2019). Cell-type-specific transcriptome and histone modification dynamics during cellular reprogramming in the Arabidopsis stomatal lineage. *Proc. Natl. Acad. Sci. U. S. A.* 116, 21914–21924. doi: 10.1073/pnas

Lin, G., Zhang, L., Han, Z., Yang, X., Liu, W., Li, E., et al. (2017). A receptor-like protein acts as a specificity switch for the regulation of stomatal development. *Genes Dev.* 31, 927–938. doi: 10.1101/gad.297580.117

MacAlister, C. A., Ohashi-Ito, K., and Bergmann, D. C. (2007). Transcription factor control of asymmetric cell divisions that establish the stomatal lineage. *Nature* 445, 537–540. doi: 10.1038/nature05491

Magyar, Z., Horváth, B., Khan, S., Mohammed, B., Henriques, R., De Veylder, L., et al. (2012). Arabidopsis E2FA stimulates proliferation and endocycle separately through RBR-bound and RBR-free complexes. *EMBO J.* 31, 1480–1493. doi: 10.1038/emboj.2012.13

Matos, J. L., Lau, O. S., Hachez, C., Cruz-Ramirez, A., Scheres, B., and Bergmann, D. C. (2014). Irreversible fate commitment in the Arabidopsis stomatal lineage requires a FAMA and RETINOBLASTOMA-RELATED module. *Elife* 10, 03271. doi: 10.7554/eLife.03271

Melotto, M., Underwood, W., Koczan, J., Nomura, K., and He, S. Y. (2006). Plant stomata function in innate immunity against bacterial invasion. *Cell* 126, 969–980. doi: 10.1016/j.cell.2006.06.054

Melotto, M., Zhang, L., Oblessuc, P. R., and He, S. Y. (2017). Stomatal defense a decade later. *Plant Physiol.* 174, 561–571. doi: 10.1104/pp.16.01853

Meng, X., Chen, X., Mang, H., Liu, C., Yu, X., Gao, X., et al. (2015). Differential function of Arabidopsis SERK family receptor-like kinases in stomatal patterning. *Curr. Biol.* 25, 2361–2372. doi: 10.1016/j.cub.2015.07.068

Nadeau, J. A., and Sack, F. D. (2002a). Control of stomatal distribution on the Arabidopsis leaf surface. *Science* 296, 1697–1700. doi: 10.1126/science.1069596

Nadeau, J. A., and Sack, F. D. (2002b). Stomatal development in Arabidopsis. *Arabidopsis Book* 1, e0066. doi: 10.1199/tab.0066

Niwa, T., Kondo, T., Nishizawa, M., Kajita, R., Kakimoto, T., and Ishiguro, S. (2013). EPIDERMAL PATTERNING FACTOR LIKE5 peptide represses stomatal development by inhibiting meristemoid maintenance in Arabidopsis thaliana. *Biosci. Biotechnol. Biochem.* 77, 1287–1295. doi: 10.1271/bbb.130145

Peterson, K. M., Shyu, C., Burr, C. A., Horst, R. J., Kanaoka, M. M., Omae, M., et al. (2013). Arabidopsis homeodomain-leucine zipper IV proteins promote stomatal development and ectopically induce stomata beyond the epidermis. *Development* 140, 1924–1935. doi: 10.1242/dev.090209

Pillitteri, L. J., and Dong, J. (2013). Stomatal development in Arabidopsis. *Arabidopsis Book* 6, e0162. doi: 10.1199/tab.0162

Pillitteri, L. J., and Torii, K. U. (2012). Mechanisms of stomatal development. *Annu. Rev. Plant Biol.* 63, 591–614. doi: 10.1146/annurev.arplant.58.032806.104023

Pillitteri, L. J., Sloan, D. B., Bogenschutz, N. L., and Torii, K. U. (2007). Termination of asymmetric cell division and differentiation of stomata. *Nature* 445, 501–505. doi: 10.1038/nature05467

Pillitteri, L. J., Peterson, K. M., Horst, R. J., and Torii, K. U. (2011). Molecular profiling of stomatal meristemoids reveals new component of asymmetric cell division and commonalities among stem cell populations in Arabidopsis. *Plant Cell* 23, 3260–3275. doi: 10.1105/tpc.111.088583

Putarjunan, A., Ruble, J., Srivastava, A., Zhao, C., Rychel, A. L., Hofstetter, A. K., et al. (2019). Bipartite anchoring of SCREAM enforces stomatal initiation by coupling MAP kinases to SPEECHLESS. *Nat. Plants* 5, 742–754. doi: 10.1038/s41477-019-0440-x

Qi, S. L., Lin, Q. F., Feng, X. J., Han, H. L., Liu, J., Zhang, L., et al. (2019). IDD16 negatively regulates stomatal initiation via trans-repression of SPCH in Arabidopsis. *Plant Biotechnol. J.* 17, 1446–1457. doi: 10.1111/pbi.13070

Qian, P., Song, W., Yokoo, T., Minobe, A., Wang, G., Ishida, T., et al. (2018). The CLE9/10 secretory peptide regulates stomatal and vascular development through distinct receptors. *Nat. Plants* 4, 1071–1081. doi: 10.1038/s41477-018-0317-4

Raissig, M. T., Abrash, E., Bettadapur, A., Vogel, J. P., and Bergmann, D. C. (2016). Grasses use an alternatively wired bHLH transcription factor network to establish stomatal identity. *Proc. Natl. Acad. Sci. U. S. A.* 113, 8326–8331. doi: 10.1073/pnas.1606728113

Shpak, E. D., McAbee, J. M., Pillitteri, L. J., and Torii, K. U. (2005). Stomatal patterning and differentiation by synergistic interactions of receptor kinases. *Science* 309, 290–293. doi: 10.1126/science.1109710

Sugano, S. S., Shimada, T., Imai, Y., Okawa, K., Tamai, A., Mori, M., et al. (2010). Stomagen positively regulates stomatal density in Arabidopsis. *Nature* 463, 241–244. doi: 10.1038/nature08682

Takada, S., Takada, N., and Yoshida, A. (2013). ATML1 promotes epidermal cell differentiation in Arabidopsis shoots. *Development* 140, 1919–1923. doi: 10.1242/dev.094417

Vaten, A., Soyars, C. L., Tarr, P. T., Nimchuk, Z. L., and Bergmann, D. C. (2018). Modulation of asymmetric division diversity through cytokinin and SPEECHLESS regulatory interactions in the Arabidopsis stomatal lineage. *Dev. Cell* 47, 53–66. doi: 10.1016/j.devcel.2018.08.007. e55.

von Groll, U. (2002). The subtilisin-like serine protease SDD1 mediates cell-to-cell signaling during Arabidopsis stomatal development. *Plant Cell* 14, 1527–1539. doi: 10.1105/tpc.001016

Wang, H., Ngwenyama, N., Liu, Y., Walker, J. C., and Zhang, S. (2007). Stomatal development and patterning are regulated by environmentally responsive mitogen-activated protein kinases in Arabidopsis. *Plant Cell* 19, 63–73. doi: 10.1105/tpc.106.048298

Wang, Y., Xue, X., Zhu, J. K., and Dong, J. (2016). Demethylation of ERECTA receptor genes by IBM1 histone demethylase affects stomatal development. *Development* 143, 4452–4461. doi: 10.1242/dev.129932

Weimer, A. K., Nowack, M. K., Bouyer, D., Zhao, X., Harashima, H., Naseer, S., et al. (2012). RETINOBLASTOMA RELATED1 regulates asymmetric cell divisions in Arabidopsis. *Plant Cell* 24, 4083–4095. doi: 10.1105/tpc.112.104620

Wu, Z., Chen, L., Yu, Q., Zhou, W., Gou, X., Li, J., et al. (2019). Multiple transcriptional factors control stomata development in rice. *New Phytol.* 223, 220–232. doi: 10.1111/nph.15766

Yamamuro, C., Miki, D., Zheng, Z., Ma, J., Wang, J., Yang, Z., et al. (2014). Overproduction of stomatal lineage cells in Arabidopsis mutants defective in active DNA demethylation. *Nat. Commun.* 5, 4062. doi: 10.1038/ncomms5062

Yang, M., and Sack, F. D. (1995). The too many mouths and four lips mutations affect stomatal production in Arabidopsis. *Plant Cell* 7, 2227–2239. doi: 10.1105/tpc.7.12.2227

Yang, K., Jiang, M., and Le, J. (2014). A new loss-of-function allele 28y reveals a role of ARGONAUTE1 in limiting asymmetric division of stomatal lineage ground cell. *J. Integr. Plant Biol.* 56, 539–549. doi: 10.1111/jipb.12154

Yang, K. Z., Jiang, M., Wang, M., Xue, S., Zhu, L. L., Wang, H. Z., et al. (2015). Phosphorylation of serine 186 of bHLH transcription factor SPEECHLESS promotes stomatal development in Arabidopsis. *Mol. Plant* 8, 783–795. doi: 10.1016/j.molp.2014.12.014

Zhang, J., Shao, F., Li, Y., Cui, H., Chen, L., Li, H., et al. (2007). A *Pseudomonas syringae* effector inactivates MAPKs to suppress PAMP-induced immunity in plants. *Cell Host Microbe* 1, 175–185. doi: 10.1016/j.chom.2007.03.006

Zhang, J. Y., He, S. B., Li, L., and Yang, H. Q. (2014). Auxin inhibits stomatal development through MONOPTEROS repression of a mobile peptide gene STOMAGEN in mesophyll. *Proc. Natl. Acad. Sci. U. S. A.* 111, E3015–E3023. doi: 10.1073/pnas.1400542111

Zhang, Y., Wang, P., Shao, W., Zhu, J. K., and Dong, J. (2015). The BASL polarity protein controls a MAPK signaling feedback loop in asymmetric cell division. *Dev. Cell* 33, 136–149. doi: 10.1016/j.devcel.2015.02.022

Zhang, Y., Guo, X., and Dong, J. (2016). Phosphorylation of the polarity protein BASL differentiates asymmetric cell fate through MAPKs and SPCH. *Curr. Biol.* 26, 2957–2965. doi: 10.1016/j.cub.2016.08.066

Conflict of Interest: The authors declare that the research was conducted in the absence of any commercial or financial relationships that could be construed as a potential conflict of interest.

frontiers in Plant Science

ORIGINAL RESEARCH
published: 06 March 2020
doi: 10.3389/fpls.2020.00255

Expression of Hexokinase in Stomata of Citrus Fruit Reduces Fruit Transpiration and Affects Seed Development

*Nitsan Lugassi[1], Gilor Kelly[1], Tal Arad[1], Chagai Farkash[1], Yossi Yaniv[1], Yelena Yeselson[1], Arthur A. Schaffer[1], Eran Raveh[2], David Granot[1] and Nir Carmi[1]**

[1] Institute of Plant Sciences, Agricultural Research Organization, The Volcani Center, Bet Dagan, Israel, [2] Department of Fruit Tree Sciences, Institute of Plant Sciences, Agricultural Research Organization, Gilat Research Center, Negev, Israel

The temporal formation and spatial distribution of stomata on the surface of citrus floral organs and, specifically, on the ovule from which the fruit develops, were analyzed using citrus plants that express green fluorescent protein (GFP) under the guard cell-specific *KST1* promoter. Stomata are found on the style, sepal, and anther of the closed flower and on ovules from the stage of anthesis. It has previously been shown that hexokinase (HXK) mediates sugar-sensing in leaf guard cells and stimulates stomatal closure. The activity and response of citrus fruit stomata to sugar-sensing by HXK was examined using plants that express HXK under the *KST1* promoter. Those plants are referred to as GCHXK plants. The transpiration of young green GCHXK citrus fruits was significantly reduced, indicating that their stomata respond to sugar similar to leaf stomata. Toward fruit maturation, fruit stomata are plugged and stop functioning, which explains why WT and GCHXK mature yellow fruits exhibited similar water loss. Seeds of the GCHXK plants were smaller and germinated more slowly than the WT seeds. We suggest that the stomata of young green citrus fruits, but not mature yellow fruits, respond to sugar levels via HXK and that fruit stomata are important for proper seed development.

Keywords: sugar-sensing, hexokinase, fruit stomata, fruit transpiration, floral organs

OPEN ACCESS

Edited by:
Scott McAdam,
Purdue University, United States

Reviewed by:
Danilo M. Daloso,
Federal University of Ceará, Brazil
Ross Deans,
University of California, Davis, United States

***Correspondence:**
Nir Carmi
nircarmi@agri.gov.il;
nircarmi@volcani.agri.gov.il

Specialty section:
This article was submitted to Plant Development and EvoDevo, a section of the journal Frontiers in Plant Science

Received: *05 December 2019*
Accepted: *18 February 2020*
Published: *06 March 2020*

Citation:
Lugassi N, Kelly G, Arad T, Farkash C, Yaniv Y, Yeselson Y, Schaffer AA, Raveh E, Granot D and Carmi N (2020) Expression of Hexokinase in Stomata of Citrus Fruit Reduces Fruit Transpiration and Affects Seed Development. Front. Plant Sci. 11:255. doi: 10.3389/fpls.2020.00255

INTRODUCTION

Stomata are the gates that allow the exchange of gases between the atmosphere and the inner tissues of the plant. During the process of gas exchange, the plant transpires water vapor into the surrounding atmosphere and CO_2 for photosynthesis enters the plant. The spatial and temporal distribution of stomata on leaves has been studied extensively over the past decades (Geisler and Sack, 2002; Nadeau and Sack, 2002; Kelly et al., 2017). In Arabidopsis, stomata appear on the cotyledons immediately after germination and, soon after, on the edges of true leaves, and the densities of the stomata on those plant parts increase in the following days (Kelly et al., 2017). Stomata are also found on the hypocotyl and stem and have been observed on Arabidopsis and *Lilium* hyb. *enchantment* anthers and the fruit skins of apple (*Malus domestica*), banana (*Musa acuminata*), passionfruit (*Passiflora edulis*), pitaya (*Hylocereus megalanthus*), and citrus (*Citrus unshiu*) (Johnson and Brun, 1966; Blanke and Lenz, 1989; Clement et al., 1997; Wilson et al., 2011;

Sánchez et al., 2013; Hiratsuka et al., 2015; Wei et al., 2018). Yet, the presence and temporal development of stomata on other flower parts, such as the petal, style, and ovule, have been the subject of very little study (Huang et al., 2018).

In most plants, leaf stomata open in response to light, to allow the entry of atmospheric CO_2 for photosynthesis, and this happens at the expense of extensive water loss via the open stomata. At night, the stomata close to prevent water loss. It has been shown that leaf stomata close in response to increasing sugar levels and that, within guard cells, this process is mediated by HXK (Kelly et al., 2013; Lugassi et al., 2015; Kottapalli et al., 2018). HXK is the only enzyme in plants that can phosphorylate glucose and may also phosphorylate fructose (Granot, 2007, 2008). In addition to its catalytic phosphorylation activity, HXK also functions as a sugar sensor independent of its phosphorylation activity (Moore et al., 2003). It is assumed that HXK senses the level of glucose and fructose and generates a signal that activates the ABA pathway that closes stomata (Kelly et al., 2013). Stomatal closure by sugars and HXK is a conserved trait that allows for coordination between photosynthesis and transpiration (Kelly et al., 2013; Lugassi et al., 2015; Kottapalli et al., 2018; Granot and Kelly, 2019). It has been shown in some fruits, such as purple passionfruit, yellow pitaya, banana, and apple, that fruit stomata respond in a similar way to leaf stomata, opening in response to light, high temperatures, and high humidity (Johnson and Brun, 1966; Blanke and Lenz, 1989; Sánchez et al., 2013). Yet, whether fruit stomata also respond to sugar is not known. We used citrus plants expressing either GFP or HXK under the guard cell-specific promoter *KST1* to follow the development of stomata on the various organs of citrus flowers and to examine the response of the stomata of citrus fruits to sugar.

MATERIALS AND METHODS

Plant Material and Growth Conditions

Experiments were conducted on *Troyer citrange* (*Citrus sinensis* "Washington" sweet orange × *Poncirus trifoliata*). *T. citrange* explants were transformed with *KSTpro:GFP* and *KSTpro:HXK1* constructs that express *GFP* or *HXK1* under the *KST1* promoter, respectively, as described previously by Lugassi et al. (2015). Plants transformed with *KSTpro:GFP* or *KSTpro:HXK1* are referred to as GCGFP and GCHXK (standing for guard-cell GFP and guard-cell HXK, respectively). Plants were grown in 10-L pots that contained (w/w) 30% vermiculite, 30% peat, 20% tuff, and 20% perlite (Even Ari, Israel). WT (untransformed), GCGFP, and GCHXK plants were vegetatively propagated by the grafting of shoots onto *T. citrange* rootstocks. Two independent lines of GCHXK plants, GCHXK1 and GCHXK5, were used in some of the experiments, based on the availability of the necessary plant material. WT, GCHXK1, and GCHXK5 plants were of the same age, were grafted at the same time, and were trimmed periodically to be similar in size. The grafted plants were grown in a temperature-controlled greenhouse (25–30°C in the summer and 15–25°C in the winter) under natural light conditions.

Confocal Microscopy Imaging

Images were acquired using the Olympus IX 81 inverted laser scanning confocal microscope (Fluoview 500; Olympus Corporation, Tokyo, Japan) equipped with a 488-nm argon ion laser and a 60 × 1.0 numerical aperture PlanApo water immersion objective (Olympus). Green fluorescent protein was excited by 488-nm light and the emission was collected using a BA 505–525 filter. A BA 660 IF emission filter was used to observe chlorophyll autofluorescence. Confocal optical sections were obtained in 0.5- to l-μm increments. The images were color-coded green for GFP and magenta for chlorophyll autofluorescence.

The image presented in **Figure 7** was made using a Leica SP8 laser-scanning microscope (Leica, Wetzlar, Germany) equipped with a solid-state laser with 488 nm light, HC PL APO CS 63×/1.2 water immersion objective (Leica, Wetzlar, Germany) and Leica

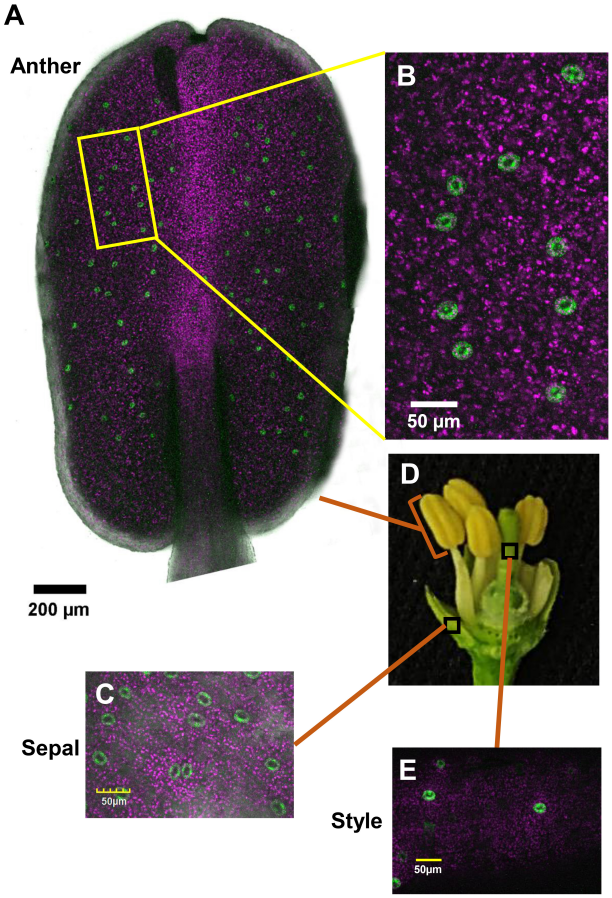

FIGURE 1 | Distribution of stomata on the organs of a closed citrus flower. The confocal images **A–C** and **E** are merged images of white light, chlorophyll autofluorescence (stained magenta), and GFP fluorescence (stained green). Flowers were harvested from GCGFP plants. **(A)** Confocal image of an anther removed from a closed flower. **(B)** Enlargement of the square in part **A**. **(C)** Confocal image of a sepal removed from a closed flower, as indicated in part **D**. **(D)** Dissection of a closed flower revealing the floral organs. **(E)** Confocal image of a style removed from a closed flower. Analyses were performed on five biological replicates.

Application Suite X software (LASX, Leica, Wetzlar, Germany). Images of GFP signal were acquired using the 488-nm laser line and emission was detected with a HyD (hybrid) detector in a range of 500–525 nm. For reflection microscopy, a 488-nm laser was used and light reflected into a band between 480 and 495 nm.

Distribution of Stomata on Various Parts of Citrus Fruits and Flowers

To evaluate the temporal formation and spatial distribution of stomata on various parts of citrus flowers, we collected five closed flowers and five open flowers and analyzed the distribution of stomata on the various floral organs. The same analyses were repeated in two sequential flowering seasons, with the same number of flowers examined each season.

Analyses of the stomata on fruit surfaces were conducted twice, with similar results. In the first analysis, a comparison was made between at least five stomata from each of three ripe fruits and three green fruits. In the second analysis, which was conducted the following season (the results of which are presented in **Figure 7**), the comparison was made between at least five stomata taken from each green or ripe parts of three breaker fruits (total of 10 stomata per fruit).

Measurement of the Transpiration of Green Fruits

Fruit transpiration rates were measured on intact 4-cm-diam. green fruits from plants grown in a greenhouse using the LI-1600 steady-state porometer (LI-COR, Lincoln, NE, United States). Measurements were conducted between 9:00 a.m. and 10:00 a.m. on all of the available fruits: eight WT fruits and 12 GCHXK1 fruits. The ambient light intensity was 550 μmol m^{-2} s^{-1}, the temperature was 23°C, and the relative humidity was 55%.

Water Loss of Ripe Yellow Fruits

Six ripe yellow fruits of similar weight from GCHXK and WT plants (average weights of 83.8 g for the WT and 82.7 g for GCHXK1) were incubated soon after harvest for 5 days under long-day conditions (16 h light/8 h dark photoperiod) at 25°C and 50% relative humidity. Weight loss during the incubation time was measured and is presented as a percentage from the initial weight (**Figure 6**).

Stomatal Measurements

Stomatal aperture and density were determined using the rapid imprinting technique described by Geisler and Sack (2002). The rapid imprinting technique with fast-drying dental resin allowed us to score a large number of stomata from independent biological samples from each experiment. In brief, light-bodied vinyl polysiloxane dental resin (Zhermack, Badia Polesine, Italy) was attached to the fruit surface and then removed as soon as it had dried (1 min). The resin epidermal imprints were

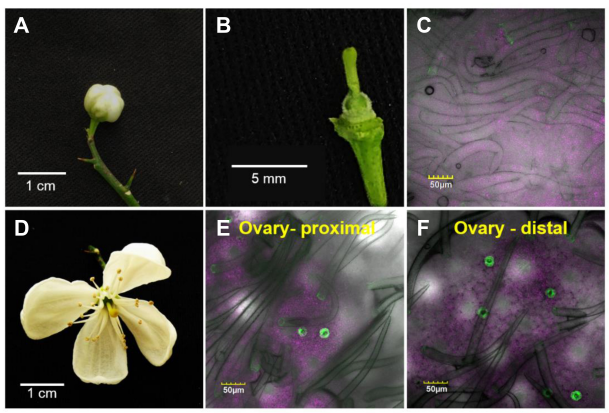

FIGURE 2 | Temporal and spatial distribution of the stomata on a citrus ovary. The confocal images **C**, **E**, and **F** are merged images of white light, chlorophyll autofluorescence (stained magenta), and GFP fluorescence (stained green). Samples were taken from GCGFP plants. The images in the lower row were taken from flowers 3 days older than the images shown in the upper row. **(A)** A closed GCGFP flower. **(B)** Binocular image of a dissected closed flower, revealing the ovary. **(C)** Confocal image of an ovary from a closed flower. **(D)** An open GCGFP flower. **(E)** Confocal image of the proximal part of an ovary from an open flower. **(F)** Confocal image of the distal part of an ovary from an open flower. Analyses were performed on five biological replicates.

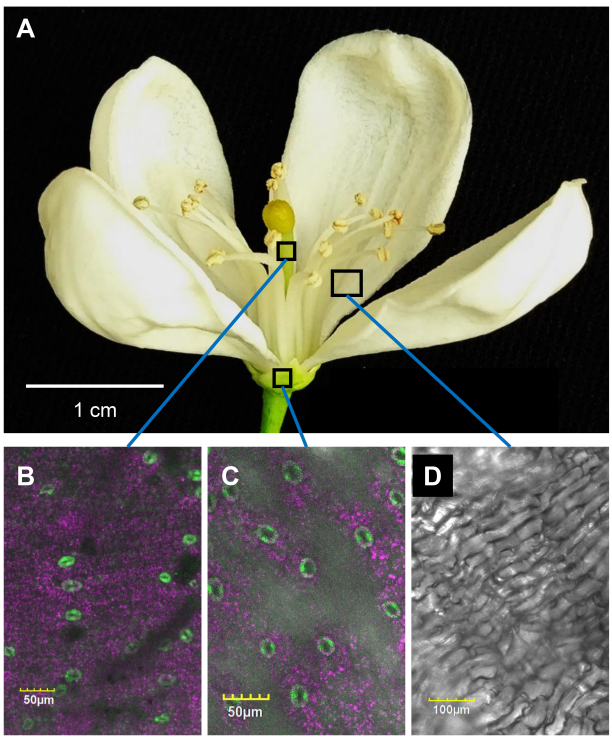

FIGURE 3 | Distribution of stomata on the organs of an open citrus flower. The confocal images **B**, **C**, and **D** are merged images of white light, chlorophyll autofluorescence (stained magenta), and GFP fluorescence (stained green). Flowers were harvested from GCGFP plants. **(A)** An open GCGFP flower. **(B)** Confocal image of a style removed from an open flower, as indicated in panel **A**. **(C)** Confocal image of a sepal removed from an open flower, as indicated in panel **A**. **(D)** Confocal image of a petal removed from an open flower, as indicated in panel **A**. Analyses were performed on five biological replicates.

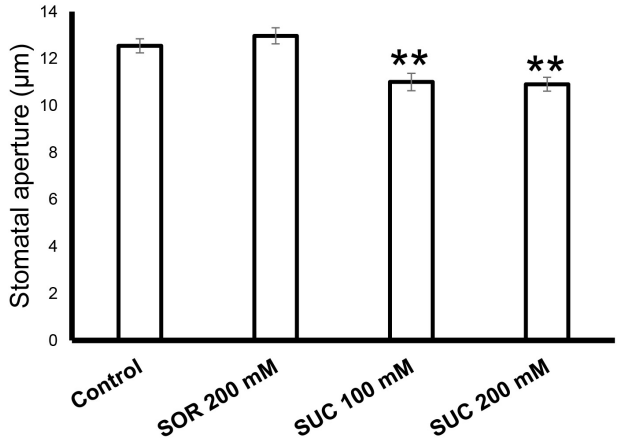

FIGURE 4 | Sugar stimulates the closure of citrus fruit stomata. The stomatal response to sucrose in WT fruit rind was assayed with rind discs (taken from six fruits) that were immersed for 2.5 h in artificial xylem sap (Wilkinson and Davies, 1997), artificial xylem sap containing 200 mM sorbitol (as an osmotic control), 100 mM sucrose (Suc), and 200 mM Suc. Epidermal imprints were then taken and the apertures of 60 stomata from each treatment were measured. Data are displayed as means ± SE. Asterisks denote significant differences relative to the WT (*t*-test, $P < 0.01$).

covered with nail polish, which was removed once it had dried and served as a mirror image of the resin imprint. The nail-polish imprints transferred to microscope slides and photographed under a bright-field inverted microscope (1M7100; Zeiss, Welwyn Garden City, Hertfordshire, United Kingdom) on which a Hitachi HV-D30 CCD camera (Hitachi, Tokyo, Japan) was mounted. Stomatal images were later analyzed using the IMAGEJ software (Bethesda, MD, United States) fit-ellipse tool to determine aperture size or stomatal density. A microscopic ruler (Olympus, Tokyo, Japan) was used for the size calibration.

The stomatal response to sucrose in WT fruit rind was assayed with rind disks taken from six different green, 4-cm-diam. fruits (one disc from each fruit in each treatment). Rind disks were each 1 cm in diameter and approximately 2 mm thick. The samples were immersed for 2.5 h in either artificial xylem sap (Wilkinson and Davies, 1997) or artificial xylem sap containing 200 mM sorbitol (as an osmotic control), 100 mM sucrose (Suc), and 200 mM Suc. Ambient light intensity was around 500 µmol m^{-2} s^{-1}. Epidermal imprints were then taken and stomatal aperture was measured. From each of the six imprints of each treatment, 10 randomly selected stomata were analyzed. Stomatal density was measured using 4-cm-diam., green fruits, with six biological repeats for the WT and seven biological repeats for each GCHXK line. More than 330 stomata were counted for each line in fields of 0.1 mm^2.

Seed Germination

The germination rate of GCHXK seeds was examined by sowing 68 seeds of the WT and GCHXK1 plants, and 40 seeds of the GCHXK5 plants. Seeds were collected from fully mature fruits. The seeds were divided into 17 groups of four seeds each for the WT and GCHXK1 (total of 68 seeds for each line) and 10 groups of 4 seeds each for the GCHXK5 line (total of 40 seeds). The proportion of seeds that germinated was calculated based on the average germination of the groups over a period of 28 days.

Assays of Sugar Levels in Fruit Juice

Juice was collected from three samples of mature yellow fruits of each line. For the WT and GCHXK1, the juice of each sample was collected from two different fruits. For GCHXK5

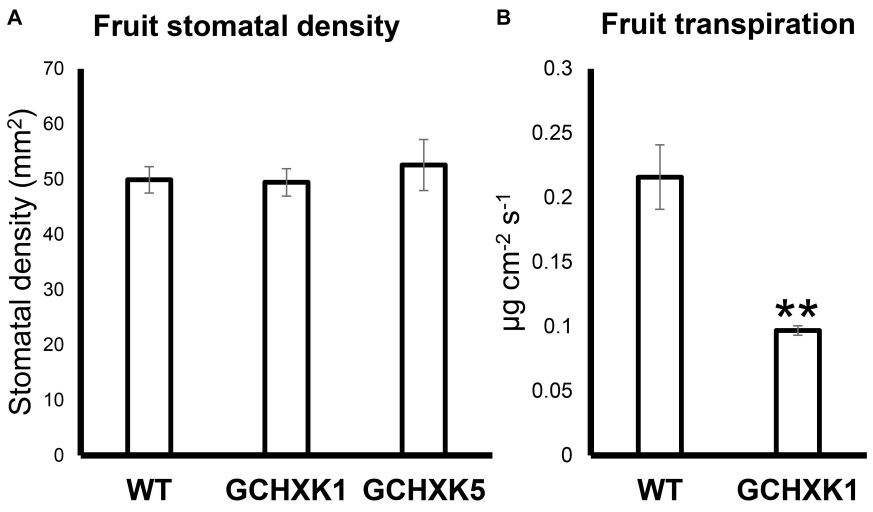

FIGURE 5 | Expression of *AtHXK1* in guard cells of citrus fruits reduced fruit transpiration with no change in stomatal density. **(A)** Stomatal densities on WT, GCHXK1, and GCHXK5 fruits. For the WT, there were six biological repeats and for each GCHXK line, there were seven biological repeats. **(B)** Transpiration of green WT and GCHXK1 fruits, as measured with the LI-1600 steady-state porometer (WT: $n = 8$; GCHXK1: $n = 12$). Data displayed as means ± SE. Asterisks denote significant differences relative to the WT (*t*-test, $P < 0.01$).

the juice of each sample was collected from one fruit. Samples were centrifuged at 15,000 rotations/min for 15 min and then filtered through a 0.22-μm nylon syringe. Sucrose, fructose, and glucose contents were determined by HPLC. The HPLC system consisted of a Shimadzu LC10AT solvent delivery system and a Shimadzu RID10A refractive index detector. Separation was carried out on an Alltech 700 CH Carbohydrate Column (Alltech, Deer-Weld, IL, United States) maintained at 90°C with a flow rate of 0.5 ml/min, according to the manufacturer's recommendations.

Measurement of Total Soluble Solids

The total soluble solids (TSS) content of the juice of mature yellow fruits was determined with a PAL-1 digital refractometer (Atago, Tokyo, Japan). Each measurement included three samples. For the WT and GCHXK1, the juice of each sample was collected from two different fruits. For GCHXK5, the juice of each sample was collected from one fruit.

RESULTS

Temporal Formation and Spatial Distribution of Stomata on Various Parts of Citrus Flowers

To monitor the appearance of stomata on citrus flowers and fruits, we used transgenic *T. citrange* (*C. sinensis* "Washington" sweet orange × *P. trifoliata*) containing the *KSTpro:GFP* that drives guard-cell expression of GFP (Lugassi et al., 2015; Kelly et al., 2017). The immediate and constitutive expression of *KSTpro:GFP* in newly formed guard cells (Kelly et al., 2017) allowed us to monitor the appearance of stomata easily and accurately. We started at early stages of flower development, when the flowers were still closed. At this stage, stomata were found on anthers, styles, and sepals (**Figure 1**), but not on stigmas, filaments, or ovules (which eventually develop into fruits; **Figures 2A–C**). When the flower opens about 3 days later (**Figures 2D**, **3A**), stomata are seen on the proximal and distal parts of the ovules (**Figures 2E,F**), but are more abundant on the style and sepal (**Figures 3B,C**). No stomata were seen on petals, filaments, or stigmas, even at later stages (**Figure 3D**). We concluded that stomata appear on the styles, anthers, and sepals of flowers that are still closed and on ovules at anthesis.

The Stomata of Young Citrus Fruits Respond to Sucrose

To check the response of citrus fruits' stomata to sugar, rind discs from green WT fruits were treated with artificial xylem sap solution (AXS, control), AXS supplemented with sorbitol (osmotic control), or AXS supplemented with 100 or 200 mM sucrose. Stomata that were treated with sucrose had significantly smaller apertures than those treated with AXS or the osmotic control (**Figure 4**). There was no significant difference between the stomatal closure of discs treated with 100 mM and the stomatal closure of discs treated with 200 mM sucrose. These results imply that the stomata on the fruit surface are functional and respond to known closing signals, similar to leaf stomata (Kelly et al., 2013).

GCHXK Fruits Exhibited Lower Transpiration Rates Than WT Fruits

It has previously been shown that sugar-sensing in guard cells is mediated by HXK and that expression of HXK in guard cells reduces leaf transpiration (Kelly et al., 2013; Lugassi et al., 2015). To examine whether HXK reduces the transpiration of fruit, we measured the stomatal density and transpiration of fruits from a previously described GCHXK citrus line (Lugassi et al., 2015). Stomatal density on 4-cm-diam., green GCHXK fruits was similar to that of WT fruits (**Figure 5A**). Yet, fruit transpiration of 4-cm-diam., green GCHXK fruits, measured using the LI-1600 steady-state porometer, was less than half of that observed for the WT fruits (**Figure 5B**).

We also measured water loss of ripened yellow fruits of similar size from GCHXK and WT plants following 5 days of exposure to long-day conditions (16 h light/8 h dark photoperiod) at 25°C (**Figure 6**). No difference in water loss was observed between

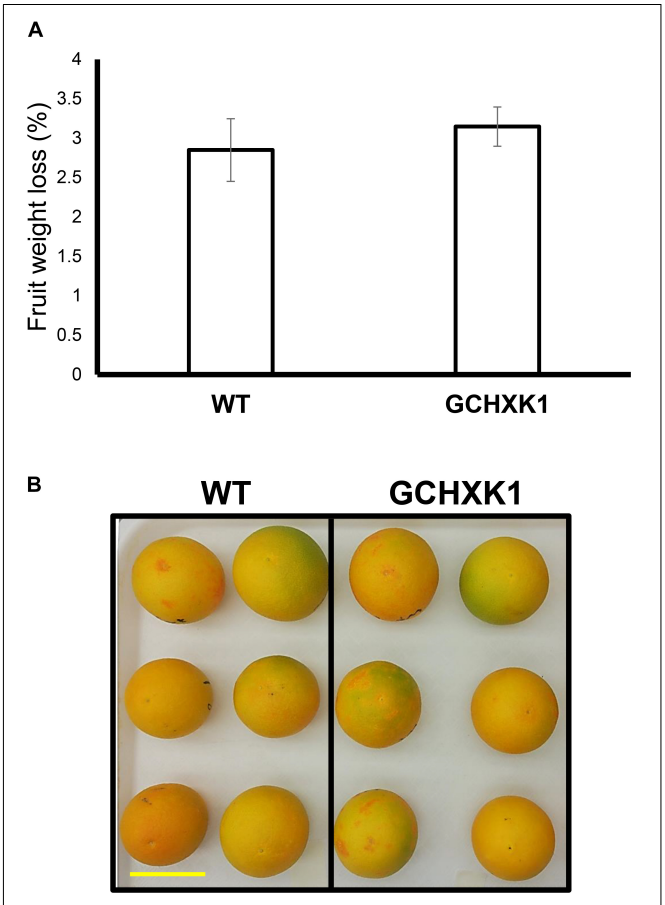

FIGURE 6 | Water loss of ripe GCHXK fruits. **(A)** Ripe, harvested WT, and GCHXK1 fruits exhibited similar water loss after 5 days of long-day conditions (16 h light/8 h dark photoperiod) at 25°C (n = 6). **(B)** Ripe, harvested WT, and GCHXK1 fruits used for the water loss experiment, scale bar is 5 cm. Data displayed as means ± SE.

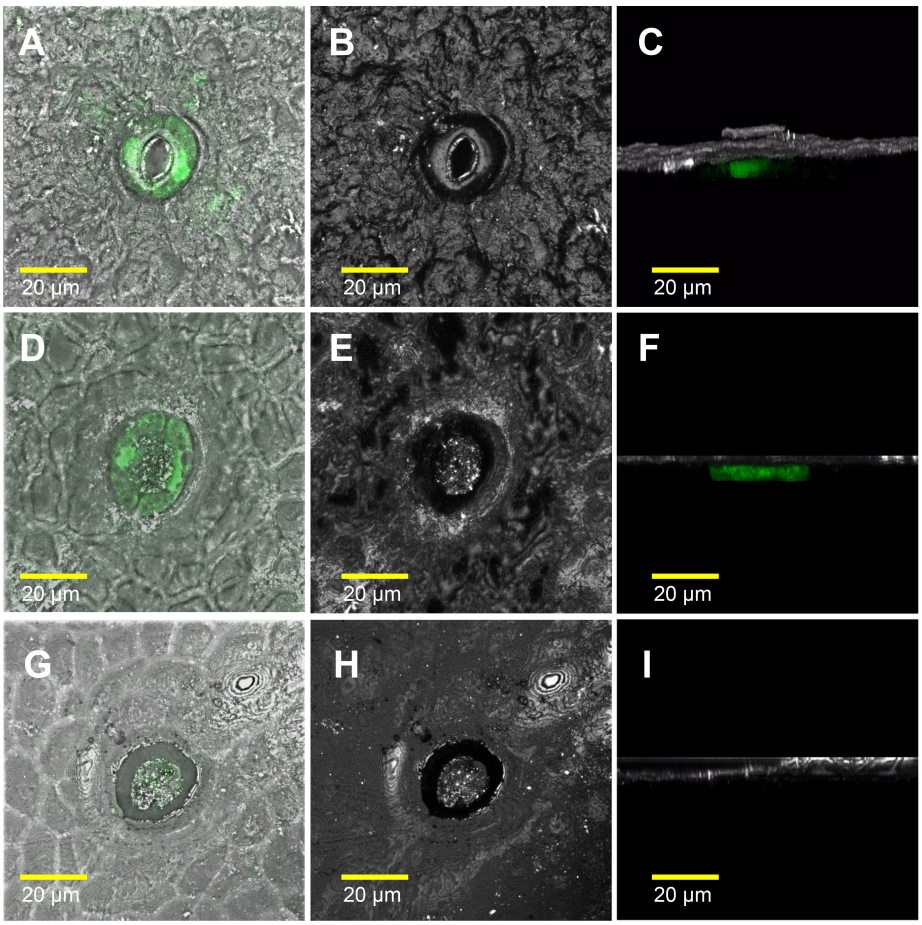

FIGURE 7 | The stomatal pores of ripe yellow fruits are plugged. The confocal images **A**, **D**, and **G** are merged images of white light, reflections of the sample, and GFP fluorescence (stained green). The confocal images **B**, **E**, and **H** are reflections of the sample. The confocal images **C**, **F**, and **I** are 3D simulations, to provide a side view of the stomata, composed of reflections of the sample and GFP fluorescence (stained green). Breaker fruits were harvested from GCGFP plants. **(A–C)** Stomata were taken from a green segment of the fruit. **(D–F)** Plugged stomata from a yellow segment of the fruit; GFP staining can still be observed within the guard cells. **(G–I)** Plugged stomata from a yellow segment of the fruit in which GFP was not detected in the guard cells. Analyses were performed on three biological replicates.

the GCHXK and WT fruits (**Figure 6**). Confocal analysis of stomata of GCGFP citrus fruits revealed that, as demonstrated previously (Ben-Yehoshua et al., 1985; Hiratsuka et al., 2015), the stomatal pores of ripened yellow fruits are plugged (**Figures 7D–I**). However, GFP signal could still be observed in some of the plugged stomata (**Figures 7D–F**). These results suggest that green GCHXK fruits had lower transpiration rates, since the stomata at this stage are functional and respond to sugar. However, the functionality of the stomata disappears toward fruit ripening, since the stomata of yellow mature fruits are plugged and the plugged stomata do not respond to sugar signals (**Figures 7A–C**, compared to **Figures 7D–I**).

GCHXK Seeds Are Smaller and Germinate More Slowly

Previous studies have suggested that the stomata of young citrus fruits allow photosynthesis and incorporation of CO_2 by fruits (Hiratsuka et al., 2015), but the contribution of fruit photosynthesis to citrus fruit development is not known. We, therefore, took advantage of the isogenic background of WT and GCHXK lines to examine the potential effect of the lower stomatal conductance of GCHXK on fruit development. No significant changes were observed in size between the GCHXK and WT fruits, and the number of seeds per fruit of GCHXK plants was similar to that of WT plants (**Figure 8D**). Yet, the seeds of the GCHXK lines were significantly smaller, with a significant change in their weight distribution (**Figures 8A–C**). In addition, GCHXK seeds germinated significantly more slowly than WT seeds (**Figure 9A**). On average, the GCHXK seeds germinated 2–3 days later than the WT seeds (**Figure 9B**).

Ripe GCHXK Fruits Do Not Show Reduction in Sugar Accumulation

To examine whether GCHXK affects the juice characteristics of mature yellow fruits, we analyzed the TSS and sugar contents of mature yellow fruits. The TSS content of the juice of one line,

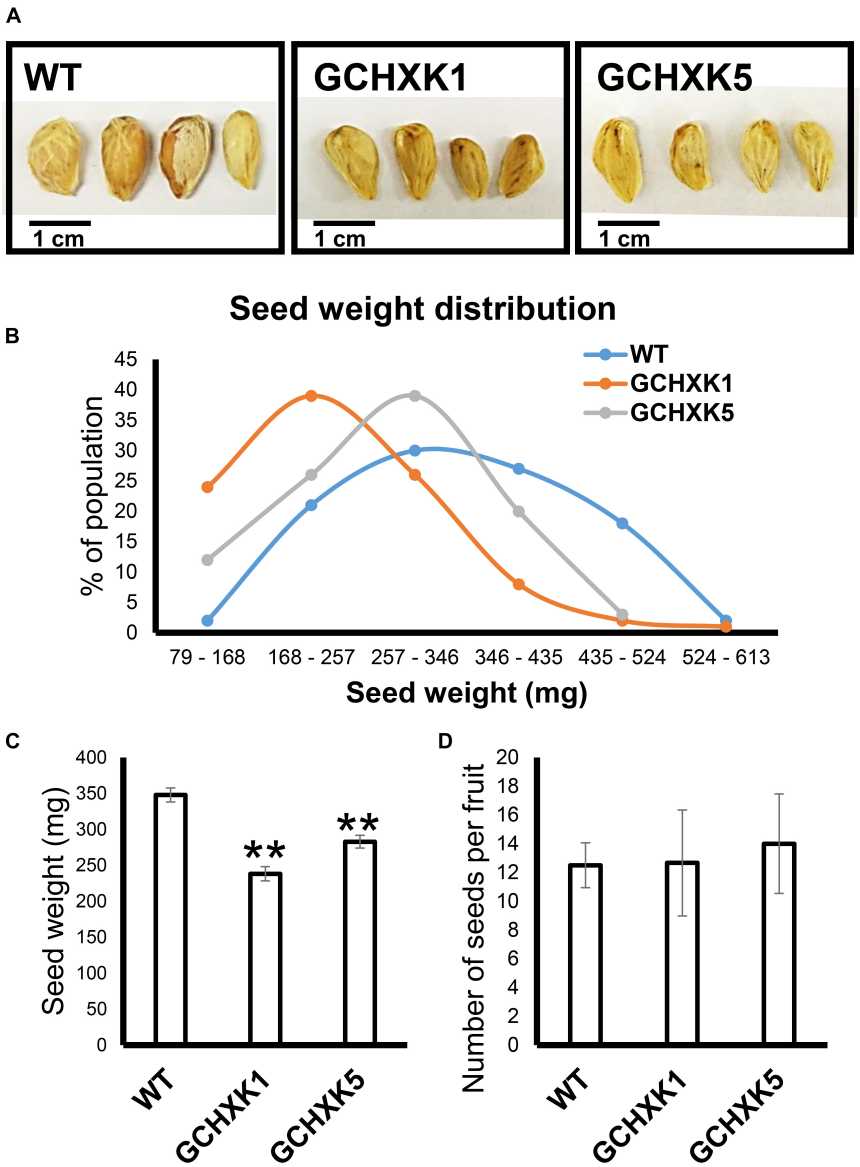

FIGURE 8 | GCHXK citrus plants produce smaller seeds. Seed weight was determined by weighing 100 individual seeds from the GCHXK1, GCHXK5, and WT plants. **(A)** Representative images of WT, GCHXK1, and GCHXK5 seeds. **(B)** Weight distribution of the seeds. **(C)** Average weights of the WT, GCHXK1, and GCHXK5 seeds. **(D)** Number of seeds per fruit (for WT and GCHK1, $n = 6$ fruits; for GCHXK5, $n = 3$ fruits). Data are displayed as means ± SE. Asterisks denote significant differences relative to the WT (*t*-test, $P < 0.01$).

GCHXK1, was significantly higher than that of the WT, while that of GCHXK5 was similar to that of WT (**Figure 10A**). Sugar analyses revealed similar sucrose and glucose levels, along with fructose levels that were higher than those observed for the WT (**Figure 10B**). These results indicate that GCHXK has no negative effect on juice parameters.

DISCUSSION

In the current study, we used GCGFP plants that express GFP under the *KST1* promoter and found that stomata are formed on floral organs early in the reproductive phase. The *KSTpro:GFP* construct has already been proven to be very useful for monitoring the formation of guard cells (Kelly et al., 2017). It drives guard cell-specific expression soon after the differentiation of guard cells from guard mother cells is expressed in all guard cells and allows easy detection of the appearance of stomata and distribution (Kelly et al., 2017). In this study, stomata were observed on the sepals, styles, and anthers of closed citrus flowers, and on ovules upon the opening of the flowers. It is likely that the stomata on citrus anthers allow desiccation and the opening of the anthers, which is required for

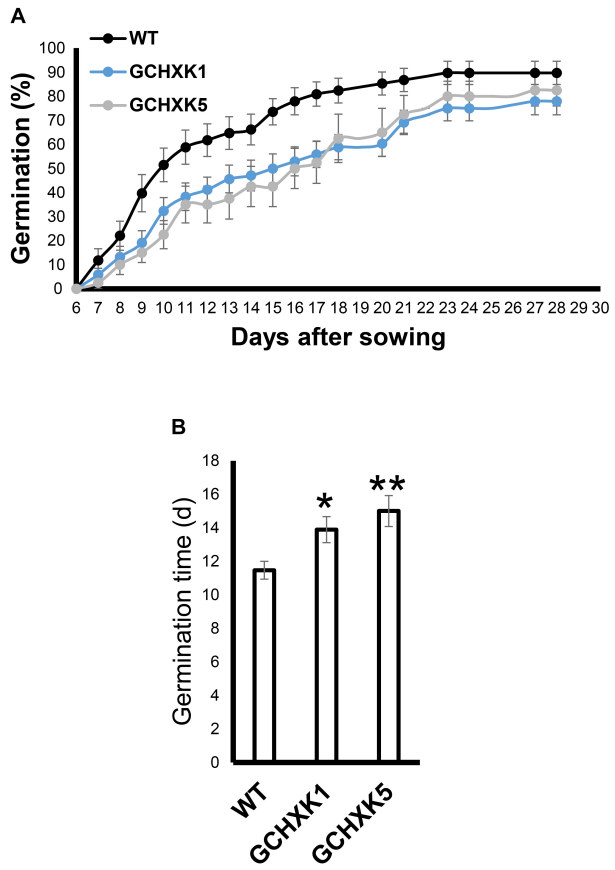

FIGURE 9 | GCHXK seeds germinate more slowly than WT seeds. The germination rates of the different seeds were examined by sowing 68 seeds of the WT and GCHXK1, and 40 GCHXK5 seeds. The seeds were divided into groups of four, and the percentage of seeds that germinated was calculated from the average of the groups. **(A)** Percentage of seed that germinated over 28 days. **(B)** Average time to germination of WT, GCHXK1, and GCHXK5 seeds. Data are displayed as means ± SE. Asterisks denote significant differences relative to the WT (*t*-test, $*P < 0.05$; $**P < 0.01$).

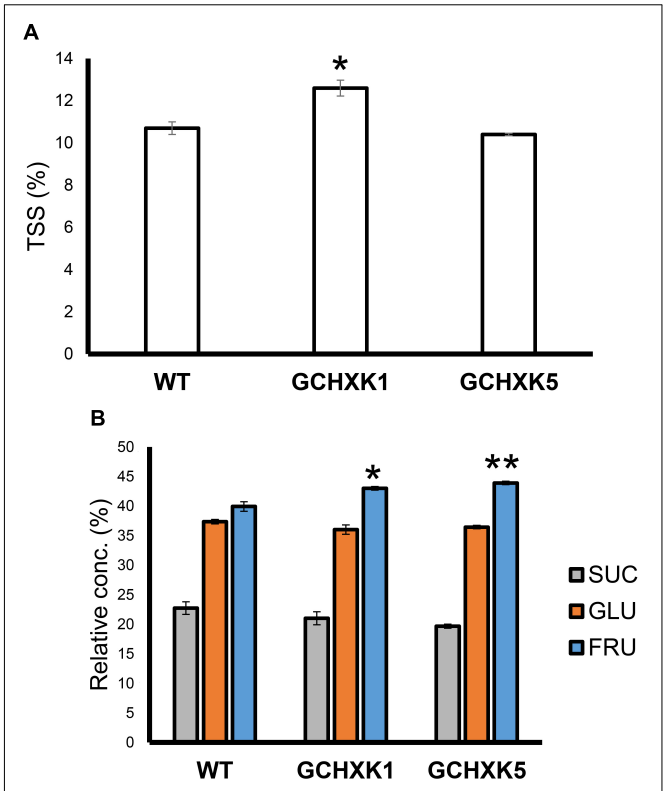

FIGURE 10 | TSS content and sugar content of GCHXK fruit. **(A)** TSS levels in the juices of GCHXK lines, compared to the WT. **(B)** Relative sucrose, fructose, and glucose levels (from total sugar content) in the juice of GCHXK lines, compared to the WT. Each measurement included three samples. For the WT and GCHXK1, the juice of each sample was collected from two different fruits. For GCHXK5, the juice of each sample was collected from one fruit (due to a lack of fruits). Data are displayed as means ± SE. Asterisks denote significant differences relative to the WT (*t*-test, $*P < 0.05$; $**P < 0.01$).

the release of pollen at anthesis, perhaps similar to the evolutionarily early role of stomata on the diploid sporophyte parts of mosses, which allow for spore desiccation and release (Sussmilch et al., 2017). Indeed, mutation of the *ICE1* transcription factor that reduces the number of mature stomata on Arabidopsis anthers has been shown to prevent anther dehiscence and the release of pollen (Wei et al., 2018). Yet, it has been suggested that stomata of closed flowers of *Lilium* hyb. *enchantment* anthers may allow assimilation of CO_2 at very early stages of pollen development, by low photon intensity that might penetrate the closed flowers (Clement et al., 1997).

The role of stomata on the green parts of the flower (i.e. the sepals, ovule, and style) might be to allow CO_2 uptake and photosynthesis (Vu et al., 1985). The functionality of fruit stomata has been demonstrated previously in several species such as banana (Johnson and Brun, 1966), purple passionfruit, yellow pitaya (Sánchez et al., 2013), and apple (Blanke and Lenz, 1989). It has also been shown that young green Satsuma mandarin (*C. unshiu*) fruits take up CO_2 (Hiratsuka et al., 2012, 2015). Accordingly, the opening of fruit stomata by light (Blanke and Bower, 1991) and the closure of those stomata by sucrose support the notion that the stomata of young green fruits allow for photosynthesis. It has been reported that, at low light intensities, the photosynthesis of Satsuma mandarin fruit is more efficient than that carried out in its leaves (Hiratsuka et al., 2015). However, the extent to which fruit photosynthesis is important for fruit development is not known. Certain orange trees (Blanke and Bower, 1991) have small fruits, whose size has been partially attributed to inefficient fruit photosynthesis (Blanke and Bower, 1991). Another study examined why bagging of Satsuma mandarin (to prevent fungal, insect, and physical damage and to promote color development of the fruit skin) leads to reduced sugar levels at harvest. It was suggested that bagging probably inhibits photosynthesis and CO_2 incorporation, leading to the lower sugar levels that were observed at harvest (Hiratsuka et al., 2012).

Yet, despite the reduced stomatal conductance, in our study, the sugar and TSS contents of mature GCHXK fruits were not lower than those of WT plants (**Figure 10**). However, the seeds of GCHXK plants were smaller and germinated more slowly, suggesting that the reduced stomatal apertures of GCHXK fruits did have a negative effect on seed development. Seed development starts at anthesis, immediately after pollination, when the fruits (ovules) are still very small, and since the stomata appear on ovules at anthesis, they may allow CO_2 incorporation that contributes to ovule and seed development. Since we observed a reduction of >50% in GCHXK fruit transpiration, it is likely that the reduced apertures of the stomata of GCHXK fruits lead to lower fruit photosynthesis rates, which negatively affect seed development. No negative effects on leaf photosynthesis rates or plant growth were observed concurrent with the vegetative growth of GCHXK plants (Lugassi et al., 2015), minimizing the possibility that the seeds were indirectly affected by fluctuations in leaf photosynthesis.

As citrus fruits mature, the fruit guard cells collapse and the stomata accumulate a wax-like substance (Hiratsuka et al., 2015). Accordingly, no difference in water loss was observed between mature yellow GCHXK and WT fruits. Based on our GCGFP line, it appears that while the stomatal pore is plugged throughout fruit yellowing, some of the guard cells do not collapse, remain intact, and even retain their GFP signal (**Figures 7D–F**). Nevertheless, the results of this study indicate that the stomata on the reproductive organs at early developmental stages of citrus flowers are not only reminiscent of their epidermal origin, but may contribute to seed development.

DATA AVAILABILITY STATEMENT

All datasets generated for this study are included in the article/supplementary material.

AUTHOR CONTRIBUTIONS

NL, GK, AS, ER, NC, and DG planned and designed the research. NL and DG wrote the manuscript. NL, GK, TA, CF, YeY, and YoY performed the experiments. NL, GK, TA, YeY, ER, NC, and DG analyzed the data.

FUNDING

This research was supported by grant no. 261-1052 from the Chief Scientist of the Israel Ministry of Agriculture and Rural Development.

ACKNOWLEDGMENTS

We wish to thank Mr. Aysheshim Malede for his dedicated and diligent care of the citrus plants grown for this research.

REFERENCES

Ben-Yehoshua, S., Burg, S. P., and Young, R. (1985). Resistance of citrus fruit to mass transport of water vapor and other gases. *Plant Physiol.* 79, 1048–1053. doi: 10.1104/pp.79.4.1048

Blanke, M. M., and Bower, J. P. (1991). Small fruit problem in citrus trees. *Tree Struct. Funct.* 5, 239–243. doi: 10.1007/bf00227531

Blanke, M. M., and Lenz, F. (1989). Fruit photosynthesis. *Plant Cell Environ.* 12, 31–46.

Clement, C., Mischler, P., Burrus, M., and Audran, J. C. (1997). Characteristics of the photosynthetic apparatus and CO2-fixation in the flower bud of Lilium. II. Anther. *Int. J. Plant Sci.* 158, 801–810. doi: 10.1086/297493

Geisler, M. J., and Sack, F. D. (2002). Variable timing of developmental progression in the stomatal pathway in *Arabidopsis cotyledons*. *New Phytol.* 153, 469–476. doi: 10.1046/j.0028-646x.2001.00332.x

Granot, D. (2007). Role of tomato hexose kinases. *Funct. Plant Biol.* 34, 564–570.

Granot, D. (2008). Putting plant hexokinases in their proper place. *Phytochemistry* 69, 2649–2654. doi: 10.1016/j.phytochem.2008.08.026

Granot, D., and Kelly, G. (2019). Evolution of guard-cell theories: the story of sugars. *Trend Plant Sci.* 24, 507–518. doi: 10.1016/j.tplants.2019.02.009

Hiratsuka, S., Suzuki, M., Nishimura, H., and Nada, K. (2015). Fruit photosynthesis in *Satsuma mandarin*. *Plant Sci.* 241, 65–69. doi: 10.1016/j.plantsci.2015.09.026

Hiratsuka, S., Yokoyama, Y., Nishimura, H., Miyazaki, T., and Nada, K. (2012). Fruit photosynthesis and phosphoenolpyruvate carboxylase activity as affected by lightproof fruit bagging in *Satsuma mandarin*. *J. Am. Soc. Hort. Sci.* 137, 215–220. doi: 10.21273/jashs.137.4.215

Huang, X., Lin, S., He, S., Lin, X., Liu, J., Chen, R., et al. (2018). Characterization of stomata on floral organs and scapes of cut 'Real' gerberas and their involvement in postharvest water loss. *Postharvest Biol. Technol.* 142, 39–45. doi: 10.1016/j.postharvbio.2018.04.001

Johnson, B. E., and Brun, W. A. (1966). Stomatal density and responsiveness of banana fruit stomates. *Plant Physiol.* 41, 99–101. doi: 10.1104/pp.41.1.99

Kelly, G., Lugassi, N., Belausov, E., Wolf, D., Khamaisi, B., Brandsma, D., et al. (2017). The *Solanum tuberosum* KST1 partial promoter as a tool for guard cell expression in multiple plant species. *J. Exp. Bot.* 68, 2885–2897. doi: 10.1093/jxb/erx159

Kelly, G., Moshelion, M., David-Schwartz, R., Halperin, O., Wallach, R., Attia, Z., et al. (2013). Hexokinase mediates stomatal closure. *Plant J.* 75, 977–988. doi: 10.1111/tpj.12258

Kottapalli, J., David-Schwartz, R., Khamaisi, B., Brandsma, D., Lugassi, N., Egbaria, A., et al. (2018). Sucrose-induced stomatal closure is conserved across evolution. *PLoS One* 13:e0205359. doi: 10.1371/journal.pone.0205359

Lugassi, N., Kelly, G., Fidel, L., Yaniv, Y., Attia, Z., Levi, A., et al. (2015). Expression of *Arabidopsis hexokinase* in citrus guard cells controls stomatal aperture and reduces transpiration. *Front. Plant Sci.* 6:1114. doi: 10.3389/fpls.2015.01114

Moore, B., Zhou, L., Rolland, F., Hall, Q., Cheng, W. H., Liu, Y. X., et al. (2003). Role of the *Arabidopsis* glucose sensor HXK1 in nutrient, light, and hormonal signaling. *Science* 300, 332–336. doi: 10.1126/science.1080585

Nadeau, J. A., and Sack, F. D. (2002). Control of stomatal distribution on the *Arabidopsis* leaf surface. *Science* 296, 1697–1700. doi: 10.1126/science.1069596

Sánchez, C., Fischer, G., and Sanjuanelo, D. W. (2013). Stomatal behavior in fruits and leaves of the purple passionfruit (Passiflora edulis Sims) and fruits and cladodes of the yellow pitaya [*Hylocereus megalanthus* (K. Schum. ex Vaupel) Ralf Bauer]. *Agron. Colombia* 31, 38–47.

Sussmilch, F. C., Brodribb, T. J., and McAdam, S. A. M. (2017). What are the evolutionary origins of stomatal responses to abscisic acid in land plants? *J. Integr. Plant Biol.* 59, 240–260. doi: 10.1111/jipb.12523

Vu, J. C. V., Yelenosky, G., and Bausher, M. G. (1985). Photosynthetic activity in the flower buds of Valencia orange (*Citrus sinensis* [L.] Osbeck). *Plant Physiol.* 78, 420–423. doi: 10.1104/pp.78.2.420

Wei, D. H., Liu, M. J., Chen, H., Zheng, Y., Liu, Y. X., Wang, X., et al. (2018). Inducer of CBF expression 1 is a male fertility regulator impacting anther dehydration in *Arabidopsis*. *PLoS Genet.* 14:e1007695. doi: 10.1371/journal.pgen.1007695

Wilkinson, S., and Davies, W. J. (1997). Xylem sap pH increase: a drought signal received at the apoplastic face of the guard cell that involves the suppression of saturable abscisic acid uptake by the epidermal symplast. *Plant Physiol.* 113, 559–573. doi: 10.1104/pp.113.2.559

Wilson, Z. A., Song, J., Taylor, B., and Yang, C. (2011). The final split: the regulation of anther dehiscence. *J. Exp. Bot.* 62, 1633–1649. doi: 10.1093/jxb/err014

Conflict of Interest: The authors declare that the research was conducted in the absence of any commercial or financial relationships that could be construed as a potential conflict of interest.

frontiers in Plant Science

ORIGINAL RESEARCH
published: 17 March 2020
doi: 10.3389/fpls.2020.00283

Physiological Changes in *Mesembryanthemum crystallinum* During the C_3 to CAM Transition Induced by Salt Stress

Qijie Guan[1,2], Bowen Tan[3], Theresa M. Kelley[2], Jingkui Tian[1,4,5] and Sixue Chen[2,6]**

[1] College of Biomedical Engineering and Instrument Science, Zhejiang University, Hangzhou, China, [2] Department of Biology, Genetics Institute, Plant Molecular and Cellular Biology Program, University of Florida, Gainesville, FL, United States, [3] Department of Biology, University of Florida, Gainesville, FL, United States, [4] Key Laboratory for Biomedical Engineering of Ministry of Education, College of Biomedical Engineering and Instrument Science, Zhejiang University, Hangzhou, China, [5] Zhejiang-Malaysia Joint Research Center for Traditional Medicine, Zhejiang University, Hangzhou, China, [6] Proteomics and Mass Spectrometry, Interdisciplinary Center for Biotechnology Research, University of Florida, Gainesville, FL, United States

Salt stress impedes plant growth and development, and leads to yield loss. Recently, a halophyte species *Mesembryanthemum crystallinum* has become a model to study plant photosynthetic responses to salt stress. It has an adaptive mechanism of shifting from C_3 photosynthesis to crassulacean acid metabolism (CAM) photosynthesis under stresses, which greatly enhances water usage efficiency and stress tolerance. In this study, we focused on investigating the morphological and physiological changes [e.g., leaf area, stomatal movement behavior, gas exchange, leaf succulence, and relative water content (RWC)] of *M. crystallinum* during the C_3 to CAM photosynthetic transition under salt stress. Our results showed that in *M. crystallinum* seedlings, CAM photosynthesis was initiated after 6 days of salt treatment, the transition takes place within a 3-day period, and plants became mostly CAM in 2 weeks. This result defined the transition period of a facultative CAM plant, laid a foundation for future studies on identifying the molecular switches responsible for the transition from C_3 to CAM, and contributed to the ultimate goal of engineering CAM characteristics into C_3 crops.

Keywords: *Mesembryanthemum crystallinum*, salt stress, photosynthesis and photorespiration, C_3 to CAM transition, physiology

OPEN ACCESS

Edited by:
Caspar Christian Cedric Chater, The University of Sheffield, United Kingdom

Reviewed by:
Luisa C. Carvalho, University of Lisbon, Portugal
Sun-Hee Woo, Chungbuk National University, South Korea

****Correspondence:***
Jingkui Tian
tjk@zju.edu.cn
Sixue Chen
schen@ufl.edu

Specialty section:
This article was submitted to Plant Development and EvoDevo, a section of the journal Frontiers in Plant Science

Received: *19 December 2019*
Accepted: *25 February 2020*
Published: *17 March 2020*

Citation:
Guan Q, Tan B, Kelley TM, Tian J and Chen S (2020) Physiological Changes in Mesembryanthemum crystallinum During the C_3 to CAM Transition Induced by Salt Stress. Front. Plant Sci. 11:283. doi: 10.3389/fpls.2020.00283

INTRODUCTION

Mesembryanthemum crystallinum can switch its photosynthetic system from C_3 photosynthesis to crassulacean acid metabolism (CAM) under drought or salt conditions. CAM is a specialized mode of photosynthesis that has nocturnal fixation of atmospheric CO_2 into organic acids (e.g., malic acid) by phosphoenolpyruvate carboxylase (PEPC), whereby the CO_2-storing organic acids are remobilized and decarboxylated to provide CO_2 for the Calvin cycle during the day (Winter et al., 2015). *M. crystallinum* is also known as a succulent plant with more succulence in leaves at adult and flowering stages than at juvenile stage (Adams et al., 1998). Because the CO_2-storing organic acids are mainly stored in mesophyll cells, some degree of succulence is required for CAM to be efficient (Males, 2017). The succulence ensures independence from limited or unpredictable water supply after the juvenile growth phase. Over the years, *M. crystallinum* has become a favorite

halophyte model for studying C_3 and CAM due to its facultative capability under stress conditions (Vinocur and Altman, 2005; Winter and Holtum, 2014; Winter et al., 2015; Males and Griffiths, 2017).

Osmotic stress and ionic stress are two main challenges for plants growing under salinity (Munns and Tester, 2008). Mature *M. crystallinum* can survive high salt concentrations because of its ability to store water and its capacity of epidermal bladder cells (EBCs) to sequester up to 1 M sodium salt for adjusting the osmotic pressure (Bohnert and Cushman, 2000). Salt tolerance combined with the high water use efficiency (WUE) makes *M. crystallinum* an efficient CAM plant (Agarie et al., 2007). A comprehensive transcriptomic analysis of EBCs showed that V-type H^+-ATPase (VHA) subunits were highly induced for vacuolar Na^+ deposition in the EBCs (Oh et al., 2015).

Stomatal behavior is another specific feature of CAM plants. Stomatal movement is controlled by many different factors, including light, CO_2 concentration, and circadian clock. In C_3 plants, stomata open in the day and close in the night, causing much water loss through diurnal transpiration during C_3 photosynthesis. Under mild stresses, plants reduce stomatal conductance, leading to decreases in CO_2 intake and mesophyll photosynthesis (Chaves et al., 2009). In CAM plants, stomata are closed in the day and open at night to minimize water loss during PEPC-mediated CO_2 fixation in the night. Then during the day, the CO_2-storing organic acids are decarboxylated to provide high concentration of CO_2 for C_3 photosynthesis with closed stomata.

Differences in gene expression, protein, and metabolite levels, as well as phenotypic changes have been studied in C_3 and CAM plants (Aragón et al., 2012; Cosentino et al., 2013; Abraham et al., 2016; Chiang et al., 2016). For example, weekly morphological and physiological changes in micropropagated pineapple under CAM-inducing conditions were characterized (Aragón et al., 2012). However, studies focusing on the physiological and molecular changes in the model plant *M. crystallinum* during the C_3 to CAM transition in a short period have not been published. Here we report the morphological and physiological changes in *M. crystallinum* under salt-stress induced transition from C_3 to CAM photosynthesis. By studying the short transition period, we were able to investigate mechanistic changes of photosynthesis, especially the regulatory triggers in facultative CAM plants. We observed that high salt concentration in the soil influences *M. crystallinum* phenotypic changes. In addition, stomatal movement combined with the leaf succulence assay during the transition period also gave us insight into how the facultative CAM plants reduce water loss, and how leaf succulence was developed to facilitate CAM photosynthesis.

MATERIALS AND METHODS

Plant Growth and Salt Stress

Mesembryanthemum crystallinum seeds were provided by Professor John C. Cushman at the University of Nevada. *M. crystallinum* seeds were germinated and grown in a plant growth chamber at 26°C during the day and 18°C at night in a 12/12 h day/night cycle. Each seedling was grown in a 946 mL foam pot with Sungro Propagation Mix soil (SunGro Horticulture, MA, United States). Plants were watered three times a week with 50 mL 0.5× Hoagland's solution (Hoagland and Arnon, 1950) for 28 days. Then plants in the control group were watered daily with 50 mL 0.5× Hoagland's solution, while those in treatment group were watered with 50 mL 0.5× Hoagland's solution containing 0.5 M NaCl following the protocol by Cushman et al. (1990). All the experiments were conducted with four biological replicates unless otherwise stated, with each individual plant being an independent biological replicate.

Relative Water Content Analysis

To obtain fresh weight of leaves, the third and fourth leaf were detached and weighed. Similarly, fresh weight of the remnant shoot was weighed and fresh weight of the whole shoot was calculated by summing the weights of the leaves and remnant shoot. The leaves and remnant shoots were wrapped in aluminum foil, immersed immediately in a 4°C distilled water bath and soaked for 12 h. After 12 h, leaf surface was quickly blotted dry using paper towels and leaf turgid weight was measured. Then leaves were dried in an 80°C oven for 12 h, and leaf dry weight was measured. RWC was calculated by RWC = [(Fresh Weight − Dry Weight)/(Turgid Weight − Fresh weight)] * 100% (González and Gonzalez-Vilar, 2001). Four biological replicates were used in both control and salt-treated groups.

Leaf Area Measurement

A python program was created using the ratio of green pixels against 1 cm^2 black spot pixels used for measuring leaf surface area with images taken by a Cannon Rebel T6 DSLR camera (**Supplementary Figure S1** and **Supplementary File S1**). Eight plants were divided into control and salt-treatment groups. They were photographed at 12 pm every day to track leaf growth, and the python program was used for leaf area measurement. Leaf area simulation was based on a model reported by Xiao et al. (1988), and parameters were calculated using minimum distances between simulation and acquired data.

Gas Exchange Measurement

Gas exchange measurements were conducted by a portable photosynthesis system (Li-Cor 6800, Li-Cor Inc., Lincoln, NE, United States) equipped with a 68H-581066 fluorescence head and a 6 cm^2 chamber. An air flow ratio was set to 800 $\mu mol\ s^{-1}$ with chamber delta P at 0.2 kPa, and a fan speed of 10,000 min^{-1}. Relative humidity in the chamber was set to 50% to be consistent with the humidity setting in the plant growth chamber, and the reference cell CO_2 concentration was set to 400 $\mu mol\ mol^{-1}$ air. Light intensity in the fluorescence head was set to track the light intensity measured by the external quantum sensor. A program was made to log parameters every 30 s and to match IRGA (infrared gas analyzer) every 30 min. The Li-Cor instrument was kept in the growth chamber for diurnal and nocturnal gas exchange monitoring. Three separate biological replicates were conducted for the gas exchange measurement.

Stomatal Phenotype Observation and Measurement

A stomata tape-peel method (Lawrence et al., 2018) was used for stomatal movement observation. A piece of transparent adhesive tape was attached to the central part of the abaxial side of the third or fourth leaf, and a razor blade was applied to scrape away non-adherent cells. The tape with a thin layer of cells was put onto a microscopy slide, and then observed under a Leica DM6000 B microscope. Fifteen images of three biological replicates were taken in Openlab 5.5.3 in RGB mode for each group at each observation time point. Diurnal and nocturnal behaviors of stomatal movement were observed at 4 pm and 4 am, respectively. ImageJ was used to analyze microscopic images[1] and150 stomata were observed from the 15 images. The stomatal aperture was measured by the width of inner pore, and the proportion of open stomata was calculated by division of the number of open stomata by that of total stomata (Eisele et al., 2016).

Leaf Succulence Measurement

Leaf succulence was measured daily at 4 am for 14 days after start of control and salt treatment. Then the second pair of leaves from one plant was used as one biological replicate, and a total of four plants were measured. The leaf area was measured using the same protocol as described above using the python program, and leaf fresh weight was measured immediately after the leaves were excised. Leaf succulence (g cm^{-2}) was calculated by leaf fresh weight/leaf area. Four biological replicates were used at each time point for each treatment.

Malondialdehyde Content Measurement

We adapted a method from Wang et al. (2019) for measuring the malondialdehyde (MDA) content. Leaves of ice plants were harvested before and after salt treatment, and then ground to a fine powder in liquid nitrogen. A total of 3 mL 10% trichloroacetic acid (TCA) was added to 0.2 g leaf tissue powder and kept in 4°C overnight. After centrifugation at 10,000 × *g*, 4°C for 20 min, the supernatant (2 mL) was transferred to a new tube. Then, 2 mL 0.6% thiobarbituric acid was added to the supernatant, and vortexed thoroughly. The mixture was heated in boiling water for 15 min, cooled to 4°C immediately and centrifuged at 10,000 × *g*, 4°C for 10 min. Absorbance of the supernatant was recorded at wavelengths of 532 and 450 nm. The MDA content (μmol L^{-1}) was calculated by 6.45 * OD_{532} – 0.56 * OD_{450}. Four biological replicates were conducted at each time point.

Statistical Analysis

Experimental values were processed using Numpy module and Scipy module installed on Python 3.5. Bars in the figures correspond to standard errors, and a star in the figures indicates *p*-value <0.05 based on Student's *t*-test, and two stars indicate *p*-value <0.01.

[1]https://imagej.nih.gov/ij/

RESULTS

Plant Growth and Leaf Area Changes

Mesembryanthemum crystallinum seedlings have different leaf shapes at different developmental stages. In this study, we used seedlings at the early developmental stage (**Figure 1**) before they shift into CAM photosynthesis. After 4 weeks of growth, the second pair of primary leaves became as large as the first pair of primary leaves. Then we applied salt treatment to one group of the plants. In the first week of treatment, there are no significant plant growth differences between the control and salt-treated groups. After 1 week of salt-treatment, the treated plants decreased the rate of leaf growth compared to the control plants (**Figure 1**). Leaf area change is closely related to plant growth, development, and water usage. Here we developed a python script (**Supplementary File S1**) using leaf images with a 1 cm^2 reference square on the same plane to accurately measure the leaf areas of *M. crystallinum* seedlings every day for a total of 56 days. Statistics analysis was performed between the leaf areas from control and treatment groups. Clearly, *M. crystallinum* seedlings had a fast growing trend (**Figure 2**) in the control group using a simulated equation: $A(\mathrm{cm}^2) = 29.7391 \times (1.0830^{D+21} - 1)$. *A* is the total leaf area and *D* is the days after treatment. After salt treatment, *M. crystallinum* leaves grew at a similar rate as the control group in the first 5 days, and then slowed down the growth after 7 days of salt-treatment with a simulated equation:

$$A\ (\mathrm{cm}^2) = 29.7391 \times (1.0830^{D+21} - 1) \quad \text{if } D \leq 0.$$

$$A\ (\mathrm{cm}^2) = 29.7391 \times (1.0830^{D+21} - 1) - 5.7849(1.2998^{D+21} - 1) \quad \text{if } D > 0.$$

Since carbon fixation plays an important role in leaf expansion, these results indicate that after 7 days of salt stress, the ice plants may have less carbon fixation compared to the C_3 plants.

CO_2 Assimilation and Transpiration

Stomata conductance to water vapor is affected by many factors, such as stomatal aperture, CO_2 concentration, light intensity, and temperature. In this study, we did gas exchange measurements for leaf assimilation rate continuously over 14 days after the salt treatment (**Figure 3A**). In control plants, the assimilation rate during the day is in the range of 6.0–12.0 μmol m^{-2} s^{-1}, and in the range of −2.0 to 0.0 μmol m^{-2} s^{-1} during the night. In contrast, in the salt-treated plants, the assimilation rate has a decreasing trend in the day and an increasing trend in the night. The gas exchange result of control plants indicates that under well-watered conditions, the 42-day-old plants did not switch to CAM photosynthesis and the photosynthetic activity was steady in the leaves. The salt treatment results showed that the assimilation rate was decreased during the day after 6 days of salt-treatment. However, the assimilation rate

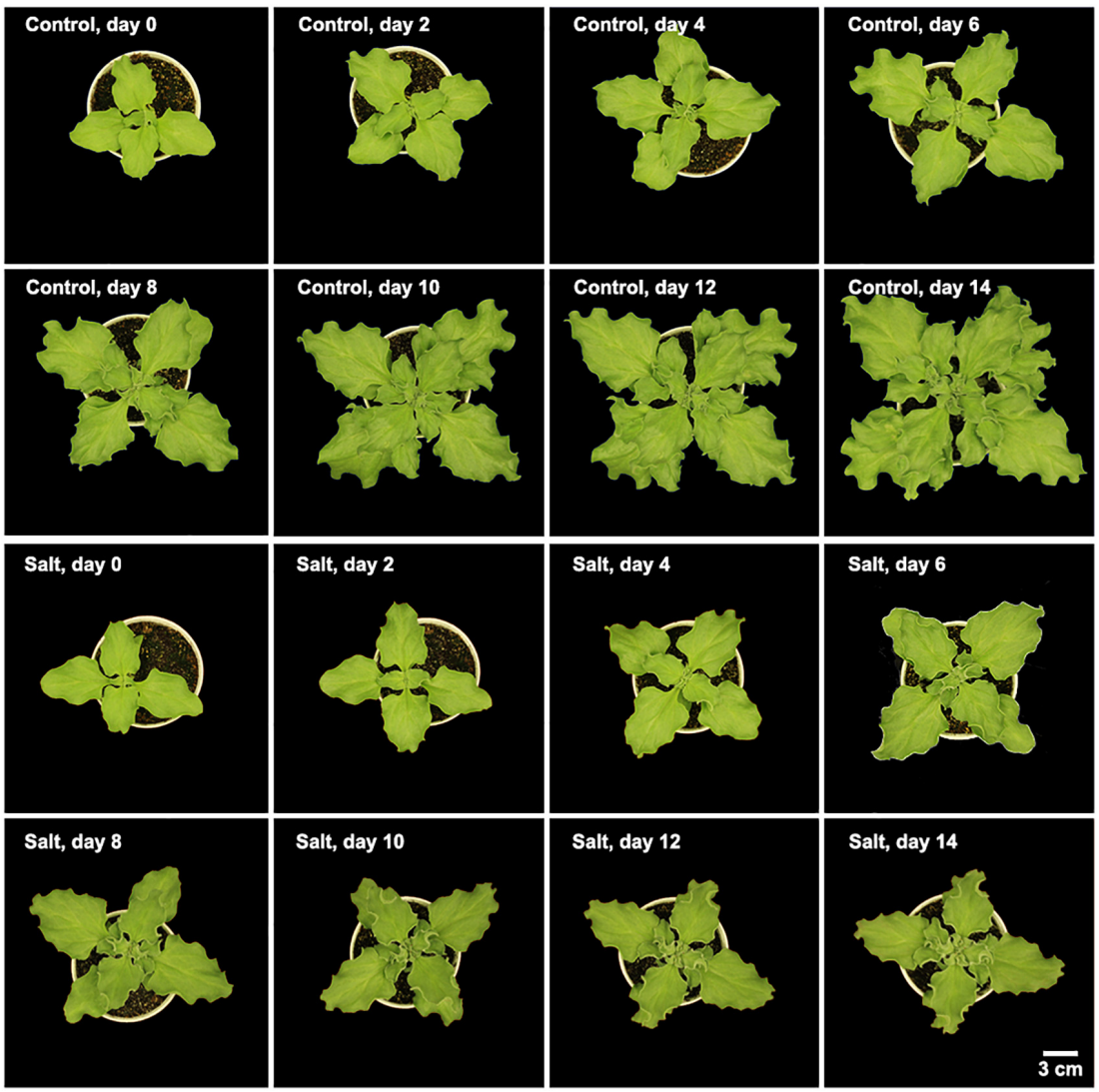

FIGURE 1 | Morphology of *M. crystallinum* seedlings growing under control and salt treatment for 14 days. Each image is representative of the seedlings at 12 pm in the four biological replicates.

during the night was increased after 6 days of treatment. After 8 days of the salt-treatment, the assimilation rate during the night was increase to almost 0.0 μmol m^{-2} s^{-1}, indicating that switching to CAM took place between 6 and 8 days after treatment.

After 9 days of salt treatment, the plants had an interesting pattern of gas exchange rate, the lowest assimilation rate during the day was lower than 0.0 μmol m^{-2} s^{-1} at 2 pm, and the highest assimilation rate during the night was higher than 0.0 μmol m^{-2} s^{-1} at 2 am. When the chamber light initially came on, the assimilation rate culminated from lower than −2.0 μmol m^{-2} s^{-1} to >2.0 μmol m^{-2} s^{-1}, and when the chamber light switched off, the assimilation rate dropped from higher than 1.0 μmol m^{-2} s^{-1} to lower than −2.0 μmol m^{-2} s^{-1} (**Figure 3A**). These results indicated the existence of the CAM circadian clock, which controlled stomata closure before the chamber light switched on and stomatal opening before the chamber light switched off.

Diurnal Stomatal Movement

We measured diurnal stomatal movement patterns through analyzing stomatal aperture and the proportion of opening stomata every 12 h during the 14-day period after the salt treatment. As shown in **Figure 3B**, the size of *M. crystallinum* stomatal aperture was in a range of 1.7–3.0 μm while stomata were open, and at a range of 0.7–1.1 μm while stomata were closed. The inversed stomatal movement behavior in the salt-treated plants was observed between 6 and 7 days after the treatment, indicating that CAM photosynthetic mechanism starts to play a role at day 7. It was noticed that the overall stomatal aperture of salt-treated plants became smaller after

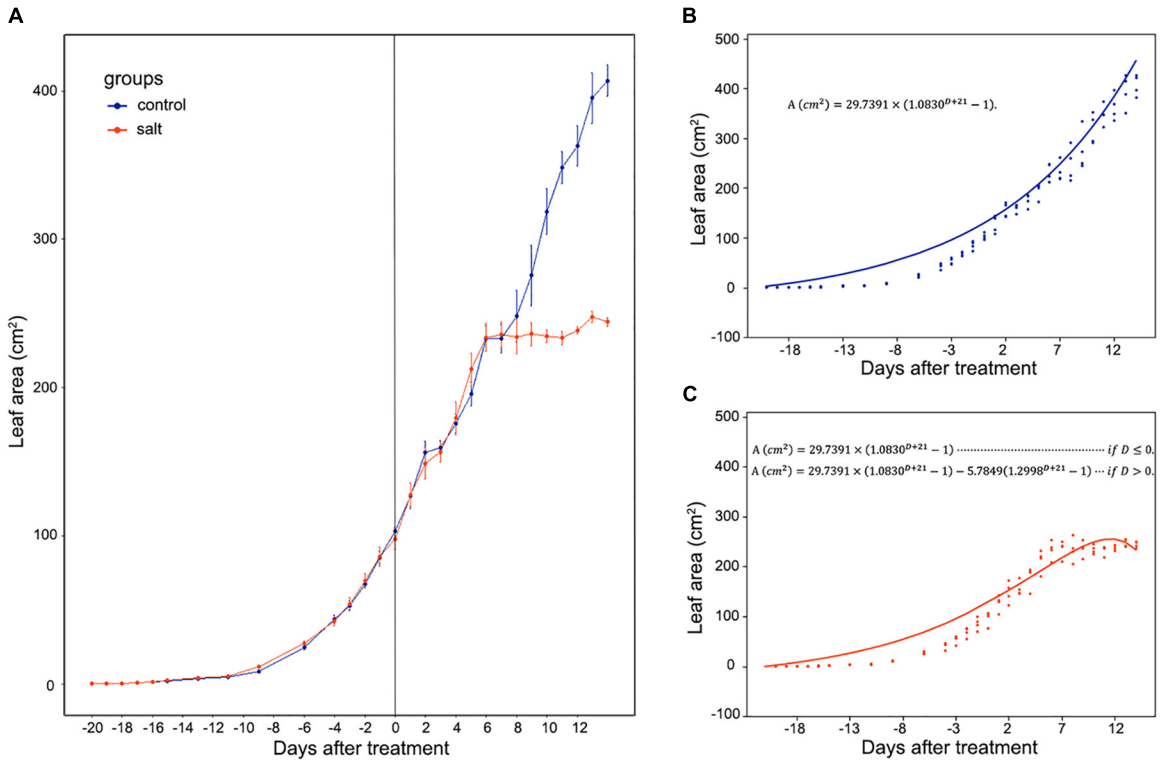

FIGURE 2 | Whole leaf area measurement of *M. crystallinum* seedlings during their growth for 42 days. The salt treatment began at day 0. **(A)** Leaf area changes in control group (blue line) and salt-treated group (orange line) of *M. crystallinum*. **(B)** Simulation of *M. crystallinum* growth of the control group. The line represents the simulation and the dots represent exact leaf area of each biological replicate. **(C)** Simulation of *M. crystallinum* growth of the salt treated group. The line represents the simulation and the dots represent exact leaf area of each biological replicate.

10 days of treatment, so did the size of the stomatal guard cells (**Supplementary Figure S2**).

Leaf Succulence and RWC

As shown in **Figure 4A**, leaf succulence of both control and salt-treated *M. crystallinum* seedlings increased slowly from 0.12 to 0.16 g cm^{-2} during the beginning 5 days. In salt-treated *M. crystallinum*, leaf succulence was significantly higher than the control group after 5 days of the salt-treatment, and it increased to 0.18 g cm^{-2} after day 11. The RWC data showed *M. crystallinum* seedlings had an increase in water storage during the leaf growth from 62.5 to 80% (**Figure 4B**), which provides a strong support of the increasing leaf succulence of *M. crystallinum* at this developmental stage. Unlike the leaf succulence result, RWC of the salt-treated plants was significantly higher than control plants from day 4 to day 11, but it dropped to similar levels as control plants after day 12.

MDA Content

The MDA contents of *M. crystallinum* leaves were in a range of 0.8–1.5 nmol g^{-1} fresh weight in the control group. From day 7 after the salt treatment, the MDA contents began to show significant increases compared to the control group. Overall, the salt-treated group had higher MDA contents than the control group, and they were in a range of 1.4–2.1 nmol g^{-1} fresh weight after day 7 of the salt treatment (**Figure 5**).

DISCUSSION

Mesembryanthemum crystallinum is a well-known facultative CAM plant, which can change its stomatal movement pattern and gas exchange profile [e.g., from direct Rubisco-mediated CO_2 assimilation to PEPC-mediated assimilation (Silvera et al., 2010; Winter and Holtum, 2014)]. Stomatal conductance mediated by guard cell circadian cycle needs to be synchronized with the mesophyll CAM cycle and the associated metabolite changes (Gallé et al., 2015; Males and Griffiths, 2017). It was reported that a relatively low nocturnal temperature may help to optimize the CAM activity (Yamori et al., 2014). To facilitate the C_3 to CAM transition after salt treatment, we applied a consistent environment with relatively high diurnal temperature (26°C) and low nocturnal temperature (18°C). Under our conditions, the *M. crystallinum* seedlings showed normal C_3 growth and development (**Figure 1**; Adams et al., 1998). When salt treatment was applied, the seedlings continue to grow at the similar rate as control for 6 days, and thereafter slowed down the growth and leaf expansion (**Figures 1**, **2**). The phenotypic data reflect the shift from C_3 to CAM, and the shift clearly compromised the seedling

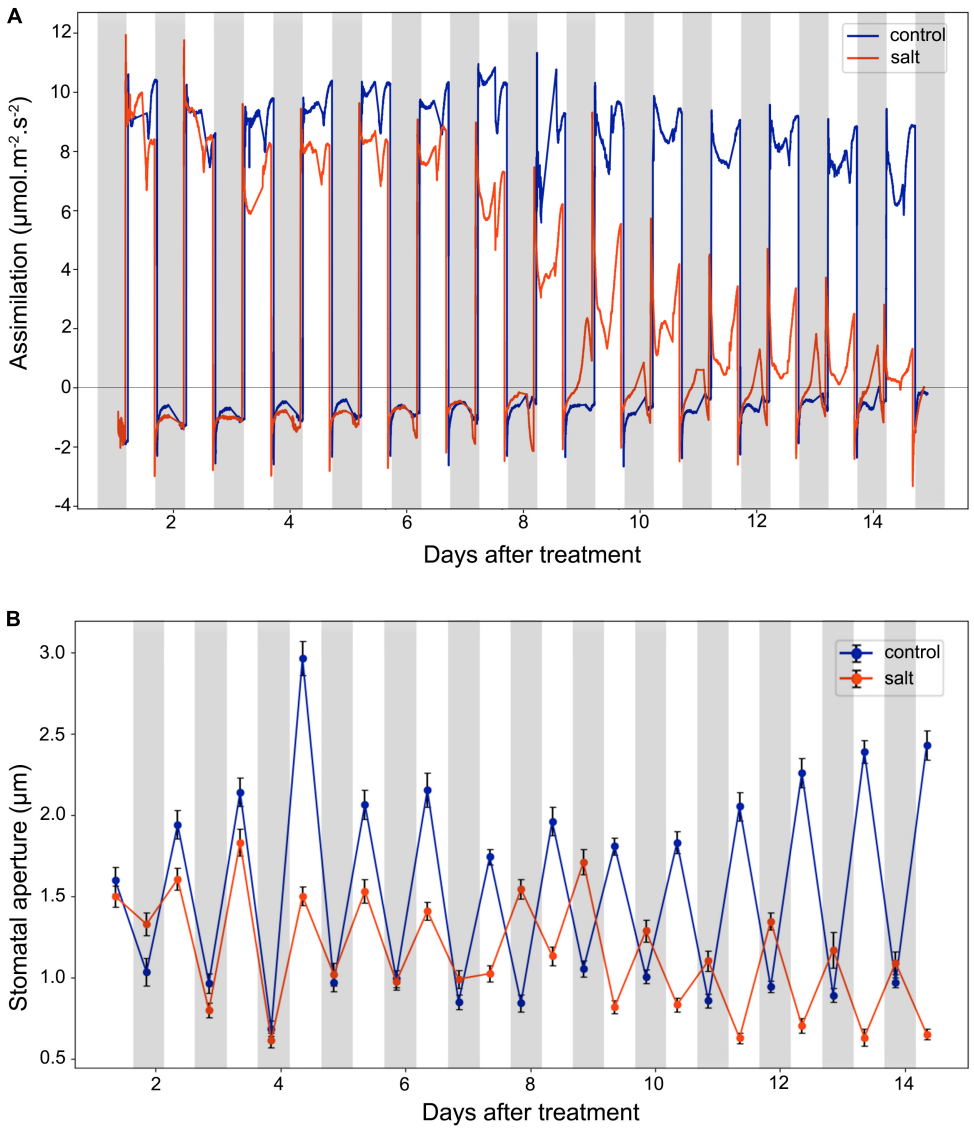

FIGURE 3 | Leaf CO_2 assimilation and stomatal aperture changes in the control and salt-treated *M. crystallinum* seedlings. **(A)** Leaf CO_2 gas exchange and **(B)** stomatal movement behavior. The blue line represents the control group and the orange line represents the salt-treated group. The gray bars represent the night time and the white bars represent the day time. The error bar represents standard error. The data were obtained from three biological replicates.

growth and development. How salt stress triggers the transition from C_3 to CAM is still a mystery. Although it is challenging to differentiate salt stress responses from the specific responses leading to the C_3 to CAM transition, studying the changes in diel patterns at molecular and physiological levels may provide important insights into the CAM initiation.

According to the net CO_2 exchange data, *M. crystallinum* plants were determined to switch from C_3 to CAM under drought stress and revert to C_3 upon re-introduction of water to plants (Winter and Holtum, 2014). Our gas exchange data showed the transition from C_3 to CAM under salt stress took place from 6 to 8 days after salt treatment and the CO_2 exchange values were consistent with those reported in Winter and Holtum (2014) at both the C_3 stage and CAM stage (**Figure 3**). Interestingly, leaf succulence and RWC increased in the salt-treatment group (**Figure 4**) before the gas exchange value had significant changes between the salt-treatment group and the control group (**Figure 3A**). These results seem to suggest succulence may be a prerequisite for the development of CAM photosynthesis (Bohnert and Cushman, 2000). During and after the C_3 to CAM transition of the salt-treated seedlings, the leaf succulence maintained at higher levels than control seedlings. This result is consistent with the report that another facultative CAM plant *Ananas comosus* (L.) Merr. var MD-2 showed high leaf succulence after 4 weeks in CAM-inducing conditions (Aragón et al., 2013). Leaf succulence due to enlarged vacuoles contributes to not only malic acid storage, but also water storage under drought or salt stress. In addition, tightly packed

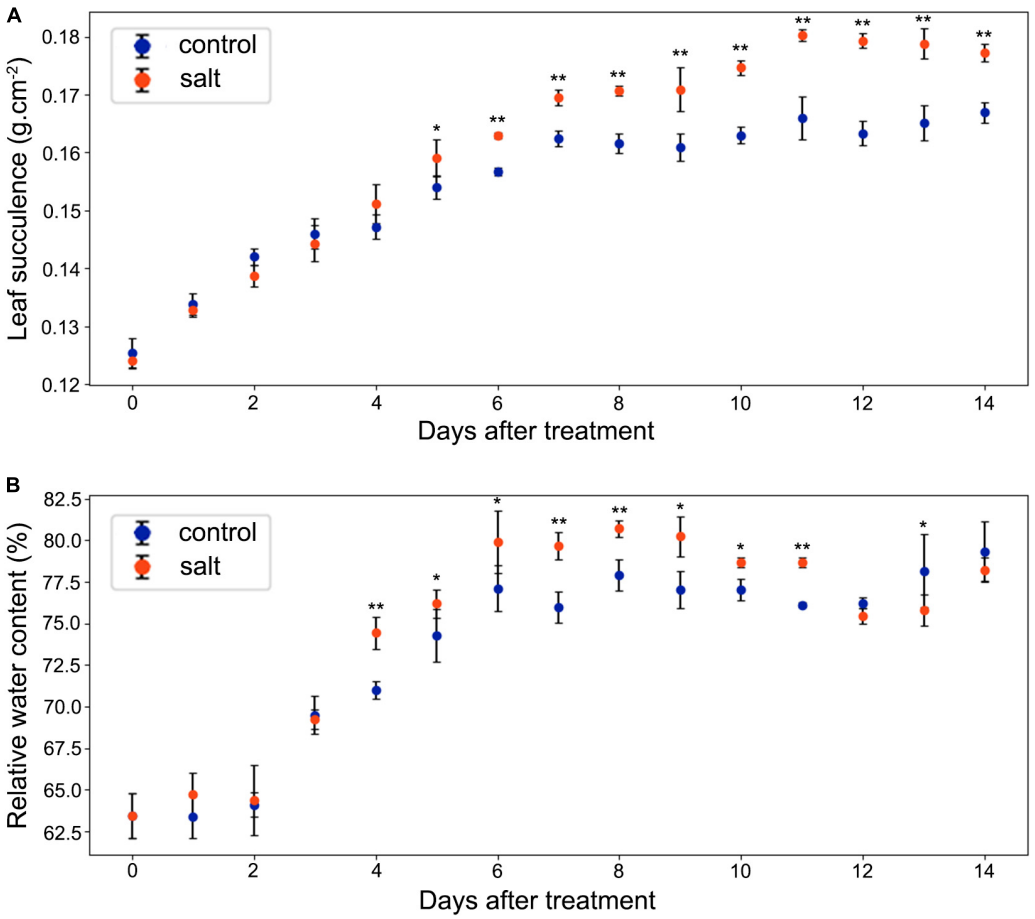

FIGURE 4 | Changes in leaf succulence and relative water content (RWC) in the control and salt-treated *M. crystallinum* seedlings. **(A)** Leaf succulence. The blue dots represent the control group and the orange dots represent the salt-treated group. The error bar represents standard error. **(B)** RWC. The blue dots represent the control group and the orange dots represent the salt-treated group. The error bar represents standard error. An asterisk indicates a Student's *t*-test ($p < 0.05$) and two asterisks indicate a Student's *t*-test ($p < 0.01$). The data were obtained from four biological replicates.

large cells restrict CO_2 efflux and enhance CO_2 assimilation efficiency (Aragón et al., 2012, 2013). It should be noted that succulence and CAM are closely associated across the tree of life, although some CAM species (e.g., bromeliads) do not have succulent photosynthetic organs (De Santo et al., 1983; Ogburn and Edwards, 2013; Edwards, 2019).

In this study, we observed that significant changes in stomatal movement behavior occurred in the night of day 7 after the salt treatment (**Figure 3B**). This inverted stomatal movement behavior is essential for the nocturnal carbon fixation of CAM plants (Males and Griffiths, 2017; Edwards, 2019). Currently, there is little experimental data on the signaling pathways that control the inverse stomatal pattern in CAM plants. What drives the inversed stomatal behavior has been under debate. It was proposed that the nocturnal stomatal opening is mediated by the low CO_2 concentration in the intercellular air space due to the PEPC activity, i.e., stomatal opening is driven by the nocturnal CO_2 fixation (Cockburn, 1979; Griffiths et al., 2007; von Caemmerer and Griffiths, 2009). There are limited experimental data providing correlation but not direct cause and effect (Cockburn, 1979; Kebeish et al., 2012). For example, expression of a *Solanum tuberosum PEPC* under the control of a dark-induced promoter Din 10 in Arabidopsis resulted in greater stomatal conductance, respiration, and transpiration in dark-adapted leaves than wild-type plants (Kebeish et al., 2012). However, there is no evidence to imply the cause of stomatal movement is CO_2. In fact, humidity should also be considered as humidity is generally high in the night (Meinzer, 2002). Other data appear to refute the role of CO_2 in CAM induction. For example, in two facultative species, *Clusia pratensis* and *M. crystallinum* at C_3 state, 100 or 800 ppm CO_2 treatment during daytime showed no effect on nocturnal CO_2 exchange, i.e., no CAM induction (Winter, 1979; Winter and Holtum, 2014). These data suggest that CO_2 concentration may not be the CAM inducing factor. In addition, mesophyll-derived apoplastic malate was recently reported to link stomatal regulation with mesophyll cell metabolism (Medeiros et al., 2016).

High salinity can induce oxidative stress in plants (AbdElgawad et al., 2016). In this study, we measured MDA content as an indication of oxidative stress. Interestingly,

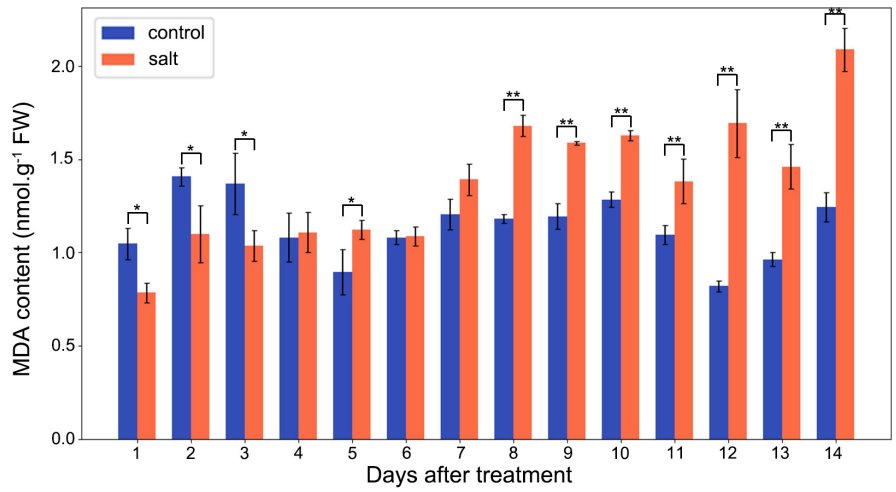

FIGURE 5 | Changes in MDA contents in the control and salt-treated *M. crystallinum* seedlings. The blue dots represent the control group and the orange dots represent the salt-treated group. The error bar represents standard error. An asterisk indicates a Student's *t*-test ($p < 0.05$) and two asterisks indicate a Student's *t*-test ($p < 0.01$). The data were obtained from four biological replicates.

MDA content did not significantly increase until day 8 after salt treatment, i.e., before the initiation of the transition from C_3 to CAM photosynthesis (**Figure 5**). Previous studies indicated that oxidative stress could facilitate the switch from C_3 to CAM (Aragón et al., 2012, 2013). After 8 days of salt treatment, the relatively high MDA content was maintained in the *M. crystallinum* seedlings, suggesting oxidative stress may be part of the CAM development and maintenance. However, it should be noted that the difference between the control group and the salt-treatment group was similar to some of the non-CAM halophytes (Ksouri et al., 2007; Amor et al., 2005), or significantly smaller than some non-halophytes (Liang, 1999; Sreenivasulu et al., 1999). Since reactive oxygen species and oxidative stress affect cellular redox state, and many biological processes including photosynthesis are regulated by redox, future studies focusing on redox regulation [e.g., using redox proteomics and metabolomics (David et al., 2019; Yu et al., 2020)] can be expected to reveal molecular mechanisms underlying the C_3 to CAM transition in *M. crystallinum* plants.

CONCLUSION

Mesembryanthemum crystallinum is a facultative CAM plant, which can switch from C_3 photosynthesis to CAM photosynthesis under salt stress treatment. Based on a combination of phenotypic and physiological measurements (including leaf area, gas exchange, stomatal aperture, leaf succulence, RWC and MDA contents), we found the critical transition time for *M. crystallinum* seedlings to shift from C_3 to CAM photosynthesis is between 6 and 8 days of salt treatment. The quick transition to CAM photosynthesis is important for the seedlings to establish tolerance to environmental stresses with CAM characteristics, such as high WUE and inverted stomatal behavior. Our study has laid a foundation for further experiments to determine the molecular switches underlying the rapid C_3 to CAM transition, and thereby engineering CAM into C_3 crops for enhanced WUE and stress tolerance.

DATA AVAILABILITY STATEMENT

All datasets generated for this study are included in the article/**Supplementary Material**.

AUTHOR CONTRIBUTIONS

QG, JT, and SC conceived and designed the research. QG, BT, and TK performed the experiments. QG, BT, and SC analyzed the data and wrote the manuscript draft. JT and SC finalized the manuscript for submission. All authors approved the manuscript.

FUNDING

This work was supported by the China Scholarship Council (201706320126), the National Natural Science Foundation of China (No. 81872973), the Zhejiang Provincial Science and Technology Planning Project (No. 2016C04005), and the University of Florida internal funds.

ACKNOWLEDGMENTS

The authors thank Ms. Hope Hersh from Plant Molecular and Cellular Biology program at the University of Florida and Mr. Daniel Chen from Honors College at the University of South Florida for editing the manuscript.

SUPPLEMENTARY MATERIAL

The Supplementary Material for this article can be found online at: https://www.frontiersin.org/articles/10.3389/fpls.2020.00283/full#supplementary-material

FIGURE S1 | Development of a method for measuring leaf area. **(A)** Positioning of the plant and 1 cm^2 reference spot. **(B)** Original image taken by a digital camera. **(C)** Border outline of the leaves, as a quality control for the pixel selection. **(D)** Total reference pixels detected in the image, and white pixels represent the reference pixels. **(E)** Total leaf pixels detected in the plant image; light yellow pixels represent the pixels detected in green.

FIGURE S2 | Stomatal aperture changes in day and night during the C_3 to CAM transition of *M. crystallinum* seedlings in the control and the salt groups. The data were collected at 4 am representing night and 4 pm representing day.

FILE S1 | A python script for detecting green pixels as leaf pixels, with black pixels as reference pixels to calculate the leaf area by green pixels * actual reference area divided by the reference pixels.

REFERENCES

AbdElgawad, H., Zinta, G., Hegab, M. M., Pandey, R., Asard, H., and Abuelsoud, W. (2016). High salinity induces different oxidative stress and antioxidant responses in maize seedlings organs. *Front. Plant Sci.* 7:276. doi: 10.3389/fpls.2016.00276

Abraham, P. E., Yin, H., Borland, A. M., Weighill, D., Lim, S. D., De Paoli, H. C., et al. (2016). Transcript, protein and metabolite temporal dynamics in the CAM plant Agave. *Nat. Plants* 2:16178. doi: 10.1038/nplants.2016.178

Adams, P., Nelson, D. E., Yamada, S., Chmara, W., JensenN, R. G., Bohnert, H. J., et al. (1998). Growth and development of *Mesembryanthemum crystallinum* (Aizoaceae). *New Phytol.* 138, 171–190. doi: 10.1046/j.1469-8137.1998.00111.x

Agarie, S., Shimoda, T., Shimizu, Y., Baumann, K., Sunagawa, H., Kondo, A., et al. (2007). Salt tolerance, salt accumulation, and ionic homeostasis in an epidermal bladder-cell-less mutant of the common ice plant *Mesembryanthemum crystallinum*. *J. Exp. Bot.* 58, 1957–1967. doi: 10.1093/jxb/erm057

Amor, N. B., Hamed, K. B., Debez, A., Grignon, C., and Abdelly, C. (2005). Physiological and antioxidant responses of the perennial halophyte *Crithmum maritimum* to salinity. *Plant Sci.* 168, 889–899. doi: 10.1016/j.plantsci.2004.11.002

Aragón, C., Carvalho, L., González, J., Escalona, M., and Amâncio, S. (2012). The physiology of ex vitro pineapple (*Ananas comosus* L. Merr. var MD-2) as CAM or C3 is regulated by the environmental conditions. *Plant Cell Rep.* 31, 757–769. doi: 10.1007/s00299-011-1195-7

Aragón, C., Pascual, P., González, J., Escalona, M., Carvalho, L., and Amancio, S. (2013). The physiology of ex vitro pineapple (*Ananas comosus* L. Merr. var MD-2) as CAM or C3 is regulated by the environmental conditions: proteomic and transcriptomic profiles. *Plant Cell Rep.* 32, 1807–1818. doi: 10.1007/s00299-013-1493-3

Bohnert, H. J., and Cushman, J. C. (2000). The ice plant cometh: lessons in abiotic stress tolerance. *J. Plant Growth Regul.* 19, 334–346. doi: 10.1007/s003440000033

Chaves, M. M., Flexas, J., and Pinheiro, C. (2009). Photosynthesis under drought and salt stress: regulation mechanisms from whole plant to cell. *Ann. Bot.* 103, 551–560. doi: 10.1093/aob/mcn125

Chiang, C. P., Yim, W. C., Sun, Y. H., Ohnishi, M., Mimura, T., Cushman, J. C., et al. (2016). Identification of ice plant (*Mesembryanthemum crystallinum* L.) microRNAs using RNA-Seq and their putative roles in high salinity responses in seedlings. *Front. Plant Sci.* 7:1143. doi: 10.3389/fpls.2016.01143

Cockburn, W. (1979). Relationships between stomatal behavior and internal carbon dioxide concentration in crassulacean acid metabolism plants. *Plant Physiol.* 63, 1029–1032. doi: 10.1104/pp.63.6.1029

Cosentino, C., Di Silvestre, D., Fischer-Schliebs, E., Homann, U., De Palma, A., Comunian, C., et al. (2013). Proteomic analysis of *Mesembryanthemum crystallinum* leaf microsomal fractions finds an imbalance in V-ATPase stoichiometry during the salt-induced transition from C3 to CAM. *Biochem. J.* 450, 407–415. doi: 10.1042/BJ20121087

Cushman, J. C., Michalowski, C. B., and Bohnert, H. J. (1990). Developmental control of crassulacean acid metabolism inducibility by salt stress in the common ice plant. *Plant Physiol.* 94, 1137–1142. doi: 10.1104/pp.94.3.1137

David, L., Kang, J., and Chen, S. (2019). Targeted metabolomics of plant hormones and redox metabolites in stomatal immunity. *Methods Mol. Biol.* 2085, 79–92. doi: 10.1007/978-1-0716-0142-6_6

De Santo, A. V., Alfani, A., Russo, G., and Fioretto, A. (1983). Relationship between CAM and succulence in some species of Vitaceae and Piperaceae. *Bot. Gaz.* 144, 342–346. doi: 10.1086/337382

Edwards, E. J. (2019). Evolutionary trajectories, accessibility and other metaphors: the case of C4 and CAM photosynthesis. *New Phytol.* 223, 1742–1755. doi: 10.1111/nph.15851

Eisele, J. F., Fäßler, F., Bürgel, P. F., and Chaban, C. (2016). A rapid and simple method for microscopy-based stomata analyses. *PLoS One* 11:e0164576. doi: 10.1371/journal.pone.0164576

Gallé, A., Lautner, S., Flexas, J., and Fromm, J. (2015). Environmental stimuli and physiological responses: the current view on electrical signalling. *Environ. Exp. Bot.* 114, 15–21. doi: 10.1016/j.envexpbot.2014.06.013

González, L., and Gonzalez-Vilar, M. (2001). "Determination of relative water content," in *Handbook of Plant Ecophysiology Techniques*, ed. M. J. R. Roger (Dordrecht: Springer), 207–212. doi: 10.1007/0-306-48057-3_14

Griffiths, H., Cousins, A. B., Badger, M. R., and von Caemmerer, S. (2007). Discrimination in the dark. Resolving the interplay between metabolic and physical constraints to phosphoenolpyruvate carboxylase activity during the crassulacean acid metabolism cycle. *Plant Physiol.* 143, 1055–1067. doi: 10.1104/pp.106.088302

Hoagland, D. R., and Arnon, D. I. (1950). The water-culture method for growing plants without soil. *Circ. Calif. Agric. Exp. Station* 347:32.

Kebeish, R., Niessen, M., Oksaksin, M., Blume, C., and Peterhaensel, C. (2012). Constitutive and dark-induced expression of *Solanum tuberosum* phosphoenolpyruvate carboxylase enhances stomatal opening and photosynthetic performance of *Arabidopsis thaliana*. *Biotechnol. Bioeng.* 109, 536–544. doi: 10.1002/bit.23344

Ksouri, R., Megdiche, W., Debez, A., Falleh, H., Grignon, C., and Abdelly, C. (2007). Salinity effects on polyphenol content and antioxidant activities in leaves of the halophyte *Cakile maritima*. *Plant Physiol. Biochem.* 45, 244–249. doi: 10.1016/j.plaphy.2007.02.001

Lawrence, S. II, Pang, Q., Kong, W., and Chen, S. (2018). Stomata tape-peel: an improved method for guard cell sample preparation. *J. Vis. Exp.* 137:e57422. doi: 10.3791/57422

Liang, Y. (1999). Effects of silicon on enzyme activity and sodium, potassium and calcium concentration in barley under salt stress. *Plant Soil* 209:217.

Males, J. (2017). Secrets of succulence. *J. Exp. Bot.* 68, 2121–2134. doi: 10.1093/jxb/erx096

Males, J., and Griffiths, H. (2017). Stomatal biology of CAM plants. *Plant Physiol.* 174, 550–560. doi: 10.1104/pp.17.00114

Medeiros, D. B., Martins, S. C., Cavalcanti, J. H., Daloso, D. M., Martinoia, E., Nunes-Nesi, A., et al. (2016). Enhanced photosynthesis and growth in atquac1 knockout mutants are due to altered organic acid accumulation and an increase in both stomatal and mesophyll conductance. *Plant Physiol.* 170, 86–101. doi: 10.1104/pp.15.01053

Meinzer, F. C. (2002). Co-ordination of vapour and liquid phase water transport properties in plants. *Plant Cell Environ.* 25, 265–274. doi: 10.1046/j.1365-3040.2002.00781.x

Munns, R., and Tester, M. (2008). Mechanisms of salinity tolerance. *Annu. Rev. Plant Biol.* 59, 651–681.

Ogburn, R. M., and Edwards, E. J. (2013). Repeated origin of three-dimensional leaf venation releases constraints on the evolution of succulence in plants. *Curr. Biol.* 23, 722–726. doi: 10.1016/j.cub.2013.03.029

Oh, D. H., Barkla, B. J., Vera-Estrella, R., Pantoja, O., Lee, S. Y., Bohnert, H. J., et al. (2015). Cell type-specific responses to salinity–the epidermal bladder cell transcriptome of *Mesembryanthemum crystallinum*. *New Phytologist* 207, 627–644. doi: 10.1111/nph.13414

Silvera, K., Neubig, K. M., Whitten, W. M., Williams, N. H., Winter, K., and Cushman, J. C. (2010). Evolution along the crassulacean acid metabolism continuum. *Funct. Plant Biol.* 37, 995–1010.

Sreenivasulu, N., Ramanjulu, S., Ramachandra-Kini, K., Prakash, H. S., Shekar-Shetty, H., Savithri, H. S., et al. (1999). Total peroxidase activity and peroxidase isoforms as modified by salt stress in two cultivars of fox-tail millet with differential salt tolerance. *Plant Sci.* 141, 1–9. doi: 10.1016/s0168-9452(98)00204-0

Vinocur, B., and Altman, A. (2005). Recent advances in engineering plant tolerance to abiotic stress: achievements and limitations. *Curr. Opin. Biotechnol* 16, 123–132. doi: 10.1016/j.copbio.2005.02.001

von Caemmerer, S., and Griffiths, H. (2009). Stomatal responses to CO2 during a diel Crassulacean acid metabolism cycle in Kalanchoe daigremontiana and Kalanchoe pinnata. *Plant Cell Environ.* 32, 567–576. doi: 10.1111/j.1365-3040.2009.01951.x

Wang, B., Bian, B., Wang, C., Li, C., Fang, H., Zhang, J., et al. (2019). Hydrogen gas promotes the adventitious rooting in cucumber under cadmium stress. *PLoS One* 14:e0212639. doi: 10.1371/journal.pone.0212639

Winter, K. (1979). Effect of different CO2 regimes on the induction of crassulacean acid metabolism in *Mesembryanthemum crystallinum*. *Austral. J. Plant Physiol.* 6, 589–594.

Winter, K., and Holtum, J. A. (2014). Facultative crassulacean acid metabolism (CAM) plants: powerful tools for unravelling the functional elements of CAM photosynthesis. *J. Exp. Bot.* 65, 3425–3441. doi: 10.1093/jxb/eru063

Winter, K., Holtum, J. A., and Smith, J. A. C. (2015). Crassulacean acid metabolism: a continuous or discrete trait? *New Phytol.* 208, 73–78. doi: 10.1111/nph.13446

Xiao, R. F., Alexander, J. I. D., and Rosenberger, F. (1988). Morphological evolution of growing crystals: A Monte Carlo simulation. *Phys. Rev. A* 38:2447. doi: 10.1103/physreva.38.2447

Yamori, W., Hikosaka, K., and Way, D. A. (2014). Temperature response of photosynthesis in C3, C4, and CAM plants: temperature acclimation and temperature adaptation. *Photosynth. Res.* 119, 101–117. doi: 10.1007/s11120-013-9874-6

Yu, J., Li, Y., Qin, Z., Guo, S., Li, Y., Miao, Y., et al. (2020). Plant chloroplast stress response: insights from thiol redox proteomics. *Antioxid. Redox Signal.* doi: 10.1089/ars.2019.7823 [Epub ahead of print].

Conflict of Interest: The authors declare that the research was conducted in the absence of any commercial or financial relationships that could be construed as a potential conflict of interest.

frontiers in Plant Science

ORIGINAL RESEARCH
published: 08 May 2020
doi: 10.3389/fpls.2020.00542

ROS of Distinct Sources and Salicylic Acid Separate Elevated CO_2-Mediated Stomatal Movements in Arabidopsis

*Jingjing He[1†], Ruo-Xi Zhang[1†], Dae Sung Kim[1], Peng Sun[1], Honggang Liu[1], Zhongming Liu[1], Alistair M. Hetherington[2] and Yun-Kuan Liang[1]**

[1] State Key Laboratory of Hybrid Rice, Department of Plant Science, College of Life Sciences, Wuhan University, Wuhan, China, [2] School of Biological Sciences, Life Sciences Building, University of Bristol, Bristol, United Kingdom

Elevated CO_2 (eCO_2) often reduces leaf stomatal aperture and density thus impacts plant physiology and productivity. We have previously demonstrated that the Arabidopsis BIG protein distinguishes between the processes of eCO_2-induced stomatal closure and eCO_2-inhibited stomatal opening. However, the mechanistic basis of this action is not fully understood. Here we show that eCO_2-elicited reactive oxygen species (ROS) production in *big* mutants was compromised in stomatal closure induction but not in stomatal opening inhibition. Pharmacological and genetic studies show that ROS generated by both NADPH oxidases and cell wall peroxidases contribute to eCO_2-induced stomatal closure, whereas inhibition of light-induced stomatal opening by eCO_2 may rely on the ROS derived from NADPH oxidases but not from cell wall peroxidases. As with JA and ABA, SA is required for eCO_2-induced ROS generation and stomatal closure. In contrast, none of these three signals has a significant role in eCO_2-inhibited stomatal opening, unveiling the distinct roles of plant hormonal signaling pathways in the induction of stomatal closure and the inhibition of stomatal opening by eCO_2. In conclusion, this study adds SA to a list of plant hormones that together with ROS from distinct sources distinguish two branches of eCO_2-mediated stomatal movements.

Keywords: elevated CO_2, stomatal movement, plant hormones, reactive oxygen species, NADPH oxidases, cell wall peroxidases

OPEN ACCESS

Edited by:
Scott McAdam, Purdue University, United States

Reviewed by:
Yunqing Yu, Donald Danforth Plant Science Center, United States
Amanda A. Cardoso, Universidade Federal de Viçosa, Brazil

***Correspondence:**
Yun-Kuan Liang
ykliang@whu.edu.cn

† These authors have contributed equally to this work

Specialty section:
This article was submitted to Plant Development and EvoDevo, a section of the journal Frontiers in Plant Science

Received: *14 December 2019*
Accepted: *09 April 2020*
Published: *08 May 2020*

Citation:
He J, Zhang R-X, Kim DS, Sun P, Liu H, Liu Z, Hetherington AM and Liang Y-K (2020) ROS of Distinct Sources and Salicylic Acid Separate Elevated CO_2-Mediated Stomatal Movements in Arabidopsis. Front. Plant Sci. 11:542. doi: 10.3389/fpls.2020.00542

INTRODUCTION

Stomata formed by a pair of guard cells regulate gas exchanges between plants and the atmosphere. Guard cells sense and integrate both extra- and intracellular signals, such as light, temperature, carbon dioxide (CO_2), plant hormones, leading to plant adaptive responses

Abbreviations: ABA, abscisic acid; CA, carbonic anhydrase; CO_2, carbon dioxide; eCO_2, elevated carbon dioxide; DPI, diphenylene iodinium; DMSO, N,N-dimethylsphingosine; H_2O_2, hydrogen peroxide; H_2DCF-DA, 2′,7′-dichlorodihydrofluorescein diacetate; JA, jasmonic acid; MES, 2-[N]-morpholinnoethane sulfonic acid; NADPH, nicotinamide adenine dinucloetide phosphate; NO, nitric oxide; PAMP, pathogen-associated molecular pattern; PAOs, polyamine oxidases; PCR, polymerase chain reaction; PRXs, peroxidases; RBOH, respiratory burst oxidase; ROS, reactive oxygen species; RT-PCR, reverse transcription-polymerase chain reaction; SHAM, salicylhydroxamic acid; SA, salicylic acid; SAR, systemic acquired resistance; WT, wild type.

(Hetherington and Woodward, 2003; Murata et al., 2015; He and Liang, 2018). The continuing rise of atmospheric CO_2 can profoundly impact plant physiology and crop yield potential via stomata, as elevated CO_2 (eCO_2) concentration in the atmosphere reduces leaf stomatal aperture and density in many species including crop plants (Woodward, 1987; Assmann, 1993; Keenan et al., 2013; Xu et al., 2016). Understanding CO_2 signaling in guard cells is important in the context of breeding "climate change ready" crop varieties with improved agricultural performance and nutritional content (Kim et al., 2010; Myers et al., 2014; Caine et al., 2018; Zhang et al., 2018). In guard cells, CO_2 signaling starts from CO_2 conversion to bicarbonate (HCO_3^-) by βCA1 (beta Carbonic Anhydrase 1) and βCA4, followed by activation of MATE type transporter RHC1 (Resistance to High CO_2), MPK4 (Mitogen-Activated Protein Kinase 4) and MPK12, subsequently leading to inhibition of HT1 (High Leaf Temperature 1), which phosphorylates and inactivates OST1 (Open Stomata 1). Repression of HT1 facilitates S-type anion channel activation by OST1 to mediate the anion effluxes resulting in stomatal closure (Hashimoto et al., 2006; Hu et al., 2010; Tian et al., 2015; Hashimoto-Sugimoto et al., 2016; Hõrak et al., 2016; Jakobson et al., 2016; Tõldsepp et al., 2018; Zhang et al., 2018).

As typified by the abscisic acid (ABA) receptors, the components in the stomatal closure induction and the stomatal opening inhibition are not necessarily the same (Assmann, 1993; Mishra et al., 2006; Yin et al., 2013; Dittrich et al., 2019). We have recently identified the Arabidopsis BIG protein as a novel component involved in eCO_2-induced stomatal closure but not of eCO_2-inhibited light-induced stomatal opening (He et al., 2018). BIG is involved in diverse processes including auxin transport, light and hormonal signaling, vesicle trafficking, endocytosis, phosphate deficiency tolerance, and the dynamic adjustment of circadian period (Li et al., 1994; Ruegger et al., 1997; Gil et al., 2001; Kanyuka et al., 2003; López-Bucio et al., 2005; Paciorek et al., 2005; Yamaguchi et al., 2007; Hearn et al., 2018). Mutations in the Arabidopsis *BIG* gene suppress eCO_2-induced stomatal closure due to the disrupted activity of S-type ion channels (He et al., 2018). Direct channel regulation has been demonstrated to be insufficient to explain the strong eCO_2-induced stomatal closing response in Arabidopsis (Wang et al., 2016). More recently, it has been shown that *big* mutants are more susceptible to bacterial pathogens that gain entry to the plant through stomata (Zhang et al., 2019). These findings point to the need to gain a better understanding of how BIG distinguishes two distinct processes of stomatal movement in response to eCO_2. Given that reactive oxygen species (ROS) play a significant role in various signaling processes, and the results of investigations have revealed a role for BIG in redox signaling (Rhee et al., 2000; Gil et al., 2001; Grek et al., 2013; Song et al., 2014; Parsons et al., 2015; Zhang et al., 2019), we hypothesized that ROS production has a central role to play in defining stomatal responses to eCO_2.

ROS including hydrogen peroxide (H_2O_2) and superoxide (O_2^-) are widely produced in different cellular compartments in plants and have been recognized as a major regulator in various aspects of plant life such as stomatal development and movement, particularly under different abiotic and biotic stress conditions (McAinsh et al., 1996; Neill et al., 2002; Foyer and Noctor, 2005; Song et al., 2014; Sierla et al., 2016). In Arabidopsis, apoplastic ROS are mainly produced by plasma membrane-localized NADPH oxidases and cell wall peroxidases (Song et al., 2014; Murata et al., 2015; Singh et al., 2017), and the activities of these different types of enzymes are strongly inhibited by diphenylene iodonium (DPI) and salicylhydroxamic acid (SHAM), respectively (Allan and Fluhr, 1997; Pei et al., 2000; Mori et al., 2001; Khokon et al., 2011; Miura et al., 2013). The evolution and maintenance of different sources for ROS production is most likely due to the requirement for intricate control of oxidative signaling, given the fact that ROS can be cytotoxic and mutagenic and for their proper function in signaling their production must be tightly regulated both temporally and spatially (Mittler, 2017).

ABA and jasmonate (JA) induce ROS accumulation in guard cells via the activities of two NADPH oxidases, RBOHD and RBOHF (Torres et al., 2002, 2006; Kwak et al., 2003; Suhita et al., 2004), whereas salicylic acid (SA) likely regulates ROS homeostasis via the peroxidases-catalyzed reactions (Mori et al., 2001; Khokon et al., 2011), and the inhibition of catalase and ascorbate peroxidase (Chen et al., 1993; Durner and Klessig, 1995). eCO_2-induced stomatal closure is suppressed in the *rbohDrbohF* double mutants (Kolla et al., 2007; Chater et al., 2015). Peroxidases are bifunctional enzymes, through two possible catalytic cycles, hydroxylic and peroxidative, to generate or detoxify and regulate H_2O_2 levels. For example, during the hydroxylic cycle, the peroxidases catalyze the generation of ·OH and HOO· from H_2O_2 by two different routes (Passardi et al., 2004). In Arabidopsis, there are 73 isoforms of cell wall peroxidases (Tognolli et al., 2002; Passardi et al., 2006). Two cell wall peroxidase-encoding genes, *PRX33* and *PRX34*, which are highly and preferentially expressed in guard cells compared with other PRXs members according to Genevestigator (an available microarray database[1]), are widely involved in H_2O_2 production against fungi-, bacteria-, SA-, and flg22-induced stomatal closure (Bindschedler et al., 2006; Daudi et al., 2012; O'Brien et al., 2012a,b; Arnaud et al., 2017). Notably, SA-mediated ROS production and stomatal closure are not impaired by DPI or in *rbohDrbohF* double mutant (Khokon et al., 2011). In contrast to NADPH oxidases, the importance of ROS-producing peroxidases to plant adaptive responses, particularly their function in regulating eCO_2-mediated stomatal movement, has largely been overlooked.

In this study, by combining pharmacological and genetic approaches, we reveal distinct roles of ROS-producing peroxidases and NADPH oxidases for eCO_2-induced stomatal movements. We also found that endogenous SA and SA-signaling components are required for eCO_2-induced stomatal closure. Neither ABA, JA, or SA are involved in regulating eCO_2-inhibited stomatal opening. In conclusion, our data suggest that plant hormones and ROS from distinct sources selectively mediate different stomatal CO_2 responses, and shed new light on ROS action and the CO_2 signaling network.

[1]https://www.genevestigator.com

MATERIALS AND METHODS

Plant Material and Growth Conditions

All Arabidopsis (*Arabidopsis thaliana* L.) lines used in this study were in the Columbia background (Col-0). Seeds of *sid2-2*, *npr1-1*, *npr3npr4,* and *rbohDrbohF* were kindly provided by Drs Shunping Yan and Honghong Hu (Huazhong Agricultural University, China). Seeds of *prx33-3* and *prx34-2* was a gift from Dr. Ildoo Hwang (Pohang University of Science and Technology, Korea). More information of the mutants used in this study are shown in **Supplementary Table S1**. Seed germination and plant growth were essentially carried out as described in He et al. (2018). For stomatal aperture bioassays, seeds were surface-sterilized and sown on half-strength Murashige and Skoog (MS) medium plates containing 0.6% agar and 1% sucrose. After stratification (4°C in the dark for 2 days), the plates were transferred to the green house at 22°C/18°C (day/night) with 10 h/14 h (light/dark) photoperiod cycle (light intensity 120 μ moles photons $m^{-2}s^{-1}$), 50% relative humidity, at ambient CO_2, approximate 450 ppm. Ten days old plants were transferred to soil and grown in the same green house for the future experiments. For the stomatal bioassays, 4–5 weeks old plants were used.

Stomatal Aperture Measurements

For elevated CO_2-induced stomatal closure, abaxial epidermis of fully expanded leaves were detached and incubated for 2.5 h under 150 μmol $m^{-2}s^{-1}$ light in 50 mM KCl, 10 mM MES/KOH (pH 6.15) at 22°C whilst being aerated with CO_2-free air by bubbling through the buffer solution to bring about stomatal opening, and then either aerated with CO_2-free air or elevated CO_2 (800 ppm) for additional 2.5 h before peels were removed, mounted on slides and stomatal aperture measurements were recorded using an inverted microscope (Olympus BX51), fitted camera (Olympus DP70), and ImageJ software v. 1.43u (NIH). For inhibition of stomatal opening, epidermal peels of abaxial epidermis floated on the 10 mM MES/KOH (pH 6.20) in 6 cm dishes at 22°C for 1 h under the dark, then directly transferred to fresh dishes and incubated for 3 h under light of 150 μmol $m^{-2}s^{-1}$ in 50 mM KCl, 10 mM MES/KOH (pH 6.15) at 22°C either aerated with CO_2-free air or elevated CO_2 (800 ppm) by bubbling directly into the buffer.

Details of the DPI, SHAM and Tiron treatments were as follows: The ROS scavenger Tiron (4,5-dihydroxy-1,3-benzenedisulfonic acid) (Sigma-Aldrich, United States) was dissolved in water and used at a final concentration of 10 mM, ROS inhibitor DPI (diphenyl iodonium chloride) (Sigma-Aldrich, United States) was dissolved in DMSO and used at a final concentration of 20 μM, SHAM (salicylhydroxamic acid) (Sigma-Aldrich, United States) was dissolved in ethanol and used at a final concentration of 2 mM, these chemicals were added 30 min prior to the addition of 800 ppm CO_2. The highest concentration of DMSO or ethanol that was used was added to the zero treatments as a control. To avoid experimenter bias, all the aperture measurements were performed blind. Forty or sixty stomatal apertures were measured per treatment and measurements from two replicates of each treatment were pooled and analyzed by GraphPad Prism 8.0.2 (GraphPad).

Measurement of ROS Production in Guard Cells

2′,7′-Dichlorofluorescein diacetate (H_2DCF-DA) (Sigma-Aldrich, United Kingdom) fluorescence was used as a measure for ROS levels as previously described (Chater et al., 2015). Briefly, epidermal peels from treated leaves were incubated in 50 mM KCl, 10 mM MES/KOH (pH 6.15) buffer in the presence of 50 μM H_2DCF-DA for 10 min at 22°C in darkness. Epidermal strips were washed with 50 mM KCl, 10 mM MES/KOH (pH 6.15) buffer at room temperature. Subsequently, the fluorescence in guard cells was detected using TCS-SP8 confocal laser scanning microscope (Leica lasertechnik GmbH, Heidelberg, Germany). The fluorescent intensities of each image were analyzed using Photoshop 7.0 (ASI). At least fifty guard cell pairs were measured per experiment and analyzed by GraphPad Prism 8.0.2 (GraphPad). To avoid experimenter bias, all the fluorescent intensities measurements were performed blind. Each experiment was done at least three independent times with similar results.

Gene Expression Analysis by Quantitative Real-Time PCR

Total RNA from aerial parts of the plants was extracted using RNeasy® total RNA mini kit (Qiagen) followed by plant genomic DNA digestion with RNase-free DNase I (Thermo scientific) according to the manufacturer's instructions. The absence of genomic DNA contamination was confirmed by PCR using RNA as template without reverse transcription. First strand cDNA was synthesized using Superscript II® reverse transcriptase (Invitrogen) and oligo $d(T)_{15-18}$ (Promega) mRNA primer with 1 μg of total RNA as the template. cDNA corresponding to 20 ng of total RNA and 300 nM of each primer were used in PCR reactions. Primer sequences used for RT-PCR and quantitative RT-PCR are listed in **Supplementary Table S2**. Experiments on independently grown plant material were carried out three times and data analyzed by GraphPad Prism 8.0.2 (GraphPad).

Statistical Analysis

The data were statistically analyzed using GraphPad Prism 8.0.2 (GraphPad). The effects of CO_2 and chemical treatments as well as their interactions on variables were analyzed using analysis of variance (ANOVA). Differences between treatments were considered significant when the *P*-value was less than 0.05 by Tukey's test.

RESULTS

Cell Wall Peroxidases and NADPH Oxidases Are Required for eCO_2-Induced Stomatal Closure

To test the hypothesis that ROS production has a central role to play in defining stomatal CO_2 responses, we started

by monitoring ROS levels in the *big* mutant and wild-type Col-0 (WT) plants using the fluorescence of H_2-DCFDA. As shown in **Supplementary Figure S1A**, the application of eCO_2 (800 ppm) resulted in rapid enhancement of fluorescence in WT guard cells, whereas the increases of ROS were greatly reduced in all *big* mutant alleles examined, including *big-1*, *doc1-1,* and *big-j588* (**Supplementary Figure S1A**), consistent with the compromised eCO_2-induced stomatal closure (He et al., 2018). Strikingly, during eCO_2 inhibited light-induced stomatal opening, we observed comparable increases of ROS levels in the guard cells of the *big* mutant and WT plants (**Supplementary Figure S1B**), in line with previous results (He et al., 2018). These data suggest that CO_2-stimulated stomatal closure and inhibition of light-induced opening both employ an increase in ROS. This suggests that the guard cells might employ different mechanisms to discriminate the types and strength of ROS signals and thereby finely tune stomatal movements in response to eCO_2.

The functioning of NADPH oxidases RBOHD and RBOHF in eCO_2-induced stomatal closure has been well documented (Kolla et al., 2007; Chater et al., 2015; Geng et al., 2016), while the function of cell wall peroxidases in CO_2 signaling remains to be investigated. **Figures 1A,B** show that eCO_2 caused an average 25% reduction in stomatal apertures, whereas this reduction was efficiently abolished by either NADPH oxidases inhibitor DPI or cell wall peroxidases inhibitor SHAM. Around 30% extra ROS were induced by eCO_2 treatments, but peels pre-treated with DPI or SHAM failed to exhibit significant ROS accumulation during eCO_2 treatment (**Figures 1C,D**). These results suggest that cell wall peroxidases function in eCO_2-induced stomatal closure. We next examined the stomatal CO_2 responses in *prx33-3* and *prx34-2* using the *rbohDrbohF* double mutants as a positive control. Similar to *rbohDrbohF*, stomatal apertures of both *prx33-3* and *prx34-2* mutant lines failed to close in response to eCO_2 (**Figure 1E**). In line with this observation, ROS accumulation was not triggered by eCO_2 in the *prx33-3*, *prx34-2*, or *rbohDrbohF* mutants in marked contrast to an over 50% ROS increase in WT (**Figure 1F**). These data not only support the notion that CO_2-induced stomatal closure is dependent on ROS (H_2O_2) production (Kolla et al., 2007; Chater et al., 2015; Geng et al., 2016), but also demonstrate an essential role of cell wall peroxidases including PRX33 and PRX34 in response to eCO_2, shedding new light on ROS action in plants. Furthermore, as with two eCO_2 inducible genes, *SLAC1* and *OST1* (Shi et al., 2015; Dittrich et al., 2019), expressions of *RBOHD*, *RBOHF*, *PRX33,* and *PRX34* were upregulated by eCO_2 (**Supplementary Figure S2**), further corroborating our view that both NADPH oxidases and cell wall peroxidases function in guard cell eCO_2 signaling.

eCO_2-Mediated Stomatal Opening Inhibition Requires ROS Generation

eCO_2-induced stomatal closure and the inhibition of light-induced stomatal opening by eCO_2 are two separate processes (He et al., 2018). **Figure 1** shows that eCO_2-induced stomatal closure requires ROS from both NADPH oxidases and cell wall peroxidases. In eCO_2-inhibited light-induced stomatal opening, eCO_2 suppressed opening induced by 36% and this was associated with an approximate 60% greater increase in ROS accumulation compared to mock treated plants (**Figures 2A,B**). eCO_2-inhibited light induced stomatal opening was virtually abolished by Tiron, a potent ROS scavenger (**Figure 2A**; Yamada et al., 2003). Consistently, the eCO_2-induced ROS accumulation was inhibited by Tiron (**Figure 2B**). Together, these data support the hypothesis that ROS production is indispensable to eCO_2-mediated inhibition of stomatal opening. DPI dampened stomatal opening inhibition presumably by blocking eCO_2-induced ROS increase, as in the presence of DPI, a 24% reduction in stomatal aperture accompanied with a slight while statistically insignificant increase (14%) of ROS production was observed (**Figures 2A,B**). However, neither eCO_2-inhibited stomatal opening nor eCO_2-induced ROS accumulation was compromised by SHAM (**Figures 2A,B**). The inhibition of stomatal opening by eCO_2 required ROS accumulation which might be dependent on NADPH oxidases but less likely on cell wall peroxidases. These data suggest that ROS from distinct sources differentially modulate eCO_2-triggered stomatal movements. Importantly, when the *rbohDrbohF*, *prx33-3,* and *prx34-2* and WT plants were analyzed, we observed similar eCO_2-inhibited stomatal opening and guard cell ROS accumulations (**Figures 2C,D**), suggesting RBOHD, RBOHF, PRX33, and PRX34 are unlikely to be involved in the inhibition of stomatal opening by eCO_2. On the basis of our results we conclude that sources of ROS, other than those described above, must be involved in eCO_2-inhibited stomatal opening.

eCO_2-Induced ROS and Stomatal Closure Require SA and SA Signaling

SA can modulate plant growth, development and responses to a wide range of biotic and abiotic stresses. To determine whether SA participates in eCO_2-induced stomatal closure, we measured stomatal apertures and ROS production using SA-deficient mutant *sid2-2* (SA Induction-Deficient 2) after eCO_2 treatments. While stomatal apertures of WT were reduced by about 10%, no significant reduction of stomatal apertures was detected in *sid2-2* by eCO_2 application (**Figure 3A**). Additionally, we tested *npr1-1*, *npr3npr4* mutants because NPR1, NPR3, and NPR4 are key components of SA signaling (Fu et al., 2012; Wu et al., 2012; Kuai et al., 2015; Ding et al., 2018). In contrast to a nearly 20% reduction of stomatal apertures in WT, *npr1-1* and *npr3npr4* mutants displayed no appreciable eCO_2-induced stomatal closure (**Figure 3B**). Consistently, eCO_2-induced ROS accumulation in guard cells was completely abolished in *sid2-2*, *npr1-1* as well as in *npr3npr4* (**Figures 3C,D** and **Supplementary Figure S3**). These results indicate that eCO_2-induced stomatal closure requires an intact SA signaling pathway, and both SA biosynthesis and SA signaling are involved in eCO_2-induced ROS production.

SA, JA, and ABA Function Differently in eCO_2-Inhibited Stomatal Opening

As shown in **Figure 4A**, stomata of WT and *sid2-2*, *npr1-1,* and *npr3npr4* exhibited a similar degree of closure as WT

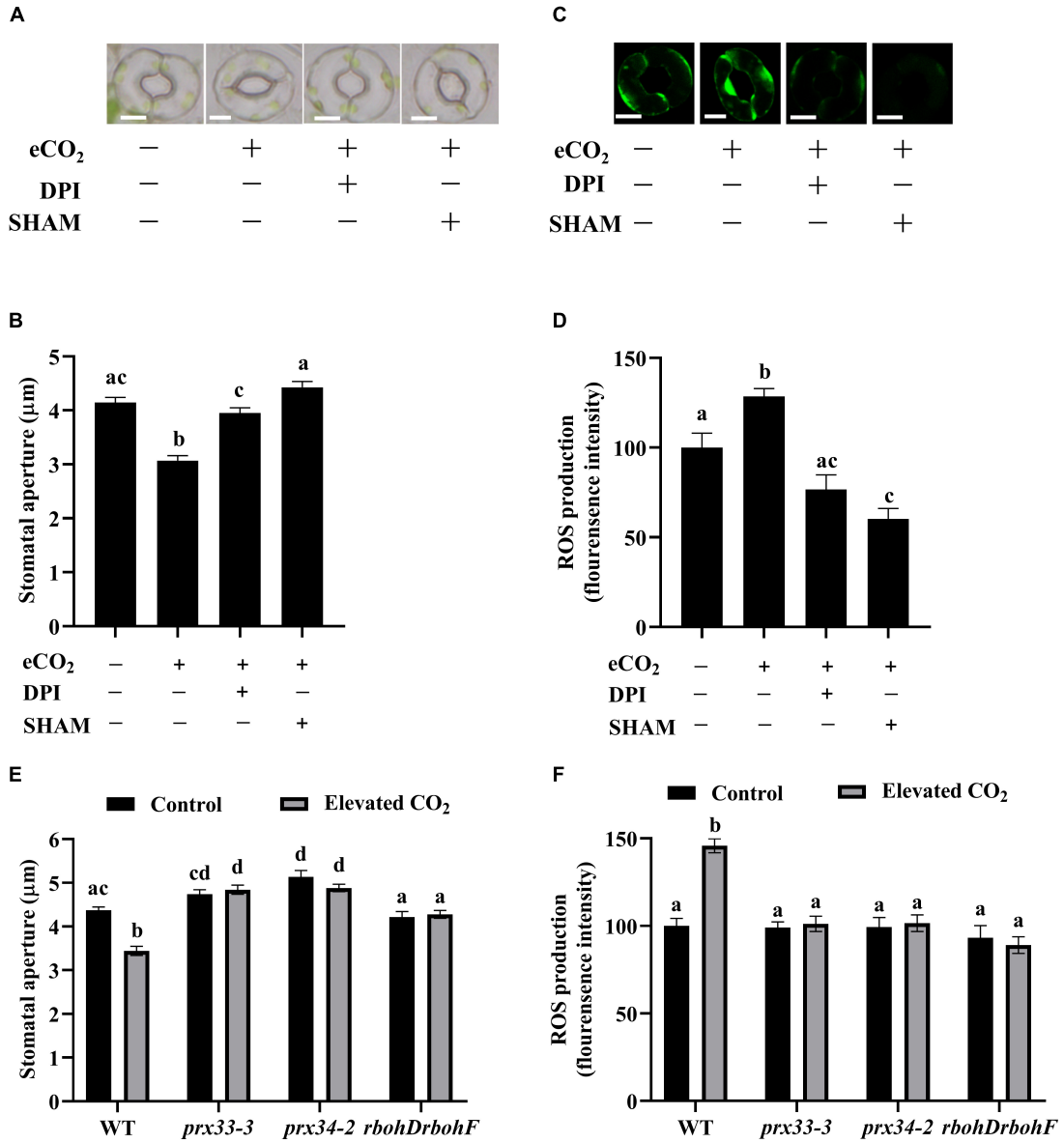

FIGURE 1 | Cell wall peroxidases and NADPH oxidases are required for elevated CO_2-induced stomatal closure. **(A)** eCO_2-induced stomatal closure is inhibited by ROS inhibitors DPI and SHAM. Representative images showing guard cells of WT: after 2.5 h light-incubation, epidermal peels of WT plants were treated with 800 ppm CO_2 for another 2.5 h before photos taken. 20 μM DPI or 2 mM SHAM added before CO_2 treatment for 30 min. Scale bar, 5 μm. **(B)** Quantitative stomatal aperture from (**A**). **(C)** Representative images showing H_2DCF-DA fluorescence of WT guard cells under control (CO_2-free air) and elevated (800 ppm) CO_2 with or without ROS inhibitors DPI or SHAM treatment. Scale bar, 5 μm. **(D)** Quantitative ROS production from **(C)**. eCO_2 stimulates an increase of H_2DCF-DA fluorescence in guard cells that is blocked in the presence of DPI/SHAM. **(E)** eCO_2-induced stomatal closure is disrupted in *prx33-3*, *prx34-2,* and *rbohDrbohF* mutants. **(F)** eCO_2-induced ROS production in guard cells is compromised in *prx33-3*, *prx34-2,* and *rbohDrbohF* mutants during stomatal closure. In **(B)** (n = 120), **(D)** (n = 50), **(E)** (n = 80), and **(F)** (n = 60), values are means ± s.e. All experiments were repeated at least three times. Different letters represent statistically significant differences at $P < 0.05$ based on a Tukey's test.

after 1 h dark treatment. Light-induced stomatal opening in *sid2-2* and *npr3npr4* was similar to WT while apertures of *npr1-1* were consistently larger than WT (**Figure 4A**). When treated with eCO_2, the reduction in stomatal aperture of either *sid2-2* (48%) or *npr3npr4* (43%) was similar to that of WT (47%), indicating that eCO_2-inhibited stomatal opening was not compromised in *sid2-2* and *npr3npr4*, but partially impaired in *npr1-1* (31% reduction) (**Figure 4A**). Based on these results we conclude that SA biosynthesis and SA signaling play no significant role in eCO_2-inhibited light-induced stomatal opening.

We next examined the involvement of ABA and JA signaling which has been reported to be essential for eCO_2-induced stomatal closure (Chater et al., 2015; Geng et al., 2016; Hsu

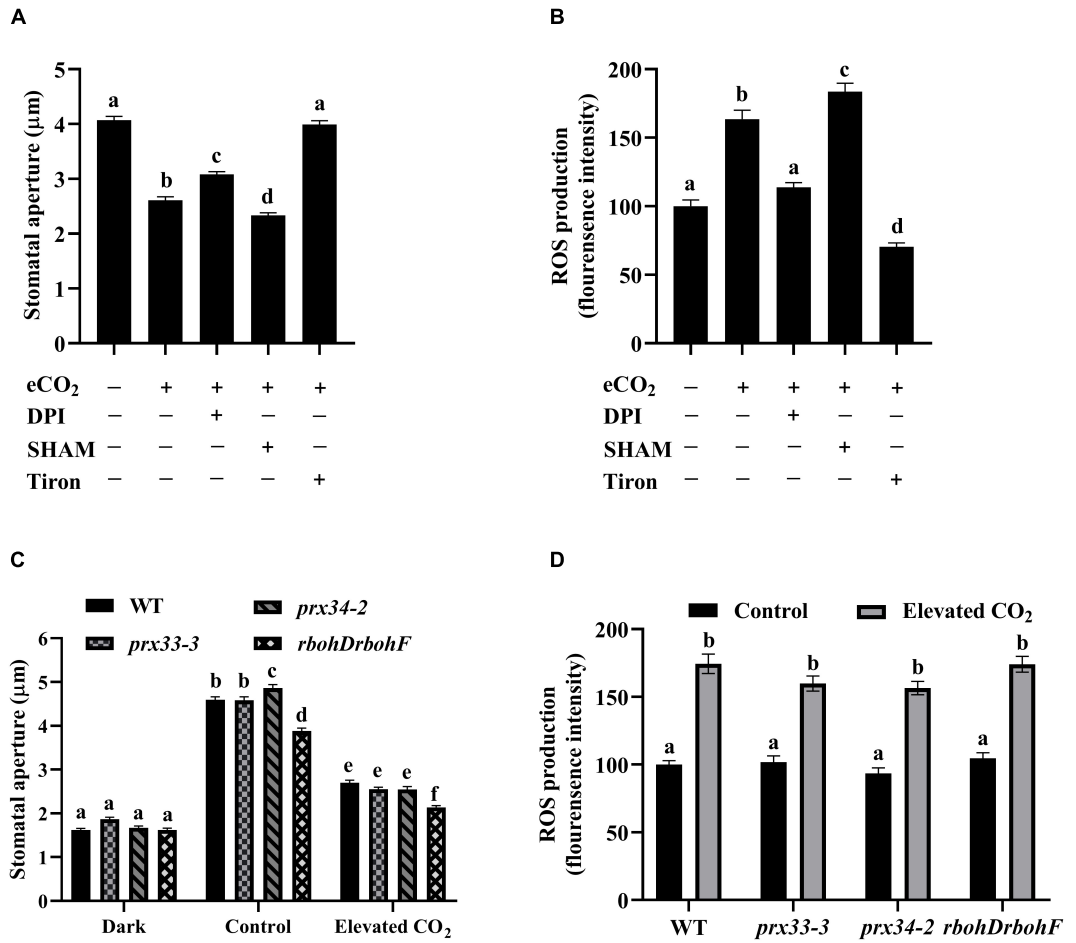

FIGURE 2 | The inhibition of light-induced stomatal opening by eCO_2 requires ROS generation. **(A)** eCO_2-inhibited stomatal opening is compromised by treatment with Tiron. Stomatal apertures were measured on light-incubated epidermal peels treated with CO_2-free (mock) or 800 ppm CO_2 (elevated CO_2) for 3 h. DPI, SHAM, and Tiron added before light treatment for 30 min. **(B)** eCO_2 stimulates an increase of H_2DCF-DA fluorescence in guard cells that is blocked in the presence of DPI and Tiron. **(C)** eCO_2-inhibited stomatal opening in *prx33-3*, *prx34-2,* and *rbohDrbohF* mutants is similar to WT. Stomatal apertures were measured on illuminated epidermal peels treated with CO_2-free (mock) or 800 ppm CO_2 (elevated CO_2) for 3 h. Dark represents 1 h dark-adapted stomata incubated in the 10 mM MES/KOH (pH 6.20) buffer. **(D)** eCO_2 stimulates an increase in guard cells of H_2DCF-DA fluorescence in WT as well as in *prx33-3*, *prx34-2,* and *rbohDrbohF* mutants. Mean fluorescence intensity was measured on light-incubated epidermal peels treated with CO_2-free (mock) or 800 ppm CO_2 (elevated CO_2) for 3 h. In **(A)** (n = 120), **(B)** (n = 60), **(C)** (n = 120), and **(D)** (n = 60), values are mean ± s.e. All experiments were repeated at least three times. Different letters represent statistically significant differences at $P < 0.05$ based on a Tukey's test.

et al., 2018) in eCO_2-inhibited stomatal opening. First we verified that JA pathway deficient mutants *coi1-1* and *jar1-1* are insensitive to eCO_2-induced stomatal closure (**Supplementary Figure S4**). These data confirmed the results of Geng et al. (2016). *myc2-2*, a loss-of-function mutant line of *MYC2,* which is a master regulator of JA signaling, and *jar1-1*, behaved similarly to WT (47, 49, 50% reduction of stomatal aperture, respectively) in eCO_2-inhibited light-induced stomatal opening (**Figure 4B**). Likewise, both the quadruple ABA receptor mutant *pyr1pyl1pyl2pyl4* (*ABA1124*) and *ost1-3* exhibited wild type (44, 49, 44% reduction of stomatal aperture, respectively) responses to eCO_2-inhibited stomatal opening (**Figure 4C**). Taken together, it appears that ABA and JA signaling pathway are not directly involved in eCO_2-inhibited light-induced stomatal opening.

DISCUSSION

Different Sources of ROS Play Different Roles in eCO_2-Induced Stomatal Movement

An increase in guard cell ROS, including H_2O_2 in response to diverse stimuli is one of the first measurable events in stomatal movements. H_2O_2 production mainly depends on two types of enzymes in guard cells, one is NADPH oxidases and the other is cell wall peroxidases (Murata et al., 2015). Similar to the bacterial pathogen-associated molecular patterns (PAMPs), flagellin (flg22) that induces stomatal closure, eCO_2-induced stomatal closure requires both NADPH oxidases- and cell wall peroxidases-generated ROS (**Figure 1**; O'Brien et al., 2012b).

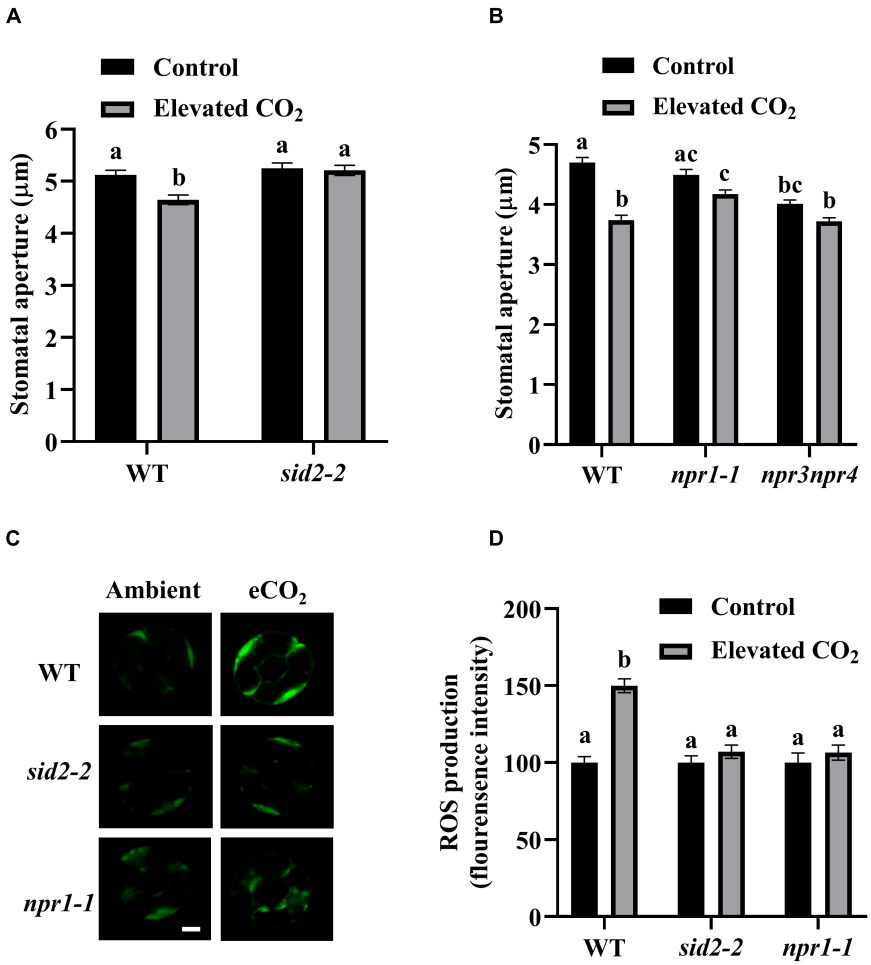

FIGURE 3 | eCO_2-induced stomatal closure requires SA and SA signaling. **(A)** eCO_2-induced stomatal closure is corrupted in *sid2-2* mutants. **(B)** eCO_2-induced stomatal closure is disrupted in *npr1-1* and *npr3npr4* mutants. **(C)** Representative images showing H_2DCF-DA fluorescence of WT, *sid2-2* and *npr1-1* mutants guard cells under control (CO_2-free air) and elevated (800 ppm) CO_2. Scale bar, 5 μm. **(D)** eCO_2 stimulates an increase of H_2DCF-DA fluorescence in WT guard cells, but is blocked in *sid2-2* and *npr1-1* mutants. Mean fluorescence intensity was measured on 2.5 h light-preincubated epidermal peels, treated with 800 ppm CO_2 for another 2.5 h. Stomatal apertures in **(A,B)** were measured on 2.5 h light-preincubated epidermal peels, treated with 800 ppm CO_2 for another 2.5 h. In **(A)** (n = 120), **(B)** (n = 120), and **(D)** (n = 60), values are mean ± s.e. All experiments were repeated at least three times. Different letters represent statistically significant differences at $P < 0.05$ based on a Tukey's test.

Intriguingly, when we analyzed *RBOHD*, *RBOHF*, *PRX33,* and *PRX34* expression levels in *rbohDrbohF*, *prx33*, and *prx34* mutant plants, we found that loss of function of any individual gene had no detectable effects on the expression of the other genes (**Supplementary Figure S5**). In addition, the disruption of one gene is not compensated by other functional ROS generation related genes, indicating there is no feedback and/or counterbalancing regulations among the expressions of NADPH oxidases and cell wall peroxidases. This is consistent with the observation that the cytokinin analog trans-zeatin induces stomatal closure and ROS accumulation in guard cells involving the apoplastic PRXs PRX4, PRX33, PRX34, and PRX71, but not the NADPH oxidases RbohD and RbohF (Arnaud et al., 2017). Thus, it is highly possible that NADPH oxidases and cell wall peroxidases function independently to generate ROS during eCO_2-/PAMP-induced stomatal closure. More dedicated experiments including the evaluation of the possible additive effects on ROS production between *prx33*/*34* and *rbohD*/*F* mutants will be needed to further assess this interpretation. Notably, it has been quantitatively determined that peroxidases are responsible for half of the ROS produced in response to PAMPs, while the other half is produced by NADPH oxidases and/or mitochondrial and chloroplastic ROS sources (O'Brien et al., 2012b).

In contrast to eCO_2-induced stomatal closure, eCO_2-inhibited stomatal opening was only partially blocked by DPI treatment but not by SHAM. These results are in line with the insights we got from working with BIG (**Supplementary Figure S1**), namely, that guard cells employ different mechanisms to discriminate the types and strength of ROS signals in order to, presumably, finely tune stomatal movements in response to eCO_2. Interestingly, a recent paper reported that neither DPI nor SHAM reduced the

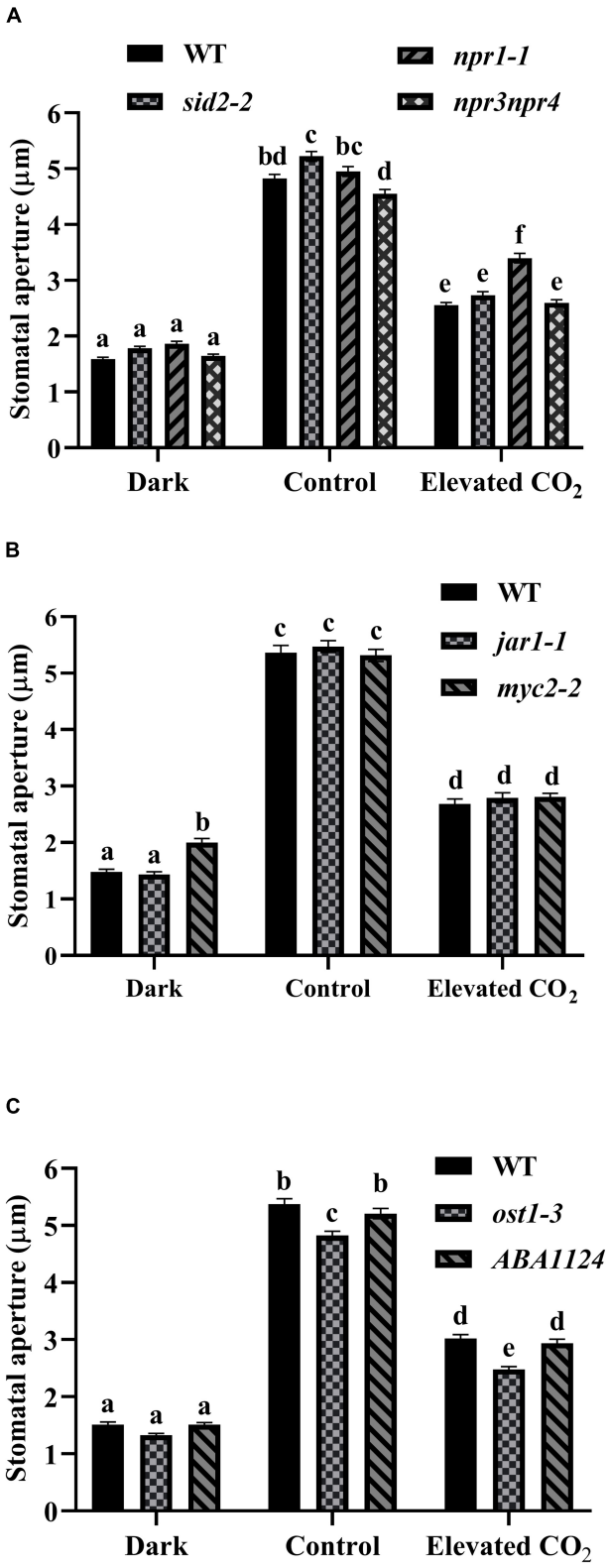

FIGURE 4 | SA, JA, and ABA are not required for the inhibition of light-stimulated stomatal opening by eCO_2. **(A)** eCO_2-inhibited stomatal *(Continued)*

FIGURE 4 | opening in *sid2-2*, *npr1-1,* and *npr3npr4* mutants is similar to WT. **(B)** eCO_2-inhibited stomatal opening in *jar1-1* and *myc2-2* mutants is similar to WT. **(C)** eCO_2-inhibited stomatal opening in *pyr1pyl1pyl2pyl4* (*ABA1124*) and *ost1-3* mutants is similar to WT. Stomatal apertures were measured on light-incubated epidermal peels treated with CO_2-free (mock) or 800 ppm CO_2 (elevated CO_2) for 3 h. Dark represents 1 h dark-adapted stomata incubated in the 10 mM MES/KOH (pH 6.20) buffer. In **(A–C)** (n = 120), the shown result is a representative of three independent biological experiments, values are mean ± s.e. Different letters represent statistically significant differences at $P < 0.05$ based on a Tukey's test.

high level of ROS in the *atg*2 mutant, which is compromised in light- and low CO_2-induced stomatal opening (Yamauchi et al., 2019). While both eCO_2-inhibited stomatal opening and ROS accumulation could be entirely abrogated by Tiron, the inhibition of stomatal opening by eCO_2 remains functional in the *rbohDrbohF* double mutant (**Figure 2**). This suggests that other ROS sources, which are inhibited by Tiron but not by DPI function in eCO_2-inhibited light-induced stomatal opening. Nitric oxide (NO) which plays a role in stomatal movement (Neill et al., 2003; Laxalt et al., 2016) has been identified to be required for eCO_2-induced stomatal closure in tomato (Shi et al., 2015). Evidently, NO production might also contribute to eCO_2-triggered stomatal movement in Arabidopsis. In addition to NADPH oxidases and cell wall peroxidases, the polyamine oxidases (PAOs) catalyze catabolism of spermidine and spermine with concomitant production of H_2O_2 (Pottosin et al., 2014; Sierla et al., 2016). An inhibitor of PAOs interferes with ABA-induced stomatal closure in French bean and ethylene-induced stomatal closure in Arabidopsis (An et al., 2008; Hou et al., 2013). Whether and how PAOs contribute to the ROS accumulations that drive eCO_2-reguated stomatal movement remains to be investigated. Another possibility is that other members of the NADPH oxidase family function in guard cell signaling in response to eCO_2. In Arabidopsis, there are 10 members of the RBOH family. When the spatiotemporal expression profile of all *RBOH* members is examined using ePlant[2], it is apparent that, in addition to *RBOHD* and *RBOHF*, *RBOHC* is highly expressed in guard cells (**Supplementary Figure S6**), suggesting a regulatory role of RBOHC in stomatal function. This suggestion is supported by work from Wei et al. (2018) who provided evidence that the activity of RBOHC is required for melatonin-induced stomatal closure and ROS production. It will be interesting to investigate whether RBOHC is involved in eCO_2-induced stomatal movement.

Apoplastic ROS are known to regulate stomatal movement, however they are sensed and transduced is not well understood. One possibility is that apoplastic ROS are sensed by yet to be characterized extracellular sensors and subsequently transduced by unknown intracellular pathways (Sierla et al., 2016). Alternatively, apoplastic ROS such as H_2O_2 can be transported into the cytoplasm via aquaporins (Tian et al., 2016), as exemplified by the aquaporin PIP2;1 which is required for ABA and flg22-induced H_2O_2 accumulation in guard cells (Rodrigues et al., 2017). Moreover, ROS can directly modify the activity

[2]http://bar.utoronto.ca/eplant/

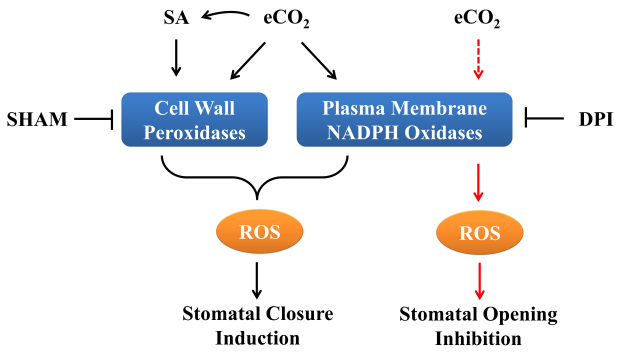

FIGURE 5 | Schematic diagram of ROS accumulation and stomatal movement in response to eCO_2 in Arabidopsis. In terms of cell wall peroxidases and NADPH oxidases it appears both of which function in eCO_2-induced stomatal closure. SA signaling is required for eCO_2-regulated stomatal closure, while eCO_2-inhibited stomatal opening may only depend on NADPH oxidases mediated ROS generation. Black lines signify induced stomatal closure and red lines signify inhibited stomatal opening. Solid lines indicate verified interactions; dashed lines indicate hypothetical interactions.

of ion channels leading to stomatal closure (Pei et al., 2000). Equally possible, however, is that ROS function through parallel mechanisms to promote CO_2 signaling in guard cells.

Plant Hormone Signals Differentially Mediate eCO_2-Regulated Stomatal Movement

Changes in SA concentration after pathogen infection affect the redox state of the cell and bring about a conformational switch of NPR1 (Cao et al., 1994) and thereby activate *PR* genes (Chen et al., 1993; Vanacker et al., 2000; Noctor et al., 2002; Mou et al., 2003). eCO_2 can induce SA production and activate SA signaling in many plant species (Matros et al., 2006; Casteel et al., 2012; Huang et al., 2012; Zhang et al., 2015; Mhamdi and Noctor, 2016; Williams et al., 2018). Our observation that eCO_2-induced stomatal closure requires endogenous SA and SA-signaling components supports a proposed link between SA and CO_2 signaling in guard cells response (Medina-Puche et al., 2017). This is in line with several reports that SABP3 (SA-binding protein 3), a chloroplast carbonic anhydrase (CA), which exhibits both CA enzymatic and SA-binding activities is indispensable to SA-mediated defense response in tomato as well as in Arabidopsis (Slaymaker et al., 2002; Wang et al., 2009). Also, NPR1 and NRB4 (Non-recognition of BTH 4, another SA signaling component) interact with βCA1 (Medina-Puche et al., 2017). In addition, it is known that the β*ca1*β*ca4* double mutant compromises CO_2 sensing (Hu et al., 2010). These, together with the fact that the quintuple mutant β*ca1*β*ca2*β*ca3*β*ca4*β*ca6* shows reduced sensitivity to SA, suggest that CAs likely function in modulating the perception of SA in plants (Medina-Puche et al., 2017). Although NPR1 and NPR3/NPR4 play opposite roles in transcriptional regulation, they all function in a SA-dependent manner for plant immune responses as NPR1, NPR3, and NPR4 are SA-binding proteins (Ding et al., 2018). Nevertheless, both *npr1-1* and *npr3npr4* are insensitive to eCO_2-induced stomatal closure (**Figure 3**), in line with the finding that the double mutant *npr3npr4* is defective in systemic acquired resistance (SAR) (Fu et al., 2012), suggesting disruption in different aspects of SA signaling components might consequently affect eCO_2-induced stomatal closure. Interestingly, eCO_2-inhibited stomatal opening was partially compromised only in *npr1-1* but not in *sid2-2* or *npr3npr4* (**Figure 4A**). It is assumed that selective SA-binding to NPR1 and NPR3/NPR4 could differentially affect eCO_2-inhibited stomatal opening. Alternatively, SA-independent NPR1 function in ER (endoplasmic reticulum) stress has been reported recently (Lai et al., 2018), thus NPR1 might function in a SA-independent manner during eCO_2-inhibited stomatal opening. PRX33 and PRX34 play a significant role in SA-mediated stomatal closure (Arnaud et al., 2017). Our observation that SA signaling pathway functions in eCO_2-induced stomatal closure rather than in eCO_2-inhibited stomatal opening (**Figures 3**, **4**), is in accordance with that cell wall peroxidases differentially mediate eCO_2-regulated stomatal movement (**Figures 1**, **2**), implicating that SA regulates eCO_2 inhibition of stomatal closure via the activities of the peroxidases, which needs to be assessed in more details in the future, for example, by examining the expression changes of PRX33 and PRX34 in response to eCO_2 in the SA mutants using RBOHD and RBOHF as experimental controls.

Multiple lines of evidence support a requirement of ABA for perceiving CO_2 concentration changes by stomata (Raschke, 1975; Webb and Hetherington, 1997; Merilo et al., 2013; Chater et al., 2015; Hsu et al., 2018). Recently, Dittrich et al. (2019) have further demonstrated that ABA receptors PYL4 and PYL5 are key to CO_2-induced stomatal closure. JA and SA signaling pathways are often mutually antagonistic, which can be induced simultaneously under eCO_2 and intracellular oxidative stresses (Han et al., 2013a,b; Mhamdi and Noctor, 2016; Williams et al., 2018). The present study shows that both SA and JA are required for mediating stomatal closure by eCO_2 (**Figure 3** and **Supplementary Figures S5**), in line with the emerging evidences that SA, JA, ABA and ROS signaling are important in linking CO_2 availability, stomatal function and the activation of plant defense responses (Li et al., 2014; Geng et al., 2016; Mhamdi and Noctor, 2016; Zhou et al., 2017; Williams et al., 2018). To further substantiate these findings, the contents of SA, JA and ABA need to be monitored in the future experiments. However, there is no evidence that eCO_2 brings about an elevation of ABA (Chater et al., 2015; Hsu et al., 2018). ABA and JA can induce ROS accumulation in guard cells via the activities of RBOHD and RBOHF, whereas SA regulates ROS homeostasis via the peroxidases-catalyzed reactions (Murata et al., 2015). ABA, JA and SA are known to be required for eCO_2-induced stomatal closure. However, our data indicate that none of these three hormones plays major roles in eCO_2-inhibited stomatal opening, a process that is dependent on ROS generation, reflecting a similar mechanism in O_3-induced ROS stress responses which are independent on SA, JA and ethylene signals (Xu et al., 2015).

In this study, by investigating ROS accumulation and stomatal movement in response to eCO_2, we demonstrated that both cell wall peroxidases and NADPH oxidases are required for ROS production during eCO_2-mediated stomatal closure, whereas eCO_2-inhibited stomatal opening might be dependent

on NADPH oxidases but not on cell wall peroxidases (**Figure 5**). The data presented here indicate that eCO_2-inhibited light-stimulated stomatal opening requires ROS. However, our data suggest that distinct sources of ROS other than NADPH oxidases and PRXs play vital roles in stomatal opening inhibition by eCO_2. Furthermore, we show that as with JA and ABA, SA signals are required for eCO_2-induced stomatal closure and ROS generation. None of these three hormones has a significant role in eCO_2-inhibited stomatal opening. Taken together, these results suggest that ROS from distinct sources and various plant hormones differentially regulate eCO_2-induced stomatal movement.

DATA AVAILABILITY STATEMENT

All datasets generated for this study are included in the article/**Supplementary Material**.

AUTHOR CONTRIBUTIONS

Y-KL conceived the research. JH, R-XZ, DK, PS, HL, and ZL conducted experiments. JH, R-XZ, AH, and Y-KL analyzed data and wrote the manuscript with the support of DK, PS, and ZL. All authors read and approved the manuscript.

FUNDING

This work was supported by the National Natural Science Foundation of China under Grant No. 31770282 and 31470360 and the UK, BBSRC, Grant No. BB/N001168/1.

SUPPLEMENTARY MATERIAL

The Supplementary Material for this article can be found online at: https://www.frontiersin.org/articles/10.3389/fpls.2020.00542/full#supplementary-material

FIGURE S1 | ROS accumulation is disrupted in the *big* mutant during stomatal closure induced by eCO_2. **(A)** eCO_2-induced ROS production during eCO_2-induced stomatal closure is reduced in comparison to WT. Mean H_2DCF-DA fluorescence intensity was measured on 2.5 h light-preincubated epidermal peels, treated with CO_2-free (mock) or 800 ppm CO_2 (elevated CO_2) for another 2.5 h. **(B)** In the inhibition of light-stimulated stomatal opening by eCO_2, ROS production in WT and *big* mutants is identical. Mean H_2DCF-DA fluorescence intensity was measured on light-incubated epidermal peels treated with CO_2-free (mock) or 800 ppm CO_2 (elevated CO_2) for 3 h. In **(A,B)** (n = 60), values are means ± s.e. All experiments were repeated at least three times. Different letters indicate significant differences at $P < 0.05$ based on a Tukey's test.

FIGURE S2 | ROS generation related genes transcription levels are induced by eCO_2. **(A–F)** four-week old intact leaves were treated with or without eCO_2 for 3 h, the transcription levels of *PRX33* **(A)**, *PRX34* **(B)**, *RBOHD* **(C),** and *RBOHF* **(D)** genes were determined by quantitative RT-PCR and normalized to *Actin3*, *OST1* **(E)** and *SLAC1* **(F)** were used as positive controls. In **(A–F)**, the shown result is a representative of three independent biological experiments, values are mean ± s.e. Means with different letters represent statistically significant differences at $P < 0.05$ based on a Tukey's test.

FIGURE S3 | eCO_2-induced ROS accumulation requires SA signaling. eCO_2 stimulates an increase H_2DCFDA fluorescence in WT guard cells, but is blocked in *npr3npr4* mutants. Mean fluorescence intensity was measured on 2.5 h light-preincubated epidermal peels, treated with 800 ppm CO_2 for another 2.5 h. Values are mean ± s.e. (n = 50). All experiments were repeated at least three times. Different letters represent statistically significant differences at $P < 0.05$ based on a Tukey's test.

FIGURE S4 | eCO_2-induced stomatal closure requires JA signaling. **(A)** eCO_2-induced stomatal closure is disrupted in *coi1-1* mutants. **(B)** eCO_2-induced stomatal closure is disrupted in *jar1-1* mutants. Stomatal apertures in **(A,B)** were measured on 2.5 h light-preincubated epidermal peels, treated with 800 ppm CO_2 for another 2.5 h. In **(A,B)**, the shown result is a representative of three independent biological experiments, values are mean ± s.e. (n = 120). Different letters represent statistically significant differences at $P < 0.05$ based on a Tukey's test.

FIGURE S5 | The expression of *PRXs* and *RBOH* gene are not affected in ROS mutants. Four-week old leaves were used to extract mRNA. The quantitative RT-PCR **(A–D)** and RT-PCR **(E)** analysis of *PRX33*, *PRX34*, *RBOHD,* and *RBOHF* transcription in leaves of 5-week-old WT, *prx33-3*, *prx34-2,* and *rbohDrbohF* mutants. For quantitative RT-PCR, the transcription levels normalized to *Actin3*; for RT-PCR, *EF1a* was used as a control for cDNA quantity. In **(A–D)**, the shown result is a representative of three independent biological experiments, values are mean ± s.e. Different letters represent statistically significant differences at $P < 0.05$ based on a Tukey's test.

FIGURE S6 | Expression of *RBOHs* genes in leaves and guard cells after treatment with ABA. Heat map showing levels of expression of *AtRBOHA-AtRBOHJ* genes (log_2 intensity) in guard cells (1–6) and leaves (7–10) according to ePlant (http://bar.utoronto.ca/eplant/). 1 represents the mock test, 2 is treated with 50 μM ABA for 20 h (reference to Böhmer and Schroeder, 2011), 3 and 7 represent mock tests, 4 and 7 are treated with 100 μM ABA for 4 h (reference to Yang et al., 2008), 5 and 9 represent mock tests, 6 and 10 are treated with 50 μM ABA for 3 h (reference to Pandey et al., 2010).

TABLE S1 | Mutants used in this study.

TABLE S2 | Primers used in this study.

REFERENCES

Allan, A. C., and Fluhr, R. (1997). Two distinct sources of elicited reactive oxygen species in tobacco epidermal cells. *Plant Cell* 9, 1559–1572. doi: 10.1105/tpc.9.9.1559

An, Z., Jing, W., Liu, Y., and Zhang, W. (2008). Hydrogen peroxide generated by copper amine oxidase is involved in abscisic acid-induced stomatal closure in *Vicia faba*. *J. Exp. Bot.* 59, 815–825. doi: 10.1093/jxb/erm370

Arnaud, D., Lee, S., Takebayashi, Y., Choi, D., Choi, J., Sakakibara, H., et al. (2017). Cytokinin-mediated regulation of reactive oxygen species homeostasis modulates stomatal immunity in *Arabidopsis*. *Plant Cell* 29, 543–559. doi: 10.1105/tpc.16.00583

Assmann, S. M. (1993). Signal transduction in guard cells. *Annu. Rev. Cell Biol.* 9, 345–375. doi: 10.1146/annurev.cb.09.110193.002021

Bindschedler, L. V., Dewdney, J., Blee, K. A., Stone, J. M., Asai, T., Plotnikov, J., et al. (2006). Peroxidase-dependent apoplastic oxidative burst in *Arabidopsis* required for pathogen resistance. *Plant J.* 47, 851–863. doi: 10.1111/j.1365-313X.2006.02837.x

Böhmer, M., and Schroeder, J. I. (2011). Quantitative transcriptomic analysis of abscisic acid-induced and reactive oxygen species-dependent expression changes and proteomic profiling in *Arabidopsis* suspension cells. *Plant J.* 67, 105–118. doi: 10.1111/j.1365-313X.2011.04579.x

Caine, R. S., Yin, X., Sloan, J., Harrison, E. L., Mohammed, U., Fulton, T., et al. (2018). Rice with reduced stomatal density conserves water and has improved

drought tolerance under future climate conditions. *New Phytol.* 22, 371–384. doi: 10.1111/nph.15344

Cao, H., Bowling, S. A., Gordon, A. S., and Dong, X. (1994). Characterization of an *Arabidopsis* mutant that is nonresponsive to inducers of systemic acquired resistance. *Plant Cell* 6, 1583–1592. doi: 10.1105/tpc.6.11.1583

Casteel, C. L., Segal, L. M., Niziolek, O. K., Berenbaum, M. R., and Delucia, E. H. (2012). Elevated carbon dioxide increases salicylic acid in *Glycine max*. *Environ. Entomol.* 41, 1435–1442. doi: 10.1603/EN12196

Chater, C., Peng, K., Movahedi, M., Dunn, J. A., Walker, H. J., Liang, Y. K., et al. (2015). Elevated CO_2-induced responses in stomata require ABA and ABA signaling. *Curr. Biol.* 25, 2709–2716. doi: 10.1016/j.cub.2015.09.013

Chen, Z., Silva, H., and Klessig, D. F. (1993). Active oxygen species in the induction of plant systemic acquired resistance by salicylic acid. *Science* 262, 1883–1886.

Daudi, A., Cheng, Z., O'Brien, J. A., Mammarella, N., Khan, S., Ausubel, F. M., et al. (2012). The apoplastic oxidative burst peroxidase in *Arabidopsis* is a major component of pattern-triggered immunity. *Plant Cell* 24, 275–287. doi: 10.1126/science.8266079

Ding, Y., Sun, T., Ao, K., Peng, Y., Zhang, Y., Li, X., et al. (2018). Opposite roles of salicylic acid receptors NPR1 and NPR3/NPR4 in transcriptional regulation of plant immunity. *Cell* 173, 1454–1467. doi: 10.1016/j.cell.2018.03.044

Dittrich, M., Mueller, H. M., Bauer, H., Peirats-Llobet, M., Rodriguez, P. L., Geilfus, C. M., et al. (2019). The role of *Arabidopsis* ABA receptors from the PYR/PYL/RCAR family in stomatal acclimation and closure signal integration. *Nat. Plants* 5, 1002–1011. doi: 10.1038/s41477-019-0490-0

Durner, J., and Klessig, D. F. (1995). Inhibition of ascorbate peroxidase by salicylic acid and 2, 6-dichloroisonicotinic acid, two inducers of plant defense responses. *Proc. Natl. Acad. Sci. U.S.A.* 92, 11312–11316. doi: 10.1073/pnas.92.24.11312

Foyer, C. H., and Noctor, G. (2005). Oxidant and antioxidant signalling in plants: a re-evaluation of the concept of oxidative stress in a physiological context. *Plant Cell Environ.* 28, 1056–1071. doi: 10.1111/j.1365-3040.2005.01327.x

Fu, Z. Q., Yan, S., Saleh, A., Wang, W., Ruble, J., Oka, N., et al. (2012). NPR3 and NPR4 are receptors for the immune signal salicylic acid in plants. *Nature* 486, 228–232. doi: 10.1038/nature11162

Geng, S., Misra, B. B., de Armas, E., Huhman, D. V., Alborn, H. T., Sumner, L. W., et al. (2016). Jasmonate−mediated stomatal closure under elevated CO_2 revealed by time-resolved metabolomics. *Plant J.* 88, 947–962. doi: 10.1111/tpj.13296

Gil, P., Dewey, E., Friml, J., Zhao, Y., Snowden, K. C., Putterill, J., et al. (2001). BIG: a calossin-like protein required for polar auxin transport in *Arabidopsis*. *Genes Dev.* 15, 1985–1997. doi: 10.1101/gad.905201

Grek, C. L., Zhang, J., Manevich, Y., Townsend, D. M., and Tew, K. D. (2013). Causes and consequences of cysteine S-glutathionylation. *J. Biol. Chem.* 288, 26497–26504. doi: 10.1074/jbc.R113.461368

Han, Y., Chaouch, S., Mhamdi, A., Queval, G., Zechmann, B., and Noctor, G. (2013a). Functional analysis of *Arabidopsis* mutants points to novel roles for glutathione in coupling H_2O_2 to activation of salicylic acid accumulation and signaling. *Antioxid. Redox Signal.* 18, 2106–2121. doi: 10.1089/ars.2012.5052

Han, Y., Mhamdi, A., Chaouch, S., and Noctor, G. (2013b). Regulation of basal and oxidative stress-triggered jasmonic acid-related gene expression by glutathione. *Plant Cell Environ.* 36, 1135–1146. doi: 10.1111/pce.12048

Hashimoto, M., Negi, J., Young, J., Israelsson, M., Schroeder, J. I., and Iba, K. (2006). *Arabidopsis* HT1 kinase controls stomatal movements in response to CO_2. *Nat. Cell Biol.* 8, 391–397. doi: 10.1038/ncb1387

Hashimoto-Sugimoto, M., Negi, J., Monda, K., Higaki, T., Isogai, Y., Nakano, T., et al. (2016). Dominant and recessive mutations in the Raf-like kinase HT1 gene completely disrupt stomatal responses to CO_2 in *Arabidopsis*. *J. Exp. Bot.* 67, 3251–3261. doi: 10.1093/jxb/erw134

He, J., and Liang, Y.-K. (2018). Stomata. *eLS* doi: 10.1002/9780470015902.a0026526

He, J., Zhang, R. X., Peng, K., Tagliavia, C., Li, S., Xue, S., et al. (2018). The BIG protein distinguishes the process of CO_2-induced stomatal closure from the inhibition of stomatal opening by CO_2. *New Phytol.* 218, 232–241. doi: 10.1111/nph.14957

Hearn, T. J., Ruiz, M. C. M., Abdul-Awal, S. M., Wimalasekera, R., Stanton, C. R., Haydon, M. J., et al. (2018). BIG regulates dynamic adjustment of circadian period in *Arabidopsis thaliana*. *Plant Physiol.* 178, 358–371. doi: 10.1104/pp.18.00571

Hetherington, A. M., and Woodward, F. I. (2003). The role of stomata in sensing and driving environmental change. *Nature* 424, 901–908.

Hõrak, H., Sierla, M., Tõldsepp, K., Wang, C., Wang, Y. S., Nuhkat, M., et al. (2016). A dominant mutation in the HT1 kinase uncovers roles of MAP kinases and GHR1 in CO_2-induced stomatal closure. *Plant Cell* 28, 2493–2509. doi: 10.1105/tpc.16.00131

Hou, Z. H., Liu, G. H., Hou, L. X., Wang, L. X., and Xin, L. I. U. (2013). Regulatory function of polyamine oxidase-generated hydrogen peroxide in ethylene-induced stomatal closure in *Arabidopsis thaliana*. *J. Integr. Agr.* 12, 251–262. doi: 10.1016/S2095-3119(13)60224-5

Hsu, P. K., Takahashi, Y., Munemasa, S., Merilo, E., Laanemets, K., Waadt, R., et al. (2018). Abscisic acid-independent stomatal CO_2 signal transduction pathway and convergence of CO_2 and ABA signaling downstream of OST1 kinase. *Proc. Natl. Acad. Sci. U.S.A.* 115, E9971–E9980. doi: 10.1073/pnas.1809204115

Hu, H., Boisson-Dernier, A., Israelsson-Nordström, M., Böhmer, M., Xue, S., Ries, A., et al. (2010). Carbonic anhydrases are upstream regulators of CO_2-controlled stomatal movements in guard cells. *Nat. Cell Biol.* 12, 87–93. doi: 10.1038/ncb2009

Huang, L., Ren, Q., Sun, Y., Ye, L., Cao, H., and Ge, F. (2012). Lower incidence and severity of tomato virus in elevated CO_2 is accompanied by modulated plant induced defence in tomato. *Plant Biol.* 14, 905–913. doi: 10.1111/j.1438-8677.2012.00582.x

Jakobson, L., Vaahtera, L., Toldsepp, K., Nuhkat, M., Wang, C., Wang, Y. S., et al. (2016). Natural variation in *Arabidopsis* Cvi-0 accession reveals an important role of MPK12 in guard cell CO_2 signaling. *PLoS Biol.* 14:e2000322. doi: 10.1371/journal.pbio.2000322

Kanyuka, K., Praekelt, U., Franklin, K. A., Billingham, O. E., Hooley, R., Whitelam, G. C., et al. (2003). Mutations in the huge *Arabidopsis* gene BIG affect a range of hormone and light responses. *Plant J.* 35, 57–70. doi: 10.1046/j.1365-313X.2003.01779.x

Keenan, T. F., Hollinger, D. Y., Bohrer, G., Dragoni, D., Munger, J. W., Schmid, H. P., et al. (2013). Increase in forest water-use efficiency as atmospheric carbon dioxide concentrations rise. *Nature* 499, 324–327. doi: 10.1038/nature12291

Khokon, M. A. R., Okuma, E. I. J. I., Hossain, M. A., Munemasa, S., Uraji, M., Nakamura, Y., et al. (2011). Involvement of extracellular oxidative burst in salicylic acid-induced stomatal closure in *Arabidopsis*. *Plant Cell Environ.* 34, 434–443. doi: 10.1111/j.1365-3040.2010.02253.x

Kim, T. H., Bömer, M., Hu, H., Nishimura, N., and Schroeder, I. (2010). Guard cell signal transduction network: advances in understanding abscisic acid, CO_2, and Ca^{2+} signaling. *Annu. Rev. Plant Biol.* 61, 561–591. doi: 10.1146/annurev-arplant-042809-112226

Kolla, V. A., Vavasseur, A., and Raghavendra, A. S. (2007). Hydrogen peroxide production is an early event during bicarbonate induced stomatal closure in abaxial epidermis of *Arabidopsis*. *Planta* 225, 1421–1429. doi: 10.1007/s00425-006-0450-6

Kuai, X., MacLeod, B. J., and Després, C. (2015). Integrating data on the *Arabidopsis* NPR1/NPR3/NPR4 salicylic acid receptors; a differentiating argument. *Front. Plant Sci.* 6:235. doi: 10.3389/fpls.2015.00235

Kwak, J. M., Mori, I. C., Pei, Z. M., Leonhardt, N., Torres, M. A., Dangl, J. L., et al. (2003). NADPH oxidase AtrbohD and AtrbohF genes function in ROS-dependent ABA signaling in *Arabidopsis*. *EMBO J.* 22, 2623–2633. doi: 10.1093/emboj/cdg277

Laxalt, A. M., García-Mata, C., and Lamattina, L. (2016). The dual role of nitric oxide in guard cells: promoting and attenuating the ABA and phospholipid-derived signals leading to the stomatal closure. *Front. Plant Sci.* 7:476. doi: 10.3389/fpls.2016.00476

Lai, Y. S., Renna, L., Yarema, J., Ruberti, C., He, S. Y., and Brandizzi, F. (2018). Salicylic acid-independent role of NPR1 is required for protection from proteotoxic stress in the plant endoplasmic reticulum. *Proc. Natl. Acad. Sci. U.S.A.* 115, E5203–E5212. doi: 10.1073/pnas.1802254115

Li, H. M., Altschmied, L., and Chory, J. (1994). *Arabidopsis* mutants define downstream branches in the phototransduction pathway. *Genes Dev.* 8, 339–349. doi: 10.1101/gad.8.3.339

Li, X., Sun, Z., Shao, S., Zhang, S., Ahammed, G. J., Zhang, G., et al. (2014). Tomato-*Pseudomonas* syringae interactions under elevated CO_2 concentration: the role of stomata. *J. Exp. Bot.* 66, 307–316. doi: 10.1093/jxb/eru420

López-Bucio, J., Hernández-Abreu, E., Sánchez-Calderón, L., Pérez-Torres, A., Rampey, R. A., Bartel, B., et al. (2005). An auxin transport independent pathway is involved in phosphate stress-induced root architectural alterations in *Arabidopsis*. Identification of BIG as a mediator of auxin in pericycle cell activation. *Plant Physiol.* 137, 681–691. doi: 10.1104/pp.104.049577

Matros, A., Amme, S., Kettig, B., Buck-Sorlin, G. H., Sonnewald, U. W. E., and Mock, H. P. (2006). Growth at elevated CO_2 concentrations leads to modified profiles of secondary metabolites in tobacco cv. SamsunNN and to increased resistance against infection with *potato virus Y*. *Plant Cell Environ.* 29, 126–137. doi: 10.1111/j.1365-3040.2005.01406.x

McAinsh, M. R., Clayton, H., Mansfield, T. A., and Hetherington, A. M. (1996). Changes in stomatal behavior and guard cell cytosolic free calcium in response to oxidative stress. *Plant Physiol.* 111, 1031–1042. doi: 10.1104/pp.111.4.1031

Medina-Puche, L., Castelló, M. J., Canet, J. V., Lamilla, J., Colombo, M. L., and Tornero, P. (2017). β-carbonic anhydrases play a role in salicylic acid perception in *Arabidopsis*. *PLoS One* 12:e0181820. doi: 10.1371/journal.pone.0181820

Merilo, E., Laanemets, K., Hu, H., Xue, S., Jakobson, L., Tulva, I., et al. (2013). PYR/RCAR receptors contribute to ozone-, reduced air humidity-, darkness-, and CO_2-induced stomatal regulation. *Plant Physiol.* 162, 1652–1668. doi: 10.1104/pp.113.220608

Myers, S. S., Zanobetti, A., Kloog, I., Huybers, P., Leakey, D. B., Bloom, A. J., et al. (2014). Increasing CO_2 threatens human nutrition. *Nature* 510, 139–142. doi: 10.1038/nature13179

Mhamdi, A., and Noctor, G. (2016). High CO_2 primes plant biotic stress defences through redox-linked pathways. *Plant Physiol.* 172, 929–942. doi: 10.1104/pp.16.01129

Mishra, G., Zhang, W., Deng, F., Zhao, J., and Wang, X. (2006). A bifurcating pathway directs abscisic acid effects on stomatal closure and opening in *Arabidopsis*. *Science* 312, 264–266. doi: 10.1126/science.1123769

Mittler, R. (2017). ROS are good. *Trends Plant Sci.* 22, 11–19. doi: 10.1016/j.tplants.2016.08.002

Miura, K., Okamoto, H., Okuma, E., Shiba, H., Kamada, H., Hasegawa, P. M., et al. (2013). SIZ1 deficiency causes reduced stomatal aperture and enhanced drought tolerance via controlling salicylic acid-induced accumulation of reactive oxygen species in *Arabidopsis*. *Plant J.* 73, 91–104. doi: 10.1111/tpj.12014

Mori, I. C., Pinontoan, R., Kawano, T., and Muto, S. (2001). Involvement of superoxide generation in salicylic acid-induced stomatal closure in *Vicia faba*. *Plant Cell Physiol.* 42, 1383–1388. doi: 10.1093/pcp/pce176

Mou, Z., Fan, W., and Dong, X. (2003). Inducers of plant systemic acquired resistance regulate NPR1 function through redox changes. *Cell* 113, 935–944. doi: 10.1016/S0092-8674(03)00429-X

Murata, Y., Mori, I. C., and Munemasa, S. (2015). Diverse stomatal signaling and the signal integration mechanism. *Annu. Rev. Plant Biol.* 66, 369–392. doi: 10.1146/annurev-arplant-043014-114707

Neill, S., Desikan, R., and Hancock, J. (2002). Hydrogen peroxide signalling. *Curr. Opin. Plant Biol.* 5, 388–395. doi: 10.1016/S1369-5266(02)00282-0

Neill, S. J., Desikan, R., and Hancock, J. T. (2003). Nitric oxide signalling in plants. *New Phytol.* 159, 11–35. doi: 10.1046/j.1469-8137.2003.00804.x

Noctor, G., Gomez, L., Vanacker, H., and Foyer, C. H. (2002). Interactions between biosynthesis, compartmentation and transport in the control of glutathione homeostasis and signalling. *J. Exp. Bot.* 53, 1283–1304. doi: 10.1093/jexbot/53.372.1283

O'Brien, J. A., Daudi, A., Butt, V. S., and Bolwell, G. P. (2012a). Reactive oxygen species and their role in plant defence and cell wall metabolism. *Planta* 236, 765–779. doi: 10.1007/s00425-012-1696-9

O'Brien, J. A., Daudi, A., Finch, P., Butt, V. S., Whitelegge, J. P., Souda, P., et al. (2012b). A peroxidase-dependent apoplastic oxidative burst in cultured *Arabidopsis* cells functions in MAMP-elicited defense. *Plant Physiol.* 158, 2013–2027. doi: 10.1104/pp.111.190140

Paciorek, T., Zažímalová, E., Ruthardt, N., Petrášek, J., Stierhof, Y. D., Kleine-Vehn, J., et al. (2005). Auxin inhibits endocytosis and promotes its own efflux from cells. *Nature* 435, 1251–1256. doi: 10.1038/nature03633

Pandey, S., Wang, R. S., Wilson, L., Li, S., Zhao, Z., Gookin, T. E., et al. (2010). Boolean modeling of transcriptome data reveals novel modes of heterotrimeric G-protein action. *Mol. Syst. Biol.* 6:372. doi: 10.1038/msb.2010.28

Parsons, K., Nakatani, Y., and Nguyen, M. D. (2015). p600/UBR4 in the central nervous system. *Cell. Mol. Life Sci.* 72, 1149–1160. doi: 10.1007/s00018-014-1788-8

Passardi, F., Penel, C., and Dunand, C. (2004). Performing the paradoxical: how plant peroxidases modify the cell wall. *Trends Plant Sci.* 9, 534–540. doi: 10.1016/j.tplants.2004.09.002

Passardi, F., Tognolli, M., De Meyer, M., Penel, C., and Dunand, C. (2006). Two cell wall associated peroxidases from *Arabidopsis* influence root elongation. *Planta* 223, 965–974. doi: 10.1007/s00425-005-0153-4

Pei, Z. M., Murata, Y., Benning, G., Thomine, S., Klüsener, B., Allen, G. J., et al. (2000). Calcium channels activated by hydrogen peroxide mediate abscisic acid signalling in guard cells. *Nature* 406, 731–734. doi: 10.1038/35021067

Pottosin, I., Velarde-Buendía, A. M., Bose, J., Zepeda-Jazo, I., Shabala, S., and Dobrovinskaya, O. (2014). Cross-talk between reactive oxygen species and polyamines in regulation of ion transport across the plasma membrane: implications for plant adaptive responses. *J. Exp. Bot.* 65, 1271–1283. doi: 10.1093/jxb/ert423

Raschke, K. (1975). Simultaneous requirement of carbon dioxide and abscisic acid for stomatal closing in *Xanthium strumarium* L. *Planta* 125, 243–259. doi: 10.1007/BF00385601

Rhee, S. G., Bae, Y. S., Lee, S. R., and Kwon, J. (2000). Hydrogen peroxide: a key messenger that modulates protein phosphorylation through cysteine oxidation. *Sci. Signal.* 2000:e1. doi: 10.1126/stke.2000.53.pe1

Ruegger, M., Dewey, E., Hobbie, L., Brown, D., Bernasconi, P., Turner, J., et al. (1997). Reduced naphthylphthalamic acid binding in the *tir3* mutant of *Arabidopsis* is associated with a reduction in polar auxin transport and diverse morphological defects. *Plant Cell* 9, 745–757. doi: 10.1105/tpc.9.5.745

Rodrigues, O., Reshetnyak, G., Grondin, A., Saijo, Y., Leonhardt, N., Maurel, C., et al. (2017). Aquaporins facilitate hydrogen peroxide entry into guard cells to mediate ABA-and pathogen-triggered stomatal closure. *Proc. Natl. Acad. Sci. U.S.A.* 114, 9200–9205. doi: 10.1073/pnas.1704754114

Shi, K., Li, X., Zhang, H., Zhang, G., Liu, Y., Zhou, Y., et al. (2015). Guard cell hydrogen peroxide and nitric oxide mediate elevated CO_2-induced stomatal movement in tomato. *New Phytol.* 208, 342–353. doi: 10.1111/nph.13621

Sierla, M., Waszczak, C., Vahisalu, T., and Kangasjärvi, J. (2016). Reactive oxygen species in the regulation of stomatal movements. *Plant Physiol.* 171, 1569–1580. doi: 10.1104/pp.16.00328

Singh, R., Parihar, P., Singh, S., Mishra, R. K., Singh, V. P., and Prasad, S. M. (2017). Reactive oxygen species signaling and stomatal movement: current updates and future perspectives. *Redox. Biol.* 11, 213–218. doi: 10.1016/j.redox.2016.11.006

Slaymaker, D. H., Navarre, D. A., Clark, D., del Pozo, O., Martin, G. B., and Klessig, D. F. (2002). The tobacco salicylic acid-binding protein 3 (SABP3) is the chloroplast carbonic anhydrase, which exhibits antioxidant activity and plays a role in the hypersensitive defense response. *Proc. Natl. Acad. Sci. U.S.A.* 99, 11640–11645. doi: 10.1073/pnas.182427699

Song, Y., Miao, Y., and Song, C. P. (2014). Behind the scenes: the roles of reactive oxygen species in guard cells. *New Phytol.* 201, 1121–1140. doi: 10.1111/nph.12565

Suhita, D., Raghavendra, A. S., Kwak, J. M., and Vavasseur, A. (2004). Cytoplasmic alkalization precedes reactive oxygen species production during methyl jasmonate-and abscisic acid-induced stomatal closure. *Plant Physiol.* 134, 1536–1545. doi: 10.1104/pp.103.032250

Tian, S., Wang, X., Li, P., Wang, H., Ji, H., Xie, J., et al. (2016). Plant aquaporin AtPIP1;4 links apoplastic H_2O_2 induction to disease immunity pathways. *Plant Physiol.* 171, 1635–1650. doi: 10.1104/pp.15.01237

Tian, W., Hou, C., Ren, Z., Pan, Y., Jia, J., Zhang, H., et al. (2015). A molecular pathway for CO_2 response in *Arabidopsis* guard cells. *Nat. Commun.* 6:6057. doi: 10.1038/ncomms7057

Tognolli, M., Penel, C., Greppin, H., and Simon, P. (2002). Analysis and expression of the class III peroxidase large gene family in *Arabidopsis thaliana*. *Gene* 288, 129–138. doi: 10.1016/S0378-1119(02)00465-1

Tõldsepp, K., Zhang, J., Takahashi, Y., Sindarovska, Y., Hõrak, H., Ceciliato, P. H., et al. (2018). Mitogen-activated protein kinases MPK4 and MPK12 are key components mediating CO_2-induced stomatal movements. *Plant J.* 96, 1018–1035. doi: 10.1111/tpj.14087

Torres, M. A., Dangl, J. L., and Jones, J. D. (2002). *Arabidopsis* gp91^{phox} homologues AtrbohD and AtrbohF are required for accumulation of reactive oxygen intermediates in the plant defense response. *Proc. Natl. Acad. Sci. U.S.A.* 99, 517–522. doi: 10.1073/pnas.012452499

Torres, M. A., Jones, J. D., and Dangl, J. L. (2006). Reactive oxygen species signaling in response to pathogens. *Plant Physiol.* 141, 373–378. doi: 10.1104/pp.106.079467

Vanacker, H., Carver, T. L., and Foyer, C. H. (2000). Early H_2O_2 accumulation in mesophyll cells leads to induction of glutathione during the hyper-sensitive response in the barley-powdery mildew interaction. *Plant Physiol.* 123, 1289–1300. doi: 10.1104/pp.123.4.1289

Wang, Y. Q., Feechan, A., Yun, B. W., Shafiei, R., Hofmann, A., Taylor, P., et al. (2009). S-nitrosylation of AtSABP3 antagonizes the expression of plant immunity. *J. Biol. Chem.* 284, 2131–2137. doi: 10.1074/jbc.M806782200

Wang, C., Hu, H., Qin, X., Zeise, B., Xu, D., Rappel, W.-J., et al. (2016). Reconstitution of CO_2 regulation of SLAC1 anion channel and function of CO_2-permeable PIP2;1 aquaporin as CARBONIC ANHYDRASE4 interactor. *Plant Cell* 28, 568–582. doi: 10.1105/tpc.15.00637

Webb, A. A., and Hetherington, A. M. (1997). Convergence of the abscisic acid, CO_2, and extracellular calcium signal transduction pathways in stomatal guard cells. *Plant Physiol.* 114, 1557–1560. doi: 10.1104/pp.114.4.1557

Wei, J., Li, D. X., Zhang, J. R., Shan, C., Rengel, Z., Song, Z. B., et al. (2018). Phytomelatonin receptor PMTR 1-mediated signaling regulates stomatal closure in *Arabidopsis thaliana*. *J. Pineal. Res.* 65:e12500. doi: 10.1111/jpi.12500

Williams, A., Pétriacq, P., Schwarzenbacher, R. E., Beerling, D. J., and Ton, J. (2018). Mechanisms of glacial-to-future atmospheric CO_2 effects on plant immunity. *New Phytol.* 218, 752–761. doi: 10.1111/nph.15018

Woodward, F. I. (1987). Stomatal numbers are sensitive to increases in CO_2 from pre-industrial levels. *Nature* 327:617. doi: 10.1038/327617a0

Wu, Y., Zhang, D., Chu, J. Y., Boyle, P., Wang, Y., Brindle, I. D., et al. (2012). The *Arabidopsis* NPR1 protein is a receptor for the plant defense hormone salicylic acid. *Cell Rep.* 1, 639–647. doi: 10.1016/j.celrep.2012.05.008

Xu, E., Vaahtera, L., and Brosché, M. (2015). Roles of defense hormones in the regulation of ozone-induced changes in gene expression and cell death. *Mol. Plant* 8, 1776–1794. doi: 10.1016/j.molp.2015.08.008

Xu, Z., Jiang, Y., Jia, B., and Zhou, G. (2016). Elevated-CO_2 response of stomata and its dependence on environmental factors. *Front. Plant Sci.* 7:657. doi: 10.3389/fpls.2016.00657

Yamada, J., Yoshimura, S., Yamakawa, H., Sawada, M., Nakagawa, M., Hara, S., et al. (2003). Cell permeable ROS scavengers, Tiron and Tempol, rescue PC12 cell death caused by pyrogallol or hypoxia/reoxygenation. *Neurosci. Res.* 45, 1–8. doi: 10.1016/S0168-0102(02)00196-7

Yamaguchi, N., Suzuki, M., Fukaki, H., Morita-Terao, M., Tasaka, M., and Komeda, Y. (2007). CRM1/BIG-mediated auxin action regulates *Arabidopsis* inflorescence development. *Plant Cell Physiol.* 48, 1275–1290. doi: 10.1093/pcp/pcm094

Yamauchi, S., Mano, S., Oikawa, K., Hikino, K., Teshima, K. M., Kimori, Y., et al. (2019). Autophagy controls reactive oxygen species homeostasis in guard cells that is essential for stomatal opening. *Proc. Natl. Acad. Sci. U.S.A.* 116, 19187–19192. doi: 10.1073/pnas.1910886116

Yang, Y., Costa, A., Leonhardt, N., Siegel, R. S., and Schroeder, J. I. (2008). Isolation of a strong *Arabidopsis* guard cell promoter and its potential as a research tool. *Plant Methods* 4:6. doi: 10.1186/1746-4811-4-6

Yin, Y., Adachi, Y., Ye, W., Hayashi, M., Nakamura, Y., Kinoshita, T., et al. (2013). Difference in abscisic acid perception mechanisms between closure induction and opening inhibition of stomata. *Plant Physiol.* 163, 600–610. doi: 10.1104/pp.113.223826

Zhang, J., De-oliveira-Ceciliato, P., Takahashi, Y., Schulze, S., Dubeaux, G., Hauser, F., et al. (2018). Insights into the molecular mechanisms of CO_2-mediated regulation of stomatal movements. *Curr. Biol.* 28, R1356–R1363. doi: 10.1016/j.cub.2018.10.015

Zhang, R. X., Ge, S., He, J., Li, S., Hao, Y., Du, H., et al. (2019). BIG regulates stomatal immunity and jasmonate production in *Arabidopsis*. *New Phytol.* 222, 335–348. doi: 10.1111/nph.15568

Zhang, S., Li, X., Sun, Z., Shao, S., Hu, L., Ye, M., et al. (2015). Antagonism between phytohormone signalling underlies the variation in disease susceptibility of tomato plants under elevated CO_2. *J. Exp. Bot.* 66, 1951–1963. doi: 10.1093/jxb/eru538

Zhou, Y., Vroegop-Vos, I., Schuurink, R. C., Pieterse, C. M., and Van Wees, S. (2017). Atmospheric CO_2 alters resistance of *Arabidopsis* to *Pseudomonas syringae* by affecting abscisic acid accumulation and stomatal responsiveness to coronatine. *Front. Plant Sci.* 8:700. doi: 10.3389/fpls.2017.00700

Conflict of Interest: The authors declare that the research was conducted in the absence of any commercial or financial relationships that could be construed as a potential conflict of interest.

frontiers in Plant Science

ORIGINAL RESEARCH
published: 08 May 2020
doi: 10.3389/fpls.2020.00478

Competition and Drought Alter Optimal Stomatal Strategy in Tree Seedlings

Nicole Zenes[1], Kelly L. Kerr[1], Anna T. Trugman[1,2] and William R. L. Anderegg[1]*

[1] School of Biological Sciences, University of Utah, Salt Lake City, UT, United States, [2] Department of Geography, University of California, Santa Barbara, Santa Barbara, CA, United States

A better understanding of plant stomatal strategies holds strong promise for improving predictions of vegetation responses to drought because stomata are the primary mechanism through which plants mitigate water stress. It has been assumed that plants regulate stomata to maintain a constant marginal water use efficiency and forego carbon gain when water is scarce. However, recent hypotheses pose that plants maximize carbon assimilation while also accounting for the risk of hydraulic damage via cavitation and hydraulic failure. This "gain-risk" framework incorporates competition in stomatal regulation because it takes into account that neighboring plants can "steal" unused water. This study utilizes stomatal models representing both the water use efficiency and carbon-maximization frameworks, and empirical data from three species in a potted growth chamber experiment, to investigate the effects of drought and competition on seedling stomatal strategy. We found that drought and competition responses in the empirical data were best explained by the carbon-maximization hypothesis and that both drought and competition affected stomatal strategy. Interestingly, stomatal responses differed substantially by species, with seedlings employing a riskier strategy when planted with a high water use competitor, and seedlings employing a more conservative strategy when planted with a low water use competitor. Lower water users in general had less stomatal sensitivity to decreasing Ψ_L compared to moderate to high water users. Repeated water stress also resulted in legacy effects on plant stomatal behavior, increasing stomatal sensitivity (i.e., conservative behavior) even when the seedling was returned to well-watered conditions. These results indicate that stomatal strategies are dynamic and change with climate and competition stressors. Therefore, incorporating mechanisms that allow for stomatal behavioral changes in response to water limitation may be an important step to improving carbon cycle projections in coupled climate-Earth system models.

Keywords: plant hydraulics, drought, competition, stomatal optimization, water stress

OPEN ACCESS

Edited by:
Elena D. Shpak, The University of Tennessee, Knoxville, United States

Reviewed by:
Caspar Christian Cedric Chater, University of Sheffield, United Kingdom
Matthew Haworth, Institute for Sustainable Plant Protection, Italian National Research Council, Italy
Michael Vincent Mickelbart, Purdue University, United States

****Correspondence:***
Nicole Zenes
Nicole.zenes@utah.edu;
nicolezenes@gmail.com

Specialty section:
This article was submitted to Plant Development and EvoDevo, a section of the journal Frontiers in Plant Science

Received: *07 December 2019*
Accepted: *31 March 2020*
Published: *08 May 2020*

Citation:
Zenes N, Kerr KL, Trugman AT and Anderegg WRL (2020) Competition and Drought Alter Optimal Stomatal Strategy in Tree Seedlings. Front. Plant Sci. 11:478. doi: 10.3389/fpls.2020.00478

INTRODUCTION

Stomata are small pores on plant leaves that control the rate at which carbon is gained and water is lost. Stomata are the primary mechanism through which plants can mitigate water stress (Jones and Sutherland, 1991) and often respond first to changes in environmental conditions and hormone signaling (Schroeder et al., 2001) by opening or closing on short timescales

(i.e., minutes) to regulate stomatal conductance and gas exchange rates. Many studies have investigated the sensitivity of stomatal conductance to environmental drivers including soil moisture (Ali et al., 1998) and humidity (Aasamaa and Sober, 2010) as well as physiological metrics that are indicative of changes in environmental stimuli including drought-induced changes in leaf abscisic acid concentrations (a stress hormone in leaves; Bahrun et al., 2002) and leaf water potential (Ψ_L; Lawlor and Tezara, 2009). While substantial progress has been made in understanding the physiology underlying stomatal regulation, we currently lack a fully mechanistic understanding. Thus, optimal stomatal behavior theories, where stomata aim to maximize fitness, hold substantial promise for mechanistically predicting stomatal behavior (Cowan and Farquhar, 1977; Katul et al., 2009; Medlyn et al., 2011; Wolf et al., 2016). The stomatal models based on optimal behavior theory are built on the critical trade-off between carbon uptake and water loss, particularly during unfavorable environmental conditions, and can inform predictions of plant productivity and survival under potential novel future climate conditions.

The literature related to optimal stomatal behavior theories is extremely rich, and largely began with seminal work by Cowan and Farquhar (1977) which has been subsequently extended to many environmental conditions and species (Katul et al., 2009; Manzoni et al., 2011; Medlyn et al., 2011; Lin et al., 2015; Buckley, 2017). The Cowan and Farquhar theory was developed using the assumption that plants maximize photosynthesis (A_N) over time while limiting transpiration (E). "Optimal" stomatal behavior occurs when $\delta A_N/\delta E$ (the marginal water use efficiency) is equal to a constant λ (or $1/\lambda$ in some formulations) (Cowan and Farquhar, 1977; Buckley, 2017). Under this water use efficiency (WUE) hypothesis, plants adjust stomatal conductance to maintain a constant $\delta A_N/\delta E$ ratio over a given period of time, which is often not specified but has been studied with timeframes spanning from a day to multiple seasons in the literature (Manzoni et al., 2013; Novick et al., 2016; Anderegg et al., 2018). This theory, however, does not account for competition between plants for a shared water supply, which is a critical component of terrestrial ecosystem dynamics given widespread root system overlap (Casper and Jackson, 1997).

More recent studies have proposed and employed a "gain-risk" carbon maximization (CM) hypothesis that optimizes stomatal conductance based on photosynthetic gain versus the cost or risks to the hydraulic continuum associated with decreases in Ψ_L (Prentice et al., 2014; Wolf et al., 2016; Sperry et al., 2017; Anderegg et al., 2018; Eller et al., 2018; Venturas et al., 2018). The carbon maximization hypothesis uses a game theory approach where plants are under selective pressure to prevent both short- and long-term consequences associated with water limitation, namely the risk of hydraulic damage via cavitation and hydraulic failure associated with low Ψ_L, to simulate the effects of competition (Wolf et al., 2016). Under the CM hypothesis, optimal stomatal behavior aims to maximize A_N while minimizing a hydraulic cost/risk term [defined here as $\theta(\Psi_L)$], at a given Ψ_L and set of environmental conditions. With this model, hydraulic cost or risk to the plant increases with declining Ψ_L. The steepness of this cost function indicates different plant physiological strategies for dealing with water stress. Plants with cost functions with steeper slopes follow a "water saver" strategy, and close stomata earlier as Ψ_L declines (**Figure 1**). Plants employing a "water spender" strategy tend to keep stomata open longer because their cost increases at a slower rate with more negative Ψ (**Figure 1**).

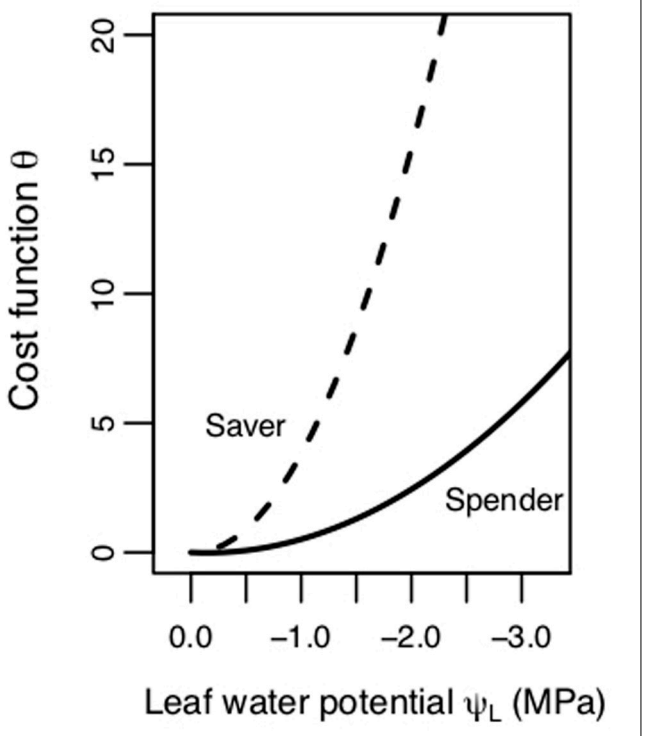

FIGURE 1 | Schematic of hydraulic cost/risk function (θ, unitless) as a function of leaf water potential (Ψ_L, MPa). One strategy is a riskier "spender" strategy (lower β_1 or slope value, shallower cost function) with stomata closing at a more negative Ψ_L. The other strategy is a more conservative "saver" strategy (higher β_1 or slope value, steeper cost function) with stomata closing faster as Ψ_L declines.

Stomatal behavior, in response to environmental and competitive cues, is modulated by a suite of physiological traits that regulate response to abiotic stress and avoid mortality while competing with neighbors for scarce resources (Piutti and Cescatti, 1997; Bottero et al., 2017). On short to moderate timescales (days to months), plant hydraulic and photosynthetic traits can plastically respond to the environment and buffer plant water stress during drought and competition (Callaway et al., 2003; Bartlett et al., 2014). These traits include the water potential at which cells lose turgor (turgor loss point, Ψ_{TLP}), leaf photosynthetic rate (expressed as the maximum rate of carboxylation, V_{cmax}), and hydraulic conductivity of different plant tissues (K). In addition, plants balance competitive capacity with the risk of hydraulic damage to xylem tissue, which can result in a long-term reduction in photosynthesis (Anderegg et al., 2014; Mackay et al., 2015; Trugman et al., 2018). Indeed, damage to water transport tissue is one major mechanism through which reduced photosynthetic capacity

(Resco et al., 2009) or even plant death (Allen et al., 2010; Phillips et al., 2010; Anderegg et al., 2015) can occur. Thus, untangling the mechanisms underlying how plants mediate hydraulic risk in balance with carbon gain is critical for predicting tree survival and productivity.

Moving forward, critical questions remain about the efficacy of different optimization hypotheses (CM vs. WUE) and whether stomatal strategy is an inherent and constrained trait with little plasticity or whether plants behavior changes with environmental conditions and competitive environment. While several studies have investigated optimized stomatal behavior in response to drought alone (Sperry and Love, 2015; Anderegg et al., 2018; Lu et al., 2019), our understanding of this behavior in response to the complex interactions between drought and competition is limited. Therefore, we ask: (1) Do stomatal responses to environmental variation support the WUE or CM stomatal theory; (2) Does competition affect the sensitivity of stomatal closure to Ψ_L (i.e., cost function steepness); (3) Do plants change their stomatal behavior following drought; and (4) Is stomatal behavior explained by concomitant changes in other hydraulic metrics? Critically, answers to these questions will significantly advance our understanding of stomatal behavior because our experiment allows us to directly examine the effects of competition on stomatal strategy.

MATERIALS AND METHODS

Study Design

We conducted a growth chamber experiment in which *Populus tremuloides*, *Populus angustifolia,* and *Pinus ponderosa* (referred to hereafter as aspen, cottonwood, and pine, respectively) seedlings were planted with a competitor or alone and subsequently subject to multiple periods of water stress. We describe the design and measurements briefly here, full details are in Kerr et al. (unpublished). We chose these species because they co-exist in natural stands where competition is likely to occur, and they employ a spectrum of water use strategies ranging from high/profligate water users (cottonwoods), to intermediate (aspen), and low/conservative (pine) (Anderegg and HilleRisLambers, 2016). Each seedling was either grown alone in an 18-l square pot with 15 l of soil or in competition with another seedling in a 36-l rectangular (i.e., two 18 L square pots connected together) pot with 30 l of soil with another seedling to maintain the same amount of relative resources (**Supplementary Figure S1**). There were six replicates of the following planting groups: aspen grown alone (A), cottonwood grown alone (C), pine grown alone (P), aspen competing with another aspen (AxA), aspen competing with cottonwood (AxC), and aspen competing with pine (AxP) (**Supplementary Figure S2**). As one of the most widespread tree species in North America, aspen is important across a vast diversity of ecosystems. However, it has been found to be sensitive to drought and susceptible to drought-induced mortality (Anderegg et al., 2012; Worrall et al., 2013). Therefore, in order to accommodate space constraints of the growth chamber, we chose aspen to be our focal species when designing the study.

The baseline conditions in the growth chamber were set to 25°C temperature, 75% relative humidity, 1150 μmol m^{-2} s^{-1} photosynthetic photon flux density, and 400 ppm ambient carbon dioxide (CO_2). Photoperiod for the growth chamber was set to closely match that of the greenhouse, where the seedlings were initially grown, with lights on from 6:00 to 19:15 using EYE HORTILUX ceramic metal halide 315 W grow lamp lights. During the predrought treatment period, we weighed a subset of pots and calculated a baseline average water volume to be given daily. Then we imposed three water limitation treatments sequentially – a low soil moisture treatment, an elevated vapor pressure deficit (VPD) treatment, and a combination of both simultaneously – on the seedlings. We took gas exchange and hydraulic measurements during the control predrought period, each treatment period, and a subsequent a post treatment recovery period. Each drought treatment lasted 5 days and seedlings were allowed to recover for 3 days in between treatments by returning to both baseline watering and growth chamber conditions. During the soil drought, we gave seedlings 50% of the water they were receiving during the predrought baseline period. During the elevated VPD treatment, watering was returned to the predrought water regime, and relative humidity was reduced from ∼75% to ∼45%. For the combination drought, reduced watering to 25% of their daily water and reduced relative humidity to 45% to impose the most significant water stress (**Supplementary Table S1**). Post drought treatments, the seedlings were returned to the predrought (control) conditions for 3 days.

We then fitted the WUE and CM optimization models to observed stomatal conductance measurements and compared the best fits to determine which hypothesis more skillfully predicted observed stomatal responses. Next, we evaluated how the hydraulic risk function related to competition treatment, water stress, and plant traits. The performance of the WUE and CM models, and how the hydraulic cost/risk function varied, provides insight into species' stomatal strategies and their dynamics. We describe the modeling approach in detail below.

Modeling Photosynthesis, Water Transport and Stomatal Conductance

We fitted our data with a stomatal optimization model that uses well-established equations for modeling photosynthesis, hydraulic conductivity, and water transport and can use either λ (i.e., the WUE theory) or θ(Ψ_L) (i.e., the CM theory) for the optimality criterion (Anderegg et al., 2018). The core components of the model are as follows. For photosynthesis, Farquhar et al. (1980) (eqn. 1) was used to model net carbon assimilation (A_N) as the smallest of two limiting factors; rubisco limitation (w_c) and light limitation (w_j).

$$A_N = \min(w_c, w_j) - R_d \quad (1)$$

where R_d is the rate of dark respiration. The relationship between carbon assimilation and stomatal conductance was calculated using Equation 2, based on Fick's Law,

$$A_N = \frac{g_S(C_a - C_i)}{1.6} \quad (2)$$

where, g_s is stomatal conductance, C_a is the atmospheric concentration of CO_2, C_i is the internal concentration of CO_2 inside the leaf, and 1.6 accounts for the difference in diffusion rates of water vapor and CO_2.

Transpiration is represented by Equation 3,

$$E = g_S(e_S - e_a) \tag{3}$$

where e_s is the saturated vapor pressure inside the leaf and e_a is the actual vapor pressure of the air.

Steady-state transpiration is modeled by Equation 4,

$$E = \int_{\psi L}^{\psi S} K(\psi) d\psi \tag{4}$$

where Ψ_S is soil water potential, and $K(\Psi)$ is the xylem conductance function. Conductance is calculated by Equation 5

$$K(\psi_L) = K_{\max} * \exp^{(-(\frac{P}{-B})^C)} \tag{5}$$

where C and B Weibull curve parameters were estimated from the stem vulnerability curves (see physiological measurements below) using a bootstrapping method (Hacke et al., 2015), P is leaf water potential, and K_{max} is the whole plant maximum xylem conductance. In our modeling framework, K_{max} was unknown, thus we estimated K_{max} assuming that plants want to maximize productivity without compromising the hydraulic system. Thus, calculated to maximize the difference between measured predawn and calculated midday Ψ_L while not exceeding the median water potential where 50% of maximum hydraulic conductivity is lost (P_{50}), and satisfy the remaining equations (Eqn. 1–5) according to the methods in Anderegg et al. (2018). For the aspen grown alone and cottonwood grown with a competitor planting groups, in order to provide solutions for the remaining equations with viable priors for β_1 and λ, the estimated K_{max} resulted in a midday Ψ_L that exceeded P50 with $\Psi_L = -3.00$ MPa (P50 = −2.69 MPa) and $\Psi_L = -1.35$ MPa (P50 = −1.31 MPa), respectively.

Modeling Plant Response to Water Stress

To understand how plants balance carbon gain versus risk/cost during water stress, we used an optimality equation that relies on measurements of stomatal conductance to estimate a "shadow cost" (or risk to future plant performance) function for both the WUE and CM theory. As described in Wolf et al. (2016) the marginal xylem tension efficiency (MXTE) is the amount of carbon gain a plant is willing to forgo to prevent a decrease in Ψ_L. Importantly, the MXTE differs between the WUE and CM optimality theories as shown by Equations 6 and 7:

$$MXTE_{WUE} = \lambda \frac{\delta E}{\delta \psi_L} \tag{6}$$

and

$$MXTE_{CM} = \frac{\delta \theta}{\delta \psi_L} \tag{7}$$

where λ is the constant marginal water use efficiency, E is transpiration, θ is the cost/risk term.

We linearized the derivative of the cost function such that

$$\frac{\delta \theta}{\delta \psi_L} = \beta_1 \psi_L + \beta_0 \tag{8}$$

where β_1 and β_0 are parameters fitted using observational stomatal conductance measurements. The linearized form of the derivative is advantageous in that it (i) distinguishes between the increasing versus decreasing responses of $\delta\theta/\delta\Psi$ to decreases in Ψ_L in the CM and WUE hypotheses, respectively, and (ii) minimizes unconstrained parameters. This linear marginal cost function implies a parabolic form of the cost/risk function with declining water potential (Anderegg et al., 2018):

$$\theta(\psi_L) = \frac{\beta_1}{2}\psi_L^2 + \beta_0 \psi_L + c \tag{9}$$

where c is the intercept of the cost function, which is not solved for because the derivative gives the necessary information to quantify stomatal strategies.

Parameter Estimation

A Markov-Chain Monte Carlo (MCMC) algorithm was used to calculate the posterior probability density function (PDF) of β_1 or λ that provided the best fit between observed and modeled stomatal conductance for the CM or WUE models, respectively. MCMCs were run for each of the WUE and CM models for species type (aspen, cottonwood, and pine) and each planting group (competition and no competition), for a total of eight different fitting groups per model. For the CM model, we found that the best β_1 and β_0 often covaried, leading to an equifinality issue (eq. 8). Therefore, we ran a series of MCMCs (∼50) each using a different fixed value of β_0 in order to estimate β_1. For each of the eight fitting groups, we determined the range of initial β_0 values (**Table 1**) that would allow a solution to the system of equations with variables in biologically realistic bounds (Ψ_L within [−10,0]) for each planting group using an initial value of $\beta_1 = 0.1$. This value was chosen because a positive β_1 represents a marginal increase in cost of damage with decreasing Ψ_L, so it is physiologically realistic, but is still a relatively uninformed initial guess . When running the series of MCMCs, our range and increment of β_0 values (**Table 1**) was chosen because it allowed us to explore the full parameter space while maintaining a level of reasonable computational efficiency. Each separate MCMC was run for 5000 steps for each of the fixed β_0. The first 1000 steps were discarded as burn in and we sampled for every tenth step to account for temporal autocorrelation to represent the posterior PDF. The mode of the posterior PDF was used as the estimated β_1.

For the WUE model, for each of the eight planting groups, we ran MCMCs with an initial guess of $\lambda = 0.1$. For some fitting groups, no solution to the system of equations could be found at small λ values so we gradually increased our initial guess by increments of 0.1 until a solution could be obtained. When proposing the next step running the MCMCs, we confine lambda to the positive parameter space as a negative value would imply a decrease in cost as Ψ_L becomes more negative. We used linear models and the Akaike Information Criterion (AIC) score for all three species to assess model performance and determined that

TABLE 1 | Range of fixed β_0 values used to estimate β_1.

Planting group	Lowest β_0	Highest β_0	Sequenced by
Aspen alone (A)	−7.9	0.6	0.1
Aspen × aspen (AxA)	−10.9	0.6	0.1
Aspen × cottonwood (AxC)	−9	0.6	0.1
Aspen × pine (AxP)	−12.4	0.4	0.2
Cottonwood alone (C)	−8.1	0.3	0.2
Cottonwood × aspen (CxA)	−15.7	0.5	0.2
Pine alone (P)	−4.6	0.5	0.1
Pine × aspen (PxA)	−4.1	0.4	0.1

Values allow the MCMC to be run with a prior start value of β_1 = 0.1. Three planting groups; aspen competing with pines (AxP), cottonwoods grown alone (C), and cottonwoods competing with aspen (CxA), were sequenced by 0.2 due to computing power available.

the CM model more skillfully predicted stomatal conductance compared to the WUE model for all three of our species. Thus, for subsequent analyses we used only the CM model.

When investigating effects of competition between planting groups, we performed one fit using all the stomatal conductance measurements for each planting group taken across the five treatment periods for the CM only. When looking at effects of treatment period within a planting group, we performed separate fits using the subset of stomatal conductance measurements taken at each treatment period; predrought, soil drought, VPD drought, combination soil and VPD drought, and post drought recovery. Because we only calculated V_{cmax} during the predrought and post drought recovery periods, we used the predrought measured V_{cmax} values for the predrought and three drought periods and the post drought measured V_{cmax} for the post drought recovery treatment period (Kerr et al., unpublished).

Physiological Measurements

At each treatment period, we took gas exchange measurements using a Li-6400 open gas exchange system with a red-blue light source and conditions set to maintain 25°C leaf temperature, 1200 μmol m^{-2} s^{-1} photosynthetic photon flux density, 400 ppm ambient CO_2, and relative humidity matching that of the growth chamber for the current treatment period. Predawn leaf water potential (Ψ_{PD}) was measured for each seedling using a Scholander-type pressure chamber before the growth

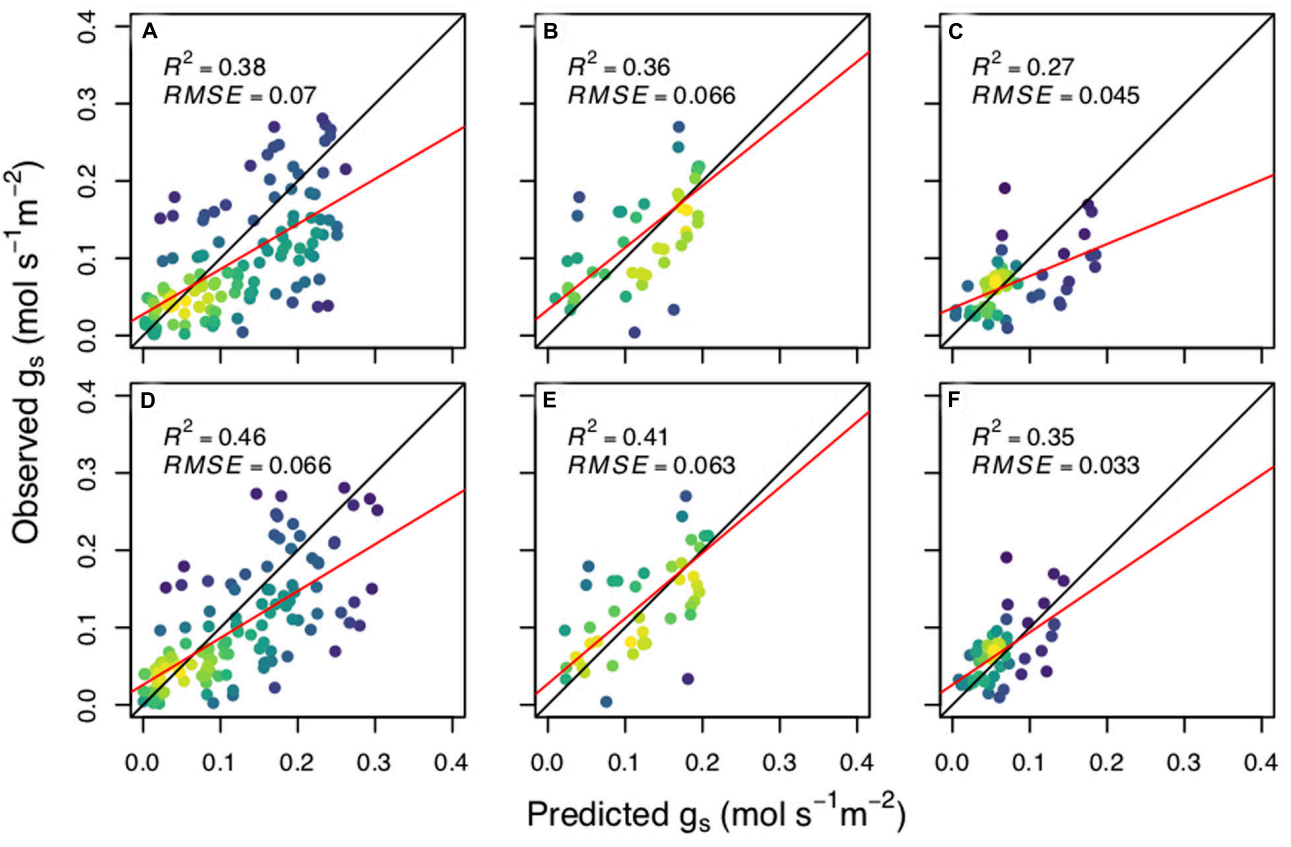

FIGURE 2 | The predicted stomatal conductance (g_s) versus observed stomatal conductance (mol s^{-1} m^{-2}). Upper panel values were calculated using the water use efficiency model for each species; *Populus tremuloides* **(A)**, *Populus angustifolia* **(B)**, and *Pinus ponderosa* **(C)**. The bottom panels were calculated using the carbon maximization model for each species (**D–F**, respectively). β_0 and best fit β_1 were estimated for each planting group and plotted together for predictive power per species. Black lines represent the 1:1 line, red lines are the best fit for linear regression and adjusted R^2 and root mean square error (RMSE) values are reported. Yellow indicates a higher density of points while purple represents a lower density.

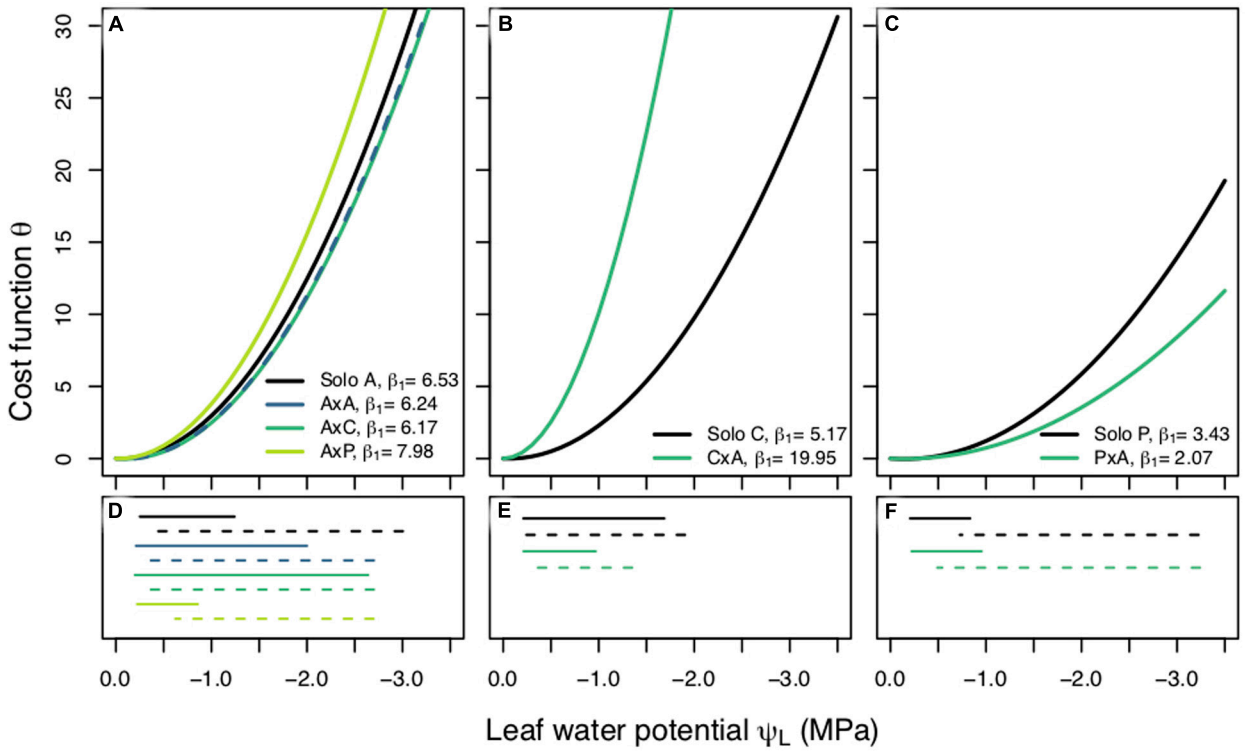

FIGURE 3 | Cost functions (θ) between planting groups within a species plotted against leaf water potential (Ψ_L, MPa). Each curve is produced using the best fit β_1 value and the corresponding fixed β_0. Best fit β_1 values are reported for each planting group. Panels are separated by species; *Populus tremuloides* **(A)**, *Populus angustifolia* **(B)**, and *Pinus ponderosa* **(C)** and each planting group is represented by a different color. Measured predawn (Ψ_{PD}, solid lines), and modeled midday (Ψ_{MD}, dashed lines), water potentials plotted under their corresponding species **(D–F)**. Legend key for planting groups: aspen grown alone (A), aspen competing with aspen (AxA), aspen competing with cottonwoods (AxC), aspen competing with pines (AxP); cottonwoods grown alone (C), cottonwoods competing with aspen (CxA); pines grown alone (P), and pines competing with aspen (PxA).

chamber lights turned on (between the hours of 0400 and 0600) (**Figures 3D–F**). Samples for Ψ_{PD} were removed from the plant, placed in a sealed plastic bag, and water potential was measured within 5 min.

In the predrought and post drought periods, we measured vulnerability curves using the centrifuge method (Alder et al., 1997) and calculated the water potential at which 50 percent of the xylem conductivity is lost (P50). Using the standard flow method, we calculated percent loss of conductivity (PLC) comparing the native stem conductivity to the maximum hydraulic conductivity. V_{cmax} was determined from constructing A-Ci curves using a Li-6400 open gas exchange system and settings of 25°C leaf temperature, 1200 μmol m^{-2} s^{-1} photosynthetic photon flux density, 400 ppm ambient CO_2, and relative humidity matching that of the growth chamber. We also calculated the Ψ_{TLP} in the predrought and recovery periods using the pressure-volume method (Tyree and Hammel, 1972) with a Scholander-type pressure chamber and mass balance to measure Ψ_L and weight as samples periodically dried.

Analyses of Results

To answer our first question, we used the best fit parameters as determined from our initial MCMC simulations using the eight planting groups for each the WUE and CM models. Separate MCMC fits were calculated for each planting group and we used linear models and the Akaike Information Criterion (AIC) score to assess relative model performance.

To answer our second and third questions, we performed non-parametric analyses of longitudinal time series data for comparisons of β_1 values over time (treatment periods), comparisons of β_1 values between planting groups, and the interaction between time and planting group using R package (nparLD) (Noguchi et al., 2012) with β_0 representing repeated measures subjects in an ANOVA analysis. ANOVA-type statistics are reported, and Tukey HSD *post hoc* pairwise comparisons were conducted. For hydraulic metrics, we performed linear regressions for mean predrought and post drought recovery β_1 and TLP, PLC, and Ψ_{PD} for each species.

RESULTS

We found that the CM model more skillfully predicted stomatal conductance compared to the WUE model for all three of our species: aspen (R^2_{WUE} = 0.38, R^2_{CM} = 0.46) (**Figures 2A,D**), cottonwood (R^2_{WUE} = 0.42, R^2_{CM} = 0.54) (**Figures 2B,E**), and pine (R^2_{WUE} = 0.27, R^2_{CM} = 0.35) (**Figures 2C,F**). The

CM model also had a lower AIC than the WUE model for all species: $aspen_{WUE} = -331.9$, $aspen_{CM} = -349.1$; $cottonwood_{WUE} = -218.5$, $cottonwood_{CM} = -235.2$; $pine_{WUE} = -201.6$, $pine_{CM} = -207.6$.

We found different responses to competition across our three species. The results of a non-parametric two-way repeated measures ANOVA for aspen showed that planting group had a significant effect on β_1 and the *post hoc* Tukey HSD pairwise test indicated that competitor identity, in addition to competitor presence, had an effect on β_1. Specifically, a high water use competitor, such as aspen and cottonwood, resulted in a riskier stomatal strategy than when aspen were grown alone or with a pine (**Figure 3A**). Cottonwoods grown with a competitor saw a shift to a larger β_1 value and cost function with a steeper slope (**Figure 3B**) ($p < 0.0001$) indicating cottonwood seedlings' stomatal behavior was more conservative under competition. Interestingly, pines had the opposite response: pines under competition employed a riskier stomatal strategy, had a small β_1 value ($p < 0.0001$), and a cost function with a shallower slope (**Figure 3C**). β_1 values also varied across species: cottonwoods had largest β_1, aspens had a more moderate β_1, and pines had the smallest β_1, indicating that water use strategy may relate to the rate of stomatal closure as Ψ_L declines.

Planting group, treatment, and their interaction all had an effect on β_1 (**Figure 4**). Repeated measures tests were significant for differences between planting groups, treatment period, and the interaction between group and period ($p < 0.0001$) for all three species. For aspen and cottonwoods, all treatment periods pairwise comparisons were significant ($p < 0.01$) indicating that both drought presence and type resulted in shifts in β_1. Pines saw less of an effect of treatment periods on β_1, likely due to the fact that pines experienced less severe water stress compared to aspens and cottonwoods (as verified through Ψ_{PD}). However, pine recovery β_1 were significantly different from predrought β_1, VPD drought β_1, and combination drought β_1 ($p < 0.0001$), indicating that there was an effect of water stress on pine stomatal behavior.

Interactions between planting group and treatment period had a variety of responses (**Table 2**). Aspen grown alone, aspen competing with cottonwoods (AxC), and aspen competing with pine (AxP) had no significant differences in β_1 values during the predrought period, but all four planting groups β_1 values were significantly different in the post-drought recovery period, indicating that there was an effect of competitor identity on changes in β_1 following drought treatments ($p < 0.0001$). Within each of the aspen planting groups, recovery β_1 values were significantly different from all other time periods providing further evidence that drought affected stomatal behavior ($p < 0.0001$). High water use competitors, such as the case when aspen competed with aspen (AxA) or cottonwood (AxC), resulted in larger recovery β_1, while the aspen grown alone and aspen competing with pine resulted in a smaller recovery β_1 (**Figure 4A**), suggesting increased competition for water stimulates a more dramatic shift toward a more conservative stomatal strategy post water stress treatment (after drought).

Within cottonwood planting groups, the majority of treatment periods were significantly different ($p < 0.05$) and their recovery β_1 values were largest, indicating that repeated drought treatments led to a shift toward a more conservative stomatal strategy. Competitors also affected how seedlings responded to each sequential drought: solo cottonwoods and competing cottonwoods had different β_1 values during all treatment periods (**Figure 4B**). Pines grown without a competitor responded to the drought treatments and shifted to a more conservative stomatal, as indicated by a larger recovery β_1 compared to pretreatment β_1, VPD treatment β_1, and combination drought treatment β_1 ($p < 0.001$). Contrary to patterns seen in the other species and planting groups, pine competing with aspen (PxA) saw a statistically significant larger β_1 in the predrought period than the drought and post drought treatment periods. Within treatment periods, pines without a competitor and pines with a competitor were always significantly different ($p < 0.05$), indicating an effect of planting group on stomatal strategy (**Figure 4C**).

We found there were relationships between changes in physiological metrics and changes in β_1 such that a decrease in drought resistance and increase in hydraulic damage lead to a more conservative strategy in aspen and cottonwoods (**Figures 5A–F**). Larger β_1 values were correlated with less negative TLP and increased PLC for aspens (**Figures 5A,B**). However, only the PLC relationship was statistically significant ($p < 0.01$). Larger β_1 values were correlated with less negative TLP, PLC, and less negative Ψ_{PD} for cottonwoods (**Figures 5D–F**), although none were statistically significant. In contrast to the aspens and cottonwoods, pines saw a non-significant negative correlation with all three measurements (**Figures 5G–I**), such that stomatal closure rate decreased in step with increased PLC and less negative TLP.

DISCUSSION

Here we show the CM model more skillfully predicted stomatal response to water stress induced through both competition and drought compared to the WUE model. Further, we found that both competition and drought influenced stomatal strategies. Critically, the effects of competition were complicated and varied by species. Surprisingly, pines exhibited a riskier, "spenders" strategy in response to competition whereas cottonwoods exhibited a more conservative, "savers" strategy, which is counterintuitive based on our current understanding of their life history strategies. However, the competitor's water use strategy helps explain the magnitude and direction of shift in cost function with seedlings adopting a riskier strategy when competing with higher water users and a more conservative strategy when competing with lower water users. All three species showed this pattern across treatment periods with varying environmental conditions and watering regimes, and the magnitude of these shifts was likely related to the strength of competition., These results illustrate that gas exchange variation in individual trees and whole forest communities is likely influenced by a complex interplay among environmental stress, competitive stress, and stomatal and trait strategies.

Shifts in the shadow cost (MXTE) and pricing hydraulic risk in response to both competition and drought were explained by competitor species and adjustments in physiological traits. The

TABLE 2 | *Post hoc* Tukey HSD pairwise interaction comparisons for *Populus tremuloides, Populus angustifolia,* and *Pinus ponderosa*.

(a) Planting group	Treatment period	Pairwise comparisons within planting groups				
A	Predrought	A				
	Soil	A				
	VPD		B			
	Combination		B			
	Recovery			C		
AxA	Predrought	A				
	Soil	A				
	VPD		B			
	Combination		B			
	Recovery			C		
AxC	Predrought	A				
	Soil		B			
	VPD			C		
	Combination				D	
	Recovery					E
AxP	Predrought	A				
	Soil	A	B			
	VPD	A	B			
	Combination		B			
	Recovery			C		
C	Predrought	A				
	Soil		B			
	VPD			C		
	Combination				D	
	Recovery					E
CxA	Predrought	A				
	Soil		B			
	VPD		B			
	Combination			C		
	Recovery				D	
P	Predrought	A				
	Soil		B			
	VPD	A				
	Combination	A				
	Recovery		B			
PxA	Predrought	A				
	Soil		B			
	VPD		B			
	Combination		B			
	Recovery		B			

(b) Treatment period	Aspen planting groups	Pairwise comparisons within treatment periods			Cottonwood planting groups	Pairwise comparisons within treatment periods		Pine planting groups	Pairwise comparisons within treatment periods	
Predrought	A	a			C	a		P	a	
	AxA		b		CxA		b	PxA		b
	AxC	a								
	AxP	a								
Soil	A	a			C	a		P	a	
	AxA		b		CxA		b	PxA		b
	AxC			c						
	AxP	a	b							
VPD	A	a			C	a		P	a	
	AxA		b		CxA		b	PxA		b

(Continued)

TABLE 2 | Continued

(b) Treatment period	Aspen planting groups	Pairwise comparisons within treatment periods			Cottonwood planting groups	Pairwise comparisons within treatment periods		Pine planting groups	Pairwise comparisons within treatment periods	
	AxC			c						
	AxP	a	b							
Combination	A	a			C	a		P	a	
	AxA		b		CxA		b	PxA		b
	AxC	a	b							
	AxP	a	b							
Recovery	A	a			C	a		P	a	
	AxA		b		CxA		b	PxA		b
	AxC			c						
	AxP			d						

Letters represent statistically significant differences ($p < 0.05$). Panel (a) shows within planting group comparisons across treatment periods. Panel (b) shows within treatment period and between planting group comparisons. Planting groups are aspen grown alone (A), aspen competing with aspen (AxA), aspen competing with cottonwoods (AxC), aspen competing with pines (AxP), cottonwoods grown alone (C), cottonwood competing with aspen (CxA), pines grown alone (P) and pines competing with aspen (PxA).

angiosperm species had a positive correlation between PLC and β_1 such that the seedlings had both a higher PLC and larger β_1 during treatment recovery compared to the pretreatment period. The coordination between PLC and β_1 could be due to an increase in embolism, which would limit the amount of water seedlings could transport, causing a shift toward a "savers" stomatal behavior to avoid additional hydraulic damage (**Figure 1**). The relationships between larger β_1 and shifts in, TLP, PLC, and Ψ_{PD} were consistent with our hypotheses that increased hydraulic damage (i.e., higher PLC) and lower drought tolerance

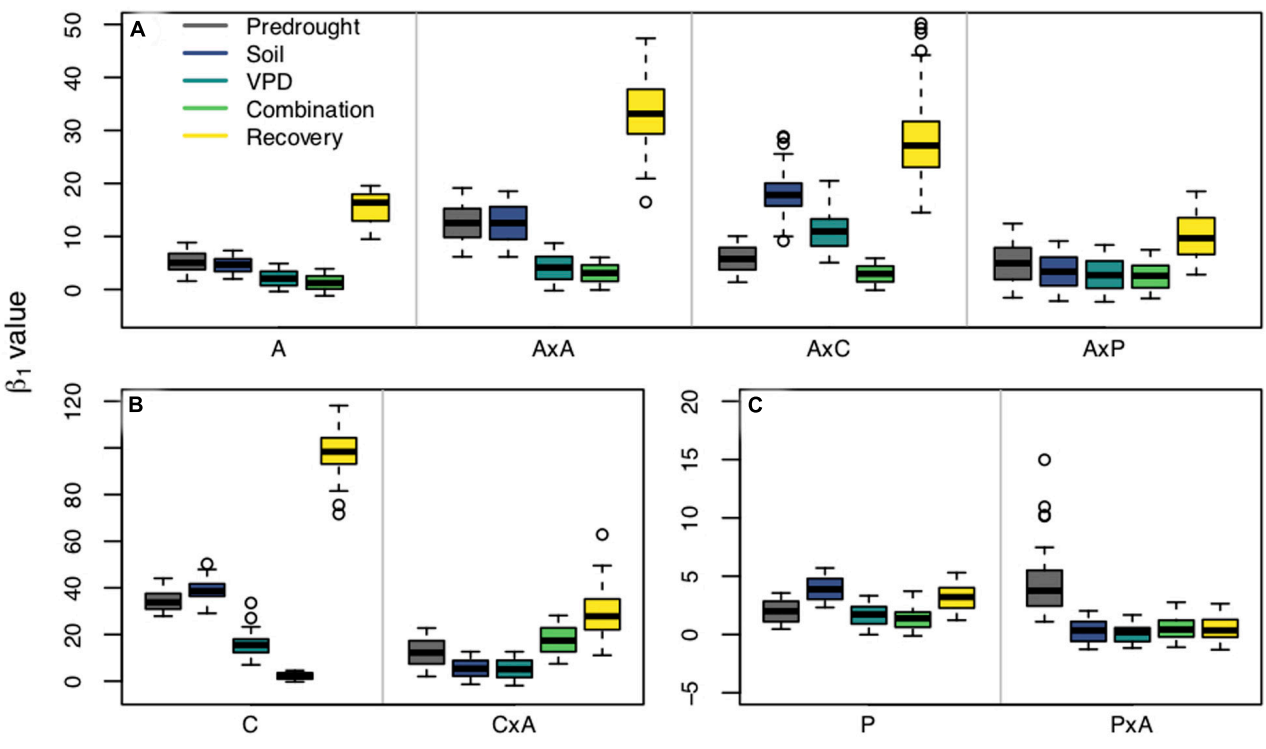

FIGURE 4 | β_1 values estimated from fixed β_0 values within planting groups across treatment periods [predrought, soil drought, vapor pressure deficit (VPD) drought, combination soil and VPD drought, and post drought recovery]. Panels are separated by species: *Populus tremuloides* **(A)**, *Populus angustifolia* **(B)**, and *Pinus ponderosa* **(C)**. Planting groups are separated within panels by gray lines: aspen grown alone (A), aspen competing with aspen (AxA), aspen competing with cottonwoods (AxC), aspen competing with pines (AxP); cottonwoods grown alone (C), cottonwoods competing with aspen (CxA); pines grown alone (P), and pine competing with aspen (PxA). Colors represent treatment periods. Boxplots show the median, 25th and 75th percentiles with whiskers extending to furthest data point up to 1.5x the interquartile range, and data points beyond this are considered outliers and represented by open circles. *Y*-axes vary between species.

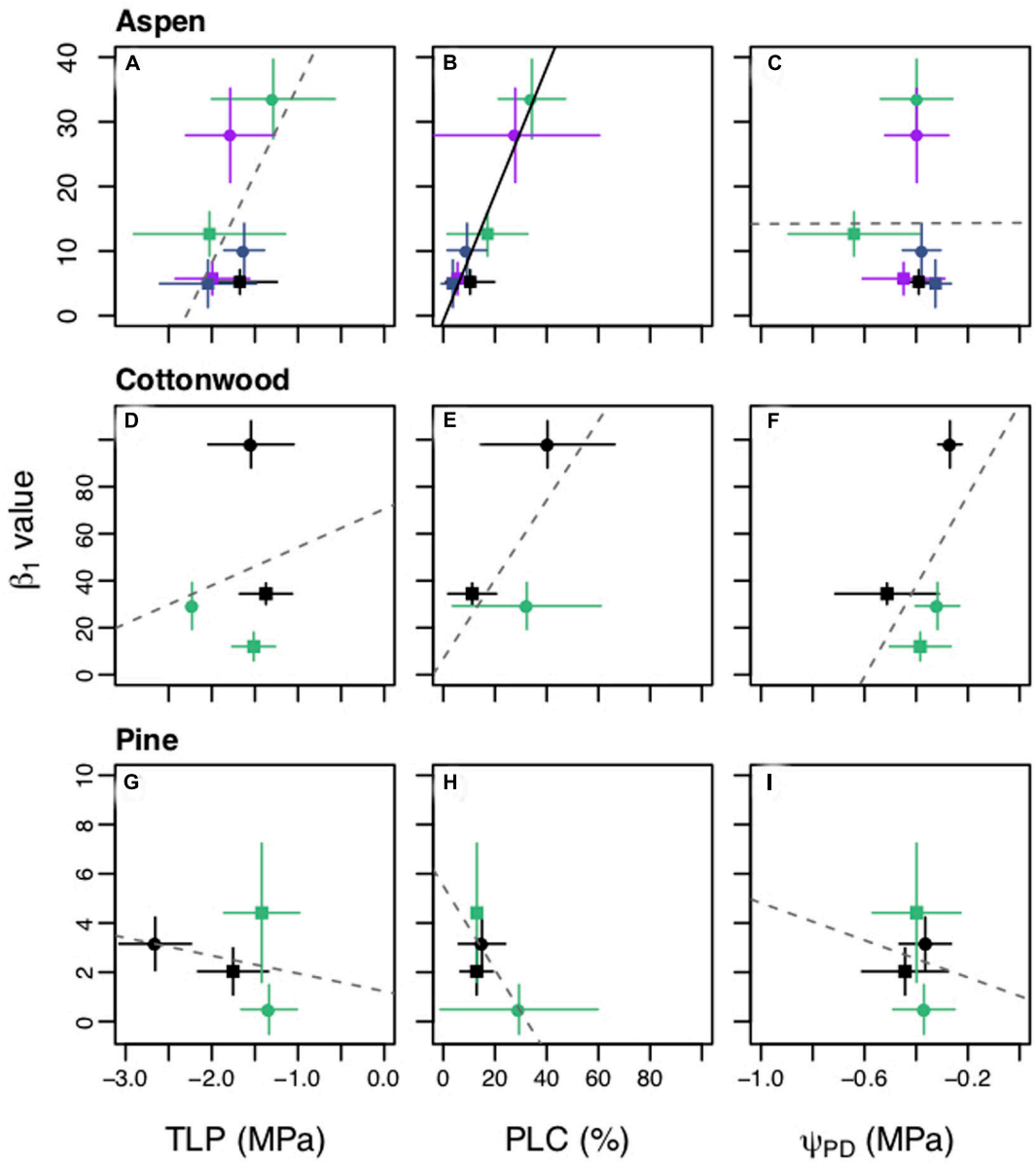

FIGURE 5 | Comparison of β_1 values with turgor loss point (TLP) **(A,D,G)**, percent loss of hydraulic conductivity (PLC) **(D,E,H)**, and predawn water potential (Ψ_{PD}) **(C,F,I)** during the predrought and post drought recovery treatment periods for each planting group. Panels are organized by species: *Populus tremuloides* **(A–C)**, *Populus angustifolia* **(D–F)**, *Pinus ponderosa* **(G–I)**. Squares (■) are predrought measurements and circles (●) are post drought measurements. Each planting group is represented by color, groups for the plants grown alone are in black. Aspen competing with aspen (AxA), cottonwood competing with aspen (CxA), and pine competing with aspen (PxA) groups are in green; aspen competing with cottonwoods (AxC) is in purple; and aspen competing with pine (AxP) is in blue. Mean values are plotted with ± one standard deviation bars shown. Solid black lines represent significant results ($p < 0.05$) and gray dashed lines for non-significant results for the best fit for ordinary least squares regression. *Y*-axes vary by species.

(less negative TLP) are associated with a shift toward a more conservative stomatal strategy. In addition, cottonwoods had less negative Ψ_{PD} in the recovery period, which is indicative of lower water stress, but also larger β_1, further supporting evidence of hydraulic damage and increased cost even at less negative Ψ_L. The pines, the only gymnosperm, had non-significant but slightly negative correlations between β_1 and TLP, PLC, and Ψ_{PD} and showed less variation in these variables, both within planting groups and across treatment periods (**Figures 5H,I**). This may be due to the fact that the pines were not significantly stressed during the drought treatments, resulting in less of a response in both β_1 and hydraulic metrics.

Increased stomatal sensitivity following drought events could have important impacts on productivity, even under well-water conditions, preventing plants from photosynthesizing and repairing hydraulic damage sustained during drought (Brodersen

and McElrone, 2013). This physiological response could help to explain a lag in growth recovery and mortality that has been observed following drought events (Anderegg et al., 2015; Peltier et al., 2016; Klockow et al., 2018; Trugman et al., 2018). This hypothesis is supported by other studies: Aasamaa and Sober (2011) found trees exposed to drought showed an increase in stomatal sensitivity to changes in environmental conditions following a recovery period. A positive correlation between PLC and β_1 would make it more difficult for trees to prepare for future drought events as they are forgoing carbon even under low atmospheric demand, due to increased stomatal sensitivity. Therefore, avoiding damage to hydraulic tissue and the increased carbon cost of recovering hydraulic conductivity could favor the selection for plants to become more conservative following drought periods (Brodribb et al., 2010). Some of these shifts in stomatal strategy could be due to changes in biochemical mechanisms, such as abscisic acid (ABA) concentrations, that have been shown to respond to drought and influence optimal stomatal behavior (Haworth et al., 2018; Brunetti et al., 2019). For example, increased foliar ABA has been shown to maintain stomatal closure when plants were returned to well-watered conditions (Tombesi et al., 2015). Investigating how long plants take to revert to their predrought strategy, as well as the mechanisms driving the adjustment, could give insight into ecosystem dynamics shifts following changes in frequency and severity of droughts.

While there have been a number of studies addressing the role of physiological traits and mechanisms affecting plant response during drought (Farooq et al., 2009), the recovery of photosynthetic rates, Ψ_{PD}, and leaf gas exchange in plant communities after natural drought has not been as thoroughly investigated (Flexas et al., 2006). The shifts we observed toward a more conservative stomatal strategy and more rapid stomatal closure as Ψ_L declined may help to explain the lag in gas exchange recovery following drought events, even when Ψ_L return to predrought levels (Pšidová et al., 2015). Indeed, Yin and Bauerle (2017) found that incomplete post-drought recovery was present across all plant functional types documented in their meta-analysis, although the magnitude varied greatly. Damage to hydraulic transport tissue has been found to be a major determinant of photosynthetic recovery in the desert perennial tree *Prosopis velutina* due to the increase in stomatal limitation even without changes to leaf biochemistry (Resco et al., 2009), which may explain the shift to a more conservative strategy with increased PLC following drought. Incorporating mechanisms that reflect underlying processes driving the changes in stomatal strategy and stomatal sensitivity into mechanistic models may help better predict changes in plant productivity following drought.

Here, we provide evidence that the CM hypothesis accurately predicts plant stomatal strategies in complex environmental and competitive stress scenarios. Further, overall stomatal behavior and shifts in stomatal strategy in response to drought were species-specific. Interestingly, higher water users showed increased sensitivity to changes in Ψ_L and had a larger shift to conservative strategies after drought had ended. Crucially, we show that drought and water stress, even on short term timescales, can have lasting effects on plant stomatal behavior even when the plants returned to favorable environmental conditions. As current climate models assume perfect plant recovery from water stress, there is a need to better describe and incorporate these stomatal behavior changes and plant recovery in order to better predict ecosystem fluxes and forest response to a changing climate.

DATA AVAILABILITY STATEMENT

The datasets generated for this study are available on request to the corresponding author.

AUTHOR CONTRIBUTIONS

All authors designed the experiment and carried out the data interpretation. WA developed the model. KK and NZ were involved in data collection. NZ performed the analyses. NZ wrote the manuscript with contributions from all other authors.

FUNDING

NZ acknowledges support from the NSF Graduate Research Fellowship Program Grant No. 1747505. KK acknowledges support from the University of Utah Global Change and Sustainability Center, and the University of Utah Rio Mesa Center. AT acknowledges support from the USDA National Institute of Food and Agriculture Postdoctoral Research Fellowship Grant No. 2018-67012-28020. WA acknowledges funding from the David and Lucile Packard Foundation, NSF Grants 1714972 and 1802880, and the USDA National Institute of Food and Agriculture, Agricultural and Food Research Initiative Competitive Programme, Ecosystem Services and Agro-ecosystem Management, grant no. 2018-67019-27850.

ACKNOWLEDGMENTS

The authors thank Grayson Badgley and Martin Venturas for assistance with interpretation of results and improving the quality of the manuscript. The authors also thank Christopher Morrow for his assistance with experiment set-up and management, and Mary Beninati, Jaycee Cappaert, Beth Blattenberger, Bryce Alex, Michaela Lemen, David Flocken, and Kailiang Yu for their assistance with greenhouse, growth chamber and laboratory work.

SUPPLEMENTARY MATERIAL

The Supplementary Material for this article can be found online at: https://www.frontiersin.org/articles/10.3389/fpls.2020.00478/full#supplementary-material

REFERENCES

Aasamaa, K., and Sober, A. (2010). Sensitivity of stem and petiole hydraulic conductance of deciduous trees to xylem sap ion concentration. *Biol. Plant.* 54, 299–307. doi: 10.1007/s10535-010-0052-9

Aasamaa, K., and Sober, A. (2011). Stomatal sensitivities to changes in leaf water potential, air humidity, CO2 concentration and light intensity, and the effect of abscisic acid on the sensitivities in six temperate deciduous tree species. *Environ. Exp. Bot.* 71, 72–78. doi: 10.1016/j.envexpbot.2010.10.013

Alder, N. N., Pockman, W. T., Sperry, J. S., and Nuismer, S. (1997). Use of centrifugal force in the study of xylem cavitation. *J. Exp. Bot.* 48, 665–674. doi: 10.1093/jxb/48.3.665

Ali, M., Jensen, C. R., and Mogensen, V. O. (1998). Early signals in field grown wheat in response to shallow soil drying. *Aust. J. Plant Physiol.* 25, 871–882.

Allen, C. D., Macalady, A. K., Chenchouni, H., Bachelet, D., Mcdowell, N., Vennetier, M., et al. (2010). A global overview of drought and heat-induced tree mortality reveals emerging climate change risks for forests. *For. Ecol. Manag.* 259, 660–684. doi: 10.1016/j.foreco.2009.09.001

Anderegg, L. D. L., and HilleRisLambers, J. (2016). Drought stress limits the geographic ranges of two tree species via different physiological mechanisms. *Glob. Change Biol.* 22, 1029–1045. doi: 10.1111/gcb.13148

Anderegg, W. R. L., Berry, J. A., Smith, D. D., Sperry, J. S., Anderegg, L. D. L., and Field, C. B. (2012). The roles of hydraulic and carbon stress in a widespread climate-induced forest die-off. *Proc. Natl. Acad. Sci. U.S.A.* 109, 233–237. doi: 10.1073/pnas.1107891109

Anderegg, W. R. L., Leander, D. L., Anderegg, J. A., Berry, D., and Field, C. B. (2014). Loss of whole-tree hydraulic conductance during severe drought and multi-year forest die-off. *Oecologia* 1, 11–23. doi: 10.1007/s00442-013-2875-5

Anderegg, W. R. L., Schwalm, C., Biondi, F., Camarero, J. J., Koch, G., Litvak, M., et al. (2015). Pervasive drought legacies in forest ecosystems and their implications for carbon cycle models. *Science* 349, 528–532. doi: 10.1126/science.aab1833

Anderegg, W. R. L., Wolf, A., Arango-Velez, A., Choat, B., Chmura, D. J., Jansen, S., et al. (2018). Woody plants optimise stomatal behaviour relative to hydraulic risk. *Ecol. Lett.* 21, 968–977. doi: 10.1111/ele.12962

Bahrun, A., Jensen, C. R., Asch, F., and Mogensen, V. O. (2002). Drought-induced changes in xylem pH, ionic composition, and ABA concentration act as early signals in field-grown maize (*Zea mays* L.). *J. Exp. Bot.* 53, 251–263. doi: 10.1093/jexbot/53.367.251

Bartlett, M. K., Zhang, Y., Kreidler, N., Sun, S., Ardy, R., Cao, K., et al. (2014). Global analysis of plasticity in turgor loss point, a key drought tolerance trait. *Ecol. Lett.* 17, 1580–1590. doi: 10.1111/ele.12374

Bottero, A., D'Amato, A. W., Palik, B. J., Bradford, J. B., Fraver, S., Battaglia, M. A., et al. (2017). Density-dependent vulnerability of forest ecosystems to drought. *J. Appl. Ecol.* 54, 1605–1614. doi: 10.1111/1365-2664.12847

Brodersen, C. R., and McElrone, A. J. (2013). Maintenance of xylem network transport capacity: a review of embolism repair in vascular plants. *Front. Plant Sci.* 4:108. doi: 10.3389/fpls.2013.00108

Brodribb, T. J., Bowman, D. J. M. S., Nichols, S., Delzon, S., and Burlett, R. (2010). Xylem function and growth rate interact to determine recovery rates after exposure to extreme water deficit. *New Phytol.* 188, 533–542. doi: 10.1111/j.1469-8137.2010.03393.x

Brunetti, C., Gori, G., Marino, P., Latini, A. P., Sobolev, A., Nardini, M., et al. (2019). Dynamic changes in ABA content in water-stressed *Populus nigra*: effects on carbon fixation and soluble carbohydrates. *Ann. Bot.* 124, 627–643. doi: 10.1093/aob/mcz005

Buckley, T. N. (2017). Modeling stomatal conductance. *Plant Physiol.* 174, 572–582. doi: 10.1104/pp.16.01772

Callaway, R. M., Pennings, S. C., and Richards, C. L. (2003). Phenotypic plasticity and interactions among plants. *Ecol. Soc. Am.* 84, 1115–1128. doi: 10.1890/0012-9658(2003)084%5B1115:ppaiap%5D2.0.co;2

Casper, B. B., and Jackson, R. B. (1997). Plant competition underground. *Annu. Rev. Ecol. Syst.* 28, 545–570. doi: 10.1146/annurev.ecolsys.28.1.545

Cowan, I. R., and Farquhar, G. D. (1977). Stomatal function in relation to leaf metabolism and environment. *Symp. Soc. Exp. Biol.* 31, 471–505.

Eller, C. B., Rowland, R. S., Oliveira, P. R. L., Bittencourt, F. V., Barros, A. C. L., Da Costa, P., et al. (2018). Modelling tropical forest responses to drought and El Niño with a stomatal optimization model based on xylem hydraulics. *Philos. Trans. R. Soc. B Biol. Sci.* 373:20170315.

Farooq, M., Wahid, N., Kobayashi, D., Fujita, S., and Basra, S. M. A. (2009). Plant drought stress: effects, mechanisms and management. *Agron. Sustain. Dev.* 29, 185–212. doi: 10.1051/agro:2008021

Farquhar, G. D., Von Caemmerer, S., and Berry, J. A. (1980). A biochemical model of photosynthetic C O 2 assimilation in leaves of C 3 species. *Planta* 149, 78–90. doi: 10.1007/bf00386231

Flexas, J., Bota, J., Galmés, H., Medrano, H., and Ribas-Carbó, M. (2006). Keeping a positive carbon balance under adverse conditions: responses of photosynthesis and respiration to water stress. *Physiol. Plant.* 127, 343–352. doi: 10.1111/j.1399-3054.2006.00621.x

Hacke, U. G., Venturas, E. D., MacKinnon, A. L., Jacobsen, J. S., Sperry, S., and Pratt, R. B. (2015). The standard centrifuge method accurately measures vulnerability curves of long-vesselled olive stems. *New Phytol.* 205, 116–127. doi: 10.1111/nph.13017

Haworth, M., Marino, S. L., Cosentino, C., Brunetti, A., De Carlo, G., Avola, E., et al. (2018). Increased free abscisic acid during drought enhances stomatal sensitivity and modifies stomatal behaviour in fast growing giant reed (*Arundo donax* L.). *Environ. Exp. Bot.* 147, 116–124. doi: 10.1016/j.envexpbot.2017.11.002

Jones, H. G., and Sutherland, R. A. (1991). Stomatal control of xylem embolism. *Plant Cell Environ.* 14, 607–612. doi: 10.1111/j.1365-3040.1991.tb01532.x

Katul, G. G., Palmroth, S., and Oren, R. (2009). Leaf stomatal responses to vapour pressure deficit under current and CO 2 -enriched atmosphere explained by the economics of gas exchange. *Plant Cell Environ.* 32, 968–979. doi: 10.1111/j.1365-3040.2009.01977.x

Klockow, P. A., Vogel, C. B., Edgar, G., and Moore, G. W. (2018). Lagged mortality among tree species four years after an exceptional drought in east Texas. *Ecosphere* 9:e02455. doi: 10.1002/ecs2.2455

Lawlor, D. W., and Tezara, W. (2009). Causes of decreased photosynthetic rate and metabolic capacity in water-deficient leaf cells: a critical evaluation of mechanisms and integration of processes. *Ann. Bot.* 103, 561–579. doi: 10.1093/aob/mcn244

Lin, Y. S., Medlyn, R. A., Duursma, I. C., Prentice, H., Wang, S., Baig, D., et al. (2015). Optimal stomatal behaviour around the world. *Nat. Clim. Change* 5, 459–464.

Lu, Y., Duursma, C. E., Farrior, B. E., Medlyn, R., and Feng, X. (2019). Optimal stomatal drought response shaped by competition for water and hydraulic risk can explain plant trait covariation. *New Phytol.* 225, 1206–1217. doi: 10.1111/nph.16207

Mackay, D. S., Roberts, B. E., Ewers, J. S., Sperry, N. G., McDowell, G., and Pockman, W. T. (2015). Interdependence of chronic hydraulic dysfunction and canopy processes can improve integrated models of tree response to drought. *Water Resour. Res.* 51, 6156–6176. doi: 10.1002/2015wr017244

Manzoni, S., Vico, G., Katul, P. A., Fay, W., Polley, S., Palmroth, S., et al. (2011). Optimizing stomatal conductance for maximum carbon gain under water stress: a meta-analysis across plant functional types and climates. *Funct. Ecol.* 25, 456–467. doi: 10.1111/j.1365-2435.2010.01822.x

Manzoni, S., Vico, S., Palmroth, A., Porporato, A., and Katul, G. (2013). Optimization of stomatal conductance for maximum carbon gain under dynamic soil moisture. *Adv. Water Resour.* 62, 90–105. doi: 10.1016/j.advwatres.2013.09.020

Medlyn, B. E., Duurama, D., Eamus, D. S., Ellsworth, C. I., Prentice, C. V. M., Barton, K. Y., et al. (2011). Reconciling the optimal and empirical approaches to modelling stomatal conductance. *Glob. Change Biol.* 17, 2134–2144. doi: 10.1111/j.1365-2486.2010.02375.x

Noguchi, K., Gel, E., Brunner, R., and Konietschke, F. (2012). nparLD : an R software package for the nonparametric analysis of longitudinal data in factorial experiments. *J. Stat. Softw.* 50:12218.

Novick, K. A., Miniat, C. F., and Vose, M. (2016). Drought limitations to leaf-level gas exchange: results from a model linking stomatal optimization and cohesion-tension theory. *Plant Cell Environ.* 39, 583–596. doi: 10.1111/pce.12657

Peltier, D. M. P., Fell, M., and Ogle, K. (2016). Legacy effects of drought in the southwestern United States: a multi-species synthesis. *Ecol. Monogr.* 86, 312–326. doi: 10.1002/ecm.1219

Phillips, O. L., Van der Heijden, S. L., Lewis, G., López-González, L. E. O. C., Aragão, J., Lloyd, Y., et al. (2010). Drought-mortality relationships for tropical forests. *New Phytol.* 187, 631–646. doi: 10.1111/j.1469-8137.2010.03359.x

Piutti, E., and Cescatti, A. (1997). A quantitative analysis of the interactions between climatic response and intraspecific competition in European beech. *Can. J. For. Res.* 27, 277–284. doi: 10.1139/x96-176

Prentice, I. C., Dong, S. M., Gleason, V., Maire, M., and Wright, I. J. (2014). Balancing the costs of carbon gain and water transport: testing a new theoretical framework for plant functional ecology. *Ecol. Lett.* 17, 82–91. doi: 10.1111/ele.12211

Pšidová, E., Ditmarová, G., Jamnická, D., Kurjak, J., Majerová, T., Czajkowski, T., et al. (2015). Photosynthetic response of beech seedlings of different origin to water deficit. *Photosynthetica* 53, 187–194. doi: 10.1007/s11099-015-0101-x

Resco, V., Ewers, W., Sun, T. E., Huxman, J. F., Weltzin, F., and Williams, D. G. (2009). Drought-induced hydraulic limitations constrain leaf gas exchange recovery after precipitation pulses in the C 3 woody legume, *Prosopis velutina*. *New Phytol.* 181, 672–682. doi: 10.1111/j.1469-8137.2008.02687.x

Schroeder, J. I., Allen, V., Hugouvieux, J. M., Kwak, M., and Waner, D. (2001). Guard cell signal transduction. *Annu. Rev. Plant Physiol. Plant Mol. Biol.* 52, 627–658.

Sperry, J. S., and Love, D. M. (2015). What plant hydraulics can tell us about responses to climate-change droughts. *New Phytol.* 207, 14–27. doi: 10.1111/nph.13354

Sperry, J. S., Venturas, W. R. L., Anderegg, M., Mencuccini, D. S., Mackay, Y., Wang, Y., et al. (2017). Predicting stomatal responses to the environment from the optimization of photosynthetic gain and hydraulic cost. *Plant Cell Environ.* 40, 816–830. doi: 10.1111/pce.12852

Tombesi, S., Nardini, T., Frioni, M., Soccolini, C., Zadra, D., Farinelli, S., et al. (2015). Stomatal closure is induced by hydraulic signals and maintained by ABA in drought-stressed grapevine. *Sci. Rep.* 5:12449. doi: 10.1038/srep12449

Trugman, A. T., Detto, M. K., Bartlett, D., Medvigy, W. R. L., Anderegg, C., Schwalm, B., et al. (2018). Tree carbon allocation explains forest drought-kill and recovery patterns. *Ecol. Lett.* 21, 1552–1560. doi: 10.1111/ele.13136

Tyree, M. T., and Hammel, H. T. (1972). The measurement of the turgor pressure and the water relations of plants by the pressure-bomb technique. *J. Exp. Bot.* 23, 267–282. doi: 10.1093/jxb/23.1.267

Venturas, M. D., Sperry, D. M., Love, E. H., Frehner, M. G., Allred, Y., Wang, M., et al. (2018). A stomatal control model based on optimization of carbon gain versus hydraulic risk predicts aspen sapling responses to drought. *New Phytol.* 220, 836–850. doi: 10.1111/nph.15333

Wolf, A., Anderegg, W. R. L., and Pacala, S. W. (2016). Optimal stomatal behavior with competition for water and risk of hydraulic impairment. *Proc. Natl. Acad. Sci. U.S.A.* 113, E7222–E7230.

Worrall, J. J., Rehfeldt, A., Hamann, E. H., Hogg, S. B., Marchetti, M., Michaelian, M., et al. (2013). Recent declines of *Populus tremuloides* in North America linked to climate. *For. Ecol. Manag.* 299, 35–51. doi: 10.1016/j.foreco.2012.12.033

Yin, J., and Bauerle, T. L. (2017). A global analysis of plant recovery performance from water stress. *Oikos* 126, 1377–1388. doi: 10.1111/oik.04534

Conflict of Interest: The authors declare that the research was conducted in the absence of any commercial or financial relationships that could be construed as a potential conflict of interest.

frontiers in Plant Science

ORIGINAL RESEARCH
published: 25 May 2020
doi: 10.3389/fpls.2020.00643

Stomata and Sporophytes of the Model Moss *Physcomitrium patens*

Robert S. Caine[1†], Caspar C. C. Chater[1†], Andrew J. Fleming[2†] and Julie E. Gray[1†]*

[1] Department of Molecular Biology and Biotechnology, University of Sheffield, Sheffield, United Kingdom, [2] Department of Animal and Plant Sciences, University of Sheffield, Sheffield, United Kingdom

Mosses are an ancient land plant lineage and are therefore important in studying the evolution of plant developmental processes. Here, we describe stomatal development in the model moss species *Physcomitrium patens* (previously known as *Physcomitrella patens*) over the duration of sporophyte development. We dissect the molecular mechanisms guiding cell division and fate and highlight how stomatal function might vary under different environmental conditions. In contrast to the asymmetric entry divisions described in *Arabidopsis thaliana*, moss protodermal cells can enter the stomatal lineage directly by expanding into an oval shaped guard mother cell (GMC). We observed that when two early stage *P. patens* GMCs form adjacently, a spacing division can occur, leading to separation of the GMCs by an intervening epidermal spacer cell. We investigated whether orthologs of Arabidopsis stomatal development regulators are required for this spacing division. Our results indicated that bHLH transcription factors PpSMF1 and PpSCRM1 are required for GMC formation. Moreover, the ligand and receptor components PpEPF1 and PpTMM are also required for orientating cell divisions and preventing single or clustered early GMCs from developing adjacent to one another. The identification of GMC spacing divisions in *P. patens* raises the possibility that the ability to space stomatal lineage cells could have evolved before mosses diverged from the ancestral lineage. This would have enabled plants to integrate stomatal development with sporophyte growth and could underpin the adoption of multiple bHLH transcription factors and EPF ligands to more precisely control stomatal patterning in later diverging plant lineages. We also observed that when *P. patens* sporophyte capsules mature in wet conditions, stomata are typically plugged whereas under drier conditions this is not the case; instead, mucilage drying leads to hollow sub-stomatal cavities. This appears to aid capsule drying and provides further evidence for early land plant stomata contributing to capsule rupture and spore release.

Keywords: stomatal development, guard cells, guard mother cell, moss, *Physcomitrella*, stomatal function, evolution

OPEN ACCESS

Edited by:
Stefan A. Rensing, University of Marburg, Germany

Reviewed by:
Rabea Meyberg, University of Marburg, Germany
Amelia Merced, International Institute of Tropical Forestry, (USDA) Forest Service, United States

***Correspondence:**
Robert S. Caine
B.caine@sheffield.ac.uk

†ORCID:
Robert S. Caine
orcid.org/0000-0002-6480-218X
Caspar C. C. Chater
orcid.org/0000-0003-2058-2020
Andrew J. Fleming
orcid.org/0000-0002-9703-0745
Julie E. Gray
orcid.org/0000-0001-9972-5156

Specialty section:
This article was submitted to Plant Development and EvoDevo, a section of the journal Frontiers in Plant Science

Received: *18 February 2020*
Accepted: *27 April 2020*
Published: *25 May 2020*

Citation:
Caine RS, Chater CCC, Fleming AJ and Gray JE (2020) Stomata and Sporophytes of the Model Moss Physcomitrium patens. Front. Plant Sci. 11:643. doi: 10.3389/fpls.2020.00643

INTRODUCTION

Stomata are microscopic pores typically consisting of a pair of guard cells which regulate a central aperture to control gas exchange for photosynthesis and water loss. They are present on the majority of land plants and evolved prior to 418 million years ago (Edwards et al., 1998; Ligrone et al., 2012; Chater et al., 2013, 2017). Along with other structural innovations such as leaves, roots and

a cuticle, stomata permitted plants to grow larger and thrive in drier environments; which in-turn resulted in vegetation increasingly impacting on, and shaping the terrestrial biosphere (Beerling, 2007; Berry et al., 2010). Vascular land plant stomata regulate plant gaseous exchange, water status, temperature, internal solute transport and can also prevent or allow pathogen entry (Yoo et al., 2010; Franks et al., 2015; Hepworth et al., 2015; Dutton et al., 2019). The role of stomata in non-vascular land plants is less well understood, but recent evidence points toward a role in aiding sporophyte capsule drying and spore release; possibly by facilitating the drying and recession of internal mucilage but does not preclude additional roles (Duckett et al., 2009; Pressel et al., 2014; Villarreal and Renzaglia, 2015; Chater et al., 2016; Duckett and Pressel, 2018). Here, we assess stomatal formation during the sporophyte development of *Physcomitrium patens*, and provide novel insights into how moss stomata develop and function. For a more specialized overview of *P. patens* sporophyte development, see Hiss et al. (2017).

The development of stomata in vascular land plants is well described, with *Arabidopsis thaliana* being particularly well characterized (Zhao and Sack, 1999; Lucas et al., 2006; Rudall et al., 2013, 2017; **Figure 1A**). Recent work in mosses and hornworts has begun to dissect the relatively simpler mechanisms of stomatal development in bryophyte species (Merced and Renzaglia, 2013, 2016, 2017; Pressel et al., 2014). Like other mosses, the model species *P. patens* (Rensing et al., 2020) employs a simple form of stomatal development (**Figure 1B**) and a number of genes orthologous to those of Arabidopsis have been shown to regulate stomatal development and patterning (MacAlister and Bergmann, 2011; Caine et al., 2016; Chater et al., 2016). Surprisingly, despite the elucidation of genetic regulators, our understanding of stomatal and epidermal ontogeny in this model moss remains limited (**Figure 1B**). This represents a significant gap in our knowledge relating to how stomatal development might have altered over the course of evolution. With a better understanding of how *P. patens* produces stomata, we will gain insight into how stomatal and epidermal cell coordination has developed over time, and may begin to understand how vascular land plants gradually built the intricate stomatal developmental and patterning modules that we marvel at today.

Most of our knowledge relating to the genetics underpinning stomatal development stems from work conducted on Arabidopsis (Qi and Torii, 2018; Zoulias et al., 2018; Lee and Bergmann, 2019). Research presented here is associated with the core signaling module regulating stomatal development, outlined in **Figure 1A**, but for an in-depth description relating to the latest findings see also Lee and Bergmann (2019) and Qi and Torii (2018). Arabidopsis stomatal development is initiated when basic helix-loop-helix (bHLH) transcription factors SPEECHLESS (SPCH) and ICE1/SCREAM (SCRM) or ICE2 (SCRM2) heterodimerize leading to a subset of protodermal cells gaining meristemoid mother cell (MMC) identity (**Figure 1A**; MacAlister et al., 2007; Kanaoka et al., 2008). MMCs undergo an asymmetric entry division to produce a smaller meristemoid cell and a larger stomatal lineage ground cell (SLGC), again regulated via SPCH-SCRM/2 (Zhao and Sack, 1999; Bhave et al., 2009; Pillitteri and Dong, 2013). SLGCs either produce satellite meristemoids via an asymmetric spacing division (regulated by SPCH-SCRM/2 activity), or can de-differentiate and form epidermal pavement cells (Pillitteri and Dong, 2013). The meristemoids formed by either entry or spacing divisions may also undergo self-renewing amplifying divisions, which leads to the production of further SLGCs, again via SPCH-SCRM/2 activity (Zhao and Sack, 1999; Berger and Altmann, 2000; MacAlister et al., 2007; Kanaoka et al., 2008).

Following these asymmetric divisions, the transition from Arabidopsis meristemoid to guard mother cell (GMC) is orchestrated by the transcriptional regulator bHLH MUTE (closely related to SPCH), in combination with SCRM/2 (**Figure 1A**; Kanaoka et al., 2008; Pillitteri et al., 2008). To form a pair of guard cells, MUTE and SCRM/2 also oversee the GMC symmetric division, and finally FAMA (related to both SPCH and MUTE), together with SCRM/2, enforces correct guard cell identity (Zhao and Sack, 1999; Ohashi-Ito and Bergmann, 2006; Kanaoka et al., 2008; Han et al., 2018). The activity of SPCH, MUTE and FAMA, in combination with either of the SCRMs, is modulated by a mitogen activated protein kinase (MAPK) pathway (Lampard, 2009; Han and Torii, 2016; Qi et al., 2017). This pathway facilitates intricate signaling within and between cells by connecting the plasma membrane to the nuclear bHLH transcription factors (Qi and Torii, 2018; Lee and Bergmann, 2019).

To coordinate the above cellular transitions and divisions, Arabidopsis uses a signaling network which includes a plasma membrane-localized receptor-like protein (RLP), receptor-like kinases (RLKs) and apoplastic signaling peptides (**Figure 1A**; Qi and Torii, 2018; Lee and Bergmann, 2019). For asymmetric divisions to commence, the RLP TOO MANY MOUTHS (TMM) in combination with the ERECTA family of RLKs [especially ERECTA (ER)] are particularly important (Yang and Sack, 1995; Shpak et al., 2005; Lee et al., 2012, 2015). These receptor components enable the transduction of signals from the apoplast across the plasma membrane. If the apoplastic signaling peptide EPIDERMAL PATTERNING FACTOR (EPF) 2 is successful in binding to TMM and ERECTAs (typically ER) then asymmetric entry divisions fail to occur and the stomatal lineage is halted because SPCH becomes phosphorylated and thus de-activated (**Figure 1A**; Hara et al., 2009; Hunt and Gray, 2009; Lee et al., 2015). Conversely, If EPF2 is out-competed for receptor binding by EPF-like 9 (EPFL9, otherwise known as STOMAGEN), then an asymmetric entry division is more likely to occur, resulting in a meristemoid and SLGC (Hunt et al., 2010; Sugano et al., 2010; Lee et al., 2015). The subsequent transition of the meristemoid to a GMC is governed by EPF1, which like EPF2, uses TMM and ERECTA family members [particularly ER-like1 (ERL1)] to convey signals into the cytoplasm that prevent GMC formation (Hara et al., 2007; Hunt and Gray, 2009; Lee et al., 2012; Pillitteri and Torii, 2012; Qi et al., 2017).

We have previously shown that *P. patens* expresses multiple genes that are orthologous to Arabidopsis equivalents that function during stomatal development and patterning (Caine et al., 2016; Chater et al., 2016). Instead of three bHLH genes akin to *SPCH*, *MUTE* and *FAMA*, *P. patens* has two genes:

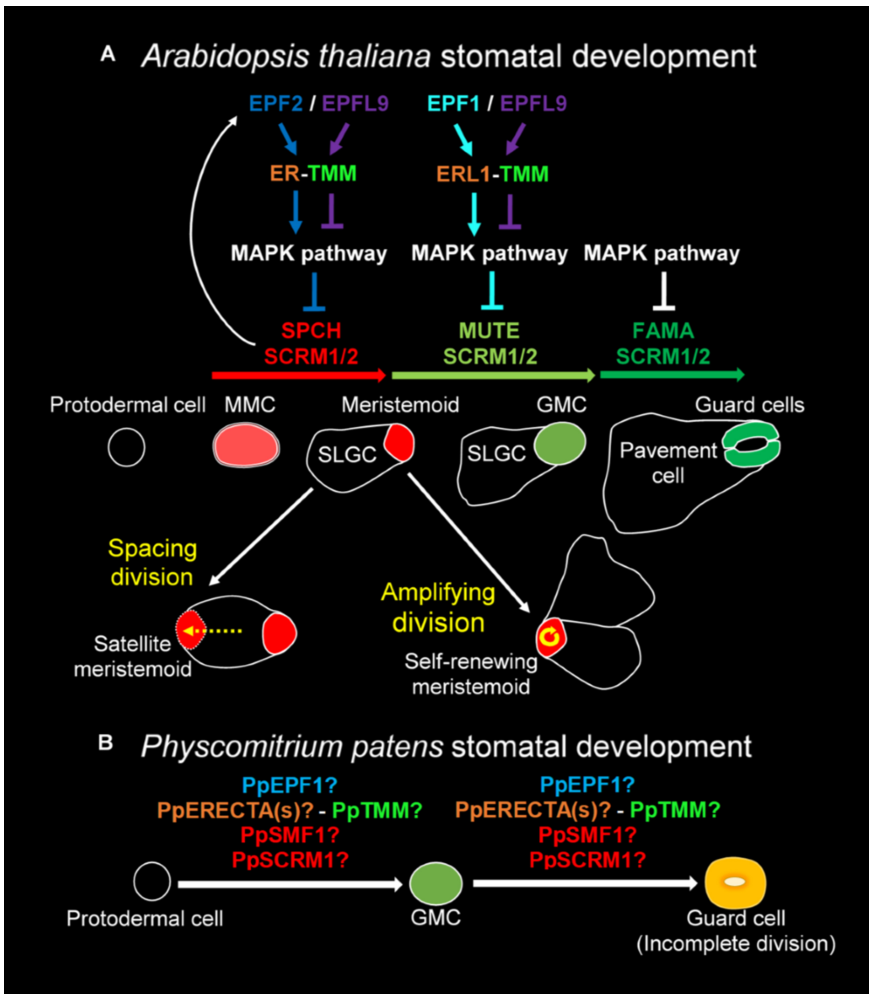

FIGURE 1 | Overview of the molecular control of stomatal development. **(A)** In *Arabidopsis thaliana* the stomatal lineage is initiated when an undifferentiated protodermal cell is specified to become a meristemoid mother cell (MMC) via the actions of a heterodimeric protein complex consisting of bHLH transcription factors SPEECHLESS (SPCH) and either SCREAM (SCRM) or SCRM2 (also referred to as ICE1 and ICE2). The MMC then undergoes an asymmetric entry division again promoted by SPCH and SCRM/2 activity. SPCH is phospho-regulated via the activity of a mitogen activated protein kinase (MAPK) pathway that facilitates signals being relayed from the plasma membrane to the nuclear-residing transcription factors. TOO MANY MOUTHS (TMM) and ERECTA family proteins act to regulate external signals that trigger the MAPK pathway from outside the cell. Binding of EPIDERMAL PATTERNING FACTOR (EPF) 2 signaling peptide to ERECTA family proteins particularly ERECTA (ER) increases MAPK activity and SPCH is phosphorylated thereby preventing stomatal lineage progression. Conversely, if EPF-like 9 (EPFL 9, also known as STOMAGEN) outcompetes EPF2, then the MAPK pathway is not activated and SPCH activity is preserved. The heterodimeric unit of SPCH and SCRM/2 is self-regulatory as SPCH drives the expression of EPF2. Additional meristemoids can be generated via spacing divisions where an SLGC divides away from an already formed meristemoid, and via self-renewing amplifying divisions of an existing meristemoid. Both of these divisions are solicited by SPCH and SCRM/2 activity. For meristemoids to advance to guard mother cell (GMC) state, the bHLH MUTE is required in combination with SCRM/2. This is again under the control of the MAPK pathway. Instead of EPF2, EPF1 competes with EPFL9 for the binding of ERECTA proteins particularly ER-like 1 (ERL1) with moderation again via TMM. EPF1 bound ERL1 leads to increased MAPK activity and prevents stomatal lineage advancement. For a GMC to symmetrically divide and form a pair of guard cells (GCs) both MUTE, and then FAMA, again in combination with SCRM/2 are required. FAMA, like SPCH and MUTE, is also regulated via MAPK activity, although how this occurs is not well understood. **(B)** A suggested model for *Physcomitrium patens* stomatal development. Mosses and hornworts initiate stomatal development module when a protodermal cell expands and becomes an ovoid GMC. For *P. patens*, the GMC then undergoes an incomplete symmetric division leading to the formation of a single ovoid shaped GC. Where the previously described *PpSMF1*, *PpSCRM1, PpTMM, PpEPF1*, and *PpERECTA1* gene products function during the developmental module remain to be determined.

PpSMF1 and *PpSMF2*, of which only *PpSMF1* is required during stomatal development. In *ppsmf1* knockout lines no stomata form on the moss sporophyte (Chater et al., 2016). For Arabidopsis SCRM/2 equivalents, there are four moss orthologs, of which, only *PpSCRM1* has thus far been identified to be involved in stomatal development. As with *ppsmf1* plants, *ppscrm1* mutants possess no stomata on the moss sporophyte (Chater et al., 2016). Whilst Arabidopsis has three *ERECTA* family genes, there are six orthologous *P. patens* genes, but to date only *PpERECTA1* has been studied (Caine et al., 2016). Like ERECTA, PpERECTA1 positively regulates stomatal development and the correct placement of stomata. The contribution of other

PpERECTA genes to stomatal and sporophyte development remains unknown.

TOO MANY MOUTHS is a single-copy gene in both Arabidopsis and *P. patens* (Caine et al., 2016). Arabidopsis *TMM* prevents stomatal clustering in a number of organs including leaves, yet at the same time promotes stomatal development in other organs, most notably on siliques and the base of inflorescence stems (Geisler et al., 1998; Abrash and Bergmann, 2010). In *pptmm* mutants, clustered stomata and zones devoid of stomata can be found on the same sporophyte, highlighting the complex mechanisms by which PpTMM titrates different stomatal developmental signals during sporophyte growth (Caine et al., 2016). Whilst at least three *EPF/L* genes regulate Arabidopsis stomatal development, only one *EPF* appears to play a role in moss stomatal development: *PpEPF1* (Chater et al., 2017). PpEPF1 negatively regulates stomatal development as *ppepf1* mutants exhibit abnormal contiguous clustering of stomata (Caine et al., 2016). To test whether a positive regulator of stomatal development could promote stomatal development in *P. patens*, Arabidopsis *EPFL9* was over-expressed, but no change in phenotype was detected (Caine et al., 2016). Based on this and phylogenetic analysis, it is likely that positive regulation of stomatal development by *EPFL9* genes evolved after the divergence of vascular plants (Chater et al., 2017). Despite these advances, the coordinated functioning of signaling components in moss stomatal development is yet to be described.

In most non-vascular land plants, stomatal development involves the specification of a protodermal cell which enlarges to become a GMC, that subsequently divides to produce a pair of guard cells (Vaten and Bergmann, 2012; Merced and Renzaglia, 2016, 2017; **Figure 1B**). GMCs have previously been termed "guard cell parent cells" (GPCs) in mosses and "stomatal mother cells" (SMC) in hornworts (Sack and Paolillo, 1985; Pressel et al., 2014). For simplicity, and to convey their similar shared identity, we refer to all bryophyte equivalents as GMCs. No asymmetric entry division appears to precede GMC formation in non-vascular plants (Rudall et al., 2013; Pressel et al., 2014; Merced and Renzaglia, 2016). Moreover, amplifying divisions and spacing divisions are also thought to be absent in mosses and hornworts. This implies that non-vascular land plant stomata are perigenous as they develop – that is, there is an absence of any neighboring cells that originally derived from the same stomatal lineage (Rudall et al., 2013). GMC development and division in mosses and hornworts appear to be intricately coordinated with chloroplast behavior, as specific chloroplast conformations have been observed prior to the symmetric division that forms the pore (Pressel et al., 2014; Merced and Renzaglia, 2016, 2017). Whilst most bryophyte GMCs divide to produce two guard cells, in the Funariaceae mosses such as *P. patens* the GMC does not fully divide and a single guard celled stomate is produced (**Figure 1B**; Sack and Paolillo, 1985; Field et al., 2015; Chater et al., 2016).

Most mosses and hornworts, but not liverworts, possess stomata on their sporophytes (Chater et al., 2017; Merced and Renzaglia, 2017; Duckett and Pressel, 2018; Brodribb et al., 2020). For a number of bryophyte species (including *P. patens*), liquid mucilage is initially detectable in the cavity formed beneath the developing stomata of young sporophytes (Pressel et al., 2014; Merced and Renzaglia, 2016; Renzaglia et al., 2017). As sporophyte expansion continues, stomatal opening occurs and typically internal mucilage recedes. This leads to a hollowing of the sub-stomatal cavity. In hornworts this is followed by stomata collapsing inwardly and cells dying as capsules mature (Renzaglia et al., 2017). Mucilage recession enables water release from both moss and hornwort capsules, and this appears to accelerate sporophyte drying and capsule rupture (Villarreal and Renzaglia, 2015; Chater et al., 2016; Merced and Renzaglia, 2017; Duckett and Pressel, 2018). Despite this, observations of near-mature *P. patens* capsules show that sub-stomatal cavity mucilage does not always recede (Chater et al., 2016), suggesting that water release during maturation is variable and possibly conditional on the surrounding environment (Merced and Renzaglia, 2017).

Based on the findings reported here, we suggest that stomatal development in moss is more complex than previously thought and is not exclusively perigenous. We observed mesoperigenous development, with non-stomatal lineage cells forming during the development of stomata (Payne, 1979; Rudall et al., 2013). Furthermore, we dissect how *P. patens* correctly initiates stomatal development and patterning in relation to GMC formation by following deviations of cell fate transitions in *ppsmf1*, *ppscrm1*, *pptmm*, and *ppepf1* knock-out mutants. By analyzing the development and maturation of guard cells and subtending cavities under differing environmental conditions, we provide further insight into the possible role of moss stomata and provide a rationale for whether stomata remain open or become plugged as sporophyte capsules mature.

MATERIALS AND METHODS

Plant Materials

Physcomitrium patens subspecies *patens* (Hedwig) Mitten (Medina et al., 2019; Rensing et al., 2020) wild-type strains Gransden 2004, Gransden D12 and Villersexel, and previously published mutants were grown under sterile conditions on 42 mm Jiffy 7 peat pellets (Amazon, London). To produce data in **Figures 2–7**, pellets were first rehydrated using 40 ml of distilled water inside Magenta GA-7 culture vessels (Sigma-Aldrich, Gillingham, United Kingdom), sealed with Micropore tape (3 M, Maplewood, Minnesota, United States) and sterilized. Post-sterilization, a further 70 ml of sterilized distilled water was added. To produce sterile protonemal homogenate, a 1 × 9 cm plate of 6–10-day old BCDAT-grown tissue (Cove et al., 2009) was scraped from a cellophane disk (AA Packaging, Preston, United Kingdom) and placed in 15 ml of sterilized distilled water and homogenized for 20 s using a Polytron PT1200 (KINEMATICA AG, Luzern, Switzerland). Peat pellets were inoculated with either 1.5 ml of protonemal homogenate (**Figures 2–6**) or a 1.5 cm^2 piece of tissue derived from 3-week-old BCDAT-grown tissue (**Figure 1**). To produce the sporophytes presented in **Figure 8**, plants were grown on agar plates (12 g l^{-1}) supplemented with Knop

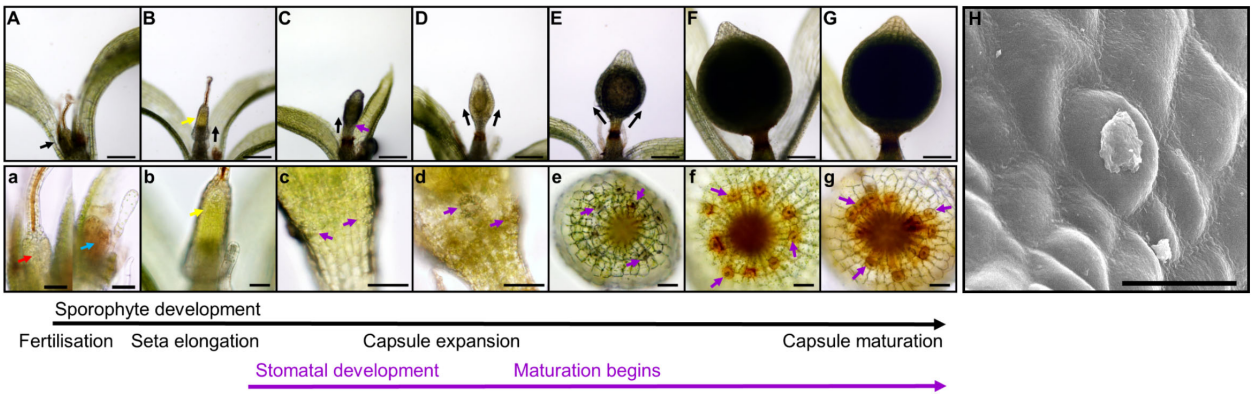

FIGURE 2 | Stomatal development during sporophyte development in *Physcomitrium patens*. **(A–G)** Overview of the developing *P. patens* sporophyte from fertilization to fully expanded brown sporophyte stage. **(a–g)** Close-ups of **(A–G)** illustrating early sporophyte development, and then once formed, stomata and their development in relation to overall sporophyte development. Representative stomata in panels **(c–g)** are marked with purple arrows. **(A)** Mature gametangia and nascent sporophyte (black arrow) surrounded by leafy gametophyte tissue. **(a)** Left image, a very young sporophyte (red arrow) resulting from the fertilization of the egg cell in the female archegonia. The gametophytic calyptra derived from the archegonia is visible and is being pushed up by the underlying nascent sporophyte. Right image, male antheridia (blue arrow) with a cloud of spermatozoids above. **(B)** Developing sporophyte (black arrow) being pushed up via a seta, with gametophyte calyptra still affixed (yellow arrow); the seta is subtending the calyptra. **(b)** A close-up of the calyptra sitting atop the gametophyte (yellow arrow). **(C)** Elongating sporophyte with a darkened central spore sac becoming visible. **(c)** Stomatal lineage cells protruding from the surface of epidermis (purple arrows). The calyptra is absent from this image, and also for subsequent images through to sporophyte maturity. Normally it remains present until the penultimate stages of sporophyte development when sporophytes remain undisturbed (Hiss et al., 2017). **(D)** As the sporophyte begins to expand outward the central spore sac becomes distinct from the surrounding tissue. **(d)** As expansion of the capsule occurs **(D)** stomatal pores can be seen in the central regions of recently formed guard cells (GCs; see centrally placed purple arrow). **(E)** As the central spore sac expands the overall shape of the sporophyte becomes more spherical. **(e)** The stomata on the expanding sporophyte begin a transition from being translucent to being filled with an orange to brown substance. **(F)** A fully expanded green sporophyte with maturing spores. **(f)** The GCs are now orange in color as the sporophyte is maturing. **(G)** The fully expanded sporophyte capsule is browned, indicating that the internal spores are mature. **(g)** Like the sporophyte capsule, the color of the stomata turns increasingly brown prior to and during senescence. **(H)** Scanning electron microscopy image of a mature *Physcomitrium patens* guard cell plugged with waxes. Scale bars are as follows: **(A–G)** = 100 μm; **(a–g)** = 50 μm; **(H)** = 25 μm.

medium (Egener et al., 2002; Frank et al., 2005) as previously described Chater et al. (2016).

Growth Conditions

Plants were grown at 25°C under continuous light (140 μmol m^{-2} s^{-1} irradiance) for 8 to 12 weeks until large gametophores were produced. To induce gametangia, plants were moved to a Medicool MPR-161D(H) cabinet (Sanyo, Osaka, Japan) fitted with Phillips Master TL-D 90 De Luxe 18W/965 fluorescent lamps (Amsterdam, Netherlands) set to 18°C, 10 h light (100 μmol m^{-2} s^{-1} irradiance) and 15°C, 14 h dark. After 2–3 weeks, 40 ml of sterile distilled water was poured over plants to fertilize archegonia. For analysis of stomata on dry or wet grown sporophyte capsules, the following procedures were undertaken. For nascent sporophytes, samples were collected approximately 3 weeks after water application. For expanded green-to-yellow spore sporophytes, collection occurred approximately 5 weeks after water application. For browning sporophytes, samples were collected at approximately 6.5 weeks. For stomatal counts of browned sporophytes, samples were fixed in modified Carnoy's solution (2:1 Ethanol: Glacial acetic acid) for 1 week prior to analysis. To identify dry grown sporophytes for **Figure 7**, capsules were located on peat pellets from lower-humidity zones of the moss canopy, identified by water repellent gametophores within the colony. Dry-and wet-grown samples were collected from similar heights and depths within colonies to minimize edge effects and micro-environments. We did not follow individual dry-grown sporophytes on individuals from fertilization until maturity. Plants cultivated on plates for results in **Figure 8** were grown at 23°C, 16 h light, 8 h dark prior to sporophyte induction as in Hohe et al. (2002).

Sample Preparation, Microscopy and Image Processing

For bright-field and fluorescence microscopy, spore capsules were excised from moss colonies and dissected in water. Imaging was performed on an Olympus BX-51 microscope fitted with Olympus DP71 camera (Tokyo, Japan). For fluorescence imaging of untreated samples, an Olympus U-RFL-T-200 UV lamp (Tokyo, Japan) with an LP 400 nm emission filter was used. To produce stacked images, multiple fields of view of a subject were obtained. Images were stacked using ImageJ (Schneider et al., 2012) and then flattened using the Z project function using either the Min Intensity or Max Intensity settings to compile flattened images. The moss colony image was taken using a Canon EOS 500D camera (Tokyo, Japan).

DPBA Staining and Imaging

Mature browning capsules were fixed in Carnoy's, and incubated for 1 h in either Diphenylboric acid-2-aminoethyl ester (DPBA; Sigma-Aldrich, Gillingham, United Kingdom) solution (0.25% DPBA, 0.02% Triton X-100 (v/v) or a control solution of 0.02% Triton X-100 solution (v/v). Dissected capsules were

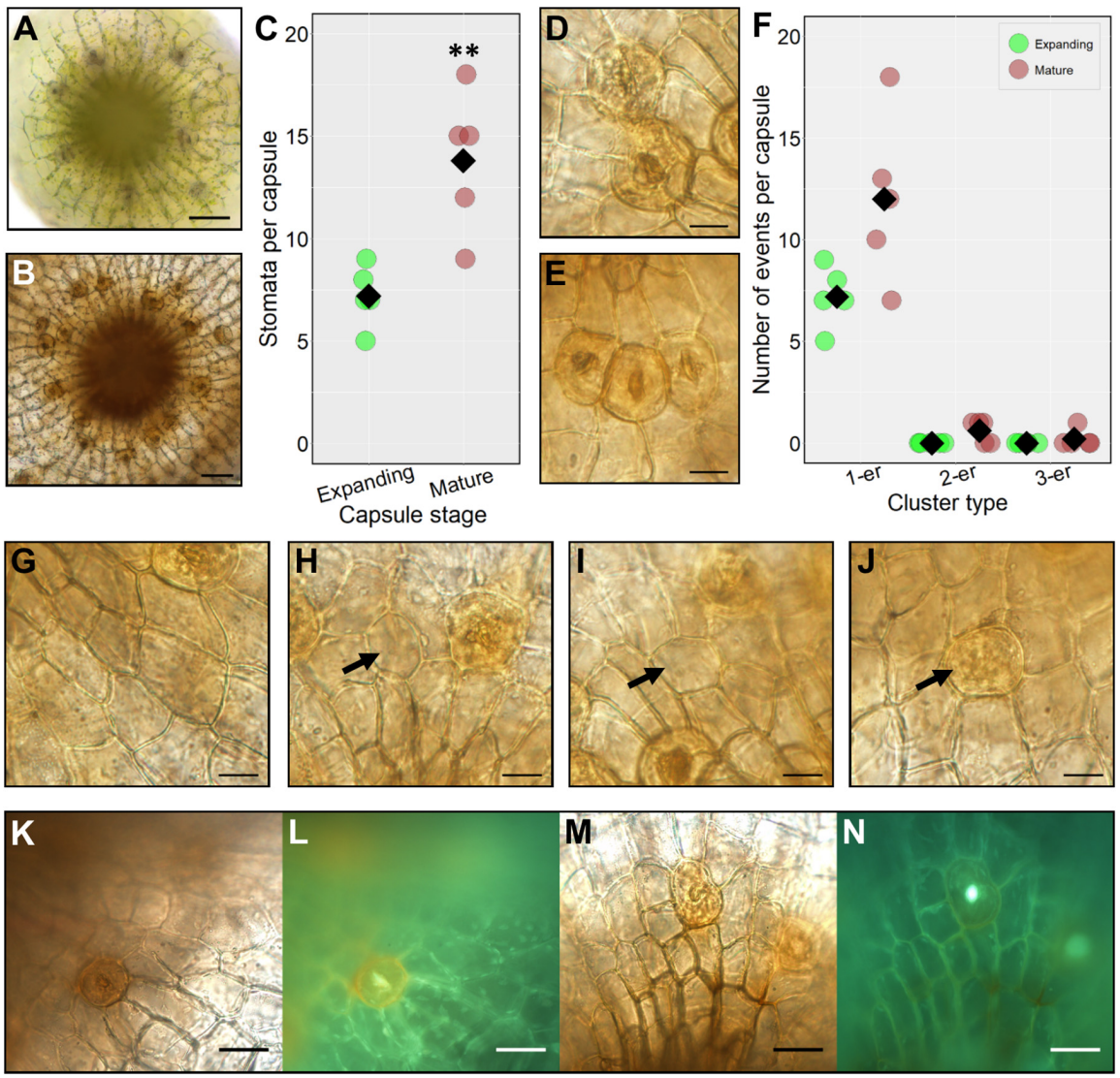

FIGURE 3 | Stomatal formation during capsule expansion and in fully expanded mature capsules. **(A)** A stacked and flattened image of an early expanding sporophyte capsule dissected and face-up. The capsules surveyed were equivalent in size to sporophytes including and between growth stages in **Figures 2D,E**. **(B)** A stacked and flattened image of an equivalent fully expanded mature brown spore capsule equivalent to **Figure 2G**. **(C)** Dot-plot of stomatal number on expanding and mature sporophyte capsules. Individual replicate values denoted by circles, means by black diamonds. A two-tailed *t*-test confirms significantly more stomata on mature brown capsules (**$P < 0.01$). **(D)** A stomatal cluster consisting of two stomata (2-er) on a mature browned wild-type sporophyte capsule. **(E)** A stomatal cluster consisting of three stomata (3-er) on a mature wild-type capsule. **(F)** Dot-plot of instances of clustering on expanding and mature brown sporophyte capsules. Symbols are as in panel **(C)**. Non-clustering stomata are counted as 1-ers. **(G–N)** All images taken from mature brown fixed capsules. **(G)** An epidermal area almost devoid of stomata. **(H,I)** Enlarged round, possibly aborted GMC cells (see black arrows). **(J)** An aborted GMC displaying the characteristic orange to brown hue akin to mature guard cells but without the central pore (see arrow). **(K)** Mature sporophyte capsule dissected and stained with diphenylboric acid 2-amino ethyl ester (DPBA). **(L)** Capsule exposed to UV light to assess flavonoid derivatives which are visible as an orange fluorescence in the guard cell. **(M)** Mock treated equivalent to panel **(K)**. **(N)** No fluorescence is emitted from the guard cell under equivalent UV light treatment. Scales bars are as follows: **(A,B)** = 50 μm; **(D,E)** and **(G–J)** = 15 μm; **(K–M)** = 25 μm.

then imaged using a pE-2 UV Fluorescence Light Source (CoolLED, Andover, United Kingdom) on an Olympus BX-51 microscope. To excite samples 400 nm wavelength was utilized. To capture fluorescence at the appropriate wavelength a 455 nm emission filter was used. Bright-field and UV images of both the stained and treated controls were obtained using the same exposure settings.

Statistical Analysis and Graphing

For comparisons of stomatal frequency, the total number of stomata were counted from 5 expanding and 5 expanded spore capsules and analyzed using a Student's *t*–test. A stoma was classified as a GC with an obvious central pore. Dot-plot graphs were produced in R using the ggplot2 data visualization package (Wickham, 2009; R Development Core Team, 2012).

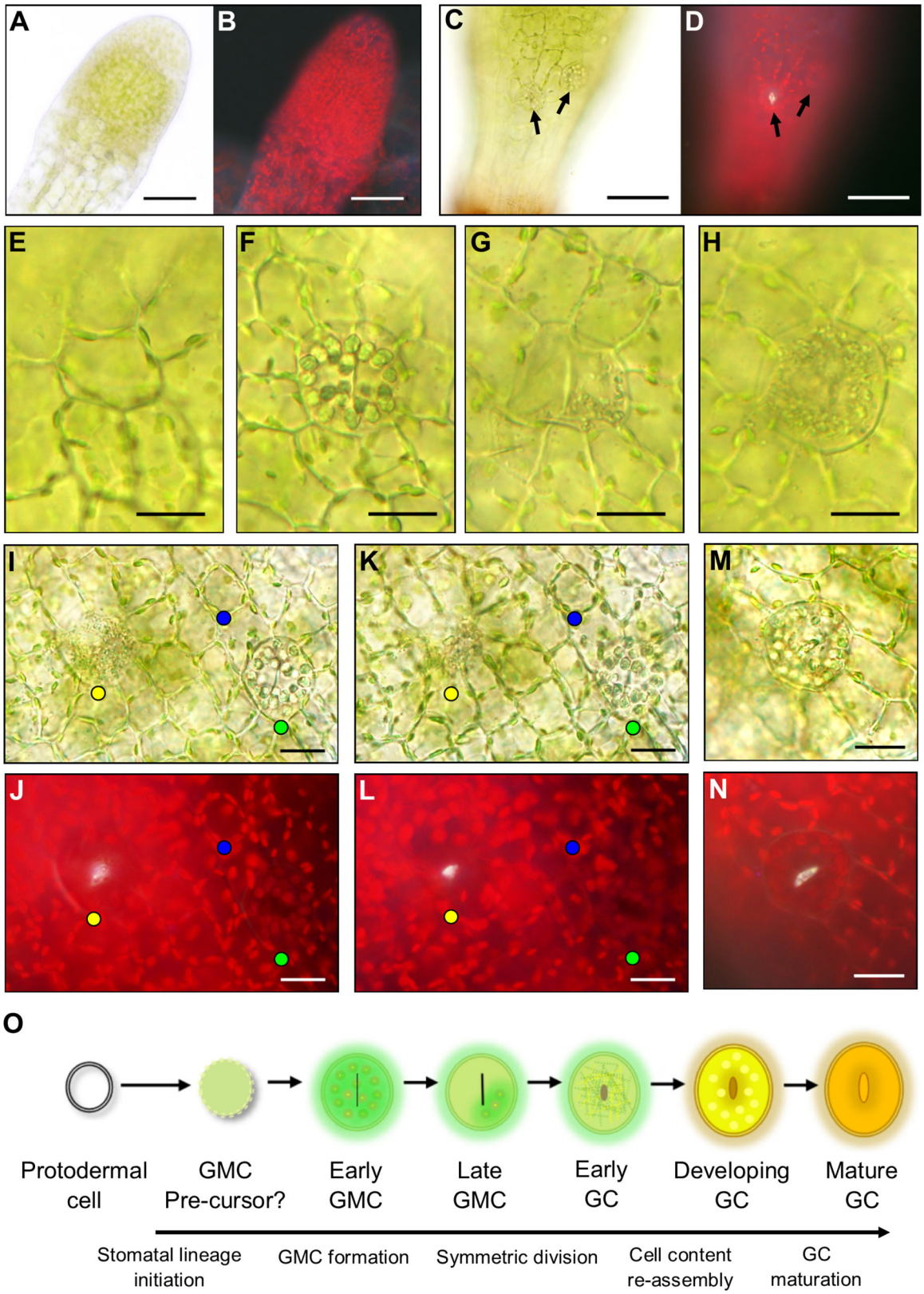

FIGURE 4 | Continued

FIGURE 4 | Stomatal lineage cells during stomatal development in *Physcomitrium patens*. **(A)** An excised apical portion of an expanding sporophyte, with calyptra removed, equivalent in size to the sporophyte in **Figure 2B**. No stomata were visible at this developmental stage. **(B)** Fluorescence image of panel **(A)**. **(C)** Representative elongating sporophyte capsule beginning to expand which is equivalent to a sporophyte between stages **Figures 2C,D**. A nascent guard cell (GC) can be seen in the central basal region of the sporophyte capsule. More apically and to the right a guard mother cell (GMC) is also present. Note: capsules equivalent to **Figure 2C** were also used during these observations and nascent stomata were found at this development stage. **(D)** Fluorescent image of the same sporophyte as **(C)** emitting a white autofluorescence coming from the open central open pore of the nascent GC, but no fluorescence was detected from the GMC located more apically and to the right. **(E–L)** Images taken from sporophytes equivalent in size to **Figure 2C** through to **Figure 2D** where sporophytes were still elongating and beginning to expand. In most cases a neatly arranged group of cells exists around the central stomatal lineage cells. **(E)** A smaller circular cell which is probably a GMC pre-cursor. **(F)** An expanded GMC with organelles radially aligned at the cell perimeter and a central cell plate. **(G)** Expanded GMC with partially fragmented organelles in one location that are dissipating and a very pronounced cell plate. **(H)** An early GC with fragmented organelles and a central indented region. **(I)** Bright-field image of an early GC with fragmented organelles (yellow dot). A GMC with aggregated organelles (green dot) and a circular cell with organelles circulating around the cell perimeter (blue dot). **(J)** Equivalent fluorescence image to bright-field in panel **(I)**. **(K,L)** Adjusted depth of field images equivalent to those in panesl **(I,J)**, illustrating a fluorescent material in the pores of the GMC with fragmenting organelles (yellow dot), but not in the cell with aggregating organelles (green dot) or the smaller circular undifferentiated cell (blue dot). The fluorescent material is used as a marker for pore formation in the early GC with fragmenting organelles, which is not present in the aggregating organelle GMC or the smaller circular cell. **(M)** Once the organelles have finished fragmenting the pore is formed leading to the reformation of aggregated organelles in the developing GC and a yellow to orange hue beginning to occur inside the developing GC. **(N)** Fluorescence image of panel **(M)** illustrating fluorescence material lining the pore lips. **(O)** Schematic representation of the transition from protodermal cell to Mature GC. Firstly, protodermal cells marginally expand and become surrounded in a very particular cellular arrangement thereby probably becoming a GMC pre-cursor. Then this cell expands further to become early GMC which has aggregated organelles and a central cell plate. As the symmetric division begins to occur, the organelles then dissipate and the late GMC is formed. In early GCs Organelles are fragmented throughout as the central pore begins to form. Organelles then reform in the developing GCs before finally maturing, the process becoming an orangey brown color. Scales bars are as follows: **(A–D)** = 50 μm; **(E–N)** = 15 μm.

RESULTS

Stomatal Development on the Sporophyte of *P. patens*

We observed the development of stomata in *P. patens*, which in common with other mosses, produces stomata only on the spore capsule of the sporophyte and not on the gametophyte (Paton and Pearce, 1957; Field et al., 2015; Caine et al., 2016; Chater et al., 2016; Merced and Renzaglia, 2017; **Figure 2**). Sporophyte development begins when a gametophytic egg cell is fertilized by a gametophyte sperm cell either via self-fertilization or from another individual (Perroud et al., 2011, 2019; Hiss et al., 2017). Post-fertilization, the diploid zygote divides asymmetrically to form a sporophyte consisting of an apical cell and basal cell (Sakakibara et al., 2008). The apical meristem derived from the apical cell is responsible for the development of the spore capsule on which stomata will form. The basal cell gives rise to the haustorium that anchors the sporophyte in the parent gametophore. An intercalary meristem implements further differentiation by producing a seta, a stalk containing conducting tissue which is responsible for elevating the developing sporophyte above the confines of the parent gametophore (**Figures 2B,b**).

As sporophyte development and expansion continues, seta development slows (**Figure 2C**). The calyptra, a gametophyte-derived protective cap (visible in **Figures 2A,B**) normally sits atop the sporophyte, and is ordinarily retained until just prior to sporophyte capsule maturity (Hiss et al., 2017). As the sporangium and stomatal regions continue to develop, the spore sac and stomatal lineage cells become increasing visible (**Figures 2D,d**). Within the spore sac, spores gradually develop (Wallace et al., 2015), and the capsule gradually matures leading to the sporophyte changing color from green to yellow, then orange, before finally browning (Chater et al., 2016; Hiss et al., 2017). Stomata also change color as the capsule matures, starting a relatively translucent color and gradually following the same color changes associated with the maturing sporophyte (**Figures 2c–g**). Following maturation, brown capsules dehisce through irregular lysis of epidermal cells, leading to rupture and spore dispersal; at this late stage of sporophyte development stomata often appeared to be "plugged" (**Figure 2H**).

Quantifying Stomatal Development and Assessing Stomata on the Mature Sporophyte Epidermis

To investigate the timing of stomatal formation during *P. patens* wild-type sporophyte development we compared the number of stomata on expanding capsules (between the stages defined in **Figures 2D,E**) with the final stomatal number on fully expanded mature brown sporophytes **Figure 2G** (**Figure 3**). During expansion, the number of stomata was just over half that on fully mature spore capsules (**Figures 3A–C**). This indicates that stomatal development continues as sporophytes expand. At the partially expanded stage, all the stomata observed were spaced, with no clustering, but on mature capsules, small clusters of stomata were occasionally observed (**Figures 3D–F**). Although pairs, and very occasionally triplets of contiguously clustered stomata were observed on mature sporophytes, the majority (85–90%) were separated by at least one epidermal cell (**Figure 3F**). In addition to the occasional clusters, small patches devoid of stomata also infrequently occurred (**Figure 3G**), although these were not as large as the stomata-less zones previously observed in *pptmm* lines (Caine et al., 2016). On occasion, stomatal precursor cells with the characteristic GMC oval shape were observed in the mature sporophyte (**Figures 3H–J**), bearing similarity to arrested GMCs observed in other land plant lineages (Zhao and Sack, 1999; Pressel et al., 2014). During this study we used Gransden 2004, Gransden D12 or Villersexel wild-type *P. patens* strains. We did not observe any obvious differences in stomatal development or patterning, and our previous work (Chater et al., 2016), revealed no differences in stomatal number between the different backgrounds.

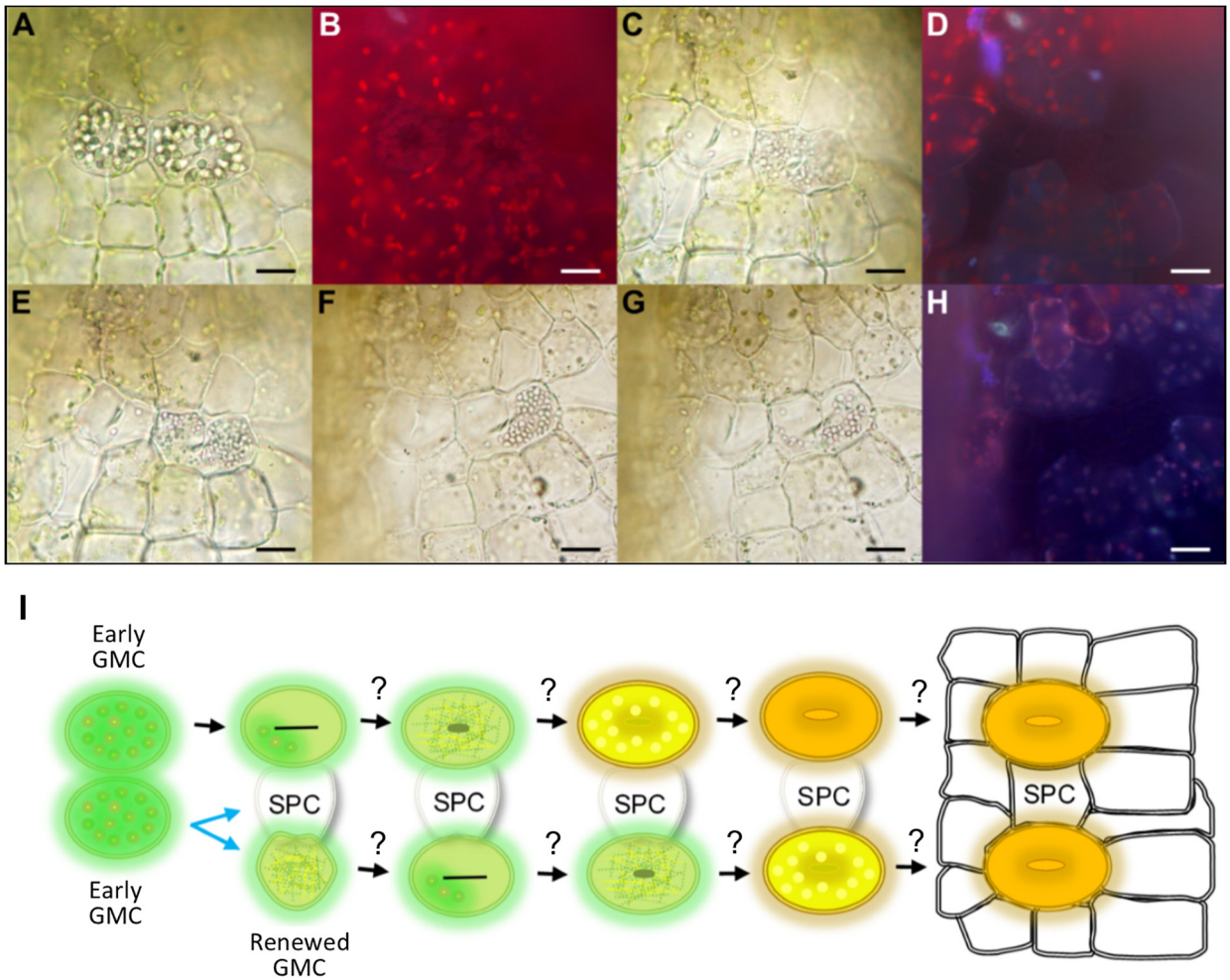

FIGURE 5 | Evidence for mesoperigenous stomatal development in *Physcomitrium patens*. A montage of images taken over approximately 2 h illustrating changes in stomatal lineage cell conformation during an asymmetric GMC spacing division. **(A)** Bright-field image illustrating two neighboring early GMC cells with aggregated cellular organelles. The right GMC is budding off and undergoing an asymmetric spacing division. A cell plate can be seen in both GMCs. **(B)** Fluorescence image of panel **(A)** with no visible build-up of fluorescence material in central pore regions of either cell, further suggesting that both cells are early GMCs (see also **Figure 4**). **(C)** The previously pronounced organelles in both GMC cells have dissipated substantially in the left-side GMC, and have fragmented in an equally distributed pattern within the right-side cell. **(D)** Fluorescence image of panel **(C)** still displaying no evidence of fluorescent material associated with pore formation. A number of the cells including the GMCs now appear darker than previously observed in panel **(B)**. **(E–G)** Over time as cell division is continuing, the fragmented organelles seem to migrate past the cell plate and become concentrated in the right of two newly forming cells. This leads to the formation of a spacer cell (SPC) in between the two previously adjacent early GMCs. **(H)** Fluorescence image of panel **(G)** still with no visible fluorescence build-up in either the left-side GMC or either of the two daughter cells formed from the spacing division of the right-side GMC parental cell. **(I)** Schematic representation of a GMC spacing division. When two early GMCs form next to each other, one early GMC will bud off and undergo an asymmetric spacing division whilst the other appears to approach mid GMC phase (see also **Figure 3**). The early GMC that buds off may or may not be able to renew early GMC identity. With an SPC in place between stomatal lineage cells, stomatal development may continue as in **Figure 3**. Scale bars = 15 μm.

Many mature guard cells acquired an orangey hue prior to full browning of the sporophyte. To ascertain the chemical nature of the coloration we stained capsules with diphenylboric acid 2-amino ethyl ester (DPBA), which fluoresces under UV light in conjugation with flavonoid derivatives (**Figures 3K–N**). A substantial fluorescent signal was detected in the mature guard cells of stained capsules relative to unstained controls indicating the presence of flavonoids (**Figure 3L**). For controls, fluorescence was only detectable in the central pore regions and not in the guard cells (**Figure 3N**).

Deciphering *P. patens* Stomatal Ontogeny

During the early stages of development, the unexpanded sporophyte was completely enclosed in a humid microenvironment provided by the calyptra (**Figure 2B**; Budke et al., 2011, 2012; Hiss et al., 2017). To ascertain whether stomatal development is initiated at this early developmental stage, the calyptra of young sporophytes was removed and the underlying epidermis was checked for the presence or absence of stomatal lineage cells (**Figures 4A,B**). At this

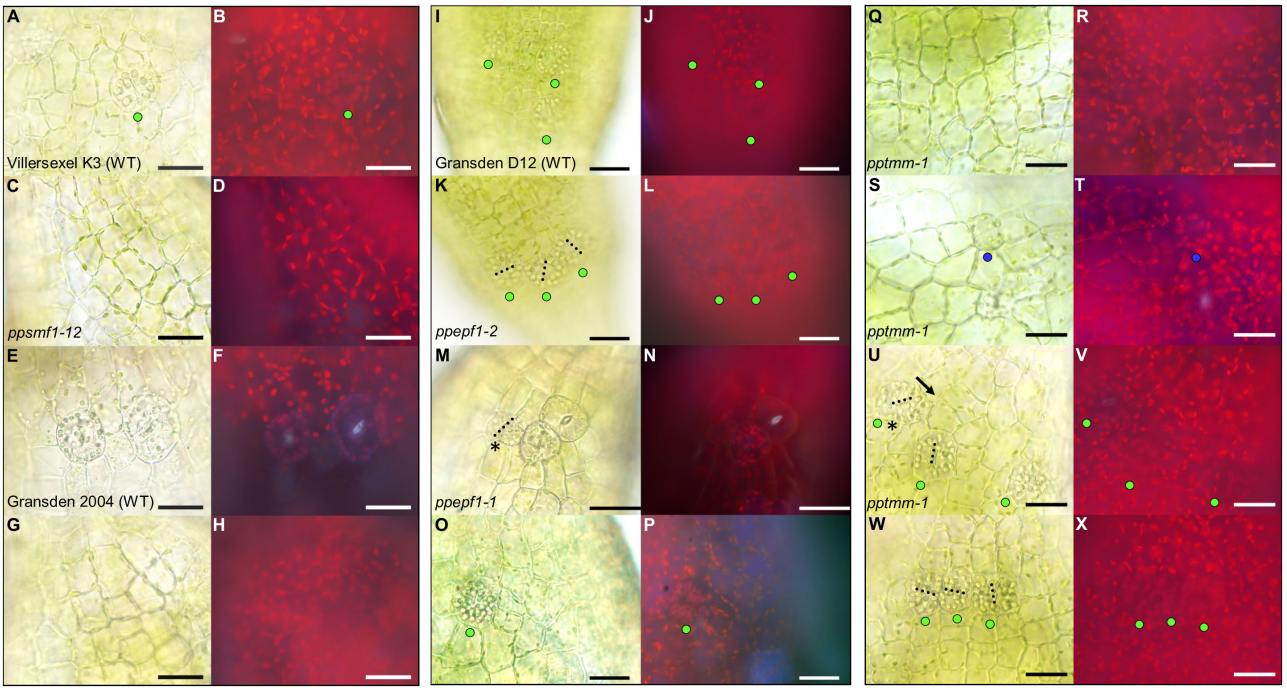

FIGURE 6 | Stomata development-associated genes *PpSMF1*, *PpSCRM1*, *PpEPF1* and *PpTMM* all regulate guard mother cell (GMC) activity. All images displayed are taken from elongating early expanding sporophytes equivalent to those pictured in **Figures 1C,D**. **(A)** Close-up of Villersexel K3 wild-type (WT) image of the epidermis with a GMC that has yet to undergo division. **(B)** Fluorescent equivalent to panel **(A)**. **(C)** *ppsmf1* epidermis with epidermal cells loosely arranged in files equivalent to wild-type in panel **(A)**. **(D)** Fluorescent image of panel **(C)**. **(E)** Representative close-up Gransden 2004 wild-type (WT) image with nascent guard cells (GCs) that have re-aggregated organelles. **(F)** Fluorescent equivalent to panel **(E)**. Note the fluorescence being emitted from the pore region of newly formed GCs where organelles have re-aggregated. In both wild types a range of different stomatal lineage cell types were detected from early GMCs to nascent GCs at the early expanding sporophyte stage. **(G)** *ppscrm1* epidermis with epidermal cells, but no GMCs, which was equivalent to wild-type in panel **(E)**. **(H)** Fluorescent equivalent to panel **(G)**. **(I)** Gransden D12 wild-type (WT) displaying early GMC cells with accompanying **(J)** fluorescence shot. **(K–X)** All images from plants in Gransden D12 background. **(K)** *ppepf1* with three early GMC cells clustering adjacently with accompanying fluorescence image **(L)**. **(M)** Bright-field and **(N)** fluorescence epidermal images showing ppepf1 nascent early GC and adjacently clustering GMCs. **(O)** *PpEPF1OE* bright-field and **(P)** fluorescence epidermal images of an expanded early GMC that may have undergone- or is in the process of- endoreduplication. **(Q–X)** Bright-field and fluorescence images of *pptmm* sporophyte epidermis's showing **(Q,R)** undifferentiated cells, **(S,T)** a putative early GMC pre-cursor, **(U,V)** an early GMC dividing toward (see asterisk) another GMC and (W+X) early GMCs clustering. Blue dots represent a probable GMC pre-cursor, green dots represent early GMCs and the yellow dots represent dividing GMCs. Black dotted lines denote cell plates. Scale bars = 25 μm.

developmental stage, no obvious stomatal lineage cells were detected using bright-field or fluorescence microscopy. The first developmental stage where stomata lineage cells were clearly apparent (**Figures 4C,D**), was on sporophytes equivalent to those in **Figure 2C**. As the young sporangium expanded further (**Figure 2D**), in addition to maturing guard cells with fluorescent cuticular pores (**Figure 4D**), other stomatal lineage cells were also present (**Figures 4E–L**). These included distinctively circular unexpanded cells that had radiating epidermal cells surrounding them (**Figure 4E**). Based on their orientation to other cells and lack of expansion, the circular cells were probably GMC precursors. Although we observed lots of variation in epidermal cell size and orientation, we did not identify asymmetric entry divisions equivalent to those described in the early stomatal lineage of vascular land plants (Zhao and Sack, 1999), in agreement with previous reports that such divisions are absent during the very earliest stages of moss stomatal development (Vaten and Bergmann, 2012).

Using our combined bright-field and fluorescence microscopy technique, we characterized the developmental changes that take place once a GMC is formed and subsequently then undergoes an incomplete division to form a GC (**Figures 4E–N**). For clarity, we defined pore opening, rather than cell plate formation, as the point when a GC formed in *P. patens*. This characterization is in line with the designation of guard cells in Arabidopsis by Zhao and Sack (1999). We detected a number of expanded oval shaped putative GMCs on the expanding sporophyte (**Figures 4F–H**) in addition to the probable GMC precursors discussed above (**Figure 4E**, also marked by blue dots in the epidermal and sub-epidermal images shown in **Figures 4I–L**). These cell conformations included; cells with prominent, radially aligned circular bodies consisting of chloroplasts and starch granules containing a centralized cell plate (**Figure 4F** and marked by green dots in **Figures 4I–L**); cells with sparse, fragmented cellular matter containing a central cell plate (**Figure 4G**); and cells with densely fragmented cellular matter (**Figure 4H**, and marked by yellow dots in **Figures 4I–L**

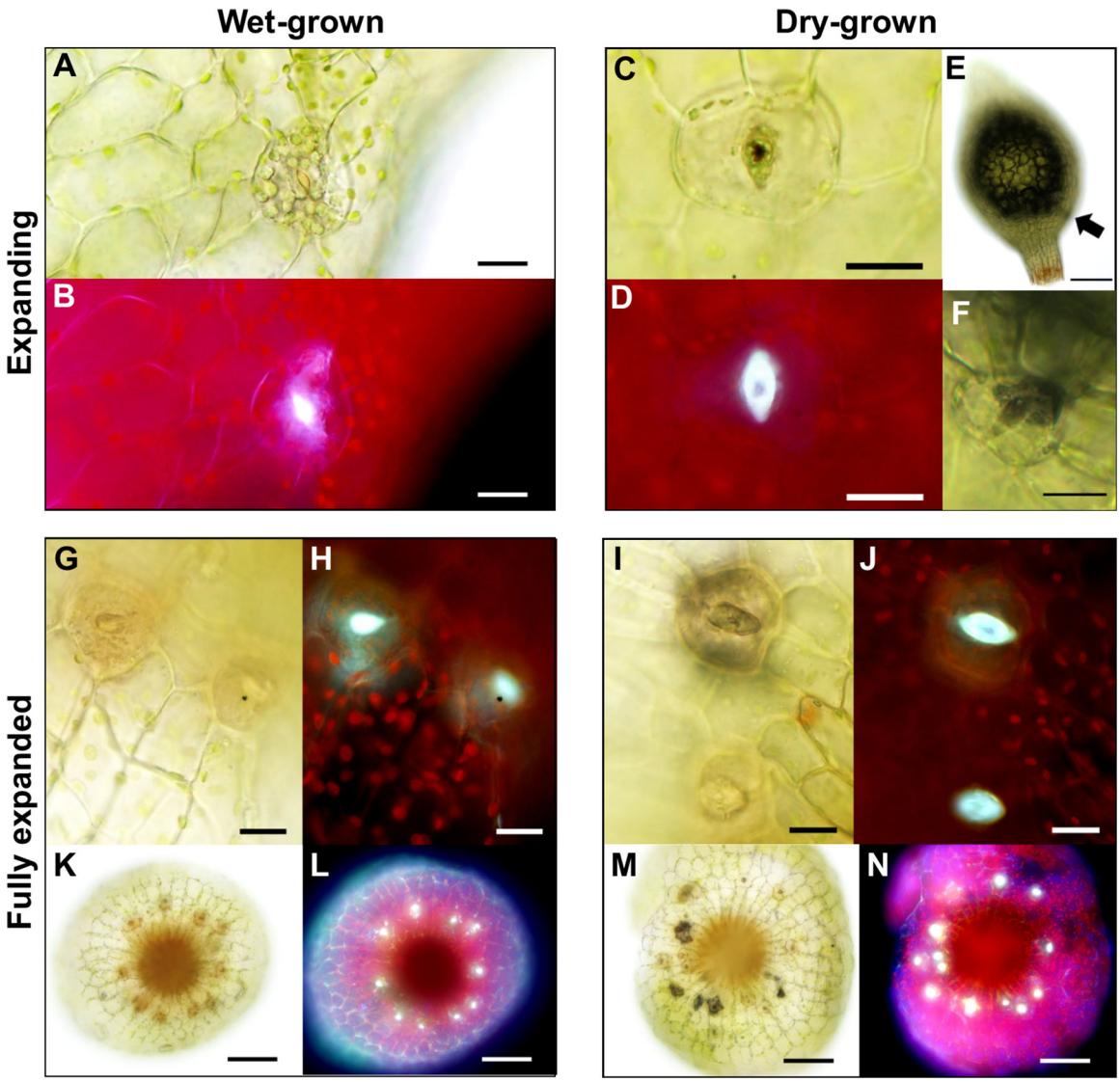

FIGURE 7 | Altered anatomical stomatal functioning in response to different environmental surroundings in *Physcomitrium patens*. **(A)** Bright-field and **(B)** fluorescence images of a nascent guard cell (GC) on an expanding sporophyte growing in wet conditions. Note. The occluded pore. **(C)** Equivalent bright-field and **(D)** fluorescence images of a GC on an expanding sporophyte growing in dry conditions. The differences in fluorescence intensity between panels **(B)** and **(D)** probably represent a difference in mucilage localization with **(D)** exhibiting receding mucilage. **(E)** An expanding sporophyte capsule with a darkened sub-epidermal region with **(F)** corresponding stomata subsequently imaged close up. **(G–J)** Close-up bright-field and fluorescence images of expanded capsules grown under wet **(G,H)** or dry **(I,J)** conditions. Note: in panels **(I,J)** the darkened sub-stomatal cavity and un-occluded pore. **(K–N)** Stacked and flattened images of capsules used to image the stomata in panels **(G–J)**. Note: the darkened cavities and increased fluorescence in **(M,N)** comparatively to **(K,L)**. Scales bars are as follows: **(A–D,F–J)** = 15 μm; **(E,K–N)** = 100 μm.

and **Supplementary Figure S1**). Using fluorescence imaging we observed stomatal pores in oval cells with fragmented cellular matter (yellow dots), but not in cells with circular organelles (green dots, early GMCs) or those with sparse fragmented cellular matter (late GMCs, **Figures 4I–L**, **5**). The composition of the observed fluorescent material is not known, but possibilities include cutin or wax deposition in the pore wall and/or pectin/mucilage build-up (Lee and Priestley, 1924; Isaac, 1941; Smith, 1955; Sack and Paolillo, 1983; Pressel et al., 2014; Merced and Renzaglia, 2017). Once incomplete symmetric division of a GMC was finished, the cellular contents of GCs re-aggregated (**Figures 4M,N** and **Supplementary Figure S1**). These data suggest that enlarged GMCs (early GMCs) first develop with aggregated circular organelles and/or starch granules which then dissipate in late GMCs, before fragmentation of contents occurs throughout the cell and pore formation occurs which marks the differentiation from GMC to GC (**Figure 4O**). The formation of the GC results in the re-assembly of the cell contents and gradual browning and flavonoid formation as the stoma matures.

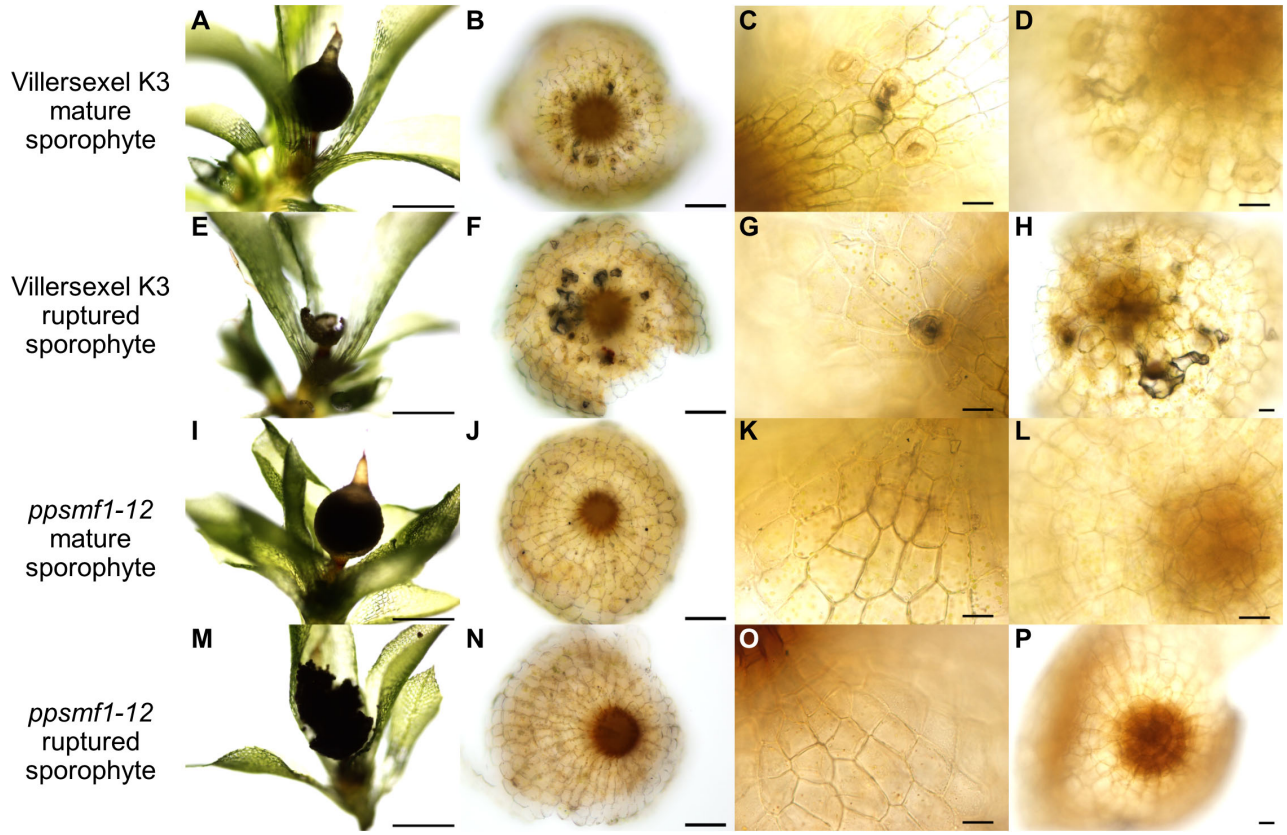

FIGURE 8 | *ppsmf1* moss sporophytes do not possess darkened and vacuous sub-stomatal cavities when grown under dry conditions. For **(A–P)** plants and corresponding sporophytes were taken from plates grown under the same conditions set out in Chater et al. (2016). **(A)** Mature brown intact Villersexel K3 wild-type sporophyte capsule attached to parental gametophyte. **(B)** A stacked and flattened image of a sporophyte capsule base of panel **(A)** dissected and face upward. **(C)** Close-up of stomata from sample in panel **(B)** illustrating darkening beneath the cavity. **(D)** Same capsule as in panels **(A–C)** mounted upside down to observe underlying sub-stomatal cavity. The darkening can be seen lining the sub-stomatal cavity which extends from the open pore into the base of capsule. **(E)** Ruptured brown Villersexel K3 sporophyte capsule attached to parental gametophyte. **(F)** A stacked and flattened image of the sporophyte capsule base in panel **(E)** dissected and faced upward. **(G)** Close-up of stomata from panel **(F)** illustrating darkening beneath the cavity. **(H)** The same capsule as in panels **(E–G)** mounted upside down. Darkening can again be seen lining large portions of the cavities which underlie the stomata. **(I)** Mature brown intact ppsmf1 sporophyte capsule attached to the parental gametophyte. **(J)** A stacked and flattened image of the sporophyte capsule base in panel **(I)** dissected and face upward. **(K)** Close-up of the astomate epidermis of *ppsmf1*. **(L)** The same capsule as in panesl **(I–K)** mounted upside down with no sub-stomatal cavities. **(M)** Ruptured *ppsmf1* sporophyte capsule attached to the parental gametophyte. **(N)** A stacked and flattened image of the sporophyte capsule base in panel **(M)** dissected and face upwards. **(O)** Close-up of the astomate epidermis of *ppsmf1*. **(P)** The same capsule as in panel **(O)** mounted upside down with no sub-stomatal cavities. Scales bars are as follows: **(A,E,I,M)** = 500 μm; **(B,F,J,N)** = 100 μm; **(C,D,G,H,K,L,O,P)** = 25 μm.

Whilst observing stomatal development, we noticed meristematic activity in early GMCs (**Figure 5**). This was in contrast to previous reports in which non-vascular land plant GMCs always divide or differentiate directly to form a GC or pair of GCs (Sack and Paolillo, 1985; Pressel et al., 2014; Merced and Renzaglia, 2016). We found that when two *P. patens* early GMCs formed adjacently, one of the GMCs had the potential to undergo a GMC spacing division resulting in the formation of an intervening spacer cell (SPC) (**Figure 5**). During a spacing division, aggregated cellular organelles in the dividing GMC were at first spread throughout the dividing cell (see right GMC in **Figures 5A,B**). As the division occurred over a 2 h-period, the organelles dissipated and migrated to the most distal part of the dividing GMC as it moved away from the previously adjacent GMC (**Figures 5C–H**). Meanwhile over the same period, in the stationary GMC the aggregated organelles dissipated (see left GMC in **Figures 5C–H**). Autofluorescence profiles of the division, taken over the 2 h period, suggest that both cells start at the early GMC stage, and at no point does pore formation begin to occur (**Figures 5B,D,H**). These data indicate that *P. patens* GMCs can undergo spacing divisions which would enable more dynamic control over stomatal patterning and development than previously thought. It remains unclear whether renewed GMCs could undergo further meristematic activity by undergoing additional GMC spacing divisions as it was not possible to continue tracking the live dissected samples over longer periods (**Figure 5L**). Similarly, it remains unknown whether the SPC produced from a GMC spacing division could maintain or revert to GMC identity and become a stoma, if spacing permitted.

Identifying Controllers of Cell Fate and Polarity: Stomatal Development Ontogeny in *P. patens* Development and Patterning Mutants

To further understand *P. patens* stomatal development and spacing processes at the molecular level, a reverse genetics approach was taken and the development of stomatal mutants generated in previous studies were studied (Caine et al., 2016; Chater et al., 2016). Observations were taken at equivalent developmental stages to the wild-type sporophytes in **Figures 4**, **5**. Both *ppsmf1* and *ppscrm1* single deletion mutants failed to form early GMCs (**Figures 6A–H**). We observed some small cells in these lines, however, it was not possible to conclude whether these were pre-cursors to GMCs or nascent epidermal cells. Observations of *ppepf1* sporophytes revealed contiguous clustering of early and more advanced GMCs which were irregularly orientated, possibly due to an inability to undergo GMC spacing divisions (**Figures 6K,N**). Conversely, over-expression of *PpEPF1* produced early GMCs with ectopic organelle formation indicative of endoreduplication, or alternatively large areas without any early GMCs (**Figures 6O,P**). Taking *ppepf1* and *PpEPF1OE* phenotypes together, it appears that PpEPF1 prevents cells adjacent to early GMCs from assuming early GMC identity. Moreover, PpEPF1 appears to govern early GMC spacing divisions by regulating GMC duplication, and also assists in setting the correct orientation of division (**Figures 6K–P**).

Mature *pptmm* mutant capsules exhibit a range of stomatal patterning phenotypes which vary both between and within individual sporophytes and between sporophytes (Caine et al., 2016). *pptmm* phenotypes were tracked during early sporophyte development (**Figures 6Q–X**). In the young *pptmm* epidermis, there were zones devoid of stomatal precursors (**Figures 6Q,R**), irregularly small GMCs (**Figures 6S,T**), early GMCs dividing toward each other (**Figures 6U,V**), and areas with clustered early GMCs with irregular cellular orientations (**Figures 6W,X**). Overall, these phenotypes suggest that PpTMM is required for the correct regulation of early GMCs in a number of ways. PpTMM enhanced entry into the stomatal lineage by promoting early GMC formation when no other GMCs were present (**Figures 6Q–T**) and once early GMCs had formed, PpTMM acted to prevent excessive ectopic spacing divisions of early GMCs (**Figures 6U,V**). PpTMM also specified the orientation of GMC divisions and regulated early GMC identity in neighboring cells, thereby preventing clustering (**Figures 6U–X**).

Growth in Wet or Dry Conditions Influences the Fate of Mature *P. patens* Stomata

As sporophyte capsules expanded (**Figures 2C–F**), guard cells continued to develop, and once formed generated a pore linking the sub-stomatal cavity with the surrounding environment (**Figure 7**). We observed that when sporophytes matured under wet conditions, GC pores were often occluded. When viewed under UV light these plugged pores displayed an enhanced autofluorescent haze, probably due to increased secretion of mucilage (**Figures 7A,B**). Conversely, sporophytes which matured under drier conditions (**Figures 7C,D**) had stomata that typically displayed autofluorescence from the inner walls of the GC pore and inner cavity (compare **Figure 7D** to **Figure 7B**). In some instances, the sub-stomatal area become darkened, perhaps due to dried mucilage (**Figure 7E**), and this was evident even from a distance (**Figure 7F**). The stomata and underlying cavities of fully expanded green-to-yellow capsules often had plugged pores when grown under wet conditions, and open pores with darkened cavities were frequently detectable in capsules grown under dry conditions (**Figures 7G,K,I,M**). Typically, the autofluorescence signals from "wet-grown" capsule stomata arose from the clogged pore, whereas dry-grown capsules emitted auto-fluorescence from the underlying sub-stomatal cavities where mucilage had receded (compare **Figures 7H,L** with **Figures 7J,N**).

To ascertain whether the darkening effect attributed to drying mucilage also occurred in *ppsmf1,* which fails to produce stomata or sub-stomatal cavities (Chater et al., 2016), we examined dry-grown mature capsules prior to- and after- sporophyte rupture (**Figure 8**). As expected, *ppsmf1* presented no darkening in either mature intact or ruptured sporophytes (Compare **Figures 8A–H** with **Figures 8I–P**). This observation suggests that stomata are essential for the induction of internal darkening during capsule dry-down in *P. patens*. These observations help to explain the delayed sporophyte rupture of *ppsmf1* mutants (Chater et al., 2016) and provide further evidence that bryophyte stomata play an important role in capsule drying and spore dispersal (Duckett et al., 2009; Pressel et al., 2014; Chater et al., 2016; Merced and Renzaglia, 2017).

DISCUSSION

Building Increasingly Robust Stomatal Developmental Modules

In Arabidopsis, as in most other land plants, stomata are spaced by at least one intervening epidermal pavement cell (Hara et al., 2007; Rudall et al., 2013; Caine et al., 2016). This is achieved through orientated amplifying and spacing divisions of stomatal precursors, so that stomatal lineage cells are typically bordered by SLGCs or epidermal pavement cells (Geisler et al., 1998, 2000; Zhao and Sack, 1999; **Figures 9A–C**). EPF2 negatively regulates SPCH-SCRM/2 activity in the early stages of the stomatal lineage; EPF1 negatively regulates MUTE-SCRM/2 as meristemoids transition to GMCs; and TMM is required for EPF signal transduction (Hara et al., 2007; Hunt and Gray, 2009; Qi et al., 2017). Our observations indicate that mosses also influence stomatal patterning via orientated asymmetric cell divisions, albeit at the early GMC stage, and this is regulated by a similar molecular signaling pathway: The one moss EPF (PpEPF1) and RLP (PpTMM) are both required for correct stomatal spacing (**Figures 4**, **5**, **6I–X**, **9D–F**). PpSMF1 and

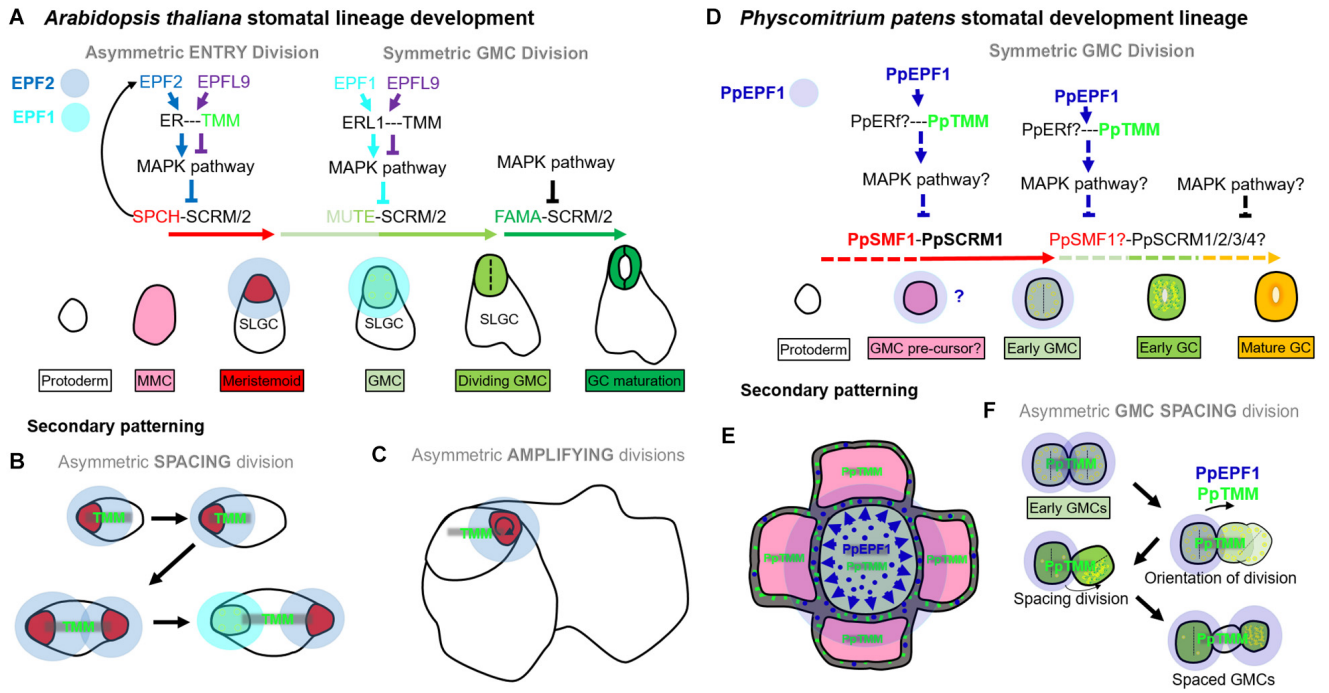

FIGURE 9 | Contrasting stomatal development in *Arabidopsis thaliana* and *Physcomitrium patens*. In Arabidopsis, asymmetric entry **(A)**, spacing **(B)**, and amplifying **(C)** divisions are regulated by SPEECHLESS (SPCH) and ICE1/SCREAM (SCRM) or SCRM2. In all three types of divisions, SPCH activity is under phospho-regulatory control, and this occurs via the MAPK pathway. The MAPK pathway facilitates signals from the plasma membrane exterior to be transduced into the nucleus. ERECTA family proteins [particularly ERECTA (ER)], modulated by TOO MANY MOUTHS (TMM) convey such signals. If the EPIDERMAL PATTERNING FACTOR (EPF), EPF2 successfully binds to ER then stomatal lineage entry is inhibited. If the EPF-like (EPFL) peptide, EPFL9 binds, the MAPK pathway activity is reduced, allowing the SPCH-SCRM/2 heterodimers to initiate asymmetric divisions from meristemoid mother cells (MMC), leading to new meristemoid formation [see red cell in entry **(A)** or spacing **(B)** division], or the renewal of an existing meristemoid [see red cell in amplifying **(C)** divisions]. SPCH also upregulates EPF2 and thus regulates its own activity through negative feedback. Later MUTE, together with SCRM/2, orchestrates the advancement of the meristemoid to GMC, and then participates in the GMC division. EPF1 inhibits MUTE activity and EPFL9 promotes it, again via elements of a MAPK pathway. What drives EPF1 expression is still unclear. Lastly, FAMA together with SCRM/2 permits correct GC identity and this stage is also governed by various elements of the MAPK pathway. Typically EPF2 is secreted from meristemoids during early stomatal development, primarily to restrict SPCH activity in neighboring stomatal lineage cells [see translucent blue circles around meristemoids in panels **(A–C)**]. EPF1 is secreted later during the meristemoid to GMC transition, and continuing into GMC division [see translucent light blue circles around GMCs in panels **(A,B)**]. **(D)** PpSMF1 and PpSCRM1 both facilitate stomatal lineage advancement to an early GMC. This may also include promoting early GMC pre-cursor fate. PpTMM promotes the initial formation of GMCs, and PpEPF1 may also be involved by preventing initial cells from obtaining early GMC fate. These signals are probably conveyed by a number of PpERECTA proteins (Caine et al., 2016) and a MAPK pathway. PpEPF1 function could normally take place once an initial GMC has been specified, although further work is required to establish whether this is the case. Downstream of the early GMC formation it is unclear as to what, if any, roles PpSMF1 and/or PpSCRM1/2/3/4 undertake. All lines which are dashed are hypothesized mechanisms as are the functions of proteins which are followed by question marks. **(E)** Secondary patterning occurs when early GMC cells may secrete PpEPF1 (blue circles) to signal to nearby early GMC pre-cursor. PpTMM, on the early GMC pre-cursor (green sticks), probably transduces PpEPF1 signal and thereby preventing adjacent early GMCs from forming. **(F)** GMC asymmetric spacing divisions occur when two early GMCs concurrently arise next to each other, maybe from cells which concurrently differentiate from GMC pre-cursor origin. PpEPF1 may be secreted by both early GMCs, and via PpTMM signaling assists in the orientation of division so that GMCs are not touching. The spacing division can then unfold and cellular organelles move in a polar fashion to the distal part of the dividing cell. This will eventually lead to GMCs which are separated via a spacer cell (SPC). PpEPF1 presence with PpTMM ensures these processes occur in the correct orientation. It is unclear whether the new SC has the capability to re-enter the stomatal lineage.

PpSCRM1 are also necessary, as without these transcription factors there is no GMC formation.

A key difference between the Arabidopsis asymmetric divisions and the observed *P. patens* spacing division mechanism (**Figures 5**, **6**) is that Arabidopsis has the ability to undergo such divisions prior to GMC formation; a stage which is characterized in both species by small cells with aggregated chloroplasts (Lucas et al., 2006; **Figures 4**, **9**). This postponement of the GMC state in angiosperms may have been made possible by the duplication(s) of members of both the *SMF* and *EPF* gene families. In particular, the evolution of *EPF2* and *SPCH* genes enabled earlier temporal control of asymmetric divisions (compare **Figures 9A–C** with **Figures 9D,F**), which led to greater developmental plasticity and more accurately spaced stomata. In some respects, PpEPF1 behaves similarly, to both EPF2 and EPF1 in that it functions to prevent neighboring cells of early GMCs, such as GMC pre-cursors, from becoming early GMCs. This is similar to how both EPF2 and EPF1 regulate Arabidopsis MMCs and SLGCs which neighbour meristemoids

and GMCs (compare **Figures 9B,E**). On the other hand, PpEPF1 also shows similarity with EPF2 functionality during amplifying divisions to maintain cell fate (**Figures 9C,F**). This is because, as highlighted, although ectopic early GMC divisions occur in *ppepf1* plants (see **Figures 5M,N**), instead of terminating as small cells as in *epf2* plants, the early GMCs of *ppepf1* carry on to become stomata and, hence, contiguous clustering occurs (Hara et al., 2009; Hunt and Gray, 2009; Caine et al., 2016).

Whilst we show PpSMF1 and PpSCRM1 regulate early GMC formation (**Figures 6A–H**), we are unable to confirm that these proteins also play a part in GMC precursor formation and the GMC symmetric division leading to GC formation. Interestingly, the E-box DNA binding domain of FAMA, which is integral for GC formation in Arabidopsis, is also present in PpSMF1 (Chater et al., 2016), and complementation studies in both Arabidopsis *mute* and *fama* have shown that PpSMF1 can partially rescue both mutant lines (MacAlister and Bergmann, 2011). Further functional motif studies are required to understand the ancestral roles of SMF and SCRM bHLHs, and their divergence and specialization across stomatal evolution.

Our data suggest that a more complex form of stomatal patterning exists in *P. patens* than was previously thought. We propose that moss GMCs have the capacity to alter their cell fate, rather than directly transitioning to GCs they may instead undergo asymmetric spacing divisions. This differs from the situation reported in the closely related *Funaria hygrometrica*, where stomata are exclusively spaced via divisions of close-by epidermal cells (Merced and Renzaglia, 2016). Our analysis of *ppsmf1* and *ppscrm1* capsules illustrates that GMCs only form when both of these key bHLH genes are present; no early GMCs were found in either of the mutant backgrounds throughout sporophyte development. This confirms that the early GMCs involved with *P. patens* spacing divisions (**Figure 5**) are indeed GMCs, and not undifferentiated epidermal cells that integrate correct stomatal patterning post-GC formation, as described in *F. hygrometrica*.

For ancient sporophytes, the evolution of a GMC spacing division would have permitted a more refined regulation of stomatal development. Later, as plant lineages evolved, regulatory control may have been modified to enable asymmetric entry divisions prior to the formation of the GMC. This would have enabled stomatal development to be corrected at an earlier time-point, thereby further optimizing stomatal placement. At the molecular level this is particularly evident in *SPCH* evolution, as this gene (and encoded protein) has many regulatory points that govern if and when stomatal development is initiated (Lampard, 2009; Sugano et al., 2010; Gudesblat et al., 2012; Tricker et al., 2012; Chater et al., 2017; Lau et al., 2018). As photosynthetic capacity became more important to increasingly large sporophytes, perhaps *EPFL9*-type genes evolved to enable signals from the mesophyll to be more tightly integrated into the stomatal development module.

Further Considerations for Stomatal Function in *P. patens*

It has been proposed that stomata are "monophyletic" structures across land plants (Raven, 2002; Caine et al., 2016). However, the possibility of convergent evolution of stomata across plant groups has also been argued (Raven, 2002; Pressel et al., 2014). Recent molecular and physiological analyses suggest that the mechanisms of stomatal function and development are broadly conserved across land plants (Chater et al., 2011, 2016; Ruszala et al., 2011; Doi et al., 2015; Lind et al., 2015; Caine et al., 2016; Harris et al., 2020). However, in earlier diverging lineages including the bryophytes, the divergent physiology and functions of stomata continue to be debated (Duckett et al., 2009; Chater et al., 2011, 2013, 2016; Pressel et al., 2014; Field et al., 2015; Chen et al., 2016; McAdam and Brodribb, 2016; Hõrak et al., 2017; Grantz et al., 2019). While this matter requires further study, it has become clear that for bryophytes stomata are important in aiding sporophyte drying and subsequent rupture for dehiscence, leading to spore dispersal (Duckett et al., 2009; Merced and Renzaglia, 2013; Chater et al., 2016), and our anatomical observations here further support this.

In addition to aiding capsule drying, it has been suggested that the positioning of stomata around the base of moss spore capsules may also aid in water and nutrient uptake from the parent gametophyte (Haig, 2013). Moreover, owing to stomata being positioned above spongy tissues, it has been further suggested that they may be important in permitting gas exchange for photosynthesis (Merced and Renzaglia, 2013). Our observations suggest that the function of moss stomata might also vary depending on the environment in which a given capsule develops, and this is related to whether stomata become occluded or not. In wet environments, stomata readily become plugged with auto-fluorescent cuticular material that perhaps prevents water and/or pathogens entering sub-stomatal cavities (**Figure 7**). Whether this inhibits gaseous exchange and impacts on matrotrophy is unknown. Conversely, in drier habitats, stomata are often open as the sporophyte capsule enlarges, perhaps enhancing expanding sporophyte gas exchange and water and nutrient acquisition from the parental gametophore (**Figures 7**, **8**). We suggest that the darkening of drying capsules is a result of receding mucilage and related to the material observed in hornwort stomata that may assist in capsule rupture (Pressel et al., 2014). Our data support this assumption, as *ppsmf1* capsules lacking stomata and their cavities demonstrate delayed rupture (Chater et al., 2016) and do not undergo sub-epidermal darkening (**Figure 8**). Taken together, these observations suggest that bryophyte stomata, like the stomata of vascular plants, permit the controlled release of water, and thereby enhance the efficiency of mature capsule drying and rupture, and increasing the distance of spore dispersal. For *P. patens*, an ephemeral moss of riparian habitats, this may translate into the improved fitness of an individual by increasing the probability for spores to reach aqueous environments such as rivers and lakes.

DATA AVAILABILITY STATEMENT

The raw data supporting the conclusions of this article will be made available by the authors, without undue reservation, to any qualified researcher.

AUTHOR CONTRIBUTIONS

RC performed the experiments. All authors interpreted the data and wrote the manuscript. AF and JG conceived the project.

FUNDING

This work was funded by the National Environmental Research Council (1241768), the Biotechnology and Biological Sciences Research Council, and the University of Sheffield QR GCRF fellowship (Research England institutional allocation). CC would like to acknowledge funding from the European Union's Horizon 2020 Research and Innovation Programme under the Marie Skłodowska-Curie grant agreement no. 700867.

ACKNOWLEDGMENTS

We thank Prof. Dr. Ralf Reski (Freiburg) for use of the *ppscrm1* mutants and Robert Brench for his advice when writing the manuscript.

SUPPLEMENTARY MATERIAL

The Supplementary Material for this article can be found online at: https://www.frontiersin.org/articles/10.3389/fpls.2020.00643/full#supplementary-material

REFERENCES

Abrash, E. B., and Bergmann, D. C. (2010). Regional specification of stomatal production by the putative ligand CHALLAH. *Development* 137, 447–455. doi: 10.1242/dev.040931

Beerling, D. J. (2007). *The Emerald Planet : How Plants Changed Earth's History*. Oxford: Oxford University Press.

Berger, D., and Altmann, T. (2000). A subtilisin-like serine protease involved in the regulation of stomatal density and distribution in *Arabidopsis thaliana*. *Genes Dev.* 14, 1119–1131.

Berry, J. A., Beerling, D. J., and Franks, P. J. (2010). Stomata: key players in the earth system, past and present. *Curr. Opin. Plant Biol.* 13, 233–240. doi: 10.1016/j.pbi.2010.04.013

Bhave, N. S., Veley, K. M., Nadeau, J. A., Lucas, J. R., Bhave, S. L., and Sack, F. D. (2009). TOO MANY MOUTHS promotes cell fate progression in stomatal development of Arabidopsis stems. *Planta* 229, 357–367. doi: 10.1007/s00425-008-0835-9

Brodribb, T. J., Carriquí, M., Delzon, S., McAdam, S. A. M., and Holbrook, N. M. (2020). Advanced vascular function discovered in a widespread moss. *Nat. Plants* 6, 273–279. doi: 10.1038/s41477-020-0602-x

Budke, J. M., Goffinet, B., and Jones, C. S. (2011). A hundred-year-old question: is the moss calyptra covered by a cuticle? A case study of *Funaria hygrometrica*. *Ann. Bot.* 107, 1279–1286. doi: 10.1093/aob/mcr079

Budke, J. M., Goffinet, B., and Jones, C. S. (2012). The cuticle on the gametophyte calyptra matures before the sporophyte cuticle in the moss *Funaria hygrometrica* Funariaceae. *Am. J. Bot.* 99, 14–22. doi: 10.3732/ajb.1100311

Caine, R. S., Chater, C. C., Kamisugi, Y., Cuming, A. C., Beerling, D. J., Gray, J. E., et al. (2016). An ancestral stomatal patterning module revealed in the non-vascular land plant *Physcomitrella patens*. *Development* 143, 3306–3314. doi: 10.1242/dev.135038

Chater, C. C. C., Caine, R. S., Fleming, A. J., and Gray, J. E. (2017). Origins and evolution of stomatal development. *Plant Physiol.* 174, 624–638. doi: 10.1104/pp.17.00183

Chater, C. C., Caine, R. S., Tomek, M., Wallace, S., Kamisugi, Y., Cuming, A. C., et al. (2016). Origin and function of stomata in the moss *Physcomitrella patens*. *Nat. Plants* 2, 16179–16179. doi: 10.1038/nplants.2016.179

Chater, C., Gray, J. E., and Beerling, D. J. (2013). Early evolutionary acquisition of stomatal control and development gene signalling networks. *Curr. Opin. Plant Biol.* 16, 638–646. doi: 10.1016/j.pbi.2013.06.013

Chater, C., Kamisugi, Y., Movahedi, M., Fleming, A., Cuming, A. C., Gray, J. E., et al. (2011). Regulatory mechanism controlling stomatal behavior conserved across 400 million years of land plant evolution. *Curr. Biol.* 21, 1025–1029. doi: 10.1016/j.cub.2011.04.032

Chen, Z.-H., Chen, G., Dai, F., Wang, Y., Hills, A., Ruan, Y.-L., et al. (2016). Molecular evolution of grass stomata. *Trends Plant Sci.* 22, 124–139.

Cove, D. J., Perroud, P.-F., Charron, A. J., McDaniel, S. F., Khandelwal, A. and Quatrano, R. S. (2009). Culturing the moss *physcomitrella patens*. *Cold Spring Harb. Protoc.* 2009:prot5136. doi: 10.1101/pdb.prot5136

Doi, M., Kitagawa, Y., and Shimazaki, K. (2015). Stomatal blue light response is present in early vascular plants. *Plant Physiol.* 169, 1205–1213. doi: 10.1104/pp.15.00134

Duckett, J. G., and Pressel, S. (2018). The evolution of the stomatal apparatus: intercellular spaces and sporophyte water relations in bryophytes-two ignored dimensions. *Philos. Trans. R. Soc. Lond. B Biol. Sci.* 373:20160498. doi: 10.1098/rstb.2016.0498

Duckett, J. G., Pressel, S., P'ng, K. M. Y., and Renzaglia, K. S. (2009). Exploding a myth: the capsule dehiscence mechanism and the function of pseudostomata in Sphagnum. *New Phytol.* 183, 1053–1063. doi: 10.1111/j.1469-8137.2009.02905.x

Dutton, C., Hõrak, H., Hepworth, C., Mitchell, A., Ton, J., Hunt, L., et al. (2019). Bacterial infection systemically suppresses stomatal density. *Plant Cell Environ.* 42, 2411–2421. doi: 10.1111/pce.13570

Edwards, D., Kerp, H., and Hass, H. (1998). Stomata in early land plants: an anatomical and ecophysiological approach. *J. Exp. Bot.* 49, 255–278.

Egener, T., Granado, J., Guitton, M.-C., Hohe, A., Holtorf, H., Lucht, J. M., et al. (2002). High frequency of phenotypic deviations in *Physcomitrella patens* plants transformed with a gene-disruption library. *BMC Plant Biol.* 2:6. doi: 10.1186/1471-2229-2-6

Field, K. J., Duckett, J. G., Cameron, D. D., and Pressel, S. (2015). Stomatal density and aperture in non-vascular land plants are non-responsive to above-ambient atmospheric CO_2 concentrations. *Ann. Bot.* 115, 915–922. doi: 10.1093/aob/mcv021

Frank, W., Ratnadewi, D., and Reski, R. (2005). *Physcomitrella patens* is highly tolerant against drought, salt and osmotic stress. *Planta* 220, 384–394. doi: 10.1007/s00425-004-1351-1

Franks, P. J., Doheny-Adams, T. W., Britton-Harper, Z. J., and Gray, J. E. (2015). Increasing water-use efficiency directly through genetic manipulation of stomatal density. *New Phytol.* 207, 188–195. doi: 10.1111/nph.13347

Geisler, M., Nadeau, J., and Sack, F. D. (2000). Oriented asymmetric divisions that generate the stomatal spacing pattern in Arabidopsis are disrupted by the *too many mouths* mutation. *Plant Cell* 12, 2075–2086. doi: 10.1105/tpc.12.11.2075

Geisler, M., Yang, M., and Sack, F. D. (1998). Divergent regulation of stomatal initiation and patterning in organ and suborgan regions of the Arabidopsis mutants too many mouths and four lips. *Planta* 205, 522–530. doi: 10.1007/s004250050351

Grantz, D. A., Linscheid, B. S., and Grulke, N. E. (2019). Differential responses of stomatal kinetics and steady-state conductance to abscisic acid in a fern:

comparison with a gymnosperm and an angiosperm. *New Phytol.* 222, 1883–1892. doi: 10.1111/nph.15736

Gudesblat, G. E., Schneider-Pizon, J., Betti, C., Mayerhofer, J., Vanhoutte, I., van Dongen, W., et al. (2012). SPEECHLESS integrates brassinosteroid and stomata signalling pathways. *Nat. Cell Biol.* 14, 548–554. doi: 10.1038/ncb2471

Haig, D. (2013). Filial mistletoes: the functional morphology of moss sporophytes. *Ann. Bot.* 111, 337–345. doi: 10.1093/aob/mcs295

Han, S. K., Qi, X., Sugihara, K., Dang, J. H., Endo, T. A., Miller, K. L., et al. (2018). MUTE directly orchestrates cell-state switch and the single symmetric division to create stomata. *Dev. Cell* 45, 303–315.e5. doi: 10.1016/j.devcel.2018.04.010

Han, S.-K., and Torii, K. U. (2016). Lineage-specific stem cells, signals and asymmetries during stomatal development. *Development* 143, 1259–1270. doi: 10.1242/dev.127712

Hara, K., Kajita, R., Torii, K. U., Bergmann, D. C., and Kakimoto, T. (2007). The secretory peptide gene EPF1 enforces the stomatal one-cell-spacing rule. *Genes Dev.* 21, 1720–1725. doi: 10.1101/gad.1550707

Hara, K., Yokoo, T., Kajita, R., Onishi, T., Yahata, S., Peterson, K. M., et al. (2009). Epidermal cell density is autoregulated via a secretory peptide, EPIDERMAL PATTERNING FACTOR$_2$ in Arabidopsis leaves. *Plant Cell Physiol.* 50, 1019–1031. doi: 10.1093/pcp/pcp068

Harris, B. J., Harrison, C. J., Hetherington, A. M., and Williams, T. A. (2020). Phylogenomic evidence for the monophyly of bryophytes and the reductive evolution of stomata. *Curr. Biol.* doi: 10.1016/j.cub.2020.03.048 [Epub ahead of print].

Hepworth, C., Doheny-Adams, T., Hunt, L., Cameron, D. D., and Gray, J. E. (2015). Manipulating stomatal density enhances drought tolerance without deleterious effect on nutrient uptake. *New Phytol.* 208, 336–341. doi: 10.1111/nph.13598

Hiss, M., Meyberg, R., Westermann, J., Haas, F. B., Schneider, L., Schallenberg-Rudinger, M., et al. (2017). Sexual reproduction, sporophyte development and molecular variation in the model moss *Physcomitrella patens*: introducing the ecotype Reute. *Plant J.* 90, 606–620. doi: 10.1111/tpj.13501

Hohe, A., Rensing, S. A., Mildner, M., Lang, D., and Reski, R. (2002). Day length and temperature strongly influence sexual reproduction and expression of a novel MADS-box gene in the moss *Physcomitrella patens*. *Plant Biol.* 4, 595–602.

Hõrak, H., Kollist, H., and Merilo, E. (2017). Fern stomatal responses to ABA and CO_2 depend on species and growth conditions. *Plant Physiol.* 174, 672–679. doi: 10.1104/pp.17.00120

Hunt, L., and Gray, J. E. (2009). The signaling peptide EPF2 controls asymmetric cell divisions during stomatal development. *Curr. Biol.* 19, 864–869. doi: 10.1016/j.cub.2009.03.069

Hunt, L., Bailey, K. J., and Gray, J. E. (2010). The signalling peptide EPFL9 is a positive regulator of stomatal development. *New Phytol.* 186, 609–614. doi: 10.1111/j.1469-8137.2010.03200.x

Isaac, I. (1941). The structure of *Anthoceros laevis* in relation to its water supply. *Ann. Bot.* 5, 339–35l.

Kanaoka, M. M., Pillitteri, L. J., Fujii, H., Yoshida, Y., Bogenschutz, N. L., Takabayashi, J., et al. (2008). SCREAM/ICE1 and SCREAM2 specify three cell-state transitional steps leading to Arabidopsis stomatal differentiation. *Plant Cell* 20, 1775–1785. doi: 10.1105/tpc.108.060848

Lampard, G. R. (2009). The missing link?: Arabidopsis SPCH is a MAPK specificity factor that controls entry into the stomatal lineage. *Plant Signal. Behav.* 4, 425–427. doi: 10.4161/psb.4.5.8296

Lau, O. S., Song, Z., Zhou, Z., Davies, K. A., Chang, J., Yang, X., et al. (2018). Direct control of SPEECHLESS by PIF4 in the high-temperature response of stomatal development. *Curr. Biol.* 28, 1273–1280.e3. doi: 10.1016/j.cub.2018.02.054

Lee, B., and Priestley, J. H. (1924). The Plant Cuticle. 1. It's structure, distribution and function. *Ann. Bot.* 38, 525–545. doi: 10.1074/jbc.M116.755330

Lee, J. S., Hnilova, M., Maes, M., Lin, Y. C. L., Putarjunan, A., Han, S. K., et al. (2015). Competitive binding of antagonistic peptides fine-tunes stomatal patterning. *Nature* 522, 439–443. doi: 10.1038/nature14561

Lee, J. S., Kuroha, T., Hnilova, M., Khatayevich, D., Kanaoka, M. M., McAbee, J. M., et al. (2012). Direct interaction of ligand-receptor pairs specifying stomatal patterning. *Genes Dev.* 26, 126–136. doi: 10.1101/gad.179895.111

Lee, L. R., and Bergmann, D. C. (2019). The plant stomatal lineage at a glance. *J. Cell Sci.* 132:jcs228551. doi: 10.1242/jcs.228551

Ligrone, R., Duckett, J. G., and Renzaglia, K. S. (2012). Major transitions in the evolution of early land plants: a bryological perspective. *Ann. Bot.* 109, 851–871. doi: 10.1093/aob/mcs017

Lind, C., Dreyer, I., Lopez-Sanjurjo, E. J., von Meyer, K., Ishizaki, K., Kohchi, T., et al. (2015). Stomatal guard cells co-opted an ancient ABA-dependent desiccation survival system to regulate stomatal closure. *Curr. Biol.* 25, 928–935. doi: 10.1016/j.cub.2015.01.067

Lucas, J. R., Nadeau, J. A., and Sack, F. D. (2006). Microtubule arrays and *Arabidopsis* stomatal development. *J. Exp. Bot.* 57, 71–79. doi: 10.1093/jxb/erj017

MacAlister, C. A., and Bergmann, D. C. (2011). Sequence and function of basic helix-loop-helix proteins required for stomatal development in *Arabidopsis* are deeply conserved in land plants. *Evol. Dev.* 13, 182–192. doi: 10.1111/j.1525-142X.2011.00468.x

MacAlister, C. A., Ohashi-Ito, K., and Bergmann, D. C. (2007). Transcription factor control of asymmetric cell divisions that establish the stomatal lineage. *Nature* 445, 537–540. doi: 10.1038/nature05491

McAdam, S. A. M., and Brodribb, T. J. (2016). Linking Turgor with ABA biosynthesis: implications for stomatal responses to vapor pressure deficit across land plants. *Plant Physiol.* 171, 2008–2016. doi: 10.1104/pp.16.00380

Medina, R., Johnson, M. G., Liu, Y., Wickett, N. J., Shaw, A. J., and Goffinet, B. (2019). Phylogenomic delineation of *Physcomitrium* (Bryophyta: Funariaceae) based on targeted sequencing of nuclear exons and their flanking regions rejects the retention of *Physcomitrella*, *Physcomitridium* and *Aphanorrhegma*. *J. Syst. Evol.* 57, 404–417.

Merced, A., and Renzaglia, K. (2017). *Structure, Function and Evolution of Stomata from a Bryological Perspective*. Aukland: Magnolia Press, 7–20.

Merced, A., and Renzaglia, K. S. (2013). Moss stomata in highly elaborated *Oedipodium* (Oedipodiaceae) and highly reduced *Ephemerum* (Pottiaceae) sporophytes are remarkably similar. *Am. J. Bot.* 100, 2318–2327. doi: 10.3732/ajb.1300214

Merced, A., and Renzaglia, K. S. (2016). Patterning of stomata in the moss Funaria: a simple way to space guard cells. *Ann. Bot.* 117, 985–994. doi: 10.1093/aob/mcw029

Ohashi-Ito, K., and Bergmann, D. C. (2006). Arabidopsis FAMA controls the final proliferation/differentiation switch during stomatal development. *Plant Cell* 18, 2493–2505. doi: 10.1105/tpc.106.046136

Paton, J. A., and Pearce, J. V. (1957). The occurrence, structure and functions of the stomata in British bryophytes. *Trans. Br. Bryol. Soc.* 3, 228–259.

Payne, W. W. (1979). Stomatal patterns in embyrophytes - Their evolution, ontogeny and interpretation. *Taxon* 28, 117–132.

Perroud, P. F., Meyberg, R., and Rensing, S. A. (2019). *Physcomitrella patens* Reute mCherry as a tool for efficient crossing within and between ecotypes. *Plant Biol.* 21(Suppl. 1), 143–149. doi: 10.1111/plb.12840

Perroud, P.-F., Cove, D. J., Quatrano, R. S., and McDaniel, S. F. (2011). An experimental method to facilitate the identification of hybrid sporophytes in the moss *Physcomitrella patens* using fluorescent tagged lines. *New Phytol.* 191, 301–306. doi: 10.1111/j.1469-8137.2011.03668.x

Pillitteri, L. J., and Dong, J. (2013). Stomatal development in arabidopsis. *Arabidopsis Book* 11:e0162.

Pillitteri, L. J., and Torii, K. U. (2012). Mechanisms of stomatal development. *Annu. Rev. Plant Biol.* 63, 591–614.

Pillitteri, L. J., Bogenschutz, N. L., and Torii, K. U. (2008). The bHLH protein, MUTE, controls differentiation of stomata and the hydathode pore in Arabidopsis. *Plant Cell Physiol.* 49, 934–943. doi: 10.1093/pcp/pcn067

Pressel, S., Goral, T., and Duckett, J. G. (2014). Stomatal differentiation and abnormal stomata in hornworts. *J. Bryol.* 36, 87–103.

Qi, X., and Torii, K. U. (2018). Hormonal and environmental signals guiding stomatal development. *BMC Biol.* 16:21. doi: 10.1186/s12915-018-0488-5

Qi, X., Han, S.-K. I., Dang, J. H., Garrick, J. M., Ito, M., Hofstetter, A. K., et al. (2017). Autocrine regulation of stomatal differentiation potential by EPF1 and ERECTA-LIKE1 ligand-receptor signaling. *eLife* 6:e24102. doi: 10.7554/eLife.24102

R Development Core Team (2012). *R: A Language and Environment for Statistical Computing*. Vienna: R Foundation for Statistical Computing.

Raven, J. A. (2002). Selection pressures on stomatal evolution. *New Phytol.* 153, 371–386.

Rensing, S. A., Goffinet, B., Meyberg, R., Wu, S.-Z., and Bezanilla, M. (2020). The Moss *Physcomitrium* (*Physcomitrella*) patens: a model organism for non-seed plants. *Plant Cell*. doi: 10.1105/tpc.19.00828 [Epub ahead of print].

Renzaglia, K. S., Villarreal, J. C., Piatkowski, B. T., Lucas, J. R., and Merced, A. (2017). Hornwort stomata: architecture and fate shared with 400-million-year-old fossil plants without leaves. *Plant Physiol.* 174, 788–797. doi: 10.1104/pp.17.00156

Rudall, P. J., Chen, E. D., and Cullen, E. (2017). Evolution and development of monocot stomata. *Am. J. Bot.* 104, 1122–1141. doi: 10.3732/ajb.1700086

Rudall, P. J., Hilton, J., and Bateman, R. M. (2013). Several developmental and morphogenetic factors govern the evolution of stomatal patterning in land plants. *New Phytol.* 200, 598–614. doi: 10.1111/nph.12406

Ruszala, E. M., Beerling, D. J., Franks, P. J., Chater, C., Casson, S. A., Gray, J. E., et al. (2011). Land plants acquired active stomatal control early in their evolutionary history. *Curr. Biol.* 21, 1030–1035. doi: 10.1016/j.cub.2011.04.044

Sack, F. D., and Paolillo, D. J. (1985). Incomplete cytokinesis in Funaria stomata. *Am. J. Bot.* 72, 1325–1333.

Sack, F., and Paolillo, D. J. (1983). Structure and development of walls in Funaria stomata. *Am. J. Bot.* 70, 1019–1030. doi: 10.1093/aob/mcu165

Sakakibara, K., Nishiyama, T., Deguchi, H., and Hasebe, M. (2008). Class 1 KNOX genes are not involved in shoot development in the moss *Physcomitrella patens* but do function in sporophyte development. *Evol. Dev.* 10, 555–566. doi: 10.1111/j.1525-142X.2008.00271.x

Schneider, C. A., Rasband, W. S., and Eliceiri, K. W. (2012). NIH image to imagej: 25 years of image analysis. *Nat. Methods* 9, 671–675. doi: 10.1038/nmeth.2089

Shpak, E. D., McAbee, J. M., Pillitteri, L. J., and Torii, K. U. (2005). Stomatal patterning and differentiation by synergistic interactions of receptor kinases. *Science* 309, 290–293. doi: 10.1126/science.1109710

Smith, G. M. (1955). *Cryptogamic Botany: Bryophytes and Pteridophytes*. New York, NY: McGraw-Hill Book Co.

Sugano, S. S., Shimada, T., Imai, Y., Okawa, K., Tamai, A., Mori, M., et al. (2010). Stomagen positively regulates stomatal density in Arabidopsis. *Nature* 463, 241–244. doi: 10.1038/nature08682

Tricker, P. J., Gibbings, J. G., Lopez, C. M. R., Hadley, P., and Wilkinson, M. J. (2012). Low relative humidity triggers RNA-directed de novo DNA methylation and suppression of genes controlling stomatal development. *J. Exp. Bot.* 63, 3799–3813. doi: 10.1093/jxb/ers076

Vaten, A., and Bergmann, D. C. (2012). Mechanisms of stomatal development: an evolutionary view. *EvoDevo* 3:11. doi: 10.1186/2041-9139-4-11

Villarreal, J. C., and Renzaglia, K. S. (2015). The hornworts: important advancements in early land plant evolution. *J. Bryol.* 37, 157–170.

Wallace, S., Chater, C. C., Kamisugi, Y., Cuming, A. C., Wellman, C. H., Beerling, D. J., et al. (2015). Conservation of Male Sterility 2 function during spore and pollen wall development supports an evolutionarily early recruitment of a core component in the sporopollenin biosynthetic pathway. *New Phytol.* 205, 390–401. doi: 10.1111/nph.13012

Wickham, H. (2009). *Ggplot2: Elegant Graphics for Data Analysis*. New York, NY: Springer.

Yang, M., and Sack, F. D. (1995). The too many mouths and four lips mutations affect stomatal production in Arabidopsis. *Plant Cell* 7, 2227–2239. doi: 10.1105/tpc.7.12.2227

Yoo, C. Y., Pence, H. E., Jin, J. B., Miura, K., Gosney, M. J., Hasegawa, P. M., et al. (2010). The Arabidopsis GTL1 transcription factor regulates water use efficiency and drought tolerance by modulating stomatal density via transrepression of SDD1. *Plant Cell* 22, 4128–4141. doi: 10.1105/tpc.110.078691

Zhao, L. M., and Sack, F. D. (1999). Ultrastructure of stomatal development in *Arabidopsis* (Brassicaceae) leaves. *Am. J. Bot.* 86, 929–939.

Zoulias, N., Harrison, E. L., Casson, S. A., and Gray, J. E. (2018). Molecular control of stomatal development. *Biochem. J.* 475, 441–454.

Conflict of Interest: The authors declare that the research was conducted in the absence of any commercial or financial relationships that could be construed as a potential conflict of interest.

frontiers in Plant Science

ORIGINAL RESEARCH
published: 28 May 2020
doi: 10.3389/fpls.2020.00567

With Over 60 Independent Losses, Stomata Are Expendable in Mosses

Karen S. Renzaglia[1], William B. Browning[1] and Amelia Merced[2]*

[1] *Plant Biology Department, Southern Illinois University, Carbondale, IL, United States,* [2] *International Institute of Tropical Forestry, USDA Forest Service, San Juan, PR, United States*

Because stomata in bryophytes are uniquely located on sporangia, the physiological and evolutionary constraints placed on bryophyte stomata are fundamentally different from those on leaves of tracheophytes. Although losses of stomata have been documented in mosses, the extent to which this evolutionary process occurred remains relatively unexplored. We initiated this study by plotting the known occurrences of stomata loss and numbers per capsule on the most recent moss phylogeny. From this, we identified 40 families and 74 genera that lack stomata, of which at least 63 are independent losses. No trends in stomata losses or numbers are evident in any direction across moss diversity. Extant taxa in early divergent moss lineages either lack stomata or produce pseudostomata that do not form pores. The earliest land plant macrofossils from 400 ma exhibit similar sporangial morphologies and stomatal distribution to extant mosses, suggesting that the earliest mosses may have possessed and lost stomata as is common in the group. To understand why stomata are expendable in mosses, we conducted comparative anatomical studies on a range of mosses with and without stomata. We compared the anatomy of stomate and astomate taxa and the development of intercellular spaces, including substomatal cavities, across mosses. Two types of intercellular spaces that develop differently are seen in peristomate mosses, those associated with stomata and those that surround the spore sac. Capsule architecture in astomate mosses ranges from solid in the taxa in early divergent lineages to containing an internal space that is directly connected to the conducing tissue and is involved in capsule expansion and the nourishment, hydration and development of spores. This anatomy reveals there are different architectural arrangements of tissues within moss capsules that are equally effective in accomplishing the essential processes of sporogenesis and spore dispersal. Stomata are not foundational to these processes.

Keywords: stomata, mosses, guard cells, intercellular space, capsule, land plant evolution

OPEN ACCESS

Edited by:
Michael T. Raissig,
Heidelberg University, Germany

Reviewed by:
Paula Rudall,
Royal Botanic Gardens, Kew, United Kingdom
Silvia Pressel,
Natural History Museum, United Kingdom

****Correspondence:***
Karen S. Renzaglia
renzaglia@siu.edu

Specialty section:
This article was submitted to Plant Development and EvoDevo, a section of the journal Frontiers in Plant Science

Received: *20 February 2020*
Accepted: *16 April 2020*
Published: *28 May 2020*

Citation:
Renzaglia KS, Browning WB and Merced A (2020) With Over 60 Independent Losses, Stomata Are Expendable in Mosses. Front. Plant Sci. 11:567. doi: 10.3389/fpls.2020.00567

INTRODUCTION

Stomata in bryophytes are located on sporangia and are restricted in their occurrence across phylogeny. Liverworts are the only extant land plants that lack stomata entirely, while stomata are widespread but not ubiquitous in hornworts and mosses. With contemporary phylogenies pointing to hornworts as the earliest divergent bryophyte group (Puttick et al., 2018; Renzaglia et al., 2018), stomata are best interpreted as plesiomorphic in land plants, especially given that *Leiosporoceros*, the sister taxon to other hornworts, possesses stomata. Within the small hornwort clade of 10–12

genera there are two well-documented losses of stomata in derived taxa (Renzaglia et al., 2017). In comparison, early diversification of the moss assemblage apparently was not dependent on the existence of stomata as Takakiales and Andreaeopsida, two of the oldest moss clades, are stomata free. Moreover, there are multiple moss orders and families that include taxa with and without stomata. Clearly stomata are not vital to the survival and were not required for the initial radiation of bryophytes.

The sporadic occurrence of stomata in bryophytes calls into question the role stomata play in the physiology and growth of bryophyte sporophytes. Recent studies reveal that diurnal cycles of opening and closing, and responses to ABA and desiccation, which are key to water relations in tracheophytes, do not occur in hornworts (Pressel et al., 2018). However, substomatal cavities and intercellular spaces that are necessary for functional stomata are always present in mosses and hornworts with stomata, while species without stomata do not have substomatal spaces (Goffinet et al., 2009; Merced and Renzaglia, 2017). Intercellular spaces are common in different tissues of land plants, and in some bryophytes are present in both gametophyte and sporophyte generations, suggesting that spaces originated multiple times in the evolution of plants (Duckett and Pressel, 2018). In tracheophytes, intercellular spaces in the form of spongy tissue are coordinated with the presence of functional stomata to facilitate gas exchange (Dow et al., 2017; Lundgren et al., 2019).

In order to better understand the evolution of stomata within mosses, we traced the number per capsule, and known absence of stomata across the range of moss diversity. Due to the lack of stomata in early divergent moss lineages, we examined the fossil record on early land plants for clues to the origin of the moss capsule with and without stomata. We tested the hypothesis that stomata were lost repeatedly throughout the history of mosses and not restricted to derived taxa. We further speculated that stomatal losses were accompanied by anatomical and developmental modification within the sporophyte. Accordingly, we identified architectural features that characterize sporophytes with and without stomata and documented the development of intercellular spaces, including substomatal cavities. Anatomical and developmental analyses identify two distinct types of internal spaces in mosses and document the loss of peripheral spaces strictly associated with guard cells and the retention of internal spaces in taxa without stomata. Our anatomical studies point to modified architectural features that accompanied stomata loss and led to fundamentally different, but equally effective, internal hydration and capsule maturation.

MATERIALS AND METHODS

Plants and Specimens Examined

Moss capsules were collected locally in Southern Illinois over the growing season to ensure observations of early and late stages of development. Prepared blocks of capsules from species not found in Illinois were sectioned and examined. Species examined include the following, with the seven taxa lacking stomata denoted by asterisks: *Takakia ceratophylla**, *Andreaea rothii**, *Sphagnum angustifolium**, *Polytrichastrum ohiensis*, *Atrichum angustatum**, *Tetraphis pellucida**, *Diphysium foliosum*, *Buxbaumia viridis*, *Physcomitrium pomiform*, *Physcomitrium* (*Physcomitrella) patens*, *Funaria hygrometrica*, *Dicranum scoparium*, *Orthotrichum pusillum*, *Plagiomnium cuspidatum*, *Ephemerum spinosum*, *Leucobryum glaucum**, *Bartramia pomiforme*, *Hypnum curvifolium*, *Brachythecium rutabulum*, *Thuidium delicatulum*, and *Neckeropsis undulata*.* A KNOX mutant of *P. patens* that lacks stomata was acquired from Dr. Neil Ashton.

Published records of fossils of the earliest land plants with sporangia and stomata were examined for comparisons with the morphology and anatomy of the extant members of early divergent moss lineages. Fossil stomata were reproduced from Edwards (1979) and Edwards et al. (1998) with permission.

Stomata Presence in the Phylogeny of Mosses

We assessed the presence and absence of stomata by mapping their occurrence across the most recent phylogeny of mosses (Liu et al., 2019). An extensive literature review (**Table 1**) identified genera and species that lack stomata, and confirmed the number of stomata reported for members of each moss family, if known. To determine the minimum number of losses in moss orders, we counted the number of families that have genera that lack stomata and assessed independent origin based on phylogenetic relationships. If a genus has species with both states (present and absent stomata) these were counted as independent losses. Losses within different families were each scored as independent. From these analyses, we estimate the minimum number and, in some cases, maximum number (in parenthesis) of losses for each order (**Figure 1**).

Light Microscopy, Electron Microscopy, and Immunogold Labeling

Protocols are described in detail in Merced and Renzaglia (2013, 2014). Sporophytes of mosses were fixed in 2% glutaraldehyde in 0.05M $NaPO_4$ buffer, washed three times in 0.05M $NaPO_4$ buffer and post-fixed for 20 min in 1% OsO4 in 0.05M $NaPO_4$ buffer. Specimens were rinsed in distilled water and dehydrated in a graded ethanol series ending with 100% ethanol. For scanning electron microscopy (SEM), fixed capsules were critical point dried and mounted on stubs, then sputter-coated for 230 s with palladium-gold. Specimens were observed using a Hitachi S570 scanning electron microscope. For light microscopy and transmission electron microscopy (TEM), specimens were infiltrated with Spurr's resin (Electron Microscopy Sciences, Hatfield, PA, United States) or LR White resin (London Resin Company, Berkshire, United Kingdom) and cured at 65°C. For light microscopy, semi-thin sections (250–750 nm) were mounted on glass slides and stained with 1.5% toluidine blue in distilled water. Slides were observed on a Leica DM5000 B compound microscope and images captured digitally. Thin sections (60–90 nm) were collected on nickel grids, incubated with 2% BSA in 0.02M PBS for immunogold labeling. Grids were transferred to the LM19 primary antibody (diluted 1: 20

TABLE 1 | Counts per capsule and 40 losses (counts of 0) of stomata in 69 families of mosses.

Family	Stomata per capsule	References (in Supplementary Material)
Oedipodiaceae	60	Paton and Pearce, 1957
Polytichaceae	0, 20, 40, 50–78, 80–***120, 200, 250***	Paton and Pearce, 1957; Duckett and Pressel, 2018
Tetraphidaceae	0, 5	Paton and Pearce, 1957
Buxbaumiaceae	20–30	Paton and Pearce, 1957, present study
Diphysciaceae	0, 10	Paton and Pearce, 1957; Schofield, 2007
Timmiaceae	30	Paton and Pearce, 1957
Disceliaceae	0, ?	Paton and Pearce, 1957
Encalyptaceae	15, 30, 50	Paton and Pearce, 1957
Funariaceae	10, 14, 60, *160, 180, 200*	Paton and Pearce, 1957; Duckett and Pressel, 2018
Catoscopiaceae	0, ?	Paton and Pearce, 1957
Distichiaceae	8–12	Paton and Pearce, 1957
Scouleriaceae	0*	Duckett and Pressel, 2018
Drummundiaceae	0, ?	Vitt, 2007
Saelaniaceae	6	Paton and Pearce, 1957
Grimmiacea	0, 6–18, 30	Paton and Pearce, 1957; Hastings and Grevens, 2007; McIntosh, 2007
Seligeriaceae	0, 4, 8	Paton and Pearce, 1957; Bartlett and Vitt, 1986; Andreas, 2013; Duckett and Pressel, 2018
Archidiaceae	0*	Paton and Pearce, 1957
Fissidentaceae	0, 12	Paton and Pearce, 1957; Egunyomi, 1982; Pursell, 1987, 2007; Pursell et al., 1988
Ditrichaceae	0, 4, 6, 8–12	Paton and Pearce, 1957; Gradstein et al., 2001
Bruchiaceae	0, 70	Tong and He, 2002
Erpodiaceae	0, ?	Gradstein et al., 2001; Milne and Klazenga, 2012
Schistostegaceae	0, 4, 5	Jennings, 1913; Paton and Pearce, 1957
Rhabdoweisiaceae	5–12	Paton and Pearce, 1957
Dicranaceae	0, 4, 6–20	Paton and Pearce, 1957; Gradstein et al., 2001; Duckett and Pressel, 2018
Micromitriaceae	0, ?	Crum and Anderson, 1981; Smith, 2004; Bryan, 2007
Leucobryaceae	0, ?	Paton and Pearce, 1957; Gradstein et al., 2001
Calymperaceae	0, 2, 15	Egunyomi, 1982
Pottiaceae	0, 3–16	Paton and Pearce, 1957; Egunyomi, 1982; Zander and Eckel, 1993; Abella et al., 1999; Gradstein et al., 2001
Pleurophascaceae	0, ?	Fife and Dalton, 2005
Splachnaceae	20, 30, 40, 50, 60, 90	Paton and Pearce, 1957; Goffinet, 2012
Meesiaceae	30, 50, 70	Paton and Pearce, 1957
Bryaceae	15, 50–70, 90, *100, 120, 185*	Paton and Pearce, 1957; Egunyomi, 1982; Duckett and Pressel, 2018, present study
Mniaceae	8–20, 40, 45, 60, *180*	Paton and Pearce, 1957, present study
Bartramiaceae	16, 28, 40, 45, 60, 70, ***100, 220–240***	Paton and Pearce, 1957
Orthotrichaceae	3–8, 12, 20, 40	Paton and Pearce, 1957, present study
Hedwigiaceae	0, 12, 24	Paton and Pearce, 1957; Vitt and Buck, 1984
Aulacomniaceae	6–12, 30	Paton and Pearce, 1957
Orthodontiaceae	14, 18	Paton and Pearce, 1957
Pterobryellaceae	0, ?	Arzeni, 1954
Orthorrhynchiaceae	0, ?	Klazenga, 2012a
Rhabdodontiaceae	0, ?	Paton and Pearce, 1957; Hattaway, 1984
Ptychomniceae	0, 5, 10	Paton and Pearce, 1957; During, 1977; Hattaway, 1984
Daltoniaceae	10	Paton and Pearce, 1957; Gradstein et al., 2001
Hookeriaceae	18	Paton and Pearce, 1957
Pilotrichaceae	0, ?	Paton and Pearce, 1957
Fontinalaceae	0*	Paton and Pearce, 1957; Allen, 2015
Climaciaceae	12	Paton and Pearce, 1957

(Continued)

TABLE 1 | Continued

Family	Stomata per capsule	References (in Supplementary Material)
Amblystegiaceae	6–50, 54, 80, ***130, 200***	Paton and Pearce, 1957; Cheney, 1897
Helodiaceae	20	Paton and Pearce, 1957
Leskeaceae	0, 4–6, 8, 20	Buck, 1981; Spence, 2015
Thuidiaceae	5, 24	Paton and Pearce, 1957; Egunyomi, 1982
Stereophyllaceae	0, 6, 23	Egunyomi, 1982
Brachytheciaceae	5–28, 30	Paton and Pearce, 1957
Myriniaceae	14	Paton and Pearce, 1957; Gradstein et al., 2001
Fabroniaceae	4	Egunyomi, 1982
Hypnaceae	3, 4, 5–10, 11, 16, 19–44	Paton and Pearce, 1957; Egunyomi, 1982, present study
Pterigynandraceae	8, 10	Klazenga, 2012b
Hylocomiaceae	6–15, 22	Paton and Pearce, 1957; Hedenäs, 2005
Plagiotheciaceae	0, 5–10, 14, 20	Paton and Pearce, 1957; Ireland, 2015
Entodontaceae	0, 8	Paton and Pearce, 1957; Gradstein et al., 2001
Pylaisiadelphaceae	4, 6, 8	Paton and Pearce, 1957; Gradstein et al., 2001
Sematophyllaceae	0, 4	Paton and Pearce, 1957; Fife, 2012
Cryphaeaceae	0, 12	Paton and Pearce, 1957; Gradstein et al., 2001
Leucodontaceae	0, 12	Paton and Pearce, 1957
Pterobryaceae	0*	Yu and Jia, 2012
Neckeraceae	0, 4, 12, 14	Paton and Pearce, 1957; Gradstein et al., 2001
Leptodontaceae	0, 6	Paton and Pearce, 1957; Stark, 2015
Lembophyllaceae	0, 10–20, 90	Paton and Pearce, 1957; Tangney, 1997; Gradstein et al., 2001
Anomodontaceae	0, 12	Gradstein et al., 2001

*For families with losses (counts of 0), "?" denotes no reports of counts in stomata-containing members and * denotes no stomata-containing members. Counts greater than 100 in six families are in bold and italicized.*

in 2% BSA/PBS) for 3 h and controls (one grid each treatment) were left in buffer during that time. All grids were rinsed in 2% BSA/PBS, then incubated in goat anti-rat IgG secondary antibody (Sigma- Aldrich, St. Louis, MO, United States) diluted 1: 20 in 2% BSA/PBS for 30 min. Grids were rinsed with PBS followed by distilled/deionized autoclaved filtered water, and dried at room temperature. Grids were observed unstained with a Hitachi H7650 transmission electron microscope at 60 kV.

RESULTS

Stomata Presence and Number in the Phylogeny of Mosses

Based on data mining from published literature, stomata are absent in 74 genera and 40 families of mosses, accounting for at least 63 independent losses in the phylogeny of mosses (**Figure 1** and **Supplementary Data**). Nearly 60% (16 of 28) of the orders of peristomate mosses have recorded losses of stomata. These losses are equally present in acrocarps and pleurocarps with high numbers in the Dicranales, Pottiales, and Hypnales (**Figure 1**). As the sister taxon to peristomate mosses, *Oedipodium* represents the earliest divergent moss lineage to possess stomata. Numbers of stomata per capsule range from 0 to 250 (**Figure 2** and **Table 1**), with the vast majority of counts (40 of 54 = 74%) ranging from 3 to 30 (**Figures 2C,D**). Numbers above 200 are rare and recorded only for three families, Polytrichaceae, Funariaceae (**Figure 2B**) and Bartramiaceae, although many members of these family have less than 70 stomata (**Figures 2C,F**) (**Table 1**). There are no evident trends in numbers in either direction with divergence time. For example, numbers vary in the first moss lineages with stomata: in *Oedipodium* the 60 or so stomata are scattered along the highly elongated neck and within the Tetraphidaceae, *Tetraphis* lacks stomata and *Tetradontium* contains only five per capsule. Members of the Polytrichales exhibit the extremes in stomata numbers per capsule, with 200 and 250 in *Polytrichum* and zero in three genera, *Atrichum*, *Pogonatum,* and *Itatalia*.

Structure of Early Divergent Moss Capsules and Comparisons With Early Fossil Plants

Capsules of extant mosses in early divergent lineages (*Takakia* and *Andreaea*) lack stomata or contain over 100 pseudostomata that do not form pores and are evenly dispersed across the capsule epidermis (Sphagnales). These capsules lack apophyses, have prominent central columellae and have solid tissue throughout without air spaces (**Figures 3A–C**). Sporophyes of *Andreaea* and *Sphagnum* have short setae, and are embedded in an elongated pseudopodium of the gametophyte (**Figures 3B,C**). Comparisons with the oldest fossil plants reveal similar capsule morphology and stomatal arrangement/anatomy as in each of these extant early divergent mosses (**Figures 3D–J**). Sporangia of *Tortilicaulis* from the Silurian are spiraled and similar in shape to *Takakia* (**Figures 3D,E**). Early Devonian sporangia approximately 400 million years old demonstrate the occurrence

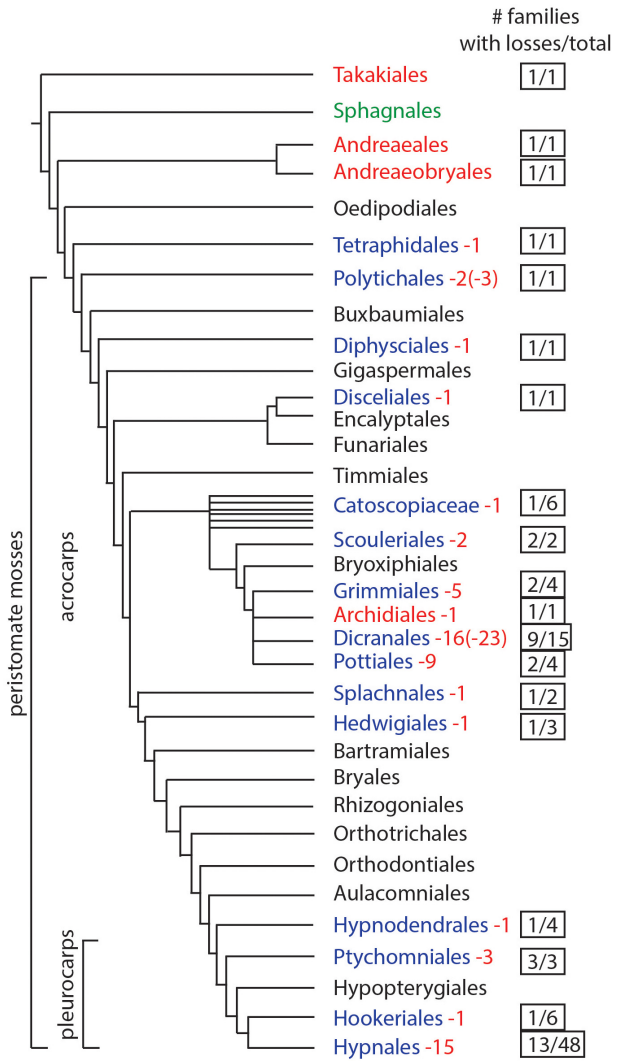

FIGURE 1 | Phylogenetic of moss orders based on Liu et al. (2019). Orders in red lack stomata, green have pseudostomata, black have stomata (no records of losses), and blue have documented losses of stomata. Numbers in red represent the minimum times stomata were lost and numbers in parentheses indicate the maximum possible number of losses. The right column indicates the number of families that include taxa without stomata, over the total number of families in the order.

of stomata scattered cross sporangia (**Figure 3G**), resembling the arrangement of pseudostomata in *Sphagnum* (**Figure 3F**), and restricted to the base similar to extant mosses (**Figure 3H**). In section, the stomatal complex of the earliest fossils have guard cells with ledges and substomatal cavities much like those of *Oedipodium*, the first moss group to possess stomata (**Figures 3I,J**).

Anatomy of Peristomate Moss Capsules

Members of the Polytrichaceae have well-developed capsule regardless of whether they lack stomata (represented by *Atrichum*) or contain stomata (represented by *Polytrichastrum* with 100+ stomata) (**Figure 4**). In *Atrichum* the capsule is brown (reddish) when mature and cylindrical, and the short calyptra is situated at the apex (**Figure 4A**). From the urn down, the neck tapers toward the seta and there is no distinct apophysis. In *Polytrichastrum*, the capsule is swollen throughout with extensive internal spaces (**Figures 4D,E**). The distinct apophysis is green with a constriction at the base where the stomata are located. The calyptra covers the capsule up to the constriction throughout development. Side-by-side sections illustrate the arrangement of tissues, including air spaces, in these closely related genera. *Atrichum* lacks peripheral spaces including substomatal cavities (**Figure 4B**) that are abundant in *Polytrichastrum* (**Figure 4E**). Chloroplasts line cells associated with substomatal cavities (**Figure 4G**). A large internal air space occurs in *Atrichum* at the base of the capsule and around the entire spore sac (**Figure 4F**). This circumsporangial space forms in the young capsule just interior to the solid capsule wall in a zone between the amphithecium and endothecium, the two primary embryonic regions (**Figure 4B**). In both genera, a well-developed conducting strand of hydroids and leptoids extends in the seta to the spore sac where it ends abruptly and presumably fills the internal space with water and nutrients (**Figures 4F,I**). Unlike *Polytrichastrum* that has stomata to draw water toward the outside, the apophysis of *Atrichum* is covered in a thick cuticle, which retards water loss through the epidermis (**Figure 4H**). Capsule dehiscence through detachment of the operculum follows drying of liquid in the circumsporangial space and the constriction of the neck at the capsule base (**Figure 4C**).

Types and Development of Intercellular Spaces

Anatomy of capsules with and without stomata reveals two types of intercellular spaces: (1) the substomatal cavity and connected spaces associated with stomata and (2) the circumsporangial cavity that surrounds the spore sac and may extend into the capsule neck and seta (**Figures 4**, **5**, **6**). No stomata-lacking capsules have substomatal cavities and associated spaces but all capsules of peristomate mosses examined in this study possess circumsporangial cavities, regardless of whether they have stomata or not (**Figures 4F**, **5**, **6**). As illustrated in *Atrichum* (**Figure 4F**), *Ephemerum* (**Figure 6A**) and *Brachythecium* (**Figure 6B**), circumsporangial cavities surround the developing sporogenous tissue and are intimately associated with conducting tissue (when present), which delivers water and food to the developing spores. In some mosses that lack stomata, like *Leucobryum*, this circumsporangial space is found only during capsule development (**Figure 5**). The circumsporangial space forms between the embryonic endothecium and amphithecium, prior to the proliferation of sporogenous tissue, and extends the length of the spore sac when the archesporium is a single cell layer (**Figures 4A**, **5A**). When the capsule is fully developed in taxa like *Leucobryum*, no space is discernible due to capsule expansion and spore differentiation (**Figure 5B**).

Both types of spaces, substomatal cavities and circumsporangial spaces form in the spear stage just before capsule expansion in mosses with stomata. In taxa with

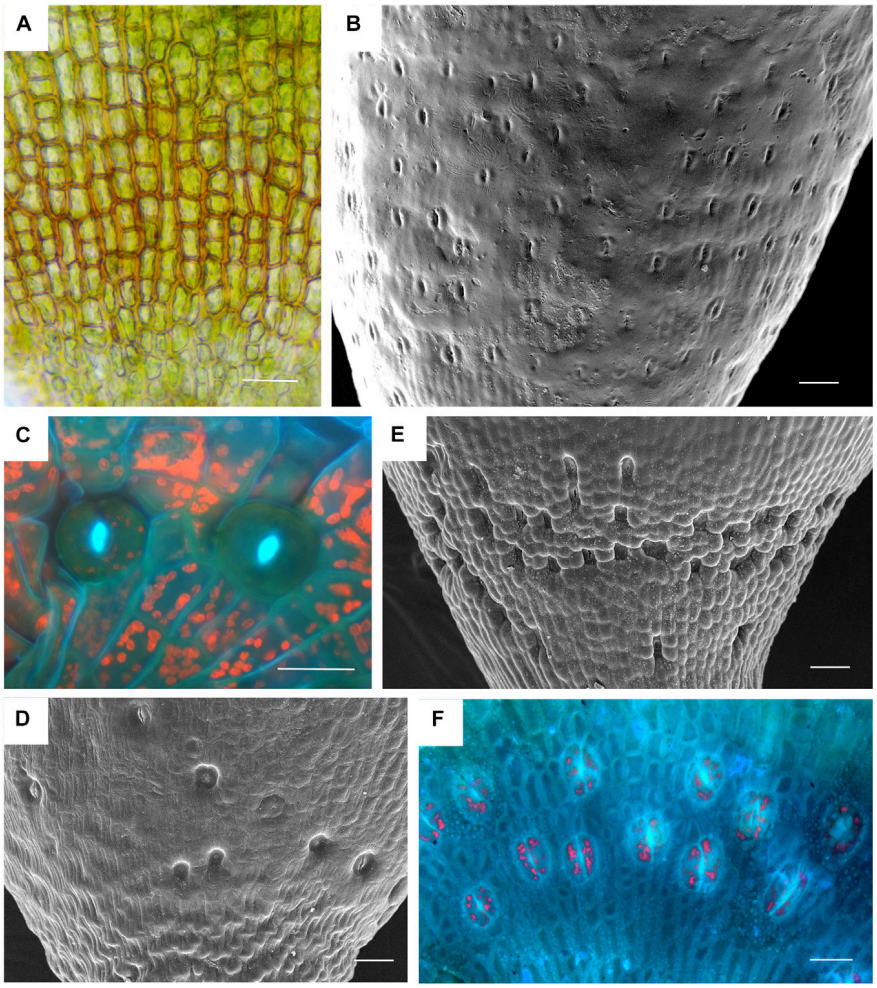

FIGURE 2 | Stomata diversity in mosses. **(A)** *Atrichum angustatum* light micrograph of stomata free epidermis. **(B)** *Funaria hygrometrica* SEM of apophysis covered with ~200 stomata. **(C)** *Physcomitrium* (*Physcomitrella*) *patens* 2 of 10 stomata in fluorescence. **(D)** *Brachythecium rutabulum* SEM of sparse scattered stomata. Image credit: Jeffrey J. Duckett. **(E)** *Plagiomnium cuspidatum* SEM showing numerous sunken stomata on the apophysis. 60 stomata estimated in the capsule. Image credit: Jeffrey J. Duckett. **(F)** *Bartramia pomiforme* group of stomata in fluorescence. 70 stomata estimated in the capsule. Bars: **(A,C,F)** = 20 μm, **(B,D,E)** = 50 μm.

stomata, stomata and liquid-filled substomatal cavities form in the expanding neck or apophysis before the sporogenous tissue develops (**Figure 7A**). Circumsporangial spaces are not associated with stomata and are found in all mosses during development. They begin with the deposition of an electron-dense fibrillar material (**Figure 7B**) that abundantly localizes with the monoclonal antibody LM19, which recognizes unesterified homogalacturonas pectin (**Figure 7C**). When the capsule begins to expand and spaces become larger, the fluid inside the space lacks substructure and no longer localizes with this antibody (Merced and Renzaglia, 2016). Substomatal cavities, in contrast, do not form in the absence of stomata and do not label with LM19 early in development (not shown). Their development is coordinated with differentiation of the guard mother cell and before the division of guard cells and pore opening (**Figure 7D**). The doughnut shaped guard cell of *P. patens* has a small round pore (**Figure 7E**) and a very reduced substomatal cavity (**Figure 7F**). *P. patens* sporophytes without stomata have no substomatal cavities but the more internal liquid-filled intercellular spaces are connected to the circumsporangial space and remain throughout development (**Figure 7G**).

DISCUSSION

Extant members of early divergent moss lineages entirely lack stomata (Takakiales and Andreaeales) or contain pseudostomata as in Sphagnales. Pseudostomata are pairs of specialized epidermal cells that lack cell wall ledges, do not completely separate to form pores and do not have underlying cavities. They collapse when mature, facilitating drying, capsule dehiscence and spore dispersal, and have been interpreted as either independent from stomata in origin (Duckett et al., 2009) or as modified stomata (Renzaglia et al., 2007; Merced, 2015;

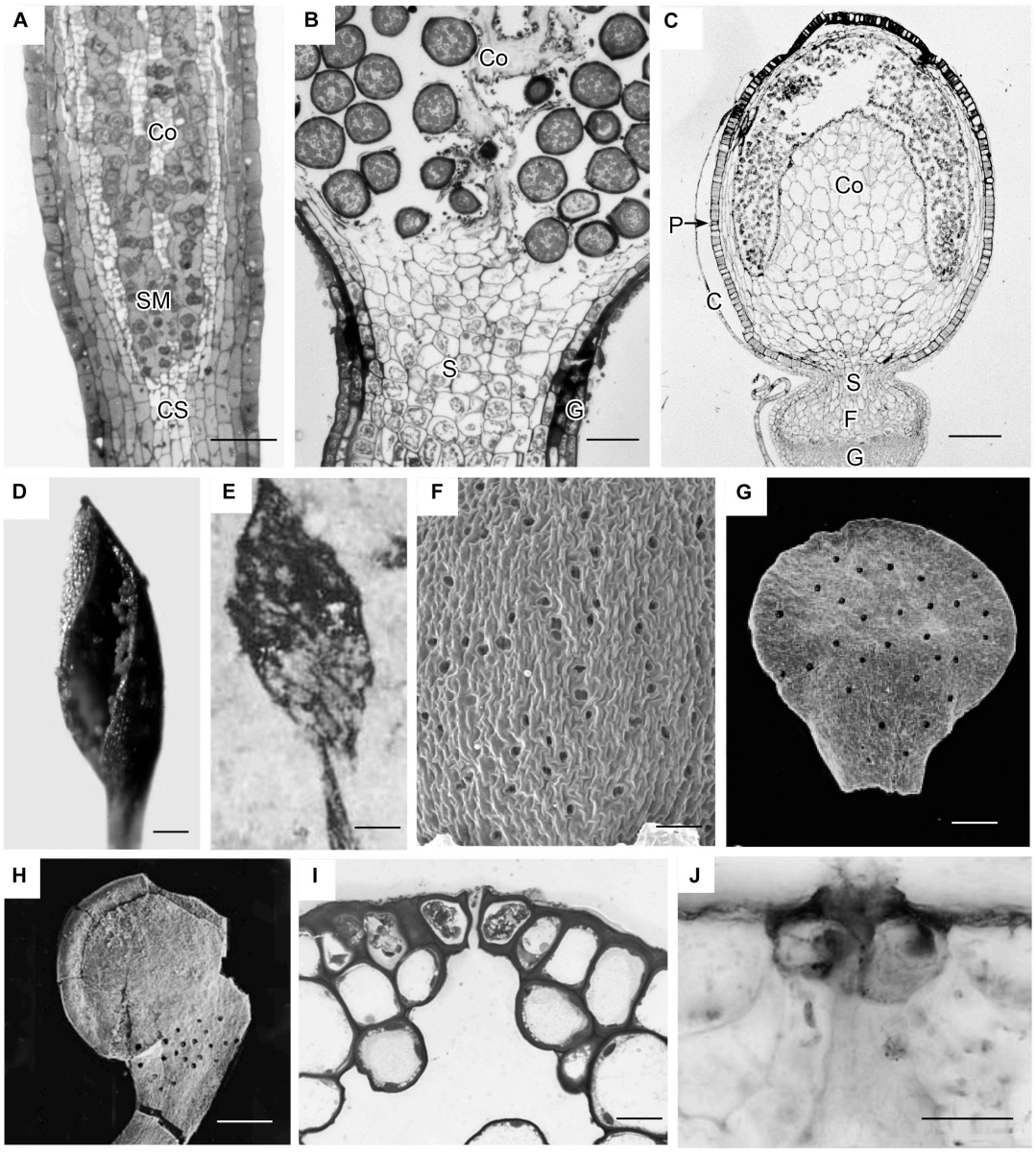

FIGURE 3 | Capsule anatomy, pseudostomata and stomata in extant members of early divergent moss lineages, and sporangia and stomata of the first fossil land plants. **(A)** *Takakia ceratophylla*. Light micrograph (LM) longitudinal section of solid cylindrical capsule with spore mother cells (SM), columella (Co) and conducting strand (CS) in seta. **(B)** *Andreaea rothii*. LM longitudinal section of solid capsule with spores, columella (Co) and short seta (S) surrounded by gametophyte (G) tissue of the pseudopodium. **(C)** *Sphagnum tenellum*. LM longitudinal section of solid capsule, covered by calyptra (C), with pseudostomata (P) in the epidermis, massive columella (Co) covered by the spore sac, and highly reduced seta (S) embedded by foot (F) into gametophyte (G) pseudopodium. **(D)** *Takakia ceratophylla* capsule with single spiraled suture and spores. **(E)** *Tortilicaulis transwalliensis* capsule from the Silurian resembles *Takakia* in **(D)**. **(F)** *Sphagnum tenellum* SEM showing scattered pseudostomata on dried capsule. **(G)** Early Devonian bivalved sporangium with scattered stomata (spots). **(H)** Early Devonian sporangium with band of stomata (spots) at base. **(I)** *Oedipodium* LM cross section of neck with guard cells with ledges over substomatal cavity. **(J)** *Aglaophyton major* from Rhynie Chert. Cross section of mature axis with stoma showing guard cells with ledges over substomatal cavity. Fossil images reproduced with permission from Journal of Experimental Botany (Edwards et al., 1998) and Paleontology (Edwards, 1979). Bars: **(A,E,H)** = 100 μm; **(B,G,J)** = 50 μm; **(C,F)** = 500 μm; **(D)**= 200 μm, **(I)** = 20 μm.

Merced and Renzaglia, 2017). Capsule anatomy in these three ancient lineages reflects the absence of pores as intercellular spaces are lacking and the capsule wall and columella are solid throughout. All of these distinctive capsules are erect, lack peristomes, do not contain a distinctive neck or swollen capsule base (apophysis) where stomata are housed, and disperse spores simultaneously with capsule dehiscence through sutures. The early divergent mosses universally lack pore-producing stomata. This includes the Sphagnales that produce high numbers of pseudostomata (100–200 per capsule) that

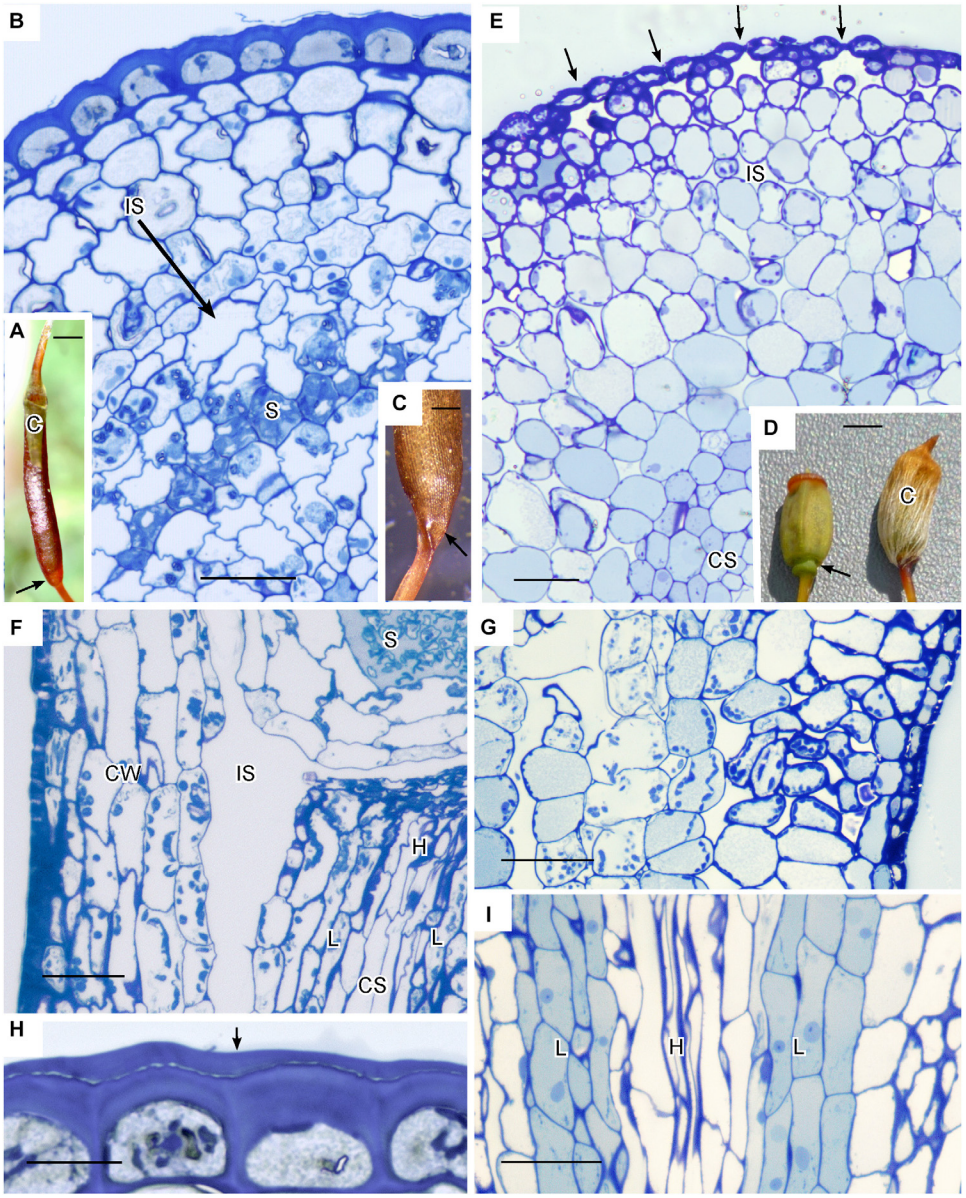

FIGURE 4 | Structure of Polytrichaceae capsule. **(A–C,F,H)** *Atrichum angustatum* that lacks stomata in left hand column. **(D,E,G,I)** *Polytrichastrum ohiensis* with approximately 100 stomata in right hand column. **(A)** Long cylindrical red-brown mature *Atrichum* capsule with inconspicuous calyptra (C) on the top and tapering neck region (arrow) connecting to seta. **(B)** LM cross section at the capsule urn showing solid capsule wall, developing sporogenous region (S) and circumsporangial space (IS) forming between the capsule wall and spore sac. **(C)** Base of recently opened *Atrichum* capsule showing constriction of neck region (arrow) due to drying in circumsporangial cavity and connecting space. **(D)** Two mature *Polytrichastrum* capsules, left without calyptra and right covered by calyptra (C). The capsule is wide and green at the base where the calyptra ends and the narrowly constricted area of the apophysis houses stomata (arrow). **(E)** LM cross section at the constriction with multiple stomata (arrows), subtended by substomatal cavities and associated intercellular spaces (IS), and central conducting strand (CS). **(F)** LM longitudinal section at the junction between spore sac with spores (S) and neck. A large circumsporangial space (IS) extends just inside the solid capsule wall (CW), along the length of the spore sac and downward into the neck. The conducting strand (CS) of hydroids (H) and leptoids (L) ends abruptly at the circumsporangial space and spore sac. **(G)** LM longitudinal section at the constriction showing chloroplast rich cells next to spaces associated with substomatal region on the right and the circumsporangial space to the far left. **(H)** Epidermis with thick walls and cuticle (arrow). **(I)** Prominent conducting strand in the apophysis with leptoids (L) around hydroids (H). Bars: **(A)** = 0.5 mm, **(B,E–G,I)** = 50 μm, **(C)** = 0.2 mm, **(D)** = 1.0 mm, **(H)** = 20 μm.

have been interpreted as either independent from stomata in origin (Duckett et al., 2009) or modified stomata (Merced, 2015; Merced and Renzaglia, 2017). Capsule anatomy reflects the absence or pores as intercellular spaces are lacking in *Takakia, Andreaea,* and *Sphagnum* and the capsule wall and columella are solid throughout. All of these distinctive capsules are erect, lack peristomes, do not contain a swollen capsule base (apophysis) or distinctive neck where stomata

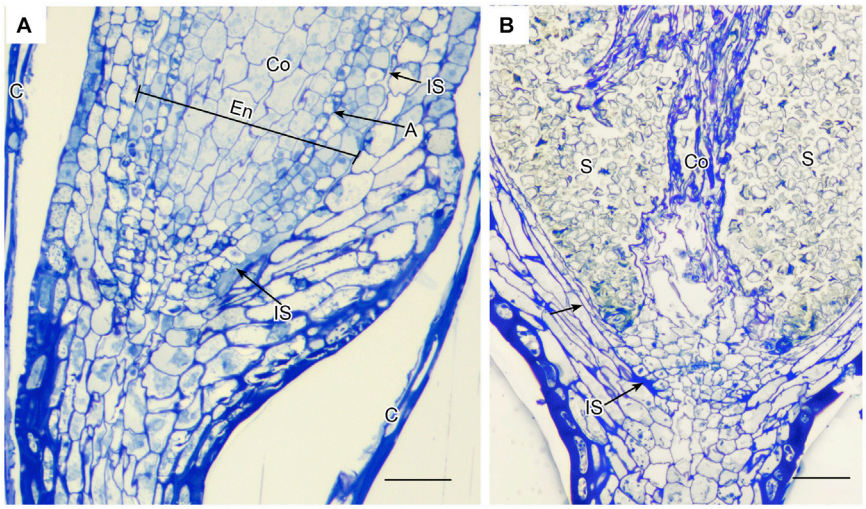

FIGURE 5 | *Leucobryum glaucum*. LM longitudinal sections of astomate capsule. **(A)** Base of immature capsule where seta meets the neck covered by calyptra (C). An inconspicuous fluid-filled intercellular space (IS) extends the entire length of the region between the amphithecium that forms the capsule wall, and the endothecium (En) that consists of a prominent columella (Co) and developing spore sac with one layer of archesporium (A) (sporogeneous tissue). **(B)** Fully expanded capsule. With development of the spore sac that contains 100s of spores (S), the columella (Co) has partially degenerated and the intercellular spaces are closed (arrow) or residual (IS). Bars = 25 μm.

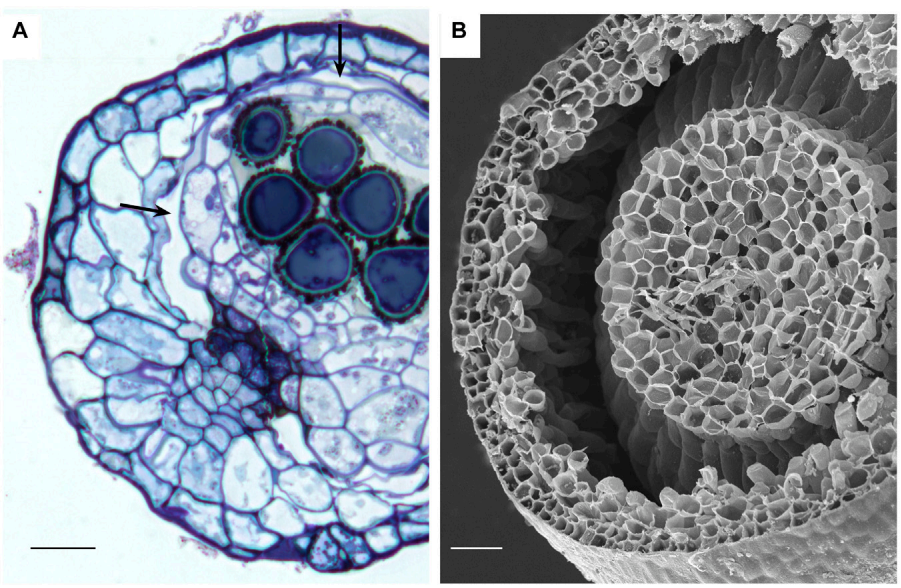

FIGURE 6 | Stomata-containing capsules showing internal circumsporangial space (arrows) that forms between the embryonic endothecium and amphithecium, extends into the neck, and is involved in hydrating and nourishing the spore sac during development. **(A)** LM *Ephemerum*. **(B)** SEM *Plagiomnium*. Image credit: Jeffrey J. Duckett. Bars: **(A)** = 35 μm; **(B)** = 50 μm.

are housed, and disperse spores simultaneously with capsule dehiscence through sutures. Across mosses, the capsules of *Sphagnum* and *Andreaea* (and Andreaeobryum not studied here) are uniquely positioned on a gametophytic extension or pseudopodium, not a sporophytic seta, and both generations lack conducting tissues. *Takakia* resembles other mosses in that gradual seta elongation elevates the capsule and there is a strand of water conducting cells that ends at the capsule base, albeit the cells in the strand are fundamentally different in development, and structure from those of moss hydroids (Renzaglia et al., 1997, 2000, 2007). These unique architectural features preclude comparisons with more derived peristomate mosses and suggest that true stomata evolved after mosses diversified (Duckett and Pressel, 2018). Consequently, we turned to the fossil record for clues as to when in moss evolution stomata evolved.

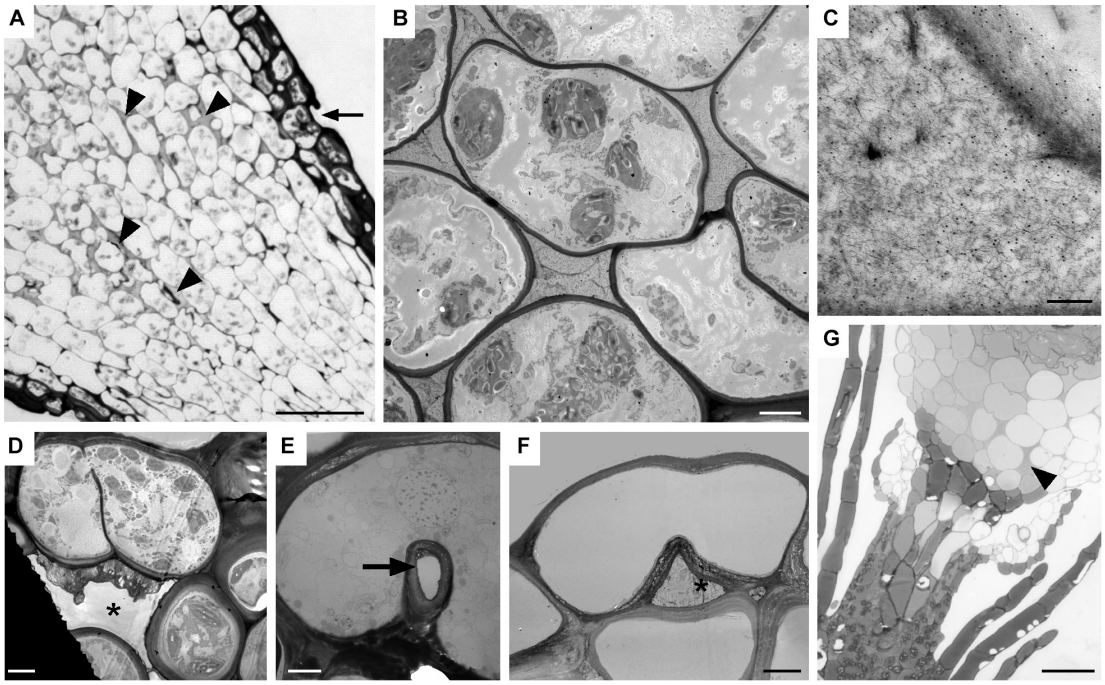

FIGURE 7 | Substomatal cavities and intercellular spaces. **(A–D)** *Dicranum scoparium*. **(A)** LM tangential section of expanding capsule showing stomata (arrow) and associated intercellular spaces are liquid-filled (arrow heads). **(B)** TEM of circumsporangial space filled with dense filamentous material. **(C)** Immunogold labeling TEM shows the liquid in the developing circumsporangial space is positive for the LM19 antibody that recognize homogalacturonan pectin (small black dots). **(D)** Substomatal cavity begins to form before pore opening. **(E,F)** TEM micrographs of *Physcomtrium patens*. **(E)** Small round pore (arrow) of the single-celled stoma. **(F)** Reduced substomatal cavity*. **(G)** LM of liquid-filled intercellular spaces (arrowhead) that are part of the circumsporangial space and not associated with the epidermis of a *P. patens* class 1 KNOX mutant that lacks stomata. Bars: **(A)** = 25 μm; **(B,D–F)** = 4 μm; **(C)** = 200 nm; **(G)** = 20 μm.

Because bryophytes exclusively bear stomata on sporangia, we surveyed the literature on the oldest fossil land plants with reference to sporangia and the occurrence, structure and anatomy of stomata. Fossil plants from the Silurian and early Devonian demonstrate that the range of variability in sporangia seen in extant mosses existed approximately 400 million years ago. These earliest fossil sporangia both bore stomata and lacked stomata, e.g., *Tortilicaulis*, which has a twisted sporangium that is remarkable similar to *Takakia* (Renzaglia et al., 1997, 2017; Edwards et al., 1998). The oldest fossil sporangia were valvate and contained stomata evenly dispersed on the surface similar to pseudostomata of *Sphagnum*, or aggregated at the base in a location that is reminiscent of those on moss necks and apophyses. Details of fossil stomata reveal guard cells and internal anatomy similar to that in *Oedipodium*, the first moss lineage with stomata. Based on the existence of stomata on sporangia in the first plant macrofossils and the similarities with architectural features of early mosses, it is quite possible/likely that stomata existed on moss capsules prior to the diversification of peristomate mosses, which occurred over 100 million years after mosses originated (Newton et al., 2009). Indeed, the estimated median stem age of *Takakia* and *Sphagnum* based on the oldest fossil land plants is 465 Ma, while those for *Tetraphis* and *Oedipodium* are 309 and 298 Ma, respectively (Laenen et al., 2014). This line of evidence identifies stomata on sporangia that resemble moss capsules when stomata first appeared in the fossil record. Early plant fossils and the high incidence of stomata loss in extant mosses are consistent with the hypothesis that stomata evolved once in bryophytes and were lost repeatedly during diversification, including in early divergent lineages and along the entire moss phylogeny.

Losses of stomata in peristomate mosses are numerous and widespread throughout acrocarps and pleurocarps (**Figure 1**). Minimally we identify 40 families and 74 genera in which stomata are absent. Of these, 63 are estimated to be independent losses based on phylogenetic relationships. This is a low estimate given the scant record of descriptions and counts of stomata in mosses. Stomata are first seen in the Oedipodiaceae, Tetraphidaceae and Polytrichaceae. The first family includes the single genus *Oedipodium*, which has the most elongated neck found in any moss and contains approximately 60 stomata (Shaw and Renzaglia, 2004). Both genera in the Tetraphidaceae have erect cylindrical capsules with simple anatomy and minimal neck. *Tetrodontium* contains five stomata while *Tetraphis* has none and has an anatomy at the short neck that is devoid of air spaces.

With 3–30 stomata in 74% of moss families (40 of the 54 families based on published counts), stomatal numbers per capsule are relatively low in most mosses. Only 9% of families with counts have more than 100 stomata per capsule. Four families include no members with stomata. Even in the groups with high numbers of stomata there are species with single digit to zero stomata. In general, higher numbers of

stomata are found in sporophytes with larger capsules, but capsules devoid of stomata are variable in size (Paton and Pearce, 1957). In the Polytrichaceae, for example, stomata-free capsules of *Atrichum* and *Pogonatum* are similar in length to those of *Polytrichum*, which has up to 250 stomata per capsule (Smith Merrill, 2007). Ecological factors do not explain the absence of stomata either as these taxa often occur side by side along forest floors. In some cases, losses of stomata appear to be associated with capsule reduction. For example, in the Pottiaceae, a transformational series of capsule and seta reduction is associated with high incidences of stomatal losses that have been reported in eight genera (Zander and Eckel, 1993). In other instances, stomatal numbers are relatively low but no known instances of loss have been documented. In the Orthotrichaceae, for example, capsules that are immersed in protective leaves still possess stomata (Merced and Renzaglia, 2017) and cleistocarpic capsules of *Ephemerum* and *P. patens* also have stomata (Merced and Renzaglia, 2013). A clear trend is the absence of stomata in aquatic bryophytes, e.g., *Fissidens* subg. *Octodiceras* and *Fontinalis* (**Supplementary Data**) or semi aquatic taxa when submerged.

Anatomy and development are foundational for understanding plant structure/function relationships and evolution. Our examinations of the internal organization of tissues and their development in capsules confirm that the mosses in early divergent lineages, *Takakia, Andreaea* and Sphagnaceae, lack any type of intercellular space in the sterile tissue of the capsule, and that peristomate mosses possess intercellular spaces some time in development even if stomata are absent (Duckett and Pressel, 2018). Although these spaces in mosses begin development with the secretion of a fluid-filled matrix, we demonstrate the existence of two distinct types of intercellular spaces in moss capsules. The first is the substomatal cavity associated only with stomata. The second is a circumsporangial space that extends between the spore sac and capsule wall and is involved in capsule expansion during sporogenesis. In many capsules with stomata such as *Funaria*, circumsporangial spaces extend into the apophysis and eventually connect with substomatal cavities, forming an elaborate system of internal spaces (Merced and Renzaglia, 2016).

We identify different origins for the two types of intercellular spaces in moss capsules. Substomatal cavities begin to develop at the spear stage in concert with guard cell differentiation before sporogenesis. The formation of substomatal cavities involves deposition of a fluid in the cavity that does not localize for pectins, suggesting it is not mucilaginous in nature (Merced and Renzaglia, 2014, 2016). These cavities are necessary for guard cells to separate, develop their unique walls, and for the pore to form. The extent of the system of substomatal cavites and circumsporangial space is related to the size of the capsule or apophysis where stomata are present. This is exemplified in the large capsules of *Oedipodium, Funaria,* and *Polytrichum* with extensive interconnected systems of substomatal cavities and underlying intercellular spaces versus the reduced capsules of *Ephemerum* and *P. patens* that have small substomatal cavities and a reduced circumsporangial space (Merced and Renzaglia, 2013, 2014, 2016). No mosses without stomata, including stomata free mutants of *P. patens*, form cavities directly beneath the epidermis that compare with substomatal cavities. Similarly, the absence of substomatal cavities in Sphagnales coincides with the absence of pores in pseudostomata.

In tracheophytes, stomata and intercellular spaces are coordinated throughout development to maximize gas exchange and minimize water lost. The molecular mechanisms controlling air spaces and stomata placement are now being elucidated, and it is hypothesized that feedback signaling between stomata and air spaces influences mesophyll arrangement (Baillie and Fleming, 2020). In mutant wheat plants with arrested stomata, when guard cells fail to divide and do not form a pore, no substomatal cavity is formed (Lundgren et al., 2019). This is similar to what we observed in mosses without stomata, i.e., that substomatal cavities fail to form. The loss of pore formation in *Sphagnum* and lack of intercellular spaces is consistent with an interpretation that pseudostomata are modified stomata (Merced, 2015).

Unlike substomatal cavities, circumsporangial spaces form in all capsules of peristomate mosses regardless of whether they have stomata or not. This internal space develops with the deposition of fluid that results in an expanding schism between capsule wall and spore sac. As illustrated in the immature *Leucobryum* and mature *Atrichum, Ephemerum* and *Plagiomnium* capsules, the circumsporangial space extends around the entire spore sac, providing a protective and nutritive matrix during spore differentiation. Unlike substomatal cavities, the fluid in this internal space contains pectins as labeled by the LM19 antibody, suggestive of mucilage, and evidence that the two types of spaces are developmentally and genetically independent. The antibody LM19 recognize epitopes of unesterified homogalacturonan, pectin, a polymer found in cell walls of all land plants that is an important component of guard cell walls and mucilage of bryophytes and angiosperms (Merced and Renzaglia, 2014, 2019; Renzaglia et al., 2017).

The separation zone that forms the circumsporangial space is determined in the formative stage of embryogenesis at the time of delineation of the endothecium, which develops into the spore sac plus columella, and amphithecium that forms the capsule wall (Smith, 1955). In comparison, intercellular spaces in hornwort sporophytes are associated with stomata only and are therefore lacking in the two hornwort clades that have lost stomata (Renzaglia et al., 2017). That no circumsporangial space occurs in hornworts is easily explained by the continued and gradual maturation of the cylindrical sporophyte from a basal meristem upward. Unlike in mosses, there is no massive capsule expansion in width in hornworts. Moreover, formative divisions in hornworts do not mimic those in mosses as the amphithecium gives rise to the sporogenous tissue and endothecium, while the endothecium produces only the columella (Renzaglia, 1978). Developmentally there are few similarities between moss and hornwort sporophytes, thus stomata loss is associated with different anatomical modifications in the two bryophyte clades.

The astomate capsule of *Atrichum* provides abundant clues to the potential role of the internal spaces in moss capsules. In this plant, large spaces remain around and below the spore sac throughout development. These are fluid-filled from their origin and dry following capsule expansion and spore maturation. The

circumsporangial spaces are strategically positioned around and above the sporogenous tissue at the region where the central strand of conducting tissue abruptly ends in the neck. The neck in turn consists of tightly packed cells with an epidermis covered by a thick cuticle. Based on this architecture, it is reasonable to deduce that water and dissolved photosynthate that is drawn up to the top of the neck fills the space around the spore sac. In this arrangement, sporogenous tissue is hydrated and provided with a constant source of nutrients. Unlike the neck or apophysis of stomata-containing mosses, there is no potential for a transpirational pull of water up and out of the capsule. Rather, water and solutes are sequestered around the developing spores, and resources are utilized and replenished as needed. This path from source to sink is unidirectional and draws nutrients and water from the gametophyte through the placenta and into the capsule throughout differentiation. The greater loss of water in astomate *Atrichum* capsules than in stomata bearing taxa as reported by Duckett and Pressel (2018) can be explained by the directed and constant use of water and nutrients in this closed systems. In the final stages of capsule differentiation, the fluid dries in the circumsporangial space, compressing the capsule urn and neck, and resulting in the detachment of the operculum and progressive spore release throughout the season.

A dearth in developmental and structural studies of moss capsules has limited comparisons across the group, making the role of specific anatomical structures in capsule function difficult to interpret. For example, there are many genera for which stomata occurrence and counts are not recorded. The existence and arrangement of key tissues such as conducting tissue are not adequately documented. Consequently, it is not verified but only speculated that hydroids occur in most moss setae (Hébant, 1977). There are mosses such as *Orthotrichum* that possess stomata but do not have conducting tissue in the sporophyte. *Grimmia*, in contrast, has been reported to have conducting tissue in the gametophyte but none in the sporophyte, while *Buxbaumia* has hydroids but no leptoids solely in the sporophyte. How these anatomical differences impact nutrient movement and capsule function are in need of further studied.

Coupled with our morphological and anatomical observations, recent studies on physiology and genetics are providing a comprehensive picture of function and evolution of stomata in bryophytes (Chater et al., 2017). Moss and hornwort stomata do not respond to environmental and endogenous cues including light intensity, water status, abscisic acid, plasmolysis, and physical damage as do angiosperm stomata (Pressel et al., 2018). In bryophytes there are no mechanisms for stomatal pores to open and close and ion changes are the same in all epidermal cells (Sussmilch et al., 2019). The preponderance of recent evidence suggests that stomata play a strategic role in capsule maturation, drying, and dehiscence without any active regulation of water loss.

The function of moss capsules in nourishing, hydrating, protecting, and dispersing spores occurs regardless of whether stomata are present. Stomata have been eliminated in over 60 moss genera/lineages in capsules that are highly modified in anatomy compared with their stomata-bearing relatives. The repeated and numerous evolutionary events that reduced and eliminated stomata on moss capsules point to the fact that unlike in tracheophytes where stomata loss is rare and restricted in occurrence (Keeley et al., 1984; Woodward, 1998), stomata are not necessary for mosses. The loss of stomata has no major consequences for the physiology of the sporophyte but results in delayed maturation and dispersion of spores in stomata-less mutants of *P. patens* (Chater et al., 2016, 2017). Capsule architecture in mosses without stomata ranges from solid in taxa in early divergent lineages to containing an internal circumsporangial space that is directly connected to the conducing tissue and is involved in capsule expansion and the nourishment, hydration and development of spores. This anatomy reveals there are different architectural arrangements of tissues within moss capsules that are equally effective in accomplishing the essential processes of sporogenesis and spore dispersal. Stomata are not foundational to these processes.

DATA AVAILABILITY STATEMENT

All datasets generated for this study are included in the article/**Supplementary Material**.

AUTHOR CONTRIBUTIONS

KR designed the study, conducted anatomical studies, prepared the figures, analyzed the data, and wrote the manuscript. AM conducted ultrastructural studies/immunogold labeling, generated the phylogenetic tree and assisted in preparing the figures and writing the manuscript. WB assisted with generating the phylogenetic tree, conducted literature searches, compiled data tables, and assisted in anatomical studies. All authors read and approved the manuscript.

FUNDING

This work was supported by grants from the National Science Foundation (NSF 1758497) and the National Institutes of Health (NIH 5R25GM107760-07).

ACKNOWLEDGMENTS

We thank Juan Larraín, Heinjo During, Richard Zander, Ida Bruggeman, Brent Mishler, Bernard Goffinet, and Jeffrey Duckett for providing information, publications and micrographs on stomata in obscure and diverse moss taxa.

SUPPLEMENTARY MATERIAL

The Supplementary Material for this article can be found online at: https://www.frontiersin.org/articles/10.3389/fpls.2020.00567/full#supplementary-material

REFERENCES

Abella, L., Alcalde, M., Estébanez, B., Cortella, A., Alfayate, C., and Ron, E. (1999). Observations on the stomatal complex in ten species of mosses (Pottiaceae, Bryopsida). *J. Hattori Bot. Lab.* 86, 179–185. doi: 10.18968/jhbl.86.0_179

Allen, B. (2015). "Fontinalaceae," in *Flora of North America North of Mexico*, Vol. 28, ed. Flora of North America Editorial Committee (New York, NY: Oxford University Press), 489–494.

Andreas, B. K. (2013). A revision of *Blindia* (*Seligeriaceae*) from Southern South America. *Bryol.* 116, 263–280. doi: 10.1639/0007-2745-116.3.263

Arzeni, C. B. (1954). The Pterobryaceae of the Southern United States, Mexico, Central America, and the West Indies. *Am. Midl. Nat.* 52, 1–67.

Baillie, A. L., and Fleming, A. J. (2020). The developmental relationship between stomata and mesophyll airspace. *New Phytol.* 225, 1120–1126. doi: 10.1111/nph.16341

Bartlett, J. K., and Vitt, D. H. (1986). A survey of species in the genus *Blindia* (Bryopsida, Seligeriaceae). *N. Z. J. Bot.* 24, 203–246. doi: 10.1080/0028825X.1986.10412674

Bryan, V. S. (2007). "Ephemeraceae," in *Flora of North America North of Mexico*, Vol. 2, ed. Flora of North America Editorial Committee (New York, NY: Oxford University Press), 646–649.

Buck, W. R. (1981). A re-interpretation of the Fabroniaceae, III: anacamptodon and Fabronidium revisited, Mamillariella, Helicodontiadelphus and Bryobartlettia gen. nov. *Brittonia* 33, 473–481.

Chater, C. C., Caine, R. S., Fleming, A. J., and Gray, J. E. (2017). Origins and evolution of stomatal development. *Plant Phys.* 174, 624–638.

Chater, C. C., Caine, R. S., Tomek, M., Wallace, S., Kamisugi, Y., Cuming, A. C., et al. (2016). Origin and function of stomata in the moss *Physcomitrella patens*. *Nat. Plants* 2, 1–7.

Cheney, L. S. (1897). North American species of Amblystegium. *Bot. Gazette* 24, 236–291. doi: 10.1086/327591

Crum, H. A., and Anderson, L. E. (1981). *Mosses of Eastern North America*. New York, NY: Columbia University Press.

Dow, G. J., Berry, J. A., and Bergmann, D. C. (2017). Disruption of stomatal lineage signaling or transcriptional regulators has differential effects on mesophyll development, but maintains coordination of gas exchange. *New Phytol.* 216, 69–75. doi: 10.1111/nph.14746

Duckett, J. G., and Pressel, S. (2018). The evolution of the stomatal apparatus: intercellular spaces and sporophyte water relations in bryophytes—two ignored dimensions. *Philos. Trans. R. Soc. Lond. B Biol. Sci.* 373:20160498.

Duckett, J. G., Pressel, S., P'ng, K. M., and Renzaglia, K. S. (2009). Exploding a myth: the capsule dehiscence mechanism and the function of pseudostomata in *Sphagnum*. *New Phytol.* 183, 1053–1063. doi: 10.1111/j.1469-8137.2009.02905.x

During, H. J. (1977). *A taxonomical Revision of the Garovaglioideae (Pterobryaceae, Musci)*. thesis, Bryophytorum Bibliotheca12, J. Cramer Verlag, Vaduz.

Edwards, D. (1979). A late Silurian flora from the lower old red sandstone of south-west dyfed. *Palaeontology* 22, 23–52.

Edwards, D., Kerp, H., and Hass, H. (1998). Stomata in early land plants: an anatomical and ecophysiological approach. *J. Exp. Bot.* 49, 255–278.

Egunyomi, A. (1982). On the stomata of some tropical African mosses. *Lindbergia* 8, 121–124.

Fife, A. J. (2012). New taxa of *Sematophyllum* and Wijkia (Musci:Sematophyllaceae), with a key to New Zealand Sematophyllaceae. *N. Z. J. Bot.* 50, 435–447. doi: 10.1080/0028825X.2012.728993

Fife, A. J., and Dalton, P. J. (2005). A reconsideration of *Pleurophascum* (Musci: *Pleurophascaceae*) and specific status for a New Zealand endemic, Pleurophascum ovalifolium stat. et nom. nov. *N. Z. J. Bot.* 43, 871–884. doi: 10.1080/0028825X.2005.9512997

Goffinet, B. (2012). *Australian Mosses Online. 53. Splachnaceae*. Avaliable online at: http://www.anbg.gov.au/abrs/Mosses_online/Splachnaceae.pdf

Goffinet, B., Buck, W. R., and Shaw, A. J. (2009). "Morphology, anatomy and classification of the Bryophyta," in *Bryophyte Biology*, eds B. Goffinet, and A. J. Shaw, (Cambridge, MA: Cambridge University Press), 55–138.

Gradstein, S. R., Churchill, S. P., and Salazar-Allen, N. (2001). *Guide to the Bryophytes of Tropical America*. The Bronx, NY: Memoirs New York Botanical Garden.

Hastings, R. I., and Grevens, H. C. (2007). "Grimmia," in *Flora of North America North of Mexico*, Vol. 27, ed. Flora of North America Editorial Committee (New York, NY: Oxford University Press), 225–257.

Hattaway, R. A. (1984). *A Monograph of the Ptychomniaceae (Bryopsida)*. Ph.D. dissertation, Pennsylvania State University, University Park, PA.

Hébant, C. (1977). The conducting tissue of bryophytes. *Bryophyt. Bibl.* 10:157.

Hedenäs, L. (2005). Bryophyte flora of Uganda. 4. Rhytidiaceae, Hylocomiaceae and Hypnaceae (Part 1). *J. Bryol.* 27, 55–66. doi: 10.1179/174328205x40734

Ireland, R. (2015). "Plagiotheciaceae," in *Flora of North America North of Mexico*, Vol. 28, ed. Flora of North America Editorial Committee (New York, NY: Oxford University Press), 483–488.

Jennings, O. E. (1913). *A Manual of the Mosses of Western Pennsylvania*. Mosses, PA: Press of the City Mission Pub. Co., doi: 10.5962/bhl.title.54494

Keeley, J. E., Osmond, C. B., and Raven, J. A. (1984). Stylites, a vascular land plant without stomata absorbs CO2 via its roots. *Nature* 310, 694–695.

Klazenga, N. (2012a). *Australian Mosses Online. 28. Orthorrhynchiaceae*. Avaliable online at: http://www.anbg.gov.au/abrs/Mosses_online/Orthorrhynchiaceae.pdf

Klazenga, N. (2012b). *Australian Mosses Online. 29. Pterigynandraceae*. Avaliable online at: http://www.anbg.gov.au/abrs/Mosses_online/Pterigynandraceae.pdf

Laenen, B., Shaw, B., Schneider, H., Goffinet, B., Paradis, E., Désamoré, A., et al. (2014). Extant diversity of bryophytes emerged from successive post-Mesozoic diversification bursts. *Nat. Commun.* 5:5134.

Liu, Y., Johnson, M. G., Cox, C. J., Medina, R., Devos, N., Vanderpoorten, A., et al. (2019). Resolution of the ordinal phylogeny of mosses using targeted exons from organellar and nuclear genomes. *Nat. Commun.* 10:1485. doi: 10.1038/s41467-019-09454-w

Lundgren, M. R., Mathers, A., Baillie, A. L., Dunn, J., Wilson, M. J., Hunt, L., et al. (2019). Mesophyll porosity is modulated by the presence of functional stomata. *Nat. Commun.* 10:2825.

McIntosh, T. T. (2007). "Schistidium," in *Flora of North America North of Mexico*, Vol. 27, ed. Flora of North America Editorial Committee (New York, NY: Oxford University Press), 207–224.

Merced, A. (2015). Novel insights on the structure and composition of pseudostomata of *Sphagnum*. *Am. J. Bot.* 102, 329–335.

Merced, A., and Renzaglia, K. (2014). Developmental changes in guard cell wall structure and pectin composition in the moss Funaria: implications for function and evolution of stomata. *Ann. Bot.* 114, 1001–1010. doi: 10.1093/aob/mcu165

Merced, A., and Renzaglia, K. S. (2013). Moss stomata in highly elaborated *Oedipodium* (Oedipodiaceae) and highly reduced Ephemerum (Pottiaceae) sporophytes are remarkably similar. *Am. J. Bot.* 100, 2318–2327. doi: 10.3732/ajb.1300214

Merced, A., and Renzaglia, K. S. (2016). Patterning of stomata in the moss *Funaria*: a simple way to space guard cells. *Ann. Bot.* 117, 985–994. doi: 10.1093/aob/mcw029

Merced, A., and Renzaglia, K. S. (2017). Structure, function and evolution of stomata from a bryological perspective. *Bryophys. Divers. Evol.* 39, 7–20.

Merced, A., and Renzaglia, K. S. (2019). Contrasting pectin polymers in guard cell walls of Arabidopsis and the hornwort Phaeoceros reflect physiological differences. *Ann. Bot.* 123, 579–585.

Milne, J., and Klazenga, N. (2012). *Australian Mosses Online. 24. Entodontaceae*. Avaliable online at: http://www.anbg.gov.au/abrs/Mosses_Online/Entodontaceae.pdf

Newton, A. E., Wikström, N., Shaw, A. J., Hedges, S. B., and Kumar, S. (2009). *Mosses (Bryophyta). The Time Tree of Life*. New York: Oxford University Press, 138–145.

Paton, J. A., and Pearce, J. V. (1957). The occurrence, structure and functions of the stomata in British bryophytes. *Trans. Br. Bryol. Soc.* 3, 228–259. doi: 10.1179/006813857804829560

Pressel, S., Renzaglia, K. S., Clymo, R. S., and Duckett, J. G. (2018). Hornwort stomata do not respond actively to exogenous and environmental cues. *Ann. Bot.* 122, 45–57. doi: 10.1093/aob/mcy045

Puttick, M. N., Morris, J. L., Williams, T. A., Cox, C. J., Edwards, D., Kenrick, P., et al. (2018). The interrelationships of land plants and the nature of the ancestral embryophyte. *Curr. Biol.* 28, 733–745. doi: 10.1016/j.cub.2018.01.063

Pursell, R. A. (1987). A taxonomic revision of *Fissidens* subgenus *Octodiceras* (Fissidentaceae). *Mem N. Y. Bot. Gard.* 45, 639–660.

Pursell, R. A. (2007). "Fissidentaceae," in *Flora of North America North of Mexico*, Vol. 27, ed. Flora of North America Editorial Committee (New York, NY: Oxford University Press), 331–357.

Pursell, R. A., Bruggeman-Nannenga, M. A., and Allen, B. H. (1988). A taxonomic revision of *Fissidens* subgenus *Sarawakia* (Bryopsidae: Fissidentacaea). *Bryologist* 91, 202–213.

Renzaglia, K. S. (1978). A comparative morphology and developmental anatomy of the Anthocerotophyta. *J. Hattori Bot. Lab.* 44, 31–90.

Renzaglia, K. S., Duff, R. J., Nickrent, D. L., and Garbary, D. J. (2000). Vegetative and reproductive innovations of early land plants: implications for a unified phylogeny. *Philos. Trans. R. Soc. Lond. B Biol. Sci.* 355, 769–793.

Renzaglia, K. S., McFarland, K. D., and Smith, D. K. (1997). Anatomy and ultrastructure of the sporophyte of *Takakia ceratophylla* (Bryophyta). *Am. J. of Bot.* 84, 1337–1350.

Renzaglia, K. S., Schuette, S., Duff, R. J., Ligrone, R., Shaw, A. J., Mishler, B. D., et al. (2007). Bryophyte phylogeny: advancing the molecular and morphological frontiers. *Bryologist* 110, 179–213.

Renzaglia, K. S., Villareal Aguilar, J. C., and Garbary, D. J. (2018). Morphology supports the setaphyte hypothesis: mosses plus liverworts form a natural group. *Bryophys. Divers. Evol.* 40, 11–17.

Renzaglia, K. S., Villarreal, J. C., Piatkowski, B. T., Lucas, J. R., and Merced, A. (2017). Hornwort stomata: architecture and fate shared with 400-million-year-old fossil plants without leaves. *Plant Physiol.* 174, 788–797. doi: 10.1104/pp.17.00156

Schofield, W. B. (2007). "Diphysciaceae," in *Flora of North America North of Mexico*, Vol. 27, ed. Flora of North America Editorial Committee (New York, NY: Oxford University Press), 162–164.

Shaw, A. J., and Renzaglia, K. S. (2004). Phylogeny and diversification of bryophytes. *Am. J. Bot.* 91, 1557–1581. doi: 10.3732/ajb.91.10.1557

Smith, G. M. (1955). *Cryptogamic Botany: Vol. II Bryophytes and Pteridophytes*. New York, NY: McGraw-Hill Book Company.

Smith, A. J. (2004). *The Moss Flora of Britain and Ireland*. Cambridge: Cambridge University Press.

Smith Merrill, G. L. (2007). "Polytrichaceae," in *Flora of North America North of Mexico*, ed. Flora of North America Editorial Committee, (New York, NY: Oxford University Press), 121–160.

Spence, J. R. (2015). "Leskeaceae," in *Flora of North America North of Mexico*, Vol. 28, ed. Flora of North America Editorial Committee (New York, NY: Oxford University Press), 340–361.

Stark, L. (2015). "Leptodontaceae," in *Flora of North America North of Mexico*, Vol. 28, ed. Flora of North America Editorial Committee (New York,NY: Oxford University Press), 623–627.

Sussmilch, F. C., Roelfsema, M. R. G., and Hedrich, R. (2019). On the origins of osmotically driven stomatal movements. *New Phyt.* 222, 84–90.

Tangney, R. S. (1997). A generic revision of the Lembophyllaceae. *J. Hattori Bot. Lab* 81, 123–153.

Tong, C., and He, S. (2002). "Ditrichaceae," in *Moss Flora of China*, Vol. 1, eds Peng-cheng, W. Crosby, and S. He (St. Louis, MO: Missouri Botanical Garden Press), 58–80.

Vitt, D. H. (2007). "Drummondia," in *Flora of North America North of Mexico*, Vol. 27, ed. Flora of North America Editorial Committee (New York, NY: Oxford University Press), 40–41.

Vitt, D. H., and Buck, W. R. (1984). The familial placement of *Bryowijkia* (Musci: Trachypodaceae). *Brittonia* 36, 300–306. doi: 10.2307/2806531

Woodward, F. I. (1998). Do plants really need stomata? *J. Exp. Bot.* 49, 471–480.

Yu, N.-N., and Jia, Y. (2012). The taxonomic status of two species of *Calyptothecium* Mitt. (Pterobryaceae, Bryopsida). *J. Bryol.* 34, 63–65. doi: 10.1179/1743282011Y.0000000044

Zander, R. H., and Eckel, P. M. (1993). *Genera of the Pottiaceae: Mosses of Harsh Environments*. Buffalo, NY: Buffalo Society of Natural Sciences.

Conflict of Interest: The authors declare that the research was conducted in the absence of any commercial or financial relationships that could be construed as a potential conflict of interest.

frontiers in Plant Science

ORIGINAL RESEARCH
published: 23 June 2020
doi: 10.3389/fpls.2020.00774

A Permeable Cuticle, Not Open Stomata, Is the Primary Source of Water Loss From Expanding Leaves

*Cade N. Kane[1], Gregory J. Jordan[2], Steven Jansen[3] and Scott A. M. McAdam[1]**

[1]Department of Botany and Plant Pathology, Purdue University, West Lafayette, IN, United States, [2]School of Natural Sciences, University of Tasmania, Hobart, TAS, Australia, [3]Institute of Systematic Botany and Ecology, Ulm University, Ulm, Germany

High rates of water loss in young, expanding leaves have previously been attributed to open stomata that only develop a capacity to close once exposed to low humidity and high abscisic acid (ABA) levels. To test this model, we quantified water loss through stomata and cuticle in expanding leaves of *Quercus rubra*. Stomatal anatomy and density were observed using scanning electron microscopy. Leaves of *Q. rubra* less than 5 days after emergence have no stomata; therefore, water loss from these leaves must be through the cuticle. Once stomata develop, they are initially covered in a cuticle and have no outer cuticular ledge, implying that the majority of water lost from leaves in this phase of expansion is through the cuticle. Foliar ABA levels are high when leaves first expand and decline exponentially as leaves expand. Once leaves have expanded to maximum size, ABA levels are at a minimum, an outer cuticular ledge has formed on most stomata, cuticular conductance has declined, and most water loss is through the stomata. Similar sequences of events leading to stomatal regulation of water loss in expanding leaves may be general across angiosperms.

Keywords: plant cuticle, Quercus-oak, leaf development, abscisic acid, stomatal development, stomata, plant physiology, cuticle development

OPEN ACCESS

Edited by:
Adriano Nunes-Nesi, Universidade Federal de Viçosa, Brazil

Reviewed by:
Mauro Guida Santos, Federal University of Pernambuco, Brazil
Georgios Liakopoulos, Agricultural University of Athens, Greece

****Correspondence:***
Scott A. M. McAdam
smcadam@purdue.edu

Specialty section:
This article was submitted to Plant Physiology, a section of the journal Frontiers in Plant Science

Received: *18 March 2020*
Accepted: *15 May 2020*
Published: *23 June 2020*

Citation:
Kane CN, Jordan GJ, Jansen S and McAdam SAM (2020) A Permeable Cuticle, Not Open Stomata, Is the Primary Source of Water Loss From Expanding Leaves. Front. Plant Sci. 11:774. doi: 10.3389/fpls.2020.00774

INTRODUCTION

Expanding leaves are highly sensitive to abiotic stresses including drought stress (Hsiao and Xu, 2000; Pantin et al., 2012). Yet, somewhat paradoxically, there are reports of extremely high rates of evaporation from young, expanding leaves (Pantin et al., 2013). High rates of water loss in young leaves have been attributed to open stomata that are unable to close because they lack sensitivity to abscisic acid (ABA) (Pantin et al., 2013). A major assumption in this model is that the physical characteristics of expanding leaves are similar to those of fully developed leaves. However, several factors challenge this assumption. Cell turgor dynamics are different between expanding and fully developed leaves, with expanding leaves maintaining high cell turgor essential for both cell expansion and the supply of nutrients to developing tissues (Shackel et al., 1987; Hsiao and Xu, 2000; Liu et al., 2003; Siebrecht et al., 2003; Sansberro et al., 2004). Cell walls in expanding leaves must be highly flexible to allow for cell expansion (Schultz and Matthews, 1993), but normal stomatal function requires rigid cell walls (Buckley et al., 2003). In addition, the cuticle, a waxy layer that forms on the outer

wall of the epidermal cells of all terrestrial plants (Raven, 1984; Gülz, 1994; Schreiber and Riederer, 1996), has been dismissed as a major source of water loss in expanding leaves (Pantin et al., 2013). This is despite reports that cuticular conductance can be very high in young leaves and decreases during leaf expansion (Hamerlynck and Knapp, 1996; Hauke and Schreiber, 1998). These ontogenetic changes may reflect changes in the cuticle during leaf expansion: during the initial phase of rapid epidermal cell expansion the cuticle remains thin, elastic, and often disjointed with epidermal cell-shaped pieces of cuticle sitting on top of epidermal cells (Sargent, 1976). Once leaf expansion ceases, the cuticle thickens, completely covering the leaf surface, while becoming firm and rigid (Sargent, 1976; Onoda et al., 2012).

The evolution of the cuticle is believed to have allowed the aquatic algal ancestors of land plants to colonize terrestrial environments (Raven, 1984; Edwards et al., 1996; Kenrick and Crane, 1997). Despite being present on all terrestrial plants, the cuticle can vary markedly in thickness, composition, and conductance at the interspecific level, and across various developmental stages and organs within an individual plant (Jeffree, 1996; Goodwin and Jenks, 2005; Buschhaus et al., 2007; Fernández et al., 2016). Being predominantly hydrophobic wax, fully developed cuticles provide a near-water tight seal on the outside of cell walls, protecting internal tissues from desiccation, blocking UV light, and acting as barrier against pathogens and physical abrasion (Edwards et al., 1996; Krauss et al., 1997; Łaźniewska et al., 2012).

Recent work suggests that cuticular organic compounds are formed within epidermal cells and transported to the outside of the cell wall *via* transport proteins, after which the cuticle self-assembles by evaporation (Lee and Priestley, 1924; Neinhuis et al., 2001; Schreiber, 2005; Yeats and Rose, 2013). While cuticles are deposited by evaporation, they also create an almost gas-tight seal around the cells (Lendzian, 1982; Lendzian and Kerstiens, 1991). The low permeability to gases severely limits CO_2 diffusion, which provided a strong selective pressure for the evolution of stomata, the epidermal valves that provide internal photosynthetic cells with access to atmospheric CO_2 (Lendzian, 1982; Lendzian and Kerstiens, 1991; Brodribb et al., 2020).

A waterproof cuticle punctuated with stomatal valves to facilitate gas exchange is essential for homoiohydry and plant growth in the desiccating environments that almost all vascular plants occupy (Lendzian, 1982; Raven, 1984; Brodribb et al., 2020). In a hydrated plant, stomata account for more than 99% of total water loss from a leaf, but once stomata close during a drought, it is believed that a considerable proportion of water lost from the plant evaporates *via* the cuticle (Körner, 1993; Duursma et al., 2019). After drought-induced closure of stomata, between 50 and 94% of the water lost from leaves is reported to be lost through the cuticle or incompletely closed stomata (Šantrůček et al., 2004; Brodribb et al., 2014). Much like the variation in maximum stomatal conductance (Körner et al., 1979), the degree of variation in cuticular conductance between species can be considerable and may be critical for determining the ecological limits of species (Schreiber and Riederer, 1996; Mayr, 2007). Highly permeable cuticles are found in moss and fern gametophytes, while very low cuticular conductance is found in species that are adapted to dry environments (Edwards et al., 1996; Jeffree, 1996; Schreiber and Riederer, 1996; Brodribb et al., 2014; Blackman et al., 2016; Carignato et al., 2020; Lee et al., 2019). Pollutants and time can degrade the leaf cuticle impacting drought resistance (Jordan and Brodribb, 2007; Burkhardt and Pariyar, 2014). In particular, the removal of outer cuticular waxes can severely decrease drought tolerance in semiarid woody species, leading to a reduction in photosynthesis, gas exchange, and plant pigment levels (Medeiros et al., 2017; Pereira et al., 2019).

Although there has long been a focus on cuticular conductance in determining drought-tolerance thresholds, almost no focus has been placed on the role of cuticular conductance in determining leaf gas exchange as leaves expand. Complete leaf expansion in *Hedera helix* occurs around the same time cuticular conductance reaches a minimum (Hauke and Schreiber, 1998). Cuticles also appear to cease developing in chemical composition once leaves cease expanding (Hauke and Schreiber, 1998). Furthermore, very young stomata are covered in a cuticle (Davis and Gunning, 1993; Nadeau and Sack, 2002; Hunt et al., 2017). Breaking of this cuticle covering layer in leaf development to form the outer cuticular ledge may be responsible for reported increases in leaf gas exchange as leaves expand (Constable and Rawson, 1980). In support of this rates of gas exchange in mutant plants of *Arabidopsis* in which stomata are occluded by a cuticle covering are half that of wild-type plants without occluded stomata (Hunt et al., 2017).

Here, we utilize the hypostomatic species *Quercus rubra* to separate cuticular and stomatal water loss from total leaf transpiration in expanding leaves. *Q. rubra* has large, fast-growing leaves, making it ideal for these experiments. We reexamine the ontogeny of the formation of the outer cuticular ledge in expanding *Arabidopsis* leaves, which is essential for the initiation of stomatal conductance. We also collected foliage ABA levels in expanding leaves to examine what, if any, role ABA may play in "priming" stomatal function.

MATERIALS AND METHODS

Plant Material

Six, 3 year-old bare-rooted *Q. rubra* plants were planted in 10 L pots containing a 1:1:1 mix of Indiana Miami topsoil, ground pine bark, and sand. Plants were grown in the glasshouses of Purdue University, IN, USA, under a 16 h photoperiod, supplemented, and extended with LED lights (Illumitex Power Harvest I4, TX, USA) that provided a photon flux density on an F3 spectrum (22.4% blue; 13.4% green; 63.9% red; and 0.4% far-red) of 150 μmol m^{-2} s^{-1} at pot level. The highest PPFD (natural and supplemental light) measured was 1,800 μmol m^{-2} s^{-1} at solar noon on a cloudless day. Plants were watered daily and received liquid nutrients once per month. Conditions in the glasshouse were set at a night/day temperature of 22/28°C. After initial bud burst, all developing leaves were tagged with the date of leaf emergence. Six plants of *Arabidopsis thaliana Col-0* were grown under a 10 h

photoperiod, supplied by LED lights (SUNCO Lighting, CA, USA), providing a photon flux density of 60 μmol m^{-2} s^{-1} at pot level. Seeds were sown directly on germination mix (Sun Gro Horticulture, MA, USA). Plants were watered from the base and given liquid nutrients once per month. Plants were imaged daily to determine leaf age. The area of eight leaves was measured daily from initial emergence until 23 days after emergence.

Determining Cuticular and Stomatal Conductance by Leaf Gas Exchange

Leaf gas exchange was measured using an infrared gas analyzer (LI-6800, Licor Biosciences, NE, USA). Conditions in the leaf cuvette were maintained as close to ambient glasshouse conditions as possible, and light conditions were set at 1,500 μmol m^{-2} s^{-1}. Measurements were taken between 09:00 till 11:00 on clear, cloudless days. Initial stomatal conductance (g_s) was measured on expanding, or fully expanded, leaves by enclosing the leaf in the chamber and measuring instantaneous leaf gas exchange parameters. After this initial measurement, the abaxial surface of the leaf was covered in petroleum jelly and plastic wrap and instantaneous leaf gas exchange was again measured in the same region of the leaf, or the whole leaf. By covering the abaxial leaf surface we only measured gas exchange through the adaxial surface which has no stomata or hydathodes, like most *Quercus* species (Bolhàr-Nordenkampf and Draxler, 1993; Ivănescu et al., 2009). All rates of leaf gas exchange were normalized by leaf area in the cuvette. Whole leaf area was also measured for each leaf analyzed by imaging leaves (12 megapixel, IPhone 7, Apple Inc., CA, USA) and measuring area using ImageJ (National 303 Institutes of Health, Bethesda, MD, USA). To avoid variation due to potential developmental variation across the leaf surface, the center of each leaf was placed in the cuvette. In younger leaves, we were able to measure the whole leaf. All measured leaves were preserved in methanol and stored at −20°C for anatomical assessment. Cuticular and stomatal conductance and the percent of total leaf conductance that occurred through the stomata were calculated according to Jordan and Brodribb (2007).

Quantifying Foliage Abscisic Acid Levels

Leaves were harvested at 11:00 and immediately wrapped in damp paper towel and bagged. A sample of tissue was taken from each leaf, weighed (±0.0001 g, OHAUS Corporation, NJ, USA) and then covered in −20°C 80% methanol in water (v v^{-1}) containing 250 mg L^{-1} butylated hydroxytoluene, chopped to fine pieces and stored at −20°C overnight. Extraction in methanol ensures that both free and fettered ABA in the chloroplasts were extracted from the sample (Georgopoulou and Milborrow, 2012). The samples were homogenized and 15 μl of deuterium labeled [$^2H_6$]ABA (OlChemim Ltd, Czech Republic) was added as an internal standard. ABA was extracted overnight at 4°C. An aliquot of supernatant was dried in a vacuum sample concentrator (Labconco, MO, USA), and ABA was resuspended in 200 μl of 2% acetic acid in water (v v^{-1}), centrifuged at 14,800 RPM for 4 min and 100 μl taken for analysis. The level of ABA and internal standard in each sample was quantified using an Agilent 6460 series triple quadrupole LC/MS (Agilent, CA, USA) according to McAdam (2015). After quantification, the plant material from which the supernatant was taken was dried down at 70°C, and leaf dry weight was estimated by subtracting the initial mass of the empty tube.

Anatomy

Stomatal anatomy was analyzed in hole punches (diameter 0.5 cm) from the center of *Q. rubra* leaves ranging from 1 to 30 days of age (including all of the leaves measured for leaf exchange) that had been stored in methanol at −20°C. Anatomical samples were collected from either the whole leaf, in young leaves or from center of the leaves when they were large enough. In *Q. rubra*, leaves expand evenly and then acropetally after reaching approximately 70% of maximum size (Tomlinson et al., 1991); our sampling protocol ensured that we avoided these regions of differential or continual expansion in larger leaves. Samples were prepared for SEM by critical point drying (E3000 Critical Point Dryer, Quorum Technologies, East Sussex, UK). Dried samples were placed on stubs and sputter coated for 60 s at 8 mA using a gold target (Balzers Union FL-9496 sputter device, Balzers, Liechtenstein). Images of stomata from the abaxial surface were taken on a Phenom XL desktop SEM (Nano Science Instruments, AZ, USA) at 1,000x magnification to determine stomatal density and the percent of stomata in which the outer cuticular ledge had formed. For stomatal density measurements, a stoma was counted if both guard cells were discernible. A stoma with an outer cuticular ledge was defined as having any form of rip, tear, or hole in the cuticular covering over the stomatal pore. Cross sections of *Q. rubra* leaves were made using a freezing microtome (Microm HM 430, Thermo Scientific, MA, USA). The cuticle on leaf sections was stained using Sudan IV (0.5 g powdered Sudan IV in 100 ml 75% Ethanol, 25% DI water) for 8 h at 25°C. Images were taken using a 40x oil emersion objective on a light microscope (AxioImagerA2, Zeiss, Germany). Observations were made from four different sections from three different leaves 6 and 21 days after emerging.

Arabidopsis leaves used for stomatal anatomy were harvested on a single day and stored in methanol at −20°C. Leaf segments were prepared to observe the abaxial leaf surface and attached to a SEM stub with 1:1 OCT Cryo-Gel and water. Leaf pieces were frozen in a liquid nitrogen slurry and moved into a Gatan Alto 2500 (Gatan 316 Inc., Pleasanton, CA, USA) cryo-preparation chamber of an SEM (FEI Nova Nano 317200, Hillsboro, OR, USA). The samples were placed under vacuum and held at −170°C. Samples were then allowed to sublimate at −90°C, while viewing to remove frost. Leaves were sputter coated for 120 s at 8 mA using a platinum target and then imaged at −140°C.

Leaf Water Potential

Midday leaf water potential was measured in young expanding leaves (6 days after leaf emergence), as well as fully expanded leaves (32 days after leaf emergence) using a Scholander pressure

chamber (PMS Instrument Company, OR, USA). Leaves were excised and wrapped in damp paper towel and immediately placed into a humid plastic bag. Leaves were allowed to equilibrate in dark, in the humid bag for 5 min before measurements were taken.

RESULTS

In the newest expanding leaves of *Q. rubra* (less than 5 days old; i.e., at ~15% of fully expanded area), whole leaf conductance was found to be relatively high, at 0.023 mol m^{-2} s^{-1}. By 10 days after leaf emergence (i.e., at 60% of fully expanded area), leaf conductance had doubled to 0.047 mol m^{-2} s^{-1} (**Figures 1, 2**). While leaf conductance was measurable in leaves that were less than 5 days old, less than 5% of total leaf conductance was found to be lost through the stomata (**Figure 1**). After 5 days of leaf expansion, the percentage of water lost from a leaf through stomata began to increase rapidly (**Figure 1**). Ten days after leaf emergence, the stomata were found to be responsible for approximately 50% of water loss from the leaf (**Figure 1**). By 15 days after leaf emergence, the percentage of water lost through the stomata accounted for more than 80% of total leaf conductance, which had increased to more than 0.075 mol m^{-2} s^{-1} (**Figure 1**). By this age leaves were fully expanded. In general, leaves had ceased to expand by day 13 (**Figure 2**). Leaves 6 days after emerging did not appear to have a very thick or well-developed cuticle when compared to leaves 21 days after emerging, which displayed a much thicker and well-developed cuticle (**Figure 1**).

Foliar ABA levels in developing *Q. rubra* leaves were approximately 21.5 μg g^{-1} dry weight on the first day following leaf emergence (**Figure 3**). As leaves expanded, this high level of initial ABA in primordial leaves declined following an

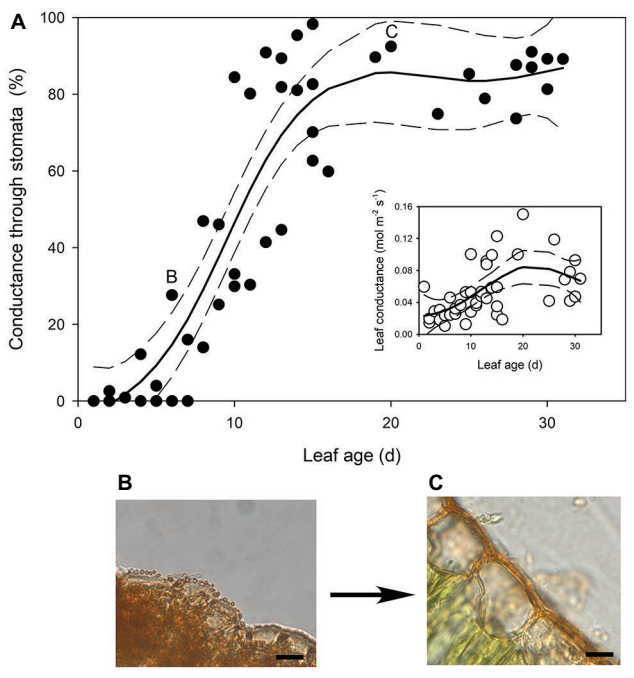

FIGURE 1 | (A) The percentage of transpired water lost through stomata as *Quercus rubra* leaves expand. The insert depicts the absolute rates of leaf conductance measured in the same leaves. Generalized additive model curves and 95% confidence intervals are represented by solid and dashed black lines, respectively. Each point represents a single leaf. Letters on the chart depict the leaf from which representative images **(B,C)** were taken. **(B)** Cross sections through the epidermis of a *Q. rubra* leaf 6 days after emerging, and **(C)** 21 days after emerging, with cuticles stained using Sudan IV (scale bars = 10 μm).

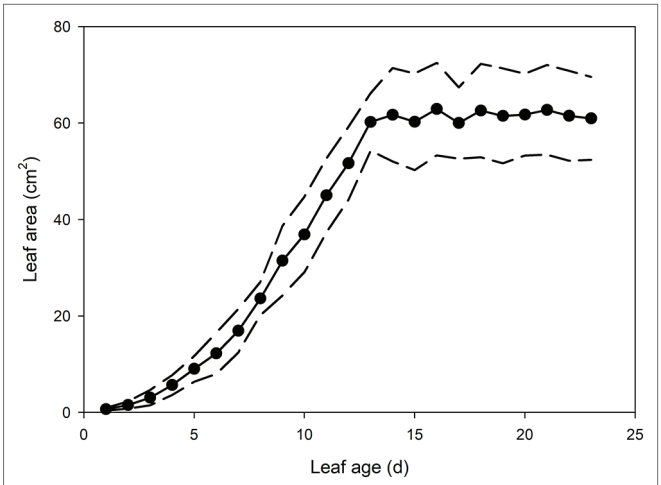

FIGURE 2 | Mean leaf area of *Q. rubra* leaves from emergence (day 0) to 23 days after leaf emergence (n = 8 leaves, ± *SD*). Dashed lines depict standard deviation.

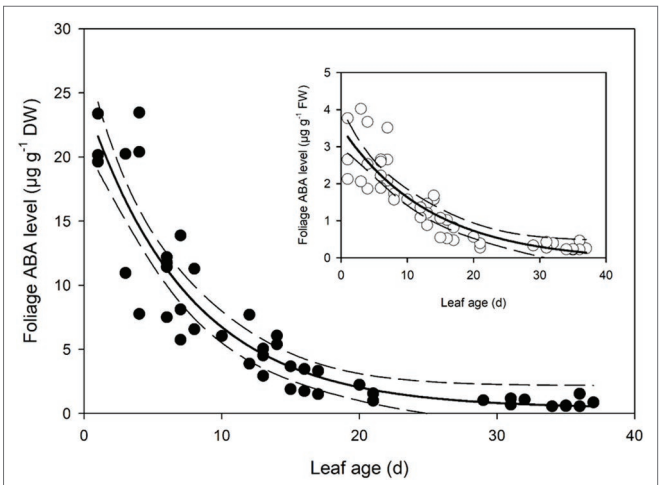

FIGURE 3 | Foliage abscisic acid (ABA) level in expanding *Q. rubra* leaves. ABA levels are expressed in terms of dry weight. A single exponential decay three parameter model (ABA level $DW = 0.3822 + 24.2829 \times e^{-0.1340 \times \text{Leaf age}}$) (solid line) with 95% confidence interval (dashed lines) is depicted (p = <0.0001, R^2 = 0.8493). The insert shows ABA levels in terms of fresh weight (FW). A single exponential decay three parameter model (ABA level $FW = -0.0982 + 3.6244 \times e^{-0.0737 \times \text{Leaf age}}$) (solid line) with 95% confidence interval (dashed line) is depicted (p = <0.0001, R^2 = 0.7912).

exponential decay curve, such that by 7 days after leaf emergence, ABA levels in terms of dry weight were half the initial level in the newest emerged leaves (**Figure 3**). ABA levels continued to decline until around 30 days after initial leaf emergence, by which time they had approached a steady-state level of around 0.55 μg g^{-1} dry weight (**Figure 3**).

The youngest *Q. rubra* leaves had very few stomata, with approximately 27 ± 2 stomata mm^{-2} by the second day following emergence (**Figure 4**). Stomatal densities remained low in expanding leaves until 5 days after leaf emergence, when densities rapidly increased by 20-fold, to approximately 575 stomata mm^{-2} (**Figure 4**). Allowing for a change in leaf area, this indicates a 200,000-fold increase in the total number of stomata over that time (**Figure 4**). The highest recorded stomatal density on an individual leaf was measured in leaves 9 days after leaf emergence, with 1,528 ± 33 stomata mm^{-2} (**Figure 4**), after which stomatal density declined as leaves continued to expand. Seventeen days after leaf emergence, stomatal density reached a steady-state mean density of 790 stomata mm^{-2} (±5) (**Figure 4**).

In all stomatal complexes on leaves younger than 7 days old, a cuticle covered the pore between the guard cells (**Figure 5**). The presence of this covering meant that these stomatal complexes did not have apertures and therefore could not be functional stomata. By 13 days after leaf emergence, in 90% of stomatal complexes, this cuticle layer had split to create an aperture and an outer cuticular ledge (**Figure 5**). Similar patterns in the formation of the outer cuticular ledge were observed in the expanding leaves of *A. thaliana Col-0* plants (**Figures 6, 7**)

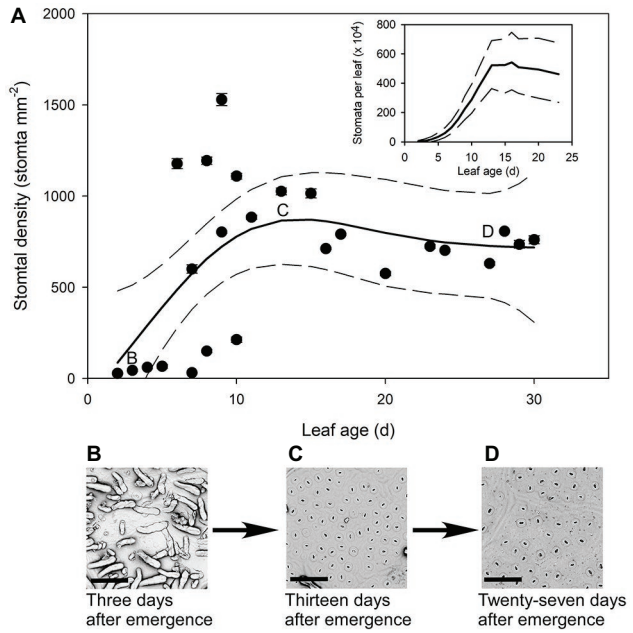

FIGURE 4 | (A) Mean stomatal density (n = 5 fields of view per leaf taken from the center of the leaf, ± *SE*) of expanding *Q. rubra* leaves. Each point represents a single leaf. Letters on the chart depict the leaf from which representative images **(B–D)** were taken. Generalized additive model curves and 95% confidence intervals are represented by solid and dashed black line respectively. The insert represents the total number of stomata per leaf of expanding *Q.rubra* leaves (solid line) flanked by the 95% confidence interval (dashed line). **(B)** An image of the abaxial surface of a *Q. rubra* leaf 3 days after emergence with visible trichomes (scale bar = 80 μm). **(C)** An image of the abaxial surface of a *Q. rubra* leaf 13 days after emergence (scale bar = 80 μm). **(D)** An image of the abaxial surface of a *Q. rubra* leaf 27 days after emergence (scale bar = 80 μm).

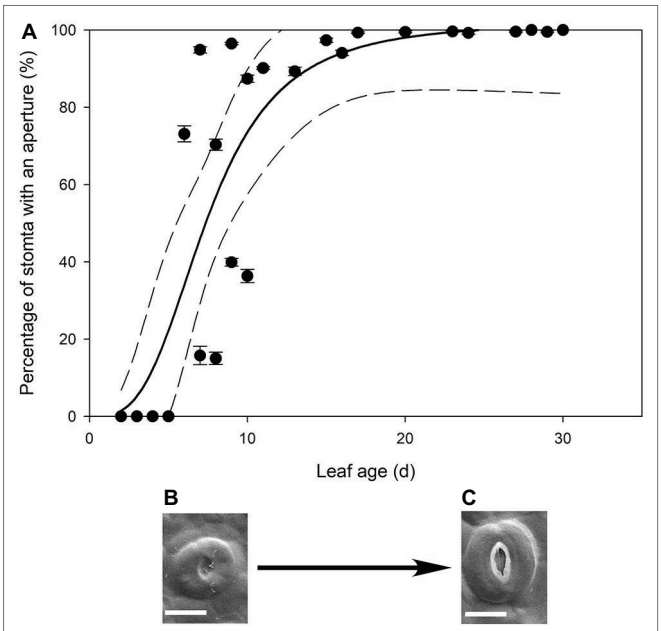

FIGURE 5 | (A) Mean percentage of stomata with an aperture (n = 5 fields of view per leaf taken from the center of the leaf, ± *SE*) in expanding leaves of *Q. rubra*. Each point represents a single leaf. A logistic three parameter sigmoidal curve (solid line) and 95% confidence interval (dashed line) is shown (p = <0.0001, R^2 = 0.7178). **(B,C)** Representative images of *Q. rubra* stomata **(B)** without an aperture and **(C)** with an aperture captured on the same leaf 10 days after emergence (scale bar = 10 μm).

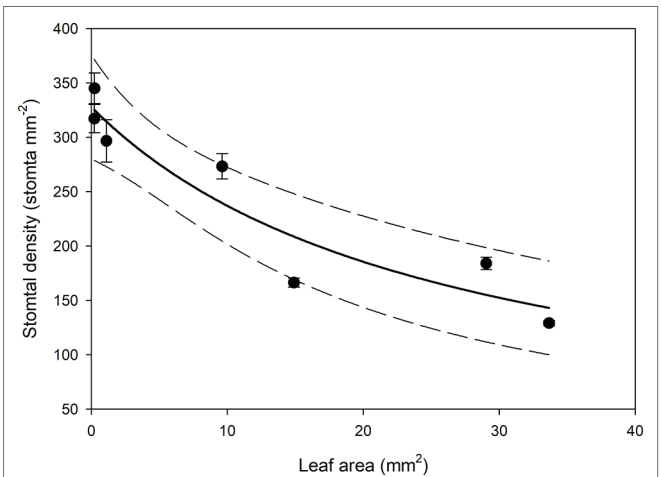

FIGURE 6 | Mean stomatal density on the abaxial surface (n = 5 fields of view from the same leaf taken from the center of the leaf, ± *SE*) in expanding *Arabidopsis thaliana Col-0* leaves. Each point represents a single leaf. A rational, 2 Parameter II curve (solid line) and 95% confidence interval (dashed line) is shown (p = <0.0015, R^2 = 0.8870).

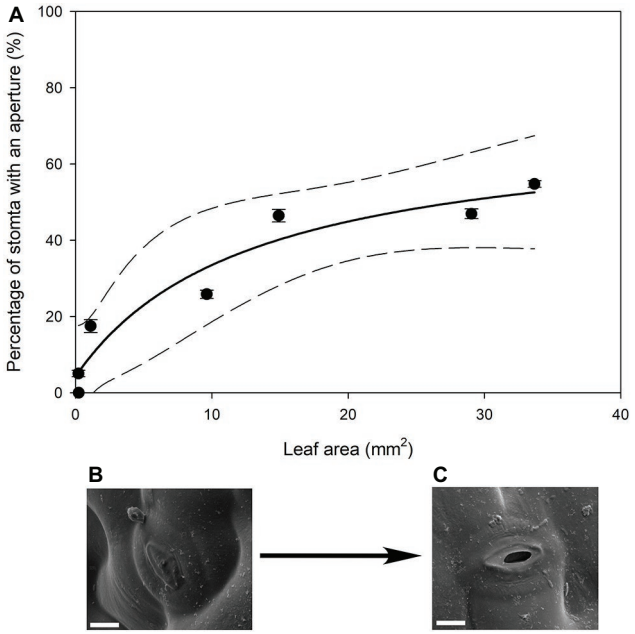

FIGURE 7 | (A) Mean percentage of stomata that have formed an aperture on the abaxial surface (n = 5 fields of view per leaf taken from the center of the leaf, ± *SE*) in young expanding leaves of *A. thaliana Col-0*. Each point represents a single leaf. A rational, 3 Parameter II (solid line) and 95% confidence interval (dashed line) is shown (p = <0.0050, R^2 = 0.9295). **(B)** Image of an *A. thaliana Col-0* stoma without an aperture on a leaf that was 29.04 mm^2, approximately 6 days after emergence (Scale bar = 5 μm). **(C)** Image of an *A. thaliana Col-0* stoma with an aperture on with the same leaf imaged in **(B)** (Scale bar = 5 μm).

with most stomata in the smallest and youngest leaves covered with cuticle (**Figure 7**). Zero to five percent of stomata had formed an outer cuticular ledge in leaves of *A. thaliana* that were <0.25 mm^2 in area and had not yet emerged from the center of the rosette. Once leaves had emerged from the rosette for approximately 1 day (being more than 10 mm^2 in area), approximately 25% of the stomata had developed an outer cuticular ledge (**Figure 7**). The number of stomata forming an outer cuticular ledge per day declined once *A. thaliana* leaves reached approximately 15 mm^2 in area.

We found that leaf water potential of young expanding leaves of *Q. rubra* was the same as that of fully expanded leaves on the same plant. Leaves 3 days after emerging had a water potential of −0.866 ± 0.113 MPa (n = 3, *SE*), while leaf water potential in leaves that emerged at least 32 days prior to the measurement, and were fully expanded, was −0.763 ± 0.089 MPa (n = 3, *SE*).

DISCUSSION

Contrary to the model of Pantin et al. (2013), based on observations in *Arabidopsis*, cuticular conductance accounts for the majority of water loss from expanding leaves in *Q. rubra*. In *Q. rubra* the youngest leaves have no stomata and once stomata form, they have no aperture as they are still covered in cuticle. Only once the stoma and aperture forms by tearing the covering cuticle do stomata become the primary source of leaf conductance to water vapor. We found no evidence in *Q. rubra* that ABA levels increased as leaves expand, thereby priming stomata to function as hypothesized by Pantin et al. (2013). In contrast, ABA levels were very high in young expanding leaves and appeared to decline thereby, presumably, allowing stomata to open.

The highly permeable cuticle in young, expanding leaves previously observed in *Quercus macrocarpa*, *Q. muehlenbergii*, and *H. helix* (Hamerlynck and Knapp, 1996; Hauke and Schreiber, 1998) may be due to the development of the cuticle (Lee and Priestley, 1924; Neinhuis et al., 2001). Mature cuticles are extremely dense with a very high breakage strength, suggesting that a weaker cuticle may be necessary to allow cells and leaves to expand (Onoda et al., 2012). The more elastic disjointed developing cuticle needed to allow cell expansion may come at the cost of a higher cuticular conductance. If this is the case, plants would have to balance the maintenance of high turgor pressure to drive cell expansion and deliver nutrients with a permeable cuticle to allow for cell expansion. Although cuticle permeance has been found to be a function of water status with high leaf water potential leading to higher levels of cuticular water loss (Boyer et al., 1997; Jordan and Brodribb, 2007), it is unlikely that the high levels of cuticular water loss in young leaves might simply be due to the higher water status of young expanding leaves as these leaves have the same water potentials as fully expanded leaves. This is in agreement with previous work in other *Quercus* species, in which there was no difference found in leaf water potential across leaf age as leaves expand (Ren and Sucoff, 1995; Hamerlynck and Knapp, 1996). In *Q. rubra* we observed much thinner cuticles in younger leaves when compared to those that were fully expanded; this anatomical change in cuticle thickness and possibly composition is the likely cause of the higher cuticular water loss measured in young expanding leaves.

Our work suggests that the formation of the outer cuticular ledge above stomata of developing leaves (and therefore formation of an aperture) could be a major determinant of the timing and relevance of stomatal function in leaf gas exchange. Here, we observed that stomatal water loss only occurs when stomata have these apertures (**Figures 1, 4**). The cuticle that covers stomata before the formation of the outer cuticular ledge likely inhibits water flux through individual stomatal pores, just as it reduces stomatal conductance in *A. thaliana* mutant plants that do not form an outer cuticular ledge (Hunt et al., 2017). Once that cuticle tears and the outer cuticular ledge is formed, *Q. rubra* stomata are capable of sustaining maximum water loss rates through the pore. These cuticle coverings in young stomata have been observed multiple times in *A. thaliana* (Serna and Fenoll, 1997; Nadeau and Sack, 2002; Hunt et al., 2017), in *Hydrocotyle bonariensis* (Koch and Barthlott, 2009), the stomata on the flowers of *Vicia faba* (Davis and Gunning, 1993), and now *Q. rubra*. Given that we observed these in both *Q. rubra* and *A. thaliana*, and stomatal development and developmental genes are highly conserved across land plants, this cuticular covering of young stomata may be a feature common to all vascular plants (Chater et al., 2017). Whether it extends to non-vascular plant stomata remains to be examined (Renzaglia et al., 2017).

The extremely high levels of ABA found in young leaves of *Q. rubra* could have several explanations all requiring future examination. It is possible that the newest expanding leaves have high levels of ABA because ABA is required to maintain bud dormancy (Kovaleski and Londo, 2019). The decreases seen here as leaves expand might be due to dilution and catabolism as bud dormancy is broken (Kovaleski and Londo, 2019). The ABA may also be playing a role in cuticle formation, as some ABA deficient tomato mutants have thinner cuticles with reduced levels of cutin that are partially restored by the application of ABA (Martin et al., 2017). Another possibility is that ABA may be responsible for maintaining low guard cell turgor during leaf development to stop the premature tearing of the cuticle covering above the stomatal pore. Exogenous applications of ABA have been found to keep stomata closed under the cuticle covering in *focl* mutants, which have much reduced formation of the outer cuticular ledge, indicating that stomata that have a cuticle covering are possibly capable of opening and closing (Hunt et al., 2017). There is the possibility that the high levels of ABA in young leaves may be sequestered in chloroplasts, and this fettered ABA is non-functional (Loveys, 1977; Georgopoulou and Milborrow, 2012). However, given the observation in an evergreen *Quercus* species and other herbaceous species that chloroplast number is very low in young, expanding leaves, increasing as leaves expand (Miyazawa et al., 2003), this possibility seems unlikely. The most likely explanation is that the high levels of ABA found in the expanding leaves of *Q. rubra* are responsible for keeping stomata closed as leaves expand; although given other signals can close stomata (Granot et al., 2013; Salmon et al., 2020), more experimental work is required to test this theory.

Based on this work, the apparent order of events in expanding *Q. rubra* leaves is that very young leaves have relatively high levels of cuticular water loss that decline as leaves cease expanding. During expansion, stomata develop, but are present in low numbers and covered with a cuticle. Foliage ABA levels are initially high and decrease through time as leaves expand, possibly keeping the youngest stomata closed under the cuticle, until the cuticle connecting the guard cells tears to form the stomatal aperture, or is torn open by the opening stomata. Once the outer cuticular ledge forms, stomata account for most of the water lost from expanded leaves. This chain of events is very different to the model proposed by Pantin et al. (2013) based on observations made in *A. thaliana*. We would argue that these differences are not due to differences in species, as we found similar morphological development in the expanding leaves of both *Quercus* and *Arabidopsis*. However, further work is required to investigate the importance of cuticular conductance in leaf gas exchange as leaves expand across a wide diversity of species and also under field conditions. We find that the model of Pantin et al. (2013) is not supported by our observations of very high levels of ABA measured in young leaves, the cuticle covering of young stomata, and the relatively late development of the outer cuticular ledge in expanding leaves of *A. thaliana* and *Q. rubra*, all of which run counter to the theory that stomata are wide open and responsible for all of the water loss from young, expanding leaves. We conclude that the cuticle plays a primary role in determining the rate of water loss from expanding leaves.

DATA AVAILABILITY STATEMENT

The datasets generated for this study are available on request to the corresponding author.

AUTHOR CONTRIBUTIONS

This work was originally conceived by SM with GJ. SJ assisted with collection of SEM images and preparation of anatomical samples. All data was collected and analyzed by CK under the supervision of SM. Manuscript was written by CK with input from SM, GJ, and SJ. All authors contributed to the article and approved the submitted version.

FUNDING

This work was supported by the USDA National Institute of Food and Agriculture Hatch Project 1014908 (SM) and a fellowship from the Alexander von Humboldt Foundation.

ACKNOWLEDGMENTS

We acknowledge the use of the facilities of the Bindley Bioscience Center (National Institutes of Health-funded Indiana Clinical and Translational Sciences Institute), particularly the Metabolite Profiling Facility. We would also like to thank Robert Seiler at the Purdue Life Science Microscopy Facility for help with the cryoSEM, Dr. Jennifer McElwain for a helpful discussion on stomatal development, and Justine Krueger for collecting insightful preliminary data that led to this study.

REFERENCES

Blackman, C. J., Pfautsch, S., Choat, B., Delzon, S., Gleason, S. M., and Duursma, R. A. (2016). Toward an index of desiccation time to tree mortality under drought. *Plant Cell Environ.* 39, 2342–2345. doi: 10.1111/pce.12758

Bolhàr-Nordenkampf, H. R., and Draxler, G. (1993). "Functional leaf anatomy" in *Photosynthesis and production in a changing environment: A field and laboratory manual*. eds. D. O. Hall, J. M. O. Scurlock, H. R. Bolhàr-Nordenkampf, R. C. Leegood and S. P. Long (Netherlands: Springer), 91–112.

Boyer, J. S., Wong, S. C., and Farquhar, G. D. (1997). CO_2 and water vapor exchange across leaf cuticle (epidermis) at various water potentials. *Plant Physiol.* 114, 185–191. doi: 10.1104/pp.114.1.185

Brodribb, T. J., McAdam, S. A. M., Jordan, G. J., and Martins, S. C. V. (2014). Conifer species adapt to low-rainfall climates by following one of two divergent pathways. *Proc. Natl. Acad. Sci. U. S. A.* 111, 14489–14493. doi: 10.1073/pnas.1407930111

Brodribb, T. J., Sussmilch, F., and McAdam, S. A. M. (2020). From reproduction to production, stomata are the master regulators. *Plant J.* 101, 756–767. doi: 10.1111/tpj.14561

Buckley, T. N., Mott, K. A., and Farquhar, G. D. (2003). A hydromechanical and biochemical model of stomatal conductance. *Plant Cell Environ.* 26, 1767–1785. doi: 10.1046/j.1365-3040.2003.01094.x

Burkhardt, J., and Pariyar, S. (2014). Particulate pollutants are capable to 'degrade' epicuticular waxes and to decrease the drought tolerance of Scots Pine (Pinus sylvestris L.). *Environ. Pollution* 184, 659–667. doi: 10.1016/j.envpol.2013.04.041

Buschhaus, C., Herz, H., and Jetter, R. (2007). Chemical composition of the epicuticular and intracuticular wax layers on adaxial sides of *Rosa canina* leaves. *Ann. Bot.* 100, 1557–1564. doi: 10.1093/aob/mcm255

Carignato, A., Vázquez-Piqué, J., Tapias, R., Ruiz, F., and Fernández, M. (2020) Variability and plasticity in cuticular transpiration and leaf permeability allow differentiation of Eucalyptus clones at an early age. *Forests* 11:9. doi: 10.3390/f11010009

Chater, C. C. C., Caine, R. S., Fleming, A. J., and Gray, J. E. (2017). Origins and evolution of stomatal development. *Plant Physiol.* 174, 624–638. doi: 10.1104/pp.17.00183

Constable, G. A., and Rawson, H. M. (1980). Effect of leaf position, expansion and age on photosynthesis, transpiration and water use efficiency of cotton. *Funct. Plant Biol.* 7, 89–100. doi: 10.1071/PP9800089

Davis, A. R., and Gunning, B. E. S. (1993). The modified stomata of the floral nectary of *Vicia faba* L. 1. Development, anatomy and ultrastructure. *Plant Biol.* 106, 241–253. doi: 10.1111/j.1438-8677.1993.tb00747.x

Duursma, R. A., Blackman, C. J., Lopéz, R., Martin-StPaul, N. K., Cochard, H., and Medlyn, B. E. (2019). On the minimum leaf conductance: its role in models of plant water use, and ecological and environmental controls. *New Phytol.* 221, 693–705. doi: 10.1111/nph.15395

Edwards, D., Abbott, G. D., and Raven, J. A. (1996). "Cuticles of early land plants: a palaeoecophysiological evaluation" in *Plant cuticles an integrated functional approach*. ed. G. Kerstiens (Oxford: BIOS Scientific Publishers), 1–31.

Fernández, V., Guzmán-Delgado, P., Graça, J., Santos, S., and Gil, L. (2016). Cuticle structure in relation to chemical composition: re-assessing the prevailing model. *Front. Plant Sci.* 7:427. doi: 10.3389/fpls.2016.00427

Georgopoulou, Z., and Milborrow, B. V. (2012). Initiation of the synthesis of 'stress' ABA by (+)-[$^2H_6$]ABA infiltrated into leaves of *Commelina communis*. *Physiol. Plant.* 146, 149–159. doi: 10.1111/j.1399-3054.2012.01630.x

Goodwin, S. M., and Jenks, M. A. (2005). "Plant cuticle function as a barrier to water loss" in *Plant abiotic stress*. eds. M. A. Jenks and P. M. Hasegawa (Oxford: Blackwell Publishing), 14–31.

Granot, D., Kelly, G., Stein, O., and David-Schwartz, R. (2013). Substantial roles of hexokinase and fructokinase in the effects of sugars on plant physiology and development. *J. Exp. Bot.* 65, 809–819. doi: 10.1093/jxb/ert400

Gülz, P.-G. (1994). Epicuticular leaf waxes in the evolution of the plant kingdom. *J. Plant Physiol.* 143, 453–464. doi: 10.1016/S0176-1617(11)81807-9

Hamerlynck, E. P., and Knapp, A. K. (1996). Early season cuticular conductance and gas exchange in two oaks near the western edge of their range. *Trees* 10, 403–409. doi: 10.1007/BF02185644

Hauke, V., and Schreiber, L. (1998). Ontogenetic and seasonal development of wax composition and cuticular transpiration of ivy (*Hedera helix* L.) sun and shade leaves. *Planta* 207, 67–75. doi: 10.1007/s004250050456

Hsiao, T. C., and Xu, L.-K. (2000). Sensitivity of growth of roots versus leaves to water stress: biophysical analysis and relation to water transport. *J. Exp. Bot.* 51, 1595–1616. doi: 10.1093/jexbot/51.350.1595

Hunt, L., Amsbury, S., Baillie, A., Movahedi, M., Mitchell, A., Afsharinafar, M., et al. (2017). Formation of the stomatal outer cuticular ledge requires a guard cell wall proline-rich protein. *Plant Physiol.* 174, 689–699. doi: 10.1104/pp.16.01715

Ivănescu, L., Lăzărescu, A. M., and Toma, C. (2009). Comparative anatomy of the foliar lamina in some taxa of *Quercus* L. genus. *Analele Ştiinţifice Ale Universităţii "Al. I. Cuza" Iaşi Tomul LV, Fasc. 2, s.II a. Biologie Vegetală*, 7.

Jeffree, C. E. (1996). "Structure and ontogeny of plant cuticles" in *Plant cuticles an integrated functional approach*. ed. G. Kerstiens (Oxford: BIOS Scientific Publishers), 33–82.

Jordan, G. J., and Brodribb, T. J. (2007). Incontinence in aging leaves: deteriorating water relations with leaf age in *Agastachys odorata* (proteaceae), a shrub with very long-lived leaves. *Funct. Plant Biol.* 34, 918–924. doi: 10.1071/FP07166

Kenrick, P., and Crane, P. R. (1997). The origin and early evolution of plants on land. *Nature* 389, 33–39. doi: 10.1038/37918

Koch, K., and Barthlott, W. (2009). Superhydrophobic and superhydrophilic plant surfaces: an inspiration for biomimetic materials. *Philos. Trans. R Soc. A Math. Phys. Eng. Sci.* 367, 1487–1509. doi: 10.1098/rsta.2009.0022

Körner, C., Scheel, J. A., and Bauer, A. (1979). Maximum leaf diffusive conductance in vascular plants. *Photosynthetica* 13, 45-82.

Körner, C. (1993). "Scaling from species to vegetation: the usefulness of functional groups" in *Biodiversity and ecosystem function*. eds. E.-D. Schulze and H. A. Mooney (Berlin Heidelberg: Springer), 117–140.

Kovaleski, A. P., and Londo, J. P. (2019). Tempo of gene regulation in wild and cultivated *Vitis* species shows coordination between cold deacclimation and budbreak. *Plant Sci.* 287:110178. doi: 10.1016/j.plantsci.2019.110178

Krauss, P., Markstädter, C., and Riederer, M. (1997). Attenuation of UV radiation by plant cuticles from woody species. *Plant Cell Environ.* 20, 1079–1085. doi: 10.1111/j.1365-3040.1997.tb00684.x

Łaźniewska, J., Macioszek, V. K., and Kononowicz, A. K. (2012). Plant-fungus interface: the role of surface structures in plant resistance and susceptibility to pathogenic fungi. *Physiol. Mol. Plant Pathol.* 78, 24–30. doi: 10.1016/j.pmpp.2012.01.004

Lee, B., and Priestley, J. H. (1924). The plant cuticle I its structure, distribution, and function. *Ann. Bot.* os-38, 525–545. doi: 10.1093/oxfordjournals.aob.a089915

Lee, S. B., Yang, S. U., Pandey, G., Kim, M.-S., Hyoung, S., Choi, D., et al. (2019). Occurrence of land-plant-specific glycerol-3-phosphate acyltransferases is essential for cuticle formation and gametophore development in *Physcomitrella patens*. *New Phytol.* 225, 2468–2483. doi: 10.1111/nph.16311

Lendzian, K. J. (1982). Gas permeability of plant cuticles: oxygen permeability. *Planta* 155, 310–315. doi: 10.1007/BF00429457

Lendzian, K. J., and Kerstiens, G. (1991). "Sorption and transport of gases and vapors in plant cuticles" in *Reviews of environmental contamination and toxicology: Continuation of residue reviews*. ed. G. W. Ware (New York: Springer), 65–128.

Liu, F., Jensen, C. R., and Andersen, M. N. (2003). Hydraulic and chemical signals in the control of leaf expansion and stomatal conductance in soybean exposed to drought stress. *Funct. Plant Biol.* 30, 65–73. doi: 10.1071/FP02170

Loveys, B. R. (1977). The intracellular location of abscisic acid in stressed and non-stressed leaf tissue. *Physiol. Plant.* 40, 6–10. doi: 10.1111/j.1399-3054.1977.tb01483.x

Martin, L. B. B., Romero, P., Fich, E. A., Domozych, D. S., and Rose, J. K. C. (2017). Cuticle biosynthesis in tomato leaves is developmentally regulated by abscisic acid. *Plant Physiol.* 174, 1384–1398. doi: 10.1104/pp.17.00387

Mayr, S. (2007). "Limits in water relations" in *Trees at their upper limit: Treelife limitation at the alpine timberline*. eds. G. Wieser and M. Tausz (Netherlands: Springer), 145–162.

McAdam, S. (2015). Physicochemical quantification of abscisic acid levels in plant tissues with an added internal standard by ultra-performance liquid chromatography. *Bio. Protoc.* 5:e1599. doi: 10.21769/BioProtoc.1599

Medeiros, C. D., Falcão, H. M., Almeida-Cortez, J., Santos, D. Y. A. C., Oliveira, A. F. M., and Santos, M. G. (2017). Leaf epicuticular wax content changes under different rainfall regimes, and its removal affects the leaf chlorophyll content and gas exchanges of *Aspidosperma pyrifolium* in a seasonally dry tropical forest. *S. Afr. J. Bot.* 111, 267–274. doi: 10.1016/j.sajb.2017.03.033

Miyazawa, S.-I., Makino, A., and Terashima, I. (2003). Changes in mesophyll anatomy and sink-source relationships during leaf development in *Quercus glauca*, an evergreen tree showing delayed leaf greening. *Plant Cell Environ.* 26, 745–755. doi: 10.1046/j.1365-3040.2003.01011.x

Nadeau, J. A., and Sack, F. D. (2002). Stomatal development in arabidopsis. *Arabidopsis Book* 1:e0066. doi: 10.1199/tab.0066

Neinhuis, C., Koch, K., and Barthlott, W. (2001). Movement and regeneration of epicuticular waxes through plant cuticles. *Planta* 213, 427–434. doi: 10.1007/s004250100530

Onoda, Y., Richards, L., and Westoby, M. (2012). The importance of leaf cuticle for carbon economy and mechanical strength. *New Phytol.* 196, 441–447. doi: 10.1111/j.1469-8137.2012.04263.x

Pantin, F., Renaud, J., Barbier, F., Vavasseur, A., Le Thiec, D., Rose, C., et al. (2013). Developmental priming of stomatal sensitivity to abscisic acid by leaf microclimate. *Curr. Biol.* 23, 1805–1811. doi: 10.1016/j.cub.2013.07.050

Pantin, F., Simonneau, T., and Muller, B. (2012). Coming of leaf age: control of growth by hydraulics and metabolics during leaf ontogeny. *New Phytol.* 196, 349–366. doi: 10.1111/j.1469-8137.2012.04273.x

Pereira, S., Figueiredo-Lima, K., Oliveira, A. F. M., and Santos, M. G. (2019). Changes in foliar epicuticular wax and photosynthesis metabolism in evergreen woody species under different soil water availability. *Photosynthetica* 57, 192–201. doi: 10.32615/ps.2019.013

Raven, J. A. (1984). Physiological correlates of the morphology of early vascular plants. *Bot. J. Linn. Soc.* 88, 105–126. doi: 10.1111/j.1095-8339.1984.tb01566.x

Ren, Z., and Sucoff, E. (1995). Water movement through *Quercus rubra* I. leaf water potential and conductance during polycyclic growth. *Plant Cell Environ.* 18, 447–453. doi: 10.1111/j.1365-3040.1995.tb00379.x

Renzaglia, K. S., Villarreal, J. C., Piatkowski, B. T., Lucas, J. R., and Merced, A. (2017). Hornwort stomata: architecture and fate shared with 400-million-year-old fossil plants without leaves. *Plant Physiol.* 174, 788–797. doi: 10.1104/pp.17.00156

Salmon, Y., Lintunen, A., Dayet, A., Chan, T., Dewar, R., Vesala, T., et al. (2020). Leaf carbon and water status control stomatal and nonstomatal limitations of photosynthesis in trees. *New Phytol.* 226, 690–703. doi: 10.1111/nph.16436

Sansberro, P. A., Mroginski, L. A., and Bottini, R. (2004). Foliar sprays with ABA promote growth of *Ilex paraguariensis* by alleviating diurnal water stress. *Plant Growth Regul.* 42, 105–111. doi: 10.1023/B:GROW.0000017476.12491.02

Šantrůček, J., Šimáňová, E., Karbulková, J., Šimková, M., and Schreiber, L. (2004). A new technique for measurement of water permeability of stomatous cuticular membranes isolated from *Hedera helix* leaves. *J. Exp. Bot.* 55, 1411–1422. doi: 10.1093/jxb/erh150

Sargent, C. (1976). The occurrence of a secondary cuticle in *Libertia elegans* (Iridaceae). *Ann. Bot.* 40, 355–359. doi: 10.1093/oxfordjournals.aob.a085138

Schreiber, L. (2005). Polar paths of diffusion across plant cuticles: new evidence for an old hypothesis. *Ann. Bot.* 95, 1069–1073. doi: 10.1093/aob/mci122

Schreiber, L., and Riederer, M. (1996). Ecophysiology of cuticular transpiration: comparative investigation of cuticular water permeability of plant species from different habitats. *Oecologia* 107, 426–432. doi: 10.1007/BF00333931

Schultz, H. R., and Matthews, M. A. (1993). Growth, osmotic adjustment, and cell-wall mechanics of expanding grape leaves during water deficits. *Crop Sci.* 33, 287–294. doi: 10.2135/cropsci1993.0011183X003300020015x

Serna, L., and Fenoll, C. (1997). Tracing the ontogeny of stomatal clusters in arabidopsis with molecular markers. *Plant J.* 12, 747–755. doi: 10.1046/j.1365-313X.1997.12040747.x

Shackel, K., Matthewes, M., and Morrison, J. (1987). Dynamic relation between expansion and cellular turgor in growing grape (*Vitis vinifera* L.) leaves. *Plant Physiol.* 84, 1166–1171. doi: 10.1104/pp.84.4.1166

Siebrecht, S., Herdel, K., Schurr, U., and Tischner, R. (2003). Nutrient translocation in the xylem of poplar—diurnal variations and spatial distribution along the shoot axis. *Planta* 217, 783–793. doi: 10.1007/s00425-003-1041-4

Tomlinson, P. T., Dickson, R. E., and Isebrands, J. G. (1991). Acropetal leaf differentiation in *Quercus rubra* (*Fagaceae*). *Am. J. Bot.* 78, 1570–1575. doi: 10.1002/j.1537-2197.1991.tb11436.x

Yeats, T. H., and Rose, J. K. C. (2013). The formation and function of plant cuticles. *Plant Physiol.* 163, 5–20. doi: 10.1104/pp.113.222737

Conflict of Interest: The authors declare that the research was conducted in the absence of any commercial or financial relationships that could be construed as a potential conflict of interest.

frontiers in Plant Science

ORIGINAL RESEARCH
published: 25 June 2020
doi: 10.3389/fpls.2020.00897

Heterogeneity of Stomatal Pore Area Is Suppressed by Ambient Aerosol in the Homobaric Species, *Vicia faba*

David A. Grantz[1,2]*, *Marcus Karr*[1] *and Juergen Burkhardt*[2]

[1] Department of Botany and Plant Sciences, Kearney Agricultural Center, University of California, Riverside, Riverside, CA, United States, [2] Institute of Crop Science and Resource Conservation, University of Bonn, Bonn, Germany

Stomatal pore area is heterogeneous across leaf surfaces. This has been considered as "patchy stomatal conductance," and may have substantial implications for photosynthetic efficiency. Aerosols have always been important elements of plant environments, but their effects on stomatal control of plant water relations, and stomatal heterogeneity specifically, have not been considered. Here we evaluate the spatial coordination of pore area in the glabrous and homobaric leaves of *Vicia faba* grown under two aerosol treatments and measured at four levels of VPD. We construct a large dataset (n > 88,000 discrete comparisons) of paired pore areas and distances between the pores. Plants were grown in ambient urban air and in filtered air (FA) to determine the effect of ambient aerosol on stomatal properties. Pore area exhibited spatial organization, as well as considerable variability among closely co-located pores. The difference between pore areas was positively correlated with the distance between the pores, in both aerosol treatments and at all VPDs. However, aerosol deposition reduced both the magnitude of variability between pores and the rate at which this variability increased with pore separation distance. These data support previous conclusions that deposition of hygroscopic aerosol may create a thin aqueous film across the leaf surface that connects neighboring stomata to each other and to the leaf interior. Aerosol impacts on stomatal heterogeneity and gas exchange are not adequately considered in current assessments of stomatal control.

Keywords: aerosol, climate change, gas exchange, humidity, particulate matter, patchy stomata, vapor pressure deficit

OPEN ACCESS

Edited by:
Graham Dow,
ETH Zürich, Switzerland

Reviewed by:
Dimitrios Fanourakis,
Technological Educational Institute of Crete, Greece
Andreas M. Savvides,
Agricultural Research Institute, Cyprus
Peter Lehmann,
ETH Zürich, Switzerland

***Correspondence:**
David A. Grantz
dagrantz@ucanr.edu

Specialty section:
This article was submitted to Plant Development and EvoDevo, a section of the journal Frontiers in Plant Science

Received: *13 December 2019*
Accepted: *02 June 2020*
Published: *25 June 2020*

Citation:
Grantz DA, Karr M and Burkhardt J (2020) Heterogeneity of Stomatal Pore Area Is Suppressed by Ambient Aerosol in the Homobaric Species, Vicia faba. Front. Plant Sci. 11:897. doi: 10.3389/fpls.2020.00897

INTRODUCTION

Heterogeneous stomatal opening across the surface of individual leaves may result in stomatal "patchiness," random variation, or spatially coherent trends in pore area across the surface. Stomatal heterogeneity has been observed in many species (Downton et al., 1988, 1990; Terashima et al., 1988; Sharkey and Seemann, 1989; Terashima, 1992; Pospisilova and Santrucek, 1994; Haefner et al., 1997; Weyers and Lawson, 1997; Beyschlag and Eckstein, 1998; Mott and Buckley, 1998, 2000). Non-uniform pore areas and resulting uneven conductance for CO_2 and water vapor complicate standard measurements and calculations of gas exchange parameters. Heterogeneity

observed at all stages of leaf elongation in *Rosa* shows that this is not a transient developmental feature (Fanourakis et al., 2015). Under conditions of high boundary layer conductance, stomatal heterogeneity may be detrimental to gas exchange efficiency, but under conditions of low wind or large leaves, which reduce boundary layer conductance, and under conditions of low overall stomatal conductance, heterogeneity may improve photosynthetic efficiency (Buckley et al., 1999). This reflects the effects of evaporative cooling of the leaf on fluxes and gradients of both water and CO_2, and the transport efficiency of those pores that remain widely open. The significance and ubiquity of stomatal heterogeneity and its relationship with environmental conditions (Cheeseman, 1991; Gunasekera and Berkowitz, 1992; Cardon et al., 1994) as well as the role of aerosol deposition (Burkhardt and Grantz, 2017) in generating such heterogeneity have not been adequately considered.

Areas of coordinated stomatal behavior may range from a few mm to a few cm in extent (Terashima, 1992; Mott and Buckley, 1998, 2000; Mott and Peak, 2007) and are often bounded by veins, particularly in heterobaric leaves (Siebke and Weis, 1995; Haefner et al., 1997; Weyers and Lawson, 1997; Mott and Buckley, 2000). Patterns of heterogeneity can be transient, with patches of coherent stomatal response migrating within and even between areoles of heterobaric leaves (Kamakura et al., 2012), even though gas diffusion is restricted to areoles defined by vasculature with bundle sheath extensions (Terashima, 1992; Mott and Buckley, 2000).

Spatially coherent stomatal behavior is also observed in homobaric leaves (Kappen et al., 1987; Loreto and Sharkey, 1990; Mott and Parkhurst, 1991; Terashima, 1992; Eckstein et al., 1996; Mott and Buckley, 2000; Kamakura and Furukawa, 2008). This heterogeneity is less patchy and more characterized by trends across the leaf surface, from leaf base to tip (Nardini et al., 2008), margin to midrib (Weyers and Lawson, 1997), and more generally across the lamina (Terashima et al., 1988). Patches observed as $^{14}CO_2$ fixation in homobaric *V. faba* (Terashima et al., 1988) were larger than in many heterobaric species and could be considered gradients across the leaf, with greater heterogeneity within the patches than in heterobaric species (Spence, 1987; Terashima et al., 1988). Stomatal aperture in homobaric *Commelina communis* (Smith et al., 1989) exhibited gradients as high as 3 μm per mm and 20 μm from leaf edge to midrib. This behavior may be observed even in epidermal peels exposed to uniform physical and chemical conditions. The distribution of pore opening often approximates a normal distribution (e.g., *V. faba*; Laisk et al., 1980). This variance within and between leaves obscures spatial patterns across individual leaves (Weyers and Lawson, 1997), so that heterogeneity in homobaric leaves remains poorly characterized.

Uneven levels of conductance across the surfaces of individual leaves have been associated with discrepancies in estimation of intercellular CO_2 (C_i). Values calculated from measured fluxes of CO_2 and water vapor exceeded directly measured values by up to 15% (Buckley et al., 1999; Boyer, 2015a,b; Hanson et al., 2016). This suggested a pathway for water efflux that was unavailable to CO_2 influx, potentially peristomatal transpiration from around the stomatal pores (Maier-Maercker, 1983; Grantz, 1990), or cuticular transpiration from across the epidermis between the pores (Kerstiens, 1996; Boyer et al., 1997; Hanson et al., 2016). Alternatively, stomatal heterogeneity could distort the calculation of C_i (Terashima et al., 1988) as measurements of steady state gas exchange reflect the leaf-wise average of highly dynamic heterogeneous individual pores and patches of pores (Siebke and Weis, 1995).

Increased evaporative demand (leaf to air vapor pressure difference; VPD) reduces stomatal conductance and increases stomatal heterogeneity (Sharkey and Seemann, 1989; Downton et al., 1990; Haefner et al., 1997). Experimentally imposed local changes in humidity at the leaf surface altered the apertures of stomata within the affected area, and those of stomata up to 0.4 cm away, outside of the directly affected area. The linkage was apparently through epidermal turgor, although this mechanism may operate most effectively over short distances (Haefner et al., 1997; Mott et al., 1997, 1999; Mott and Franks, 2001). Variability in mesophyll biochemistry (Osmond et al., 1999) and xylem water relations may become more effective at larger scales of leaf or branch (Buckley and Mott, 2000).

Aerosol deposition (Burkhardt and Grantz, 2017) may affect both the asymmetric flux pathways for water and CO_2 (Grantz et al., 2018) and stomatal heterogeneity. Deposition of hygroscopic, particularly chaotropic, aerosol (Tsigaridis et al., 2006; Pringle et al., 2010; Burkhardt and Grantz, 2017) reduces surface tension and results in development of thin liquid films on leaf surfaces (Eiden et al., 1994; Dutcher et al., 2010; Burkhardt and Hunsche, 2013; Burkhardt and Grantz, 2017; Fernandez et al., 2017). The liquid films penetrate into stomatal pores (Eichert et al., 1998, 2008; Basi et al., 2014; Kaiser, 2014), providing a liquid phase linkage between the saturated leaf apoplast and the dry atmosphere. This pathway is not under diffusional (i.e., stomatal) control and thus water loss from this pathway through evaporation at the leaf surface increases as VPD increases, even in species such as *V. faba* that exhibit strong closing response to increasing VPD (Pariyar et al., 2013; Grantz et al., 2018). The presence of liquid films can be visualized by electrical conductance measurements (Burkhardt and Eiden, 1994; Burkhardt et al., 1999; Burkhardt and Hunsche, 2013) and by electron micrography (Burkhardt and Grantz, 2017; Burkhardt et al., 2018; Grantz et al., 2018). Aerosol deposition reduces stomatal apertures (Burkhardt et al., 2001a; Burkhardt, 2010; Burkhardt and Grantz, 2017; Grantz et al., 2018) while increasing both water flux (Burkhardt et al., 2001a; Grantz et al., 2018) and minimum (cuticular) leaf conductance (Burkhardt and Pariyar, 2014, 2016; Grantz et al., 2018).

We hypothesized that aerosol-induced surface moisture may link individual pores across the leaf surface by providing a more homogeneous hydraulic and vapor pressure environment, thereby reducing stomatal heterogeneity despite potential desiccating effects of liquid phase water loss and the previously documented reduction in pore area (Grantz et al., 2018). Here we characterize the distribution of stomatal pore areas, a subject of previous consideration (Laisk et al., 1980; Spence, 1987; Gorton et al., 1989; Terashima, 1992; Weyers and Lawson, 1997) and the role of aerosol deposition on this heterogeneity, which has not

previously been considered. We analyze a previously available dataset of 3600 direct microscopic pore area measurements (Grantz et al., 2018) to create a novel database of 88,200 discrete pore to pore comparisons of distances between the pores (d) and the differences between their pore areas (ΔA). We evaluate the distribution of pore areas, the local and larger scale heterogeneity of stomatal opening, and the effect of four levels of VPD and two levels of ambient aerosol on these characteristics.

MATERIALS AND METHODS

Plant Material

Plants of *Vicia faba* (L.) were grown from seed as described previously (Grantz et al., 2018) in plastic pots in greenhouses at the University of Bonn, Germany. Plants received complete nutrient solution (Ferty 3, Planta Düngemittel GmbH, Hohenstauf, Germany) weekly and irrigation as needed.

Plants were randomly assigned either to a greenhouse ventilated with ambient air (AA) or an adjacent greenhouse ventilated with filtered air (FA). Filtration removed nearly all particles (Pariyar et al., 2013; Grantz et al., 2018). The aerosol was typical of ambient particulate matter in central Europe (about 35% ionic; see Grantz et al., 2018 and references therein). Aerosol concentration in the AA greenhouse (cloud chamber condensation nuclei counter; TSI 3783; TSI, Shoreview, MN, United States) was 6–7 $\times$ 10^9 particles m^{-3}. This was reduced in the FA greenhouse by 99% to 5–10 $\times$ 10^6 m^{-3}; confirming previous measurements (e.g., Pariyar et al., 2013). Other environmental parameters including temperature, relative humidity and concentrations of ozone were similar in the greenhouses (see Supplementary Figures S1, S2 in Grantz et al., 2018). Plants were exposed to natural daylength and sunlight (approximately 70% of ambient irradiance).

Measurements were obtained 5 weeks after planting on one leaflet of leaf 5 or 6 (youngest fully expanded; mean leaflet area about 32 cm^2) when plants had been exposed for 3–4 weeks in the greenhouses. Leaflets remained attached to intact plants during all measurements.

Measurement of Pore Area at Controlled VPD

Plants were transported from Bonn to Kiel, Germany. Pore area measurements (see Grantz et al., 2018 for further details) were obtained while leaf to air VPD was controlled in a flow-through gas exchange system with an integrated inverted video microscope (Kaiser and Kappen, 1997, 2000; Kaiser, 2009). The gas exchange cuvette was held at constant temperature (25°C $\pm$ 0.1°C) and irradiance (PPFD = 450 $\pm$ 25 μmol m^{-2} s^{-1}). Dew point was held at 23.15, 19.0, 14.0, and 5.0°C (±0.05°C), yielding VPD of 0.33, 0.97, 1.6, and 2.3 kPa and RH of 90%, 68%, 50%, and 27%, at abaxial leaf temperature (25°C; Type K thermocouple, 0.075 mm). Air circulation in the cuvette (1 m s^{-1}) yielded laminar boundary layer conductance of 1300 mmol m^{-2} s^{-1} (Kaiser, 2009).

Nine plants were used for each of the AA and FA treatments (Experiment 1, Grantz et al., 2018). Measurements on plants subjected to the two aerosol treatments were alternated on successive days. Pore area was measured on 50 stomata per leaflet, on the abaxial surface, within the 1 cm^2 area of a predefined grid. The sample area was located away from major veins and leaf margins. The 50 stomata represented about 0.2% of the stomata in the 1 cm^2 viewing area. The location (pore center) and focus depth (narrowest part of the pore center) of each pore was stored electronically (Kaiser, 2009) to allow rapid re-imaging at each VPD.

Data Analysis

Data were stored with plant, leaf and pore identifiers, pore area, and pore coordinates in the Cartesian framework defined across the microscope stage (Kaiser, 2009). The area of each pore was determined as an idealized ellipse determined by the directly measured length and width of each pore, taken as the major and minor axes (Grantz et al., 2018). The difference in pore area (ΔA) between pairs of stomata was evaluated as a function of their separation distance (d) across the leaf surface.

Values of d were calculated from the coordinates of the center of each pore using the Pythagorean Theorem executed in a custom Python program (v. 3.6; Python Software Foundation[1]). Unique pair comparisons [C(50,2) = (50)(50-1)/2 = 1225 per leaflet] were evaluated. With 9 leaflets/aerosol treatment, 2 treatments, and 50 pores/leaflet, there were 900 unique pores and with 4 levels of VPD there were 88,200 unique comparisons of ΔA vs. d. The maximum value of d was about 1.4 cm, representing the diagonal of the 1 cm^2 square examined on each leaf.

Regressions of ΔA on d were calculated in Sigma Plot, v. 13.0 (Systat Software, San Jose, CA, United States; Regression Wizard). Normality [Kolmogorov–Smirnov (K–S) Test] and equality of variance (Brown–Forsythe Test) were generally not satisfied ($P < 0.050$). The sole exception was FA at low VPD, which was normally distributed. Mean ΔA (**Table 1**) and regression coefficients (**Table 2**) were evaluated by Two-Way ANOVA (Sigma Plot) with mean separation using the Holm-Sidak Multiple Range Test.

[1]https://www.python.org/

TABLE 1 | Means of the differences between pore areas (ΔA).

	Mean difference in pore area (ΔA; μm^2)		
VPD	**Ambient Air (AA)**	**Filtered Air (FA)**	**AA vs. FA**
0.33 kPa	37.6 ± 0.32 **(a)**	47.6 ± 0.37 **(b)**	$P < 0.001$
0.97 kPa	42.5 ± 0.36 **(c)**	56.1 ± 0.45 **(d)**	$P < 0.001$
1.6 kPa	43.6 ± 0.37 **(d)**	53.6 ± 0.43 **(c)**	$P < 0.001$
2.3 kPa	39.9 ± 0.39 **(b)**	45.7 ± 0.40 **(a)**	$P < 0.001$

Lower case letters within columns refer to differences between VPD levels within each aerosol treatment. P values in the right hand column refer to differences between aerosol treatments within VPD levels. Means were analyzed by Two-Way ANOVA with mean separation (right hand column) by the Holm-Sidak method. The ΔA × VPD interaction was generally significant.

RESULTS

Pore Location

The imaging system facilitated collection of a large number of clear photomicrographs (**Figure 1**). At all levels of stomatal opening, both within each VPD and across the levels of VPD, the pores were well characterized as ellipses, allowing the area (A) of each pore to be calculated from the directly measured length and width. Leaves of *V. faba* exhibited uniformly kidney-shaped guard cells (**Figure 1**), lacking specialized stomatal subsidiary cells and the bundle sheath extensions that play a role in stomatal patchiness in heterobaric species.

The distances (d) between pores were distributed approximately normally (**Figure 2**). Neither the shape of the distribution nor the magnitude of the distance scale differed between leaves exposed during leaf development to ambient aerosol (AA) or to FA (cf. **Figures 2A,B**). These characteristics were also stable across the levels of VPD (not shown), despite the potential for leaf shrinkage due to reduced leaf water content (not measured) at elevated VPD.

Pore Area

The large data set available for this study allowed a robust characterization of the distributions of pore area (A) in the two aerosol treatments over a range of VPDs (**Figure 3**). At low VPD (0.33 kPa) the distributions of A in both AA (**Figure 3A**) and FA (**Figure 3B**) treatments were approximately bell shaped, although only the FA treatment (**Figure 3B**) formally satisfied the Kolmogorov–Smirnov test for normality (K–S statistic of 0.661). All other distributions exhibited K–S < 0.001.

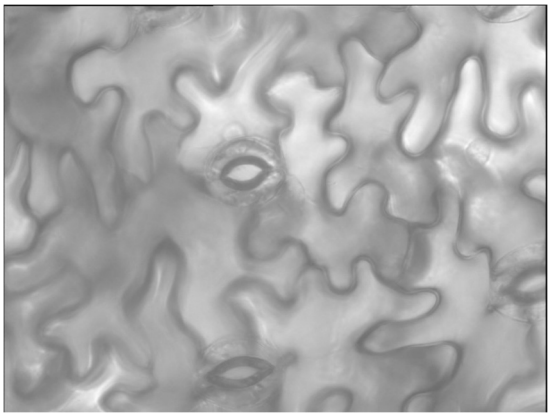

FIGURE 1 | Typical stomatal pores whose areas (A) were measured. Representative example at low VPD (0.33 kPa). Micrograph dimensions 300 × 300 μm.

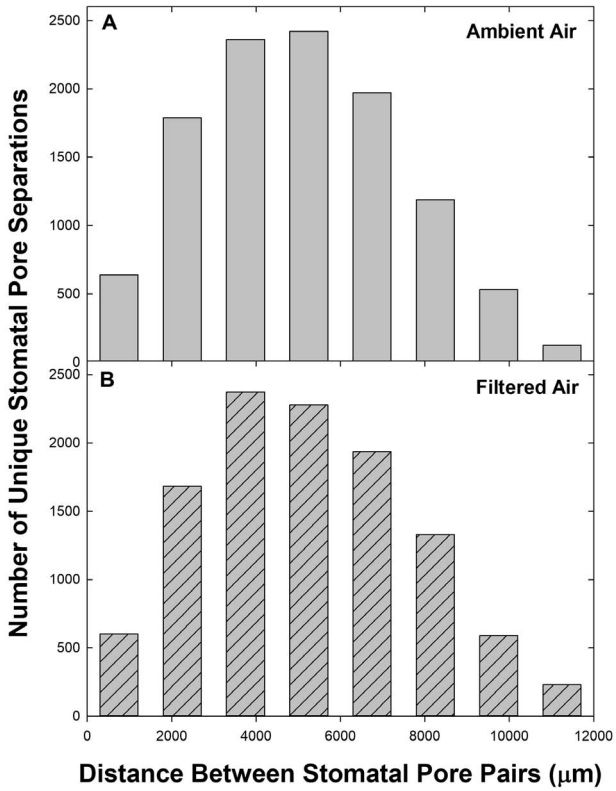

FIGURE 2 | Frequency distribution of pore separations (d) among the 50 stomata measured on each of 9 leaves (n = 11,025 per panel). Distance classes: $0 \leq d < 1500$ to $10500 \leq d < 12000$, centered at 750–11250. For $d \geq 12000$ (n = 20 for AA and 55 for FA) frequencies were pooled with $10500 \leq d < 12000$. **(A)** Ambient air; **(B)** filtered air.

TABLE 2 | Linear regression coefficients of the relationships between the difference in pore area (ΔA) and the distance between the pores (d).

VPD	Ambient Air (AA)	Filtered Air (FA)	AA vs. FA
(A) Intercept (μm²)			
0.33 kPa	35.2 ± 0.75 **(a)** [$P < 0.0001$]	40.4 ± 0.88 **(a)** [$P < 0.0001$]	$P < 0.001$
0.97 kPa	36.8 ± 0.85 **(a)** [$P < 0.0001$]	48.7 ± 1.07 **(b)** [$P < 0.0001$]	$P < 0.001$
1.6 kPa	41.0 ± 0.87 **(b)** [$P < 0.0001$]	48.2 ± 1.01 **(b)** [$P < 0.0001$]	$P < 0.001$
2.3 kPa	36.6 ± 0.93 **(a)** [$P < 0.0001$]	44.4 ± 0.94 **(c)** [$P < 0.0001$]	$P < 0.001$
(B) Slope (μm² cm⁻¹)			
0.33 kPa	4.6 ± 1.34 **(a)** Adj r^2 = 0.0010 [P = 0.0007]	13.6 ± 1.50 **(a)** Adj r^2 = 0.0072 [$P < 0.0001$]	$P < 0.001$
0.97 kPa	11.1 ± 1.51 **(b)** Adj r^2 = 0.0048 [$P < 0.0001$]	14.1 ± 1.84 **(a)** Adj r^2 = 0.0052 [$P < 0.0001$]	P = 0.208
1.6 kPa	5.1 ± 1.55 **(a)** Adj r^2 = 0.0009 [P = 0.001]	10.3 ± 1.74 **(a)** Adj r^2 = 0.0031 [$P < 0.0001$]	P = 0.026
2.3 kPa	6.4 ± 1.66 **(ab)** Adj r^2 = 0.0013 [P = 0.0001]	2.5 ± 1.62 **(b)** Adj r^2 = 0.0001 [P = 0.1188]	P = 0.093

P values in brackets refer to the individual regression coefficients. Lower case letters within columns refer to differences between VPD levels within each aerosol treatment. P values in the right hand column refer to differences between coefficients for each aerosol treatment within VPD levels. Coefficients were analyzed by Two-Way ANOVA with mean separation by the Holm-Sidak method.

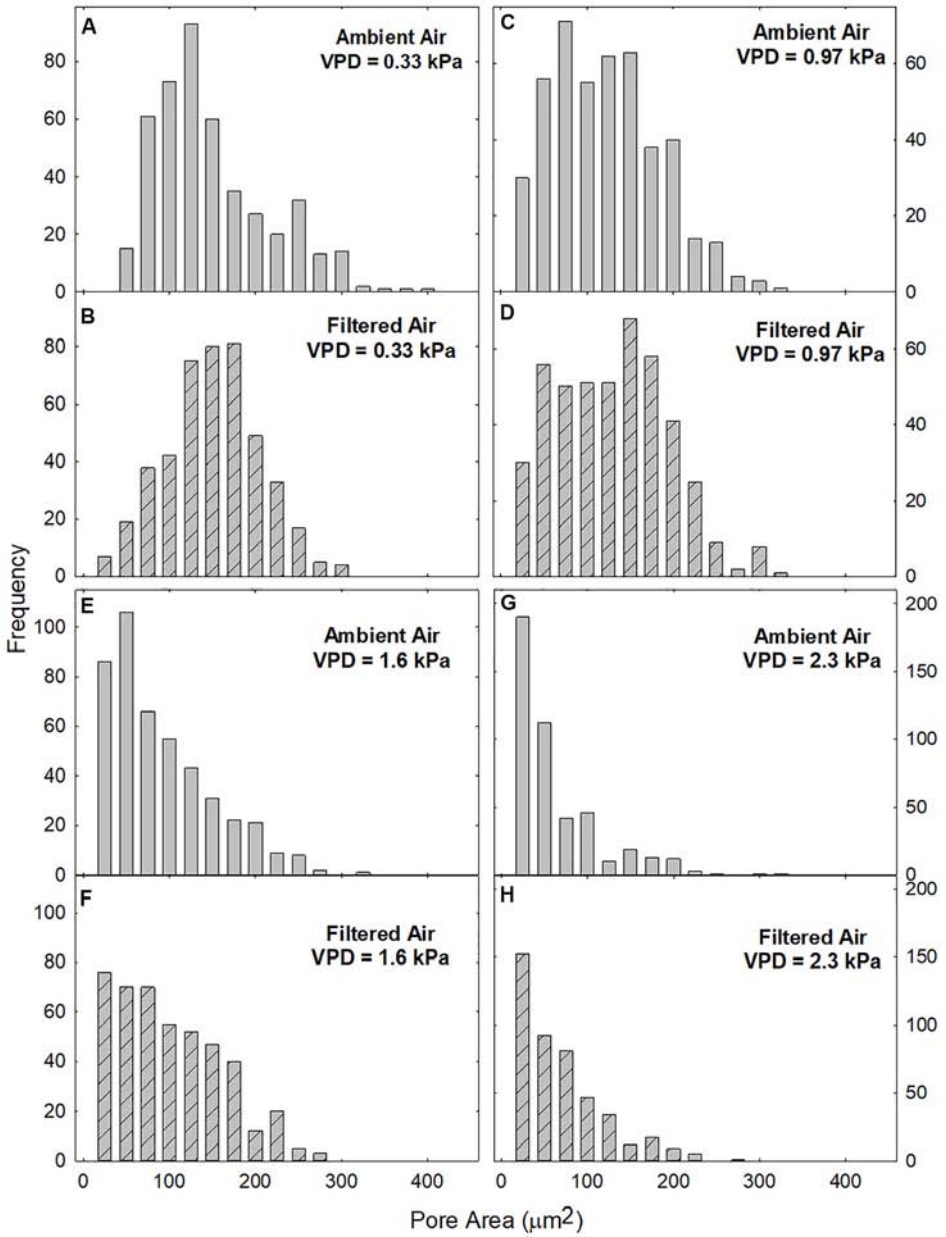

FIGURE 3 | Frequency distribution of pore areas (A) at different levels of evaporative demand (VPD), in leaves exposed to ambient (gray bars; **A,C,E,G**) or filtered (hatched bars; **B,D,F,H**) air. Area classes: $0 \leq A < 50$ to $400 \leq A < 450$, centered at 25–425. The smallest visible bars represent 1 pore.

The distributions of A were similar in AA and FA leaves at all levels of VPD (cf. **Figures 3A–H**). VPD did not differ during plant growth between the AA and FA treatments but was varied experimentally during measurement of pore areas. Skewing toward the origin increased with VPD (**Figure 3**) so that the quasi-bell shaped distribution was no longer evident at 1.6 kPa (**Figures 3E,F**) or 2.3 kPa (**Figures 3G,H**) in either aerosol treatment.

In most cases, increasing VPD reduced pore area, i.e., with greater deviation below the 1:1 line (**Figure 4**). In FA at 0.97 kPa the pattern was different. The less open pores closed in response to increased VPD, but pores initially exhibiting $A > 190\ \mu m^2$ (**Figure 4A**; red circles) did not close below the initial A. Individual stomata behaved consistently over the range of VPDs. Those with small pore areas at 0.33 kPa exhibited small areas at higher VPD. Many that were only slightly open at low VPD closed completely at higher VPD. With increasing VPD, the number of such stomata and their initial pore areas increased (horizontal part in lower left end of each curve; **Figure 4**).

Leaves exposed to ambient aerosol also exhibited greater skewing toward the origin. This reduction in magnitude was

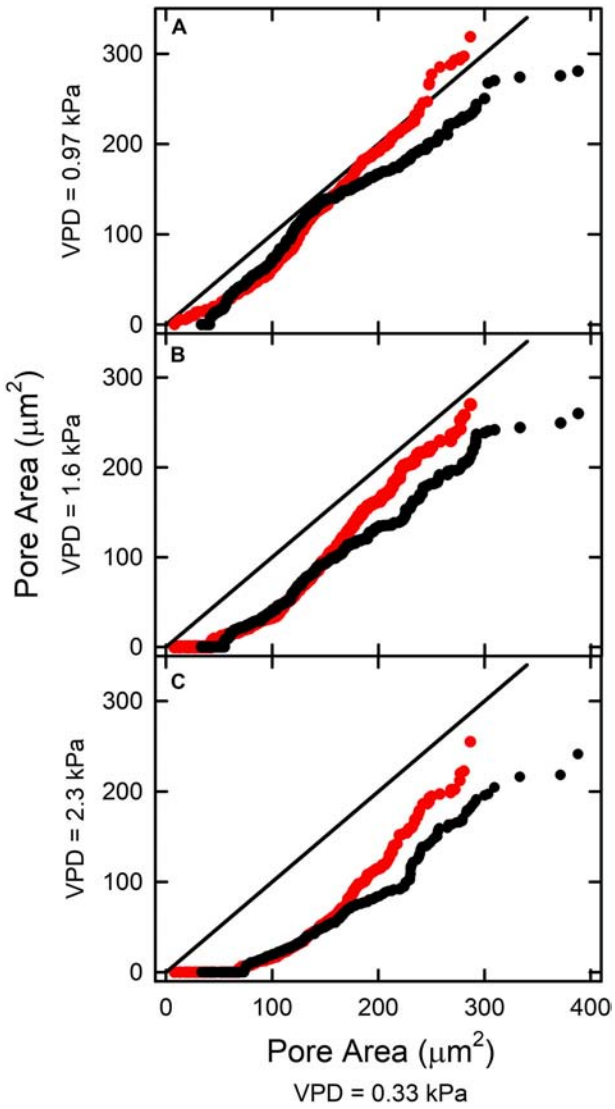

FIGURE 4 | The relationship between stomatal pore area at elevated VPD [**(A)** 0.97 kPa; **(B)** 1.6 kPa; **(C)** 2.3 kPa] and pore area measured at low VPD (0.33 kPa). The AA treatment is shown in black, and the FA treatment in red. The solid line represents the 1:1 line.

reflected in reduced mean ΔA between pores in AA relative to FA observed at all levels of VPD (**Table 1**). In general, the AA treatment closed more substantially than the FA as VPD was increased, particularly at greater initial pore area at low VPD (**Figure 4**). Among stomata with areas below 180 μm^2 at 0.33 kPa, there was little effect of aerosol on the relationships between pore area at low VPD and at higher VPD. This point of divergence between AA and FA was similar at all VPD (**Figures 4A–C**). Above this value of initial opening, pore areas in FA and AA diverged, with AA smaller than FA. This was observed from 0.33 kPa to 0.97 kPa (**Figure 4A**), even though the response of FA to VPD was minimal among the more open pores. The sensitivity to aerosol increased with pore area observed at low VPD, but did not change substantially with increasing VPD.

Stomatal Heterogeneity

We had hypothesized that stomatal heterogeneity, both ΔA between closely co-located pores and the increase of ΔA with d between more distant pores, would be reduced by aerosol deposition. The suggested mechanism, involving liquid films on the leaf surface, is illustrated in **Figure 5** showing an open stoma at the left and a closed stoma at the right. Regardless of pore area, water evaporates from the surface of the leaf (blue arrows), potentially drawing both from the surface water (**Figure 5**; blue lines) and from soil, tissue, and apoplastic storage (continuity indicated by green lines). Conventional transpiration from the apoplast (green arrows) occurs through the open pore (left side) but this diffusive transport is almost completely blocked by stomatal closure (right side).

In contrast, a continuous liquid film developing from deliquescence of deposited hygroscopic aerosol may spread across large areas of the leaf and penetrate into the stomatal pores. This liquid path through the pore reduces stomatal control of water loss. This may degrade epidermal water status by enhancing water loss, while also reducing the variability in the hydraulic and humidity environments across the leaf surface (**Figure 5**). While reduced epidermal water content might increase stomatal heterogeneity, the uniform environment under the liquid film might lead to more uniform epidermal water status and reduce heterogeneity.

We observed a reduction in heterogeneity in the ambient aerosol treatment. The intercept of ΔA on d was significantly lower in AA than FA at all VPD (**Table 2A**), reflecting reduced heterogeneity among closely co-located pores (extrapolated to zero separation). Exposure to aerosol also significantly reduced both mean ΔA (**Table 1** and **Figure 6**) and median ΔA (**Figure 7**) at all levels of VPD. The considerable local variability is illustrated by the closely positioned pores in **Figure 1**, exhibiting ΔA of about 25% despite the guard cells bordering on the same epidermal cell.

Although there were fewer pores at small and large separations (**Figure 2**), the distributions of both mean ΔA (**Figure 6**) and median ΔA (**Figure 7**) revealed a consistent increase with d over the entire range. This was observed in both AA and FA leaves, but the increase in ΔA with d was reduced by aerosol (**Figures 6**, **7**). The slope of ΔA on d was significantly reduced in AA relative to FA at VPD of 0.33 kPa and 1.6 kPa (**Table 2B**; c.f. **Figures 6G,H**, **7G,H**). Slopes did not differ at 0.97 kPa or 2.3 kPa. This reflects a general reduction in the increase in heterogeneity with distance within the 1 cm^2 sample area caused by aerosol exposure. The median analysis is presented, along with the mean, because the data often varied from normality.

The impact of VPD was less consistent. In AA, mean ΔA (**Table 1**) and the intercept of ΔA at $d = 0$ (**Table 2A**) increased with initial increase of VPD from 0.33 kPa through 0.97 to 1.6 kPa but declined at 2.3 kPa. In contrast, in FA, the mean and intercept of ΔA increased with VPD from 0.33 to 0.97 kPa, but began to decline at 1.6 kPa and declined further at 2.3 kPa. The pattern of response of ΔA over all pores (mean) and among closely spaced

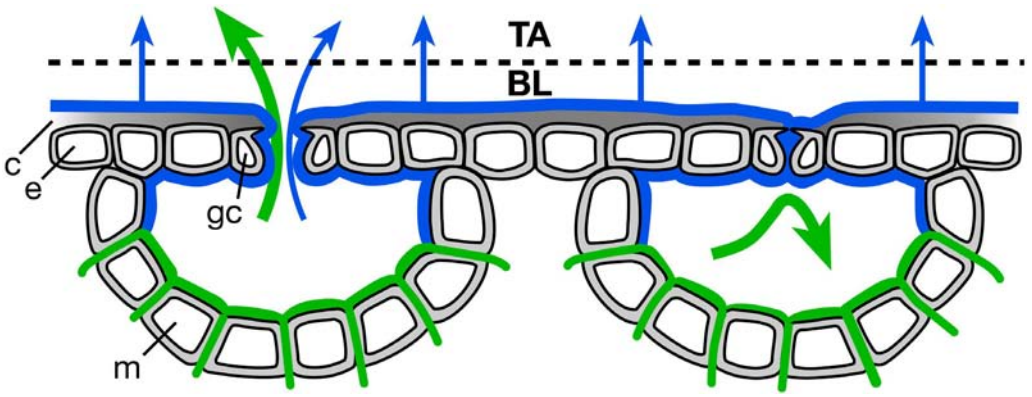

FIGURE 5 | The hypothesized role of thin liquid films in reducing microenvironmental variability across the leaf surface. Blue lines represent liquid formed by condensation to deposited hygroscopic aerosol on the leaf surface, including that which penetrates the stomatal pores; blue arrows represent the evaporative flux of water derived from this liquid. Green lines represent conventional apoplastic liquid water derived from the soil-root-xylem pathway passing through and around mesophyll cells (m); green arrows represent the much larger evaporative flux of this water when stomata are open (left side) and its elimination by stomatal closure (right side). Evaporation occurs from aerosol-condensed water with both open (left side) and closed (right side) stomata, as liquid continuity between leaf interior and exterior is maintained largely independently of stomatal pore area determined by guard cell (gc) turgor. The leaf boundary layer (BL) is uniformly humidified across the leaf surface and the osmotic environment of the cuticle (c) and underlying epidermis (e) is made more homogeneous by the presence of a liquid film. All fluxes (blue and green arrows) eventually pass through the BL and enter the mixed free atmosphere (TA), representing water loss from the leaf.

pores (intercept) was similar in the aerosol treatments, but the decline began at lower VPD in the absence of aerosol. In contrast, the slope of ΔA on d, reflecting larger scale heterogeneity, did not differ consistently between levels of VPD (**Table 2B**).

Heterogeneity of stomatal pore area was composed of two components, variability among pore areas that was not related to the distance between the pores (**Table 2A**; left-most bars, **Figures 6**, **7**), and variability which trended systematically with d (**Table 2B**; distributions, **Figures 6**, **7**). The first type of variability was expressed both as local heterogeneity between closely co-located pores, and as a component of the magnitude of ΔA between more distant pores. Large values of ΔA (>35 μm^2) were observed among neighboring pores in both AA and FA. In all cases, local variability in ΔA among neighboring pores was greater than the increase in ΔA with d across the observation area of 1.4 cm (**Figures 6**, **7**).

DISCUSSION

This study had two objectives, to characterize the distribution of individual pore areas over a range of VPD levels, and to elucidate the role of ambient aerosol in stomatal regulation of plant water relations. The first objective is advanced through analysis of an unusually large number of non-destructively imaged pore areas, acquired previously (Grantz et al., 2018). Previous experiments have approached this objective by imaging many fewer pores, either the same pores repeated over time in epidermal peels (Gorton et al., 1989) or different pores at different times in leaf impressions (Smith et al., 1989). We advance the second objective with a novel analysis of aerosol impacts on stomatal heterogeneity. We showed previously that transpiration per unit stomatal aperture and minimum leaf conductance both increased following aerosol deposition (Burkhardt et al., 2001a; Grantz et al., 2018). No previous analyses have considered whether aerosol deposition might also affect the uniformity of stomatal opening.

Pore Area Distribution

Stomatal opening is characterized by a strong element of randomness that often results in a quasi-normal (bell-shaped) distribution of pore areas (Gorton et al., 1989; Terashima, 1992; Weyers and Lawson, 1997). Our observations confirm earlier reports, including in *V. faba* (Laisk et al., 1980; Kappen et al., 1987; Spence, 1987), of large within-leaf variability with quasi-normally distributed pore areas, particularly at VPD = 0.33 kPa and 0.97 kPa. There was large heterogeneity even among nearly contiguous pores, as observed previously in *V. faba* and other species. For example, adjacent stomata of homobaric tobacco (*Nicotiana tabacum*) ranged from fully closed to fully open (Pospisilova and Santrucek, 1994).

At higher VPD (1.6 kPa and 2.3 kPa), the distributions skewed toward the origin, with a larger proportion of closed pores and reduced mean and median values, as described previously (Grantz, 1990; Grantz et al., 2018). These highly skewed distributions may also belong to theoretically normal distributions that extend into the imaginary territory of negative pore area (Laisk et al., 1980). The maintenance of the bell-shaped distribution even as mean and median pore area declined, reflects synchronous, parallel, and potentially coordinated responses, of similar magnitude by pores of different initial areas and in different locations across the leaf (Saxe, 1979; Spence et al., 1983; Kappen et al., 1987; Spence, 1987). This coherent behavior resembles an emergent property (Mott and Buckley, 2000; Mott and Peak, 2007) but the mechanism of such coordination remains unknown. Elevated VPD increases transpiration and degrades epidermal water status, suggesting metabolic and hydropassive

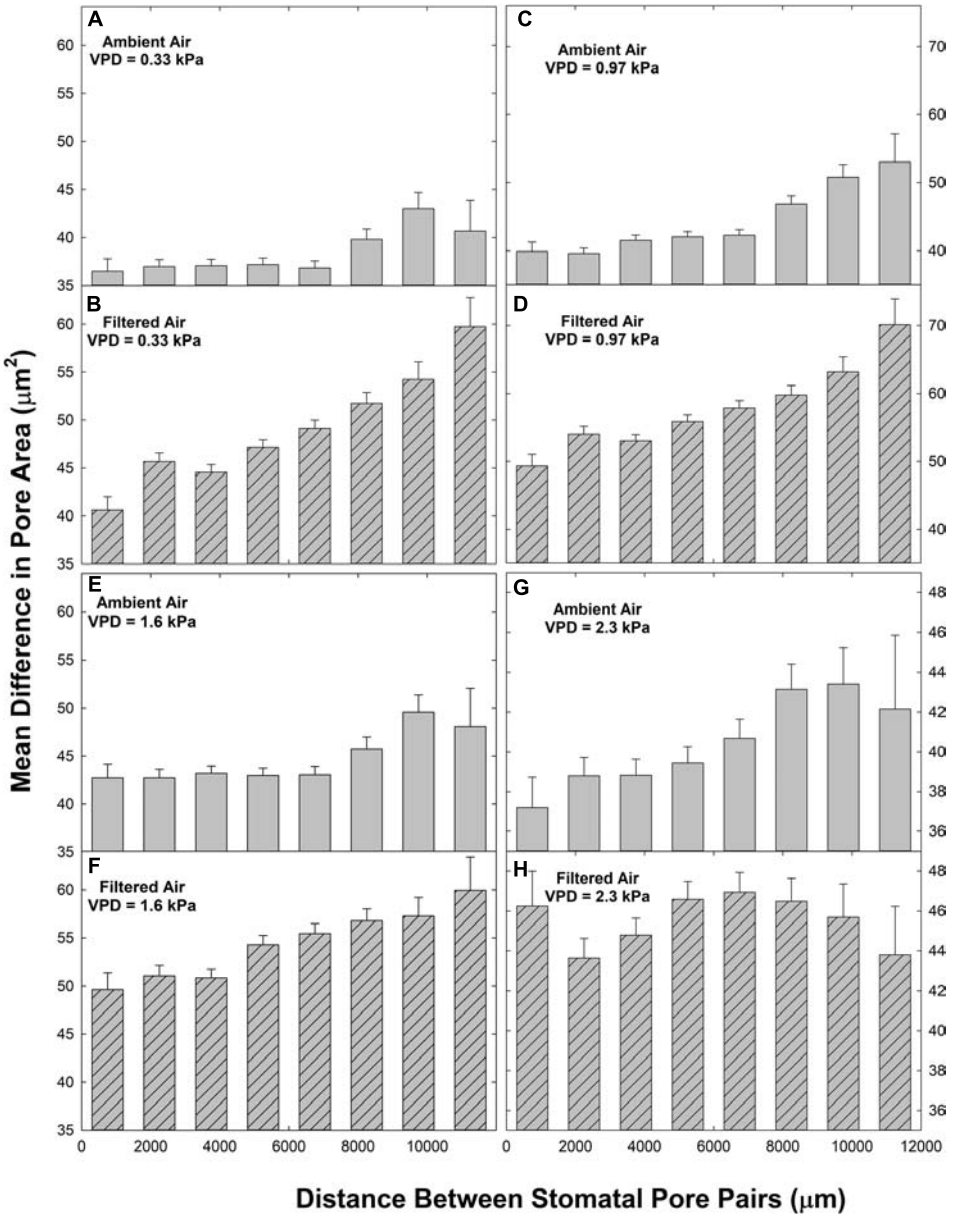

FIGURE 6 | Relationships between the paired difference between pore area (ΔA) and the distance separating the pores (d) in ambient air (AA; gray bars; **A,C,E,G**) and filtered air (FA; hatched bars, **B,D,F,H**) at different levels of evaporative demand (VPD), presented as mean ± s.e. Distance classes as in **Figure 2**.

responses of guard cells to epidermal water relations (Mott and Franks, 2001; Buckley, 2005, 2019).

The deposition of hygroscopic aerosol on the leaf surface may act similarly. The presence of thin liquid films lining stomatal pores provides a non-diffusive liquid pathway for water loss (Burkhardt et al., 2001b; Grantz et al., 2018), potentially increasing transpiration and degrading epidermal water status. Hygroscopic, particularly chaotropic, aerosol enhances the formation of such films by deliquescence and facilitates their spread across the leaf surface and into stomatal pores by reducing the surface tension of the liquid on the leaf surface (Monteith, 1957; Eiden et al., 1994; Dutcher et al., 2010; Burkhardt and Hunsche, 2013; Burkhardt and Grantz, 2017; Fernandez et al., 2017). Electrical conductance measurements (Burkhardt and Eiden, 1994; Burkhardt et al., 1999; Burkhardt and Hunsche, 2013) and electron micrography (Grantz et al., 2018) demonstrate these films and their penetration into stomatal pores (Eichert et al., 1998, 2008; Basi et al., 2014; Kaiser, 2014). The resulting hydraulic linkage of apoplast to the leaf boundary layer is associated with a reduction of mean pore area and skewing of areas toward the origin (Burkhardt et al., 2001a, 2012; Burkhardt, 2010; Pariyar et al., 2013; Grantz et al., 2018).

The current study demonstrates an apparent 3-way synergy between elevated VPD, initial stomatal opening at low VPD,

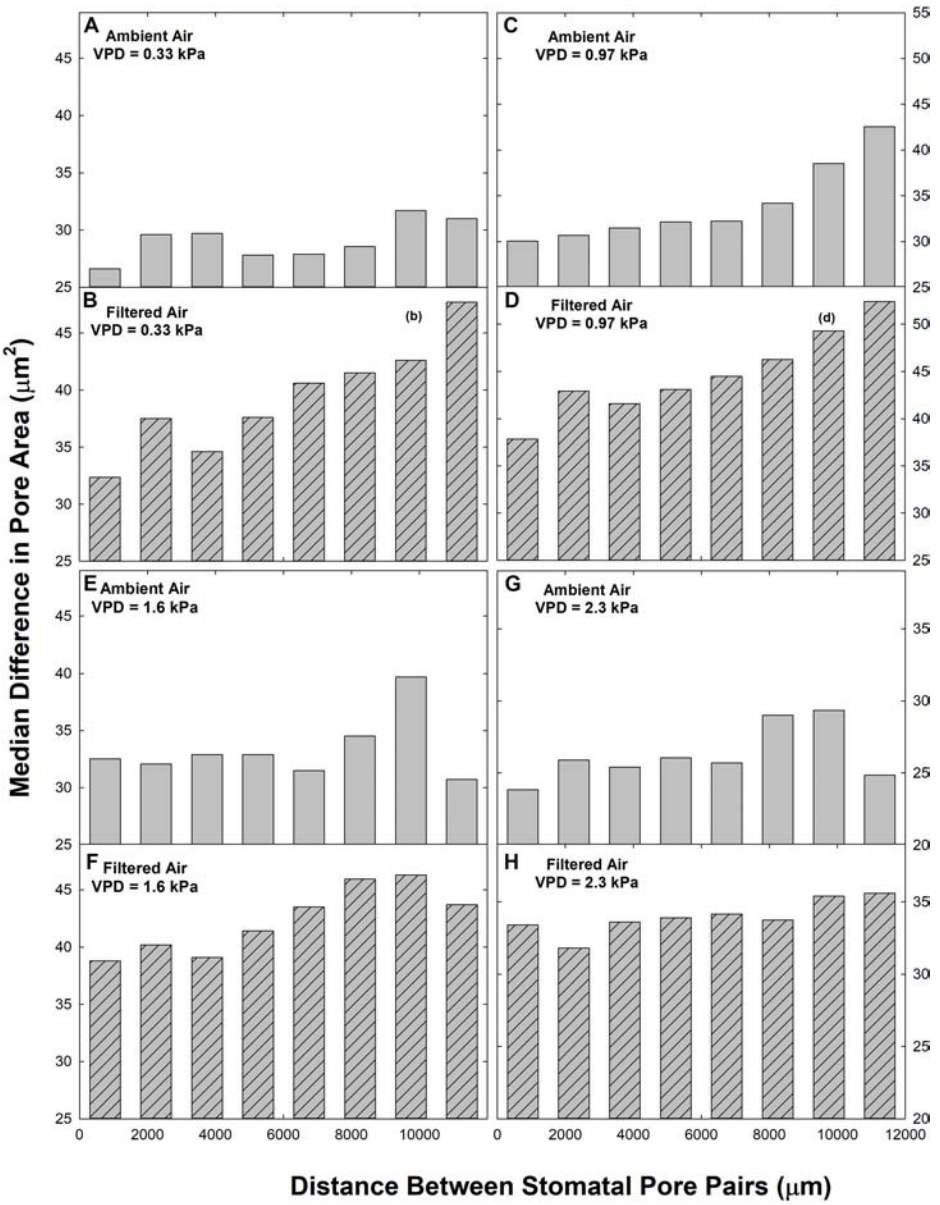

FIGURE 7 | Relationships between the paired difference between pore area (ΔA) and the distance separating the pores (d) in ambient air (AA; gray bars; **A,C,E,G**) and filtered air (FA; hatched bars, **B,D,F,H**) at different levels of evaporative demand (VPD), presented as median. Distance classes as in **Figure 2**.

and deposition of aerosol, consistent with a cumulative effect on epidermal water relations. At pore areas above about 180 μm^2 (at VPD = 0.33 kPa) the dynamics of AA and FA differ as VPD increased. The role of initial opening may reside in the conditions required to sustain liquid water on the leaf surface. This depends on the humidity of the BL which is substantially affected by transpiration. The role of aerosol deposition is to induce water accumulation on the leaf surface from unsaturated air, which becomes more significant at elevated VPD. In the absence of aerosol (FA), condensation on the leaf surface requires approximately 100% RH, but the presence of hygroscopic aerosol (AA) reduces this requirement substantially (e.g., to 75% RH for deliquescence of NaCl aerosol; Burkhardt and Grantz, 2017).

Pore Area Heterogeneity

Vicia faba is homobaric, without bundle sheath extensions or specialized stomatal subsidiary cells. This removes within-areole coordination of gaseous and water potential environments and suggests weaker coordination among stomata at local scale and potentially greater coordination at larger scale than in heterobaric species. In the present study, variability among closely co-located pores was large. This baseline level of ΔA was a dominant component of mean and median ΔA at all levels of pore

separation and at all levels of VPD. At larger scale, there was a consistent increase of ΔA with d at all VPD and both aerosol treatments. However, the increase in ΔA with distance was less than the local variability observed between closely spaced stomata. This reflects poor coordination between individual pores that was degraded further with greater separation within the 1.4 cm scale of our observations.

Degraded epidermal water status is associated with increased stomatal heterogeneity (Sharkey and Seemann, 1989; Downton et al., 1990; Haefner et al., 1997). However, in the present study, VPD did not consistently increase the magnitude of ΔA among neighboring pores, increasing only at moderate levels then declining.

The increased water loss per unit stomatal opening observed in the AA treatment (Grantz et al., 2018), suggested that aerosol could increase stomatal heterogeneity. However, this was not observed. Aerosol decreased heterogeneity among neighboring pores at all levels of VPD and reduced the rate of increase of ΔA with d at all VPD.

The liquid film at the leaf surface in the presence of aerosol may link stomata over potentially large areas of the leaf surface by making the near-surface micro-environment more homogeneous. This unifying effect may be more significant than the effect of the liquid film on increased water loss and potential impacts on epidermal water status.

Theories of stomatal optimization (Cowan and Farquhar, 1977) and of cavitation avoidance (Sperry et al., 2017), implicitly consider stomata as a population, whether at the leaf, branch or larger scale (Mott and Peak, 2007). Under conditions of high boundary layer conductance, heterogeneity may be detrimental, but in low wind or with large leaves it may improve gas exchange efficiency. This may explain similar growth of plants grown in AA or FA conditions (unpublished observations) in the slowly ventilated greenhouse, but degraded water use efficiency of AA leaves in the rapidly stirred cuvette of a gas exchange system (Pariyar et al., 2013). By reducing heterogeneity, aerosol deposition could reduce the errors in calculated values of C_i, potentially a factor that distinguishes gas exchange measurements made under controlled environment conditions from those made in more aerosol-rich field conditions.

CONCLUSION

Stomatal heterogeneity and patchy conductance remain enigmatic (Gunasekera and Berkowitz, 1992). Stomatal patchiness represents stronger stomatal coordination at local scale and poorer coordination at larger scale than predicted by true randomness (Sharkey and Seemann, 1989; Downton et al., 1990; Haefner et al., 1997; Lawson et al., 1998; Mott and Buckley, 2000; Mott and Peak, 2007). While heterogeneity among individual pore areas has been considered as noise (e.g., Cheeseman, 1991) it has more recently been seen as informative regarding the physiological bases of stomatal opening mechanics (Laisk et al., 1980), responses to environment (Mott et al., 1997; Mott and Buckley, 2000) and of the signal processing required for attainment of quasi-optimal stomatal behavior (Cheeseman, 1991; Cardon et al., 1994; Siebke and Weis, 1995; Kaiser and Kappen, 1997; Mott and Peak, 2007). Environmental drivers of coordination among individual members of populations of stomatal pores, including light and VPD, have been considered critical components of the stomatal regulatory system. Aerosol deposition to leaves has not been considered as often, but may play an important role.

We demonstrate, using a very large data set, that stomatal pore areas may be described as quasi-normally distributed, even as mean and median values change with VPD and aerosol deposition. We show that VPD and aerosol deposition both reduce mean pore area and the differences among pores, both at local and greater scale within individual leaves of homobaric *V. faba*. Synergy of these two ubiquitous environmental factors with the previously unexplored factor of initial stomatal opening, suggests linkage through impacts on epidermal water relations. The aerosol exposure in this experiment was typical of regional European particulate pollution (Putaud et al., 2010), and the study material a short-lived herbaceous annual. These effects may be greater in more hirsute and longer-lived leaves, and in more heavily polluted environments (Kuki et al., 2008; Yang et al., 2015). Aerosol impacts on leaf water relations and gas exchange, mediated by the degree of stomatal opening and its heterogeneity, may be more significant than commonly realized. Further research focused on the control elements regulating stomatal pore area (e.g., Buckley, 2019) and on their interactions with aerosol deposition (e.g., Burkhardt and Grantz, 2017) may be increasingly relevant to characterization of local and global budgets of water and carbon.

DATA AVAILABILITY STATEMENT

The datasets generated for this study are available on request to the corresponding author.

AUTHOR CONTRIBUTIONS

DG and JB conceived of the experiments. DG conducted the gas exchange and pore dimension experiments and analyzed the data. MK developed the software for spatial analysis. All authors contributed to interpretation of the results and wrote the manuscript.

FUNDING

The authors acknowledge funding from the University of California, Riverside Research Allocation Process, the Deutsche Forschungsgemeinschaft (DFG; BU 1099/7-2), and from USDA NIFA Project No. CA-R-BPS-5005-H.

ACKNOWLEDGMENTS

The authors thank H. Kaiser for interesting discussions leading up to this analysis as well as considerable assistance with the measurements.

REFERENCES

Basi, S., Burkhardt, J., Noga, G., and Hunsche, M. (2014). Hygroscopic salts support the stomatal penetration of glyphosate and influence its biological efficacy. *Weed Biol. Manag.* 14, 186–197. doi: 10.1111/wbm.12046

Beyschlag, W., and Eckstein, J. (1998). Stomatal patchiness. *Prog. Bot.* 59, 283–298. doi: 10.1007/978-3-642-80446-5_10

Boyer, J. S. (2015a). Impact of cuticle on calculations of the CO2 concentration inside leaves. *Planta* 242, 1405–1412. doi: 10.1007/s00425-015-2378-1

Boyer, J. S. (2015b). Turgor and the transport of CO2 and water across the cuticle (epidermis) of leaves. *J. Exp. Bot.* 66, 2625–2633. doi: 10.1093/jxb/erv065

Boyer, J. S., Wong, S. C., and Farquhar, G. D. (1997). CO2 and water vapor exchange across leaf cuticle (epidermis) at various water potentials. *Plant Physiol.* 114, 185–191. doi: 10.1104/pp.114.1.185

Buckley, T. N. (2005). The control of stomata by water balance. *New Phytol.* 168, 275–292. doi: 10.1111/j.1469-8137.2005.01543.x

Buckley, T. N. (2019). How do stomata respond to water status? *New Phytol.* 224, 21–36. doi: 10.1111/nph.15899

Buckley, T. N., Farquhar, G. D., and Mott, K. A. (1999). Carbon-water balance and patchy stomatal conductance. *Oecologia* 118, 132–143. doi: 10.1007/s004420050711

Buckley, T. N., and Mott, K. A. (2000). Stomatal responses to non-local changes in PFD: evidence for long distance hydraulic interactions. *Plant Cell Environ.* 23, 301–309. doi: 10.1046/j.1365-3040.2000.00552.x

Burkhardt, J. (2010). Hygroscopic particles on leaves: nutrients or desiccants? *Ecol. Monogr.* 80, 369–399. doi: 10.1890/09-1988.1

Burkhardt, J., Basi, S., Pariyar, S., and Hunsche, M. (2012). Stomatal penetration by aqueous solutions – an update involving leaf surface particles. *New Phytol.* 196, 774–787. doi: 10.1111/j.1469-8137.2012.04307.x

Burkhardt, J., and Eiden, R. (1994). Thin water films on coniferous needles. *Atmos. Environ.* 28, 2001–2011. doi: 10.1016/1352-2310(94)90469-3

Burkhardt, J., and Grantz, D. A. (2017). Plants and atmospheric aerosols. *Prog. Bot.* 78, 369–406. doi: 10.1007/124_2016_12

Burkhardt, J., and Hunsche, M. (2013). "Breath figures" on leaf surfaces-formation and effects of microscopic leaf wetness. *Front. Plant Sci.* 4:422. doi: 10.3389/fpls.2013.00422

Burkhardt, J., Kaiser, H., Goldbach, H., and Kappen, L. (1999). Measurements of electrical leaf surface conductance reveal recondensation of transpired water vapour on leaf surfaces. *Plant Cell Environ.* 22, 189–196. doi: 10.1046/j.1365-3040.1999.00387.x

Burkhardt, J., Kaiser, H., Kappen, L., and Goldbach, H. E. (2001a). The possible role of aerosols on stomatal conductivity for water vapour. *Basic Appl. Ecol.* 2, 351–364. doi: 10.1078/1439-1791-00062

Burkhardt, J., Koch, K., and Kaiser, H. (2001b). Deliquescence of deposited atmospheric particles on leaf surfaces. *Water Air Soil Pollut. Focus* 1, 313–321. doi: 10.1007/978-94-010-9026-1_31

Burkhardt, J., and Pariyar, S. (2014). Particulate pollutants are capable to 'degrade' epicuticular waxes and to decrease the drought tolerance of Scots pine (*Pinus sylvestris* L.). *Environ. Pollut.* 184, 659–667. doi: 10.1016/j.envpol.2013.04.041

Burkhardt, J., and Pariyar, S. (2016). How does the VPD response of isohydric and anisohydric plants depend on leaf surface particles? *Plant Biol.* 18, 91–100. doi: 10.1111/plb.12402

Burkhardt, J., Zinsmeister, D., Grantz, D. A., Vidic, S., Sutton, M. A., Hunsche, M., et al. (2018). Camouflaged as 'degraded wax', hygroscopic aerosols contribute to leaf desiccation, tree mortality, and forest decline. *Environ. Res. Lett.* 13:085001. doi: 10.1088/1748-9326/aad346

Cardon, Z. G., Mott, K. A., and Berry, J. A. (1994). Dynamics of patchy stomatal movements, and their contribution to steady-state and oscillating stomatal conductance calculated with gas-exchange techniques. *Plant Cell Environ.* 17, 995–1007. doi: 10.1111/j.1365-3040.1994.tb02033.x

Cheeseman, J. M. (1991). PATCHY: simulating and visualizing the effects of stomatal patchiness on photosynthetic CO2 exchange studies. *Plant Cell Environ.* 14, 593–599. doi: 10.1111/j.1365-3040.1991.tb01530.x

Cowan, I. R., and Farquhar, G. D. (1977). Stomatal function in relation to leaf metabolism and environment. *Symp. Soc. Exp. Biol.* 31, 471–505.

Downton, W. J., Loveys, B. R., and Grant, W. J. R. (1990). Salinity effects on the stomatal behaviour of grapevine. *New Phytol.* 116, 499–503. doi: 10.1111/j.1469-8137.1990.tb00535.x

Downton, W. J. S., Loveys, B. R., and Grant, W. J. R. (1988). Non-uniform stomatal closure induced by water stress causes putative non-stomatal inhibition of photosynthesis. *New Phytol.* 110, 503–509. doi: 10.1111/j.1469-8137.1988.tb00289.x

Dutcher, C. S., Wexler, A. S., and Clegg, S. L. (2010). Surface tensions of inorganic multicomponent aqueous electrolyte solutions and melts. *J. Phys. Chem. A* 114, 12216–12230. doi: 10.1021/jp105191z

Eckstein, J., Beyschlag, W., Mott, K. A., and Ryel, R. J. (1996). Changes in photon flux can induce stomatal patchiness. *Plant Cell Environ.* 19, 1066–1075.

Eichert, T., Goldbach, H. E., and Burkhardt, J. (1998). Evidence for the uptake of large anions through stomatal pores. *Bot. Acta* 111, 461–466. doi: 10.1111/j.1438-8677.1998.tb00733.x

Eichert, T., Kurtz, A., Steiner, U., and Goldbach, H. E. (2008). Size exclusion limits and lateral heterogeneity of the stomatal foliar uptake pathway for aqueous solutes and water suspended nanoparticles. *Physiol. Plant.* 134, 151–160. doi: 10.1111/j.1399-3054.2008.01135.x

Eiden, R., Burkhardt, J., and Burkhardt, O. (1994). Atmospheric aerosol particles and their role in the formation of dew on the surface of plant leaves. *J. Aerosol Sci.* 25, 367–376. doi: 10.1016/0021-8502(94)90087-6

Fanourakis, D., Heuvelink, E., and Carvalho, S. M. P. (2015). Spatial heterogeneity in stomatal features during leaf elongation: an analysis using *Rosa hybrida*. *Funct. Plant Biol.* 42, 737–745.

Fernandez, V., Bahamonde, H. A., Peguero-Pina, J. J., Gil-Pelegrin, E., Sancho-Knapik, D., Gil, L., et al. (2017). Physico-chemical properties of plant cuticles and their functional and ecological significance. *J. Exp. Bot.* 19, 5293–5306. doi: 10.1093/jxb/erx302

Gorton, H. L., Williams, W. E., and Binns, M. E. (1989). Repeated measurements of aperture for individual stomates. *Plant Physiol.* 89, 387–390. doi: 10.1104/pp.89.2.387

Grantz, D. A. (1990). Plant-response to atmospheric humidity. *Plant Cell Environ.* 13, 667–679. doi: 10.1111/j.1365-3040.1990.tb01082.x

Grantz, D. A., Zinsmeister, D., and Burkhardt, J. (2018). Ambient aerosol increases minimum leaf conductance and alters the aperture–flux relationship as stomata respond to vapor pressure deficit (VPD). *New Phytol.* 219, 275–286. doi: 10.1111/nph.15102

Gunasekera, D., and Berkowitz, G. A. (1992). Heterogeneous stomatal closure in response to leaf water deficits is not a universal phenomenon. *Plant Physiol.* 98, 660–665. doi: 10.1104/pp.98.2.660

Haefner, J. W., Buckley, T. N., and Mott, K. A. (1997). A spatially explicit model of patchy stomatal responses to humidity. *Plant Cell Environ.* 20, 1087–1097. doi: 10.1046/j.1365-3040.1997.d01-137.x

Hanson, D. T., Stutz, S. S., and Boyer, J. S. (2016). Why small fluxes matter: the case and approaches for improving measurements of photosynthesis and (photo)respiration. *J. Exp. Bot.* 67, 3027–3039. doi: 10.1093/jxb/erw139

Kaiser, H. (2009). The relation between stomatal aperture and gas exchange under consideration of pore geometry and diffusional resistance in the mesophyll. *Plant Cell Environ.* 32, 1091–1098. doi: 10.1111/j.1365-3040.2009.01990.x

Kaiser, H. (2014). Stomatal uptake of mineral particles from a sprayed suspension containing an organosilicone surfactant. *J. Plant Nutr. Soil Sci.* 177, 869–874. doi: 10.1002/jpln.201300607

Kaiser, H., and Kappen, L. (1997). *In situ* observations of stomatal movements in different light-dark regimes: the influence of endogenous rhythmicity and long-term adjustments. *J. Exp. Bot.* 48, 1583–1589. doi: 10.1093/jexbot/48.313.1583

Kaiser, H., and Kappen, L. (2000). In situ observation of stomatal movements and gas exchange of *Aegopodium podagraria* L. In the understorey. *J. Exp. Bot.* 51, 1741–1749. doi: 10.1093/jexbot/51.351.1741

Kamakura, M., and Furukawa, A. (2008). Responses of individual stomata in *Ipomoea pes-caprae* to various CO2 concentrations. *Physiol. Plant.* 132, 255–261. doi: 10.1111/j.1399-3054.2007.01003.x

Kamakura, M., Kosugi, Y., Muramatsu, K., and Muraoka, H. (2012). Simulations and observations of patchy stomatal behavior in leaves of *Quercus crispula*, a cool-temperate deciduous broad-leaved tree species. *J. Plant Res.* 125, 339–349. doi: 10.1007/s10265-011-0460-8

Kappen, L., Andresen, G., and Losch, R. (1987). In situ observations of stomatal movements. *J. Exp. Bot.* 38, 126–141.

Kerstiens, G. (1996). Cuticular water permeability and its physiological significance. *J. Exp. Bot.* 47, 1813–1832. doi: 10.1093/jxb/47.12.1813

Kuki, K. N., Oliva, M. A., Pereir, A. E. G., Costa, A. C., and Cambraia, J. (2008). Effects of simulated deposition of acid mist and iron ore particulate matter on photosynthesis and the generation of oxidative stress in *Schinus terebinthifolius* Radii and *Sophora tomentosa* L. *Sci. Total Environ.* 403, 207–214. doi: 10.1016/j.scitotenv.2008.05.004

Laisk, A., Oja, V., and Kull, K. (1980). Statistical distribution of stomatal apertures of *Vicia faba* and *Hordeum vulgare* and the *Spannungsphase* of stomatal opening. *J. Exp. Bot.* 31, 49–58.

Lawson, T., Weyers, J., and A'Brook, R. (1998). The nature of heterogeneity in the stomatal behavior of *Phaseolus vulgaris* L. primary leaves. *J. Exp. Bot.* 49, 1387–1395. doi: 10.1093/jxb/49.325.1387

Loreto, F., and Sharkey, T. D. (1990). Low humidity can cause uneven photosynthesis in olive (*Olea europaea* L.) leaves. *Tree Physiol.* 6, 409–415. doi: 10.1093/treephys/6.4.409

Maier-Maercker, U. (1983). The role of peristomatal transpiration in the mechanism of stomatal movement. *Plant Cell Environ.* 6, 369–380. doi: 10.1111/j.1365-3040.1983.tb01269.x

Monteith, J. L. (1957). Dew. *Q. J. R. Meteorol. Soc.* 83, 322–341.

Mott, K. A., and Buckley, T. N. (1998). Stomatal heterogeneity. *J. Exp. Bot.* 49, 407–417. doi: 10.1093/jexbot/49.suppl_1.407

Mott, K. A., and Buckley, T. N. (2000). Patchy stomatal conductance: emergent collective behavior of stomata. *Trends Plant Sci.* 5, 258–262. doi: 10.1016/s1360-1385(00)01648-4

Mott, K. A., Denn, E. F., and Powell, J. (1997). Interactions among stomata in response to perturbations in humidity. *Plant Cell Environ.* 20, 1098–1107. doi: 10.1046/j.1365-3040.1997.d01-138.x

Mott, K. A., and Franks, P. J. (2001). The role of epidermal turgor in stomatal interactions following a local perturbation in humidity. *Plant Cell Environ.* 24, 657–662. doi: 10.1046/j.0016-8025.2001.00705.x

Mott, K. A., and Parkhurst, D. F. (1991). Stomatal responses to humidity in air and helox. *Plant Cell Environ.* 14, 509–515. doi: 10.1111/j.1365-3040.1991.tb01521.x

Mott, K. A., and Peak, D. (2007). Stomatal patchiness and task-performing networks. *Ann. Bot.* 99, 219–226. doi: 10.1093/aob/mcl234

Mott, K. A., Shope, J. C., and Buckley, T. N. (1999). Effects of humidity on light-induced stomatal opening: evidence for hydraulic coupling among stomata. *J. Exp. Bot.* 50, 1207–1213. doi: 10.1093/jxb/50.336.1207

Nardini, A., Gortan, E., Ramani, M., and Salleo, S. (2008). Heterogeneity of gas exchange rates over the leaf surface in tobacco: an effect of hydraulic architecture? *Plant Cell Environ.* 31, 804–812. doi: 10.1111/j.1365-3040.2008.01798.x

Osmond, C. B., Kramer, D., and Luttge, U. (1999). Reversible, water stress-induced non-uniform chlorophyll fluorescence quenching in wilting leaves of *Potentilla reptans* may not be due to patch stomatal responses. *Plant Biol.* 1, 618–624. doi: 10.1111/j.1438-8677.1999.tb00272.x

Pariyar, S., Eichert, T., Goldbach, H. E., Hunsche, M., and Burkhardt, J. (2013). The exclusion of ambient aerosols changes the water relations of sunflower (*Helianthus annuus*) and bean (*Vicia faba*) plants. *Environ. Exp. Bot.* 88, 43–52. doi: 10.1016/j.envexpbot.2011.12.031

Pospisilova, J., and Santrucek, J. (1994). Stomatal patchiness. *Biol. Plant.* 36, 481–510. doi: 10.1007/bf02921169

Pringle, K. J., Tost, H., Pozzer, A., Poschl, U., and Lelieveld, J. (2010). Global distribution of the effective aerosol hygroscopicity parameter for CCN activation. *Atmos. Chem. Phys.* 10, 5241–5255. doi: 10.5194/acp-10-5241-2010

Putaud, J.-P., Van Dingenen, R., Alastuey, A., Bauer, H., Birmili, W., Cyrys, J., et al. (2010). A European aerosol phenomenology 3. Physical and chemical characteristics of particulate matter from 60 rural, urban, and kerbside sites across Europe. *Atmos. Environ.* 44, 1308–1320. doi: 10.1016/j.atmosenv.2009.12.011

Saxe, H. (1979). A structural and functional study of the coordinated reactions of individual *Commelina communis* L. stomata (Commelinaceae). *Am. J. Bot.* 66, 1044–1052. doi: 10.1002/j.1537-2197.1979.tb06320.x

Sharkey, D. T., and Seemann, J. R. (1989). Mild water stress effects on carbon-reduction-cycle intermediates, ribulose bisphosphate carboxylase activity, and spatial homogeneity of photosynthesis in intact leaves. *Plant Physiol.* 89, 1060–1065. doi: 10.1104/pp.89.4.1060

Siebke, K., and Weis, E. (1995). Assimilation images of leaves of *Glechoma hederacea*: analysis of nonsynchronous stomata related oscillations. *Planta* 196, 155–165.

Smith, S., Weyers, J. D. B., and Berry, W. G. (1989). Variation in stomatal characteristics over the lower surface of *Commelina communis* leaves. *Plant Cell Environ.* 12, 653–659.

Spence, R. D. (1987). The problem of variability in stomatal responses, particularly aperture variance, to environmental and experimental conditions. *New Phytol.* 107, 303–315. doi: 10.1111/j.1469-8137.1987.tb00182.x

Spence, R. D., Sharpe, P. J. H., Powell, R. D., and Rogers, C. A. (1983). Epidermal and guard cell interactions on stomatal aperture in epidermal strips and intact leaves. *Ann. Bot.* 52, 1–12. doi: 10.1093/oxfordjournals.aob.a086538

Sperry, J. S., Venturas, M. D., Anderegg, W. R. L., Mencuccini, M., Mackay, D. S., Wang, Y., et al. (2017). Predicting stomatal responses to the environment from the optimization of photosynthetic gain and hydraulic cost. *Plant Cell Environ.* 40, 816–830. doi: 10.1111/pce.12852

Terashima, I. (1992). Anatomy of non-uniform leaf photosynthesis. *Photosynth. Res.* 31, 195–212. doi: 10.1007/bf00035537

Terashima, I., Wong, S.-C., Osmond, C. B., and Farquhar, G. D. (1988). Characterization of non-uniform photosynthesis induced by abscisic acid in leaves having different mesophyll anatomies. *Plant Cell Physiol.* 29, 385–394.

Tsigaridis, K., Krol, M., Dentener, F. J., Balkanski, Y., Lathiere, J., Metzger, S., et al. (2006). Change in global aerosol composition since preindustrial times. *Atmos. Chem. Phys.* 6, 5143–5162. doi: 10.5194/acp-6-5143-2006

Weyers, J. D. B., and Lawson, T. (1997). Heterogeneity in stomatal characteristics. *Adv. Bot. Res.* 26, 317–351.

Yang, J., Chang, Y. M., and Yan, P. B. (2015). Ranking the suitability of common urban tree species for controlling PM2.5 pollution. *Atmos. Pollut. Res.* 6, 267–277. doi: 10.5094/apr.2015.031

Conflict of Interest: The authors declare that the research was conducted in the absence of any commercial or financial relationships that could be construed as a potential conflict of interest.

frontiers in Plant Science

MINI REVIEW
published: 30 June 2020
doi: 10.3389/fpls.2020.00968

The Role of ROS Homeostasis in ABA-Induced Guard Cell Signaling

*Anthony E. Postiglione and Gloria K. Muday**

Department of Biology and the Center for Molecular Signaling, Wake Forest University, Winston Salem, NC, United States

The hormonal and environmental regulation of stomatal aperture is mediated by a complex signaling pathway found within the guard cells that surround stomata. Abscisic acid (ABA) induces stomatal closure in response to drought stress by binding to its guard cell localized receptor, initiating a signaling cascade that includes synthesis of reactive oxygen species (ROS). Genetic evidence in Arabidopsis indicates that ROS produced by plasma membrane respiratory burst oxidase homolog (RBOH) enzymes RBOHD and RBOHF modulate guard cell signaling and stomatal closure. However, ABA-induced ROS accumulates in many locations such as the cytoplasm, chloroplasts, nucleus, and endomembranes, some of which do not coincide with plasma membrane localized RBOHs. ABA-induced guard cell ROS accumulation has distinct spatial and temporal patterns that drive stomatal closure. Productive ROS signaling requires both rapid increases in ROS, as well as the ability of cells to prevent ROS from reaching damaging levels through synthesis of antioxidants, including flavonols. The relationship between locations of ROS accumulation and ABA signaling and the role of enzymatic and small molecule ROS scavengers in maintaining ROS homeostasis in guard cells are summarized in this review. Understanding the mechanisms of ROS production and homeostasis and the role of ROS in guard cell signaling can provide a better understanding of plant response to stress and could provide an avenue for the development of crop plants with increased stress tolerance.

Keywords: guard cell, reactive oxygen species, stomata, abscisic acid, flavonols, respiratory burst oxidase homolog

OPEN ACCESS

Edited by:
Scott McAdam,
Purdue University, United States

Reviewed by:
Fouad Lemtiri-Chlieh,
University of Connecticut, United States
Yuree Lee,
Seoul National University, South Korea

***Correspondence:**
Gloria K. Muday
muday@wfu.edu

Specialty section:
This article was submitted to Plant Development and EvoDevo, a section of the journal Frontiers in Plant Science

Received: *19 December 2019*
Accepted: *12 June 2020*
Published: *30 June 2020*

Citation:
Postiglione AE and Muday GK (2020) The Role of ROS Homeostasis in ABA-Induced Guard Cell Signaling. Front. Plant Sci. 11:968. doi: 10.3389/fpls.2020.00968

INTRODUCTION

Stomatal aperture must be tightly regulated to ensure optimal CO_2 entry for photosynthesis while protecting plants against excess water loss and pathogen attack (Nilson and Assmann, 2007). The opening and closing of stomata are mediated by changes in turgor pressure inside guard cells that surround the stomatal pore (Schroeder et al., 2001). Guard cell turgor is controlled by signal transduction cascades that are induced by many environmental signals, including water availability (Xu et al., 2014; Xu et al., 2016; Li et al., 2017; Qi et al., 2018; Qu et al., 2018; Tõldsepp et al., 2018). Decreased water availability increases abscisic acid (ABA) synthesis, which induces stomatal closure and a myriad of other plant responses (Zhu, 2016; Vishwakarma et al., 2017).

Guard cells have an elegant signaling cascade induced upon ABA binding to a family of soluble receptor proteins including PYRABACTIN RESISTANCE 1 (PYR1) (Park et al., 2009), which is summarized in **Figure 1A**. The ABA-bound receptor inhibits Clade A protein phosphatases type 2C

(PP2Cs), such as ABI1 (Ma et al., 2009; Park et al., 2009; Nishimura et al., 2010). The inhibition of PP2Cs prevents protein dephosphorylation and negative regulation of ABA signaling (Park et al., 2009). Targets of PP2Cs include Sucrose nonfermenting Related Kinase 2 family members (SnRK2s), with the best characterized target being OPEN STOMATA 1 (OST1)/SnRK2.6 (Mustilli et al., 2002). OST1 transmits the ABA signal through phosphorylation of downstream targets, ultimately triggering a rapid burst of Reactive Oxygen Species (ROS) (Pei et al., 2000), which can then stimulate guard cell ion channels (Geiger et al., 2009; Demidchik, 2018). In this review, we summarize the current literature on ABA-induced ROS

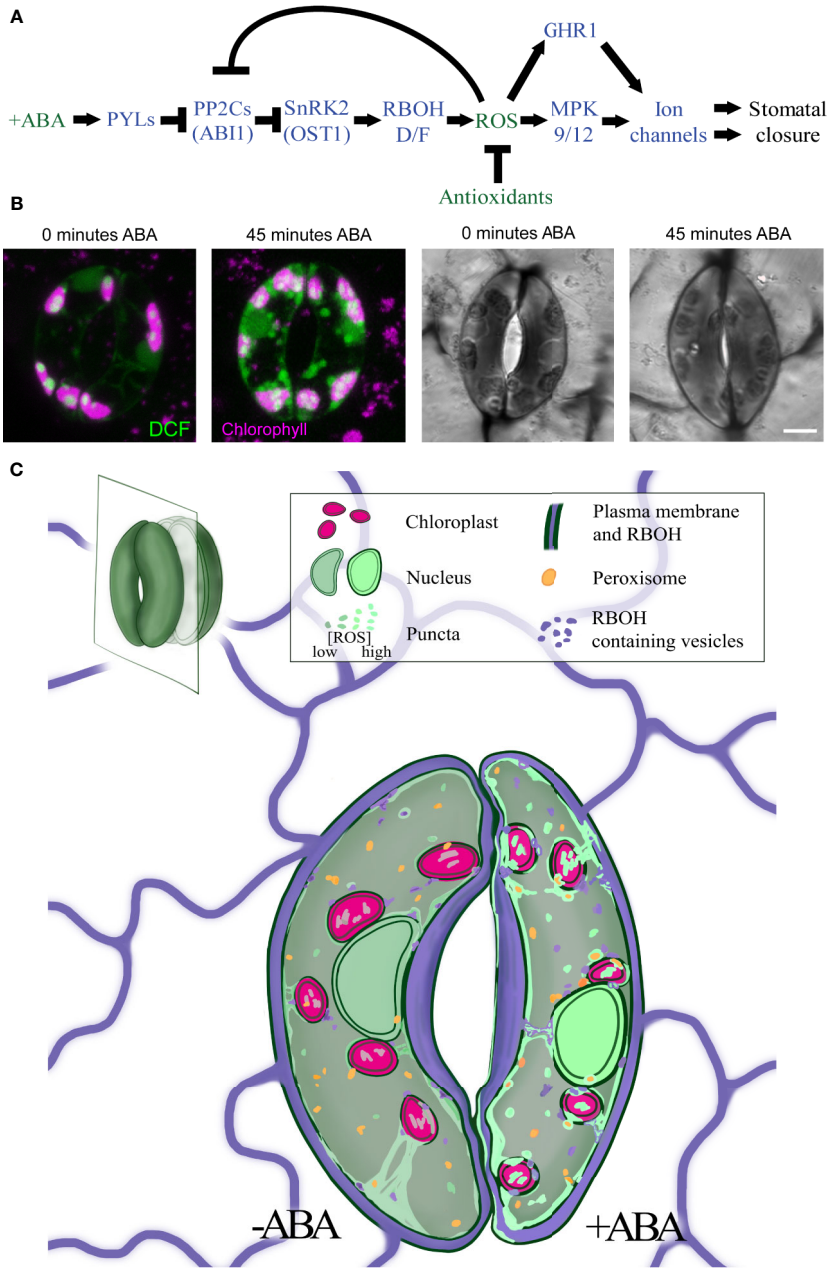

FIGURE 1 | ABA increases ROS levels in guard cells in multiple subcellular locations. **(A)** A schematic model of the ABA signaling pathway during stomatal closure. Blue fonts represent proteins, while green fonts represent molecules. **(B)** Treatment with ABA for 45 min increases DCF fluorescence and decreases stomatal aperture in tomato guard cells. **(C)** The signal of the generic ROS sensor, DCF (green), is detected in the cytosol, nucleus, chloroplasts (pink), and endomembranes, with rapid and dramatic increases in all these locations in response to ABA treatment. RBOH enzymes (purple) produce ROS at the plasma membrane but can be internalized into endosomes. ROS signal also overlays peroxisome (orange), but whether this signal increases with ABA has not yet been reported. Central vacuole is not shown in illustration.

production, targets of ROS signaling pathways, and how ROS homeostasis is maintained to keep ROS concentration appropriate for productive guard cell signaling.

ABA INDUCED ROS IN GUARD CELLS DRIVES STOMATAL CLOSURE

ROS can act as a developmental and hormonal response signal (Mittler, 2017; Huang et al., 2019) with ABA-induced ROS bursts emerging as an elegant example (Singh et al., 2017). ABA-induced ROS accumulation in guard cells is most frequently visualized by fluorescence of the ROS sensor 2′,7′-dichlorofluorescein (DCF) (Pei et al., 2000; Murata et al., 2001; Watkins et al., 2014; Watkins et al., 2017). Improvements in the resolution of confocal microscopy have revealed ABA-induced ROS signals in the guard cell nucleus, cytoplasm, chloroplasts, and endomembrane bodies (Watkins et al., 2017), (**Figure 1B**). ABA-dependent increases in DCF fluorescence are rapid, having been reported within 2 min after ABA treatment (Pei et al., 2000), although other studies detect slower changes observed within 15 min and maximal after 45 min (**Figure 1B**) (Watkins et al., 2017). These DCF changes are slower than changes in ion movements detected at 1 min after ABA treatment *via* electrophysiology (Hamilton et al., 2000). This difference may reflect the methodology used for these measurements.

It is important to understand which ROS are increased in response to ABA as they each have distinct functions. ROS as they each have distinct functions are highly reactive derivatives of molecular oxygen, which include hydroxyl radical (·OH), singlet oxygen ($^1O_2$), superoxide anion ($O_2^{\cdot -}$), and hydrogen peroxide (H_2O_2). DCF is a general ROS sensor as it is oxidized by multiple ROS (Chen et al., 2010). A recent study used the H_2O_2 specific probe Peroxy Orange1 (PO1) and showed that the pattern of H_2O_2 accumulation parallels the total ROS profile detected by DCF, except in the nucleus where little PO1 signal was observed (Watkins et al., 2017) (**Figure 2B**).

ABA induced stomatal closure has been shown to be dependent on ROS increases using several approaches. Guard cell closure is reduced, but not totally abolished, by treatment with ROS scavengers (Zhang et al., 2001) and inhibitors of or mutants in ROS producing enzymes (Pei et al., 2000; Watkins et al., 2017; Iwai et al., 2019). These partial effects are consistent with ROS independent closure and/or multiple sources of guard cell ROS. The most intriguing results were obtained *via* genetic mutants of Respiratory Burst Oxidase Homolog (RBOH)/NADPH Oxidase (NOX) enzymes, suggesting RBOH dependent ROS synthesis drives the ABA response (Kwak et al., 2003).

EXPRESSION AND FUNCTION OF RBOH ENZYMES IN ABA SIGNALING

The *Arabidopsis* genome encodes 10 RBOH family members, RBOHA-RBOHJ that have important roles in signaling induced ROS synthesis (Suzuki et al., 2011; Chapman et al., 2019). RBOH enzymes have distinct expression patterns and regulate development and signaling (Chapman et al., 2019). These plasma membrane (PM)-localized proteins have six transmembrane domains, a C-terminal FAD-binding domain and two N-terminal calcium-binding EF hands (Torres and Dangl, 2005). RBOHs produce extracellular superoxide by transferring electrons from NADPH or $FADH_2$ to oxygen (Suzuki et al., 2011). Superoxide can then be converted to H_2O_2 spontaneously or by Superoxide Dismutase (SOD). This extracellular H_2O_2 enters the plant cells through PM aquaporins (Bienert et al., 2007; Tian et al., 2016; Rodrigues et al., 2017).

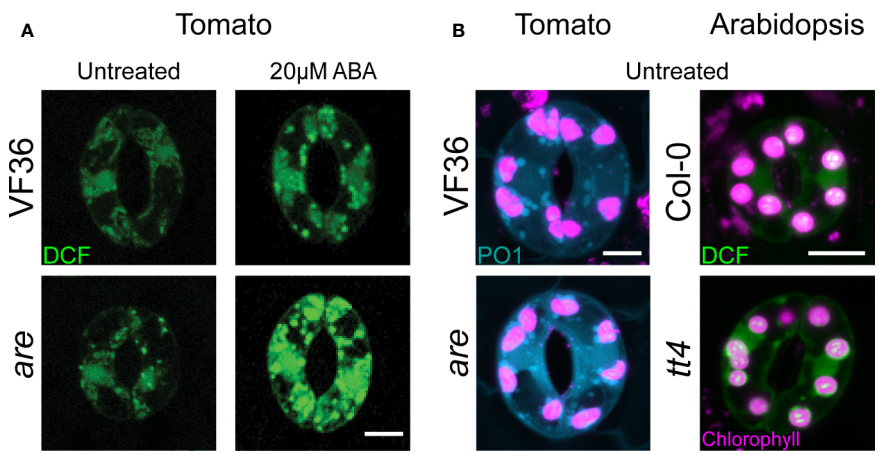

FIGURE 2 | Arabidopsis and tomato mutants with decreased flavonoid antioxidants have increased ROS accumulation. **(A)** Confocal micrographs of DCF-stained guard cells of 4-week-old VF36 (wild-type) and *are* plants show that flavonol deficient mutants have increased ROS levels both in the absence or presence of 20 μM ABA. **(B)** Confocal micrographs of DCF and PO1 fluorescence in guard cells of 4-week-old tomato and Arabidopsis leaves show tomato and Arabidopsis with decreased flavonol levels have increased total ROS and H_2O_2 levels. Scale bars = 5 μm. DCF signal is shown in green, PO1 signal in blue, and chlorophyll autofluorescence in magenta. Images obtained from experiments completed in (Watkins et al., 2014; Watkins et al., 2017).

Genetic approaches have demonstrated the importance of RBOHD and RBOHF in ABA-induced stomatal closure (Kwak et al., 2003). An *rbohf* single mutant and an *rbohd/f* double mutant show reduced rates of ABA-induced ROS synthesis and partial impairment in stomatal closure, while the *rbohd* single mutant had wild-type responses (Kwak et al., 2003). Treatment with an RBOH inhibitor, diphenyleneiodonium (DPI), also impaired ROS production and ABA-induced stomatal closure in Arabidopsis (Zhang et al., 2001) and tomato (Watkins et al., 2017). Together these results implicate RBOHs as important modulators of ABA-dependent stomatal closure.

REGULATION OF RBOH SYNTHESIS AND ACTIVITY

The synthesis of RBOHs is regulated transcriptionally (Yun et al., 2011; Hao et al., 2014; Qu et al., 2017). In Arabidopsis, *RBOHD* and *RBOHF*, the two RBOHs with known function in guard cells, are expressed in this cell type as judged by transcript abundance and transcriptional reporters (Kwak et al., 2003; Chapman et al., 2019). The abundance of *RBOHD* and *RBOHF* transcripts has been reported to be increased by ABA treatment and abiotic stress including drought, salt, and elevated osmoticum (Kwak et al., 2003; Kilian et al., 2007).

RBOH activity is also posttranslationally regulated to coordinate the timing and magnitude of the ROS burst. Mutants in *phospholipase Dα1* (*PLDα1*) have decreased phosphatidic acid synthesis, which impaired ABA-induced ROS production and stomatal closure (Zhang et al., 2009). Treatment with DPI did not affect the *plda1* mutant further, implicating phosphatidic acid as a positive regulator of RBOHs (Zhang et al., 2009). RBOHF is regulated by Ca^{2+} dependent phosphorylation by Calcineurin B-Like (CBL) which interacts with CBL-Interacting Protein Kinases (CIPKs) (Kimura et al., 2013). One report indicated that this complex negatively regulated ROS synthesis (Kimura et al., 2013), while a second report showed that coexpression of *CIPK26* and *CBL1* or *CBL9* increased RBOHF-dependent ROS production, while *CIPK26* alone had no effect (Drerup et al., 2013). Additionally, activated OST1 phosphorylates RBOHF, which may be required for its activation (Sirichandra et al., 2009). Nitrosylation of RBOHD at Cysteine 890 eliminates ROS production to block guard cell apoptosis when these cells are undergoing a pathogen induced immune response in Arabidopsis (Yun et al., 2011).

ROS INTEGRATION WITH ABA SIGNALING MACHINERY

A central question is where ABA-induced ROS integrates with guard cell signaling machinery. Two PP2C enzymes, ABA insensitive 1 (ABI1) and ABI2, which were identified in mutant screens for ABA insensitivity in stomatal closure assays, are negative regulators of ABA signaling. Both proteins are inactivated by H_2O_2 (Meinhard and Grill, 2001; Meinhard et al., 2002). The *abi1-1* and *abi2-1* mutants are defective in interactions with ABA receptors resulting in constitutive SnRK2 inactivation, blocking ABA signaling and stomatal closure (Umezawa et al., 2009). In *abi1-1*, ABA treatment failed to induce ROS production and stomatal closure (Murata et al., 2001). Impaired stomatal closure in *abi1-1* was restored by exogenous H_2O_2 treatment, suggesting that ROS is downstream of ABI1 (**Figure 1A**). However, in this same study, ABA induced a ROS burst in *abi2-1*, and the impaired stomatal closure was not rescued by H_2O_2 treatment, suggesting ABI2 may be downstream of the ABA-induced ROS burst.

ROS can regulate plant signaling cascades by modulating the activity of target proteins through reversible oxidation of cysteine residues (Waszczak et al., 2015). ABA-induced ROS activates the plasma membrane-localized Guard Cell Hydrogen Peroxide Resistant1 (GHR1) receptor-like kinase which controls calcium channel activation (Pei et al., 2000; Hua et al., 2012; Sierla et al., 2018). Mitogen Activated Protein Kinases (MAPKs) are also downstream targets of ROS in guard cells (Lee et al., 2016). Treatment with both ABA and H_2O_2 activated the guard cell specific MPK12, which works with MPK9 to positively regulate ABA-induced stomatal closure (Jammes et al., 2009). Two other guard cell map kinases, MPK3 and MPK6, are implicated in guard cell response to pathogen attack and have increased activity after H_2O_2 treatment (Kovtun et al., 2000; Yuasa et al., 2001). MPK3 and MPK6 activation is unaffected in the *rbohd/f* double mutant following treatment with flg22, a pathogen elicitor, suggesting that MPK3/MPK6 activation during pathogen response is not RBOH dependent (Xu et al., 2014). Altogether, the current evidence suggests that ABI1 is upstream of ABA-induced ROS synthesis (and feedback inhibited by ROS) while ABI2, GHR1, and MAPKs are downstream of ROS (**Figure 1A**), although aspects of this model need further experimentation.

ANTIOXIDANTS REGULATE ROS HOMEOSTASIS TO MODULATE STOMATAL APERTURE

For ROS to serve as productive signaling molecules, they need to increase to drive signaling and development (Chapman et al., 2019), but if ROS increases are left unchecked, ROS can accumulate to dangerous levels resulting in oxidative damage of proteins, DNA, and lipids (Betteridge, 2000). Guard cells contain both enzymatic and nonenzymatic machinery to maintain ROS homeostasis to prevent ROS from reaching damaging levels (Chen and Gallie, 2004; Watkins et al., 2014; Singh et al., 2017; Watkins et al., 2017; Yamauchi et al., 2019). These antioxidants regulate the responses to ABA in guard cells.

Flavonols are a class of plant specialized antioxidant metabolites that reduce ROS accumulation in guard cells to regulate stomatal closure (Watkins et al., 2014; Watkins et al., 2017). Mutants in tomato and Arabidopsis with decreased flavonol production had increased guard cell ROS (Watkins et al., 2014) and were more sensitive to ABA-induced stomatal closure (Watkins et al., 2017) (**Figure 2**). Mutants with elevated

levels of flavonols have decreased ROS accumulation and decreased ABA sensitivity (Watkins et al., 2017) as visualized using DCF and PO1. ROS signals in flavonol deficient mutants were increased in chloroplasts and unidentified endomembrane structures with both sensors, while DCF, but not PO1, was elevated in the nucleus (**Figure 2**).

Guard cells also maintain ROS homeostasis during ABA signaling *via* antioxidant enzymes such as catalases, SODs, thioredoxin reductases, glutathione peroxidases, and ascorbate peroxidases (APX) (Chen and Gallie, 2004; Miao et al., 2006; Jannat et al., 2011; Tiew et al., 2015). The H_2O_2 scavengers, APX1 and catalases 1 and 3 are abundant enzymatic antioxidants in guard cells (Chen and Gallie, 2004; Jannat et al., 2011) and mutants deficient in these enzymes have enhanced ABA responses (Pnueli et al., 2003; Jannat et al., 2011). The *calmodulin-like20* (*cml20*) mutant showed decreased APX2 expression and increased ROS levels, resulting in an ABA hypersensitive stomatal phenotype (Wu et al., 2017), consistent with the absence of antioxidant enzyme synthesis.

DISTINCT LOCATIONS OF ABA-INDUCED ROS

ABA-induced ROS accumulates in the cytoplasm, chloroplasts, nucleus, and endomembrane structures; many of these locations are highlighted by DCF and PO1 accumulation shown in **Figures 1** and **2** (Watkins et al., 2017). In addition to membrane-localized RBOHs, chloroplasts and peroxisomes are also major sources of plant cell ROS that are produced by organelle-localized metabolic processes and enzymatic machinery (Foyer and Noctor, 2003; Asada, 2006). The following sections explore organelle specific ABA-regulated ROS accumulation and signaling.

Nuclear ROS

ABA treatment increases ROS levels in guard cell nuclei (Leshem et al., 2010; Watkins et al., 2014; Watkins et al., 2017), although the mechanisms for this increase are unknown. Isolated tobacco nuclei have increased H_2O_2 following calcium application (Ashtamker et al., 2007), consistent with ROS synthesized within this organelle. Nuclear ROS may also increase *via* diffusion from the cytosol, retrograde signal transport from other organelles (see *Chloroplast* section), or through trafficking of ROS-producing enzymes to the nucleus. The mammalian NOX1 and NOX4 localize to the nucleus to produce ROS necessary for regulating gene expression, (Chamulitrat et al., 2003; Kuroda et al., 2005; Saez et al., 2016), but whether plants share this mechanism is unclear.

Nuclear ROS may function to regulate transcriptional cascades through reversible cysteine oxidation of transcription factors (TFs) to change their activity and/or localization (Peleg-Grossman et al., 2010; Poole, 2015). In plants, several stress responsive TF families such as WRKY, MYB, NAC, heat shock factors (HSF), and ZAT are redox regulated (He et al., 2018). Additionally, ABA-induced ROS could function to oxidize proteases that degrade TFs or modulate kinase or phosphatase activity that target TFs through mechanisms that have been demonstrated in other systems (Schieber and Chandel, 2014).

Endosomes and Endomembrane Trafficking

ABA increases ROS in small endomembrane structures, visualized with both DCF and PO1, which share common features with endosomes (Leshem et al., 2010; Hao et al., 2014; Watkins et al., 2017). In mammalian systems, redox-activated endosomes, termed "redoxosomes", contain NOX family components that deliver ROS where it is needed for productive signaling (Oakley et al., 2009). While literature surrounding endosomal ROS in plants is scarce, endomembrane trafficking has been shown to play a role in ABA-induced stomatal closure. Knockdown of vesicle associated membrane protein 71 family (VAMP71), which mediates endosome fusion to the central vacuole, resulted in increased quantities of ROS-containing vesicles in the cytoplasm, although the magnitude of total ROS was similar to the wild-type. VAMP71 knockdown also impaired stomatal closure following ABA treatment (Leshem et al., 2010). RBOH trafficking may drive these localized ROS increases.

ABA treatment results in clathrin-dependent endocytosis of GFP-RBOHD (Hao et al., 2014). Similarly, salt stress resulted in RBOH endocytosis and increased ROS levels in endosomes (Leshem et al., 2007). Trafficking of ion channels to and from the PM regulates guard cell turgor to modulate stomatal opening (Meckel et al., 2004). Together these findings suggest that the internalization of RBOHs and ion channels into endosomes may be a mechanism to spatially regulate intracellular ROS-mediated signaling. In tomato guard cells, ABA was shown to induce unidentified ROS-containing endomembrane structures that were in greater quantities in mutants with reduced synthesis of flavonol antioxidants (Watkins et al., 2017). Determination of the organelle identity of these endomembrane structures is an important area of future study.

Two other endomembrane organelles may participate in ROS signaling in guard cells. The guard cell central vacuole has recently been suggested to be a site of ROS synthesis *via* a copper amine oxidase (CuAOδ) involved in ABA-dependent vacuolar ROS increases and stomatal closure (Fraudentali et al., 2019). It is not yet clear how vacuolar ROS signals integrate into ABA signaling and guard cell closure. Guard cell ROS may also be regulated by autophagy of aggregated peroxisomes formed under oxidative stress (Yamauchi et al., 2019). Autophagy impaired mutants had increased ROS levels, increased number of oxidized peroxisomes, and decreased sensitivity to light-dependent stomatal opening. Antioxidant treatments rescued this phenotype (Yamauchi et al., 2019), yet whether this is linked to ABA-induced closure was not reported.

Chloroplasts

ABA biosynthesis begins in chloroplasts (Finkelstein, 2013) and ABA signaling and ROS production also occur in this organelle (Asada, 2006; Pornsiriwong et al., 2017). Mg-chelatase H subunit (CHLH) is a chloroplast protein that functions in communicating

chloroplast signals to the nucleus, or retrograde signaling, and positively regulating ABA signaling. A *CHLH* RNAi line has impaired stomatal closure and drought tolerance (Shen et al., 2006). It is still unclear whether CHLH affects ABA-induced ROS production, though *OST1* expression was decreased following CHLH knockdown, suggesting there is crosstalk with positive regulators of ABA-induced ROS (Shen et al., 2006). Initially CHLH was suggested to act as an ABA receptor, but was later shown to modulate ABA signaling without binding ABA directly (Tsuzuki et al., 2011) suggesting additional studies are needed (Cutler et al., 2010).

Other signals that originate within guard cell chloroplasts have been shown to stimulate ROS increases and stomatal closure in Arabidopsis (Zhao et al., 2019). The molecule 3′-phosphoadenosine 5′-phosphate (PAP) shows oxidative stress-induced synthesis and restores ABA-induced ROS production and stomatal phenotypes to the ABA insensitive mutants *ost1*-2 and *abi1-1*. PAP may function in parallel to the canonical ABA machinery by upregulating Ca^{2+} signaling proteins that activate SLAC1 and other ion channels to regulate stomatal closure (Pornsiriwong et al., 2017).

H_2O_2 can be a chloroplast retrograde signal by moving through stromules, which are tubules that extend from chloroplasts to the nucleus (Kwok and Hanson, 2004; Caplan et al., 2015) at a sufficient concentration to induce programmed cell death during pathogen response (Caplan et al., 2015). Stromule formation was induced by ABA and other oxidative signals (Gray et al., 2012; Brunkard et al., 2015), but whether stromules can transport ROS to the nucleus in other stress responses still needs to be evaluated. ROS produced through photorespiration have also been shown to be necessary for stomatal closure (Iwai et al., 2019). Treatment with two photosynthetic electron transport inhibitors in Arabidopsis led to reduced guard cell ROS and stomatal closure in the wild-type and the *rbohd/f* double mutant (Iwai et al., 2019). Together these findings highlight the importance of chloroplast signaling on ABA-induced ROS production and stomatal closure.

CONCLUSION AND FUTURE DIRECTIONS

It is an exciting time to study the role of ROS as second messengers in guard cell signaling. Genetic approaches have shown that ROS produced by RBOH enzymes at the PM plays a significant role in ABA-induced stomatal closure, although there may be other ROS sources that regulate this response. Changes in ROS levels in many of the organelles discussed in this review have been identified *via* colocalization of ROS dyes with organelle-specific probes and reporters. ROS accumulation and how it changes in guard cells in response to elevated ABA in nuclei, chloroplasts, and endosomes are illustrated in **Figure 1C**, which synthesizes results from multiple experiments summarized in this review. While fluorescent dyes provide beneficial spatial information for ROS levels, limitations such as dye irreversibility, working concentration, and incubation time for uptake restrict insights into the temporal dynamics of ROS regulation in guard cells. Moving forward, it will be valuable to apply new tools such as organelle localized, genetically encoded ROS sensors to fully elucidate this information (Anjum et al., 2020). Mutants defective in ROS synthesis and signaling and antioxidant synthesis highlight roles for each organelle in ROS-dependent stomatal closure. Defining the contribution of each ROS source to ABA signaling will allow better understanding of how ABA-induced ROS signals are generated, communicated, and balanced in the guard cell signaling circuit.

AUTHOR CONTRIBUTIONS

AP wrote and edited the article. GM provided scientific and editorial input.

FUNDING

This work was supported by a grant from the National Science Foundation IOS-1558046 to GM and a Center for Molecular Signaling Graduate Research Fellowship to AP.

ACKNOWLEDGMENTS

We acknowledge Xiaotian Jiao for creating the illustration in **Figure 1C** and for helpful discussions. We appreciate the imaging insight from Heather Brown-Harding and the editorial feedback of Jordan Chapman, Allison Delange, and Sheena Gayomba.

REFERENCES

Anjum, N. A., Amreen,, Tantray, A. Y., NA, K., and Ahmad, A. (2020). Reactive oxygen species detection-approaches in plants: Insights into genetically encoded FRET-based sensors. *J. Biotechnol.* 308, 108–117. doi: 10.1016/j.jbiotec.2019.12.003

Asada, K. (2006). Production and Scavenging of Reactive Oxygen Species in Chloroplasts and Their Functions. *Plant Physiol.* 141, 391–396. doi: 10.1104/pp.106.082040

Ashtamker, C., Kiss, V., Sagi, M., Davydov, O., and Fluhr, R. (2007). Diverse subcellular locations of cryptogein-induced reactive oxygen species production in tobacco Bright Yellow-2 cells. *Plant Physiol.* 143, 1817–1826. doi: 10.1104/pp.106.090902

Betteridge, D. J. (2000). What is oxidative stress? *Metabol.: Clin. Exp.* 49, 3–8. doi: 10.1016/S0026-0495(00)80077-3

Bienert, G. P., Moller, A. L., Kristiansen, K. A., Schulz, A., Moller, I. M., Schjoerring, J. K., et al. (2007). Specific aquaporins facilitate the diffusion of hydrogen peroxide across membranes. *J. Biol. Chem.* 282, 1183–1192. doi: 10.1074/jbc.M603761200

Brunkard, J. O., Runkel, A. M., and Zambryski, P. C. (2015). Chloroplasts extend stromules independently and in response to internal redox signals. *Proc. Natl. Acad. Sci.* 112, 10044–10049. doi: 10.1073/pnas.1511570112

Caplan, J. L., Kumar, A. S., Park, E., Padmanabhan, M. S., Hoban, K., Modla, S., et al. (2015). Chloroplast Stromules Function during Innate Immunity. *Dev. Cell.* 34, 45–57. doi: 10.1016/j.devcel.2015.05.011

Chamulitrat, W., Schmidt, R., Tomakidi, P., Stremmel, W., Chunglok, W., Kawahara, T., et al. (2003). Association of gp91phox homolog Nox1 with anchorage-independent growth and MAP kinase-activation of transformed human keratinocytes. *Oncogene* 22, 6045–6053. doi: 10.1038/sj.onc.1206654

Chapman, J. M., Muhlemann, J. K., Gayomba, S. R., and Muday, G. K. (2019). RBOH-Dependent ROS Synthesis and ROS Scavenging by Plant Specialized Metabolites To Modulate Plant Development and Stress Responses. *Chem. Res. Toxicol.* 32, 370–396. doi: 10.1021/acs.chemrestox.9b00028

Chen, Z., and Gallie, D. R. (2004). The ascorbic acid redox state controls guard cell signaling and stomatal movement. *Plant Cell.* 16, 1143–1162. doi: 10.1105/tpc.021584

Chen, X., Zhong, Z., Xu, Z., Chen, L., and Wang, Y. (2010). 2',7'-Dichlorodihydrofluorescein as a fluorescent probe for reactive oxygen species measurement: Forty years of application and controversy. *Free Radical Res.* 44, 587–604. doi: 10.3109/10715761003709802

Cutler, S. R., Rodriguez, P. L., Finkelstein, R. R., and Abrams, S. R. (2010). Abscisic Acid: Emergence of a Core Signaling Network. *Annu. Rev. Plant Biol.* 61, 651–679. doi: 10.1146/annurev-arplant-042809-112122

Demidchik, V. (2018). ROS-Activated Ion Channels in Plants: Biophysical Characteristics, Physiological Functions and Molecular Nature. *Int. J. Mol. Sci.* 19, 1263. doi: 10.3390/ijms19041263

Drerup, M. M., Schlücking, K., Hashimoto, K., Manishankar, P., Steinhorst, L., Kuchitsu, K., et al. (2013). The Calcineurin B-Like Calcium Sensors CBL1 and CBL9 Together with Their Interacting Protein Kinase CIPK26 Regulate the Arabidopsis NADPH Oxidase RBOHF. *Mol. Plant* 6, 559–569. doi: 10.1093/mp/sst009

Finkelstein, R. (2013). Abscisic Acid synthesis and response. *Arabidopsis Book* 11, e0166–e0166. doi: 10.1199/tab.0166

Foyer, C. H., and Noctor, G. (2003). Redox sensing and signalling associated with reactive oxygen in chloroplasts, peroxisomes and mitochondria. *Physiol. Plant.* 119, 355–364. doi: 10.1034/j.1399-3054.2003.00223.x

Fraudentali, I., Ghuge, S. A., Carucci, A., Tavladoraki, P., Angelini, R., Cona, A., et al. (2019). The Copper Amine Oxidase AtCuAOδ Participates in Abscisic Acid-Induced Stomatal Closure in Arabidopsis. *Plants (Basel).* 8, 183. doi: 10.3390/plants8060183

Geiger, D., Scherzer, S., Mumm, P., Stange, A., Marten, I., Bauer, H., et al. (2009). Activity of guard cell anion channel SLAC1 is controlled by drought-stress signaling kinase-phosphatase pair. *Proc. Natl. Acad. Sci. U. S. A.* 106, 21425–21430. doi: 10.1073/pnas.0912021106

Gray, J. C., Hansen, M. R., Shaw, D. J., Graham, K., Dale, R., Smallman, P., et al. (2012). Plastid stromules are induced by stress treatments acting through abscisic acid. *Plant J. Cell Mol. Biol.* 69, 387–398. doi: 10.1111/j.1365-313X.2011.04800.x

Hamilton, D. W. A., Hills, A., Köhler, B., and Blatt, M. R. (2000). Ca2+ channels at the plasma membrane of stomatal guard cells are activated by hyperpolarization and abscisic acid. *Proc. Natl. Acad. Sci.* 97, 4967–4972. doi: 10.1073/pnas.080068897

Hao, H., Fan, L., Chen, T., Li, R., Li, X., He, Q., et al. (2014). Clathrin and Membrane Microdomains Cooperatively Regulate RbohD Dynamics and Activity in Arabidopsis. *Plant Cell.* 26, 1729–1745. doi: 10.1105/tpc.113.122358

He, H., Van Breusegem, F., and Mhamdi, A. (2018). Redox-dependent control of nuclear transcription in plants. *J. Exp. Bot.* 69, 3359–3372. doi: 10.1093/jxb/ery130

Hua, D., Wang, C., He, J., Liao, H., Duan, Y., Zhu, Z., et al. (2012). A plasma membrane receptor kinase, GHR1, mediates abscisic acid- and hydrogen peroxide-regulated stomatal movement in Arabidopsis. *Plant Cell.* 24, 2546–2561. doi: 10.1105/tpc.112.100107

Huang, H., Ullah, F., Zhou, D.-X., Yi, M., and Zhao, Y. (2019). Mechanisms of ROS Regulation of Plant Development and Stress Responses. *Front. Plant Sci.* 10, 800. doi: 10.3389/fpls.2019.00800

Iwai, S., Ogata, S., Yamada, N., Onjo, M., Sonoike, K., and Shimazaki, K.-I. (2019). Guard cell photosynthesis is crucial in abscisic acid-induced stomatal closure. *Plant Direct* 3, e00137–e00137. doi: 10.1002/pld3.137

Jammes, F., Song, C., Shin, D., Munemasa, S., Takeda, K., Gu, D., et al. (2009). MAP kinases MPK9 and MPK12 are preferentially expressed in guard cells and positively regulate ROS-mediated ABA signaling. *Proc. Natl. Acad. Sci.* 106, 20520–20525. doi: 10.1073/pnas.0907205106

Jannat, R., Uraji, M., Morofuji, M., Islam, M. M., Bloom, R. E., Nakamura, Y., et al. (2011). Roles of intracellular hydrogen peroxide accumulation in abscisic acid signaling in Arabidopsis guard cells. *J. Plant Physiol.* 168, 1919–1926. doi: 10.1016/j.jplph.2011.05.006

Kilian, J., Whitehead, D., Horak, J., Wanke, D., Weinl, S., Batistic, O., et al. (2007). The AtGenExpress global stress expression data set: protocols, evaluation and model data analysis of UV-B light, drought and cold stress responses. *Plant J. Cell Mol. Biol.* 50, 347–363. doi: 10.1111/j.1365-313X.2007.03052.x

Kimura, S., Kawarazaki, T., Nibori, H., Michikawa, M., Imai, A., Kaya, H., et al. (2013). The CBL-interacting protein kinase CIPK26 is a novel interactor of Arabidopsis NADPH oxidase AtRbohF that negatively modulates its ROS-producing activity in a heterologous expression system. *J. Biochem.* 153, 191–195. doi: 10.1093/jb/mvs132

Kovtun, Y., Chiu, W.-L., Tena, G., and Sheen, J. (2000). Functional analysis of oxidative stress-activated mitogen-activated protein kinase cascade in plants. *Proc. Natl. Acad. Sci. U. S. A.* 97, 2940–2945. doi: 10.1073/pnas.97.6.2940

Kuroda, J., Nakagawa, K., Yamasaki, T., Nakamura, K., Takeya, R., Kuribayashi, F., et al. (2005). The superoxide-producing NAD(P)H oxidase Nox4 in the nucleus of human vascular endothelial cells. *Genes Cells Devoted Mol. Cell. Mech.* 10, 1139–1151. doi: 10.1111/j.1365-2443.2005.00907.x

Kwak, J. M., Mori, I. C., Pei, Z. M., Leonhardt, N., Torres, M. A., Dangl, J. L., et al. (2003). NADPH oxidase AtrbohD and AtrbohF genes function in ROS-dependent ABA signaling in Arabidopsis. *EMBO J.* 22, 2623–2633. doi: 10.1093/emboj/cdg277

Kwok, E. Y., and Hanson, M. R. (2004). Plastids and stromules interact with the nucleus and cell membrane in vascular plants. *Plant Cell Rep.* 23, 188–195. doi: 10.1007/s00299-004-0824-9

Lee, Y., Kim, Y. J., Kim, M.-H., and Kwak, J. M. (2016). MAPK Cascades in Guard Cell Signal Transduction. *Front. Plant Sci.* 7, 80–80. doi: 10.3389/fpls.2016.00080

Leshem, Y., Seri, L., and Levine, A. (2007). Induction of phosphatidylinositol 3-kinase-mediated endocytosis by salt stress leads to intracellular production of reactive oxygen species and salt tolerance. *Plant J.* 51, 185–197. doi: 10.1111/j.1365-313X.2007.03134.x

Leshem, Y., Golani, Y., Kaye, Y., and Levine, A. (2010). Reduced expression of the v-SNAREs AtVAMP71/AtVAMP7C gene family in Arabidopsis reduces drought tolerance by suppression of abscisic acid-dependent stomatal closure. *J. Exp. Bot.* 61, 2615–2622. doi: 10.1093/jxb/erq099

Li, Q., Wang, Y.-J., Liu, C.-K., Pei, Z.-M., and Shi, W.-L. (2017). The crosstalk between ABA, nitric oxide, hydrogen peroxide, and calcium in stomatal closing of Arabidopsis thaliana. *Biologia* 72, 1140. doi: 10.1515/biolog-2017-0126

Ma, Y., Szostkiewicz, I., Korte, A., Moes, D., Yang, Y., Christmann, A., et al. (2009). Regulators of PP2C phosphatase activity function as abscisic acid sensors. *Sci. (New York NY)* 324, 1064–1068. doi: 10.1126/science.1172408

Meckel, T., Hurst, A. C., Thiel, G., and Homann, U. (2004). Endocytosis against high turgor: intact guard cells of Vicia faba constitutively endocytose fluorescently labelled plasma membrane and GFP-tagged K+-channel KAT1. *Plant J.* 39, 182–193. doi: 10.1111/j.1365-313X.2004.02119.x

Meinhard, M., and Grill, E. (2001). Hydrogen peroxide is a regulator of ABI1, a protein phosphatase 2C from Arabidopsis. *FEBS Lett.* 508, 443–446. doi: 10.1016/S0014-5793(01)03106-4

Meinhard, M., Rodriguez, P. L., and Grill, E. (2002). The sensitivity of ABI2 to hydrogen peroxide links the abscisic acid-response regulator to redox signalling. *Planta* 214, 775–782. doi: 10.1007/s00425-001-0675-3

Miao, Y., Lv, D., Wang, P., Wang, X. C., Chen, J., Miao, C., et al. (2006). An Arabidopsis glutathione peroxidase functions as both a redox transducer and a scavenger in abscisic acid and drought stress responses. *Plant Cell.* 18, 2749–2766. doi: 10.1105/tpc.106.044230

Mittler, R. (2017). ROS Are Good. *Trends Plant Sci.* 22, 11–19. doi: 10.1016/j.tplants.2016.08.002

Murata, Y., Pei, Z. M., Mori, I. C., and Schroeder, J. (2001). Abscisic acid activation of plasma membrane Ca(2+) channels in guard cells requires cytosolic NAD(P)H and is differentially disrupted upstream and downstream of reactive oxygen species production in abi1-1 and abi2-1 protein phosphatase 2C mutants. *Plant Cell.* 13, 2513–2523. doi: 10.1105/tpc.010210

Mustilli, A. C., Merlot, S., Vavasseur, A., Fenzi, F., and Giraudat, J. (2002). Arabidopsis OST1 protein kinase mediates the regulation of stomatal aperture by abscisic acid and acts upstream of reactive oxygen species production. *Plant Cell.* 14, 3089–3099. doi: 10.1105/tpc.007906

Nilson, S. E., and Assmann, S. M. (2007). The Control of Transpiration. Insights from Arabidopsis. *Plant Physiol.* 143, 19–27. doi: 10.1104/pp.106.093161

Nishimura, N., Sarkeshik, A., Nito, K., Park, S.-Y., Wang, A., Carvalho, P. C., et al. (2010). PYR/PYL/RCAR family members are major in-vivo ABI1 protein phosphatase 2C-interacting proteins in Arabidopsis. *Plant J. Cell Mol. Biol.* 61, 290–299. doi: 10.1111/j.1365-313X.2009.04054.x

Oakley, F. D., Abbott, D., Li, Q., and Engelhardt, J. F. (2009). Signaling components of redox active endosomes: the redoxosomes. *Antioxidants Redox Signaling* 11, 1313–1333. doi: 10.1089/ars.2008.2363

Park, S. Y., Fung, P., Nishimura, N., Jensen, D. R., Fujii, H., Zhao, Y., et al. (2009). Abscisic acid inhibits type 2C protein phosphatases via the PYR/PYL family of START proteins. *Sci. (New York NY)* 324, 1068–1071. doi: 10.1126/science.1173041

Pei, Z. M., Murata, Y., Benning, G., Thomine, S., Klusener, B., Allen, G. J., et al. (2000). Calcium channels activated by hydrogen peroxide mediate abscisic acid signalling in guard cells. *Nature* 406, 731–734. doi: 10.1038/35021067

Peleg-Grossman, S., Melamed-Book, N., Cohen, G., and Levine, A. (2010). Cytoplasmic H2O2 prevents translocation of NPR1 to the nucleus and inhibits the induction of PR genes in Arabidopsis. *Plant Signaling Behav.* 5, 1401–1406. doi: 10.4161/psb.5.11.13209

Pnueli, L., Liang, H., Rozenberg, M., and Mittler, R. (2003). Growth suppression, altered stomatal responses, and augmented induction of heat shock proteins in cytosolic ascorbate peroxidase (Apx1)-deficient Arabidopsis plants. *Plant J. Cell Mol. Biol.* 34, 187–203. doi: 10.1046/j.1365-313X.2003.01715.x

Poole, L. B. (2015). The basics of thiols and cysteines in redox biology and chemistry. *Free Radic. Biol. Med.* 80, 148–157. doi: 10.1016/j.freeradbiomed.2014.11.013

Pornsiriwong, W., Estavillo, G. M., Chan, K. X., Tee, E. E., Ganguly, D., Crisp, P. A., et al. (2017). A chloroplast retrograde signal, 3'-phosphoadenosine 5'-phosphate, acts as a secondary messenger in abscisic acid signaling in stomatal closure and germination. *eLife* 6, e23361. doi: 10.7554/eLife.23361

Qi, J., Song, C. P., Wang, B., Zhou, J., Kangasjärvi, J., Zhu, J. K., et al. (2018). Reactive oxygen species signaling and stomatal movement in plant responses to drought stress and pathogen attack. *J. Integr. Plant Biol.* 60, 805–826. doi: 10.1111/jipb.12654

Qu, Y., Yan, M., and Zhang, Q. (2017). Functional regulation of plant NADPH oxidase and its role in signaling. *Plant Signaling Behav.* 12, e1356970–e1356970. doi: 10.1080/15592324.2017.1356970

Qu, Y., Song, P., Hu, Y., Jin, X., Jia, Q., Zhang, X., et al. (2018). Regulation of stomatal movement by cortical microtubule organization in response to darkness and ABA signaling in Arabidopsis. *Plant Growth Regul.* 84, 467–479. doi: 10.1007/s10725-017-0353-5

Rodrigues, O., Reshetnyak, G., Grondin, A., Saijo, Y., Leonhardt, N., Maurel, C., et al. (2017). Aquaporins facilitate hydrogen peroxide entry into guard cells to mediate ABA- and pathogen-triggered stomatal closure. *Proc. Natl. Acad. Sci.* 114, 9200–9205. doi: 10.1073/pnas.1704754114

Saez, F., Hong, N. J., and Garvin, J. L. (2016). Luminal flow induces NADPH oxidase 4 translocation to the nuclei of thick ascending limbs. *Physiol. Rep.* 4, e12724. doi: 10.14814/phy2.12724

Schieber, M., and Chandel, N. S. (2014). ROS function in redox signaling and oxidative stress. *Curr. Biol. CB.* 24, R453–R462. doi: 10.1016/j.cub.2014.03.034

Schroeder, J. I., Allen, G. J., Hugouvieux, V., Kwak, J. M., and Waner, D. (2001). GUARD CELL SIGNAL TRANSDUCTION. *Annu. Rev. Plant Physiol. Plant Mol. Biol.* 52, 627–658. doi: 10.1146/annurev.arplant.52.1.627

Shen, Y.-Y., Wang, X.-F., Wu, F.-Q., Du, S.-Y., Cao, Z., Shang, Y., et al. (2006). The Mg-chelatase H subunit is an abscisic acid receptor. *Nature* 443, 823–826. doi: 10.1038/nature05176

Sierla, M., Horak, H., Overmyer, K., Waszczak, C., Yarmolinsky, D., Maierhofer, T., et al. (2018). The Receptor-like Pseudokinase GHR1 Is Required for Stomatal Closure. *Plant Cell.* 30, 2813–2837. doi: 10.1105/tpc.18.00441

Singh, R., Parihar, P., Singh, S., Mishra, R. K., Singh, V. P., and Prasad, S. M. (2017). Reactive oxygen species signaling and stomatal movement: Current updates and future perspectives. *Redox Biol.* 11, 213–218. doi: 10.1016/j.redox.2016.11.006

Sirichandra, C., Gu, D., Hu, H. C., Davanture, M., Lee, S., Djaoui, M., et al. (2009). Phosphorylation of the Arabidopsis AtrbohF NADPH oxidase by OST1 protein kinase. *FEBS Lett.* 583, 2982–2986. doi: 10.1016/j.febslet.2009.08.033

Suzuki, N., Miller, G., Morales, J., Shulaev, V., Torres, M. A., and Mittler, R. (2011). Respiratory burst oxidases: the engines of ROS signaling. *Curr. Opin. Plant Biol.* 14, 691–699. doi: 10.1016/j.pbi.2011.07.014

Tõldsepp, K., Zhang, J., Takahashi, Y., Sindarovska, Y., Hõrak, H., Ceciliato, P. H. O., et al. (2018). Mitogen-activated protein kinases MPK4 and MPK12 are key components mediating CO2-induced stomatal movements. *Plant J.* 96, 1018–1035. doi: 10.1111/tpj.14087

Tian, S., Wang, X., Li, P., Wang, H., Ji, H., Xie, J., et al. (2016). Plant Aquaporin AtPIP1;4 Links Apoplastic H2O2 Induction to Disease Immunity Pathways. *Plant Physiol.* 171, 1635–1650. doi: 10.1104/pp.15.01237

Tiew, T. W.-Y., Sheahan, M. B., and Rose, R. J. (2015). Peroxisomes contribute to reactive oxygen species homeostasis and cell division induction in Arabidopsis protoplasts. *Front. Plant Sci.* 6, 658. doi: 10.3389/fpls.2015.00658

Torres, M. A., and Dangl, J. L. (2005). Functions of the respiratory burst oxidase in biotic interactions, abiotic stress and development. *Curr. Opin. Plant Biol.* 8, 397–403. doi: 10.1016/j.pbi.2005.05.014

Tsuzuki, T., Takahashi, K., Inoue, S.-i., Okigaki, Y., Tomiyama, M., Hossain, M. A., et al. (2011). Mg-chelatase H subunit affects ABA signaling in stomatal guard cells, but is not an ABA receptor in Arabidopsis thaliana. *J. Plant Res.* 124, 527–538. doi: 10.1007/s10265-011-0426-x

Umezawa, T., Sugiyama, N., Mizoguchi, M., Hayashi, S., Myouga, F., Yamaguchi-Shinozaki, K., et al. (2009). Type 2C protein phosphatases directly regulate abscisic acid-activated protein kinases in Arabidopsis. *Proc. Natl. Acad. Sci.* 106, 17588–17593. doi: 10.1073/pnas.0907095106

Vishwakarma, K., Upadhyay, N., Kumar, N., Yadav, G., Singh, J., Mishra, R. K., et al. (2017). Abscisic Acid Signaling and Abiotic Stress Tolerance in Plants: A Review on Current Knowledge and Future Prospects. *Front. Plant Sci.* 8, 161. doi: 10.3389/fpls.2017.00161

Waszczak, C., Akter, S., Jacques, S., Huang, J., Messens, J., and Van Breusegem, F. (2015). Oxidative post-translational modifications of cysteine residues in plant signal transduction. *J. Exp. Bot.* 66, 2923–2934. doi: 10.1093/jxb/erv084

Watkins, J. M., Hechler, P. J., and Muday, G. K. (2014). Ethylene-induced flavonol accumulation in guard cells suppresses reactive oxygen species and moderates stomatal aperture. *Plant Physiol.* 164, 1707–1717. doi: 10.1104/pp.113.233528

Watkins, J. M., Chapman, J. M., and Muday, G. K. (2017). Abscisic Acid-Induced Reactive Oxygen Species Are Modulated by Flavonols to Control Stomata Aperture. *Plant Physiol.* 175, 1807–1825. doi: 10.1104/pp.17.01010

Wu, X., Qiao, Z., Liu, H., Acharya, B. R., Li, C., and Zhang, W. (2017). CML20, an Arabidopsis Calmodulin-like Protein, Negatively Regulates Guard Cell ABA Signaling and Drought Stress Tolerance. *Front. Plant Sci.* 8, 824–824. doi: 10.3389/fpls.2017.00824

Xu, J., Xie, J., Yan, C., Zou, X., Ren, D., and Zhang, S. (2014). A chemical genetic approach demonstrates that MPK3/MPK6 activation and NADPH oxidase-mediated oxidative burst are two independent signaling events in plant immunity. The. *Plant J. Cell Mol. Biol.* 77, 222–234. doi: 10.1111/tpj.12382

Xu, Z., Jiang, Y., Jia, B., and Zhou, G. (2016). Elevated-CO2 Response of Stomata and Its Dependence on Environmental Factors. *Front. Plant Sci.* 7, 657–657. doi: 10.3389/fpls.2016.00657

Yamauchi, S., Mano, S., Oikawa, K., Hikino, K., Teshima, K. M., Kimori, Y., et al. (2019). Autophagy controls reactive oxygen species homeostasis in guard cells that is essential for stomatal opening. *Proc. Natl. Acad. Sci.* 116, 19187–19192. doi: 10.1073/pnas.1910886116

Yuasa, T., Ichimura, K., Mizoguchi, T., and Shinozaki, K. (2001). Oxidative stress activates ATMPK6, an Arabidopsis homologue of MAP kinase. *Plant Cell Physiol.* 42, 1012–1016. doi: 10.1093/pcp/pce123

Yun, B.-W., Feechan, A., Yin, M., Saidi, N. B. B., Le Bihan, T., Yu, M., et al. (2011). S-nitrosylation of NADPH oxidase regulates cell death in plant immunity. *Nature* 478, 264–268. doi: 10.1038/nature10427

Zhang, X., Zhang, L., Dong, F., Gao, J., Galbraith, D. W., and Song, C. P. (2001). Hydrogen peroxide is involved in abscisic acid-induced stomatal closure in Vicia faba. *Plant Physiol.* 126, 1438–1448. doi: 10.1104/pp.126.4.1438

Zhang, Y., Zhu, H., Zhang, Q., Li, M., Yan, M., Wang, R., et al. (2009). Phospholipase Dα1 and Phosphatidic Acid Regulate NADPH Oxidase Activity and Production of Reactive Oxygen Species in ABA-Mediated Stomatal Closure in Arabidopsis. *Plant Cell.* 21, 2357–2377. doi: 10.1105/tpc.108.062992

Zhao, C., Wang, Y., Chan, K. X., Marchant, D. B., Franks, P. J., Randall, D., et al. (2019). Evolution of chloroplast retrograde signaling facilitates green plant adaptation to land. *Proc. Natl. Acad. Sci.* 116, 5015–5020. doi: 10.1073/pnas.1812092116

Zhu, J.-K. (2016). Abiotic Stress Signaling and Responses in Plants. *Cell* 167, 313–324. doi: 10.1016/j.cell.2016.08.029

Conflict of Interest: The authors declare that the research was conducted in the absence of any commercial or financial relationships that could be construed as a potential conflict of interest.

frontiers in Plant Science

REVIEW
published: 02 July 2020
doi: 10.3389/fpls.2020.00881

Flanking Support: How Subsidiary Cells Contribute to Stomatal Form and Function

Antonia Gray†, Le Liu† and Michelle Facette†*

Department of Biology, University of Massachusetts Amherst, Amherst, MA, United States

Few evolutionary adaptations in plants were so critical as the stomatal complex. This structure allows transpiration and efficient gas exchange with the atmosphere. Plants have evolved numerous distinct stomatal architectures to facilitate gas exchange, while balancing water loss and protection from pathogens that can egress via the stomatal pore. Some plants have simple stomata composed of two kidney-shaped guard cells; however, the stomatal apparatus of many plants includes subsidiary cells. Guard cells and subsidiary cells may originate from a single cell lineage, or subsidiary cells may be recruited from cells adjacent to the guard mother cell. The number and morphology of subsidiary cells varies dramatically, and subsidiary cell function is also varied. Subsidiary cells may support guard cell function by offering a mechanical advantage that facilitates guard cell movements, and/or by acting as a reservoir for water and ions. In other cases, subsidiary cells introduce or enhance certain morphologies (such as sunken stomata) that affect gas exchange. Here we review the diversity of stomatal morphology with an emphasis on multi-cellular stomata that include subsidiary cells. We will discuss how subsidiary cells arise and the divisions that produce them; and provide examples of anatomical, mechanical and biochemical consequences of subsidiary cells on stomatal function.

Keywords: stomata, subsidiary cell, guard cell, plant development, cell division

OPEN ACCESS

Edited by:
Scott McAdam,
Purdue University, United States

Reviewed by:
Fulton Rockwell,
Harvard University, United States
Danilo M. Daloso,
Federal University of Ceara, Brazil

***Correspondence:**
Michelle Facette
mfacette@umass.edu

†ORCID:
Antonia Gray
orcid.org/0000-0002-1001-3898
Le Liu
orcid.org/0000-0002-4262-5063
Michelle Facette
orcid.org/0000-0002-6214-9359

Specialty section:
This article was submitted to Plant Development and EvoDevo, a section of the journal Frontiers in Plant Science

Received: *21 December 2019*
Accepted: *29 May 2020*
Published: *02 July 2020*

Citation:
Gray A, Liu L and Facette M (2020) Flanking Support: How Subsidiary Cells Contribute to Stomatal Form and Function. Front. Plant Sci. 11:881. doi: 10.3389/fpls.2020.00881

INTRODUCTION: WHAT IS A SUBSIDIARY CELL?

Subsidiary cells are non-guard cells within the stomatal complex. But how do we determine which cells are subsidiary cells? Guard cells flank the stomatal pore and therefore are easily identified. Guard cells have rightly been the focus of scientific inquiry into stomatal function. Turgor-driven movements of guard cell pairs regulate stomatal aperture, and over the last two decades our knowledge of guard cell function has improved dramatically (reviewed in Munemasa et al., 2015; Eisenach and De Angeli, 2017; Jezek and Blatt, 2017). However, relatively little progress has been made toward understanding the role of subsidiary cells. Moreover, identifying and defining exactly which cells comprise the stomatal complex (and even which plants possess them) has proven non-trivial. Taxonomists, anatomists, physiologists, and developmental biologists are likely to have different perspectives on what defines a subsidiary cell. We best identify as developmental biologists, but in this review attempt to synthesize information on subsidiary cells from several perspectives. We choose to define subsidiary cells broadly: cells that are adjacent to guard cells (but not necessarily touching) and are distinct from other epidermal cells. "Distinct" is most easily

identified by a unique morphology, but may also be identified by a unique molecular signature. As part of the stomatal complex, subsidiary cells may support guard cell function – but how subsidiary cells do this is likely to be varied and may be biochemical, mechanical or anatomical. In fact, in many cases the definition is taxonomic, but without a complete understanding of the physiological contributions subsidiary cells offer guard cells, a precise definition is difficult.

Ambiguity in subsidiary cell identification is not a recent development. Pant defines a subsidiary cell as any cell that is "recognizably modified" and touching a guard cell; he calls specialized cells surrounding the subsidiary that do not touch a guard cell an "encircling cell" (Pant, 1965). In her classic textbook, Esau identifies subsidiary cells as those that "appear to be associated functionally [. . .] and are morphologically distinct from other epidermal cells" (Esau, 1965) and may include cells that do not touch. Unfortunately, even these relatively simple definitions can be ambiguous or conflicting – both rely on subjective assessments of whether a subsidiary cell has a "distinct" or "recognizably modified" morphology. We use language consistent with Tomlinson (1969) and term all of these subsidiary cells. We consider any cell associated with guard cells that has an identity distinct from neighboring cells a subsidiary cell. A distinct identity can be defined not only by a unique morphology, but by a unique molecular signature (such as genes or proteins expressed). The division sequence of subsidiary cells may produce anatomically distinct cells. In our inclusive definition, we consider taxonomic and anatomical contributions as important as physiological contributions, but realize as our understanding of subsidiary cell function expands more refined definitions will likely develop.

Contrasting the stomatal apparatus between the model systems *Arabidopsis thaliana* and *Zea mays* highlights some of the difficulty in identifying subsidiary cells. In many cases it is simple to identify morphologically distinct cells flanking the guard cells, such as the case in *Z. mays* (corn or maize). In *Z. mays* and other grasses subsidiary cells are always in pairs flanking the guard cells, are uniquely shaped, are more pectin-rich and are therefore readily identified (**Figure 1A**). However, in the *Brassicaceae* – which includes the model species *A. thaliana* – subsidiary cells are subtly different from epidermal cells. The subsidiary cells are unequal in size and variable in shape, making them difficult to identify (**Figure 1B**). Not every stomatal complex within the same *A. thaliana* leaf includes subsidiary cells (Nadeau and Sack, 2002). This morphological ambiguity has led to disagreement as to whether *A. thaliana* has subsidiary cells at all (Serna and Fenoll, 2000; Nunes et al., 2020). Given the subtle shape differences in putative subsidiary cells in *A. thaliana,* molecular markers may be a good way to identify subsidiary cells. Gene-specific expression may be considered evidence supporting an identity distinct from other epidermal cells, which may in turn be indicative of a unique function. PATROL1 controls protein trafficking including that of the plasma membrane proton pump AHA1, which is important for guard cell function (Hashimoto-Sugimoto et al., 2013). *PATROL1* is expressed in guard cells and a subset of adjacent cells – which are subsidiary cells (Higaki et al., 2014). Since not all guard-cell adjacent cells express *PATROL1*, but rather it appears in the smaller cells previously identified as subsidiary cells, this indicates these cells have a unique molecular identity and should be considered part of the stomatal complex. Additional molecular markers of subsidiary cell fate will help clarify if (and which) guard-cell adjacent cells have identities distinct from other epidermal cells, but none are currently known in *A. thaliana*. In *Z. mays,* where subsidiary cells are morphologically obvious, there are potential molecular markers of subsidiary cell identity. A SWEET-family protein is expressed in subsidiary cells (Wang et al., 2019b). A gene encoding a specific *Shaker*-family potassium channel is also specifically expressed in maize subsidiary cells (Büchsenschütz et al., 2005). Whether expression of these genes – and subsidiary cell identity in general – is conserved across species is unknown. We predict that while some characteristics might be preserved, there is likely to be a large variation in the molecular components within subsidiary cells since they are varied in morphology, size, and ontogeny. A more thorough understanding of subsidiary cell function will help in accurate classification.

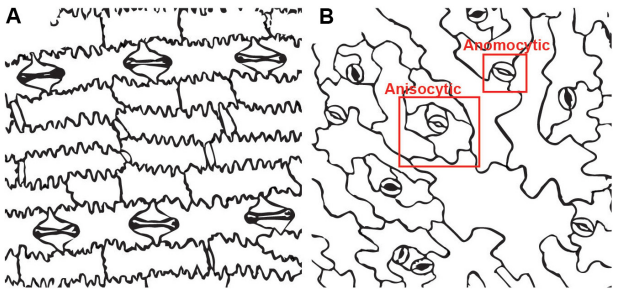

FIGURE 1 | Stomatal complexes in two model systems. **(A)** *Zea mays* (maize) has paracytic stomata. The subsidiary cells dominate the stomatal complex while the guard cells are a pair of small dumbbell shaped cells in the center.**(B)** *Arabidopsis thaliana* has both anisocytic stomata with three subsidiary cells and anomocytic stomata with no subsidiary cells. The anisocytic stomatacan be difficult to detect, since the subsidiary cells are variable in size.

WHAT DO SUBSIDIARY CELLS LOOK LIKE?

Subsidiary cells vary widely in number, arrangement and potential function. The diversity in stomatal apparatus morphology is due primarily to diversity in subsidiary cell features, which has led to accepted definitions of subsidiary cell arrangements. Stomatal terminology was originally associated with certain taxonomic groups; thus, the language of stomatal subtypes is elaborate. It can be confusing at best, and conflicting at times. Our coverage of stomatal complexes will not be exhaustive; rather we will highlight stomatal patterns that either illustrate different ontogenies or stomatal morphologies, especially those that we feel are interesting from a developmental perspective or highlight physiological contributions. A recent survey of stomatal complex morphologies, from a variety of monocot plant lineages and their cell divisions, is reviewed in Rudall et al. (2013). Texts that cover stomatal complex

morphology that we have found particularly informative include: (Pant, 1965; Tomlinson, 1969, 1974; Fryns-Claessens and Van Cotthem, 1973; Ziegler, 1987; Prabhakar, 2004; Carpenter, 2005).

Examples of known stomatal morphologies imaged via confocal microscopy, including reconstructed side views through the stomatal pore, are in **Figures 2**, **3**. Division patterns to achieve different stomatal morphologies are in **Figure 4**. Lateral subsidiary cells run parallel to the stomatal pore whereas polar subsidiary cells are perpendicular to the stomatal pore. Stomata that have no discernable subsidiary cells are called anomocytic, such as those in *Selaginella uncinata* (**Figure 2A**). Previously, anomocytic stomata were termed ranunculaceous (Metcalfe and Chalke, 1957). *A. thaliana* has both anomocytic stomata and anisocytic stomatal complexes (**Figure 1A**). Anisocytic stomatal complexes have three unequally sized subsidiary cells associated with the guard cell pair, where one of these three cells is smaller than the other two. Previously, anisocytic stomata were termed cruciferous because this arrangement is typical of crucifers such as *A. thaliana* (Metcalfe and Chalke, 1957). Wild tomato (*Solanum spp.)* may also have both anomocytic and anisocytic stomata (**Figure 2B**; Sampaio et al., 2014). Comparison of the physiological responses of different adjacent stomata – those with and without subsidiary cells – in species such as *A. thaliana* or tomato would help illustrate the functional contributions of subsidiary cells in a species where only subtle morphological differences exist.

Stomatal complexes with a pair of lateral subsidiary cells are called paracytic (previously rubiaceous) (Metcalfe and Chalke, 1957). *Coffea rubiacea* (coffee) has paracytic stomata (**Figure 2C**). Grass stomata are not only paracytic, but also have dumbbell-shaped guard cells and therefore are termed Graminacious (**Figure 2D**). The contributions of subsidiary cells in grasses are arguably the best studied (e.g., Raschke and Fellows, 1971; Majore et al., 2002; Raissig et al., 2017; Wang et al., 2019b). The subsidiaries align along the outer edge of the guard cell and maintain the symmetrically parallel arrangement of guard cells. It is easy to imagine how the extended cell-cell contact might help support guard cells mechanically and biochemically. Graminaceous stomata have been recognized for their rapid movements, which is thought to be attributable to both their paracytic subsidiary cells and the unique shape of the guard cells (Johnsson et al., 1976; Franks and Farquhar, 2007; Vico et al., 2011). *Musa acuminata* (banana) stomata are an example of how stomatal form can be difficult to classify (**Figure 2E**). A pair of obvious lateral subsidiary cells indicate paracytic stomata; however, in some cases it appears there may be a pair of polar subsidiary cells as well, or in some cases even up to six subsidiaries (hexacytic). In side view, lateral subsidiary cells overarch the stomatal pore, whereas none of the other adjacent cells do so; hence we predict all these stomatal complexes are paracytic. As-of-yet unidentified molecular markers would help clarify these cells' identities.

Stomata with a pair of polar subsidiary cells perpendicular to the guard cell pore orientation are called diacytic (previously caryophyllaceous), such as those in *Dianthus chinensis* (**Figure 2F**). Note the cuticular ledges of *D. chinensis* (magenta) that are set back from the pore (**Figure 2Fi**) and can be seen in side view (**Figure 2Fii**). In contrast, these cuticular ledges are quite close to the center of the pore in coffee and tomato.

More complicated stomatal architectures are shown in **Figure 3**. Subsidiary cells in *Kalanchoe* spp. are easy to identify and this plant displays several stomatal types within a single leaf (**Figure 3A**). **Figure 3Ai** shows an anisocytic stomatal complex, but often stomatal complexes with a spiral pattern of additional subsidiary cells can be observed, such as in the upper right corner of **Figure 3Aiii**. This spiraling pattern is termed heliocytic (Fryns-Claessens and Van Cotthem, 1973); although spiral stomatal complexes in *Kalanchoe* spp. have been otherwise classified (Inamdar and Patel, 1970; Xu et al., 2018; Nunes et al., 2020). Stomata in *Begonia* spp. are likewise heliocytic (**Figure 3B**) and may be found in clusters or individually (**Figure 5**). The pattern of cell divisions that produce anisocytic and heliocytic stomata are initially similar (discussed in the section below) therefore it is notable that *Kalanchoe* spp. has both stomatal architectures. Stomatal complexes of *Didierea madagascariensis* are unique; they may be paracytic but often will have additional C-shaped subsidiary cells (**Figure 3C**).

Stomata with four stomata are often termed tetracytic, although the cell arrangements vary. For example, *Anacampseros rufescens* has 4 lateral subsidiary cells (**Figure 3D**) while *Agave bracena* has 2 lateral and 2 polar subsidiaries (**Figure 3E**). The stomata of *Agave* are dramatically sunken, as seen in the side view in **Figure 2Fii**. The guard cell pair lies well below the epidermal surface, and the subsidiary cells extend upward to create the walls of the pore, and the cuticular stomatal ledges are on the subsidiary cells. Here, the main contribution of subsidiary cells is perhaps anatomical. Likewise, the gymnosperm *Ginkgo biloba* has sunken stomata (**Figure 3F**). The many subsidiary cells of gingko are variable in number and are arranged in a circular pattern that reaches over the recessed guard cells, which is called cyclocytic.

Even without a thorough examination of all the possible stomatal complex arrangements, the terminology is dense and classification can become challenging. Within some families stomatal morphology is highly conserved while in others it can be quite variable (Baranova, 1992). This variability, coupled with the difficulty in identifying subsidiary cells, led to the suggestion that the division patterns leading to stomatal complex formation is a more accurate classification system because the division sequence is more conservative than the final structure (Rasmussen, 1981; Ziegler, 1987). Stomatal ontogeny – that is, the divisions that generate stomata – are distinct from stomatal complex classification based on subsidiary cell arrangement.

HOW DO SUBSIDIARY CELLS ARISE?

Plant stomatal complexes are derived from a carefully controlled series of asymmetric cell divisions (Sack, 1987; Facette and Smith, 2012; Torii, 2015; Shao and Dong, 2016; Simmons and Bergmann, 2016; Chater et al., 2017). Stebbins and Shah noted the importance of understanding the mechanisms behind stomatal complex formation, and the utility of studying them as a model system for asymmetric cell divisions 60 years ago (Stebbins and Shah, 1960). Stomatal divisions have been used as a model

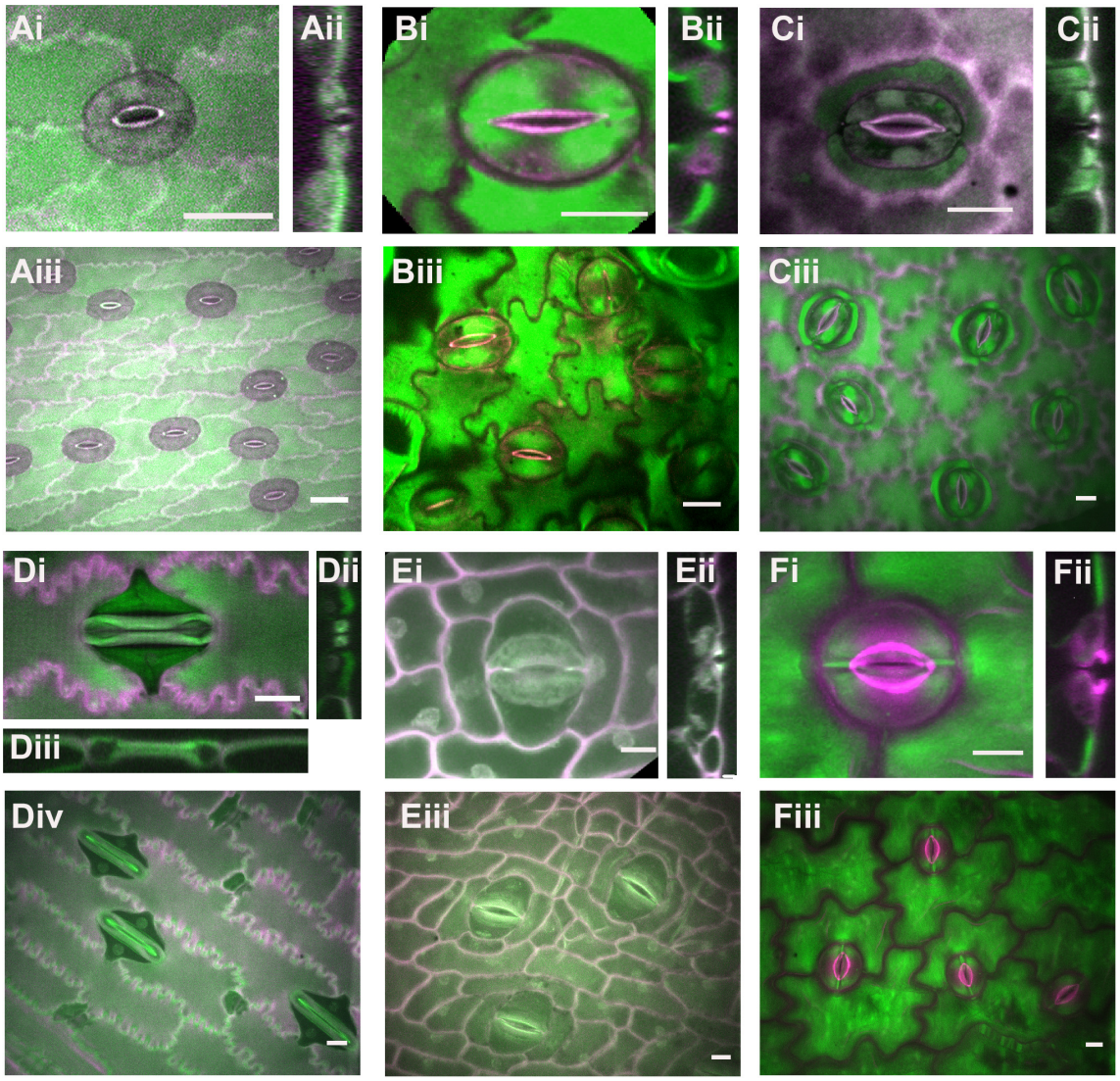

FIGURE 2 | Stomatal complex types, part 1. All images are imaged via confocal microscopy. Images **(i,iii)** are full or partial z-projections while image **(ii)** is a 3D-reconstructed side view through the stomatal pore. **(A)** *Selaginella uncinata* – anomocytic. **(B)** *Solanum* spp. (wild tomato) – anomocytic. **(C)** *Coffea rubiaceae* (coffee) – paracytic **(D)** *Zea mays* (maize/corn) – paracytic **(E)** *Musa acuminate* (banana) – paracytic **(F)** *Dianthus chinensis*; diacytic. Green = Calcofluor White and Magenta = Direct Red, except for **(Di,Dii)** where Green = Aniline Blue and Magenta = Direct Red. All scale bars are 15 micrometers.

for asymmetric division in large number of model systems as they present opportunities to study cell polarity, cell-cell communication, and cell division (Pickett-Heaps, 1969; Zeiger and Stebbins, 1972; Palevitz and Hepler, 1974; Apostolakos and Galatis, 1987; Cleary, 1995; Geisler et al., 2000; Shpak et al., 2004; MacAlister et al., 2007; Dong et al., 2009; Hunt and Gray, 2009; Chater et al., 2016; Raissig et al., 2016).

Generation of guard cell pairs occurs in a stereotypical fashion. A protodermal cells in the epidermis of immature leaves differentiates into a meristemoid mother cells (MMC); the MMC divides asymmetrically to give a small meristemoid and a stomatal lineage cell. The meristemoid differentiates into a guard mother cell (GMC), which divides via a symmetric oriented division to yield the two guard cells. Prior to the division of the GMC, subsidiary cells (if present) arise. Subsidiary cells may be generated via divisions of the meristemoid or MMC, in which case they are termed mesogenous (Metcalfe and Chalke, 1957). In mesogenous stomata the subsidiary cells and guard cells are derived from the same cell lineage. In other cases, protodermal cells adjacent to the meristemoid or GMC are recruited, and subsidiary cells therefore are derived from a lineage that is distinct from the guard cells. In this case, subsidiary cells are of perigenous origin (Metcalfe and Chalke, 1957). Necessarily, stomata of perigenous origin require cell-cell communication with the neighboring epidermal cells – very often particular neighbors on certain sides of the GMC – that are recruited into the stomatal complex. Mesoperigenous stomata have both subsidiary cells

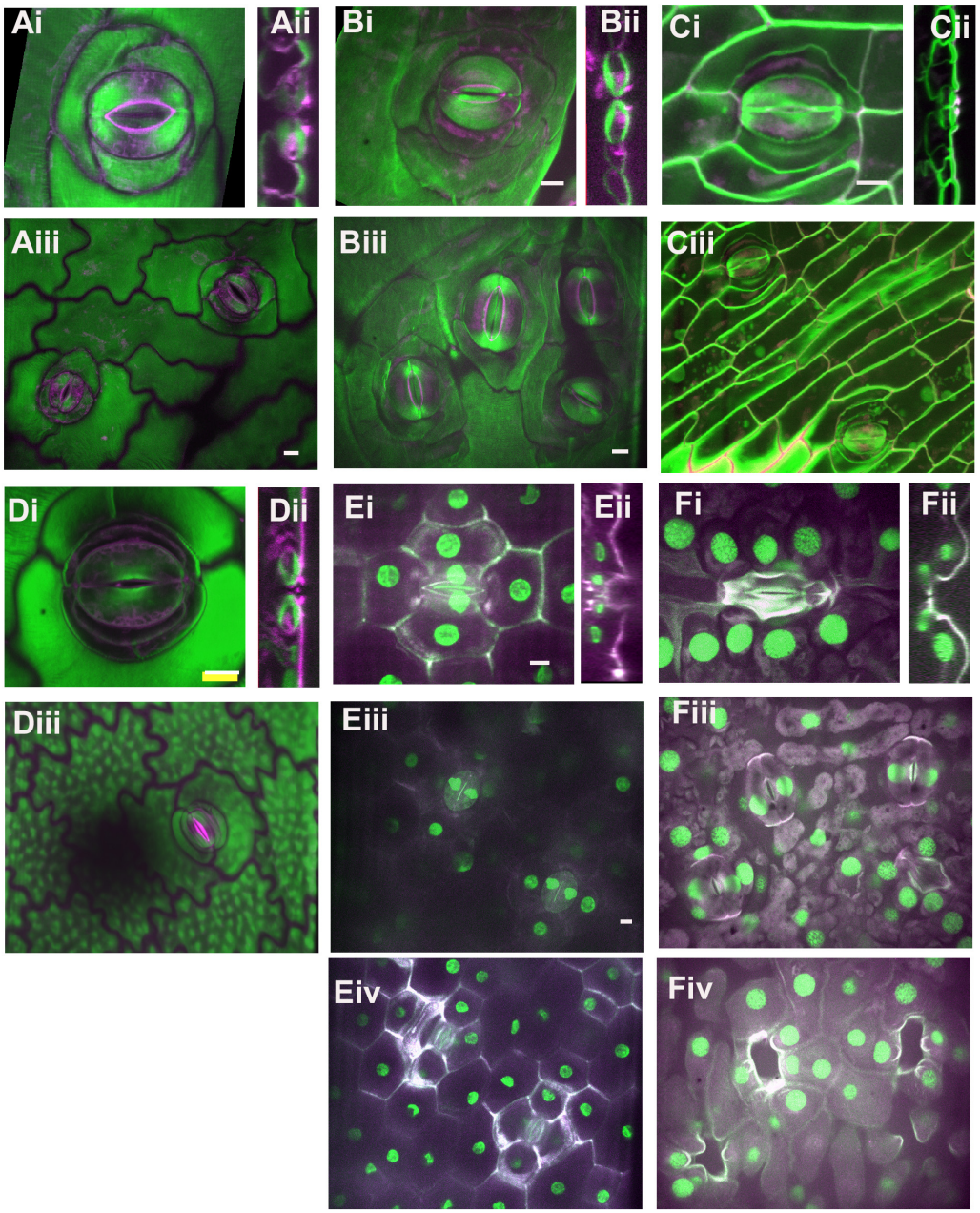

FIGURE 3 | Stomatal complex types, part 2. All images are imaged via confocal microscopy. Images **(i,iii)** are full or partial z-projections while image **(ii)** is a 3D-reconstructed side view through the stomatal pore. For sunken stomata in *Agave* and gingko **(E,F)** a lower focal plane containing the guard cells **(iii)** and a higher focal plane showing epidermal and subsidiary cells **(iv)** are shown. **(A)** *Kalanchoe* spp. (common unknown variety from garden center); anisocytic and heliocytic. **(B)** *Begonia spp*. (common unknown variety from garden center) – heliocytic **(C)** *Didierea madagascariensis* - unusual type **(D)** *Anacampseros rufescens* – tetracytic with four lateral subsidiary cells **(E)** *Agave bracena* – tetracytic with 2 lateral and 2 polar subsidiary cells. **(F)** *Ginkgo biloba* – cyclocytic. Green = Calcofluor White and Magenta = Direct Red, except for **(E,F)** where Green = Propidium Iodide and Magenta = Calcafluor White. All scale bars are 15 micrometers.

that arise from the same stomatal lineage as the GMC and subsidiary cells that are recruited from neighboring cells. More detailed and complex subclassifications of stomatal ontogenies exist (Pant, 1965; Tomlinson, 1974; Rasmussen, 1981). Regardless of whether the stomatal complex is of mesogenous or perigenous origin, the number of times a cell divides (in addition to which cells divide) has ramifications for final stomatal morphology.

A few contrasting examples of stomatal divisions are provided in **Figure 4**. Many reviews regarding *A. thaliana* cell divisions as well as the molecular factors (transcriptional regulators, signaling and scaffolding molecules, and cell cycle regulators)

exist and thus will not be covered extensively here. Many fate factors appear to be conserved across phyla (Harris et al., 2020). The divisions that create anisocytic stomata such as those in *A. thaliana* are illustrated in **Figure 4A**. An asymmetric division of a meristemoid mother cell produces a small meristemoid and a larger stomatal lineage cell. Anisocytic stomata with three subsidiary cells are created when an "amplifying division" occurs (Pillitteri and Dong, 2013). The meristemoid divides asymmetrically two more times, creating surrounding subsidiary cells (**Figure 4A**). The GMC finally divides symmetrically to form a pair of guard cells surrounded by three subsidiary cells. Anomocytic stomata are formed in *A. thaliana* when amplifying divisions are absent. Expression patterns of the PATROL1 in mature leaves (Higaki et al., 2014) suggest perhaps the stomatal lineage cell that is sister to the meristemoid may acquire subsidiary cell identity, although a careful analysis of cell lineage and PATROL1 expression in the same leaf needs to be performed to confirm this.

In certain stomata the meristemoid undergoes additional divisions to form a concentric ring of subsidiary cells to form a heliocytic stomatal complex (**Figure 4B**; Rudall et al., 2018). Heliocytic stomata are observed in some species of begonia and follow a very similar developmental pattern to those in *A. thaliana,* but with additional regenerations of the meristemoid. Interestingly, the meristemoid is often the larger of the two daughter cells after a division in this type of stomatal complex, which is highly unusual (Rudall et al., 2018). The pattern created by the amplified divisions form a spiral that raises the stoma above the leaf surface (**Figure 4B**). Contrasting the divisions of anomocytic stomata in **Figure 4A** and heliocytic stomata in **Figure 4B**, highlights the additional rounds of successive divisions of the meristemoid prior to it's differentiation to a GMC. In *A. thaliana* the transcription factor MUTE controls the transition from meristemoid to GMC (Pillitteri et al., 2007). In *A. thaliana mute* mutants, excessive rounds of asymmetric meristemoid divisions produce a cluster of cells that look similar to mid-developmental stages of heliocytic stomata depicted in **Figure 4B** – however, *mute* mutants arrest at this stage. In heliocytic stomata the meristemoid successfully differentiates into a GMC, which then goes on to undergo a successful single oriented division. Comparing the expression and function of MUTE in heliocytic stomata of *Begonia* or in *Kalanchoe*, which possesses both heliocytic and anisocytic stomata, is likely to provide insights into the developmental mechanisms of different cell patterns.

Stomatal divisions in the grasses *Z. mays, Oryza sativa*, and *Brachypodium distachyon* and the monocot *Tradescantia virginiana* have been used as models and undergo an identical division sequence (**Figure 4C**; Cleary, 1995; Facette and Smith, 2012; Apostolakos et al., 2018; Hepworth et al., 2018; Nunes et al., 2020). A meristemoid mother cell within a stomatal cell file undergoes an asymmetric division to produce a guard mother cell and a sister interstomatal cell. Stomatal divisions in grasses are perigenous; the subsidiary mother cells (SMCs) are recruited from adjacent protodermal cells. Presumably, there is an inductive signal sent from the GMC to lateral neighboring protodermal cells that stimulates them to become SMCs. The SMCs polarize toward the GMC and each SMC divides asymmetrically – exactly once – to give a small subsidiary cell and larger pavement cell. It is presumed that the GMC sends out a polarizing cue that induces the adjacent protodermal cells to differentiate, polarize and divide asymmetrically (Stebbins and Shah, 1960). Once the subsidiary cell is formed, the GMC undergoes its final symmetric division. In both *A. thaliana* and grasses, fate regulators SPEECHLESS, ICE/SCRM, MUTE,

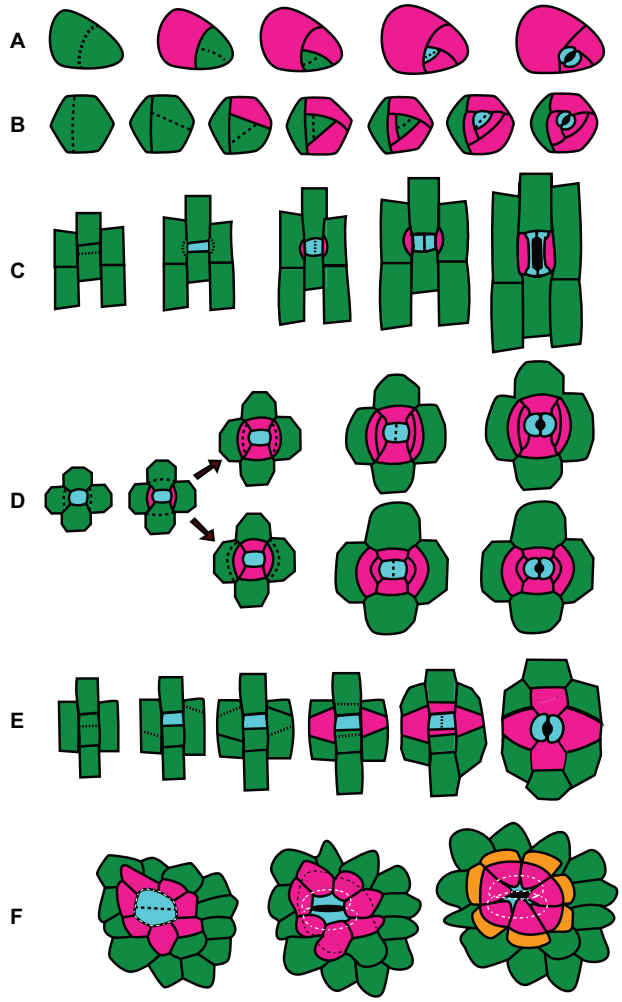

FIGURE 4 | Division patterns in stomata. Divisions outlined left (youngest cells) to right (oldest cells). GMC and guard cells are cyan; subsidiary cells are pink or orange; other cells are green. **(A)** Amplified anisocytic divisions. This type of division is common among eudicots such as *Arabidopsis thaliana*. **(B)** Helicocytic divisions. This type of stomatal complex is seen in some eudicots such as begonia. **(C)** Gramineous (grass) divisions. Paracytic divisions, as seen in other monocots like lily or *Tradescantia virginiana*, follow the same pattern but have kidney shaped guard cells rather than the dumbbell shaped guard cells characteristic of grasses. **(D)** Two possible patterns of hexacytic stomatal generation. The generation of lateral subsidiaries is identical, however in the upper panel the cell closest to the GMC divides, while in the lower panel the cell distal from the GMC divides. **(E)** Tetracytic divisions in *Agave* spp. and some other monocots and feature unusual oblique divisions in the formation of the lateral subsidiary cells. **(F)** Recruitment of subsidiary cells in cyclocytic gingko.

and FAMA are important for stomatal development, but play subtly different roles (Liu et al., 2009; Raissig et al., 2016, 2017; Wang et al., 2019a). The transcription factor MUTE is important in *A. thaliana* for specifying GMC identity but in *B. distachyon* and *Z. mays* is important for subsidiary cell differentiation as well. BdMUTE is produced in the GMC and moves, presumably through plasmodesmata, to adjacent subsidiary mother cells (Raissig et al., 2017; Wang et al., 2019a). MUTE might be the polarizing cue that induces adjacent protodermal cells to differentiate into SMCs, divide and polarize. Polarity markers accumulate in or at the plasma membrane of the SMC adjacent to the GMC, with the branched-actin regulator BRK1 polarizing immediately after GMC formation (Facette et al., 2015). Is MUTE the inductive signal the GMC sends to the neighboring cell, that induces expression or localization of these polarity factors? Since BRK appears polarized so soon after the meristemoid-generating division, this means MUTE must travel even earlier. Determining the relative timing of MUTE-BRK appearance/polarization in SMCs, and whether one is dependent on the other, will help crystallize our understanding of the process of SMC recruitment in grasses.

Consider the potential role of factors known to be important in grass divisions in the formation of certain tetracytic stomata – those that have two lateral and two polar subsidiary cells. Often, the lateral subsidiary cells form via an asymmetric division of recruited neighboring cells similar to that seen in grasses – perhaps MUTE also shows cell-to-cell movement in these tetracytic stomata. Cell-to-cell movement of MUTE does not occur in *A. thaliana,* which does not recruit neighboring cells; it would be interesting to know if the same movement occurs in other plants that have perigenous divisions or if other mechanisms evolved. Likewise, investigation of whether SMC-polarized proteins important for subsidiary-generating divisions in grasses such as BRK1 (Facette et al., 2015) or receptor-like proteins PAN1 and PAN2 (Cartwright et al., 2009; Zhang et al., 2012) also polarize in lateral SMC recruitment would indicate if common or independent mechanisms stimulate perigenous divisions in different plants. These tetracytic stomata also have polar subsidiary cells that are generated via an asymmetric division of stomatal lineage cells lying in the opposite orientation of the lateral subsidiary cells (Tomlinson, 1974). Therefore, these tetracytic stomata form via 2 additional divisions that grasses do not undergo but are otherwise similar. Do the same factors play a role in the mesogenous division? For example, in tetracytic stomata, is MUTE traveling to polarly adjacent cells in addition to laterally adjacent cells? If so, why does MUTE only travel to the lateral protodermal cells (and not the polar cells) in grasses to induce SMC fate? Notably, ectopic overexpression of BdMUTE in *B. distachyon* results in many excess divisions throughout the epidermis; but up to 4 layers of cells surrounding the guard cells appear as if they may be associated subsidiary cells in both lateral and polar directions (Raissig et al., 2017). This suggests that if BdMUTE is present in the polar cells, it is sufficient for subsidiary cell fate, and its movement or stability is somehow regulated. Markers of terminal subsidiary cell fate in *B. distachyon*, coupled with examination of MUTE localization in species with tetracytic stomata could shed light on how the diversity of stomatal form is achieved.

In the tetracytic stomata of *A. rufescens* (**Figure 3D**) there are no polar subsidiary cells and instead there are two pairs of lateral subsidiary cells. It is easy to imagine how the pair of subsidiary cells closest to the guard cells could be generated in a manner like grasses, where adjacent protodermal cells are recruited and divide asymmetrically. But how do the outer pair of subsidiary cells arise? The initial division of a SMC adjacent to the SMC would give a small subsidiary cell and a larger pavement cell – but then which of these cells divides to give another subsidiary cell? We don't know the answer in the case of *A. rufescens*, but Tomlinson (1974) showed that in hexacytic stomata, either scenario is possible. Hexacytic stomata found in the *Geogenanthus* and *Commelina* have two pairs of lateral subsidiary cells, as well as a pair of polar subsidiary cells (**Figure 4D**). In *Geogenanthus,* after an initial asymmetric division of the lateral SMC, the smaller cell divides again. Reciprocally, in *Commelina*, the larger daughter divides again. The patterns of division are conserved within families, indicating different evolutionary paths.

During all stomatal divisions described thus far, one division is required to form one subsidiary cell. *Agave* spp. initiates a meristemoid in a manner similar to other monocots, but then lateral subsidiary cells are formed via two unusual oblique asymmetric divisions that result in trapezoid shaped lateral subsidiary cells (Tomlinson, 1974). Therefore two coordinated divisions are required to make a single subsidiary cell – a developmental process that seems fundamentally different from a single division. Since the lateral subsidiary cell are recruited (as in grasses) from an adjacent row of non-stomatal lineage cells, they are of perigenous origin. On the other hand, polar subsidiary cells are generated from an asymmetric division of stomatal lineage cells (**Figure 4F**). This is an example of a mesoperigenous stomatal complex.

There are some unusual cases of stomata with many subsidiary cells arranged radially but without the spiral amplifying division pattern seen in begonia (Carpenter et al., 2005). *Banksia conferta* has these rare actinocytic stomata where subsidiary cells are recruited from neighboring protodermal cells. Here, a presumptive cue from the GMC induces differentiation but no cell division. These stomatal complexes develop in such a way that the subsidiary cells underlie the guard cells to a degree, pushing the stoma above the leaf epidermis. *Platanus orientalis* has a similar stomatal complex and appears to produce stomatal clusters (Carpenter et al., 2005). It has been suggested that actinocytic stomata are simply a variant of anomocytic (no subsidiary cells) stomata (Stace, 1965). Because these cells raise the guard cells within the epidermis, they have a unique anatomical contribution to the stomata. The recruited cells are likely to have a unique molecular signature since they differentiate differently than other epidermal cells and we therefore consider them subsidiary cells.

Cyclocytic stomata can be observed in both gingko (**Figures 3F**, **4F**) and cycads (Pant and Mehra, 1964). These stomata are very similar to the actinocytic type but the subsidiary cells are above the guard cells rather than below and thus create a

sunken stomatal complex. The subsidiary cells also divide leaving smaller, polygonal cells distal to the guard cells (**Figure 4C**).

WHAT DO SUBSIDIARY CELLS DO?

Form follows function. The diversity in subsidiary cell arrangement and shapes may reflect diverse subsidiary cell function, as well as diverse ways to achieve the same function. Ultimately, the function of the stomatal apparatus is to facilitate gas exchange with the environment. Because plants' environments vary, stomatal adaptations also vary. We will discuss three potential roles for subsidiary cells: anatomical roles that raise or lower guard cells relative to the epidermal surface, mechanical roles during stomatal movements, and molecular roles involving ion and water flux in the stomatal complex.

Stomata are often not flush with the epidermal surface but rather may lie below or above it. Stomatal crypts are large invaginations in the epidermis spanning many cells, typically containing many stomata and often will also have trichomes. Subsidiary cells do not contribute directly to the formation of crypts, but stomatal crypts and sunken stomata (which rely on subsidiary cell architecture) have several conceptual parallels. It was generally accepted that crypts are an adaptation to limit water loss by increasing the boundary layer and were primarily associated with plants growing in water-limiting conditions (i.e., xerophytes) (Katherine, 1977). However, it has become evident that crypts are more widespread and might not limit water loss (Roth-Nebelsick et al., 2009); although certain morphological features of the crypts may affect whether the crypts are indeed a xeromorphic trait (Jordan et al., 2008). An alternative function of crypts may be that they facilitate diffusion of carbon dioxide in thick leaves (Hassiotou et al., 2009).

Sunken stomata are distinct from stomatal crypts; rather than an invagination or depressed area of the epidermis, just the stomata (or guard cells within the stomatal complex) are below the epidermal surface. Sunken stomata in *Agave* are seen in **Figure 3E** by confocal microscopy and in **Figures 5A,D** by scanning electron microscopy. **Figure 3Eiii** shows a reconstructed side view of the stomata, where the guard cells are well below the rest of the leaf epidermal cells. The subsidiary cells partially cover the pore and extend up above the rest of the epidermal cells. In *Agave* the polar and lateral subsidiary cells are essential to creating the sunken stomatal morphology. Subsidiary cells in gingko (**Figure 3F**) likewise are essential to creating the recessed stoma. Like stomatal crypts, sunken stomata were thought to be associated with arid climates, but can also be found in humid climates. Sunken stomata are particularly prevalent within the gymnosperms (Sack, 1987) where they can become plugged with wax or cutin. Like crypts, sunken stomata are thought to increase the transfer resistance by increasing the boundary layer; the net effect is less water loss. However, this fails to explain why sunken stomata would be found in humid environments. In a tropical gymnosperm, leaves with plugged stomata actually had a higher stomatal conductance at high vapor pressure deficit than leaves without plugged stomata (Feild et al., 1998). Moreover, plugged stomata had higher maximal photosynthetic rates. This led to the hypothesis that hydrophobic plugs prevent stomata from filling with water in very humid environments (Feild et al., 1998). It is plausible that sunken stomata represent multiple adaptations – although in every case subsidiary cells are integral to obtaining the sunken morphology.

The opposite of sunken stomata are raised or elevated stomata. In *Begonia*, the heliocytic stomata are raised – either in clusters or singly (**Figure 5**; Papanatsiou et al., 2017; Rudall et al., 2018). The functional significance of raised stomata is unclear, but perhaps it is the reciprocal of sunken stomata – in water-replete conditions it decreases the size of the boundary layer, increasing transpiration. It has been suggested that the raised, clustered stomata in begonia increase the size of the substomatal chamber, facilitating gas exchange within the leaf (Papanatsiou et al., 2017). In begonia, the many subsidiary cells generated by multiple successive rounds of division result in the subsidiary cells creating a base that raises the clustered guard cells up. A different adaptation of raised stomata can be seen in floating leaves of aquatic plants (Ziegler, 1987). The guard cells are supported high on the subsidiary cells, above the epidermal surface, presumably to prevent flooding of the stomatal chamber.

In addition to altering the boundary layer, the morphological arrangement of subsidiary cells in angiosperms affects the mechanical properties of stomata. Turgor-driven guard cell movements are dependent on the wall properties of guard cells. All guard cell walls are thick relative to other epidermal cells, although there is a wall anisotropy that drives stomatal movements. The outer wall is more flexible while the inner wall is thickened and less flexible. In angiosperms in particular, the outer wall distends laterally into neighboring cells during opening. The subsidiary cells are compressed and either displaced laterally and/or basally into the substomatal cavity (Ziegler, 1987). Via mathematical modeling, DeMichele and Sharpe proposed that surrounding epidermal (including subsidiary) cells have a "mechanical advantage" over guard cells (DeMichele and Sharpe, 1973) which was later demonstrated experimentally (Edwards et al., 1976). The mechanical advantage of subsidiary cells is one where turgor pressure of subsidiary cells counterbalances that of guard cells, and subsidiary cell turgor has a greater effect on stomatal aperture than guard cell turgor due to physical properties of the guard cell (DeMichele and Sharpe, 1973; Edwards et al., 1976). Hence, neighboring epidermal cells constrain lateral guard cell movements and limit stomatal opening. Guard cells in non-angiosperms (such as gymnosperms and lycophytes) do not extend laterally into neighboring cells, but rather swell up or down and therefore do not have to overcome the mechanical advantages of neighboring cells (Ziegler, 1987). Using pressure-probe measurements, cryo-SEM imaging and modeling techniques, Franks and Farquhar (Franks and Farquhar, 2007) demonstrated that two species with laterally moving, paracytic guard cells must overcome large mechanical advantages to fully open their stomata. The subsidiary cells were observed to undergo large deformations, and therefore allowing the guard cells to overcome the mechanical advantage of the neighboring cells. One way to achieve these deformations is by altering the osmotic potential of the cells via active transport. Franks and Farquhar suggest a see-sawing mechanism where

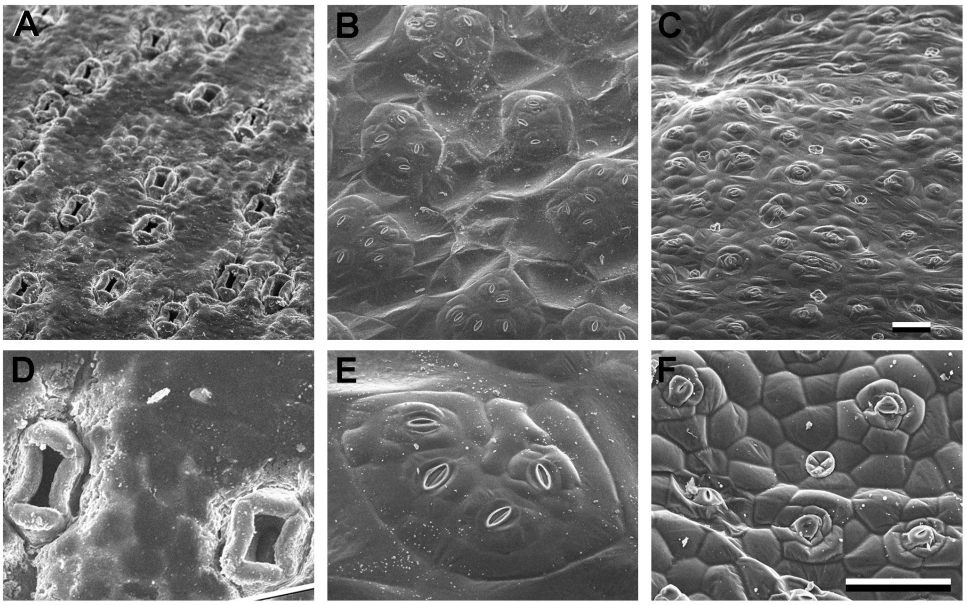

FIGURE 5 | Sunken and raised stomata **(A–D)** *Agave bracena*. **(B–E)** *Begonia* spp. (common house plant), **(C,F)** *Pellionia repens* (Trailing watermelon begonia). Panels **(A–C)** are identical scale; **(D–F)** are identical scale. Scale bars are 100 microns.

water and potassium are exchanged, which is discussed more fully below.

An important consideration in the mechanical properties of stomatal complex function is cell wall properties. Subsidiary cells can have different cell wall compositions from other epidermal cells. This is clearly evidenced in maize, where the polychromatic dye Toluidine Blue O stains guard cells blue (which correlates with more lignified walls) but subsidiary cells pink (which correlates with more pectinaceous walls); this has been used as a marker for subsidiary cell fate (Gallagher and Smith, 2000). Based on this staining, the pectinaceous subsidiary cell walls are perhaps more flexible. Recent investigations on the mechanical properties of cell walls have led to insight into guard cell properties and movements (Carter et al., 2017; Yi et al., 2018). Notably, patterns of cellulose in guard cells change during opening and closing (Rui and Anderson, 2016), and cellulose orientation patterns in subsidiary cells appear to run perpendicular to those in guard cells (Shtein et al., 2017). Extending these analyses to both guard and subsidiary cells during stomatal movements would further our understanding of how subsidiary cells support stomatal function. Indeed, Sharpe et al. (1987) point out how differing elastic forces in guard cell and adjacent cell walls are instrumental for stomatal function.

As summarized above, overcoming the mechanical advantage of neighboring cells is likely due to changes in osmotic potential in subsidiary cells. Early studies investigating the mechanism of turgor changes in maize guard cells examined cellular potassium levels cellular by cobaltinitrite precipitation. In open stomata of maize, cellular potassium is high in guard cells while in closed stomata potassium is high in subsidiary cells (Raschke and Fellows, 1971). A reciprocal exchange of potassium between guard and subsidiary cells allows stomatal complexes to overcome the mechanical advantage of neighboring cells, and is also a potential reservoir of water and ions for guard cells. A similar exchange of potassium between guard cells and subsidiary cells has been seen in many other species (Willmer and Pallas, 1972; Dayanandan and Kaufman, 1975). In certain species, potassium is concentrated only in subsidiary cells – and not other epidermal cells touching the guard cell – of closed stomata. However, in other species such as *Selaginella spp.*, which do not have clear subsidiary cells, potassium was seen in many surrounding epidermal cells, up to several cell layers deep. How do we distinguish between an indiscriminate uptake of extracellular potassium pumped out from the guard cell versus an explicit role for subsidiaries in actively exchanging solutes with guard cells? Cell specificity of uptake is one indicator. Raschke and Fellows also examined kinetics to ensure the time scale of subsidiary cell potassium uptake matched stomatal kinetics. However, additional evidence from maize supports subsidiary cell-specific adaptation. Patch clamping (Majore et al., 2002) and gene expression studies (Büchsenschütz et al., 2005) indicate that maize subsidiary cells possess specific potassium channels. A more thorough indexing of any pumps and channels specific to subsidiary cells would strengthen the argument that subsidiary cells indeed undergo an exchange of molecules with guard cells.

The change in potassium levels likely helps drive the turgor changes observed in grass subsidiary cells, but raises several questions. For example, a principle of guard cell identity is that they lose plasmodesmata as part of their development, becoming symplastically isolated. Subsidiary cells, however, maintain their plasmodesmal connections to adjacent epidermal cells (Majore et al., 2002). Under water-limiting conditions, when stomates must be closed, the subsidiary cells must be kept turgid and not lose water and solutes to adjacent epidermal cell. Under

water-limiting conditions, failure to keep subsidiary cells turgid would have disastrous consequences, as modeled by Franks and Farquhar (2007). This implicates active mechanisms to maintain subsidiary cell turgor. At least one potassium channel is unique to maize subsidiary cells (Büchsenschütz et al., 2005) but are there other unique channels and pumps? What about other molecules important for guard cell function? Chloride was also seen to shuttle between guard and subsidiary cells (Raschke and Fellows, 1971; Dayanandan and Kaufman, 1975). CST1 is a maize subsidiary cell-specific glucose transporter in the SWEET family that promotes stomatal opening (Wang et al., 2019b). The precise role of CST1 in stomatal regulation is difficult to test but the authors offer several plausible roles for CST1. Proposals include: sequestering glucose in subsidiary cells so it does not induce guard cell hexokinase-induced stomatal closing; increasing the osmolarity of the apoplast via glucose export to decrease subsidiary cell turgor; or providing subsidiary cells with sugar to power their own ion channels. Notably, this gene is duplicated in grasses and the single ortholog in *A. thaliana* to play a role in stomatal function, suggesting a possible grass-specific role.

At least in maize, there are unique transporters within its easily-identifiable subsidiary cells. However, in maize at least some potassium channels are shared by both guard cells and subsidiary cells (Büchsenschütz et al., 2005). Given the observed see-saw localization of potassium, are the same proteins functionally oppositely in guard cells and subsidiary cells, through differential regulation or simply by the existing concentration gradients? In *A. thaliana, PATROL1* is expressed in both guard cells and subsidiary cells. The role of PATROL1 in guard cells includes trafficking the proton pump AHA1 – is PATROL1 AHA1 differentially in these two cell types during opening and closing? Or is PATROL1 trafficking different proteins? Identification of cell-specific and common transporters and regulatory proteins between subsidiary cells versus guard cells should help indicate functional roles and potential regulation of subsidiary cells.

CONCLUSION AND OUTLOOK

Turgor-driven guard cell movements, and the contribution of subsidiary cells, has been long studied; Heath (1938) identified contributions of cells via puncture experiments nearly 90 years ago. The advent of molecular genetics rapidly exploded our knowledge of guard cell biology, but subsidiary cell biology was ignored. This is likely, at least partially, due to the fact that most experimental advances were accomplished in *A. thaliana,* where subsidiary cells are difficult to identify and do not appear to contribute to the same extent in organisms such as grasses. The rapid stomatal movements of grass stomata are partially attributable to their subsidiary cells, but also due to their unique dumbbell shape considering other species (such as *T. virginiana*) also possess paracytic stomata but are not as rapid (Franks and Farquhar, 2007). Current active research in stomatal development and function in model systems like *B. distachyon, Z. mays,* and *O. sativa* will contribute to understanding of subsidiary cell mechanisms in the economically important grasses (Chen et al., 2016; Hepworth et al., 2018; Nunes et al., 2020). Studies in other models with diverse stomatal architectures like *Begonia* (Rudall et al., 2018) and *Kalanchoe* (Xu et al., 2018) will be just as important. Clearly, the same basic arrangements can be obtained several different ways (e.g., hexacytic stomatal morphology) and similar architectures may have different functions (e.g., sunken stomata). Examination of stomatal complexes in totality, including subsidiary cells, in a diverse array of species will provide a more complete picture of stomatal function. Fortunately, genomic and genetic tools are being developed for a broader array of species meaning we are poised to consider the diversity of stomata examined by botanists and taxonomists.

AUTHOR CONTRIBUTIONS

MF and AG wrote the manuscript. MF prepared the **Figures 1**, **5**. LL prepared the **Figures 2**, **3**. AG prepared the **Figure 4**. All authors contributed to the article and approved the submitted version.

FUNDING

This work was supported by NSF-IOS 1754665 awarded to MF.

ACKNOWLEDGMENTS

We wish to thank the staff at the Ray Ethan Torrey Botanical Greenhouse, part of the UMass Amherst Natural History Collection, for supplying samples and aiding in identification of species (Curator: Madelaine Bartlett; Manager: Chris Phillips; and Staff: Dan Jones).

REFERENCES

Apostolakos, P., and Galatis, B. (1987). Induction, polarity and spatial control of cytokinesis in some abnormal subsidiary cell mother cells of Zea Mays. *Protoplasma* 140, 26–42. doi: 10.1007/BF01273253

Apostolakos, P., Livanos, P., Giannoutsou, E., Panteris, E., and Galatis, B. (2018). The intracellular and intercellular cross-talk during subsidiary cell formation in zea mays: existing and novel components orchestrating cell polarization and asymmetric division. *Ann. Bot.* 122, 679–696. doi: 10.1093/aob/mcx193

Baranova, M. (1992). Principles of comparative stomatographic studies of flowering plants. *The Botanical Review* 58, 49–99. doi: 10.1007/BF02858543

Büchsenschütz, K., Marten, I., Becker, D., Philippar, K., Ache, P., and Hedrich, R. (2005). Differential Expression of K+ channels between guard cells and subsidiary cells within the maize stomatal complex. *Planta* 222, 968–976. doi: 10.1007/s00425-005-0038-6

Carpenter, K. J. (2005). Stomatal architecture and evolution in basal angiosperms. *Am. J. Bot.* 92, 1595–1615. doi: 10.3732/ajb.92.10.1595

Carpenter, R. J., Hill, R. S., and Jordan, G. J. (2005). Leaf cuticular morphology links platanaceae and proteaceae. *Int. J. Plant Sci.* 166, 843–855.

Carter, R., Woolfenden, H., Baillie, A., Amsbury, S., Carroll, S., Healicon, E., et al. (2017). Stomatal opening involves polar, not radial, stiffening of guard cells. *Curr. Biol.* 27, 2974.e–2983.e. doi: 10.1016/j.cub.2017.08.006

Cartwright, H. N., Humphries, J. A., and Smith, L. G. (2009). A receptor-like protein that promotes polarization of an asymmetric cell division in maize. *Science* 323, 649–651.

Chater, C. C., Caine, R. S., Tomek, M., Wallace, S., Kamisugi, Y., Cuming, Y. C., et al. (2016). Origin and function of stomata in the moss physcomitrella patens. *Nat. Plants* 2:16179. doi: 10.1038/nplants.2016.179

Chater, C. C. C., Caine, R. S., Fleming, A. J., and Gray, J. E. (2017). Origins and evolution of stomatal development. *Plant Physiol.* 174, 624–638. doi: 10.1104/pp.17.00183

Chen, Z.-H., Chen, G., Dai, F., Wang, Y., Hills, A., Ruan, Y.-L., et al. (2016). Molecular evolution of grass stomata. *Trends Plant Sci.* 22, 124–139. doi: 10.1016/j.tplants.2016.09.005

Cleary, A. L. (1995). F-actin redistributions at the division site in livingtradescantia stomatal complexes as revealed by microinjection of rhodamine-phalloidin. *Protoplasma* 185, 152–165.

Dayanandan, P., and Kaufman, P. B. (1975). Stomatal movements associated with potassium fluxes. *Am. J. Bot.* 62, 221–231.

DeMichele, D. W., and Sharpe, P. J. H. (1973). An analysis of the mechanics of guard cell motion. *J. Theor. Biol.* 41, 77–96. doi: 10.1016/0022-5193(73)90190-2

Dong, J., MacAlister, C. A., and Bergmann, D. C. (2009). BASL controls asymmetric cell division in Arabidopsis. *Cell* 137, 1320–1330.

Edwards, M., Meidner, H., and Sheriff, D. W. (1976). Direct measurements of turgor pressure potentials of guard cells: ii. the mechanical advantage of subsidiary cells, the spannunqsphase, and the optimum leaf water deficit. *J. Exp. Bot.* 27, 163–171. doi: 10.1093/jxb/27.1.163

Eisenach, C., and De Angeli, A. (2017). Ion transport at the vacuole during stomatal movements. *Plant Physiol.* 174, 520–530. doi: 10.1104/pp.17.00130

Esau, K. (1965). *Plant Anatomy*. New York, NY: John Wiley and Sons.

Facette, M. R., Park, Y., Sutimantanapi, D., Luo, A., Cartwright, H. N., Yang, B., et al. (2015). The SCAR/WAVE complex polarises PAN receptors and promotes division asymmetry in maize. *Nat. Plants* 1:14024. doi: 10.1038/nplants.2014.24

Facette, M. R., and Smith, L. G. (2012). Division polarity in developing stomata. *Curr. Opin. Plant Biol.* 15, 585–592. doi: 10.1016/j.pbi.2012.09.013

Feild, T. S., Zwieniecki, M. A., Donoghue, M. J., and Holbrook, N. M. (1998). Stomatal Plugs of Drimys Winteri (Winteraceae) protect leaves from mist but not drought. *Proc. Natl. Acad. Sci. U.S.A.* 95, 14256–14259. doi: 10.1073/pnas.95.24.14256

Franks, P. J., and Farquhar, G. D. (2007). The mechanical diversity of stomata and its significance in gas-exchange control. *Plant Physiol.* 143, 78–87. doi: 10.1104/pp.106.089367

Fryns-Claessens, E., and Van Cotthem, W. (1973). A New Classification of the Ontogenetic Types of Stomata. *Bot. Rev.* 39, 71–138.

Gallagher, K., and Smith, L. G. (2000). Roles for polarity and nuclear determinants in specifying daughter cell fates after an asymmetric cell division in the maize leaf. *Curr. Biol.* 10, 1229–1232.

Geisler, M., Nadeau, J., and Sack, F. D. (2000). Oriented asymmetric divisions that generate the stomatal spacing pattern in arabidopsis are disrupted by the too many mouths mutation. *Plant Cell Online* 12, 2075–2086. doi: 10.1105/tpc.12.11.2075

Harris, B. J., Harrison, C. J., Hetherington, A. M., and Williams, T. A. (2020). Phylogenomic evidence for the monophyly of bryophytes and the reductive evolution of Stomata. *Curr. Biol.* 30:2001-2012.e2. doi: 10.1016/j.cub.2020.03.048

Hashimoto-Sugimoto, M., Higaki, T., Yaeno, T., Nagami, A., Irie, M., Fujimi, M., et al. (2013). A Munc13-like Protein in Arabidopsis Mediates H + -ATPase translocation that is essential for stomatal responses. *Nat. Commun.* 4, 1–9. doi: 10.1038/ncomms3215

Hassiotou, F., Evans, J. E., Ludwig, M., and Veneklaas, E. J. (2009). Stomatal Crypts May Facilitate Diffusion of CO2 to Adaxial Mesophyll Cells in Thick Sclerophylls. *Plant Cell Environ.* 32, 1596–1611. doi: 10.1111/j.1365-3040.2009.02024.x

Heath, O. V. S. (1938). An experimental investigation of the mechanism of stomatal movement, with some preliminary observations upon the response of the guard cells to 'Shock.'. *New Phytol.* 37, 385–395.

Hepworth, C., Caine, R. S., Harrison, E. L., Sloan, J., and Gray, J. E. (2018). Stomatal development: focusing on the grasses. *Curr. Opin. Plant Biol. Growth Dev.* 41, 1–7. doi: 10.1016/j.pbi.2017.07.009

Higaki, T., Hashimoto-Sugimoto, M., Akita, K., Iba, K., and Hasezawa, S. (2014). Dynamics and environmental responses of PATROL1 in Arabidopsis subsidiary cells. *Plant Cell Physiol.* 55, 773–780. doi: 10.1093/pcp/pct151

Hunt, L., and Gray, J. E. (2009). The Signaling Peptide EPF2 controls asymmetric cell divisions during stomatal development. *Curr. Biol.* 19, 864–869. doi: 10.1016/j.cub.2009.03.069

Inamdar, J. A., and Patel, R. C. (1970). Structure and development of stornata in vegetative and floral organs of three species of kalanchoe. *Ann. Bot.* 34, 965–974.

Jezek, M., and Blatt, M. R. (2017). The membrane transport system of the guard cell and its integration for stomatal dynamics. *Plant Physiol.* 174, 487–519. doi: 10.1104/pp.16.01949

Johnsson, M., Issaias, S., Brogardh, T., and And Johnsson, A. (1976). Rapid, blue-light-induced transpiration response restricted to plants with grass-like stomata. *Physiol. Plant.* 36, 229–232. doi: 10.1111/j.1399-3054.1976.tb04418.x

Jordan, G. J., Weston, P. H., Carpenter, R. J., Dillon, R. A., and Brodribb, T. J. (2008). The Evolutionary Relations of Sunken, Covered, and Encrypted Stomata to Dry Habitats in Proteaceae. *Am. J. Bot.* 95, 521–530. doi: 10.3732/ajb.2007333

Katherine, E. (1977). *Anatomy of Seed Plants*, 2nd Edn. New York, NY: Wiley.

Liu, T., Ohashi-Ito, K., and Bergmann, D. C. (2009). Orthologs of *Arabidopsis thaliana* stomatal bhlh genes and regulation of stomatal development in grasses. *Development* 136, 2265–2276. doi: 10.1242/dev.032938

MacAlister, C. A., Ohashi-Ito, K., and Bergmann, D. C. (2007). Transcription factor control of asymmetric cell divisions that establish the stomatal lineage. *Nature* 445, 537–540. doi: 10.1038/nature05491

Majore, I., Wilhelm, B., and Marten, I. (2002). Identification of K+ channels in the plasma membrane of maize subsidiary cells. *Plant Cell Physiol.* 43, 844–852. doi: 10.1093/pcp/pcf104

Metcalfe, C. R., and Chalke, L. (1957). *Anatomy of the Dicotyledons: Leaves, Stem and Wood in Relation to Taxonomy Wiht Notes on Economic Uses*, Vol. I. London: Oxford University Press.

Munemasa, S., Hauser, F., Park, J., Waadt, R., Brandt, B., and Schroeder, J. I. (2015). Mechanisms of abscisic acid-mediated control of stomatal aperture. *Curr. Opin. Plant Biol. Cell Biol.* 28, 154–162. doi: 10.1016/j.pbi.2015.10.010

Nadeau, J. A., and Sack, F. D. (2002). Stomatal development in Arabidopsis. *Arabidopsis Book* 1, e0066. doi: 10.1199/tab.0066

Nunes, T. D. G., Zhang, D., and Raissig, M. Y. (2020). Form, development and function of grass stomata. *Plant J.* 101, 780–799.

Palevitz, B. A., and Hepler, P. K. (1974). The control of the plane of division during stomatal differentiation in allium. I. I. Spindle Reorientation. *Chromosoma* 46, 297–326. doi: 10.1007/BF00284884

Pant, D. D. (1965). On the ontogeny of stomata and other homologous structures. *Plant Sci. Ser.* 1:1024.

Pant, D. D., and Mehra, B. (1964). Development of stomata in leaves of three species of cycas and Ginkgo Biloba L. *Bot. J. Linnean Soc.* 58, 491–497. doi: 10.1111/j.1095-8339.1964.tb00917.x

Papanatsiou, M., Amtmann, A., and Blatt, M. R. (2017). Stomatal clustering in begonia associates with the kinetics of leaf gaseous exchange and influences water use efficiency. *J. Exp. Bot.* 68, 2309–2315. doi: 10.1093/jxb/erx072

Pickett-Heaps, J. D. (1969). Preprophase microtubules and stomatal differentiation; some effects of centrifugation on symmetrical and asymmetrical cell division. *J. Ultrastruct. Res.* 27, 24–44. doi: 10.1016/S0022-5320(69)90018-90015

Pillitteri, L. J., and Dong, J. (2013). Stomatal development in Arabidopsis. *Am. Soc. Plant Biol.* 11:e0066. doi: 10.1199/tab.0162

Pillitteri, L. J., Sloan, D. B., Bogenschutz, N. L., and Torii, K. U. (2007). Termination of asymmetric cell division and differentiation of stomata. *Nature* 445, 501–505. doi: 10.1038/nature05467

Prabhakar, M. (2004). Structure, delimitation, nomenclature and classification of stomata. *Acta Bot. Sin.* 46, 242–252.

Raissig, M. T., Abrash, E., Bettadapur, A., Vogel, J. P., and Bergmann, D. C. (2016). Grasses use an alternatively wired BHLH transcription factor network to establish stomatal identity. *Proc. Natl. Acad. Sci. U.S.A.* 113, 8326–8331. doi: 10.1073/pnas.1606728113

Raissig, M. T., Matos, J. L., Gil, M. X. A., Kornfeld, A., Bettadapur, A., Abrash, E., et al. (2017). Mobile MUTE specifies subsidiary cells to build physiologically improved grass stomata. *Science* 355, 1215–1218. doi: 10.1126/science.aal3254

Raschke, K., and Fellows, M. P. (1971). Stomatal movement in zea mays: shuttle of potassium and chloride between guard cells and subsidiary cells. *Planta* 101, 296–316. doi: 10.1007/BF00398116

Rasmussen, H. (1981). Terminology and classification of stomata and stomatal development—a critical survey. *Bot. J. Linnean Soc.* 83, 199–212. doi: 10.1111/j.1095-8339.1981.tb0093.x

Roth-Nebelsick, A., Hassiotou, F., and Veneklaas, E. J. (2009). Stomatal crypts have small effects on transpiration: a numerical model analysis. *Plant Physiol.* 151, 2018–2027. doi: 10.1104/pp.109.146969

Rudall, J., Hilton, J., and Bateman, M. (2013). Several developmental and morphogenetic factors govern the evolution of stomatal patterning in land plants. *New Phytol.* 200, 598–614.

Rudall, P. J., Julier, A. C. M., and Kidner, C. A. (2018). Ultrastructure and development of non-contiguous stomatal clusters and helicocytic patterning in begonia. *Ann. Bot.* 122, 767–776. doi: 10.1093/aob/mcx146

Rui, Y., and Anderson, C. T. (2016). Functional analysis of cellulose and xyloglucan in the walls of stomatal guard cells of Arabidopsis. *Plant Physiol.* 170, 1398–1419. doi: 10.1104/pp.15.01066

Sack, F. (1987). Development and structure of stomata," in *Stomatal Function*, eds E. Zeiger, G. D. Farquhar, and I. R. Cowan (Stanford: Stanford University Press).

Sampaio, V. S., Araújo, N. D., and Agra, M. F. (2014). Characters of leaf epidermis in Solanum (Clade Brevantherum) Species from Atlantic Forest of Northeastern Brazil. *South Afr. J. Bot.* 94, 108–113. doi: 10.1016/j.sajb.2014.06.004

Serna, L., and Fenoll, C. (2000). Stomatal development and patterning in Arabidopsis Leaves. *Physiol. Plant.* 109, 351–358. doi: 10.1034/j.1399-3054.2000.100317.x

Shao, W., and Dong, J. (2016). Polarity in plant asymmetric cell division: division orientation and cell fate differentiation. *Dev. Biol.* 419, 121–131. doi: 10.1016/j.ydbio.2016.07.020

Sharpe, P. J. H., Wu, H.-I., and Spence, R. D. (1987). Stomatal mechanics," in *Stomatal Function*, eds E. Zeiger, G. D. Farquhar, and I. R. Cowan (Stanford: Stanford University Press), 91–114.

Shpak, E. D., Berthiaume, C. T., Hill, E. J., and Torii, K. U. (2004). Synergistic interaction of Three ERECTA-family receptor-like kinases controls arabidopsis organ growth and flower development by promoting cell proliferation. *Development* 131, 1491–1501. doi: 10.1242/dev.01028

Shtein, I., Shelef, Y., Marom, Z., Zelinger, E., Schwartz, A., Popper, Z. A., et al. (2017). Stomatal Cell wall composition: distinctive structural patterns associated with different phylogenetic groups. *Ann. Bot.* 119, 1021–1033. doi: 10.1093/aob/mcw275

Simmons, A. R., and Bergmann, D. C. (2016). Transcriptional control of cell fate in the stomatal lineage. *Curr. Opin. Plant Biol. Growth Dev.* 29, 1–8. doi: 10.1016/j.pbi.2015.09.008

Stace, C. A. (1965). Cuticular studies as an aid to plant taxonomy. *Bull. Br. Museum* 4, 37–40.

Stebbins, G. L., and Shah, S. S. (1960). developmental studies of cell differentiation in the epidermis of monocotyledons: II. Cytological Features of Stomatal Development in the Gramineae. *Dev. Biol.* 2, 477–500.

Tomlinson, P. B. (1969). *Anatomy of the Monocotyldeons. III Commelinales - Zingiberales*. Oxford: Clarendon Press.

Tomlinson, P. B. (1974). Development of the stomatal complex as a taxonomic character in the monocotyledons. *TAXON* 23, 109–128. doi: 10.2307/1218094

Torii, K. U. (2015). Stomatal differentiation: the beginning and the end. *Curr. Opin. Plant Biol. Cell Biol.* 28, 16–22. doi: 10.1016/j.pbi.2015.08.005

Vico, G., Manzoni, S., Palmroth, S., and Katul, G. (2011). Effects of stomatal delays on the economics of leaf gas exchange under intermittent light regimes. *New Phytol.* 192, 640–652. doi: 10.1111/j.1469-8137.2011.03847.x

Wang, H., Guo, S., Qiao, X., Guo, J., Li, Z., Zhou, Y., et al. (2019a). BZU2/ZmMUTE Controls symmetrical division of guard mother cell and specifies neighbor cell fate in maize. *PLoS Genet.* 15:e1008377. doi: 10.1371/journal.pgen.1008377

Wang, H., Yan, S., Xin, H., Huang, W., Zhang, H., Teng, S., et al. (2019b). A subsidiary cell-localized glucose transporter promotes stomatal conductance and photosynthesis. *Plant Cell* 31, 1328–1343. doi: 10.1105/tpc.18.00736

Willmer, C. M., and Pallas, J. E. Jr. (1972). A survey of stomatal movements and associated potassium fluxes in the plant kingdom. *Can. J. Bot.* 51, 37–24.

Xu, M., Chen, F., Qi, S., Zhang, L., and Wu, S. (2018). Loss or duplication of key regulatory genes coincides with environmental adaptation of the stomatal complex in Nymphaea Colorata and Kalanchoe Laxiflora. *Horticult. Res.* 5, 1–16. doi: 10.1038/s41438-018-0048-48

Yi, H., Rui, Y., Kandemir, B., Wang, J. Z., Anderson, C. T., and Puri, V. M. (2018). Mechanical effects of cellulose, xyloglucan, and pectins on stomatal guard cells of Arabidopsis Thaliana. *Front. Plant Sci.* 9:1566. doi: 10.3389/fpls.2018.01566

Zeiger, E., and Stebbins, G. L. (1972). Developmental genetics in barley: a mutant for stomatal development. *Am. J. Bot.* 59, 143–148.

Zhang, X., Facette, M., Humphries, J. A., Shen, Z., Park, Y., Sutimantanapi, D., et al. (2012). Identification of PAN2 by quantitative proteomics as a leucine-rich repeat–receptor-like kinase acting upstream of PAN1 to polarize cell division in maize. *Plant Cell* 24, 4577–4589.

Ziegler, H. (1987). The evolution of stomata," in *Stomatal Function*, eds E. Zeiger, G. D. Farquhar, and I. R. Cowan (Stanford: Stanford University Press), 29–58.

Conflict of Interest: The authors declare that the research was conducted in the absence of any commercial or financial relationships that could be construed as a potential conflict of interest.

frontiers in Plant Science

HYPOTHESIS AND THEORY
published: 29 October 2020
doi: 10.3389/fpls.2020.518991

A Stomatal Model of Anatomical Tradeoffs Between Gas Exchange and Pathogen Colonization

*Christopher D. Muir**

School of Life Sciences, University of Hawai'i, Honolulu, HI, United States

Stomatal pores control leaf gas exchange and are one route for infection of internal plant tissues by many foliar pathogens, setting up the potential for tradeoffs between photosynthesis and pathogen colonization. Anatomical shifts to lower stomatal density and/or size may also limit pathogen colonization, but such developmental changes could permanently reduce the gas exchange capacity for the life of the leaf. I developed and analyzed a spatially explicit model of pathogen colonization on the leaf as a function of stomatal size and density, anatomical traits which partially determine maximum rates of gas exchange. The model predicts greater stomatal size or density increases the probability of colonization, but the effect is most pronounced when the fraction of leaf surface covered by stomata is low. I also derived scaling relationships between stomatal size and density that preserves a given probability of colonization. These scaling relationships set up a potential anatomical conflict between limiting pathogen colonization and minimizing the fraction of leaf surface covered by stomata. Although a connection between gas exchange and pathogen defense has been suggested empirically, this is the first mathematical model connecting gas exchange and pathogen defense via stomatal anatomy. A limitation of the model is that it does not include variation in innate immunity and stomatal closure in response to pathogens. Nevertheless, the model makes predictions that can be tested with experiments and may explain variation in stomatal size and density among plants. The model is generalizable to many types of pathogens, but lacks significant biological realism that may be needed for precise predictions.

Keywords: anatomy, leaf gas exchange, model, pathogen, photosynthesis, scaling, stomata, tradeoff

OPEN ACCESS

Edited by:
Graham Dow,
ETH Zürich, Switzerland

Reviewed by:
Athena McKown,
University of British Columbia, Canada
Karl C. Fetter,
University of Georgia, United States

***Correspondence:**
Christopher D. Muir
cdmuir@hawaii.edu

Specialty section:
This article was submitted to Plant Development and EvoDevo, a section of the journal Frontiers in Plant Science

Received: *10 December 2019*
Accepted: *01 October 2020*
Published: *29 October 2020*

Citation:
Muir CD (2020) A Stomatal Model of Anatomical Tradeoffs Between Gas Exchange and Pathogen Colonization. Front. Plant Sci. 11:518991. doi: 10.3389/fpls.2020.518991

INTRODUCTION

Stomata evolved to regulate gas exchange in and out of the leaf (Hetherington and Woodward, 2003; Berry et al., 2010; Chater et al., 2017), but many foliar pathogens take advantage of these chinks in the leaf cuticular armor to infect prospective hosts (Zeng et al., 2010; McLachlan et al., 2014; Melotto et al., 2017). The stomatal and mesophyll conductance to CO_2 are two major limits to photosynthesis (Flexas et al., 2018; Lawson et al., 2018) that are partially determined by stomatal anatomy. Since CO_2 conductance limits photosynthesis (Farquhar and Sharkey, 1982; Jones, 1985) and pathogen infection can reduce fitness (Gilbert, 2002), this sets up a potential tradeoff between increased photosynthesis and defense against pathogens mediated by stomatal anatomy (McKown et al., 2014; Dutton et al., 2019; Fetter et al., 2019; Tateda et al., 2019). For example, plants could increase photosynthetic rate by developing more stomata, but more stomata could result in more

pathogen colonization. The optimal stomatal density, size, and arrangement on the leaf will depend on the fitness gains from increased gas exchange and fitness losses imposed by foliar pathogens, both of which depend on the environment. In the next two paragraphs I will review the relationship between stomatal anatomy, gas exchange, and foliar pathogen colonization. Then I will discuss why two anatomical traits, stomatal size and density, might be crucial components of a broader tradeoff between photosynthesis and pathogen defense.

The stomatal density and maximum pore area set an anatomical upper limit on stomatal conductance (Brown and Escombe, 1900; Parlange and Waggoner, 1970; Franks and Farquhar, 2001; Franks and Beerling, 2009b; Lehmann and Or, 2015; Sack and Buckley, 2016; Harrison et al., 2019), but stomatal shape, distribution, and patterning also affect gas exchange. Smaller guard cells and dumbbell-shaped stomata of grasses can respond faster to environmental changes (Drake et al., 2013), but responsiveness is further modulated by subsidiary cell anatomy and physiology (Franks and Farquhar, 2007; Raissig et al., 2017; Gray et al., 2020). Stomatal clustering reduces gas exchange and photosynthesis because adjacent stomata interfere with one another (Dow et al., 2014b), diffusion shells overlap (Lehmann and Or, 2015), and limitations on lateral diffusion of CO_2 in the mesophyll (Lawson and Blatt, 2014 and references therein). However, sparse clusters of small stomata could allow a leaf with low rates of gas exchange to have faster stomatal response compared to a leaf with large, low-density stomata (Papanatsiou et al., 2017). Leaves with stomata on both lower and upper surfaces (amphistomatous) supply more CO_2 to the mesophyll than hypostomatous leaves that only have stomata on the lower surface (Parkhurst, 1978; Gutschick, 1984; Parkhurst and Mott, 1990; Oguchi et al., 2018). In addition to anatomy, the pore area shrinks and expands in response to internal and external factors to regulate gas exchange dynamically (Buckley, 2019). For example, stomata typically open during the day and close at night in C_3/C_4 plants, but the opposite is true for CAM plants. Shade, high vapor pressure deficits, dry soil and other factors can cause stomata to (partially) close even in the middle of the day. Variation in how stomata respond to internal and external signals may explain as much of the variation in gas exchange across leaves as anatomy (Lawson and Blatt, 2014).

Many types of foliar pathogens, including viruses (Murray et al., 2016), bacteria (Melotto et al., 2006; Underwood et al., 2007), protists (Fawke et al., 2015), and fungi (Hoch et al., 1987; Zeng et al., 2010) use stomatal pores to gain entry into the leaf. For example, rust fungi hyphae recognize the angle at which guard cells project from the leaf surface and use it as a cue for appressorium formation (Allen et al., 1991). Oomycete pathogens can target open stomata on a leaf (Kiefer et al., 2002). Plants can limit colonization through innate immunity, called stomatal defense (recently reviewed in Melotto et al., 2017), by closing stomata after they recognize microbe-associated molecular patterns (MAMPs) on pathogen cells. Some bacterial pathogens have responded by evolving the ability to prevent stomatal closure, increasing their colonization of the leaf interior (Melotto et al., 2006). In addition to stomatal closure, anatomical changes in stomatal density and/or size might provide another layer of defense against pathogen colonization. For example, infection increases in leaves with higher stomatal density (McKown et al., 2014; Dutton et al., 2019; Fetter et al., 2019; Tateda et al., 2019). The positive effect of stomatal density on infection suggests that infection is limited by the number or size of locations for colonization, meaning that many individual pathogens must usually be unable to find stomata or other suitable locations for colonization. This is actually somewhat surprising given the ability of some pathogens to search for and sense stomata (see above).

Stomatal anatomy could be a key link between gas exchange and pathogen colonization. Although many anatomical factors and stomatal movement affect gas exchange (see above), here I focus on the density and size of stomata in a hypostomatous leaf. Stomatal size refers to both the area of guard cells when fully open, from which one can calculate the pore area for gas exchange (see Model). For simplicity, I model a hypostomatous leaf, but consider the implications for amphistomatous leaves in the Discussion. Stomatal size and density not only determine the theoretical maximum stomatal conductance ($g_{s,max}$), but are also proportional to the operational stomatal conductance ($g_{s,op}$) in many circumstances (Franks et al., 2009, 2014; Dow et al., 2014a; McElwain et al., 2016; Murray et al., 2019). $g_{s,op}$ is the actual stomatal conductance of plants in the field and is almost always below $g_{s,max}$ because stomata are usually not fully open. Although they are not the same, the strong empirical relationship between $g_{s,max}$ and $g_{s,op}$ means that anatomical $g_{s,max}$ can be used as a proxy for $g_{s,op}$ without explicitly modeling dynamic changes in stomatal aperture (see Discussion). Stomatal size and density have also been measured on many more species than stomatal responsiveness, which may make it easier to test predictions.

After a pathogen reaches a host, it must survive on the leaf surface and colonize the interior (Beattie and Lindow, 1995; Tucker and Talbot, 2001). For analytical tractability, I restrict the focus here to colonization by a pathogen using a random search on a leaf without stomatal defense (i.e., a leaf that cannot recognize pathogens and close stomata). Obviously, these simplifications ignore a lot of important plant-pathogen interaction biology. In the Discussion, I delve further into these limitations and suggest future work to overcome these limitations. In order for pathogen-mediated selection on stomatal anatomy, I assume that the pathogen reduces host fitness once it colonizes (Gilbert, 2002). Susceptible hosts can lose much of their biomass or die, but even resistant hosts must allocate resources to defense or reduce photosynthesis because of defoliation, biotrophy, or necrosis around sites of infection (Bastiaans, 1991; Mitchell, 2003).

The purpose of this study is to develop a theoretical framework to test whether variation in stomatal size and density arises from a tradeoff between gas exchange and pathogen colonization. Since stomatal size and density affect both gas exchange and pathogen colonization, selection to balance these competing demands could shape stomatal size-density scaling relationships. Botanists have long recognized that stomatal size and density are inversely correlated (Weiss, 1865; Tichá, 1982; Hetherington and Woodward, 2003; Sack et al., 2003; Franks and Beerling, 2009a; Brodribb et al., 2013; Boer et al., 2016),

but the evolutionary origin of this relationship is not yet known. Here I argue that deleterious effects of pathogen infection could shape selection on this relationship. Explanations for inverse size-density scaling are usually cast in terms of preserving $g_{s,max}$ and/or stomatal cover (f_S), defined at the fraction of epidermal area allocated to stomata (Boer et al., 2016), because there are many combinations of stomatal size and density that have same $g_{s,max}$ or same f_S:

$$g_{s,max} = bmDS^{0.5} \quad (1)$$

$$f_S = DS. \quad (2)$$

D and S are stomatal density and size, respectively (see **Table 1** for a glossary of mathematical symbols and units). b and m are assumed to be biophysical and morphological constants, *sensu* (Sack and Buckley, 2016; see **Supplementary Material**). f_S is proportional to the more widely used stomatal pore area index (Sack et al., 2003; see **Supplementary Material**). If size and density also affect pathogen colonization, then selection from foliar pathogens could significantly alter the size-density scaling relationship. The empirical size-density scaling relationship is linear on a log-log scale, determined by an intercept α and slope β:

$$D = e^{\alpha} S^{-\beta}; \quad (3)$$

$$d = \alpha - \beta S. \quad (4)$$

For brevity, $d = \log(D)$ and $s = \log(S)$. Rearranging Equations 1 and 2, a scaling relationship where $\beta = 0.5$ preserves $g_{s,max}$ while $\beta = 1$ preserves f_S.

TABLE 1 | Glossary of mathematical symbols.

Symbol	R	Units	Description
D	`D`	mm^{-2}	Stomatal density
d	`d`	mm^{-2}	Stomatal density (log-scale, $d = \log D$)
f_S	`f_s`	none	Stomatal cover ($f_s = DS$)
$g_{s,max}$	`g_smax`	mol m^{-2} s^{-1}	Theoretical maximum stomatal conductance
$g_{s,op}$	`g_sop`	mol m^{-2} s^{-1}	Operational stomatal conductance
H	`H`	μm^{-1}	Death rate of pathogen on leaf surface
R	`R`	μm	Stomatal radius ($S = \pi R^2$)
S	`S`	μm^2	Stomatal size
s	`s`	μm^2	Stomatal size (log-scale, $s = \log S$)
θ_i	`theta_i`	radians	Angles between pathogen (x_p, y_p) and lines tangent to the circumference of stomate i
U	`U`	μm	Interstomatal distance
v_i	`v_i`	μm	Distance between pathogen (x_p, y_p) and stomate i
x_i, y_i	`x_i,y_i`	μm	Position of stomate i
x_p, y_p	`x_p,y_p`	μm	Starting position of pathogen

The columns indicate the mathematical symbol used in the paper, the associated symbol used in R scripts, scientific Units, and a verbal description.

How would adding pathogens alter these predicted scaling relationships? For simplicity, consider two environments, one without foliar pathogens and one with lots. In the absence of foliar pathogens, we expect size-density scaling to preserve $g_{s,max}$, f_S, or some least-cost combination of them. What happens when we introduce pathogens? If stomatal size and density increase pathogen colonization, then selection will favor reduced size and/or density. This would change the intercept α but not the slope. The effect of foliar pathogens on the slope depends on the relationship between size, density, and probability of colonization. If the probability of colonization is proportional to the product of *linear* stomatal size ($S^{0.5}$) and density ($\propto DS^{0.5}$ as for $g_{s,max}$) then it has the same effect on the slope as $g_{s,max}$ because there are many combinations of D and $S^{0.5}$ that have same probability of colonization. If the probability of colonization is proportional to the product of *areal* stomatal size (S) and density ($\propto DS$ as for f_S) then it has the same effect on the slope as f_S because there are many combinations of D and S that have same probability of colonization. Alternatively, the probability of colonization may have a different scaling relationship (neither 0.5 nor 1) or may be non-linear on a log-log scale. Unlike $g_{s,max}$ and f_S, we do not have theory to predict a stomatal size-density relationship that preserves the probability of colonization.

In summary, the physical relationship between stomatal size, density, and conductance is well-established (Harrison et al., 2019). Size and density also likely affect the probability of pathogen colonization, but we do not have a theoretical model that makes quantitative predictions. The inverse stomatal size-density relationship has usually been explained in terms of preserving stomatal conductance and/or stomatal cover, but selection by pathogens might alter scaling. To address these gaps, the goals of this study are to (1) introduce a spatially explicit model pathogen colonization on the leaf surface; (2) use the model to predict the relationship between $g_{s,max}$, f_S, and the probability of colonization; (3) work out what these relationships predict about stomatal size-density scaling. I analyzed an idealized, spatially explicit Model of how a pathogen lands on a leaf and finds a stomate to colonize the leaf using a random search. To my knowledge, this is the first model that makes quantitative predictions about the relationship between stomatal anatomy, the probability of colonization, and their impact on stomatal size-density scaling.

MODEL

For generality, I refer to a generic "pathogen" that lands on leaf and moves to a stomate. The model is agnostic to the type of pathogen (virus, bacterium, fungus, etc.) and the specific biological details of how it moves. For example, motile bacterial cells can land and move around (Beattie and Lindow, 1995) whereas fungi may germinate from a cyst and grow until they form an appresorium for infection (Tucker and Talbot, 2001). These very different tropic movements on the leaf are treated identically here. I do not model photosynthesis explicitly, but assume that stomatal conductance limits carbon fixation, even

though the relationship is non-linear. I used Sympy version 1.6.1 (Meurer et al., 2017) for symbolic derivations.

Spatial Representation of Stomata

Stomata develop relatively equal spacing to minimize resistance to lateral diffusion (Morison et al., 2005), allow space between stomata (Dow et al., 2014b), and prevent stomatal interference (Lehmann and Or, 2015). Here I assume that stomata are arrayed in an equilateral triangular grid with a density D and size (area) S on the abaxial surface only, since most leaves are hypostomatous (Muir, 2015; but see Discussion). This assumption ignores veins, trichomes, and within-leaf variation in stomatal density. Stomata are therefore arrayed in an evenly spaced grid (**Figure 1A**). The interstomatal distance U, measured as the distance from the center of one stomata to the next, is the maximal diagonal of the hexagon in μm that forms an equal area boundary between neighboring stomata. The area of a hexagon is $A_{\text{hexagon}} = \frac{\sqrt{3}}{2}U^2$. By definition the stomatal density is the inverse of this area, such that $D = A_{\text{hexagon}}^{-1} = \frac{2}{\sqrt{3}}U^{-2}$. Therefore, interstomatal distance can be derived from the stomatal density as:

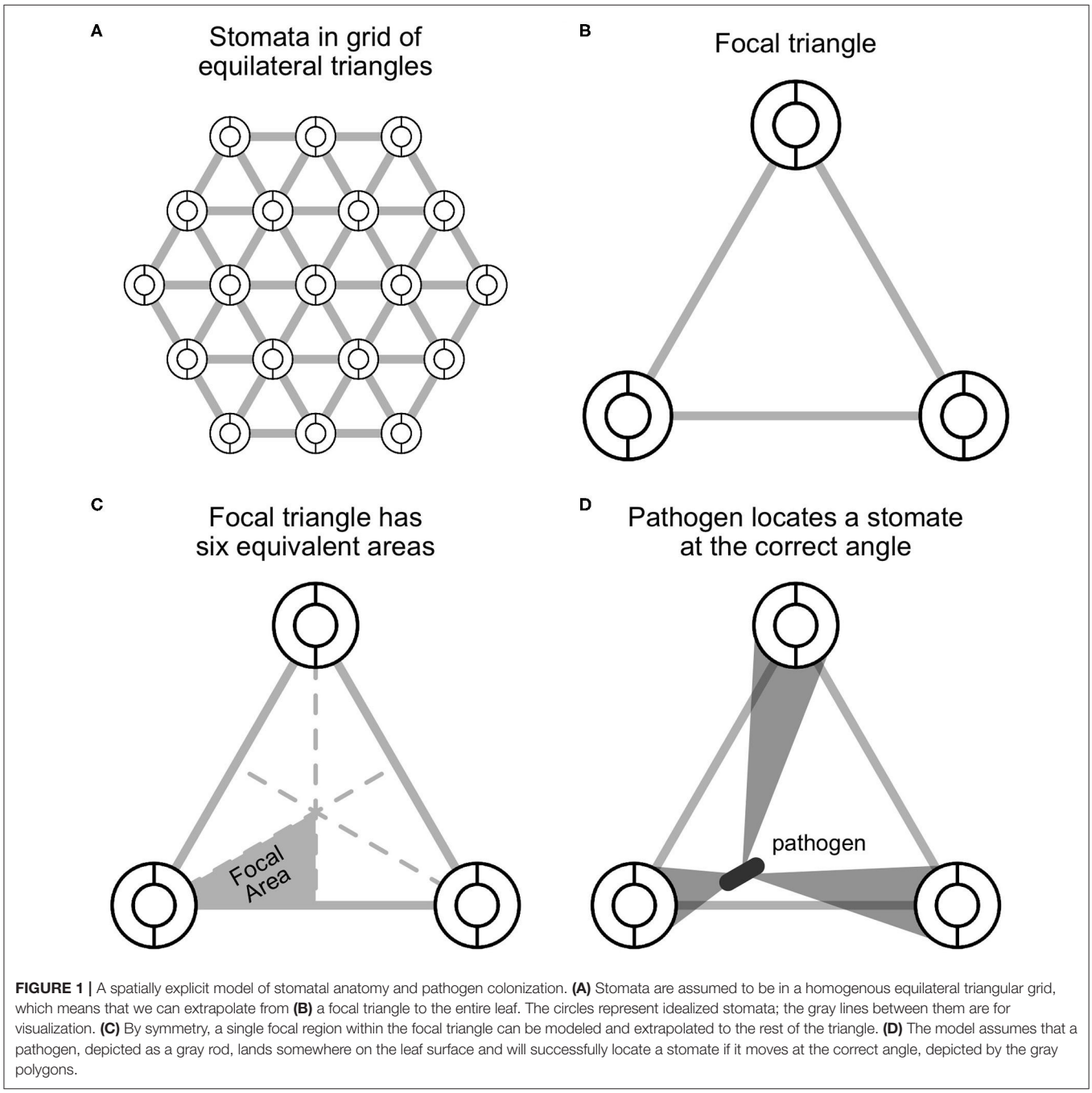

FIGURE 1 | A spatially explicit model of stomatal anatomy and pathogen colonization. **(A)** Stomata are assumed to be in a homogenous equilateral triangular grid, which means that we can extrapolate from **(B)** a focal triangle to the entire leaf. The circles represent idealized stomata; the gray lines between them are for visualization. **(C)** By symmetry, a single focal region within the focal triangle can be modeled and extrapolated to the rest of the triangle. **(D)** The model assumes that a pathogen, depicted as a gray rod, lands somewhere on the leaf surface and will successfully locate a stomate if it moves at the correct angle, depicted by the gray polygons.

$$D = \frac{2}{\sqrt{3}} U^{-2}$$

$$U = \left(\frac{2}{\sqrt{3}} D^{-1} \right)^{0.5}$$

For example, if the density is $D = 10^2$ mm^{-2} $= 10^{-4}$ μm^{-2}, then U is 107.5 μm. Parkhurst (1994) described this result previously. I also make the simplifying assumption that stomata are perfectly circular with radius R when fully open. This may be approximately true for fully open stomata with kidney-shaped guard cells (Sack and Buckley, 2016 and references therein). Although I assume stomata are circular here, in calculating $g_{s,max}$, I assume typical allometric relationships between length, width, and pore area (Sack and Buckley, 2016; see **Supplementary Material**).

Spatial Representation of Pathogen Search

Since stomata are arrayed in a homogeneous grid, we can focus on single focal triangle (**Figures 1B,C**). Suppose that an individual pathogen (e.g., bacterial cell or fungal spore) lands at a uniform random position within the focal triangle and must arrive at a stomate to colonize. If it lands on a stomate, then it infects the leaf with probability 1; if it lands between stomata, then it infects the leaf with probability p_{locate}. This is the probability that it locates a stomate, which I will derive below. The probabilities of landing on or between a stomate are f_S and $1 - f_S$, respectively. Hence, the total probability of colonization is:

$$p_{\text{colonize}} = f_S + (1 - f_S) p_{\text{locate}}. \quad (5)$$

I assume that the pathogen cannot sense where stomata are and orients at random, thereafter traveling in that direction. If it successfully locates a stomate, it colonizes the leaf, but otherwise does not infect. If there is a high density of stomata and/or large stomata, the probability of locating a stomate increases. By assuming that stomata form an equilateral triangular grid (see above), we can extrapolate what happens in the focal triangle (**Figure 1B**) by symmetry. Further, since an equilateral triangle can be broken up into six identical units (**Figure 1C**), we can simply calculate p_{locate} in this focal area. This implicitly assumes that the probability of colonizing stomata outside the focal area is 0 because they are too far away. This assumption may be unrealistic for larger pathogens, such as fungi, whose hyphae can travel longer distances on the leaf surface (Brand and Gow, 2012). In **Appendix 1**: Spatially Implicit Model I derive a simpler, but spatially *implicit* model that relaxes the assumption the pathogens must colonize a stomate within their focal triangle.

Consider a pathogen that lands in position (x_p, y_p) within the triangle. The centroid of the triangle is at position (x_c, y_c) and a reference stomate is at position $(0, 0)$ (**Figure 2A**). Therefore $x_c = U/2$ and $y_c = \sqrt{3}U/6$. The other stomata are at positions $(U/2, \sqrt{3}U/2)$ and $(U, 0)$ (**Figure 2**). x_p and y_p are defined as the horizontal and vertical distances, respectively, from the pathogen to the reference stomate at position $(0, 0)$.

Given that the pathogen starts at position (x_p, y_p), what's the probability of contacting one of the stomata at the vertices of the

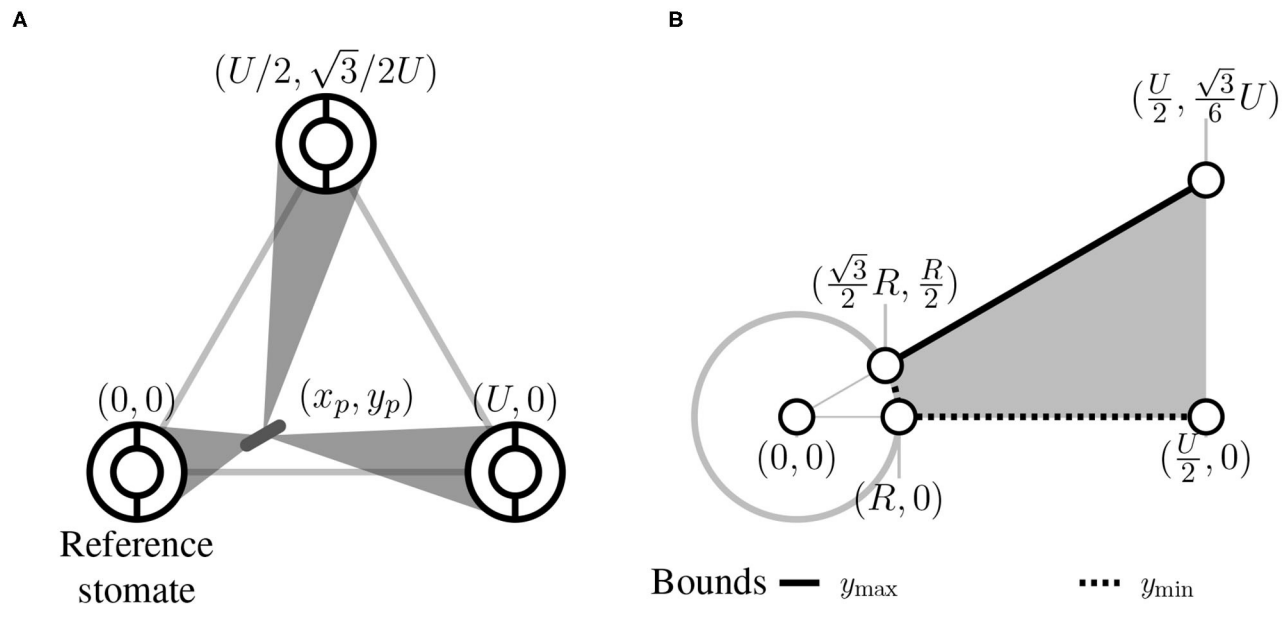

FIGURE 2 | Spatial representation of stomata and pathogen. **(A)** The pathogen starts at a uniform random position within the focal region denoted (x_p, y_p). Within the focal triangle, the reference stomate is at position (0,0) by definition, and other stomatal positions are determined by the interstomatal distance U. **(B)** Within the focal region, a pathogen can land within the stomate (white circle with gray outline and radius R) or in the gray area. The outer borders of this area are shown and depend on R and U. For a given position x, there is a minimum y-value ($y_{\min}$, dashed line) and maximum y-value ($y_{\max}$, solid line).

focal triangle? I assume the probability of contacting a stomate is equal to the proportion of angular directions that lead to a stomate (**Figure 1D**). I solved this by finding the angles $(\theta_1, \theta_2, \theta_3)$ between lines that are tangent to the outside of the three stomata and pass through (x_p, y_p) (**Figure 2A**). If stomate i is centered at (x_i, y_i), the two slopes of tangency as function of pathogen position are:

$$t_{i,1}(x_p, y_p) = \frac{-Re_{i,2}(x_p, y_p) + e_{i,3}(x_p, y_p)}{e_{i,1}(x_p, y_p)} \tag{6}$$

$$t_{i,2}(x_p, y_p) = \frac{Re_{i,2}(x_p, y_p) + e_{i,3}(x_p, y_p)}{e_{i,1}(x_p, y_p)} \tag{7}$$

where

$$e_{i,1}(x_p, y_p) = (R^2 - x_i^2 + 2x_i x_p - x_p^2), \tag{8}$$

$$e_{i,2}(x_p, y_p) = \sqrt{-e_{i,1} + (y_i - y_p)^2}, \tag{9}$$

$$e_{i,3}(x_p, y_p) = -x_i y_i + x_i y_p + x_p y_i - x_p y_p. \tag{10}$$

Note that $i \in \{1, 2, 3\}$, indexing the three stomata in the focal triangle. The angle in radians between $t_{i,1}(x_p, y_p)$ and $t_{i,2}(x_p, y_p)$ is:

$$\theta_i(x_p, y_p) = \arctan\left(\frac{t_{i,1}(x_p, y_p) - t_{i,2}(x_p, y_p)}{1 + (t_{i,1}(x_p, y_p) t_{i,2}(x_p, y_p))}\right) \tag{11}$$

I further assumed that the longer distance a pathogen must travel, the less likely it would be to locate a stomate. For example, if stomata are at very low density, then a pathogen may die before it reaches a stomate because of UV, desiccation, or another factor. I included this effect by assuming the probability of reaching a stomate declines exponentially at rate H with the Euclidean distance $v_i(x_p, y_p)$ between the pathogen location and the edge of stomata i, which is distance R from its center at x_i, y_i:

$$v_i(x_p, y_p) = \sqrt{(x_i - x_p)^2 + (y_i - y_p)^2} - R. \tag{12}$$

The probability of locating a stomate as a function of pathogen position (x_p and y_p) is the sum of the angles divided by 2π, discounted by their distance from the stomate:

$$f_{\text{locate}}(x_p, y_p) = \frac{1}{2\pi} \sum_{i=1}^{3} e^{-Hv_i(x_p, y_p)} \theta_i(x_p, y_p) \tag{13}$$

When there is no pathogen death ($H = 0$), p_{locate} is the fraction of angles that lead from (x_p, y_p) to a stomate. When $H > 0$, p_{locate} is proportional to this fraction, but less than it depending on stomatal density, size, and starting location of the pathogen.

To obtain the average p_{locate}, we must integrate $f_{\text{locate}}(x_p, y_p)$ over all possible starting positions (x_p, y_p) within the focal area. The focal area is a 30–60–90 triangle with vertices at the center of the reference stomate $(0, 0)$, the midpoint of baseline $(U/2, 0)$, and the centroid of the focal triangle $(U/2, \sqrt{3}/6U)$ (**Figure 1C**). Colonization occurs with probability 1 if the pathogen lands in the reference stomate, so we need to integrate the probability of colonization if it lands elsewhere. This region extends from the edge of the stomate, at $\sqrt{3}/2R$ to $U/2$ (**Figure 2B**). At any x, we integrate from the bottom of the focal area ($y_{\min}$) to the top ($y_{\max}$):

$$y_{\min} = f(x) = \begin{cases} \sqrt{R^2 - x^2}, & \text{if } \frac{\sqrt{3}}{2}R < x < R \\ 0, & \text{if } R \leq x \leq \frac{U}{2} \end{cases} \tag{14}$$

$$y_{\max} = f(x) = \frac{\sqrt{3}}{3}x \tag{15}$$

The integral is:

$$p_{\text{locate}} = \frac{1}{a_{\text{focal}}} \int_{\frac{\sqrt{3}}{2}R}^{U/2} \int_{y_{\min}}^{y_{\max}} f_{\text{locate}}(x, y)\, dx\, dy \tag{16}$$

a_{focal} is the area of the focal region depicted in gray in **Figure 2B**:

$$a_{\text{focal}} = \frac{U^2}{8\sqrt{3}} - \frac{\pi R^2}{12}$$

MATERIALS AND METHODS

The Model calculates a probability of host colonization (Equation 5) as a function of stomatal density, size, and position of a pathogen on the leaf. I solved p_{colonize} by importing symbolic derivations from Sympy into R with **reticulate** version 1.16 (Ushey et al., 2020) and used the `integral2()` function in the **pracma** package version 2.2.9 (Borchers, 2019) for numerical integration. I used R version 4.0.2 (R Core Team, 2020) for all analyses and wrote the paper in **rmarkdown** version 2.3 (Xie et al., 2018; Allaire et al., 2020). Citations for additional R software packages are in **Appendix 2**. Source code is deposited on GitHub (https://github.com/cdmuir/stomata-tradeoff) and archived on Zenodo (https://doi.org/10.5281/zenodo.4102283).

What Is the Relationship Between Stomatal Size, Density, and Colonization?

I calculated p_{colonize} over a biologically plausible grid of stomatal size and density for hypostomatous species based on Boer et al. (2016). Stomatal density (D) ranges from 10^1 to $10^{3.5}$ mm^{-2}; stomatal size (S) ranges from 10^1 to $10^{3.5}$ μm^2. I only considered combinations of size and density where stomatal cover (f_S) was $<1/3$, which is close to the upper limit in terrestrial plants (Boer et al., 2016). I crossed stomatal traits with three levels of $H \in \{0, 0.01, 0.1\}$. When $H = 0$, a pathogen persists indefinitely on the leaf surface. $H = 0.01$ and $H = 0.1$ correspond to low and high death rates, respectively. These values are not necessarily realistic, but illustrate qualitatively how a hostile environment on the leaf surface alters model predictions.

How Do Pathogens Alter Optimal Stomatal Size-Density Scaling?

The stomatal size-density scaling relationship can be explained in terms of preserving a constant stomatal conductance ($g_{s,\max}$)

that is proportional to $DS^{0.5}$ when bm is constant (Equation 1). In other words, there are infinitely many combinations of D and $S^{0.5}$ with the same $g_{s,max}$. If $g_{s,max}$ is held constant at C_g, then the resulting size-density scaling relationship on a log-log scale is:

$$d = c_g - 0.5s$$

where lowercase variables are log-transformed equivalents of their uppercase counterparts (**Table 1**). The scaling exponent $\beta_g = 0.5$ preserves C_g.

Next, suppose there is a scaling exponent β_p that preserves $p_{colonize}$ for the product DS^{β_p}. If $\beta_p = 0.5$, then $p_{colonize}$ is always proportional to $g_{s,max}$. If $\beta_p > 0.5$, small, densely packed stomata would be more resistant to colonization (lower $p_{colonize}$) compared to larger, sparsely spaced stomata with the same $g_{s,max}$. If $\beta_p < 0.5$, small, densely packed stomata would be less defended (higher $p_{colonize}$) compared to larger, sparsely spaced stomata with the same $g_{s,max}$. I refer to the three outcomes ($\beta_p = 0.5$, $\beta_p < 0.5$, and $\beta_p > 0.5$) as iso-, hypo-, and hyper-conductance, respectively. I was unable to solve analytically for β_p, so I numerically calculated isoclines of $p_{colonize}$ over the grid of D and S values described in the preceding subsection. I numerically calculated the scaling relationships at a constant $p_{colonize} \in \{0.025, 0.1, 0.4\}$ for $H \in \{0, 0.01, 0.1\}$.

RESULTS

Non-linear Relationships Between Colonization, Stomatal Cover, and Conductance

The probability of colonization ($p_{colonize}$) is not simply proportional to stomatal cover (f_S). At low f_S, $p_{colonize}$ increases rapidly relative to f_S at first (**Figure 3A**). At higher f_S, $p_{colonize}$ increases linearly with f_S. When pathogens persist indefinitely ($H = 0$), any combination of stomatal size (S) and density (D) with the same f_S have the same effect on $p_{colonize}$. When $H > 0$, pathogens are less likely to land close enough to a stomate to infect before dying, so $p_{colonize}$ is closer to f_S (**Figure 3A**). The maximum $p_{colonize}$ under the range of parameters considered was ~ 0.6 when $H = 0$ and f_S is at its maximum value of 1/3. When f_S is low, $p_{colonize}$ is also low. The relationship between $p_{colonize}$, f_S, and $g_{s,max}$is qualitatively similar in the spatially implicit model, but the values for $p_{colonize}$ are substantially higher because pathogens can potentially colonize any stomate on the leaf rather than only those in the focal triangle (see **Appendix 1**: Spatially Implicit Model for more detail). Bear in mind that this is the probability for a single individual searching randomly; if enough individuals reach the leaf and/or they can actively find stomata, it's almost certain that at least some will colonize the leaf. However, reducing $p_{colonize}$ may help plants limit the damage since fewer total individual pathogens will colonize the leaf interior.

$p_{colonize}$ is not directly proportional to f_S because it depends on D and S in quantitatively different ways (**Supplementary Figure 1**). For the same f_S, leaves with greater D have higher $p_{colonize}$ (**Figure 3A**). Holding f_S constant, leaves with lower D and higher S will have a greater distance (v_i) between a pathogen and its stomata. When $H > 0$, this extra distance leads more pathogens to die before they can find a stomate. However, this result is inconsistent with the spatially implicit model (**Appendix 1**) because S and D have identical effects on f_S.

In contrast to f_S, $p_{colonize}$ increases at a greater than linear rate with stomatal conductance ($g_{s,max}$). Greater D (smaller S) is associated with lower $p_{colonize}$ for a given value of $g_{s,max}$ (**Figure 3B**). This happens because $p_{colonize}$ increases approximately linearly with S whereas $g_{s,max}$ is proportional to $S^{0.5}$. Therefore, $p_{colonize}$ increases exponentially with $g_{s,max}$ at all stomatal densities, but the rate of growth is lower at greater D for a given value of $g_{s,max}$.

Hyper-Conductance Size-Density Scaling

The scaling relationship between S and D that preserves $p_{colonize}$ is always >0.5 (hyper-conductance), but usually <1. When $H = 0$, the scaling relationship is essentially 1 (**Figure 4**), which means that an increase f_S leads to a proportional increase in $p_{colonize}$. Because the scaling relationship is >0.5, leaves with greater stomatal density will have lower $p_{colonize}$ than leaves lower stomatal density but the same $g_{s,max}$. In other words, increasing D and lowering S allows plants to reduce $p_{colonize}$ while maintaining $g_{s,max}$. The scaling relationship is slightly <1, but still >0.5, when $H > 0$ (**Figure 4**). In this area of parameter space, lower stomatal density can reduce f_S while $p_{colonize}$ is constant, but this will still result in lower $g_{s,max}$. In the spatially implicit model, the size-density scaling exponent was always exactly 1 except when $H = 0$ (**Appendix 1**).

DISCUSSION

Stomatal density and size set the upper limit on gas exchange in leaves (Harrison et al., 2019) and is often closely related to operational stomatal conductance in nature (Murray et al., 2019). Despite the fact that many foliar pathogens infect through stomata, the relationship between stomatal anatomy and resistance to foliar pathogens is less clear than it is for gas exchange. I used a spatially explicit model of a pathogen searching for a stomate to colonize a host. From this Model, I derived predictions about the relationship between stomatal anatomy and the probability of colonization, a component of disease resistance. The model predicts that the probability of colonization is not always proportional to the surface area of leaf covered by stomata (f_S), as one might intuitively predict. If the leaf surface is a hostile environment and pathogens have a limited time to search, lower stomatal density decreases the probability of colonization even if f_S is constant. However, $g_{s,max}$ decreases proportionally more than the probability of colonization. The model highlights the potential for conflicting demands of minimizing pathogen colonization, minimizing stomatal cover, and maintaining stomatal conductance. Including the effect of anatomy on pathogen colonization therefore has the potential to change our understanding of how stomatal size-density scaling evolves in land plants.

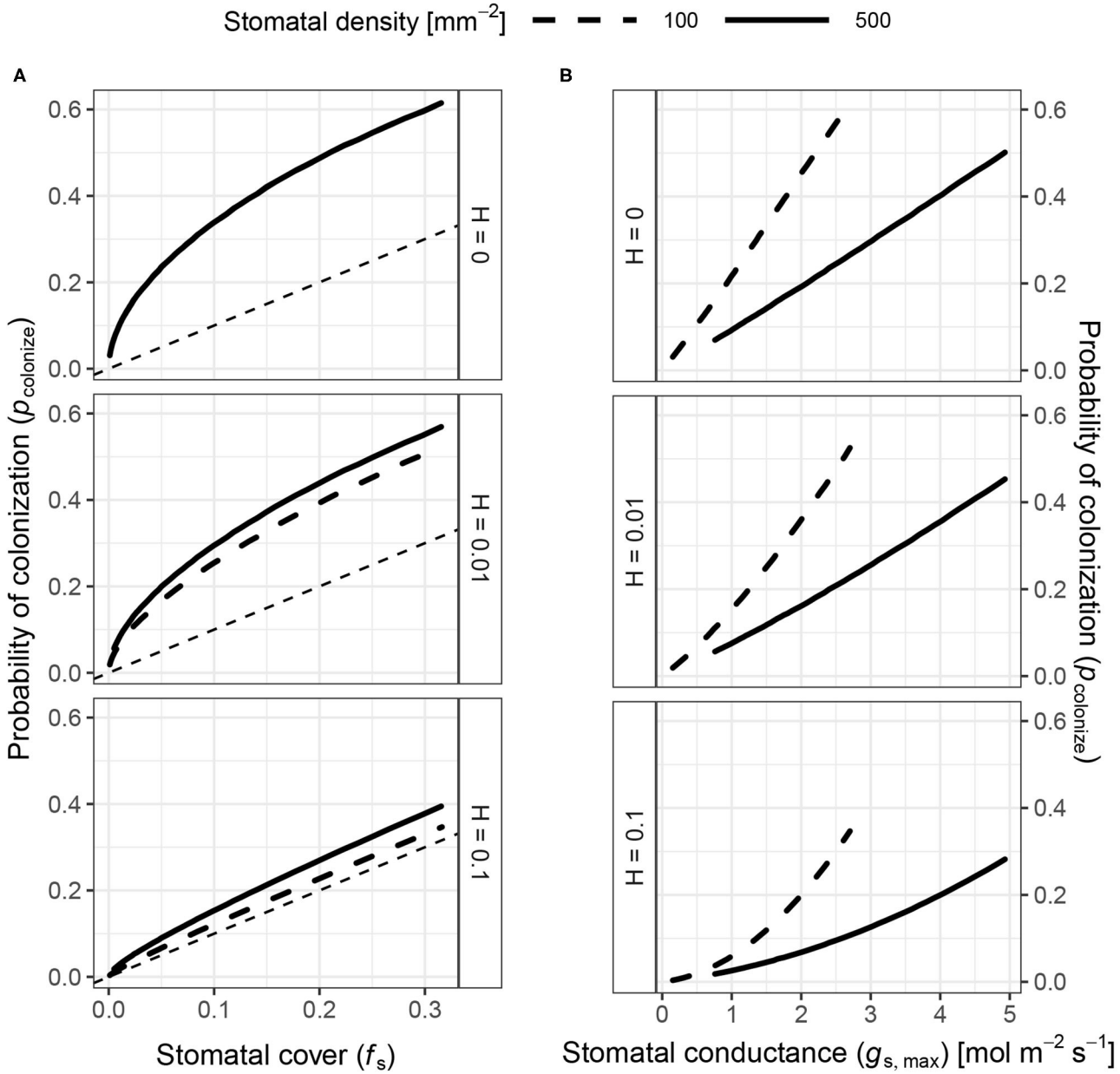

FIGURE 3 | The probability of colonization increases with both stomatal cover and conductance. I simulated the probability of colonization ($p_{colonize}$, *y*-axis) over a range of stomatal densities and sizes (see Materials and Methods), but a subset of results are shown here. Stomatal size and density determine stomatal cover (f_S; Equation 1) and theoretical maximum stomatal conductance ($g_{s,max}$; Equation 1). **(A)** $p_{colonize}$ initially increases rapidly with f_S (*x*-axis), then slows down to a linear relationship. Overall, $p_{colonize}$ is lower when pathogens can die on the leaf surface ($H > 0$). The relationship between f_S and $p_{colonize}$ is the same regardless of stomatal density when $H = 0$ (upper facet), which is why the lines overlap. When $H > 0$, higher density (solid lines) increase $p_{colonize}$ (lower facets). **(B)** $p_{colonize}$ increases exponentially with $g_{s,max}$ at all stomatal densities, but $p_{colonize}$ is much lower at higher densities for a given $g_{s,max}$. The relationship between $g_{s,max}$ and $p_{colonize}$ is similar for all values of *H*.

The model predicts that in most cases, increasing stomatal cover should lead to a proportional increase in colonization, which agrees with empirical studies (e.g., McKown et al., 2014; Dutton et al., 2019; Fetter et al., 2019; Tateda et al., 2019). It also makes new, testable predictions that are less intuitive (**Table 2**). At very low f_S, there is a rapid increase in colonization (**Figure 3A**). If there are no stomata, the probability of colonization is 0, so the first few stomata dramatically increase the probability. This is less likely to be significant for abaxial (lower) leaf surfaces, which usually have most of the stomata (Salisbury, 1928; Metcalfe and Chalk, 1950; Mott et al., 1984; Peat and Fitter, 1994; Jordan et al., 2014; Muir, 2015; Bucher

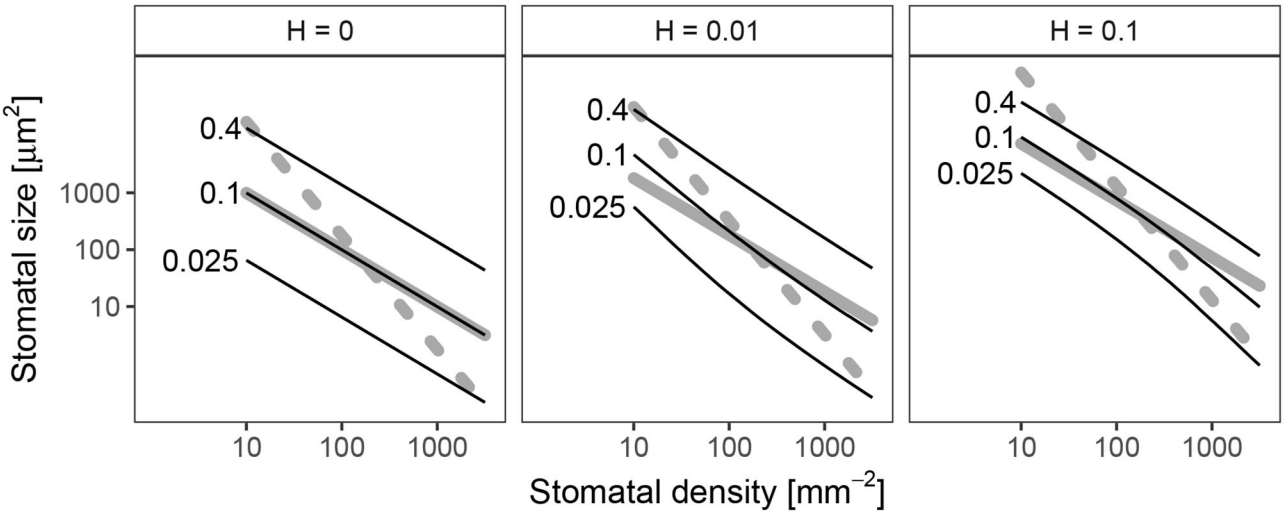

FIGURE 4 | Log-log scaling relationships between stomatal density (D, x-axis) and size (S, y-axis) that preserve the probability of colonization ($p_{colonize}$). In each panel, solid lines indicate values of D and S where $p_{colonize}$ is 0.025 (lowest line), 0.1, or 0.4 (highest line). For reference, dashed gray lines show scaling relationships that preserve f_S ($\beta = 1$, slope $= -1/\beta = -1$) and $g_{s,max}$ ($\beta = 0.5$, slope $= -1/\beta = -2$) drawn through the centroid of the plotting region. When the death rate on the leaf surface is low ($H = 0$), the scaling exponent is very close to $\beta = 1$. When $H > 0$, $0.5 < \beta < 1$ and is slightly non-linear on a log-log scale.

TABLE 2 | New testable model predictions and suggested experiments to test them.

Model prediction	How to test it
Increasing stomatal size and/or density will have a larger effect on pathogen colonization in leaves with low stomatal cover.	Compare the effect of changing stomatal size and/or density on pathogen colonization in leaves with low and high stomatal cover.
Increasing stomatal size and/or density will have a smaller effect on pathogen colonization in ephiphytic environments more hostile to pathogens.	Compare the effect of changing stomatal size and/or density on pathogen colonization in more hostile environments (e.g., drier, higher light)
When selection against pathogen colonization is stronger, the stomatal size-density scaling exponent should be lower	Measure stomatal anatomy in environments that differ in pathogen colonization using comparative or experimental approaches

et al., 2017; Drake et al., 2019). However, many adaxial (upper) leaf surfaces have zero or very few stomata. Using adaxial leaf surfaces, it should be possible to test if small changes in stomatal size or density have a larger effect on pathogen colonization when f_S is low. Such experiments could use natural genetic variation (McKown et al., 2014) or mutant lines (Dow et al., 2014b). The non-linear increase in $p_{colonize}$ is less apparent when $H > 0$ (**Figure 3A**). A more hostile microenvironment (e.g., drier, higher UV) should therefore reduce the effect of increased size or density at low f_S. If true, the diminishing marginal effect of f_S on colonization could explain why stomatal ratio on the upper and lower surface is bimodal (Muir, 2015). The initial cost of adaxial (upper) stomata is relatively high, but if the benefits outweigh the costs, then equal stomatal densities on each surface maximize CO_2 supply for photosynthesis (Parkhurst, 1978; Gutschick, 1984; Parkhurst and Mott, 1990). The costs and benefits will certainly vary with environmental conditions as well. Future work should extend this model, which considered hypostomatous leaves, to address stomatal size and density in amphistomatous leaves, since leaf surfaces may differ in the type of pathogens present and microenvironment (McKown et al., 2014; Fetter et al., 2019).

An effect of stomatal size and density on foliar pathogen colonization could change our understanding of stomatal size-density scaling. Since allocating leaf epidermis to stomata may be costly (Assmann and Zeiger, 1987; Franks and Farquhar, 2007; Dow et al., 2014b; Lehmann and Or, 2015; Baresch et al., 2019), selection should favor leaves that achieve a desired $g_{s,max}$ while minimizing f_S (Boer et al., 2016). Because of their different scaling exponents (Equation 1, 2), smaller, densely packed stomata can achieve the same $g_{s,max}$ at minimum f_S. However, many leaves have larger, sparsely packed stomata. Incorporating pathogen colonization may explain why. If pathogens have a limited time to find stomata before dying ($H > 0$), then the scaling exponent between size and density that keeps $p_{colonize}$ constant is between 0.5 and 1, the scaling exponents for $g_{s,max}$ and f_S, respectively (**Figure 4**). Greater density of smaller stomata can increase $g_{s,max}$ while keeping $p_{colonize}$ constant, but this will

increase f_S. Conversely, f_S could decrease while keeping $p_{colonize}$ constant, but this will decrease $g_{s,max}$. This sets up the potential for conflict between competing goals. The optimal stomatal size and density will therefore depend on the precise costs and benefits of infection, stomatal conductance, and stomatal cover. This may explain why many leaves have large, sparsely packed stomata despite the fact that they could achieve the same $g_{s,max}$ and lower f_S with smaller, more densely packed stomata.

The model examines the probability of colonization for a single pathogen. The calculated probabilities of colonization should not be interpreted as exact predictions, but rather as depicting qualitative relationships between stomatal anatomy and infection severity. The energetic cost and lost photosynthetic capacity (closed stomata, necrosis, etc.) of dealing with a pathogen is assumed to be proportional to the amount of infection. The actual fitness cost will be modulated by the number of pathogens landing on the leaf and the cost of infection, all else being equal. In environments with fewer or less virulent pathogens, the fitness cost of infection will be less than in environments with more abundant, virulent pathogens. The model is less relevant to very susceptible host plants that can be severely damaged or killed by a small number of colonizations that spread unchecked throughout the host tissue.

CONCLUSION

The model makes two non-intuitive predictions. First, the effect of increased stomatal density or size on susceptibility to foliar pathogens is greatest when stomatal cover is very low. Second, maximizing disease resistance sets up a potential conflict between minimizing stomatal cover and maximizing stomatal conductance. The first prediction is consistent with results in *Populus trichocarpa* (McKown et al., 2014) and may be relatively straightforward to test experimentally with adaxial (upper) stomata that occur at low and moderate densities within the same or closely related species (Muir et al., 2014; Fetter et al., 2019). The second prediction about size-density scaling is more complex because we would need to know the relationships between colonization, stomatal cover, stomatal conductance, and fitness in natural conditions. There is growing evidence that stomata mediate tradeoffs between photosynthesis and defense in *Populus trichocarpa* (McKown et al., 2019), but testing these predictions in a variety of species will help determine whether pathogens have played an important role shaping stomatal anatomy in land plants.

DATA AVAILABILITY STATEMENT

Source code is deposited on GitHub (https://github.com/cdmuir/stomata-tradeoff) and archived on Zenodo (https://doi.org/10.5281/zenodo.4102283).

AUTHOR CONTRIBUTIONS

The author confirms being the sole contributor of this work and has approved it for publication.

FUNDING

I am grateful startup funds from the University of Hawai'i for supporting this work.

ACKNOWLEDGMENTS

I would like to thank Athena McKown and Karl Fetter for valuable feedback that improved this manuscript.

SUPPLEMENTARY MATERIAL

The Supplementary Material for this article can be found online at: https://www.frontiersin.org/articles/10.3389/fpls.2020.518991/full#supplementary-material

Appendix 1 | Supplemental methods and spatially implicit model.

Appendix 2 | Additional R packages.

REFERENCES

Allaire, J., Xie, Y., McPherson, J., Luraschi, J., Ushey, K., Wickham, H., et al. (2020). *Rmarkdown: Dynamic Documents for R*. Available online at: https://github.com/rstudio/rmarkdown.

Allen, E. A., Hazen, B. E., Hoch, H. C., Kwon, Y., Leinhos, G. M. E., Staples, R. C., et al. (1991). Appressorium formation in response to topographical signals by 27 rust species. *Phytopathology* 81:323. doi: 10.1094/Phyto-81-323

Assmann, S. M., and Zeiger, E. (1987). "Guard call bioenergetics," in *Stomatal Function*, eds E. Zeiger, G. D. Farquhar, and I. R. Cowan (Stanford, CA: Stanford University Press), 163–193.

Baresch, A., Crifò, C., and Boyce, C. K. (2019). Competition for epidermal space in the evolution of leaves with high physiological rates. *New Phytol.* 221, 628–639. doi: 10.1111/nph.15476

Bastiaans, L. (1991). Ratio between virtual and visual lesion size as a measure to describe reduction in leaf photosynthesis of rice due to leaf blast. *Phytopathology* 81:611. doi: 10.1094/Phyto-81-611

Beattie, G. A., and Lindow, S. E. (1995). The secret life of foliar bacterial pathogens on leaves. *Annu. Rev. Phytopathol.* 33, 145–172.

Berry, J. A., Beerling, D. J., and Franks, P. J. (2010). Stomata: key players in the earth system, past and present. *Curr. Opin. Plant Biol.* 13, 232–239. doi: 10.1016/j.pbi.2010.04.013

Boer, H. J. de, Price, C. A., Wagner-Cremer, F., Dekker, S. C., Franks, P. J., and Veneklaas, E. J. (2016). Optimal allocation of leaf epidermal area for gas exchange. *New Phytol.* 210, 1219–1228. doi: 10.1111/nph.13929

Borchers, H. W. (2019). *Pracma: Practical Numerical Math Functions*. R package version 2.2.9. Available online at: https://CRAN.R-project.org/package=pracma.

Brand, A., and Gow, N. A. R. (2012). "Tropic orientation responses of pathogenic fungi," in *Morphogenesis and Pathogenicity in Fungi*, eds J. Pérez-Martín and A. Di Pietro (Berlin; Heidelberg: Springer Berlin Heidelberg), 21–41. doi: 10.1007/978-3-642-22916-9_2

Brodribb, T. J., Jordan, G. J., and Carpenter, R. J. (2013). Unified changes in cell size permit coordinated leaf evolution. *New Phytol.* 199, 559–570. doi: 10.1111/nph.12300

Brown, H. T., and Escombe, F. (1900). Static diffusion of gases and liquids in relation to the assimilation of carbon and translocation in plants. *Proc. R. Soc. Lond.* 67, 124–128.

Bucher, S. F., Auerswald, K., Grün-Wenzel, C., Higgins, S. I., Garcia Jorge, J., and Römermann, C. (2017). Stomatal traits relate to habitat preferences of herbaceous species in a temperate climate. *Flora* 229, 107–115. doi: 10.1016/j.flora.2017.02.011

Buckley, T. N. (2019). How do stomata respond to water status? *New Phytol.* 224, 21–36. doi: 10.1111/nph.15899

Chater, C. C. C., Caine, R. S., Fleming, A. J., and Gray, J. E. (2017). Origins and evolution of stomatal development. *Plant Physiol.* 174, 624–638. doi: 10.1104/pp.17.00183

Dow, G. J., Bergmann, D. C., and Berry, J. A. (2014a). An integrated model of stomatal development and leaf physiology. *New Phytol.* 201, 1218–1226. doi: 10.1111/nph.12608

Dow, G. J., Berry, J. A., and Bergmann, D. C. (2014b). The physiological importance of developmental mechanisms that enforce proper stomatal spacing in *Arabidopsis thaliana*. *New Phytol.* 201, 1205–1217. doi: 10.1111/nph.12586

Drake, P. L., Boer, H. J., Schymanski, S. J., and Veneklaas, E. J. (2019). Two sides to every leaf: Water and CO_2 transport in hypostomatous and amphistomatous leaves. *New Phytol.* 222, 1179–1187. doi: 10.1111/nph.15652

Drake, P. L., Froend, R. H., and Franks, P. J. (2013). Smaller, faster stomata: scaling of stomatal size, rate of response, and stomatal conductance. *J. Exp. Bot.* 64, 495–505. doi: 10.1093/jxb/ers347

Dutton, C., Hõrak, H., Hepworth, C., Mitchell, A., Ton, J., Hunt, L., et al. (2019). Bacterial infection systemically suppresses stomatal density. *Plant Cell Environ.* 42, 2411–2421. doi: 10.1111/pce.13570

Farquhar, G. D., and Sharkey, T. D. (1982). Stomatal conductance and photosynthesis. *Annu. Rev. Plant Physiol.* 33, 317–345. doi: 10.1146/annurev.pp.33.060182.001533

Fawke, S., Doumane, M., and Schornack, S. (2015). Oomycete interactions with plants: infection strategies and resistance principles. *Microbiol. Mol. Biol. Rev.* 79, 263–280. doi: 10.1128/MMBR.00010-15

Fetter, K. C., Nelson, D. M., and Keller, S. R. (2019). *Trade-Offs and Selection Conflicts in Hybrid Poplars Indicate the Stomatal Ratio as an Important Trait Regulating Disease Resistance*. Burlington, VT: University of Vermont.

Flexas, J., Cano, F. J., Carriquí, M., Coopman, R. E., Mizokami, Y., Tholen, D., et al. (2018). "CO_2 diffusion inside photosynthetic organs," in *The Leaf: A Platform for Performing Photosynthesis Advances in Photosynthesis and Respiration*, eds W. W. Adams III and I. Terashima (Cham: Springer International Publishing), 163–208. doi: 10.1007/978-3-319-93594-2_7

Franks, P. J., and Beerling, D. J. (2009a). CO_2 -forced evolution of plant gas exchange capacity and water-use efficiency over the Phanerozoic. *Geobiology* 7, 227–236. doi: 10.1111/j.1472-4669.2009.00193.x

Franks, P. J., and Beerling, D. J. (2009b). Maximum leaf conductance driven by CO_2 effects on stomatal size and density over geologic time. *Proc. Natl. Acad. Sci. U.S.A.* 106, 10343–10347. doi: 10.1073/pnas.0904209106

Franks, P. J., Drake, P. L., and Beerling, D. J. (2009). Plasticity in maximum stomatal conductance constrained by negative correlation between stomatal size and density: an analysis using *Eucalyptus globulus*. *Plant Cell Environ.* 32, 1737–1748. doi: 10.1111/j.1365-3040.2009.002031.x

Franks, P. J., and Farquhar, G. D. (2001). The effect of exogenous abscisic acid on stomatal development, stomatal mechanics, and leaf gas exchange in *Tradescantia virginiana*. *Plant Physiol.* 125, 935–942. doi: 10.1104/pp.125.2.935

Franks, P. J., and Farquhar, G. D. (2007). The mechanical diversity of stomata and its significance in gas-exchange control. *Plant Physiol.* 143, 78–87. doi: 10.1104/pp.106.089367

Franks, P. J., Royer, D. L., Beerling, D. J., Van de Water, P. K., Cantrill, D. J., Barbour, M. M., et al. (2014). New constraints on atmospheric CO_2 concentration for the Phanerozoic. *Geophys. Res. Lett.* 41, 4685–4694. doi: 10.1002/2014GL060457

Gilbert, G. S. (2002). Evolutionary ecology of plant diseases in naturalecosystems. *Annu. Rev. Phytopathol.* 40, 13–43. doi: 10.1146/annurev.phyto.40.021202.110417

Gray, A., Liu, L., and Facette, M. (2020). Flanking support: how subsidiary cells contribute to stomatal form and function. *Front. Plant Sci.* 11:881. doi: 10.3389/fpls.2020.00881

Gutschick, V. P. (1984). Photosynthesis model for C_3 leaves incorporating CO_2 transport, propagation of radiation, and biochemistry 1. Kinetics and their parameterization. *Photosynthetica* 18, 549–568.

Harrison, E. L., Arce Cubas, L., Gray, J. E., and Hepworth, C. (2019). The influence of stomatal morphology and distribution on photosynthetic gas exchange. *Plant J.* 101, 768–779. doi: 10.1111/tpj.14560

Hetherington, A. M., and Woodward, F. I. (2003). The role of stomata in sensing and driving environmental change. *Nature* 424, 901–908. doi: 10.1038/nature01843

Hoch, H. C., Staples, R. C., Whitehead, B., Comeau, J., and Wolf, E. D. (1987). Signaling for growth orientation and cell differentiation by surface topography in uromyces. *Science* 235, 1659–1662.

Jones, H. G. (1985). Partitioning stomatal and non-stomatal limitations to photosynthesis. *Plant Cell Environ.* 8, 95–104. doi: 10.1111/j.1365-3040.1985.tb01227.x

Jordan, G. J., Carpenter, R. J., and Brodribb, T. J. (2014). Using fossil leaves as evidence for open vegetation. *Palaeogeogr. Palaeoclimatol. Palaeoecol.* 395, 168–175. doi: 10.1016/j.palaeo.2013.12.035

Kiefer, B., Riemann, M., Büche, C., Kassemeyer, H.-H., and Nick, P. (2002). The host guides morphogenesis and stomatal targeting in the grapevine pathogen *Plasmopara viticola*. *Planta* 215, 387–393. doi: 10.1007/s00425-002-0760-2

Lawson, T., and Blatt, M. R. (2014). Stomatal size, speed, and responsiveness impact on photosynthesis and water use efficiency. *Plant Physiol.* 164, 1556–1570. doi: 10.1104/pp.114.237107

Lawson, T., Terashima, I., Fujita, T., and Wang, Y. (2018). "Coordination between photosynthesis and stomatal behavior," in *The Leaf: A Platform for Performing Photosynthesis Advances in Photosynthesis and Respiration*, eds W. W. Adams III and I. Terashima (Cham: Springer International Publishing), 141–161. doi: 10.1007/978-3-319-93594-2_6

Lehmann, P., and Or, D. (2015). Effects of stomata clustering on leaf gas exchange. *New Phytol.* 207, 1015–1025. doi: 10.1111/nph.13442

McElwain, J. C., Yiotis, C., and Lawson, T. (2016). Using modern plant trait relationships between observed and theoretical maximum stomatal conductance and vein density to examine patterns of plant macroevolution. *New Phytol.* 209, 94–103. doi: 10.1111/nph.13579

McKown, A. D., Guy, R. D., Quamme, L., Klápště, J., La Mantia, J., Constabel, C. P., et al. (2014). Association genetics, geography and ecophysiology link stomatal patterning in *Populus trichocarpa* with carbon gain and disease resistance trade-offs. *Mol. Ecol.* 23, 5771–5790. doi: 10.1111/mec.12969

McKown, A. D., Klápště, J., Guy, R. D., Corea, O. R. A., Fritsche, S., Ehlting, J., et al. (2019). A role for *SPEECHLESS* in the integration of leaf stomatal patterning with the growth vs disease trade-off in poplar. *New Phytol.* 223, 1888–1903. doi: 10.1111/nph.15911

McLachlan, D. H., Kopischke, M., and Robatzek, S. (2014). Gate control: guard cell regulation by microbial stress. *New Phytol.* 203, 1049–1063. doi: 10.1111/nph.12916

Melotto, M., Underwood, W., Koczan, J., Nomura, K., and He, S. Y. (2006). Plant stomata function in innate immunity against bacterial invasion. *Cell* 126, 969–980. doi: 10.1016/j.cell.2006.06.054

Melotto, M., Zhang, L., Oblessuc, P. R., and He, S. Y. (2017). Stomatal defense a decade later. *Plant Physiol.* 174, 561–571. doi: 10.1104/pp.16.01853

Metcalfe, C. R., and Chalk, L. (1950). *Anatomy of the Dicotyledons*, Vols. 1 & 2. Oxford: Oxford University Press.

Meurer, A., Smith, C. P., Paprocki, M., Čertík, O., Kirpichev, S. B., Rocklin, M., et al. (2017). SymPy: symbolic computing in Python. *PeerJ Comput. Sci.* 3:e103. doi: 10.7717/peerj-cs.103

Mitchell, C. E. (2003). Trophic control of grassland production and biomass by pathogens. *Ecol. Lett.* 6, 147–155. doi: 10.1046/j.1461-0248.2003.00408.x

Morison, J. I. L., Emily Gallouët, Lawson, T., Cornic, G., Herbin, R., and Baker, N. R. (2005). Lateral diffusion of CO$_2$ in leaves is not sufficient to support photosynthesis. *Plant Physiol.* 139, 254–266. doi: 10.1104/pp.105.062950

Mott, K. A., Gibson, A. C., and O'Leary, J. W. (1984). The adaptive significance of amphistomatic leaves. *Plant Cell Environ.* 5, 455–460.

Muir, C. D. (2015). Making pore choices: repeated regime shifts in stomatal ratio. *Proc. R. Soc. B Biol. Sci.* 282:20151498. doi: 10.1098/rspb.2015.1498

Muir, C. D., Hangarter, R. P., Moyle, L. C., and Davis, P. A. (2014). Morphological and anatomical determinants of mesophyll conductance in wild relatives of

tomato (*solanum* sect. *Lycopersicon*, sect. *Lycopersicoides*; Solanaceae). *Plant Cell Environ.* 37, 1415–1426. doi: 10.1111/pce.12245

Murray, M., Soh, W. K., Yiotis, C., Spicer, R. A., Lawson, T., and McElwain, J. C. (2019). Consistent relationship between field-measured stomatal conductance and theoretical maximum stomatal conductance in C_3 woody angiosperms in four major biomes. *Int. J. Plant Sci.* 181:706260. doi: 10.1086/706260

Murray, R. R., Emblow, M. S. M., Hetherington, A. M., and Foster, G. D. (2016). Plant virus infections control stomatal development. *Sci. Rep.* 6:34507. doi: 10.1038/srep34507

Oguchi, R., Onoda, Y., Terashima, I., and Tholen, D. (2018). "Leaf anatomy and function," in *The Leaf: A Platform for Performing Photosynthesis Advances in Photosynthesis and Respiration*, eds W. W. Adams III and I. Terashima (Cham: Springer International Publishing), 97–139. doi: 10.1007/978-3-319-93594-2_5

Papanatsiou, M., Amtmann, A., and Blatt, M. R. (2017). Stomatal clustering in Begonia associates with the kinetics of leaf gaseous exchange and influences water use efficiency. *J. Exp. Bot.* 68, 2309–2315. doi: 10.1093/jxb/erx072

Parkhurst, D. F. (1978). The adaptive significance of stomatal occurrence on one or both surfaces of leaves. *J. Ecol.* 66:367. doi: 10.2307/2259142

Parkhurst, D. F. (1994). Diffusion of CO_2 and other gases inside leaves. *New Phytol.* 126, 449–479.

Parkhurst, D. F., and Mott, K. A. (1990). Intercellular diffusion limits to CO_2 uptake in leaves: studies in Air and Helox. *Plant Physiol.* 94, 1024–1032. doi: 10.1104/pp.94.3.1024

Parlange, J.-Y., and Waggoner, P. E. (1970). Stomatal dimensions and resistance to diffusion. *Plant Physiol.* 46, 337–342. doi: 10.1104/pp.46.2.337

Peat, H. J., and Fitter, A. H. (1994). A comparative study of the distribution and density of stomata in the British flora. *Biol. J. Linn. Soc.* 52, 377–393.

R Core Team (2020). *R: A Language and Environment for Statistical Computing*. Vienna: R Foundation for Statistical Computing. Available online at: http://www.R-project.org/.

Raissig, M. T., Matos, J. L., Anleu Gil, M. X., Kornfeld, A., Bettadapur, A., Abrash, E., et al. (2017). Mobile MUTE specifies subsidiary cells to build physiologically improved grass stomata. *Science* 355, 1215–1218. doi: 10.1126/science.aal3254

Sack, L., and Buckley, T. N. (2016). The developmental basis of stomatal density and flux. *Plant Physiol.* 171, 2358–2363. doi: 10.1104/pp.16.00476

Sack, L., Cowan, P. D., Jaikumar, N., and Holbrook, N. M. (2003). The 'hydrology' of leaves: co-ordination of structure and function in temperate woody species. *Plant Cell Environ.* 26, 1343–1356. doi: 10.1046/j.0016-8025.2003.01058.x

Salisbury, E. J. (1928). On the causes and ecological significance of stomatal frequency, with special reference to the Woodland Flora. *Philos. Trans. R. Soc. B Biol. Sci.* 216, 1–65. doi: 10.1098/rstb.1928.0001

Tateda, C., Obara, K., Abe, Y., Sekine, R., Nekoduka, S., Hikage, T., et al. (2019). The host stomatal density determines resistance to *Septoria gentianae* in Japanese Gentian. *Mol. Plant Microbe Interact.* 32, 428–436. doi: 10.1094/MPMI-05-18-0114-R

Tichá, I. (1982). Photosynthetic characteristics during ontogenesis of leaves 7. Stomata density and sizes. *Photosynthetica* 16, 375–471.

Tucker, S. L., and Talbot, N. J. (2001). Surface attachment and pre-penetration stage development by plant pathogenic fungi. *Annu. Rev. Phytopathol.* 39, 385–417. doi: 10.1146/annurev.phyto.39.1.385

Underwood, W., Melotto, M., and He, S. Y. (2007). Role of plant stomata in bacterial invasion. *Cell. Microbiol.* 9, 1621–1629. doi: 10.1111/j.1462-5822.2007.00938.x

Ushey, K., Allaire, J. J., and Tang, Y. (2020). *Reticulate: Interface to 'Python'*. Available online at: https://CRAN.R-project.org/package=reticulate.

Weiss, A. (1865). Untersuchungen über die Zahlen- und Grössenverhältnisse der Spaltöffnungen. *Jahr. Wissensch. Bot.* 4, 125–196.

Xie, Y., Allaire, J. J., and Grolemund, G. (2018). *R Markdown: The Definitive Guide*. Boca Raton, FL: Taylor & Francis, CRC Press.

Zeng, W., Melotto, M., and He, S. Y. (2010). Plant stomata: a checkpoint of host immunity and pathogen virulence. *Curr. Opin. Biotechnol.* 21, 599–603. doi: 10.1016/j.copbio.2010.05.006

Conflict of Interest: The author declares that the research was conducted in the absence of any commercial or financial relationships that could be construed as a potential conflict of interest.

Advantages of publishing in Frontiers

OPEN ACCESS
Articles are free to read for greatest visibility and readership

FAST PUBLICATION
Around 90 days from submission to decision

HIGH QUALITY PEER-REVIEW
Rigorous, collaborative, and constructive peer-review

TRANSPARENT PEER-REVIEW
Editors and reviewers acknowledged by name on published articles

Frontiers
Avenue du Tribunal-Fédéral 34
1005 Lausanne | Switzerland

Visit us: www.frontiersin.org
Contact us: frontiersin.org/about/contact

REPRODUCIBILITY OF RESEARCH
Support open data and methods to enhance research reproducibility

DIGITAL PUBLISHING
Articles designed for optimal readership across devices

FOLLOW US
@frontiersin

IMPACT METRICS
Advanced article metrics track visibility across digital media

EXTENSIVE PROMOTION
Marketing and promotion of impactful research

LOOP RESEARCH NETWORK
Our network increases your article's readership